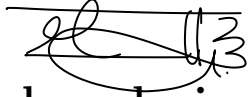


Self attested
Dr. Gopikrishnan Chirappurathu Ramesan

 27/08/2021

**Modelling and numerical analysis of complex tumour
models**

Submitted in partial fulfillment of the requirements
of the degree of
Doctor of Philosophy
of the
Indian Institute of Technology Bombay, India
and
Monash University, Australia

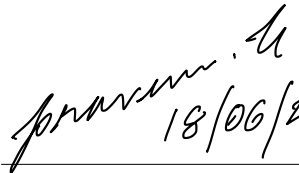


The course of study for this award was developed jointly by Monash University, Australia and the Indian Institute of Technology Bombay, India and was given academic recognition by each of them. The programme was administrated by The IITB-Monash Research Academy

(Year 2021)

Thesis Approval

The thesis entitled “*Modelling and numerical analysis of complex tumour models*” by Gopikrishnan Chirappurathu Remesan (Roll No. 164094001) is approved for the degree of Doctor of Philosophy.


18/06/2021

(Prof. Praveen Chandrasekhar)
External examiner


18-06-2021

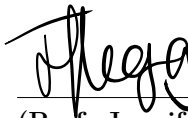
(Prof. Suresh Kumar K)
Internal examiner


18/06/2021

(Prof. Neela Nataraj)
IITB supervisor


20/06/21

(Prof. Jérôme Drinou)
Monash Supervisor


20/6/21

(Prof. Jennifer Flegg)
Monash supervisor


21/06/2021

(Prof. Swati Patankar)
Chairperson

Copyright notice

Notice 1

© Gopikrishnan Chirappurathu Remesan (2021)

Under the Copyright Act 1968, this thesis must be used only under the normal conditions of scholarly fair dealing. In particular no results or conclusions should be extracted from it, nor should it be copied or closely paraphrased in whole or in part without the written consent of the author. Proper written acknowledgement should be made for any assistance obtained from this thesis.

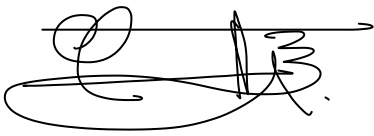
Notice 2

© Gopikrishnan Chirappurathu Remesan (2021)

I certify that I have made all reasonable efforts to secure copyright permissions for third-party content included in this thesis and have not knowingly added copyright content to my work without the owners permission.

Declaration

I declare that this written submission represents my ideas in my own words and where others ideas or words have been included, I have adequately cited and referenced the original sources. I also declare that I have adhered to all principles of academic honesty and integrity and have not misrepresented or fabricated or falsified any idea/data/fact/source in my submission. I understand that any violation of the above will be cause for disciplinary action by the institute and can also evoke penal action from the sources which have thus not been properly cited or from whom proper permission has not been taken when needed.



Student name: Gopikrishnan Chirappurathu Remesan
Date: 12 April 2021

Abstract

In the biphasic models presented in this thesis, a tumour is a continuous agglomeration of a cell phase and an interstitial fluid phase. The model variables are cell volume fraction, cell velocity (plus pressure in 2D/3D), and nutrient concentration governed by a hyperbolic, elliptic, and parabolic equation, respectively. The time-dependent tumour boundary is specified by an ordinary differential equation.

The first part of this dissertation deals with biphasic tumour growth models in 1D. Expensive re-meshing enforced by the time-dependent boundary, lack of uniform bounds on variables, and nonlinearity are a few challenges offered by the biphasic model. Also, the current framework does not facilitate theoretical results, such as the existence of a solution. To address these difficulties, two variant models are presented in which the model equations are defined on an extended domain. In the first (extended model) and second variants (threshold model), the time-dependent boundary is recovered as a curve in the time-space domain at which the cell volume fraction becomes zero and less than a small threshold value, respectively. The source terms in the threshold model are also slightly modified to enable a convergence analysis. A numerical scheme based on a combination of finite element and finite volume methods is employed to obtain the discrete solutions. Under a suitable Courant–Friedrichs–Lewy condition the discrete scheme for the threshold model is shown to converge to a weak solution defined in an appropriate sense.

The second part of the thesis focusses on tumour growth problems in 2D and 3D. A biphasic model is introduced with a well-posed cell velocity equation, the absence of which was a significant drawback in the predecessor models. The notion of the threshold model and a discrete scheme that employs a search method to locate the tumour boundary is extended to the higher dimensions. However, the computational efficiency achieved in 2D is more significant than that in 1D, as the re-meshing was considerably expensive in 2D. Several numerical experiments that illustrate the numerical scheme’s versatility, such as capturing the evolution of tumours with varying topologies are conducted. The lack of a uniform bounded variation estimate for the finite volume solutions of nonlinear multidimensional scalar conservation laws was a challenge in proving the existence of a weak solution to 2D tumour growth models. In this thesis, this goal is achieved and the result is employed to establish the existence of a weak solution to a 2D tumour growth model.

In the third part of the thesis, a modelling framework for tumour growth in an external polymeric medium is derived. The nonlinear elasticity theory and biphasic approach are used to model the polymeric medium and tumour, respectively. Several numerical simulations are conducted, and they are in good agreement with the previous results in the literature.

A long sustained gap between tumour growth modelling and numerical analysis is partially bridged in this dissertation. The attention on computational efficiency facilitates statistical estimation of model parameters, and the findings could be used in real-life medical applications in future.

Acknowledgements

Let me take a moment to express my gratitude to all the people who have supported me during various stages of my research.

I am deeply indebted to my supervisors, Prof. Neela Nataraj, Prof. Jérôme Droniou, and Prof. Jennifer Flegg for their valuable guidance and constant support throughout this study. Their contributions have been vital in providing direction to this thesis and have helped me transform abstract ideas into mathematical results. With their expert knowledge, clarity of thought and gentle words of encouragement they have made sure that I stayed on course during these past four years.

I am extremely grateful to Prof. Helen Byrne, University of Oxford, for giving me the opportunity to collaborate with.

I truly appreciate the insights and comments provided by my Research Progress Committee members, Prof. K. Suresh Kumar and Prof. Janosch Rieger, during my annual progress seminar presentations.

I would also like to express my gratitude to the staff members of IITB-Monash Research Academy, IIT Bombay for providing administrative support during the course of my research. I am thankful to the teaching and non-teaching staff members of the Department of Mathematics, IIT Bombay and School of Mathematical Sciences, Monash University for their kind assistance.

I would like to thank my friends for their invaluable friendship, encouragement and moral support. In particular, I would like to mention Rekha Mallappa Khot, Ruma Rani Maity, Venkitesh S. Iyer, Devika S., Unnikrishnan S., Ansaf V. Karim, Vishnu Narayan S., Rohit James and all my other colleagues from both the institutes for their assistance, understanding and support.

Special thanks to my parents, sisters, and wife for their love and support. I am also grateful to all the other people who I have not mentioned by name for their support, help and advice during my research.

Contents

1	Introduction	1
1.1	Motivation	1
1.2	Review of literature	3
1.2.1	Multiphase modelling in tumour growth	3
1.2.2	Existence results	5
1.3	Organisation and contributions of the thesis	8
1.4	Preliminaries	13
1.4.1	Definitions	13
1.4.2	Identities and inequalities	14
1.4.3	Key results	15
1.5	A biphasic tumour growth model	17
1.5.1	Model derivation	18
1.5.2	Model simplification	23
1.5.3	Nondimensionalisation	24
1.5.4	Domain fixing transformation	26
1.5.5	Finite difference method (FDM) in C. J. W. Breward et al. [1]	27
1.5.6	Modified numerical scheme	30
2	Extended model and numerical scheme	34
2.1	Introduction	34
2.2	The extended model	36
2.3	Weak solutions	37
2.4	Numerical scheme and implementation results	39
2.4.1	Numerical experiment 1	42
2.4.2	Numerical experiment 2	44
2.5	Conclusion	45
3	Threshold model and numerical scheme	46
3.1	Introduction	46
3.2	Threshold model	47
3.2.1	Difference between extended and threshold models	49
3.3	Threshold solution	50
3.4	Numerical solution	52

3.4.1	Physical properties of the threshold model	55
3.4.2	Comments on the numerical method	58
3.5	Numerical example	59
3.6	Conclusion	61
4	Convergence analysis of the numerical scheme for threshold model	62
4.1	Introduction	62
4.2	Main theorems	63
4.3	Proof of Theorem 4.2	65
4.3.1	Existence, uniqueness, and boundedness of the iterates	65
4.3.2	Compactness results	72
4.4	Proof of Theorem 4.3	82
4.5	Maximal time of existence	88
4.6	Conclusion	90
5	Numerical solution of a tumour growth model in two spatial dimensions	91
5.1	Introduction	91
5.2	Model presentation	94
5.2.1	Common features of NUM and NLM models	95
5.2.2	Nutrient unlimited model (NUM)	97
5.2.3	Nutrient limited model (NLM)	97
5.3	Preliminaries and notations	97
5.3.1	Function spaces and norms	98
5.4	Weak solutions and equivalence theorem	99
5.4.1	Well-posedness of velocity-pressure system	99
5.4.2	Equivalence of weak solutions	102
5.5	Numerical scheme	104
5.5.1	Discretisation	104
5.5.2	Mesh-locking effect	105
5.5.3	Approximation of the initial domain	105
5.6	Numerical results	112
5.6.1	Setting for NUM simulations (Set-NUM)	112
5.6.2	Setting for NLM simulations (Set-NLM)	112
5.6.3	Discussion on numerical results	115
5.7	Conclusions	124
6	Strong BV estimates for FV approximations of scalar conservation laws and applications	125
6.1	Introduction	125
6.2	Applications	128
6.3	Main results	130
6.3.1	Preliminaries	130
6.3.2	Presentation of the numerical scheme	131

6.4	Proof of Theorem 6.4	135
6.5	BV estimate for conservation laws with fully nonlinear flux	144
6.6	Numerical examples	146
6.6.1	Observations	148
6.6.2	A remark on strong BV estimate for non–Cartesian grids	153
6.7	Extension to three spatial dimensions	154
6.8	Existence result for a ductal carcinoma model	155
6.8.1	Compactness	158
6.8.2	Convergence	163
6.9	Conclusions	165
7	Two–phase model of compressive stress induced on a surrounding hyperelastic medium by an expanding tumour	166
7.1	Introduction	166
7.2	Mathematical model	169
7.2.1	Deformations in the hydrogel	170
7.2.2	Biphasic tumour growth	172
7.3	Dimensionless model	175
7.4	Discrete scheme	177
7.5	Numerical simulations	180
7.5.1	Free suspension growth	180
7.5.2	Stress controlled growth for tumours	182
7.5.3	Behaviour of tumour radius near the box boundary	185
7.6	Conclusions	187
8	Summary and future work	188
8.1	Summary	188
8.2	Future Work	191
A	Appendix A	193
A.1	Monotone upwind scheme for conservation laws	193
A.2	BV estimate for 3D conservation laws	194
B	Appendix B	
	Biphasic model formulation in higher spatial dimensions	202
	Bibliography	206
	Articles	206
	Books and monographs	215
	Subject index	216
	Author index	218
	List of publications	223

Chapter 1

Introduction

In this chapter, we provide a description of mathematical modelling of different occurrences of tumour development, such as free suspension, *in vitro*, and *in vivo* growth. The motivation of designing and mathematically analysing numerical schemes for such models is discussed. A survey of existing literature, derivation of a standard one-dimensional model [1], standard notations and results, organisation of the thesis, and chapter-wise descriptions are also included.

Biological terminology

In the sequel, *in vivo* refers to a process or experiment that takes place inside a living organism. *In vitro* refers to a process or experiment conducted in a controlled laboratory environment such as a tumour culture in a petri dish. *Vasculature* means a system of blood vessels. The adjectives *vascular* and *avascular* indicate the presence and absence of blood supply, respectively.

1.1 Motivation

In the earliest stage, a tumour consists of a group of proliferating cells without any well-developed vascular network. External nutrients that diffuse into the tumour tissue act as the nutritional supply that triggers cell mitosis. This is called the *avascular stage*. When the tumour attains a threshold size and is no longer able to sustain its constituent cells by a diffusing nutrient alone, it develops a complex vascular system interlaced with that of the host, which marks the onset of malignancy. Therefore, it is crucial to understand the features of the *avascular stage* and the role of various internal and external factors to inhibit tumour proliferation. Moreover, a better understanding of the avascular stage acts as a precursor to the modelling of complex vascular and metastatic stages.

In this thesis, the tumour is modelled as a biphasic mixture of a cell and a fluid phase, that represent the tumour cells and the extracellular fluid, respectively, see Figure 1.1. The fluid is consumed by the tumour cells to grow and proliferate. The dead cells are assimilated into the fluid phase. Since the material constitution of the cell and fluid phases are the same,

both of the phases are assumed to have identical densities. An external nutrient diffuses through the tumour, which controls the rate of cell proliferation and cell death. The mass and momentum balance applied to the solid and fluid phases yield a coupled system of governing equations. Generic variables associated with tumour models considered in this thesis are the cell volume fraction, cell velocity, fluid pressure, and nutrient concentration. The normal velocity of the tumour boundary is the same as the normal velocity of the tumour cells, which characterises the time-dependent tumour boundary.

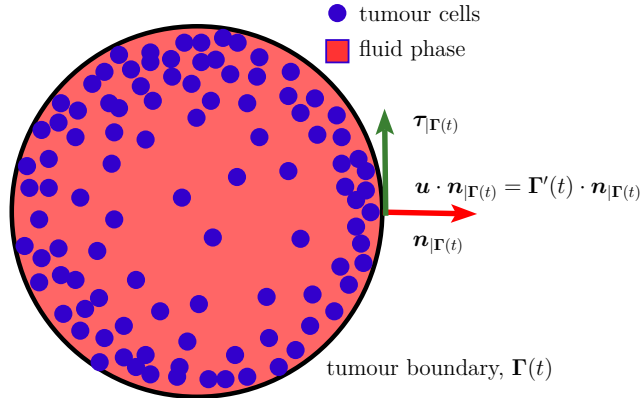


Figure 1.1: Biphase mixture of tumour cells and fluid. Here, $\Gamma(t)$ is the time-dependent boundary of the tumour at time t , $\mathbf{n}_{|\Gamma(t)}$ and $\boldsymbol{\tau}_{|\Gamma(t)}$ are unit normal and tangent vectors to $\Gamma(t)$, respectively. The cell velocity is denoted by \mathbf{u} .

Though the modelling of tumour spheroids was initiated in the 1970s, the theoretical literature available is scarce. Mathematical modelling of tumour growth as a discipline became well established by 2010. However, the well-posedness results and numerical analysis are still lagging behind. One of the main challenges in obtaining theoretical results is the presence of a time-dependent boundary associated with the problem, which also manifests as an unknown variable. The lack of information of regularity of the time-dependent domain significantly reduces the applicability of many standard theorems and analytical results. In fact, characterisation of the time-dependent boundary that enables a proof of the existence of solutions to the model itself is an involved task. The next challenge is the heterogeneous nature of the partial differential equations (PDE) based system that models tumour growth. Usually, the model is governed by a system of hyperbolic, elliptic, parabolic PDEs and a time-dependent ordinary differential equation (ODE). The model variables that are represented by these PDEs are cell volume fraction, cell velocity (and fluid pressure when $d \geq 2$), and nutrient concentration, respectively. For each class of these equations, one employs different mathematical techniques to derive analytical properties. When they appear as a coupled system, a fundamental difficulty is to adapt individual units of analytical tools appropriately to deal with the system.

The heterogeneous nature of models and the time-dependent boundary also offer challenges in designing numerical schemes and the subsequent analysis. A numerical scheme that respects the local conservation of mass such as finite volume method is employed

to discretise the hyperbolic equation. The choice of a finite element methods for cell velocity, pressure, and nutrient concentration has to be stable and not computationally expensive, as the scheme needs to be run over multiple time steps. Also, such a scheme should provide easy access to the velocity vectors needed to compute the boundary fluxes associated with the finite volume scheme. In general, the highest nutrient concentration that can be achieved will be set as unity in most dimensionless models. Therefore, the discrete nutrient concentration obtained from the finite element method should also be bounded by unity and preserve positivity.

Another difficulty associated with the time-dependent boundary is the remeshing associated with the evolving spatial domain. Constructing a proper unstructured mesh with triangles that satisfies properties like shape regularity is computationally intense and should be avoided if possible.

The fundamental theme of this thesis to address the modelling, numerical, and analytical aspects of avascular tumour growth, and the construction of a robust framework. The major goals are summarised below:

- Develop mathematical models for tumours growing in various conditions such as *in vitro*, *in vivo*, in an external polymeric medium. A combination of multiphase mixture theory and linear and nonlinear elasticity theory is employed to devise these models.
- Develop numerical methods with mathematical justifications to obtain approximate solutions of different tumour growth models. A combination of finite element and finite volume methods is used to construct the discrete schemes.
- Establish the existence of a solution to the model and prove convergence of the numerical schemes.

1.2 Review of literature

We classify the literature survey into two subsections. In Subsection 1.2.1, a review of works associated with multiphase modelling of avascular and vascular tumour growths is provided. A review of the state of the art of numerical approximations of tumour growth models is also provided. In Subsection 1.2.2, a survey of literature that study analytical properties such as well-posedness and regularity properties of tumour growth models (not necessarily biphasic) is conducted. Figure 1.2 illustrates key references used in this thesis and their relationship with thesis chapters.

1.2.1 Multiphase modelling in tumour growth

H. P. Greenspan [2] proposed an early model of avascular tumour growth. In this article, it is assumed that a diffusing nutrient solely controls the growth of a multicellular tumour

spheroid. The concentration of the nutrient is governed by a diffusion equation with a source term that depends on the concentration of the nutrient, the size of the tumour, and time. The time-dependent boundary follows an ordinary differential equation derived from balancing the rate of volume change of the tumour spheroid and the net production rate of tumour cells. However, this model considers only a single phase of tumour cells. Many other important aspects of tumour growth such as mechanical interactions between tumour cells and the influence of extra cellular fluid were not accounted in this model.

The earliest biphasic model for avascular growth was proposed by J. P. Ward and J. R. King [3] to the best of our knowledge. In this model, an avascular tumour is a continuous mixture of proliferating and dead cells with distinct volume fractions. Here, the tumour is assumed to contain no other components or vacuous space, which implies that the volume fractions of dead and proliferating cells add up to unity. The mass balance of dead and proliferating cells is employed to derive hyperbolic conservation laws with net production rates of respective phases as source terms. An external diffusing nutrient controls the production rate of tumour cells, which follows a reaction-diffusion equation. The cell velocity follows a Darcy equation. The velocity of tumour radius is set as the velocity of the tumour cells located at the tumour boundary. The Ward and King's model provides a robust framework to construct more complex models that account for viscous effects of tumour cells, mechanical drag between tumour cells and extra cellular fluid, and development of vasculature.

Mathematical modelling achieved further momentum after a series of articles were published by H. M. Byrne et al. [1, 4–7] during the period 2000–2003. A biphasic model with proliferating and dead cells as the constituent phases that depicts the evolution of a vascular tumour was published by C. J. W. Beward in [5]. This one-dimensional model also consists of a hyperbolic conservation law that governs the volume fraction of tumour cells, a Darcy equation that governs cell velocity, and a reaction-diffusion equation that governs the nutrient concentration. The thickness of a blood vessel located at the tumour periphery acts as a time-dependent boundary function.

The framework for the avascular tumour growth model [1] was laid out by the works [5], [3], and [8]. In [1], the avascular tumour is modelled as a one spatial dimensional mixture of a cell and fluid phase. The cell phase constituted by tumour cells is assumed to be a viscous phase, whilst the fluid phase is assumed to be inviscid. The mass balance leads to hyperbolic conservation laws in the volume fractions of the cell and fluid phases. The velocity of the tumour cells is modelled by a steady state linear elasticity equation. The fluid phase follows a Darcy equation. The nutrient is governed by a steady state diffusion equation. Also, in this model the velocity of the tumour boundary is set as the velocity of tumour cells located at the tumour boundary. A higher dimensional version of this model is presented in [7] without any numerical simulations.

Except [7], the articles reviewed above intrinsically assumed that the tumour grows radially symmetrically, which enables reduction of the system to one spatial dimension. However, this is not a valid assumption in many practical cases. Some aspects of asymmetric tumour growth is explored by H. M. Byrne et al. in [4], where the authors consider radially

symmetric solutions of avascular tumour growth and then attempt to introduce asymmetry as perturbations involving spherical harmonics. However, a complete asymmetric study without reducing dimensionality was not conducted. The detailed description of multiphase mixture theory and tumour growth is provided in [6]. In [9], S. Astanin et al. review multiphase models of tumour growth with detailing of mathematical derivations. Though the work presented in these articles accelerated the progress of avascular and vascular tumour growth modelling, the well-posedness was not investigated. Moreover, the stability and convergence analysis of the numerical methods used to solve these models were not studied.

A framework of multiphase fluid flow models with a time-dependent boundary is proposed by J. M. Osborne et al. in [10]. Here, the authors solve the hyperbolic conservation law using a discrete version of the characteristic equation, cell velocity–pressure system using a Taylor–Hood finite element method, and nutrient concentration by a Lagrange \mathbb{P}_1 finite element method. Then, this discrete scheme is applied in [10] to the biphasic model proposed by H. M. Byrne et al. However, the stability and convergence of the numerical scheme are not discussed in this work. This framework is used by M. E. Hubbard et al. [11] to numerically solve a vascular tumour growth model. Here, the authors employ an upwind finite volume method to discretise the hyperbolic conservation law. The analytical properties of the numerical scheme is not discussed in this work as well.

J. A. MacKenzie et al. [12] conducted the stability and convergence analysis of a finite difference scheme for a reaction–diffusion problem on a one-dimensional domain with a time-dependent boundary.

In fact, scientific literature that explicitly study the convergence analysis of numerical schemes for multiphase flow models with time-dependent boundary are rare. *An aim of this thesis is to bridge this gap and develop a strategy to numerically analyse heterogeneous models with a time-dependent boundary.*

1.2.2 Existence results

In this subsection, the literature pertaining to mathematical analysis of tumour growth models from 2003 to 2020 is reviewed. However, there could be missing references which are not directly related to the work in this thesis. Frameworks other than multiphase mixture theory employed to model tumour growth are also briefly mentioned.

Elliptic–Hyperbolic–Parabolic models

In 2003, B. Bazaliy et al. [13] considered a tumour growth model that consists of a coupled system of elliptic and parabolic equations. The nutrient concentration is modelled as a parabolic equation and the pressure exerted by the proliferating cells is modelled as an elliptic equation. The moving boundary is transformed to a fixed domain using the Hanzawa transformation. The existence of a unique solution to this problem is established under strong regularity assumptions that the nutrient concentration belong to $H^5(\Omega(0))$, where $\Omega(0)$ is the initial domain of sufficient regularity. S. Cui et al. [14] considered a tumour growth model driven by nutrient supply, which follows a steady state elliptic equation.

The proliferating cells, quiescent cells, and dead cells follow hyperbolic equations with appropriate source terms. The authors proved global and local existence of solutions by assuming that the initial data is continuously differentiable. A free boundary problem in \mathbb{R}^d , $d \geq 1$, is considered by A. Friedman in 2004 [15]. Here, a hyperbolic conservation law is used to model cell volume fraction and a Darcy equation to model the cell velocity. The normal velocity of tumour boundary is set as normal velocity of the tumour cells present in the boundary. The existence of global spherically symmetric solutions is also proved. Asymptotic estimates for the tumour radius is derived in a sequel article by X. Chen et al. [16]. Y. Tao et al. [17] studied a radially symmetric tumour growth model that accounts for the effect of a therapeutic drug in 2004. The authors assume that the tumour consists of drug, partially drug resistant tumour cells, drug sensitive tumour cells, and intratumoural blood vessels. The dimensionless model is elliptic–hyperbolic, wherein the drug follows a steady state elliptic equation and cells follow a hyperbolic equation. Local and global existence of solutions is proved under the assumption that the initial data has \mathcal{C}^1 regularity.

Phase field and Cahn–Hilliard models

In 2015, P. Colli [18] studied a phase field system of tumour growth, wherein the volume fraction of the tumour cells and healthy cells are modelled using Cahn–Hilliard type equations. The nutrient concentration follows a convection–diffusion equation. The equations are defined in a bounded connected domain and sufficient smoothness is assumed on the boundary. The existence and uniqueness of a weak solution at each finite time is established. The volume fraction and nutrient concentrations are proved to be $H^2(\Omega)$ in space, where Ω is the domain of tumour growth. Another Cahn–Hilliard based model was studied by H. Garcke and K. F. Lam [19] in 2016, in which the existence of a global weak solution of a tumour growth model that consists of tumour cells, healthy cells, and nutrient supply is established. The volume fractions of the tumour and healthy cells are modelled using a Cahn–Hilliard type system. The tumour velocity follows a Darcy equation. A convection–diffusion equation governs the nutrient concentration. The existence of weak solutions in two and three dimensions is established by a Galerkin type approach. The authors have assumed that domain of tumour growth $\Omega \subset \mathbb{R}^d$, $d \in \{2, 3\}$, is bounded with a \mathcal{C}^3 –regular boundary. The Cahn–Hilliard formulation aids to obtain an $L^2(0, T; H^3(\Omega))$ regularity on volume fraction. M. Dai et al. [20] also studied a Cahn–Hilliard based model for tumour growth. In this model, the velocity–pressure system follows Darcy kinetics and nutrient concentration follows steady–state reaction–diffusion equation. The existence of weak solution for each finite time is proved using a combination of compactness techniques and fixed point arguments. The tumour cell volume fraction is shown to be of $\mathcal{C}^0(0, T; H^1(\Omega)) \cap L^2(0, T; W^{2,6}(\Omega))$ regularity.

Porous media model

A model based on diffusion on porous media is developed by I. C. Kim et al [21] in 2016. The cell proliferation rate is a function of the pressure within the tumour. With the assumption that the initial data is in $L^1(\mathbb{R}^d)$, $d \geq 1$, the authors prove the existence of a unique solution by employing viscosity approach. Moreover, the existence of a weak solution

to the limit problem is also established in a bounded domain by assuming H^1 -regularity for the boundary data in time and space.

Optimal control models

In 2017, A. Belmiloudi [22] constructed a model based on optimal control framework that describes the distribution of a drug administered in a brain tumour. Here, the brain tumour consists of normal and cancerous cells. The author employed a set of reaction–diffusion equations to model the interactions between the tumour cells, normal cells, and the drug. The advection velocity is assumed to be in the space $L^\infty(0, T; W^{1, \infty}(\Omega))$, where T is the final time and Ω is a bounded domain of sufficient boundary regularity. Under the assumption that the initial data is in the space $L^\infty(\Omega) \cap H^1(\Omega)$ and positive, the existence and uniqueness of positive solutions to the reaction–diffusion system in the space $H^{2,1}(Q) \cap L^\infty(Q)$, where $Q = (0, T) \times \Omega$ are proved. The existence of an optimal control, that minimizes a cost functional, which measures the concentration of the tumour cells and the difference between observed data from medical imaging such as magnetic resonance imaging (MRI) and the corresponding variables in the reaction–diffusion system, is also proved in this article. S. I. Oke et al. [23] studied a breast cancer model with the effect of chemotherapy. In this model, the amount of drug to be administered is presented as an optimal control problem, wherein the tumour cell concentration is governed by a system of ordinary differential equations. The existence of an optimal control is proved with a stability estimate on the state variables. A wide range of sensitivity analysis experiments are also carried out to understand the dependence of parameters on solutions.

Integro–differential equation models

In 2019, T. Hillen et al. [24] developed a tumour growth model by assuming that the tumour consists of two types of cells: cancer stem cells and tumour cells. A coupled system of integro–differential equations is used to simulate the dynamics of the cancer stem cells and tumour cells. A comprehensive review of this article is carried out by I. Padilla et al. [25]. L. Maddalena [26] has shown existence of solutions (see [25, Theorem 2.3] or [26, Theorem 1]) for this system with homogeneous Neumann boundary conditions and initial data with $H^2(\Omega)$ regularity, where Ω is a bounded domain of sufficient boundary regularity. This result can also be proved for an initial data with $L^2(\Omega)$ regularity (see [25, Theorem 2.4]) at the price of reduced regularity of the solutions. The existence of solutions for a one–dimensional version of the model with homogeneous Dirichlet boundary conditions was proved by A. Fasano et al. [27]. A similar model that studies the role of cancer stem cells in the relapse of tumour growth is proposed by I. Borsi et al. [28]. The cancer cell and cancer stem cell density are modelled by a system of integro–differential equations. With the assumption that the initial conditions are globally continuous up to boundary, the authors have established the existence of a unique global solution.

Nonlinear models

More recently, the existence of a radially symmetric solution to a nonlinear vascular tumour growth model was established by H. Song et al. [31]. The model consists of a nonlinear

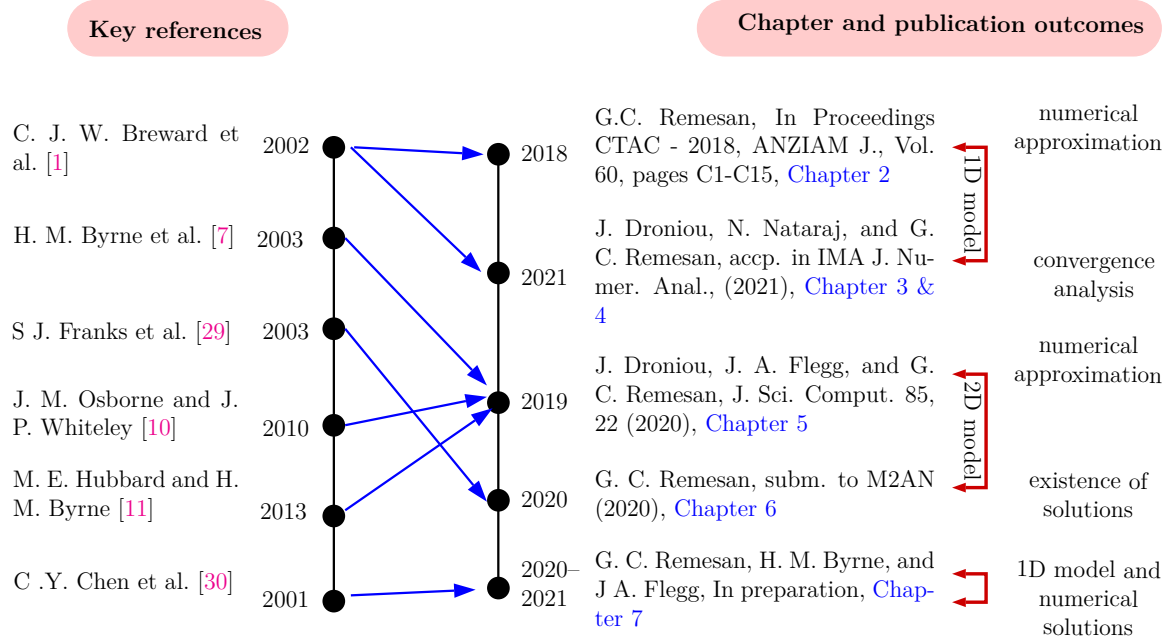


Figure 1.2: Chapters, publications and key references. Arrows indicate the key reference used in the corresponding chapter or publication.

system of stationary Poisson equations that depict the evolution of nutrient concentration and pressure inside the tumour tissue. The tumour cell velocity and pressure are related by a Darcy equation. The authors also consider a linearised problem around the radially symmetric solution and establish estimates of the solution in $\mathcal{C}^k(\Omega)$ spaces.

One of the characteristic features of the aforementioned works is the assumption of high regularity on initial and boundary conditions and on time-dependent boundary. Though the scientific literature on this direction aids to advance the analytical study, the applicability of such works to practical problems is limited. For instance, in general the natural regularity that can be imposed on initial volume fraction of tumour cells is $L^\infty(\Omega(0))$, where $\Omega(0)$ is the initial tumour domain. Similarly, it not very realistic to impose high regularity on the time-dependent boundary. *In this thesis, we impose the natural regularity on the data. Since the time-dependent boundary is an unknown in the framework employed in this thesis, only minimal regularity is assumed on it.*

1.3 Organisation and contributions of the thesis

The models and numerical schemes employed in each chapter with main contributions are presented in Table 1.1. Figure 1.3 classifies the models in each chapter into free suspension, *in vitro*, and *in vivo*. The free suspension model is an idealistic description of tumour growth that serves as a precursor to both *in vivo* and *in vitro* cases.

Chapter 2

Chapter 2 deals a different variant of the Breward–Byrne–Lewis (BBL) model (1.21) termed

as *extended model*, its numerical approximation, and simulations. The spatial domain, $(0, \ell(t))$, evolves with respect to time. To avoid the computational cost incurred from remeshing, an equivalent model is presented, wherein the cell volume fraction equation is defined on a fixed domain $(0, \ell_m)$ and the boundary point $\ell(t)$ is characterised as $\ell(t) := \min\{y : \forall y \leq x \leq \ell_m, \alpha(t, x) = 0\}$. To obtain the numerical solutions, a fixed discretisation of the domain $(0, \ell_m)$ is employed. The cell volume fraction equation is approximated using an upwind and *monotone upwind for scalar conservation laws* (MUSCL) scheme. The discrete tumour boundary is defined as $\ell(t_n) := \min\{y : \forall y \leq x \leq \ell_m, \alpha_h(t_n, x) \leq \alpha_{\text{thr}}\}$ at a time step t_n , where $\alpha_h(t_n, \cdot)$ is the discrete volume fraction at time t_n and α_{thr} is a small positive number. The elliptic (cell velocity) and parabolic equation (nutrient concentration) are solved using Lagrange \mathbb{P}_1 finite element method and a mass lumped \mathbb{P}_1 finite element method, respectively. The threshold value, α_{thr} , is crucial in improving the accuracy of $\ell(t_n)$ and obtaining many theoretical results on the model. The numerical results are tested against test cases with *a priori* known exact solutions.

The extended model removes the explicit tracing of the time-dependent boundary. Moreover, the numerical scheme in Chapter 2 does not increase the model complexity contrary to standard methods such as level set. Since no domain transformation mapping are used [1], the fundamental nature of the PDEs are preserved. Computational cost is reduced by eliminating remeshing altogether.

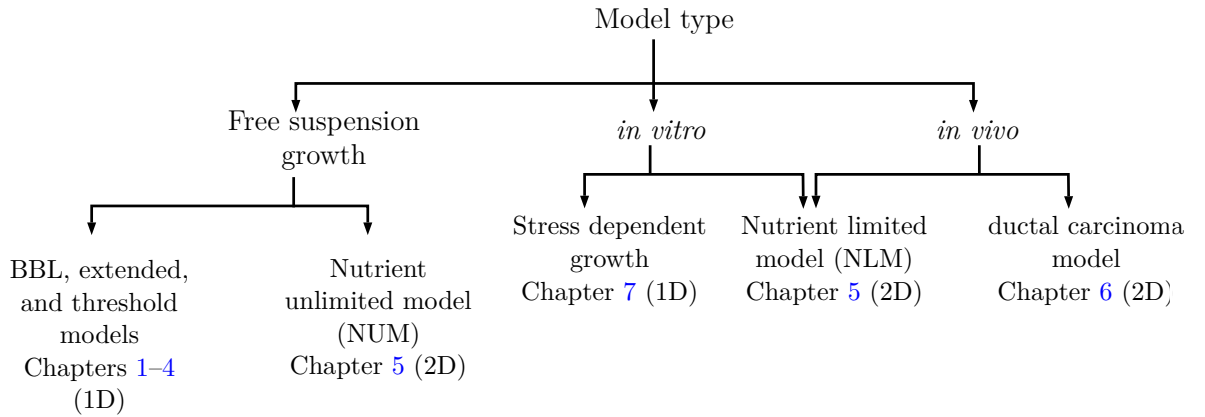


Figure 1.3: Model types in each chapter

Chapter 3

In Chapter 3, another variant of the BBL model called the *threshold model* is introduced. Though the extended model facilitates a faster numerical scheme without the need of remeshing, the lack of uniform bounds of cell volume fraction and coercivity of the cell velocity inside the computational domain $\mathcal{D}_T := (0, T) \times (0, \ell_m)$ hinders a possible convergence analysis. In the threshold model, the tumour boundary is defined as $\tilde{\ell}(t) = \min\{x : \alpha(t, x) \leq \alpha_{\text{thr}} \text{ on } (x, \ell_m)\}$, the source term of the volume fraction is modified as $(\alpha - \alpha_{\text{thr}})f(\alpha, c)$, and force term $\mathcal{H}(\alpha)$ is modified as $(\alpha - \alpha_{\text{thr}})^+ / (1 - \alpha)^2$. The modified

In Table 1.1, the abbreviations Ch., FS, and Dim. stand for Chapter, free suspension, and spatial dimension of the model.

Ch.	Type	Model (Dim.)	Model variables and numerical schemes	Key contributions
1	FS	BBL model (1D)	1. FDM for all variables 2. FDM for cell volume fraction, FEM for cell velocity and nutrient concentration	Introduction and use of finite element method to discretise the BBL model
2	FS	Extended model (1D)	FVM for cell volume fraction, FEM for cell velocity and nutrient concentration	BBL model without the need for explicit tracking of the time-dependent boundary
3	FS	Threshold model (1D)	FVM for cell volume fraction, FEM for cell velocity and nutrient concentration	Source terms are modified using the threshold value
4	FS	Threshold model (1D)	FVM for cell volume fraction, FEM for cell velocity and nutrient concentration	Convergence analysis of numerical scheme in Chapter 3 and existence of a threshold solution
5	<i>in vitro</i> , <i>in vivo</i>	Threshold model (2D)	FVM for cell volume fraction, FEM for cell velocity and nutrient concentration	Developing a well-posed 2D moving boundary model without the explicit tracking of the boundary, design of a numerical scheme for asymmetric tumour growth
6	<i>in vivo</i>	Ductal carcinoma model (2D)	Semi discrete scheme: FVM for cell volume fraction, weak solutions of velocity–pressure system and nutrient equation	Strong BV estimates in 2D, existence of a weak solution to the tumour model
7	<i>in vitro</i>	BBL model on an external polymeric medium (1D)	FVM for cell volume fraction, FEM for cell velocity and nutrient concentration, FDM for tumour radius	Modelling of polymeric medium using nonlinear elasticity, introduction of biphasic approach in stress-dependent growth models

Table 1.1: Summary of models and numerical schemes used in each chapter and key contributions.

equations are justified for theoretical reasons as explained in Section 3.4.2. Also, sufficient emphasis has been provided to keep the model as realistic as possible. A weak solution for the threshold model, termed as *threshold solution*, is presented. A discrete scheme is presented for the threshold model, which is based on the scheme introduced in Chapter 2 for the extended model.

The main contribution of Chapter 3 is the design of the threshold model, wherein the modified model coefficients facilitates a possible convergence analysis. Construction of a discrete scheme that respects the physical properties of the model variables is also a novelty. Additionally, the notion of a variational solution that nicely patch up hyperbolic, elliptic, and parabolic equations associated with the threshold model is introduced, which to the best of our knowledge is first for tumour growth models.

Chapter 4

In Chapter 4, existence of a threshold solution is established by a Galerkin type approach. It is shown that the discrete solutions obtained from Chapter 3 are uniformly bounded in appropriate normed spaces, which aids to extract weakly convergent subsequences. The limit of any convergent subsequence is established to be a threshold solution. The main challenge in Chapter 4 is to prove bounded variation regularity for discrete versions of α and $\partial_x u$, and boundedness of discrete versions of u and $\partial_x u$. The BV regularity is crucial since the term $(\alpha - \alpha_{\text{thr}})f(\alpha, c)$ in the hyperbolic equation is nonlinear and weak- \star convergence is not sufficient to ensure convergence of the numerical scheme. The boundedness and BV results on u and $\partial_x u$ is needed to ensure the BV regularity of α . A discrete Aubin–Simon theorem is used to establish the strong L^2 convergence of c , which is also necessary to account for the nonlinearity in $(\alpha - \alpha_{\text{thr}})f(\alpha, c)$ in the hyperbolic equation.

The convergence analysis of numerical solutions for a tumour growth model that accounts for cell volume fraction, cell velocity, and the nutrient concentration is the main contribution of Chapter 4. To the best of our knowledge, this is the first convergence analysis of its kind. The proof of existence of a threshold solution has not been presented in the previous literature. Chapter 4 provides a generic framework to conduct theoretical and numerical analysis of multiphase tumour growth models.

Chapter 5

Chapter 5 deals with a two and three spatial dimensional versions of the extended model. The main drawback of the model [7] considered in this chapter is that the cell velocity equation is not well-posed due to lack of necessary boundary conditions. In Chapter 5, the well-posedness of the velocity–pressure system at each time is established by supplementing the system with a homogeneous tangential boundary condition. Similar to Chapter 2, we show that the model is equivalent to a variant wherein the hyperbolic equation is defined on a fixed domain and the tumour boundary is obtained as the interface, where the cell volume fraction has a jump from a positive value to zero. The model is discretised using upwind finite volume for the hyperbolic equation, Taylor–Hood finite element method for velocity–pressure system, and mass-lumped \mathbb{P}_1 finite element method for nutrient concentration. The spatial triangulation needs to be unstructured to avoid grid orientation effects associated

with finite volume methods. Chapter 5 also describes numerical difficulties associated with structured triangulation and how to choose an unstructured triangulation.

The development of a mathematically well-defined model without the presumption of symmetric tumour growth and design of a numerical scheme that eliminates expensive remeshing in 2D and seamlessly simulates tumours (*in vivo and in vitro*) with irregular shapes and changing topological structures are the main contributions of Chapter 5. The equivalence of the original model and a variant that removes the time-dependent boundary from the system altogether, is proved. While doing so the complexity of the model is not increased. Such a model and discrete scheme is novel in literature.

Chapter 6

In Chapter 6, a strong bounded variation estimate for finite volume solutions of nonlinear hyperbolic conservation laws of the form $\partial_t \alpha + \mathbf{F}(t, \mathbf{x}, \alpha) = 0$ and $\alpha(0, \cdot) = \alpha_0$ in Ω on nonuniform Cartesian grids in \mathbb{R}^d , $d \geq 2$, is derived. The lack of such a result was a major difficulty in obtaining a convergence result in higher dimensional models of tumour growth. A major change from previously available literature is the relaxation of the classical assumption that $\operatorname{div}_{\mathbf{x}} \mathbf{F} = 0$. The existence of weak solution to a two-dimensional tumour growth problem is proved by employing the strong bounded variation estimate on the cell volume fraction (concentration). The model is adapted from [29] and depicts the evolution of tumour growth in a two-dimensional rectangular domain. A hyperbolic conservation law, viscous stokes system, and Poisson equation that respectively governs the cell volume fraction, cell velocity–pressure system, and nutrient concentration constitute the model.

The strong *BV* estimate on finite volume schemes for nonlinear scalar conservation laws in 2D and 3D over nonuniform Cartesian grids is the main contribution of Chapter 6. The velocity vector has non-zero divergence in the proofs, which is an improvement over the existing literature with zero divergence. Chapter 6 complements the state of the art of theoretical analysis of tumour growth models by establishing the existence of a weak solution to a 2D tumour growth problem.

Chapter 7

In *in vitro* tumour growth experiments, cells are cultured in a gelatinous medium, referred to as hydrogel, that mimics the properties of tissues. An expanding tumour compresses the hydrogel against the boundaries of the culture dish. The stress generated in the hydrogel by this compression hinders the tumour growth. In Chapter 7, a mathematical model that describes how mechanical deformations in the hydrogel affect tumour growth is presented. The tumour is modelled as a two-phase mixture of a viscous tumour cell phase and an isotropic inviscid interstitial fluid phase. The hydrogel is modelled as a nonlinear elastic material. For simplicity and as an initial analysis, we restrict the attention to a one-dimensional Cartesian geometry. The model variables are cell volume fraction, cell velocity, nutrient concentration, and tumour radius. These variables are respectively governed by a hyperbolic conservation law, a generalised Stokes equation, a parabolic diffusion equation, and an ordinary differential equation. Continuity of stress at the tumour–hydrogel interface manifests as a Neumann boundary condition for the generalised Stokes equation. A

combination of a finite volume method for the hyperbolic conservation law, Lagrange \mathbb{P}_1 finite element method for the generalised Stokes equation and mass lumped finite element method for the diffusion equation is used to construct numerical solutions. The qualitative behaviour of tumour growth depends on the hydrogel compressibility. It is observed that the tumour either evolves to a stable equilibrium size or it is compressed and eventually eliminated. The numerical simulations are consistent with previous findings from the literature, such as limited growth in an external medium.

Chapter 7 contributes to the mathematical modelling of tumour growth by coupling the multiphase tumour growth driven by an external limiting nutrient with the kinetics of a nonlinear elastic external medium. The novel model aids investigating into different aspects of tumour growth in an external medium such as influence of hydrogel compressibility and stabilisation of tumour radius. Moreover, it paves a basic groundwork for the construction of higher dimensional analogues.

Chapter 8 and appendices

Chapter 8 presents the summary and conclusions of the thesis. The prospective extensions of different variants of tumour growth models are discussed. A summary of future plans on numerical analysis of tumour growth models in one and higher spatial dimensions is also presented. Appendix A contains a brief derivation of the monotone upwind schemes for scalar conservation laws and a proof of strong bounded variation estimate for finite volume schemes in 3D. A brief derivation of the biphasic tumour growth model in higher dimensions is presented Appendix B.

1.4 Preliminaries

Identities, definitions, and results used in this thesis are listed here. Subsection 1.4.1 contains definitions of function spaces, inner products, and norms. The identities and inequalities are provided in Subsection 1.4.2. Key lemmas and theorems are listed in Subsection 1.4.3.

1.4.1 Definitions

The definitions of Lebesgue and Sobolev spaces used in this dissertation are standard; see H. Brezis [96] and L. C. Evans [97] for further details. Let $\Omega \subset \mathbb{R}^d$ be an open and bounded in \mathbb{R}^d ($d \geq 1$) with boundary $\partial\Omega$, where d is the dimension. The regularity of $\partial\Omega$ varies in each chapter and it is explicitly mentioned where ever required. The set $\{\Omega(t)\}_{0 \leq t \leq T}$ denotes a family of open and bounded time-dependent domains in \mathbb{R}^d ($d \geq 1$); the boundary of $\Omega(t)$ is denoted by $\partial\Omega(t)$.

The Euclidean norm on \mathbb{R}^d is denoted by $\|\bullet\|_d$. The Lebesgue measure in \mathbb{R}^d is denoted by μ_d and the measure of measurable set $A \subset \mathbb{R}^d$ is written as $\mu_d(A) =: \text{meas}(A)$. Let $\alpha = (\alpha_1, \dots, \alpha_d)$ be a multi-index in \mathbb{N}^d and its length is defined as $|\alpha| = \sum_{i=1}^d |\alpha_i|$.

Define the Sobolev space $W^{m,p}(\Omega)$, where $m \geq 0$ and $1 \leq p < \infty$ as

$$W^{m,p}(\Omega) := \{f \in L^p(\Omega) : \partial^\alpha f \in L^p(\Omega), |\alpha| \leq m\}$$

and norm $\|f\|_{W^{m,p}(\Omega)}$ as

$$\|f\|_{W^{m,p}(\Omega)} := \|f\|_{m,p,\Omega} := \left(\sum_{|\alpha| \leq m} \|\partial^\alpha f\|_{L^p(\Omega)}^p \right)^{1/p}.$$

For $p = \infty$, define

$$\|f\|_{W^{m,\infty}(\Omega)} := \max_{|\alpha| \leq m} \|\partial^\alpha f\|_{L^\infty(\Omega)}.$$

The Hilbert space $W^{m,2}(\Omega)$ is denoted by $H^m(\Omega)$. For any $k \geq 0$, $\mathcal{C}^k(\Omega)$ denotes k -times continuously differentiable functions up to the boundary $\partial\Omega$. The class of all smooth functions is denoted by $\mathcal{C}^\infty(\Omega)$ and those have a compact support by $\mathcal{C}_c^\infty(\Omega)$. The closure of $\mathcal{C}_c^\infty(\Omega)$ in $W^{m,p}(\Omega)$ is denoted by $W_0^{m,p}(\Omega)$.

The product spaces are defined as $\mathbf{W}^{m,p}(\Omega) := \prod_{i=1}^d W^{m,p}(\Omega)$ and $\mathbf{H}^m(\Omega) := \prod_{i=1}^d H^m(\Omega)$. For $\mathbf{u} = (u_1, \dots, u_d) \in \mathbf{W}^{m,p}(\Omega)$, $d \in \{1, 2\}$, define the norm

$$\|\mathbf{u}\|_{m,p,\Omega} := \sum_{i=1}^d \sum_{|\beta| \leq m} \|\partial^\beta u_i\|_{L^p(\Omega)},$$

where $\beta \in \mathbb{N}^d$ is a multi-index. Locally regular Sobolev spaces are defined as

$$X_{\text{loc}}(\Omega) := \{v \in L^2(\Omega) : v|_\omega \in X(\omega) \ \forall \omega \subset\subset \Omega\},$$

where $X = W^{m,p}$ or $X = \mathbf{W}^{m,p}$. The space $\mathcal{C}_c^1(\Omega; \mathbb{R}^d)$ is collection of smooth and compactly supported functions from Ω to \mathbb{R}^d . The bounded variation seminorm of a function $f \in L^1(\Omega)$, where $\Omega \subset \mathbb{R}^d$ is defined by

$$|f|_{BV(\Omega)} := \sup \left\{ \int_\Omega f \operatorname{div}(\boldsymbol{\varphi}) \, d\mathbf{x} : \boldsymbol{\varphi} \in \mathcal{C}_c^1(\Omega; \mathbb{R}^d), \|\boldsymbol{\varphi}\|_{L^\infty(\Omega)} \leq 1 \right\}.$$

The space of real valued functions on Ω with bounded variation is denoted by $BV(\Omega)$.

1.4.2 Identities and inequalities

The algebraic identities are presented here.

I. **Grouping identities.** If $a, b, c, d \in \mathbb{R}$, then the following identities hold:

$$ab - cd = \frac{(a+c)(b-d)}{2} + \frac{(a-c)(b+d)}{2} \quad \text{and} \quad (1.1a)$$

$$ab - cd = (a-c)b + (b-d)c. \quad (1.1b)$$

II. **Young's inequalities.** [96, Theorem 4.33] Let $a, b \in \mathbb{R}$ and $p > 1$. Then, the following hold:

$$|ab| \leq \frac{|a|^p}{p} + \frac{|b|^q}{q} \quad \text{and} \quad |ab| \leq \frac{a^2}{2\epsilon} + \frac{\epsilon b^2}{2} \quad \forall \epsilon > 0.$$

III. **Max–Min identities.** Let $a \in \mathbb{R}$. Define $a^+ = \max(a, 0)$ and $a^- = -\min(a, 0)$. Then, the following identities hold:

$$a = a^+ - a^- \quad \text{and} \quad |a| = a^+ + a^-.$$

IV. **Discrete integration by parts formula.** [98, Section D.1.7] For any families $(a_n)_{n=0, \dots, N}$ and $(b_n)_{n=0, \dots, N}$ of real numbers, it holds

$$\sum_{n=0}^{N-1} (a_{n+1} - a_n)b_n = - \sum_{n=0}^{N-1} a_{n+1}(b_{n+1} - b_n) + a_N b_N - a_0 b_0. \quad (1.4)$$

V. **Hölder's inequality.** [96, Theorem 4.6] Let $1 \leq p, q \leq \infty$ and $1 = 1/p + 1/q$. If $f \in L^p(\Omega)$ and $g \in L^q(\Omega)$, then $fg \in L^1(\Omega)$ and

$$\|fg\|_{L^1(\Omega)} \leq \|f\|_{L^p(\Omega)} \|g\|_{L^q(\Omega)}.$$

VI. **Korn's second inequality.** [99, Theorem 3.78]. If $\Omega \subset \mathbb{R}^d$, where $d = 2, 3$ is a domain, then there exists a positive constant \mathcal{C}_K such that, for every $\mathbf{v} \in \mathbf{H}_d^1(\Omega)$,

$$\mathcal{C}_K \|\mathbf{v}\|_{1, \Omega} \leq \|\nabla_s \mathbf{v}\|_{0, \Omega} + \|\mathbf{v}\|_{0, \Omega}.$$

VII. **Poincaré inequality.** [100, Theorem 2.3.4] For all $u \in W_0^{1,p}(\Omega)$, it holds

$$\|u\|_{L^p(\Omega)} \leq \mathcal{C}_p \|\nabla u\|_{L^p(\Omega)},$$

where the constant $\mathcal{C}_p := \text{diam}(\Omega)$ is independent of u .

1.4.3 Key results

The key lemmas and theorems employed in this dissertation are collected here. They are classified into compactness and convergence results and regularity results.

Compactness and convergence results

I. **Helly's selection theorem.** [101, Theorem 4, p. 176]. Let $\Omega \subset \mathbb{R}^d$ ($d \geq 1$) be an open and bounded set with a Lipschitz boundary $\partial\Omega$, and $(f_n)_{n \in \mathbb{N}}$ be a sequence in $BV(\Omega)$ such that $(\|f_n\|_{BV(\Omega)}, \|f_n\|_{L^1(\Omega)})_n$ is uniformly bounded. Then, there exists a subsequence $(f_n)_n$ up to re-indexing and a function $f \in BV(\Omega)$ such that as $n \rightarrow \infty$, $f_n \rightarrow f$ in $L^1(\Omega)$ and almost everywhere in Ω .

II. Discrete Aubin–Simon theorem. [98, Theorem C.8].

The following Definition is required in this theorem.

Definition 1.1 (Compactly–continuously embedded sequence). [98, Definition C.6]. *Let B be a Banach space. The families of Banach spaces $\{X_h, \|\cdot\|_{X_h}\}_h$ and $\{Y_h, \|\cdot\|_{Y_h}\}_h$ are such that $Y_h \subset X_h \subset B$. We say that the family $\{(X_h, Y_h)\}_h$ is compactly embedded in B if the following conditions hold.*

- Any sequence $\{u_h\}_h$ such that $u_h \in X_h$ and $\{\|u_h\|_{X_h}\}_h$ uniformly bounded is relatively compact in B .
- Any sequence $\{u_h\}_h$ such that $u_h \in X_h$, $\{\|u_h\|_{X_h}\}_h$ uniformly bounded, $\{u_h\}_h$ converges in B , and $\|u_h\|_{Y_h} \rightarrow 0$, converges to zero in B .

Statement of the theorem: Let $p \in [1, \infty)$, $(X_m, Y_m)_{m \in \mathbb{N}}$ be a compactly-continuously embedded sequence in a Banach space B , and $(f_m)_{m \in \mathbb{N}}$ be a sequence in $L^p(0, T; B)$, where $T > 0$, and assumptions (a), (b), and (c) are satisfied.

- (a) Corresponding to each $m \in \mathbb{N}$, there exists an $N \in \mathbb{N}$, a partition $0 = t_0 < \dots < t_N = T$, and a finite sequence $(g_n)_{n=0, \dots, N}$ in X_m such that $\forall n \in \{0, \dots, N-1\}$ and almost every $t \in (t_n, t_{n+1})$, $f_m(t) = g_n$. Then, the discrete derivative $\delta_m f_m$ is defined almost everywhere by $\delta_m f_m(t) := (g_{n+1} - g_n)/(t_{n+1} - t_n)$ on (t_n, t_{n+1}) for all $n \in \{0, \dots, N-1\}$.
- (b) The sequence $(f_m)_{m \in \mathbb{N}}$ is bounded in $L^p(0, T; B)$.
- (c) The sequences $(\|f_m\|_{L^p(0, T; X_m)})_m$ and $(\|\delta_m f_m\|_{L^1(0, T; Y_m)})_m$ are bounded.

Then, $(f_m)_{m \in \mathbb{N}}$ is relatively compact in $L^p(0, T; B)$.

- ## III. (a) Weak–strong convergence lemma. [98, Lemma D.8].
- If $p \in [0, \infty)$ and $q := p/(1-p)$ are conjugate exponents, $f_n \rightarrow f$ strongly in $L^p(X)$, and $g_n \rightarrow g$ weakly in $L^q(X)$, where (X, μ) is a measured space, then

$$\int_X f_n g_n d\mu \rightarrow \int_X f g d\mu.$$

- (b) **Bounded–strong convergence lemma.** If $f_n \rightarrow f$ in $L^2(X)$, $g_n \rightarrow g$ almost everywhere on X , and $\|g_n\|_{L^\infty(X)}$ is uniformly bounded, then $f_n g_n$ converges to $f g$ in $L^2(X)$.
- (c) **Discrete positivity lemma [32, Theorems 3.1, 3.2].** Let D be an $n \times n$ diagonal matrix with positive entries, A be an $n \times n$ matrix with all off-diagonal entries nonpositive, and \mathbb{I}_n be $n \times n$ identity matrix. Then, the operator $(\mathbb{I}_n + kD^{-1}A)^{-1}$ is positive for sufficiently small $k > 0$.

Regularity results and estimates

- I. **Internal regularity of Poisson equation.** [102, Theorem III.4.2] Let $f \in L^2(\Omega)$ and $\Omega \subset \mathbb{R}^2$ be an open and bounded set. If $u \in H^1(\Omega)$ is a solution of the Poisson equation $-\Delta u = f$, then $u \in H_{\text{loc}}^2(\Omega)$. Also, for every bounded and open sets $\overline{\Omega}_1 \subset \Omega_2 \subset \overline{\Omega}_2 \subset \Omega$ there exists a constant $\mathcal{C}(\Omega_1, \Omega_2) > 0$ independent of u such that $\|u\|_{2,2,\Omega_1} \leq \mathcal{C}\|f\|_{0,2,\Omega_2}$.
- II. **Global regularity of Poisson equation.** [103, Corollary 8.3.3] Set $m \geq 2$ and $p \geq 1$. Let Ω be a rectangle and $f \in W^{m-2,p}(\Omega)$. If $u \in H^1(\Omega)$ is a solution of the boundary value problem $-\Delta u = f$ in Ω with $(\lambda - 1)\nabla u \cdot \mathbf{n} + \lambda u = 0$ on $\partial\Omega$, where $\lambda \in \{0, 1\}$, then $u \in W^{m,p}(\Omega)$.
- III. **Internal regularity of Stokes equation.** [102, Theorems IV.5.8, IV.6.1] Let Ω be an open and bounded set and $g \in H_{\text{loc}}^{k+1}(\Omega)$, $k \geq 0$. Let $(\mathbf{u}, p) \in \mathbf{H}_{\text{loc}}^1(\Omega) \times L_{\text{loc}}^2(\Omega)$ be a solution to the compressible Stokes system

$$-\mu \left(\Delta \mathbf{u} + \frac{1}{3} \nabla(\text{div}(\mathbf{u})) \right) + \nabla p = 0 \text{ and } \text{div}(\mathbf{u}) = g.$$

Then, it holds $(\mathbf{u}, p) \in \mathbf{H}_{\text{loc}}^{k+2,2} \times H_{\text{loc}}^{k+1}(\Omega)$. Also, for every bounded and open sets $\overline{\Omega}_1 \subset \Omega_2 \subset \overline{\Omega}_2 \subset \Omega$ there exists a constant $\mathcal{C}(\Omega_1, \Omega_2) > 0$ independent of \mathbf{u} and p such that $\|\mathbf{u}\|_{k+2,2,\Omega_1} + \|p\|_{k+1,2,\Omega_1} \leq \mathcal{C}\|g\|_{k+1,2,\Omega_2}$.

- IV. **Petree–Tartar lemma.** [99, Lemma A.38]. If X, Y , and Z are Banach spaces, $A : X \rightarrow Y$ is an injective operator, $T : X \rightarrow Z$ is a compact operator, and there exists a positive constant \mathcal{C}_1 such that $\mathcal{C}_1\|x\|_X \leq \|Ax\|_Y + \|Tx\|_Z$, then there exists a positive constant \mathcal{C}_{PT} such that $\mathcal{C}_{PT}\|x\|_X \leq \|Ax\|_Y$.
- V. **Lax–Milgram Theorem.** [97, Section 6.2]. Let H be a Hilbert space and $B : H \times H \rightarrow \mathbb{R}$ be a bilinear map such that $|B(u, v)| \leq \alpha\|u\|_H\|v\|_H$ (continuity) and $\beta\|u\|_H^2 \leq B(u, u)$ (coercivity) for every $u, v \in H$, where $\alpha > 0$ and $\beta > 0$ are fixed constants. Let $f : H \rightarrow \mathbb{R}$ be bounded linear functional on H . Then there exists a unique element $u \in H$ such that $B(u, v) = f(v)$ for every $v \in H$.

1.5 A biphasic tumour growth model

The avascular tumour growth model derived by C. J. W. Breward et al. [1] is presented here. The detailed derivation of the model, simplification, and nondimensionalisation is discussed. The physical motivations of choosing source terms and constitutive relations are also presented. This model from [1] and further reproduced in (1.21) is referred to as Breward–Byrne–Lewis (BBL) model in the sequel. The models considered in this dissertation are motivated from the BBL model. Therefore, it is crucial to understand how the BBL model is derived in the first place. Also, a brief prologue on the BBL model aids

to understand how the adapted models in Chapter 2 and Chapter 3 are different. The robustness of the numerical schemes designed in this thesis are compared with the finite difference method based solutions of the BBL model presented in [1]. To make comparisons easy, the schemes used in [1] are presented and the results are reproduced in this section.

1.5.1 Model derivation

In C. J. W. Breward et al. [1], a tumour is construed as a continuous agglomeration of two phases. The phase that consists of tumour cells is called the cell phase. The fluid medium that surrounds the cells is called the fluid phase. The cell phase is assumed to be viscous owing to surface irregularities, and the fluid phase is assumed to be inviscid. The tumour cells and fluid medium follow the conservation of mass and momentum. Cells undergo mitotic division by consuming the extracellular fluid. Dead cells disintegrate and meld into the fluid phase. The pressures in the two phases are different from each other. The cell phase receives an additional pressure factor due to cell–cell viscous interactions. The relative distance between the cells determines the nature of force experienced between them. Remotely located cells exhibit little interaction. If the cells are within a threshold distance, the filopodial (locomotive structures associated with cell membrane) action brings them together, and the force is attractive. When cells exceed their natural close packing density, the proximity produces repulsive interactions between them. The repulsion drives cells away and releases the mechanical stress. Oxygen – the representative nutrient – is the limiting factor in cell growth and division. It is assumed that cells and fluid phases have the same constant density, which is reasonable considering each phase act as a source and sink of the other. Therefore, the unknown variables in the conservation laws are volume fractions of each phase rather than their absolute masses. The inertial effects are neglected due to low Reynolds number [1, p. 128], so that the momentum conservation laws are in the steady-state form. The model variables and parameters used in this thesis, meaning, and dimensions are provided in Table 1.2.

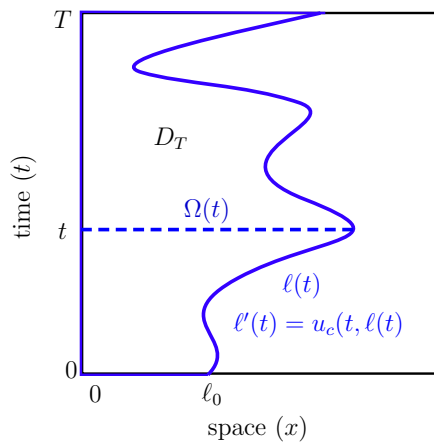


Figure 1.4: Time–space domain D_T and time–dependent boundary $\ell(t)$.

Notation	Meaning	Dimension
α	cell volume fraction	1
β	fluid volume fraction	1
u_α	cell velocity	LT^{-1}
u_β	fluid velocity	LT^{-1}
q_α	production rate of tumour cells	T^{-1}
q_β	production rate of fluid	T^{-1}
σ_α	stress in cell phase	$\text{ML}^{-1}\text{T}^{-2}$
σ_β	stress fluid phase	$\text{ML}^{-1}\text{T}^{-2}$
p_α	pressure in cell phase	$\text{ML}^{-1}\text{T}^{-2}$
p_β	pressure in fluid phase	$\text{ML}^{-1}\text{T}^{-2}$
Σ	pressure in the cell phase due to cell–cell interactions	$\text{ML}^{-1}\text{T}^{-2}$
f_α	momentum source term in cell phase	$\text{ML}^{-2}\text{T}^{-2}$
f_β	momentum source term in fluid phase	$\text{ML}^{-2}\text{T}^{-2}$
c	nutrient concentration	$\text{ML}^{-1}\text{T}^{-1}$
Q_c	rate of change of nutrient concentration	$\text{ML}^{-3}\text{T}^{-1}$
μ_α	viscosity of cell phase	$\text{ML}^{-1}\text{T}^{-2}$

Table 1.2: Notations and dimensions of model variables. Here, M, L, and T are dimensions of mass, length, and time.

We study the evolution of the avascular tumour growth over the finite time interval $(0, T)$. The tumour occupies the domain $(0, \ell(t))$ at each finite time $t \in [0, T)$. The tumour radius is defined by the following ordinary differential equation:

$$\ell'(t) = u_\alpha(t, \ell(t)) \quad \text{and} \quad \ell(0) = \ell_0. \quad (1.5)$$

Define the time–space domain of tumour growth by $D_T := \cup_{0 < t < T} (\{t\} \times \Omega(t))$, where $\Omega(t) := (0, \ell(t))$ and $\ell(t)$ is referred to as the *tumour radius* at time t in the sequel, see Figure 1.4. The governing equations for volume fractions, velocities, and nutrient concentration in D_T are derived next.

Conservation laws

The conservations laws are derived based on Reynold’s transportation theorem, see Theorem 1.2.

Theorem 1.2 (Reynold’s transportation theorem [104, p. 22]). *Let $V(t)$, $t \geq 0$, be a time–dependent domain and $B(t, \cdot) : V(t) \rightarrow \mathbb{R}$ be a scalar quantity associated with a fluid flowing with velocity $u(t, \cdot) : V(t) \rightarrow \mathbb{R}$. Then, it holds that*

$$\frac{d}{dt} \int_{V(t)} B(t, x) dx = \int_{V(t)} \left(\frac{\partial B}{\partial t} + \frac{\partial}{\partial x} (Bu) \right) dx.$$

An application of Theorem 1.2 and (1.5) to the cell volume fraction $\alpha(t, \cdot) : (0, \ell(t)) \rightarrow \mathbb{R}$ yields

$$T_1 := \frac{d}{dt} \int_0^{\ell(t)} \alpha(t, x) dx = \int_0^{\ell(t)} (\partial_t \alpha + \partial_x(\alpha u_\alpha)) dx.$$

It is assumed that there is no inflow or outflow across the boundary points $(t, 0)$ and $(t, \ell(t))$. Therefore, the differential T_1 is same as the net production rate of the tumour cells, which is equal to $\int_0^{\ell(t)} q_\alpha dx$. As a result, we obtain

$$\int_0^{\ell(t)} (\partial_t \alpha + \partial_x(\alpha u_\alpha)) dx = \int_0^{\ell(t)} q_\alpha dx,$$

which translates to the PDE

$$\frac{\partial \alpha}{\partial t} + \frac{\partial}{\partial x}(\alpha u_\alpha) = q_\alpha \quad \text{in } D_T. \quad (1.6a)$$

Follow similar steps to derive the conservation law for the fluid volume fraction, over D_T

$$\frac{\partial \beta}{\partial t} + \frac{\partial}{\partial x}(\beta u_\beta) = q_\beta \quad \text{in } D_T. \quad (1.6b)$$

The assumption that the tumour contains no voids implies $\alpha(x, t) + \beta(x, t) = 1$ for every $(t, x) \in D_T$. Since the inertial effects are negligible, the conservation of momentum yields

$$f_\alpha + \frac{\partial}{\partial x}(\alpha \sigma_\alpha) = 0 \quad \text{and} \quad f_\beta + \frac{\partial}{\partial x}(\beta \sigma_\beta) = 0 \quad \text{in } D_T. \quad (1.7a)$$

Here, f_α (resp. f_β) is the body force density acting on the cell phase (resp. fluid phase). The second term $\partial_x(\alpha \sigma_\alpha)$ (resp. $\partial_x(\beta \sigma_\beta)$) is the surface stress density acting on cell phase (resp. fluid phase) represented in divergence form.

Constitutive laws

We provide the constitutive laws that describe the terms q_α , q_β , σ_α , σ_β , f_α , and f_β . Cell death is the only internal source that creates fluid volume inside the tumour mass and so it follows that $q_\alpha = -q_\beta$. The term q_α is defined by

$$q_\alpha := \underbrace{\alpha(1-\alpha) \frac{S_0 c}{1+S_1 c}}_{\mathfrak{B}(\alpha, c)\text{-birth rate}} - \underbrace{\frac{S_2 + S_3 c}{1+S_4 c} \alpha}_{\mathfrak{D}(\alpha, c)\text{-death rate}}. \quad (1.8)$$

Here, S_0, S_1, S_2, S_3 , and S_4 are positive parameters. In (1.8), the first and second terms represent the cell birth and death rates, respectively. When $\alpha = 0$, that is, when no cell is present or when the nutrient concentration approaches zero, the birth rate becomes zero.

Denote $b(c) = S_0c/(1 + S_1c)$ and $d(c) = (S_2 + S_3c)/(1 + S_4c)$. Since $b'(c) = S_0/(1 + S_1c)^2$, the birth rate, $\mathfrak{B}(\alpha, c)$, increases with respect to the nutrient concentration. In the limiting case, where c approaches infinity, the birth rate becomes $\alpha(1 - \alpha)S_0/S_1$. The condition $S_3/S_4 \leq S_2$ is imposed, so that the death rate, $\mathfrak{D}(\alpha, c)$, remains a decreasing function of the nutrient concentration. If $c = 0$, then $\mathfrak{D}(\alpha, c)$ becomes αS_2 and when c approaches infinity, $\mathfrak{D}(\alpha, c)$ becomes $\alpha S_3/S_4$. The variations of $b(c)$ and $d(c)$ are depicted in Figure 1.5.

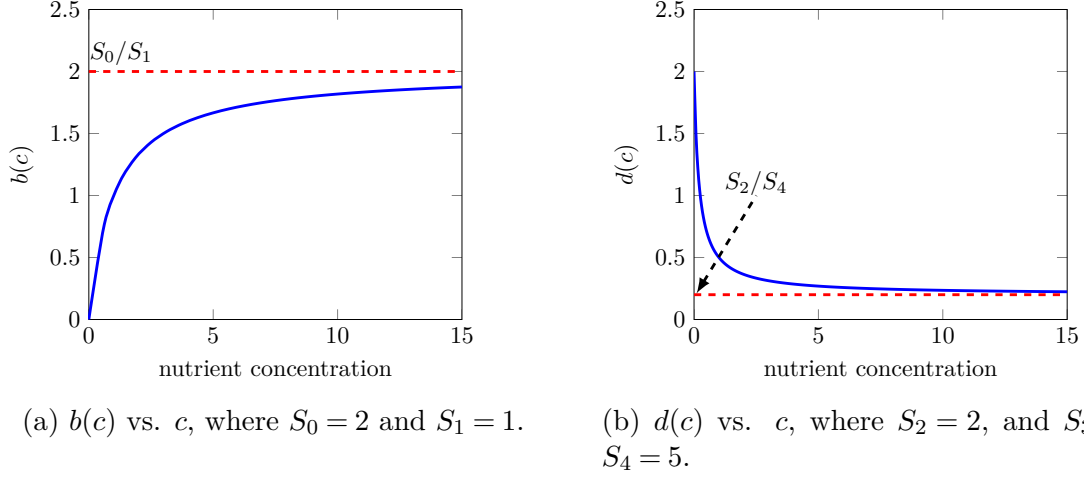


Figure 1.5: Variation of $b(c)$ and $d(c)$. The blue thick lines indicate the variation of $b(c)$ and $d(c)$, while the red dotted lines show the asymptotes as c approaches infinity.

Stress Tensors

Stresses in the cell and fluid phases are described by

$$\sigma_\alpha = -p_\alpha + 2\mu_\alpha \frac{\partial u_\alpha}{\partial x}, \quad \text{and} \quad \sigma_\beta = -p_\beta, \quad (1.9a)$$

wherein pressures in the cell and fluid phases are related by

$$p_\alpha = p_\beta + \gamma \mathcal{H}(\alpha), \quad (1.9b)$$

$\mathcal{H} : (0, 1) \rightarrow \mathbb{R}$ quantifies the cell–cell interactions, and

$$\mathcal{H}(\alpha) := \frac{\alpha - \alpha^R}{(1 - \alpha)^2} \text{Heav}(\alpha - \alpha_{\min}). \quad (1.9c)$$

Here, the Heaviside step function is defined as $\text{Heav}(x) := 1$ if $x \geq 0$ and $\text{Heav}(x) := 0$ otherwise. The quantity α^R is the volume fraction of the cells at their natural close packing. If the cell volume fraction exceeds α^R , then the cells experience mechanical stress which

drives them away from one another. On the other hand, if the cell volume fraction is below a threshold value α_{\min} , then the cells are sparsely distributed and cell–cell interactions are negligible. If $\alpha^R > \alpha > \alpha_{\min}$, then the cells experience a nonzero attractive interaction quantified by \mathcal{H} .

The variation of \mathcal{H} with respect to α is plotted in Figure 1.6 for $\alpha_{\min} = 0.7$ and $\alpha^R = 0.8$.

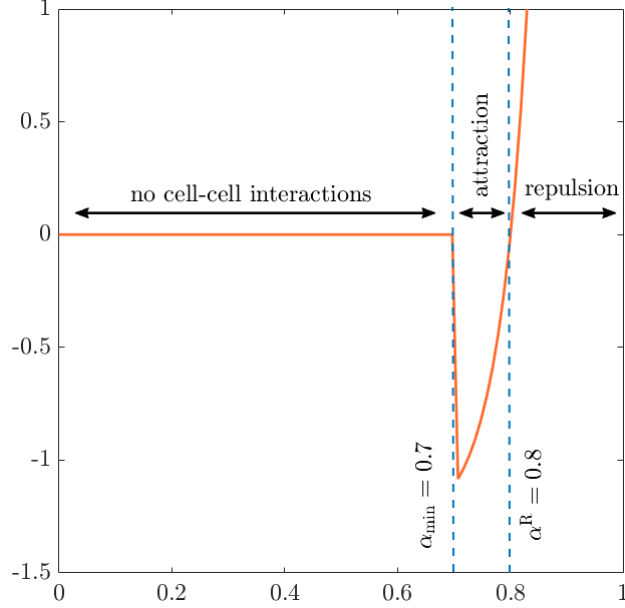


Figure 1.6: Figure showing the variation of the cell–cell interaction term $\mathcal{H}(\alpha)$ (y -axis) with respect to the cell volume fraction α (x -axis).

Momentum source terms

The relative movement of the cells and fluid phase imparts a Darcy-style drag, which serves as the source of momentum. The momentum source terms in the cell and fluid phases are

$$f_\alpha = p_\beta \frac{\partial \alpha}{\partial x} + k_1 \alpha \beta (u_\beta - u_\alpha), \quad \text{and} \quad (1.10a)$$

$$f_\beta = p_\beta \frac{\partial \beta}{\partial x} - k_1 \alpha \beta (u_\beta - u_\alpha), \quad (1.10b)$$

where k_1 is the drag coefficient which is proportional to the viscosity of fluid phase. Here, $\alpha\beta$ is included as a proportionality constant, since there is no viscous drag in the absence of either phase. The terms $p_\beta \frac{\partial \alpha}{\partial x}$ and $p_\beta \frac{\partial \beta}{\partial x}$ represent the interfacial pressure in the cell and fluid phase, respectively.

Nutrient concentration and consumption rate

The nutrient required for cell growth is obtained through diffusion. An application of Theorem 1.2 and Fick's law of diffusion to the nutrient concentration leads to

$$\frac{\partial c}{\partial t} + \frac{\partial(cu_\alpha)}{\partial x} = \frac{\partial}{\partial x} \left(\bar{\eta} \frac{\partial c}{\partial x} \right) - Q_c, \quad (1.11)$$

where $\bar{\eta}$ is the diffusivity constant. The nutrient consumption rate by the tumour cells is governed by the equation $Q_c = \frac{Q_0 \alpha c}{1 + Q_1 c}$, where Q_0 and Q_1 are nonnegative constants.

Initial and boundary conditions

We assume that the tumour growth is symmetric about $x = 0$, which yields $u_\alpha = 0 = u_\beta$ and $\frac{\partial c}{\partial x} = 0$ at $x = 0$. Stress is assumed to be continuous and fluid is allowed to pass freely across the tumour radius. As a result, we obtain the condition; $p_\beta = 0$ at $x = \ell(t)$. Therefore, the first equation in (1.9a) leads to $-\sigma_\alpha + 2\mu_\alpha \frac{\partial u_\alpha}{\partial x} = \gamma \mathcal{H}(\alpha)$. Since $\sigma_\alpha = 0$ at $x = \ell(t)$, we use (1.9c) to arrive at

$$2\mu_\alpha \frac{\partial u_\alpha}{\partial x} = \gamma \mathcal{H}(\alpha).$$

Since the nutrient is constant outside the tumour, it holds that $c = c_{\text{out}}$ at $x = \ell(t)$. The initial data for cell volume fraction and nutrient concentration are $\alpha(0, x) = \alpha_0(x)$ and $c(0, x) = c_0(x)$, for every $x \in (0, \ell_0)$.

1.5.2 Model simplification

In this section, the model is simplified to four unknowns; cell volume fraction, cell velocity, nutrient concentration, and tumour radius. Add (1.6a) and (1.6b) and use $q_\alpha = -q_\beta$ and $\alpha(x, t) + \beta(x, t) = 1$ to obtain

$$\frac{\partial}{\partial x} (u_\alpha \alpha + u_\beta \beta) = 0. \quad (1.12)$$

Integrate both sides of (1.12) to obtain $\alpha u_\alpha + (1 - \alpha) u_\beta = k$, where k is a constant. Since $u_\alpha(t, 0) = 0 = u_\beta(t, 0)$, we obtain $k = 0$ and

$$u_\beta = -\alpha u_\alpha / (1 - \alpha). \quad (1.13)$$

Add the members of (1.7a) to obtain

$$\frac{\partial(\alpha \sigma_\alpha + \beta \sigma_\beta)}{\partial x} + f_\alpha + f_\beta = 0. \quad (1.14)$$

Since $\sigma_\beta = -p_\beta$ and $\sigma_\alpha = -p_\alpha + 2\mu_\alpha \frac{\partial u_\alpha}{\partial x}$ from (1.9a), (1.14) reads as

$$\frac{\partial}{\partial x} \left(\alpha(-p_\alpha + 2\mu_\alpha \frac{\partial u_\alpha}{\partial x}) + \beta(-p_\beta) \right) + f_\alpha + f_\beta = 0. \quad (1.15)$$

Add (1.10a) and (1.10b) to obtain $f_\alpha + f_\beta = 0$. Apply this to (1.15) to obtain

$$\frac{\partial}{\partial x}(-\alpha p_\alpha) + \frac{\partial}{\partial x}\left(2\alpha\mu_\alpha \frac{\partial u_\alpha}{\partial x}\right) - \frac{\partial}{\partial x}(\beta p_\beta) = 0.$$

Use (1.9b) and (1.9c) to write

$$\begin{aligned} 2\mu_\alpha \frac{\partial}{\partial x}\left(\alpha \frac{\partial u_\alpha}{\partial x}\right) &= \frac{\partial}{\partial x}\left(\alpha(p_\beta + \gamma\mathcal{H}(\alpha))\right) + \frac{\partial}{\partial x}(\beta p_\beta) \\ &= \frac{\partial p_\beta}{\partial x} + \gamma \frac{\partial}{\partial x}(\alpha\mathcal{H}(\alpha)). \end{aligned} \quad (1.16)$$

From the second equation in (1.7a), we obtain $f_\beta + \frac{\partial}{\partial x}(\beta\sigma_\beta) = 0$. This along with the second equation in (1.9a), (1.10b), and (1.13) yields

$$\frac{\partial p_\beta}{\partial x} + k_1\alpha \left(\frac{-\alpha u_\alpha}{1-\alpha} - u_\alpha\right) = 0.$$

Rearrange the terms in the above equation to obtain

$$u_\alpha = \frac{1-\alpha}{k_1\alpha} \frac{\partial p_\beta}{\partial x}. \quad (1.17)$$

Substitute (1.17) in (1.16) to obtain

$$2\mu_\alpha \frac{\partial}{\partial x}\left(\alpha \frac{\partial u_\alpha}{\partial x}\right) = k_1 \frac{\alpha u_\alpha}{1-\alpha} + \gamma \frac{\partial}{\partial x}(\alpha\mathcal{H}(\alpha)). \quad (1.18)$$

The simplified model is described by (1.6a), (1.18), (1.11), and (1.5) with initial and boundary conditions.

1.5.3 Nondimensionalisation

Scale the independent and dependent variables to obtain corresponding dimensionless quantities denoted with a prime symbol as follows:

$$\begin{aligned} t &= \frac{1+S_1c_{\text{out}}}{S_0c_{\text{out}}}t', \quad x = \ell_0x', \quad \ell = \ell_0\ell', \quad \alpha = \alpha', \\ u_\alpha &= \frac{\ell_0S_0c_{\text{out}}}{1+S_1c_{\text{out}}}u'_\alpha, \quad \text{and} \quad c = c_{\text{out}}c'. \end{aligned}$$

The spatial and temporal derivatives of cell volume fraction transforms into

$$\frac{\partial \alpha}{\partial t} = \frac{\partial \alpha'}{\partial t'} \frac{S_0c_{\text{out}}}{1+S_1c_{\text{out}}} \quad \text{and} \quad \frac{\partial}{\partial x}(u_\alpha\alpha) = \frac{S_0c_{\text{out}}}{1+S_1c_{\text{out}}} \frac{\partial}{\partial x'}(u'_\alpha\alpha'),$$

which yield

$$\frac{\partial \alpha}{\partial t} + \frac{\partial}{\partial x}(u_\alpha \alpha) = \frac{S_0 c_{\text{out}}}{1 + S_1 c_{\text{out}}} \left(\frac{\partial \alpha'}{\partial t'} + \frac{\partial}{\partial x'}(u'_\alpha \alpha') \right). \quad (1.19)$$

Use $c' = c/c_{\text{out}}$ in (1.19) to arrive at

$$\frac{\partial \alpha'}{\partial t'} + \frac{\partial}{\partial x'}(u'_\alpha \alpha') = \frac{(1 + s_1)\alpha'(1 - \alpha')c'}{1 + s_1 c'} - \frac{s_2 + s_3 c'}{1 + s_4 c'} \alpha', \quad (1.20)$$

where

$$s_1 = S_1 c_{\text{out}}, \quad s_2 = \frac{1 + S_1 c_{\text{out}}}{S_0 c_{\text{out}}} S_2, \quad s_3 = S_3 \frac{1 + S_1 c_{\text{out}}}{S_0}, \quad \text{and} \quad s_4 = S_4 c_{\text{out}}.$$

We relabel the variables by removing the prime symbol to avoid notational clumsiness. Therefore, (1.20) reads as

$$\frac{\partial \alpha}{\partial t} + \frac{\partial}{\partial x}(u_\alpha \alpha) = \alpha f(\alpha, c)$$

where

$$f(\alpha, c) = (1 + s_1)\alpha(1 - \alpha)c/(1 + s_1 c) - \alpha(s_2 + s_3 c)/(1 + s_4 c).$$

Follow similar steps to obtain the dimensionless version of (1.18), which is

$$\frac{k u_\alpha \alpha}{1 - \alpha} - \mu \frac{\partial}{\partial x} \left(\alpha \frac{\partial u_\alpha}{\partial x} \right) = \frac{\partial}{\partial x} (\alpha \mathcal{H}(\alpha)),$$

where $k = k_1 \ell_0^2 S_0 c_{\text{out}} / (\gamma(1 + S_1 c_{\text{out}}))$ and $\mu = 2\mu_\alpha S_0 c_{\text{out}} / (\gamma(1 + S_1 c_{\text{out}}))$. Set $Q = Q_0 \frac{1 + S_1 c_{\text{out}}}{S_0 c_{\text{out}}}$, $\widehat{Q}_1 = Q_1 c_{\text{out}}$, and $\eta := \bar{\eta}(\ell_0^{-2}) \frac{1 + S_1 c_{\text{out}}}{S_0 c_{\text{out}}}$. Then, the dimensionless version of (1.11) is

$$\frac{\partial c}{\partial t} + \frac{\partial (c u_\alpha)}{\partial x} = \frac{\partial}{\partial x} \left(\eta \frac{\partial c}{\partial x} \right) - \frac{Q \alpha c}{1 + \widehat{Q}_1 c}.$$

In this thesis, we do not consider the effect of the advection term of nutrient $\partial_x(u_\alpha c)$ to maintain conformity with the previous works [1, 7]. For notational easiness, we replace u_α by u and μ_α by μ . The consolidated dimensionless model is

$$\frac{\partial \alpha}{\partial t} + \frac{\partial}{\partial x}(u \alpha) = \alpha f(\alpha, c), \quad (1.21a)$$

$$\frac{k u \alpha}{1 - \alpha} - \mu \frac{\partial}{\partial x} \left(\alpha \frac{\partial u}{\partial x} \right) = - \frac{\partial}{\partial x} (\alpha \mathcal{H}(\alpha)), \quad (1.21b)$$

$$\frac{\partial c}{\partial t} - \frac{\partial}{\partial x} \left(\eta \frac{\partial c}{\partial x} \right) = \frac{Q \alpha c}{1 + \widehat{Q}_1 c}, \quad \text{and} \quad (1.21c)$$

$$\ell'(t) = u(t, \ell(t)). \quad (1.21d)$$

The initial conditions are

$$\alpha(0, x) = \alpha_0(x), \quad c(0, x) = c_0(x) \quad \forall x \in \Omega(0), \quad (1.21e)$$

$$\ell(0) = 1, \tag{1.21f}$$

and the boundary conditions are

$$u(t, 0) = 0, \quad \mu \frac{\partial u}{\partial x}(t, \ell(t)) = \mathcal{H}(\alpha(t, \ell(t))), \tag{1.21g}$$

$$\frac{\partial c}{\partial x}(t, 0) = 0, \quad \text{and } c(t, \ell(t)) = 1 \quad \forall t \in (0, T). \tag{1.21h}$$

The model (1.21a)–(1.21h) is referred to as Breward–Byrne–Lewis (BBL) model.

1.5.4 Domain fixing transformation

In this subsection, we discuss numerical methods constructed using finite difference, finite element, and finite volume methods to compute discrete solutions of the BBL model (1.21a)–(1.21h). In the rest of this chapter, we consider the steady state version of (1.21c) and set the diffusivity constant $\eta = 1$. The steady–state formulation of (1.21c) is justified since the time scale for the nutrient diffusion is much faster than the time scale for cell division.

The main challenge in discretising the one–dimensional model (1.21a)–(1.21d) is the time–dependent boundary governed by (1.21d). A classical way to eliminate the time dependent boundary is to apply a change of variable to time and space so that $(0, \ell(t))$ is transformed to a fixed interval irrespective of $t \in [0, T]$. Transform (t, x) to (τ, ξ) as follows: for every $t \geq 0$

$$\xi := x/\ell(t) \quad \text{and} \quad \tau := t. \tag{1.22}$$

Note that the time dependent domain $(0, \ell(t))$ is scaled to $(0, 1)$ under (1.22). The transformed model is as follows: for every $(\tau, \xi) \in (0, T) \times (0, 1)$, it holds

$$\frac{\partial \alpha}{\partial \tau} - \frac{\xi}{\ell} \frac{d\ell}{d\tau} \frac{\partial \alpha}{\partial \xi} + \frac{1}{\ell} \frac{\partial(u\alpha)}{\partial \xi} = \alpha f(\alpha, c), \tag{1.23a}$$

$$\frac{\ell^2 k \alpha u}{1 - \alpha} - \mu \frac{\partial}{\partial \xi} \left(\alpha \frac{\partial u}{\partial \xi} \right) = -\ell \frac{\partial}{\partial \xi} (\alpha \mathcal{H}(\alpha)), \tag{1.23b}$$

$$\frac{\partial^2 c}{\partial \xi^2} = \frac{Q \ell^2 \alpha c}{1 + \widehat{Q}_1 c}. \tag{1.23c}$$

The transformed initial and boundary conditions are

$$\begin{aligned} \ell = 1, \quad \alpha = \alpha_0 \quad c = c_0 \quad \text{at} \quad \tau = 0, \\ u = 0 = \frac{\partial c}{\partial \xi} \quad \text{at} \quad \xi = 0, \\ \mu \frac{\partial u}{\partial \xi} = \ell \mathcal{H}(\alpha), \quad c = 1 \quad \text{at} \quad \xi = 1, \quad \text{and} \quad \frac{d\ell}{d\tau} = u(t, 1). \end{aligned} \tag{1.23d}$$

1.5.5 Finite difference method (FDM) in C. J. W. Breward et al. [1]

The finite difference discretisation for (1.23a)–(1.23c) is first described in [1]. Let $0 = \xi_0 < \dots < \xi_M = 1$ and $0 = \tau_0 < \dots < \tau_N = T$ be uniform discretisations of $(0, 1)$ and $(0, T)$, respectively. Set $h = \xi_{i+1} - \xi_i$ and $\delta = \tau_{n+1} - \tau_n$. Split the third term in (1.23a) and group the terms appropriately to obtain

$$\frac{\partial \alpha}{\partial \tau} + \frac{\partial \alpha}{\partial \xi} \left(\frac{u}{\ell} - \frac{d\ell}{d\tau} \frac{\xi}{\ell} \right) + \frac{\alpha}{\ell} \frac{\partial u}{\partial \xi} = \alpha f(\alpha, c). \quad (1.24)$$

In (1.24), discretise the temporal derivative using a backward difference approximation and spatial derivative by an upwind scheme, wherein $\partial_x \alpha$ is discretised using backward difference (resp. forward difference) if $S_i^n \geq 0$ (resp. $S_i^n < 0$). The discretisation of (1.24) is as follows: set $S_i^n := \left(\frac{u_i^n}{\ell} - \frac{\ell_n - \ell_{n-1}}{\delta} \frac{\xi_i}{\ell_n} \right)$.

Case 1 $S_i^n \geq 0$:

$$\alpha_i^{n+1} \left(\frac{1}{\delta} + \left(\frac{u_i^n - \xi_i u_M^n}{\ell \delta} \right) + \left(\frac{u_{i+1}^n - u_{i-1}^n}{2\ell h} \right) - \frac{(1+s_1)(1-\alpha_i^{n+1})c_i^n}{1+s_1c_i^n} + \frac{s_2+s_3c_i^n}{1+s_4c_i^n} \right) - \alpha_{i-1}^{n+1} \left(\frac{u_i^n - \xi_i u_M^n}{\ell \delta} \right) = \frac{\alpha_i^n}{\delta}. \quad (1.25)$$

Case 2 $S_i^n < 0$:

$$\alpha_i^{n+1} \left(\frac{1}{\delta} - \left(\frac{u_i^n - \xi_i u_M^n}{\ell \delta} \right) + \left(\frac{u_{i+1}^n - u_{i-1}^n}{2\ell h} \right) - \frac{(1+s_1)(1-\alpha_i^{n+1})c_i^n}{1+s_1c_i^n} + \frac{s_2+s_3c_i^n}{1+s_4c_i^n} \right) + \alpha_{i+1}^{n+1} \left(\frac{u_i^n - \xi_i u_M^n}{\ell \delta} \right) = \frac{\alpha_i^n}{\delta}. \quad (1.26)$$

In the limiting case $\xi \rightarrow 0$, (1.24) becomes

$$\frac{\partial \alpha}{\partial \tau} + \frac{\alpha}{\ell} \frac{\partial u}{\partial \xi} = \frac{(1+s_1)\alpha(1-\alpha)c}{1+s_1c} - \frac{s_2+s_3c}{1+s_4c} \alpha, \quad (1.27)$$

which yields the following discretisation at $\xi = 0$

$$\alpha_0^{n+1} \left(\frac{1}{\delta} + \left(\frac{u_1^n - u_0^n}{\ell h} \right) - \frac{(1+s_1)(1-\alpha_1^{n+1})c_0^n}{1+s_1c_0^n} + \frac{s_2+s_3c_0^n}{1+s_4c_0^n} \right) = \frac{\alpha_0^n}{\delta}.$$

At $\xi = 1$, $\left(\frac{u}{\ell} - \frac{d\ell}{d\tau}\frac{\xi}{\ell}\right) = 0$ and (1.24) becomes (1.27). Therefore, the discretisation at $\xi = 1$ is

$$\alpha_M^{n+1} \left(\frac{1}{\delta} + \left(\frac{u_M^n - u_{M-1}^n}{\ell h} \right) - \frac{(1+s_1)(1-\alpha_M^{n+1})c_M^n}{1+s_1c_M^n} + \frac{s_2+s_3c_M^n}{1+s_4c_M^n} \right) = \frac{\alpha_M^n}{\delta}. \quad (1.28)$$

Write (1.23b) as

$$\frac{\ell^2 k \alpha u}{1-\alpha} - \mu \alpha \frac{\partial^2 u}{\partial \xi^2} - \mu \frac{\partial u}{\partial \xi} \frac{\partial \alpha}{\partial \xi} = -\ell \frac{\partial}{\partial \xi} (\alpha \mathcal{H}(\alpha)). \quad (1.29)$$

Discretise (1.29) using central difference method to obtain, for $i = 1$ to $M-1$

$$\begin{aligned} \frac{\ell_n^2 k \alpha_i^{n+1} u_i^{n+1}}{1-\alpha_i^{n+1}} - \mu \alpha_i^{n+1} \frac{u_{i+1}^{n+1} - 2u_i^{n+1} + u_{i-1}^{n+1}}{h^2} - \mu \frac{u_{i+1}^{n+1} - u_{i-1}^{n+1}}{2h} \frac{\alpha_{i+1}^{n+1} - \alpha_{i-1}^{n+1}}{2h} \\ = -\frac{\ell_n}{2h} (\alpha_{i+1}^{n+1} \mathcal{H}(\alpha_{i+1}^{n+1})) + \frac{\ell_n}{2h} (\alpha_{i-1}^{n+1} \mathcal{H}(\alpha_{i-1}^{n+1})) \end{aligned} \quad (1.30)$$

Since $u(t, 0) = 0$, we impose $u_0^{n+1} = 0$. From (1.23d), $\mu \frac{\partial u_c}{\partial \xi} = \ell \mathcal{H}(\alpha)$ at $\xi = 1$, which upon discretisation yields

$$-\frac{\mu}{h} u_{M-1}^{n+1} + \frac{\mu}{h} u_M^{n+1} = \ell_h \mathcal{H}(\alpha_M^{n+1}). \quad (1.31)$$

Consider (1.23c) in the steady state form and discretise using central difference to obtain, for $1 \leq i \leq M-1$

$$c_{i+1}^{n+1} \frac{1}{h^2} + c_i^{n+1} \left(-\frac{2}{h^2} - \frac{Q \ell_n^2 \alpha_i^{n+1}}{1 + \widehat{Q}_1 c_i^n} \right) + c_{i-1}^{n+1} \frac{1}{h^2} = 0. \quad (1.32)$$

Since $c = 1$ at $\xi = 1$ from equation (1.23d), we impose $c_M^n = 1$. Introduce a ghost point c_{-1}^{n+1} to impose the boundary condition $\frac{\partial c}{\partial \xi} = 0 \approx (c_0^{n+1} - c_{-1}^{n+1})/h$ at $\xi = 0$. Then, set $i = 0$ in (1.32) to obtain

$$c_1^{n+1} \frac{1}{h^2} + c_0^{n+1} \left(-\frac{1}{h^2} - \frac{Q \ell_n^2 \alpha_0^{n+1}}{1 + \widehat{Q}_1 c_0^n} \right) = 0. \quad (1.33)$$

Algorithm for finite difference method

Since α_0 and c_0 is *a priori* known, at the time step $n = 0$ it is sufficient to compute $(u_i^0)_{\{0 \leq i \leq M\}}$. Use (1.30), (1.31), and $u_0^0 = 0$ to obtain $(u_i^0)_{\{0 \leq i \leq M\}}$. Algorithm 1.1 provides the finite difference steps.

Algorithm 1.1 (FDM for BBL model). **Input:** $(\alpha_i^0)_{1 \leq i \leq M}$ and $(c_i^0)_{1 \leq i \leq M}$.

Step 1: Compute $(u_i^0)_{\{0 \leq i \leq M\}}$ with (1.30), (1.31), and $u_0^0 = 0$.

Step 2: Computation of the iterates:

for $0 \leq n < N$

Step 2.1 Define $\ell_{n+1} = \ell_n + \delta u_M^n$

Step 2.2 Compute $(\alpha_i^{n+1})_{\{1 \leq i \leq M-1\}}$ with (1.26)–(1.28)

Step 2.3 Compute $(c_i^{n+1})_{\{0 \leq i \leq M-1\}}$ with (1.32), (1.33), and $c_M^{n+1} = 1$

Step 2.4 Compute $(u_i^{n+1})_{\{1 \leq i \leq M\}}$ with (1.30), (1.31), and $u_0^{n+1} = 0$

end for

Output: $(\alpha_i^n)_{1 \leq i \leq M}$, $(u_i^n)_{1 \leq i \leq M}$, $(c_i^n)_{1 \leq i \leq M}$, and (ℓ_n) for $1 \leq n \leq N$.

Numerical experiments

The constants α^R and α_{\min} are fixed at 0.8. The final time T is chosen as $T = 225$. Set $s_1 = 10$, $s_2 = 0.5$, $s_3 = 0.5$, $s_4 = 10$, $\mu = 1$, and $k = 1$. The spatial and temporal discretisation factors are $h = 0.01$ and $\delta = 0.005$. The variation of the model variables with respect to time and space is provided in Figure 1.7. The variation of $\alpha(t, \cdot)$, $u(t, \cdot)$, and $c(t, \cdot)$ at different time values are plotted against $0 \leq x \leq \ell(t)$, where $t \in (0, T)$. The attractive interaction

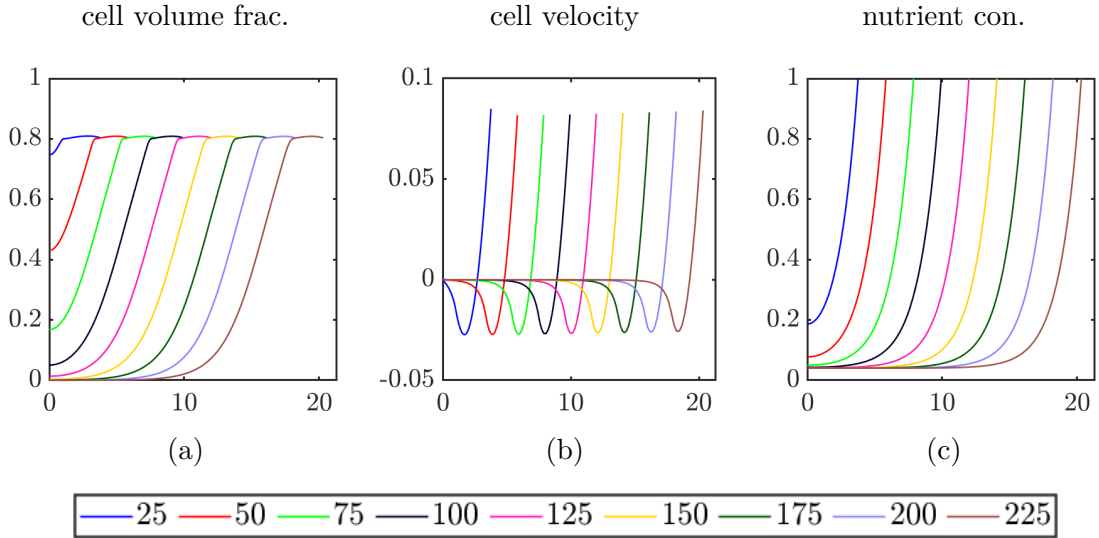


Figure 1.7: Graphs showing the variation of discrete solution obtained from FDM with respect to $x = \xi \ell(t)$ where, $0 \leq \xi \leq 1$ for different time values. Each coloured line represent the variation of model variables at a fixed time as indicated in the legend.

between the cells is assumed to be zero since $\alpha^R = \alpha_{\min}$. From Figure 1.7(a) it is clear that, as time evolves, the cell volume fraction at the tumour centre approaches zero. This region is called the central necrotic region. Most of the tumour cells occupy an annular region around the central necrotic core. In the necrotic core, the nutrient concentration is

very low and it increases to the maximum value at the tumour boundary. The variation of tumour radius with respect to time is shown in Figure 1.8. It can be observed that the the tumour radius shows a linear increase with respect to time, which is a characteristic feature of early tumour growth with abundant nutritional supply.

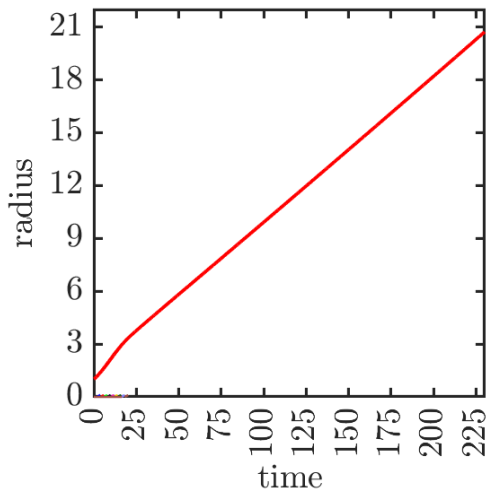


Figure 1.8: Variation of the tumour radius with respect to time for FDM.

1.5.6 Modified numerical scheme

The finite difference method, despite its simplicity and relative easiness to perform computations, offers a few undesirable difficulties. The applicability of finite difference methods depends very much on the domain in which the partial or ordinary differential equations are defined. It is challenging to construct a proper finite difference discretisation in domains with boundaries that are nonparallel to the Cartesian axes, and are computationally intensive in such cases. This shortcoming can be significantly mitigated by employing finite element methods, which are constructed on the foundation of variational techniques. Finite element methods do not seek strong regularity requirements on the unknown function and hence apply to a wide range of problems. Moreover, finite element methods offer a robust framework to establish many theoretical properties, such as the existence of a solution and error control.

We describe the discretisation of (1.23b) and (1.23c) using \mathbb{P}_1 -Lagrange elements. The cell volume fraction equation (1.23a) is discretised using FDM.

Weak formulation

The variational formulations and finite element discretisations of (1.23b) and (1.23c) are discussed here. Define $I = (0, 1)$ and $V = \{v \in H^1(I) : v(0) = 0\}$. Multiply (1.23b) by

a test function $v \in V$, apply integration by parts, and use (1.23d) to obtain

$$\int_{\mathbf{I}} a_0(\xi) u v d\xi + \int_{\mathbf{I}} a_1(\xi) \frac{\partial u}{\partial \xi} \frac{\partial v}{\partial \xi} d\xi = \int_{\mathbf{I}} a_2(\xi) \frac{\partial v}{\partial \xi} d\xi,$$

where

$$a_0(\xi) := \frac{\ell^2 k \alpha}{1 - \alpha}, a_1(\xi) := \mu \alpha, \text{ and } a_2(\xi) := \ell \alpha \mathcal{H}(\alpha). \quad (1.34)$$

The weak solution is defined as $u \in V$ such that (1.34) is satisfied for every $v \in V$. Set $I_i = (\xi_{i-1}, \xi_i)$, $1 \leq i \leq M$. Define $\mathbb{P}_1(I_i)$ as the set of all affine polynomials on I_i and the finite element space $V_h \subset V$ by

$$V_h := \left\{ v_h : v_h \in \mathcal{C}^0(\mathbf{I}), v_h|_{I_i} \in \mathbb{P}_1(I_i), 1 \leq i \leq M \text{ and } v_h(0) = 0 \right\}.$$

The discrete problem seeks $u_h \in V_h$ such that, for every $v_h \in V_h$ it holds.

$$\int_{\mathbf{I}} a_0(\xi) u_h v_h d\xi + \int_{\mathbf{I}} a_1(\xi) \frac{\partial u_h}{\partial \xi} \frac{\partial v_h}{\partial \xi} d\xi = \int_{\mathbf{I}} a_2(\xi) \frac{\partial v_h}{\partial \xi} d\xi. \quad (1.35)$$

Define $W = \left\{ v \in H^1(0, 1) : v(1) = 0 \right\}$. Multiply (1.23c) by a test function $w \in W$, apply integration by parts and (1.23d) to obtain

$$\int_{\mathbf{I}} \frac{\partial c}{\partial \xi} \frac{\partial w}{\partial \xi} d\xi = - \int_{\mathbf{I}} \frac{Q \alpha \ell^2}{1 + \widehat{Q}_1 c} c w d\xi. \quad (1.36)$$

The weak solution to (1.23c) is defined by $c \in H^1(0, 1)$ such that $c(1) = 1$ and (1.36) is satisfied for every $w \in W$. Define the finite dimensional subspace

$$W_h := \left\{ v_h : v_h \in \mathcal{C}^0(\mathbf{I}), v_h|_{I_i} \in \mathbb{P}_1(I_i), 1 \leq i \leq M, v_h(1) = 0 \right\}.$$

The discrete problem seeks $c_h \in \left\{ v_h : v_h \in \mathcal{C}^0(\mathbf{I}), v_h|_{I_i} \in \mathbb{P}_1(I_i), 1 \leq i \leq M \right\}$ with $c_h(1) = 1$ such that for every $w_h \in W_h$

$$\int_{\mathbf{I}} \frac{\partial c_h}{\partial \xi} \frac{\partial w_h}{\partial \xi} d\xi = \int_{\mathbf{I}} \frac{Q \alpha \ell^2}{1 + \widehat{Q}_1 c_h} c_h w_h d\xi.$$

Algorithm for finite element method

The numerical results obtained by using the Algorithm 1.2 is provided in Figure 1.9. The constants and mesh parameters remain the same as in FDM.

Algorithm 1.2 (Modified scheme for BBL model). *Input:* $(\alpha_i^0)_{1 \leq i \leq M}$ and $(c_i^0)_{1 \leq i \leq M}$

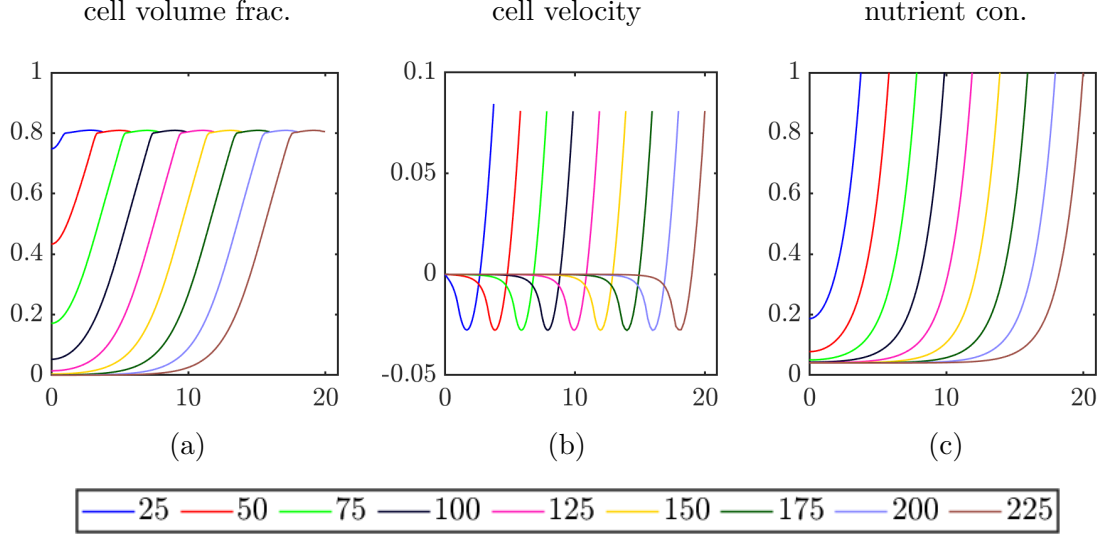


Figure 1.9: Graphs showing the variation of discrete solution obtained from modified numerical scheme with respect to $x = \xi\ell(t)$ where, $0 \leq \xi \leq 1$ for different time values. Each coloured line represent the variation of model variables at a fixed time as indicated in the legend.

Step 1: Define the piecewise constant function $\alpha_h^0 : I \rightarrow \mathbb{R}$ by, for $1 \leq i \leq M - 1$

$$\alpha_{h|I_i}^0 = \int_{I_i} \alpha_0(\xi) d\xi.$$

Step 2: Define the velocity function $u_h^0 : I \rightarrow \mathbb{R}$ as the solution of (1.35), wherein α is replaced by α_h^0 and ℓ by $\ell(0) = 1$.

Step 3: Computation of the iterates:

for $1 \leq n < N$

Step 2.1 Define $\ell_n = \ell_{n-1} + \delta u_h^n(1)$.

Step 2.2 Set $u_i^n = u_h^n(\xi_i)$. Use the finite difference scheme (1.25)–(1.28) to obtain $(\alpha_i^n)_{\{0 \leq i \leq M\}}$. Define the piecewise constant function $\alpha_h^n : I \rightarrow \mathbb{R}$ by, for $0 \leq i \leq M - 1$, $\alpha_{h|I_i}^n = (\alpha_i^n + \alpha_{i+1}^n)/2$.

Step 2.3 Define $c_h^n : I \rightarrow \mathbb{R}$ as the solution of (1.36), wherein α is replaced by α_h^n , ℓ is replaced by ℓ_n , and c_h in the denominator of the right hand side of (1.36) is replaced by c_h^{n-1} .

Step 2.4 Define $u_h^n : I \rightarrow \mathbb{R}$ as the solution of (1.35), wherein α is replaced by α_h^n and ℓ is replaced by ℓ_n .

end for

Output: $(\alpha_i^n)_{1 \leq i \leq M}$, $(u_i^n)_{1 \leq i \leq M}$, $(c_i^n)_{1 \leq i \leq M}$, and (ℓ_n) for $1 \leq n \leq N$.

It is evident from Figures 1.9 and 1.7 that numerical solutions obtained by employing finite element method to cell velocity and nutrient tension equations agree well with the finite difference solutions obtained by C. J. W. Breward et al. in [1].

Chapter 2

Extended model and numerical scheme

In this chapter, a biphasic tumour growth model, referred to as *extended model*, is presented, by which the time-dependent boundary (2.1f) can be eliminated¹. Extended model describes free suspension growth.

2.1 Introduction

The biphasic fluid flow model of avascular tumour growth was introduced and popularised by a series of articles published by C. J. W. Breward et al. [1, 5, 33] and H. M. Byrne et al. [6, 7]. The model is derived by applying conservation of mass and momentum to different phases in a proliferating tumour. The details of the derivation are provided in Section 1.5. The net production rate of tumour cells is quantified as the difference between the birth and death rates, which are controlled by the concentration of an external nutrient. The prolonged mitosis creates a closely packed tissue of tumour cells. When the natural close-packing density of tumour cells is exceeded, the resulting mechanical stress drives the cells apart. The inner stressed cells move towards the tumour periphery resulting in an expanding tissue.

Literature

Multiphase flow models with and without time-dependent boundaries are used to describe various physical and biomedical phenomena, see [9] and the references therein. The review articles by H. B. Stewart and B. Wendroff [34] and D. A. Drew [35] provide a comprehensive account of mathematical modelling of biphasic flow with different examples. The time-dependent boundary appears as an intrinsic variable in many multiphase flow models. A

¹The results in this chapter have been published as: G. C. Remesan. Numerical solution of the two-phase tumour growth model with moving boundary. *In: Proceedings of the 18th Biennial Computational Techniques and Applications Conference, CTAC-2018*. Ed. by B. Lamichane, T. Tran, and J. Bunder. Vol. 60. ANZIAM J. 2019, pp. C1–C15. <https://doi.org/10.21914/anziamj.v60i0.13936>.

review of two-phase flows with a free surface is presented in [36]. Biphasic-free boundary models of liquid-vapour interactions in heat pumps is described in the works by E. W. Grald and J. W. MacArthur [37] and [38]. A one dimensional model is studied by L. Yao and C. J. Zhu [39], wherein the authors consider a viscous two-phase liquid and gas model. Stefan problems also involve a biphasic approach, where the free boundary often appears as a separation between the phases [40]; however the governing equations are parabolic.

Motivation

Recall the BBL model from Section 1.5, with $D_T = \cup_{0 < t < T}(\{t\} \times (0, \ell(t)))$,

$$\frac{\partial \alpha}{\partial t} + \frac{\partial}{\partial x}(u\alpha) = \alpha f(\alpha, c) \text{ in } D_T, \quad \alpha(0, x) = \alpha_0(x) \quad \forall x \in \Omega(0), \quad (2.1a)$$

$$\frac{ku\alpha}{1-\alpha} - \mu \frac{\partial}{\partial x} \left(\alpha \frac{\partial u}{\partial x} \right) = - \frac{\partial}{\partial x} (\alpha \mathcal{H}(\alpha)) \text{ in } D_T, \quad (2.1b)$$

$$u(t, 0) = 0, \quad \mu \frac{\partial u}{\partial x}(t, \ell(t)) = \mathcal{H}(\alpha(t, \ell(t))) \quad \forall t \in (0, T), \quad (2.1c)$$

$$\frac{\partial c}{\partial t} - \frac{\partial}{\partial x} \left(\eta \frac{\partial c}{\partial x} \right) = \frac{Q\alpha c}{1 + \widehat{Q}_1 c} \text{ in } D_T, \quad c(0, x) = c_0(x) \quad \forall x \in \Omega(0), \quad (2.1d)$$

$$\frac{\partial c}{\partial x}(t, 0) = 0, \quad c(t, \ell(t)) = 1 \quad \forall t \in (0, T), \quad (2.1e)$$

$$\ell'(t) = u(t, \ell(t)), \text{ and } \ell(0) = 1. \quad (2.1f)$$

A drawback associated with the BBL model is the presence of a time-dependent boundary associated with it. In numerical computations, the time-dependent boundary necessitates the remeshing of the spatial domain at each time step and thereby increases the computational cost; though less intense compared to 2D and 3D situations.

The transformation to a fixed domain removes this issue in 1D. A change of variable $x \rightarrow \xi := x/\ell(t)$, see Subsection 1.5.4, is used to transform the model equations (2.1a)–(2.1f) into the fixed domain $(0, 1)$. Though this is a standard method used to solve many time-dependent boundary problems [3, 8, 33, 41], the method suffers from a few drawbacks. Firstly, the change of variable is computable only when the domain geometry is simple enough, which is practically applicable in the 1D case only. In two and three dimensions, the domain geometry is often asymmetric and complex, and a feasible transformation may not be available. Secondly, for the choice of $x \rightarrow \xi := x/\ell(t)$ in the 1D case, the discretisation error is proportional to $\ell(t)\Delta\xi$, where $\Delta\xi$ is the spatial discretisation factor. This indicates that the discretisation error may be undesirably high for larger values of $\ell(t)$. An alternative choice is to discretise $(0, \ell(t))$ and construct a numerical scheme on $(0, \ell(t))$ for each fixed time. However, this remeshing procedure at each fixed time step is computationally expensive and requires projections from one time step to another. Also, the transformation modifies the model coefficients that renders the analysis difficult.

Contributions

To mitigate these difficulties, a modification of the BBL model is introduced. We present the notion of solutions on a larger domain $(0, \ell_m)$ that contains all the time-dependent domains $\Omega(t)$ for every $t \in (0, T)$. In the modified model, the need to explicitly track the tumour boundary is eliminated via a search method, which reduces the computational complexity. It should be noted that, no additional variable is introduced in the model, contrary to level set methods, to track the boundary. The domain $(0, \ell_m)$, referred to as the *extended domain*, is time-independent and requires only one initial spatial discretisation. As a result, it is possible to eliminate the need to remesh the domain at each time step. Also, the discretisation error becomes free from the dependence on $\ell(t)$. The modified model is called the *extended model*. It is established that weak solutions of the *extended model* and that of BBL model are equivalent under appropriate conditions, which are specified later in Theorem 2.3.

Organisation

The extended model of tumour growth is described in Section 2.2. The weak solutions of the BBL model (2.1) and extended model, and the equivalence between them, are presented in Section 2.3. The numerical solutions of the extended model are presented in Section 2.4.

2.2 The extended model

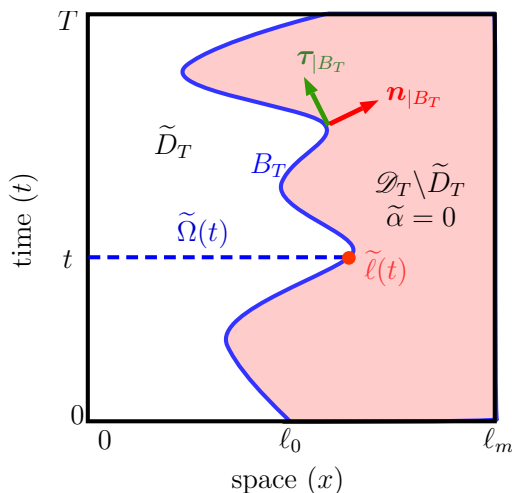


Figure 2.1: Tumour radii and time–space domains in the extended model: \tilde{D}_T is the time–space domain (region to the left of the blue curve) defined by (2.2d) and \mathcal{D}_T is the bounding box $(0, T) \times (0, \ell_m)$. The curve B_T is the boundary $\{(t, \ell(t)) : t \in (0, T)\}$. The unit normal and tangent vectors to B_T are $\mathbf{n}_{|B_T}$ and $\boldsymbol{\tau}_{|B_T}$, respectively.

Define the bounding box $\mathcal{D}_T := (0, T) \times (0, \ell_m)$, where $\ell_m > \tilde{\ell}(t)$ for $t \in (0, T)$, where $\tilde{\ell}(t)$ is the tumour radius, which is defined by (2.2d). Define $\tilde{\Omega}(t) = (0, \tilde{\ell}(t))$ and time–space domain $\tilde{D}_T = \cup_{0 < t < T} (\{t\} \times \tilde{\Omega}(t))$, see Figure 2.1. The extended model seeks variables $\tilde{\alpha}, \tilde{u}$, and \tilde{c} , which are functions of time and space on \mathcal{D}_T and $\tilde{\Omega}$, which is a function of time on $(0, T)$. The governing equations are as follows:

$$\frac{\partial \tilde{\alpha}}{\partial t} + \frac{\partial}{\partial x}(\tilde{u}\tilde{\alpha}) = \tilde{\alpha}f(\tilde{\alpha}, \tilde{c}) \text{ in } \mathcal{D}_T, \quad (2.2a)$$

$$\frac{k\tilde{u}\tilde{\alpha}}{1-\tilde{\alpha}} - \mu \frac{\partial}{\partial x} \left(\tilde{\alpha} \frac{\partial \tilde{u}}{\partial x} \right) = -\frac{\partial}{\partial x}(\tilde{\alpha}\mathcal{H}(\tilde{\alpha})) \text{ in } \tilde{D}_T \text{ and } \tilde{u} := \tilde{u}(t, \tilde{\ell}(t)) \text{ in } \mathcal{D}_T \setminus \tilde{D}_T, \quad (2.2b)$$

$$\frac{\partial \tilde{c}}{\partial t} - \eta \frac{\partial^2 \tilde{c}}{\partial x^2} = -\frac{Q\tilde{\alpha}\tilde{c}}{1+\hat{Q}_1|\tilde{c}|} \text{ in } \tilde{D}_T \text{ and } \tilde{c} := 1 \text{ in } \mathcal{D}_T \setminus \tilde{D}_T; \text{ and} \quad (2.2c)$$

$$\tilde{\ell}(t) = \min \{x : \tilde{\alpha}(t, x) = 0 \text{ on } (x, \ell_m)\}. \quad (2.2d)$$

The initial conditions are

$$\tilde{\alpha}(0, x) = \alpha_0^e(x) \text{ on } (0, \ell_m), \quad c(0, x) = c_0(x) \quad \forall x \in \tilde{\Omega}(0), \quad \tilde{\ell}(0) = \ell_0,$$

where

$$\alpha_0^e(x) := \begin{cases} \alpha_0(x) & \text{if } x \in \tilde{\Omega}(0), \\ 0 & \text{otherwise,} \end{cases}$$

and the boundary conditions are

$$\begin{aligned} \tilde{u}(t, 0) &= 0, \quad \mu \frac{\partial \tilde{u}}{\partial x}(t, \tilde{\ell}(t)) = \mathcal{H}(\tilde{\alpha}(t, \tilde{\ell}(t))), \\ \frac{\partial \tilde{c}}{\partial x}(t, 0) &= 0, \quad \text{and } \tilde{c}(t, \tilde{\ell}(t)) = 1 \quad \forall t \in (0, T). \end{aligned}$$

It is assumed in the sequel that $0 < m_{01} < \alpha_0 \leq m_{02} < 1$, where m_{01} and m_{02} are constants. Observe that the ODE (2.1f) is replaced by the search condition (2.2d) in the extended model. This replacement enables us to capture the tumour boundary without explicitly resorting to solving a differential equation.

2.3 Weak solutions

In this section, the time–dependent function spaces required to define a weak solution of the BBL and extended models are presented. The weak solution of the BBL and extended models are provided in Definitions 2.1 and 2.2, respectively. It is shown in Theorem 2.3 that these two weak solutions are equivalent. Define $A_T := \cup_{0 < t < T} (\{t\} \times (0, \ell_r(t)))$ (with $\ell_r = \ell$ (resp. $\ell_r = \tilde{\ell}$), $A_T = D_T$ (resp. $A_T = \tilde{D}_T$)) and the associated Hilbert spaces

$$\begin{aligned} H_u^1(A_T) &:= \left\{ u \in L^2(A_T) : \partial_x u \in L^2(A_T) \text{ and } u(t, 0) = 0 \forall t \in (0, T) \right\} \text{ and} \\ H_c^1(A_T) &:= \left\{ c \in L^2(A_T) : \partial_x c \in L^2(A_T) \text{ and } c(t, \tilde{\ell}(t)) = 0 \forall t \in (0, T) \right\}. \end{aligned}$$

Definition 2.1 (weak solution (BBL model)). *A weak solution of the BBL model in D_T is a four-tuple (α, u, c, Ω) such that (BM.1)–(BM.4) hold.*

(BM.1) *The volume fraction satisfies $\alpha \in L^\infty(D_T)$, $0 < m_{11} \leq \alpha \leq m_{12} < 1$, where $m_{11} \leq m_{01}$ and $m_{02} \leq m_{12}$ are constants, and for all $\varphi \in \mathcal{C}_c^\infty(\overline{D_T} \setminus (\{T\} \times \Omega(T)))$,*

$$\int_{D_T} \left(\alpha f(\alpha, c) \varphi + (\alpha, u\alpha) \cdot \nabla_{(t,x)} \varphi \right) dx dt + \int_{\Omega(0)} \varphi(0, x) \alpha_0(x) dx = 0. \quad (2.3)$$

(BM.2) *The velocity $u \in H_u^1(D_T)$ satisfies, for every $v \in H_u^1(D_T)$ and every $t \in (0, T)$,*

$$\int_{\Omega(t)} \left(k \frac{\alpha}{1-\alpha} uv + \mu \frac{\partial u}{\partial x} \frac{\partial v}{\partial x} \right) dx = \int_{\Omega(t)} \alpha \mathcal{H}(\alpha) \frac{\partial v}{\partial x} dx. \quad (2.4)$$

(BM.3) *The nutrient concentration is such that $c - 1 \in H_c^1(D_T)$ and, for every $\zeta \in H_c^1(D_T)$ with $\partial_t \zeta \in L^2(D_T)$,*

$$\begin{aligned} - \int_{D_T} c \partial_t \zeta dx dt - \int_{D_T} \eta \partial_x c \partial_x \zeta dx dt + \int_{\Omega(0)} c_0(x) \zeta(0, x) dx \\ + \int_{D_T} \frac{Q\alpha c}{1 + \widehat{Q}_1 c} \zeta dx dt = 0. \end{aligned} \quad (2.5)$$

(BM.4) *The tumour radius $\ell(t)$ satisfies (1.21d).*

Definition 2.2 (weak solution (extended model)). *A weak solution of the extended model in \mathcal{D}_T is a four-tuple $(\tilde{\alpha}, \tilde{u}, \tilde{c}, \tilde{\Omega})$ such that (EM.1)–(EM.4) hold.*

(EM.1) *The volume fraction satisfies $\alpha \in L^\infty(\mathcal{D}_T)$, $\tilde{\alpha} \geq 0$ and for all $\tilde{\varphi} \in \mathcal{C}_c^\infty([0, T] \times (0, \ell_m))$*

$$\int_{\mathcal{D}_T} \left(\tilde{\alpha} f(\tilde{\alpha}, \tilde{c}) \tilde{\varphi} + (\tilde{\alpha}, \tilde{u}\tilde{\alpha}) \cdot \nabla_{(t,x)} \tilde{\varphi} \right) dx dt + \int_0^{\ell_m} \tilde{\varphi}(0, x) \alpha_0^e(x) dx = 0. \quad (2.6)$$

(EM.2) *For a fixed t , define $\tilde{\Omega}(t) := (0, \tilde{\ell}(t))$, $\tilde{\ell}(t) := \min \{x : \tilde{\alpha}(t, x) \leq 0 \text{ on } (x, \ell_m)\}$, and $\tilde{D}_T := \cup_{0 < t < T} (\{t\} \times \tilde{\Omega}(t))$. Then, it holds $\tilde{u}|_{\mathcal{D}_T \setminus \tilde{D}_T} = 0$ and $\tilde{c}|_{\mathcal{D}_T \setminus \tilde{D}_T} = 1$.*

(EM.3) *The velocity $\tilde{u}|_{\tilde{D}_T} \in H_u^1(\tilde{D}_T)$ satisfies (2.4) for every $v \in H_u^1(\tilde{D}_T)$ and every $t \in (0, T)$, with α and $\Omega(t)$ set as $\tilde{\alpha}$ and $\tilde{\Omega}(t)$, respectively.*

(EM.4) *The nutrient concentration is such that $\tilde{c} - 1 \in H_c^1(\tilde{D}_T)$ and for every $\zeta \in H_c^1(\tilde{D}_T)$, with $\partial_t \zeta \in L^2(\tilde{D}_T)$ satisfies (2.5) with α and D_T set as $\tilde{\alpha}$ and \tilde{D}_T , respectively.*

Next, the equivalence between the weak solutions (BM) and (EM) is presented.

Theorem 2.3 (Equivalence). 1. If (α, u, c, Ω) is a weak solution of the BBL model, then $(\tilde{\alpha}, \tilde{u}, \tilde{c}, \tilde{\Omega})$ defined by $\tilde{\Omega} := \Omega$, and $\tilde{\alpha} := \alpha$, $\tilde{u} := u$, $\tilde{c} := c$ in D_T , and $\tilde{\alpha} := 0$, $\tilde{u} := 0$, $\tilde{c} := 1$ in $\mathcal{D} \setminus D_T$, is a weak solution of the extended model.

2. Let $(\tilde{\alpha}, \tilde{u}, \tilde{c}, \tilde{\Omega})$ be a weak solution of the extended model. Define (α, u, c, Ω) as $\Omega := \tilde{\Omega}$ and $\alpha := \tilde{\alpha}|_{D_T}$, $u := \tilde{u}|_{D_T}$ and $c := \tilde{c}|_{D_T}$. If there exists constants $0 < \tilde{m}_{11} \leq m_{01}$ and $m_{02} \leq \tilde{m}_{12} < 1$ such that $\tilde{m}_{11} \leq \tilde{\alpha}|_{D_T} \leq \tilde{m}_{12}$, then (α, u, c, Ω) is a weak solution of the BBL model.

Proof. 1. Let (α, u, c, Ω) be a weak solution in the sense of Definition 2.1 and $\tilde{\varphi} \in \mathcal{C}_c^\infty([0, T) \times (0, \ell_m))$. Since $\tilde{\varphi}|_{D_T} \in \mathcal{C}_c^\infty(\overline{D_T} \setminus (\{T\} \times \Omega(T)))$ and $\tilde{\alpha} = 0$ in $\mathcal{D}_T \setminus D_T$ it holds

$$\int_{D_T} (\tilde{\alpha} f(\tilde{\alpha}, \tilde{c}) \tilde{\varphi} + (\tilde{\alpha}, \tilde{u} \tilde{\alpha}) \cdot \nabla_{(t,x)} \tilde{\varphi}) dt dx + \int_{\Omega(0)} \tilde{\varphi}(0, x) \alpha_0(x) dx = 0, \quad (2.7)$$

$$\int_{\mathcal{D} \setminus D_T} (\tilde{\alpha}, \tilde{u} \tilde{\alpha}) \cdot \nabla_{(t,x)} \tilde{\varphi} dt dx + \int_{\mathcal{D} \setminus D_T} \tilde{\alpha} f(\tilde{\alpha}, \tilde{c}) \tilde{\varphi} dt dx = 0. \quad (2.8)$$

Add (2.7) and (2.8) to obtain (2.6). The conditions on \tilde{u} and \tilde{c} , see (EM.3) and (EM.4), follow naturally from Definition 2.1. Since $\tilde{\alpha} > 0$ in D_T and $\tilde{\alpha} = 0$ in $\mathcal{D} \setminus D_T$ the condition (EM.2) holds.

2. Let $\varphi \in \mathcal{C}_c^\infty(\overline{D_T} \setminus (\{T\} \times \Omega(T)))$. Define $\tilde{\varphi} \in \mathcal{C}_c^\infty([0, T) \times (0, \ell_m))$ such that $\tilde{\varphi} = \varphi$ in D_T . Since $\Omega(t) = \tilde{\Omega}(t)$ for every t , it holds $\tilde{\alpha} = 0$ in $\mathcal{D} \setminus D_T$. Therefore, (2.6) implies (2.3).

To recover (1.21d) define a vector field $\mathbf{F} : \mathcal{D}_T \rightarrow \mathbb{R}^2$ by $\mathbf{F}(t, x) := (\tilde{\alpha}, \tilde{u} \tilde{\alpha})$. Set $\mathbf{F}|_{B_T^+} = (\mathbf{F}|_{D_T})|_{B_T}$ and $\mathbf{F}|_{B_T^-} = (\mathbf{F}|_{\mathcal{D} \setminus D_T})|_{B_T}$. Since the weak divergence of the vector field \mathbf{F} is $-\tilde{\alpha} f(\tilde{\alpha}, \tilde{c}) \in L^2(\mathcal{D}_T)$, the normal flux of \mathbf{F} is continuous across B_T . Since $\tilde{\alpha} = 0$ in $\mathcal{D}_T \setminus D_T$, $\mathbf{F}|_{B_T^-} = \mathbf{0}$ holds. Therefore, $(\mathbf{F}|_{B_T^+} - \mathbf{F}|_{B_T^-}) \cdot \mathbf{n}|_{B_T} = (\alpha, u \alpha) \cdot \mathbf{n}|_{B_T} = 0$. Here, $\mathbf{n}|_{B_T} := \left(|\tilde{\ell}'(t)|^2 + 1 \right)^{-1/2} (-\tilde{\ell}'(t), 1)$ is the normal to B_T , see Figure 2.1. Therefore, $(\alpha, u \alpha) \cdot \mathbf{n}|_{B_T} = 0$ holds. Since $\alpha > 0$, $\tilde{\ell}'(t) = u(t, \tilde{\ell}(t))$ follows. The conditions (EM.3) and (EM.4) follow naturally from Definition 2.2. \square

2.4 Numerical scheme and implementation results

Theorem 2.3 provides an alternative method to construct a numerical scheme that does not require an explicit solution of (2.1f) and computationally intense re-meshing. The idea is to numerically solve the extended model and take appropriate restrictions as prescribed in the second part of Theorem 2.3 to obtain the numerical solutions of the BBL model. The

cell volume fraction equation (2.2a) is solved using cell-centred finite volume methods. In particular, we employ two methods: upwinding with Godunov flux [105, p. 135] (method U), and monotone upwinding (MUSCL) with Godunov flux [105, p. 146] (method M). A brief derivation of the MUSCL method is provided in Appendix A.1.

Choose a positive number $\alpha_{\text{thr}} \in (0, 1)$ and fix it. The number α_{thr} is referred to as the threshold value. The space and time variables are discretised as follows. Let $0 = x_0 < \dots < x_J = \ell_m$ be a uniform spatial discretisation with $h := x_{j+1} - x_j$, and $0 = t_0 < \dots < T_N = T$ be a uniform temporal discretisation with $\delta := t_{n+1} - t_n$. The numbers h and δ are called the spatial and temporal discretisation factors. Define the intervals $\mathcal{X}_j := (x_j, x_{j+1})$ and $\mathcal{T}_n := [t_n, t_{n+1})$. The node-centred intervals are defined by $\widetilde{\mathcal{X}}_j := (x_j - h/2, x_j + h/2)$ for $j = 1, \dots, J-1$, $\widetilde{\mathcal{X}}_0 := [x_0, x_0 + h/2]$, and $\widetilde{\mathcal{X}}_J := [x_J - h/2, x_J]$. The space and time stepping are uniform in the discrete schemes in Chapter 2–4 for the sake of simplicity. It should be noted that the computations in Chapters 2 and 3 and analysis in Chapter 4 carry forward with nonuniform time and space stepping as well. Let $\chi_{\widetilde{\mathcal{X}}_j}$ be the characteristic function of $\widetilde{\mathcal{X}}_j$, that is, $\chi_{\widetilde{\mathcal{X}}_j} = 1$ on $\widetilde{\mathcal{X}}_j$, and $\chi_{\widetilde{\mathcal{X}}_j} = 0$ outside $\widetilde{\mathcal{X}}_j$. For any real valued function f on \mathbb{R} , define the pointwise average $\{\{f\}\}_{\mathcal{X}_j} = (f(x_j) + f(x_{j+1}))/2$. Define the extended initial data for the nutrient concentration as follows: $\forall x \in (0, \ell_m)$, $c_0^e(x) := c_0(x)$ for every $x \in \Omega(0)$ and $c_0^e(x) := 1$ otherwise.

A detailed discussion on principles employed in selecting appropriate numerical schemes is provided in Subsection 3.4.2.

Definition 2.4 (Discrete scheme). *Initial data approximation:* Define

- α_h^0 by $\alpha_h^0 := \alpha_j^0 = \frac{1}{h} \int_{\mathcal{X}_j} \alpha_0^e(x) dx$ on \mathcal{X}_j for $0 \leq j \leq J-1$,
- c_h^0 by $c_h^0 \in \mathbb{P}_1(\mathcal{X}_j)$ for $0 \leq j \leq J-1$ and $c_h^0(x_j) := c_0^e(x_j)$ for $0 \leq j \leq J$, and
- $\Omega_h^0 := (0, \ell_h^0)$, where $\ell_h^0 = 1$.
- Choose ℓ_m such that $\ell_0 < \ell_m$. Obtain u_h^0 from (DS.c) below by taking $n = 0$.

Updation: Construct a finite sequence of 3-tuple of functions $(\alpha_h^n, u_h^n, c_h^n)_{\{0 < n \leq N-1\}}$ on $(0, \ell_m)$ as in (DS.a)–(DS.d) described now.

(DS.a) Set $\alpha_h^n := \alpha_j^n$ on \mathcal{X}_j for $0 \leq j \leq J-1$, where

$$\frac{1}{\delta}(\alpha_j^n - \alpha_j^{n-1}) + \frac{1}{h} [\mathfrak{F}_{j+1}^{n-1} - \mathfrak{F}_j^{n-1}] = \alpha_j^{(n-1)+} (1 - \alpha_j^{n-1}) b_j^{n-1} - \alpha_j^{n+} d_j^{n-1}. \quad (2.9)$$

For every $0 \leq j \leq J-1$, the flux \mathfrak{F}_j^{n-1} for upwind and MUSCL schemes are

Upwind: $\mathfrak{F}_j^{n-1} = u_j^{(n-1)+} \alpha_{j-1}^{n-1} - u_j^{(n-1)-} \alpha_j^{n-1}$ and

MUSCL: $\mathfrak{F}_j^{n-1} = u_j^{(n-1)+} (p_{j-1}^n(h/2) + \alpha_{j-1}^{n-1}) - u_j^{(n-1)-} (-p_j^n(h/2) + \alpha_j^{n-1})$, where $p_j^{n-1} = \text{minmod}((\alpha_{j+1}^{n-1} - \alpha_j^{n-1})/h, (\alpha_j^{n-1} - \alpha_{j-1}^{n-1})/h)$ and

$$\text{minmod}(a, b) := \begin{cases} \text{sgn}(a) \min(|a|, |b|) & \text{if } ab \geq 0, \\ 0 & \text{otherwise.} \end{cases}$$

Here, $u_j^n = u_h^n(x_j)$, $b_j^n = \{(1 + s_1)c_h^n/(1 + s_1c_h^n)\}\chi_j$, and $d_j^n = \{(s_2 + s_3c_h^n)/(1 + s_4c_h^n)\}\chi_j$. Note that, when $j = 0$, $u_0^{(n-1)} = 0$ and thus the value of α_{-1}^{n-1} can be arbitrarily fixed, say for example $\alpha_{-1}^{n-1} = m_{11}$.

(DS.b) Set $\Omega_h^n := (0, \ell_h^n)$, where the recovered radius at step n , ℓ_h^n , is provided by $\ell_h^n = \min\{x_j : \alpha_j^n < \alpha_{\text{thr}} \text{ on } (x_j, \ell_m)\}$.

(DS.c) Set the conforming \mathbb{P}_1 finite element space on Ω_h^n , and its subspace with homogeneous boundary condition at $x = 0$, by

$$\begin{aligned} \mathcal{S}_h^n &:= \left\{ v_h^n \in \mathcal{C}^0(\overline{\Omega_h^n}) : v_h^n|_{\mathcal{X}_j} \in \mathbb{P}_1(\mathcal{X}_j) \text{ for } 0 \leq j < J_n := \ell_h^n/h \right\} \text{ and} \\ \mathcal{S}_{0,h}^n &:= \{v_h^n \in \mathcal{S}_h^n : v_h^n(0) = 0\}. \end{aligned}$$

Then,

$$u_h^n := \begin{cases} \tilde{u}_h^n & \text{on } \Omega_h^n, \\ 0 & \text{on } (0, \ell_m) \setminus \overline{\Omega_h^n}, \end{cases}$$

where $\tilde{u}_h^n \in \mathcal{S}_{0,h}^n$ satisfies

$$a_h^n(\tilde{u}_h^n, v_h^n) = \mathcal{L}_h^n(v_h^n) \quad \forall v_h^n \in \mathcal{S}_{0,h}^n,$$

with $a_h^n : \mathcal{S}_h^n \times \mathcal{S}_h^n \rightarrow \mathbb{R}$ and $\mathcal{L}_h^n : \mathcal{S}_h^n \rightarrow \mathbb{R}$ defined by

$$\begin{aligned} a_h^n(w, v) &= k \left(\frac{\alpha_h^n}{1 - \alpha_h^n} w, v \right)_{\Omega_h^n} + \mu (\alpha_h^n \partial_x w, \partial_x v)_{\Omega_h^n} \text{ and} \\ \mathcal{L}_h^n(v) &= (\alpha_h^n \mathcal{H}(\alpha_h^n), \partial_x v)_{\Omega_h^n}. \end{aligned}$$

(DS.d) Define the finite dimensional vector spaces

$$\begin{aligned} \mathcal{S}_{h,0}^n &:= \{v_h^n \in \mathcal{S}_h^n : v_h^n(\ell_h^n) = 0\} \text{ and} \\ \mathcal{S}_{h,\text{ML}} &:= \left\{ w_h : w_h = \sum_{j=0}^J w_j \chi_{\tilde{\mathcal{X}}_j}, w_j \in \mathbb{R}, 0 \leq j \leq J \right\}, \end{aligned}$$

and the mass lumping operator $\Pi_h : \mathcal{C}^0([0, \ell_m]) \rightarrow \mathcal{S}_{h,\text{ML}}$ such that $\Pi_h w = \sum_{j=0}^J w(x_j) \chi_{\tilde{\mathcal{X}}_j}$.

Then,

$$c_h^n := \begin{cases} \tilde{c}_h^n & \text{on } \Omega_h^n, \\ 1 & \text{on } (0, \ell_m) \setminus \overline{\Omega_h^n}, \end{cases}$$

where $\tilde{c}_h^n \in \mathcal{S}_h^n$ satisfies the boundary condition $\tilde{c}_h^n(\ell_h^n) = 1$ and the following discrete equation, in which $\Pi_h \tilde{c}_h^n := (\Pi_h c_h^n)|_{\Omega_h^n}$: for all $v_h^n \in \mathcal{S}_{h,0}^n$, it holds

$$\begin{aligned} &(\Pi_h \tilde{c}_h^n, \Pi_h v_h^n)_{\Omega_h^n} - (\Pi_h c_h^{n-1}, \Pi_h v_h^n)_{\Omega_h^n} + \delta \lambda (\partial_x \tilde{c}_h^n, \partial_x v_h^n)_{\Omega_h^n} \\ &= -Q \delta \left(\frac{\alpha_h^n \Pi_h \tilde{c}_h^n}{1 + \hat{Q}_1 \Pi_h c_h^{n-1}}, \Pi_h v_h^n \right)_{\Omega_h^n}. \end{aligned} \quad (2.10)$$

The threshold value, α_{thr} , is crucial in establishing the analytical properties of the numerical solutions and reducing error in the numerical solution. In particular, if α_{thr} is set as zero, then the numerical diffusion associated with the finite volume schemes produce significant error in the discrete tumour radius ℓ_h^n .

In all numerical tests the values of the parameters are set to be $s_1 = 10 = s_4$, $s_2 = 0.5 = s_3$, $k = 1 = \mu$, $Q = 0.5$, $\widehat{Q}_1 = 0$, and $\ell_0 = 1$.

2.4.1 Numerical experiment 1

In this case, the cell velocity u and the nutrient concentration c are assumed to be unity. Here, (2.2a) reduces to a semi-linear advection equation, which is solved analytically by the method of characteristics. The analytical solution is compared with the numerical solutions in Figure 2.2. The influence of α_{thr} on locating the tumour radius is also studied.

Set $u = c = 1$. The analytical solution to (2.2a) is

$$\alpha(t, x) = \frac{(c_2 - c_1)\alpha_0(x - t)\exp((c_1 - c_2)t)}{c_1\alpha_0(x - t)(1 - \exp((c_1 - c_2)t)) + c_2 - c_1},$$

where $c_1 = 1$ and $c_2 = \frac{s_2 + s_3}{1 + s_4}$. The initial data considered are

- (i) $\alpha_0(t, x) = 0.5 \left(0.02 + \cos^2(x)\right) \chi_{[0,1]}$,
- (ii) $\alpha_0(t, x) = 0.5 \left(0.02 + \sin^2(x)\right) \chi_{[0,1]}$, and
- (iii) $\alpha_0(t, x) = \frac{\chi_{[0,1]}}{2} \frac{1 + \exp(x - 0.5)^2}{1 + \exp(2(x - 0.5)^2)}$,

where $\chi_{[0,1]} = 1$ in $[0, 1]$ and 0 otherwise. Here, $T = 5$, $\ell_m = 6$, $\delta = 0.01$, $h = 0.02$, $\alpha_{\text{thr}} = 0.04$ (method U), and $\alpha_{\text{thr}} = 0.004$ (method M). It is well known that the second order method MUSCL significantly reduces the numerical diffusion [42]. The reduction in the numerical diffusion from method U to method M explains the reduction in the threshold value.

h	α_{thr}				
	0.01	0.008	0.006	0.004	0.002
0.01	1.67E-3	1.67E-3	1.67E-3	1.67E-3	5.00E-3
0.02	3.33E-3	3.33E-3	6.67E-3	1.33E-3	2.00E-2
0.04	6.67E-3	6.67E-3	2.00E-2	2.67E-2	4.00E-2
0.06	4.31E-2	1.58E-2	2.59E-2	4.60E-2	6.61E-2
0.08	2.10E-2	7.66E-3	1.92E-2	3.26E-2	5.93E-2
0.1	3.33E-2	1.67E-2	1.67E-2	5.00E-2	8.33E-2

Table 2.1: $\Delta\ell_h$ for case 1, method M.

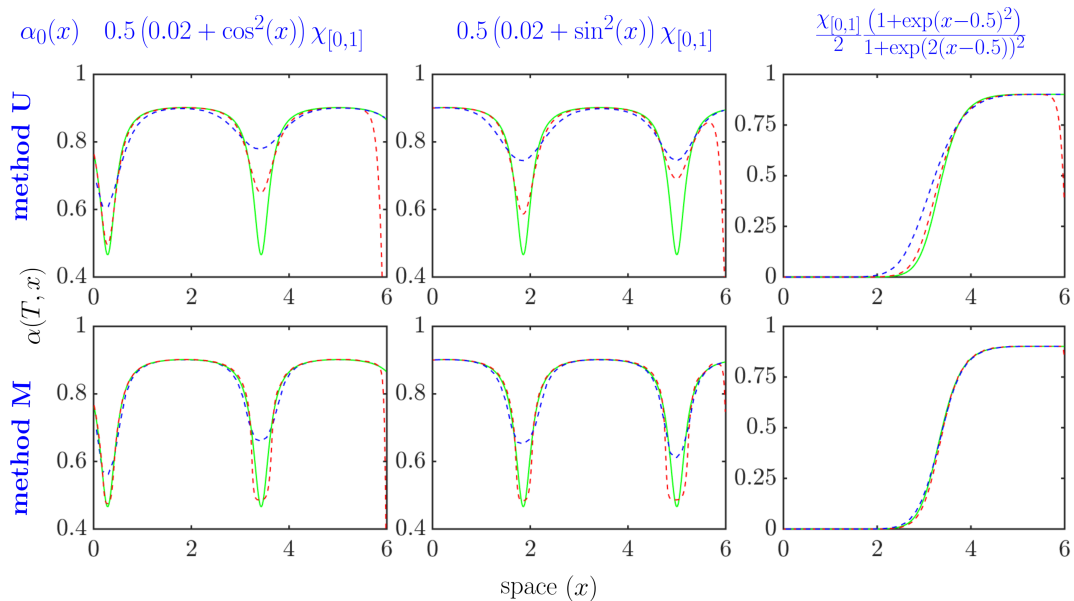


Figure 2.2: Case 1: Numerical solutions to the method U and method M are respectively given in the upper and lower rows. The red and blue lines represent the numerical solutions using threshold value and domain fixing transformation $x \rightarrow \xi := x/\ell(t)$. Green line is the analytical solution.

h	α_{thr}			
	0.04	0.03	0.02	0.01
0.01	3.33E-3	3.33E-3	1.66E-2	3.83E-2
0.02	3.33E-2	3.33E-3	1.33E-2	5.68E-2
0.04	1.20E-1	7.33E-2	6.66E-3	6.00E-2

Table 2.2: $\Delta\ell_h$ for case 1, method U.

The approximate solution obtained in the extended domain captures the properties of the analytical solution better than the one obtained in the scaled domain, see Figure 2.2, though it is less accurate towards the discontinuity at ℓ_h^N in method U due to numerical diffusion. However, method M overcomes this disadvantage; the extended solution agrees well with the scaled solution towards the discontinuity, and remarkably better in the interior region, see Figure 2.2. The recovered radius, ℓ_h^n , on the other hand, is in excellent agreement with the exact radius for both method M and U with a proper choice of the threshold values, see Tables 2.1 and 2.2.

We analyse the dependency of recovered radius ℓ_h^n on the threshold value α_{thr} for the MUSCL method. The relative error, $\Delta\ell_h = \frac{|\ell(T) - \ell_h^N|}{\ell(T)}$, at $T = 5$ is used as a quantification of the error in the recovered radius.

Two sets of experiments are conducted; (a) varying α_{thr} at a fixed h (b) varying h

at a fixed α_{thr} . Table 2.1 shows that there exists a wide range of α_{thr} and h for which the error remains below $1\text{E}-2$. This observation assures the accuracy of the proposed numerical method using the threshold value. For method U the ranges of α_{thr} and h over which the error remains low are small, which is expected considering the high numerical diffusion associated with this method.

2.4.2 Numerical experiment 2

In the second case, numerical solutions of the extended model are computed.

The extended model, wherein all variables treated as unknowns is now considered. The parameters are $\delta = 0.01$, $h = 0.01$, $T = 228$, $\ell_m = 25$, $\alpha_{\text{thr}} = 0.004$ (method M), and $\alpha_{\text{thr}} = 0.01$ (method U). The threshold values are chosen based on Tables 2.1 and 2.2. The initial condition is $\alpha_0(x) = 0.8$ for $0 \leq x \leq 1$ and 0 otherwise. Since the exact value of $\ell(T)$ is not available, the error is quantified as the relative difference between tumour radius obtained from Algorithm 1.1. The relative difference for method U is $6.18\text{E}-3$ and method M is $5.69\text{E}-3$. Therefore, the moving boundary ℓ is well captured by methods U and M. The numerical solution in the extended domain is in good agreement with the solution obtained from Section 1.5, see Figure 1.7.

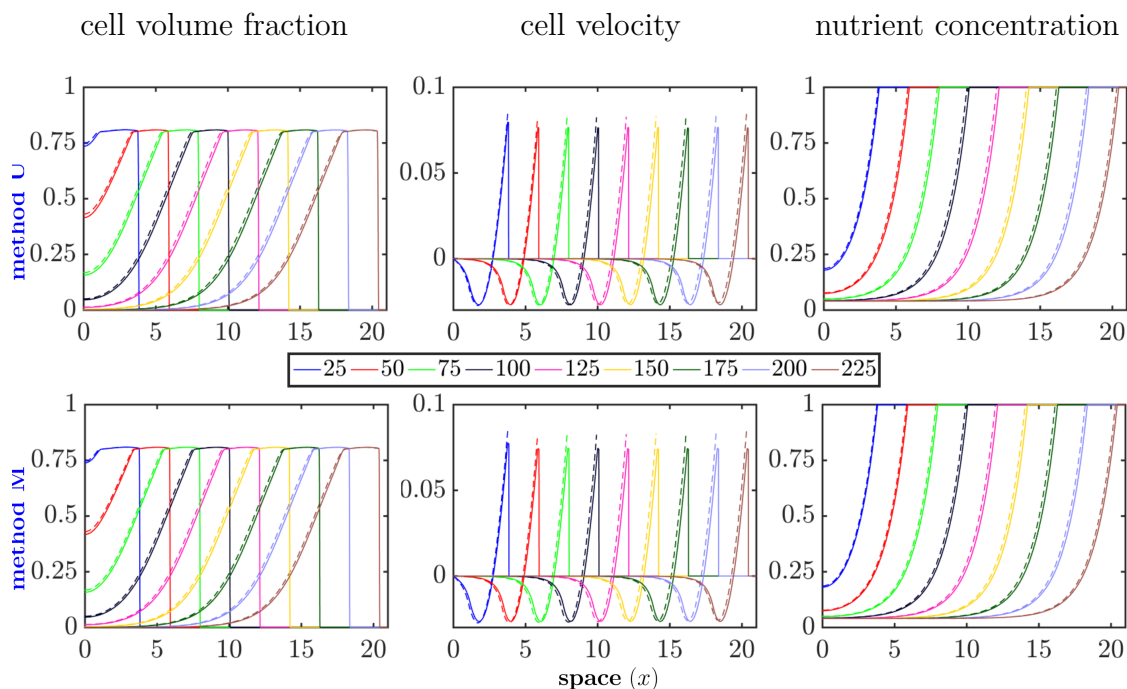


Figure 2.3: Case 2: Numerical solutions to the method U and method M are respectively given in the upper and lower rows with solid lines. The numerical solution of the BBL model using the domain fixing transformation, see Section 1.5, is denoted using dotted lines. Each curve represents the variation of the corresponding variable with respect to space at fixed times $t = 25, 50, \dots, 225$.

2.5 Conclusion

The novel numerical technique developed to solve the two phase tumour growth problem is tested against problems for which analytical solutions are known. For a fixed spatial mesh size the new method provides more accurate solutions than the standard method of solving in a scaled domain. The moving boundary is recovered from the numerical solution by comparing with a threshold value. It is found that an appreciable range of threshold values can be used along with higher order methods like MUSCL so that the error in the recovered radius can be kept low. The solutions obtained from this new technique show very good agreement with solutions obtained using standard methods. The reliability of this new approach should be beneficial when extending the method to tumour growth problems in higher dimensions while not solving for the boundary explicitly.

Chapter 3

Threshold model and numerical scheme

3.1 Introduction

One-spatial dimensional tumour growth models are usually obtained by assuming that a higher spatial dimensional tumour grows radially [4, 43–45]. Such one-dimensional models are much simpler than their intricate higher dimensional versions [11, 46–48]. However, theoretical and computational difficulties offered by even these simplified one-dimensional versions are severe. The time-dependent boundary, noncoercive coefficient functions, nonlinearities, and the strong coupling between the equations are a few of the challenges worth mentioning. Though the model in this chapter also describes free suspension growth, it is different from the *extended model* in Chapter 2. The source terms are designed so as to address the issues mentioned above. Chapter 4 discusses convergence analysis of this novel model¹

Literature

The models that truncate variables by threshold value, referred to as *cut-off* model in literature, to obtain estimates that can ensure coercivity, is a rather classical technique in the variational analysis of PDEs, see for example the work by D. Kroener and S. Luckhaus [49]. The authors prove the existence of a weak solution to a quasilinear degenerate partial differential equation that models the flow of two immiscible fluids in a porous medium using a cut-off technique. Later, it is shown that the limiting solution as the cut-off threshold approaches zero is a weak solution of the original model (without any cut-off). A similar analysis is presented in X. Cao and I. S. Pop [50]. It needs to be noted that the cut-off models considered in [50] and [49] are relatively simple, which enables an easy proof of existence of a weak solution. An analogous analysis for the threshold model

¹The results in this chapter along with that of Chapter 4 is published in IMA J. Numer. Anal.: J. Droniou, N. Nataraj, and G. C. Remesan, Convergence analysis of a numerical scheme for a tumour growth model, IMA J. Numer. Anal., (49 pages), URL: <https://doi.org/10.1093/imanum/drab016>.

is much harder, see Chapter 4, with the presence of a time dependent boundary.

Contributions

It is shown in Chapter 2 that the model (2.1) can be recast into an extended model, by which the time-dependent boundary can be eliminated from the system. However, this model does not allow for any uniform lower bounds on cell volume fraction inside the computational domain \mathcal{D}_T , which means that the velocity equation (2.2b) can lose its coercivity properties. In this chapter, we consider a modification of this extended model, hereafter called the *threshold model*, in which we introduce a (small) threshold which determines the computational domain used for cell velocity and nutrient concentration (see Figure 3.1(b)). The formulation of a numerical scheme for the threshold model with a suitable notion of solution is the primary objective of this chapter. The numerical scheme is designed in such a way that the iterates converge in appropriate norms, up to a subsequence, and that the limit is a solution to the threshold model.

Though the notion threshold value, α_{thr} , is also employed in Chapter 2 to compute the numerical solutions (see Definition 2.4) the extended model (2.2) is independent of the threshold value. Since estimates on the discrete solutions depend on the threshold value non-uniformly, it is generally difficult to obtain compactness results free from α_{thr} and subsequential convergence as α_{thr} approaches zero (similar to vanishing viscosity methods [106, p. 45]). Therefore, it is highly challenging to prove that a limit of discrete solutions, if it exists, as α_{thr} approaches zero solves the extended model weakly. The main contribution of this chapter is the identification and justification of a tumour growth model based on the threshold value, of which a subsequential limit of solutions from the Definition 3.2 (discrete scheme) serves as a weak solution. It seems heuristically that the threshold solutions converge to an extended solution as α_{thr} approaches zero; however, a rigorous analysis on this front is yet an open problem.

Organisation

In Section 3.2, the threshold model is introduced. The weak solution to the threshold model namely *threshold solution* is presented in Section 3.3. The discrete scheme is described in Section 3.4 followed by numerical results in Section 3.5.

3.2 Threshold model

We now present the slight modification of the extended model, see Section 2.2. Define the bounding box $\mathcal{D}_T := (0, T) \times (0, \ell_m)$, where $\ell_m > \hat{\ell}(t)$ for $t \in (0, T)$ – see Figure 3.1(b). Define $\hat{\Omega}(t) = (0, \hat{\ell}(t))$ and the time-space domain $\widehat{\mathcal{D}}_T^{\text{thr}} = \cup_{0 < t < T} (\{t\} \times \hat{\Omega}(t))$.

A constant and positive parameter, α_{thr} , characterises the threshold model, that seeks variables α, u , and c (functions of time and space on \mathcal{D}_T) and $\hat{\ell}(t)$ (function of time on $(0, T)$). The governing equations are as follows.

$$\frac{\partial \alpha}{\partial t} + \frac{\partial}{\partial x}(u\alpha) = (\alpha - \alpha_{\text{thr}})^+ f(\alpha, c) \text{ in } \mathcal{D}_T, \quad (3.1a)$$

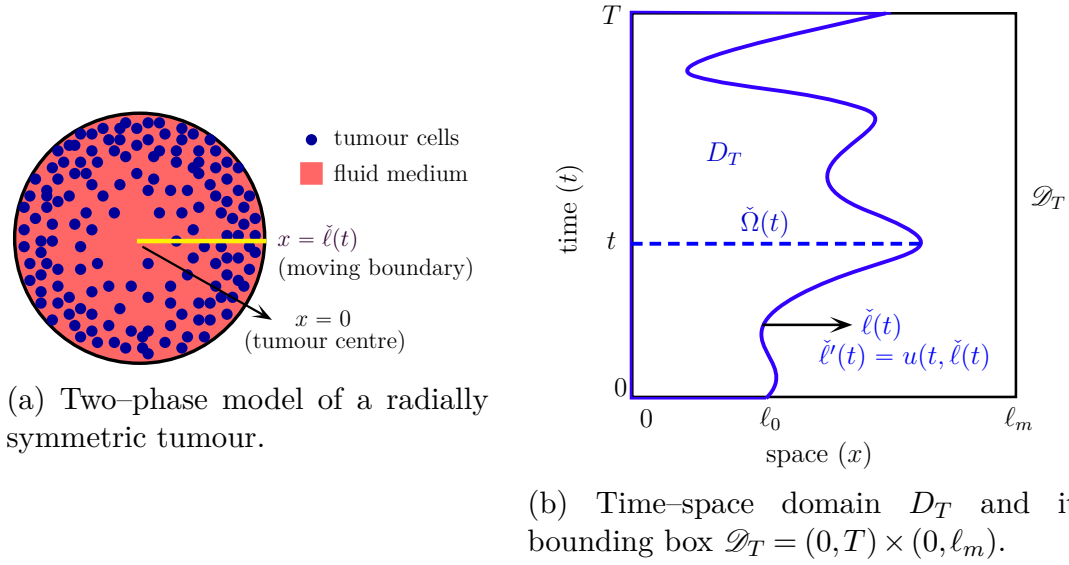


Figure 3.1: Radially symmetric tumour and corresponding time-space domains.

$$\frac{ku\alpha}{1-\alpha} - \mu \frac{\partial}{\partial x} \left(\alpha \frac{\partial u}{\partial x} \right) = - \frac{\partial}{\partial x} (\alpha \mathcal{H}(\alpha)) \text{ in } \widehat{D}_T^{\text{thr}} \text{ and } u := u(t, \ell(t)) \text{ in } \mathcal{D}_T \setminus \widehat{D}_T^{\text{thr}}, \quad (3.1b)$$

$$\frac{\partial c}{\partial t} - \lambda \frac{\partial^2 c}{\partial x^2} = - \frac{Q\alpha c}{1 + \widehat{Q}_1 |c|} \text{ in } \widehat{D}_T^{\text{thr}} \text{ and } c := 1 \text{ in } \mathcal{D}_T \setminus \widehat{D}_T^{\text{thr}}; \text{ and} \quad (3.1c)$$

$$\widehat{\ell}(t) = \min \{x : \alpha(t, x) \leq \alpha_{\text{thr}} \text{ on } (x, \ell_m)\}. \quad (3.1d)$$

Here, $\mathcal{H}(\alpha)$ is redefined by $\mathcal{H}(\alpha) := \frac{(\alpha - \alpha^{\text{R}})^+}{(1 - \alpha)^2}$. Observe, that this definition is consistent with $\mathcal{H}(\alpha) := \frac{(\alpha - \alpha^{\text{R}})}{(1 - \alpha)^2} \text{Heav}(\alpha - \alpha_{\text{min}})$ when $\alpha_{\text{min}} = \alpha^{\text{R}}$. The initial conditions are

$$\alpha(0, x) = \alpha_0^{\text{e}}(x) \text{ on } (0, \ell_m), \quad c(0, x) = c_0(x) \quad \forall x \in \widehat{\Omega}(0), \quad \ell(0) = \ell_0, \quad (3.1e)$$

where

$$\alpha_0^{\text{e}}(x) := \begin{cases} \alpha_0(x) & \text{if } x \in \widehat{\Omega}(0), \\ 0 & \text{otherwise.} \end{cases}$$

The boundary conditions are

$$\begin{aligned} u(t, 0) = 0, \quad \mu \frac{\partial u}{\partial x}(t, \widehat{\ell}(t)) &= \mathcal{H}(\alpha(t, \widehat{\ell}(t))), \\ \frac{\partial c}{\partial x}(t, 0) = 0, \quad \text{and } c(t, \widehat{\ell}(t)) &= 1 \quad \forall t \in (0, T). \end{aligned} \quad (3.1f)$$

In the sequel, it is assumed that

$$0 < m_{01} \leq \alpha_0 \leq m_{02} < 1 \quad \text{on } \widehat{\Omega}(0), \quad (3.2)$$

where m_{01} and m_{02} are constants.

Differences between the threshold and extended models, and their physical implications, are described in the next subsection.

3.2.1 Difference between extended and threshold models

Cell volume fraction and tumour radius

The cell fraction is governed by (3.1a) in the domain \mathcal{D}_T . The tumour radius $\widehat{\ell}(t)$ at time t is the smallest number in $(0, \ell_m)$ such that $\alpha(t, x)$ is below α_{thr} for every $x \geq \widehat{\ell}(t)$. The source term $\alpha f(\alpha, c)$ in (2.2a) is modified to $(\alpha - \alpha_{\text{thr}})^+ f(\alpha, c)$ in (3.1a). These modifications are motivated by population dynamics. The new source term accounts for the fact that, in the absence of a sufficient amount of cells, the reaction term that drives their growth remains dormant. Avascular tumour growth causes nutrient-limited growth, and away from the proliferating rim of high cellular volume fraction, tumour cells are known to become quiescent and even further from the proliferating rim, they become part of the necrotic core [51]. This effect is also accurately captured by modifying the source term. Moreover, at the mathematical level, the modification plays a crucial role in obtaining the boundedness of cell volume fraction. In the limiting case where α_{thr} approaches zero, the continuous function $(\alpha - \alpha_{\text{thr}})^+ f(\alpha, c)$ approaches $\alpha f(\alpha, c)$, and the tumour radius is the smallest number above which no tumour cells are present.

Cell velocity

The term $\mathcal{H}(\alpha)$ in (2.2b) is replaced by $(\alpha - \alpha^{\text{R}})^+ / (1 - \alpha)^2$ in (3.1b). In the case $\alpha_{\text{min}} \neq \alpha^{\text{R}}$, the nonlinear term $(\alpha - \alpha^{\text{R}}) \text{Heav}(\alpha - \alpha_{\text{min}})$ in $\mathcal{H}(\alpha)$ is discontinuous with respect to α , which makes proving the existence of a solution to (3.1) difficult. The major part of simulations in [1] were done under the assumption that $\alpha_{\text{min}} = \alpha^{\text{R}}$. Also, the instability created by the discontinuity of $\mathcal{H}(\alpha)$ (with $\alpha_{\text{min}} \neq \alpha^{\text{R}}$) is not observed in [1, Figure 8] since the numerical solution of cell volume fraction remains greater than the parameter value $\alpha_{\text{min}} = 0.6$ and the values of μ and k are properly chosen. Hence, $\mathcal{H}(\alpha)$ behaves throughout in [1] as a continuous function. We ran simulations with $\alpha_{\text{min}} \neq \alpha_{\text{thr}}$ and, when the cell volume fraction crosses the discontinuity at α_{min} , clear instability of the model was observed. The continuity of $\mathcal{H}(\alpha)$ is essential to obtain *a priori* estimates (see in particular the proof of Proposition 4.15), and to apply limit arguments to the numerical scheme. Physically, this modification means that tumour cells only exhibit repulsive interactions. The analysis hereafter could be done with other choices of \mathcal{H} , in particular choices that reproduce the attractive/repulsive features of the original model, provided that \mathcal{H} is (Lipschitz)-continuous.

Nutrient concentration

The original nutrient source term $-Q\alpha c / (1 + \widehat{Q}_1 c)$ in (2.2c) is modified in (3.1c) to ensure the nonnegativity of nutrient concentration (which represents a concentration). Each nonnegative solution c of (3.1c) also satisfies (3.1c) with the original source term $-Q\alpha c / (1 + \widehat{Q}_1 c)$, since $c = |c|$. Therefore, to establish the existence of a solution to (3.1c) with the original source term $-Q\alpha c / (1 + \widehat{Q}_1 c)$, it is sufficient to establish the existence of a nonnegative solution to (3.1c). The convergence analysis in Chapter 4 shows that (3.1c) indeed has a nonnegative weak solution, which is thus a solution of (3.1c) with the original source term $-Q\alpha c / (1 + \widehat{Q}_1 c)$.

3.3 Threshold solution

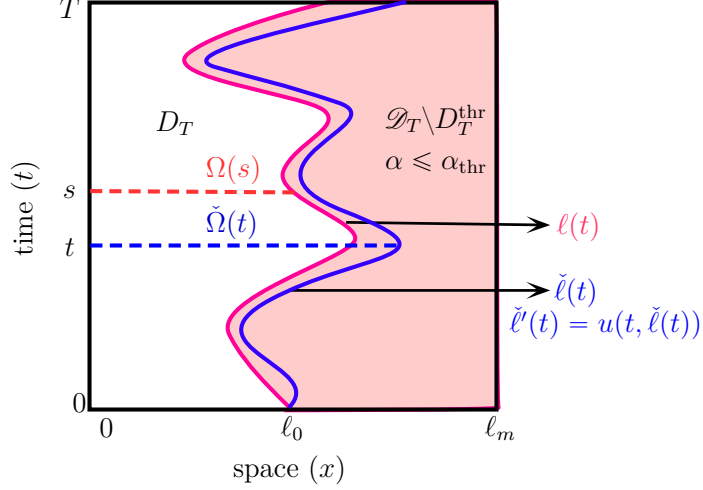


Figure 3.2: Tumour radii and time–space domains: D_T is time–space domain (region to the left of the blue curve) defined by (2.2d), D_T^{thr} (region to the left of the pink curve) is the time–space domain defined by the Threshold solution, Definition 3.1, and \mathcal{D}_T is the bounding box $(0, T) \times (0, \ell_m)$.

We define the notion of a weak solution for the threshold model (3.1), which is further referred to as the *threshold solution*, see Definition 3.1, wherein the condition to be satisfied by the tumour radius is further relaxed. Here, it is only demanded that the volume fraction of the tumour cells outside the time–space domain must be less than or equal to α_{thr} , see Figure 3.2. The convergence analysis in Chapter 4 ensures the existence of such a domain. It remains open whether such a domain is unique and coincides with the time–space domain wherein the tumour radius satisfies (2.2d) or (3.1d). Three different notions of tumour radii have been discussed so far and are summarised in Table 3.1 for clarity.

The introduction of the threshold into the definition of the domain and in the source term helps in Chapter 4 to obtain boundedness and bounded variation estimates for the numerical solution of (3.1a), and thus enables the numerical scheme to converge to the weak form (3.4a). The details presented in Subsection 3.4.2 complement this discussion.

Each threshold solution in the sense of Definition 3.1 corresponds to a pair of fixed constants m_{11} and m_{12} , which ensure the positivity and boundedness (strictly below 1) of the volume fraction in $D_T^{\text{thr}} = \cup_{0 < t < T} (\{t\} \times (0, \ell(t)))$ defined by (TS.2) in Definition 3.1.

Let $(\cdot, \cdot)_X$ be the standard L^2 inner product on a set $X \subset \mathbb{R}^d$, $d \geq 1$. The domain D_T^{thr} defined by (TS.2) in Definition 3.1 is open and bounded. Define the following vector spaces on D_T^{thr} :

$$H_{\partial_x}^{1,u}(D_T^{\text{thr}}) := \{v \in L^2(D_T^{\text{thr}}) : \partial_x v \in L^2(D_T^{\text{thr}}) \text{ and } v(t, 0) = 0 \forall t \in (0, T)\}, \text{ and}$$

$$H_{\partial_x}^{1,c}(D_T^{\text{thr}}) := \{v \in L^2(D_T^{\text{thr}}) : \partial_x v \in L^2(D_T^{\text{thr}}) \text{ and } v(t, \ell(t)) = 0 \forall t \in (0, T)\}.$$

Notation	Description
ℓ (BBL model, Section 1.5)	Solution to the ordinary differential equation $\ell'(t) = u(t, \ell(t)), \ell(0) = \ell_0$ Tumour radius defined in the BBL model.
$\hat{\ell}$ (Threshold model)	$\min \{x : \alpha(t, x) \leq \alpha_{\text{thr}} \text{ on } (x, \ell_m)\}$ Definition of tumour radius in the threshold model (3.1).
ℓ (Threshold solution)	$\forall x \geq \ell, \alpha(t, x) \leq \alpha_{\text{thr}}$ The condition above is to be satisfied by $\ell = \ell(t)$, so that (α, c, u, Ω) with $\Omega(t) = (0, \ell(t))$ is a Threshold solution in the sense of Definition 3.1.

Table 3.1: Description of various notions of tumour radii.

Define the inner product on the vector space $H_{\partial x}^{1,\varrho}(D_T^{\text{thr}})$, where $\varrho \in \{u, c\}$, as follows: for $w, v \in H_{\partial x}^{1,\varrho}(D_T^{\text{thr}})$

$$(w, v)_{H_{\partial x}^{1,\varrho}(D_T^{\text{thr}})} := (w, v)_{D_T^{\text{thr}}} + (\partial_x w, \partial_x v)_{D_T^{\text{thr}}}. \quad (3.3)$$

The inner product (3.3) induces a norm $\|w\|_{H_{\partial x}^{1,\varrho}(D_T^{\text{thr}})}$ for which $H_{\partial x}^{1,\varrho}(D_T^{\text{thr}})$ is a Hilbert space. Since for each $v \in H_{\partial x}^{1,\varrho}(D_T^{\text{thr}})$ and each $t \in (0, T)$ the time slice $v(t, \cdot)$ belongs to $H^1(0, \ell(t))$, the traces are well defined and the quantities $v(t, 0)$ and $v(t, \ell(t))$ are meaningful.

Definition 3.1 (Threshold solution). *Let $0 < m_{11} < m_{12} < 1$ be fixed constants that satisfy $m_{11} \leq m_{01}$ and $m_{12} \geq m_{02}$, where m_{01}, m_{02} satisfy (3.2). Fix a threshold value $\alpha_{\text{thr}} \in (0, 1)$. A threshold solution (with threshold α_{thr}) and domain D_T^{thr} of the threshold model in \mathcal{D}_T corresponding to the constants m_{11} and m_{12} is a 4-tuple (α, u, c, Ω) such that the following conditions hold.*

(TS.1) *The volume fraction $\alpha \in L^\infty(\mathcal{D}_T)$ is such that, for all $\varphi \in \mathcal{C}_c^\infty([0, T] \times (0, \ell_m))$,*

$$\int_{\mathcal{D}_T} ((\alpha, u\alpha) \cdot \nabla_{t,x} \varphi + (\alpha - \alpha_{\text{thr}})^+ f(\alpha, c) \varphi) dt dx + \int_{\Omega(0)} \varphi(0, x) \alpha_0(x) dx = 0, \quad (3.4a)$$

and it holds $0 < m_{11} \leq \alpha|_{\Omega(t)} \leq m_{12} < 1$ for every $t \in [0, T)$.

(TS.2) *The set D_T^{thr} is of the form $D_T^{\text{thr}} = \cup_{0 < t < T} (\{t\} \times \Omega(t))$, where $\Omega(t) = (0, \ell(t))$, and we have $\alpha \leq \alpha_{\text{thr}}$ on $\mathcal{D}_T \setminus D_T^{\text{thr}}$.*

(TS.3) The velocity u is such that $u \in H_{\partial x}^{1,u}(D_T^{\text{thr}})$ and, for all $v \in H_{\partial x}^{1,u}(D_T^{\text{thr}})$,

$$\int_0^T a^t(u(t, \cdot), v(t, \cdot)) dt = \int_0^T \mathcal{L}^t(v(t, \cdot)) dt, \quad (3.4b)$$

where $a^t : H^1(\Omega(t)) \times H^1(\Omega(t)) \rightarrow \mathbb{R}$ is the bilinear form and $\mathcal{L}^t : H^1(\Omega(t)) \rightarrow \mathbb{R}$ is the linear form defined by:

$$a^t(u, v) = k \left(\frac{\alpha}{1-\alpha} u, v \right)_{\Omega(t)} + \mu (\alpha \partial_x u, \partial_x v)_{\Omega(t)} \quad \text{and}$$

$$\mathcal{L}^t(v) = (\alpha \mathcal{H}(\alpha), \partial_x v)_{\Omega(t)}.$$

We extend u to \mathcal{D}_T by setting $u|_{\mathcal{D}_T \setminus \overline{D_T^{\text{thr}}}} := 0$.

(TS.4) The nutrient concentration c is such that $c - 1 \in H_{\partial x}^{1,c}(D_T^{\text{thr}})$, $c \geq 0$ and, for all $v \in H_{\partial x}^{1,c}(D_T^{\text{thr}})$ such that $\partial_t v \in L^2(D_T^{\text{thr}})$,

$$- \int_{D_T^{\text{thr}}} c \partial_t v dx dt + \lambda \int_{D_T^{\text{thr}}} \partial_x c \partial_x v dx dt - \int_{\Omega(0)} c_0(x) v(0, x) dx$$

$$+ Q \int_{D_T^{\text{thr}}} \frac{\alpha c v}{1 + \widehat{Q}_1 |c|} dx dt = 0. \quad (3.4c)$$

We extend c to \mathcal{D}_T by setting $c|_{\mathcal{D}_T \setminus \overline{D_T^{\text{thr}}}} := 1$.

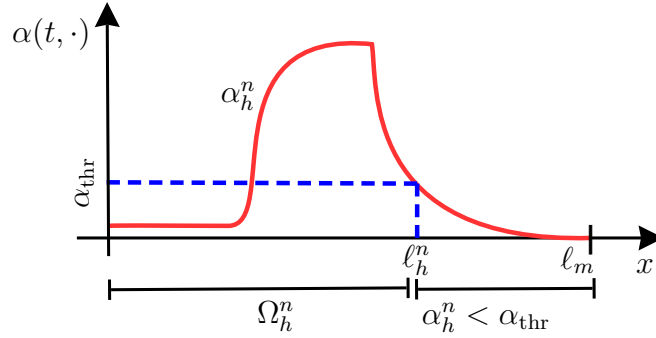


Figure 3.3: Selection of ℓ_h^n based on the value of α_h^n .

The existence of a threshold solution through the convergence of discrete solutions (Definition 3.2) is established in Chapter 4.

3.4 Numerical solution

The model equations are discretised using the principles in Chapter 2, see Section 2.4. We discretise (3.1a) using a finite volume method, (3.1b) using a Lagrange \mathbb{P}_1 -finite element

method, and (3.1c) using backward Euler in time and mass lumped \mathbb{P}_1 finite element method in space.

Recall the space and time discretisation from Section 2.4. Let $0 = x_0 < \dots < x_J = \ell_m$ be a uniform spatial discretisation with $h := x_{j+1} - x_j$, and $0 = t_0 < \dots < T_N = T$ be a uniform temporal discretisation with $\delta := t_{n+1} - t_n$. The numbers h and δ are called the spatial and temporal discretisation factors. Define the intervals $\mathcal{X}_j := (x_j, x_{j+1})$ and $\mathcal{T}_n := [t_n, t_{n+1})$. The node-centred intervals are defined by $\widetilde{\mathcal{X}}_j := (x_j - h/2, x_j + h/2)$ for $j = 1, \dots, J-1$, $\widetilde{\mathcal{X}}_0 := [x_0, x_0 + h/2]$, and $\widetilde{\mathcal{X}}_J := [x_J - h/2, x_J]$. We let $\chi_{\widetilde{\mathcal{X}}_j}$ be the characteristic function of $\widetilde{\mathcal{X}}_j$, that is, $\chi_{\widetilde{\mathcal{X}}_j} = 1$ on $\widetilde{\mathcal{X}}_j$, and $\chi_{\widetilde{\mathcal{X}}_j} = 0$ outside $\widetilde{\mathcal{X}}_j$. For any real valued function f on \mathbb{R} , define the pointwise average $\{f\}_{\mathcal{X}_j} = (f(x_j) + f(x_{j+1}))/2$. Define the extended initial data as follows: $\forall x \in (0, \ell_m)$

$$\alpha_0^e(x) := \begin{cases} \alpha_0(x) & \text{if } x \in \Omega(0), \\ 0 & \text{otherwise.} \end{cases} \quad \text{and} \quad c_0^e(x) := \begin{cases} c_0(x) & \text{if } x \in \Omega(0), \\ 1 & \text{otherwise.} \end{cases}$$

Definition 3.2 (Discrete scheme). *Fix a threshold $\alpha_{\text{thr}} \in (0, 1)$ and $\ell_m > \ell_0$ such that $(0, \ell_0) \subset (0, \ell_m)$ and $D_T^{\text{thr}} \subset \mathcal{D}_T$.*

Initial data approximation: *Define*

- α_h^0 by $\alpha_h^0 := \alpha_j^0 = \frac{1}{h} \int_{\mathcal{X}_j} \alpha_0^e(x) dx$ on \mathcal{X}_j for $0 \leq j \leq J-1$,
- c_h^0 by $c_h^0 \in \mathbb{P}_1(\mathcal{X}_j)$ for $0 \leq j \leq J-1$ and $c_h^0(x_j) := c_0^e(x_j)$ for $0 \leq j \leq J$, and
- $\Omega_h^0 := (0, \ell_h^0)$, where $\ell_h^0 = 1$.
- Obtain u_h^0 from (DS.c) below by taking $n = 0$.

Updation: *Then, construct a finite sequence of 3-tuple of functions $(\alpha_h^n, u_h^n, c_h^n)_{\{0 < n \leq N-1\}}$ on $(0, \ell_m)$ as in (DS.a)–(DS.d) described now.*

(DS.a) *Set $\alpha_h^n := \alpha_j^n$ on \mathcal{X}_j for $0 \leq j \leq J-1$, where*

$$\begin{aligned} & \frac{1}{\delta} (\alpha_j^n - \alpha_j^{n-1}) \\ & + \frac{1}{h} \left[u_{j+1}^{(n-1)+} \alpha_j^{n-1} - u_{j+1}^{(n-1)-} \alpha_{j+1}^{n-1} - u_j^{(n-1)+} \alpha_{j-1}^{n-1} + u_j^{(n-1)-} \alpha_j^{n-1} \right] \\ & = (\alpha_j^{n-1} - \alpha_{\text{thr}})^+ (1 - \alpha_j^{n-1}) b_j^{n-1} - (\alpha_j^n - \alpha_{\text{thr}})^+ d_j^{n-1}, \quad (3.5) \end{aligned}$$

where $u_j^n = u_h^n(x_j)$, $b_j^n = \{(1 + s_1)c_h^n / (1 + s_1c_h^n)\}_{\mathcal{X}_j}$, and $d_j^n = \{(s_2 + s_3c_h^n) / (1 + s_4c_h^n)\}_{\mathcal{X}_j}$. Note that, when $j = 0$, $u_0^{(n-1)} = 0$ and thus the value of α_{-1}^{n-1} can be arbitrarily fixed, say for example $\alpha_{-1}^{n-1} = m_{11}$.

(DS.b) *Set $\Omega_h^n := (0, \ell_h^n)$, where the recovered radius at step n is provided by $\ell_h^n = \min\{x_j : \alpha_j^n < \alpha_{\text{thr}} \text{ on } (x_j, \ell_m)\}$, see Figure 3.3.*

(DS.c) Set the conforming \mathbb{P}_1 finite element space on Ω_h^n , and its subspace with homogeneous boundary condition at $x = 0$, by

$$\begin{aligned}\mathcal{S}_h^n &:= \left\{ v_h^n \in \mathcal{C}^0(\overline{\Omega_h^n}) : v_h^n|_{\mathcal{X}_j} \in \mathbb{P}_1(\mathcal{X}_j) \text{ for } 0 \leq j < J_n := \ell_h^n/h \right\} \text{ and} \\ \mathcal{S}_{0,h}^n &:= \{ v_h^n \in \mathcal{S}_h^n : v_h^n(0) = 0 \}.\end{aligned}$$

Then,

$$u_h^n := \begin{cases} \tilde{u}_h^n & \text{on } \Omega_h^n, \\ 0 & \text{on } (0, \ell_m) \setminus \overline{\Omega_h^n}, \end{cases}$$

where $\tilde{u}_h^n \in \mathcal{S}_{0,h}^n$ satisfies

$$a_h^n(\tilde{u}_h^n, v_h^n) = \mathcal{L}_h^n(v_h^n) \quad \forall v_h^n \in \mathcal{S}_{0,h}^n, \quad (3.6)$$

with $a_h^n : \mathcal{S}_h^n \times \mathcal{S}_h^n \rightarrow \mathbb{R}$ and $\mathcal{L}_h^n : \mathcal{S}_h^n \rightarrow \mathbb{R}$ defined by

$$\begin{aligned}a_h^n(w, v) &= k \left(\frac{\alpha_h^n}{1 - \alpha_h^n} w, v \right)_{\Omega_h^n} + \mu (\alpha_h^n \partial_x w, \partial_x v)_{\Omega_h^n} \text{ and} \\ \mathcal{L}_h^n(v) &= (\alpha_h^n \mathcal{H}(\alpha_h^n), \partial_x v)_{\Omega_h^n}.\end{aligned} \quad (3.7)$$

(DS.d) Define the finite dimensional vector spaces

$$\begin{aligned}\mathcal{S}_{h,0}^n &:= \{ v_h^n \in \mathcal{S}_h^n : v_h^n(\ell_h^n) = 0 \} \text{ and} \\ \mathcal{S}_{h,\text{ML}} &:= \left\{ w_h : w_h = \sum_{j=0}^J w_j \chi_{\tilde{\mathcal{X}}_j}, w_j \in \mathbb{R}, 0 \leq j \leq J \right\},\end{aligned}$$

and the mass lumping operator $\Pi_h : \mathcal{C}^0([0, \ell_m]) \rightarrow \mathcal{S}_{h,\text{ML}}$ such that

$$\Pi_h w = \sum_{j=0}^J w(x_j) \chi_{\tilde{\mathcal{X}}_j}.$$

Then,

$$c_h^n := \begin{cases} \tilde{c}_h^n & \text{on } \Omega_h^n, \\ 1 & \text{on } (0, \ell_m) \setminus \overline{\Omega_h^n}, \end{cases}$$

where $\tilde{c}_h^n \in \mathcal{S}_h^n$ satisfies the boundary condition $\tilde{c}_h^n(\ell_h^n) = 1$ and the following discrete equation, in which $\Pi_h \tilde{c}_h^n := (\Pi_h c_h^n)|_{\Omega_h^n}$: for all $v_h^n \in \mathcal{S}_{h,0}^n$, it holds

$$\begin{aligned}(\Pi_h \tilde{c}_h^n, \Pi_h v_h^n)_{\Omega_h^n} - (\Pi_h c_h^{n-1}, \Pi_h v_h^n)_{\Omega_h^n} + \delta \lambda (\partial_x \tilde{c}_h^n, \partial_x v_h^n)_{\Omega_h^n} \\ = -Q \delta \left(\frac{\alpha_h^n \Pi_h \tilde{c}_h^n}{1 + \hat{Q}_1 |\Pi_h c_h^{n-1}|}, \Pi_h v_h^n \right)_{\Omega_h^n}.\end{aligned} \quad (3.8)$$

Remark 3.3 (Comparison between Definitions 3.2 and 2.4). *Though the discrete schemes in Chapter 3 and Chapter 2 (Definitions 3.2 and 2.4, respectively) are similar, two key differences needs to be noted. The source terms in (3.5) involves the threshold value, which is not the case with (2.9). Similarly, the source term in (3.8) has absolute value of $\Pi_h c_h^{n-1}$ in the denominator, while (2.10) has not. These modifications ensure that the discrete scheme (Definition 3.2) converge to a threshold solution.*

The Definition 3.2 (discrete scheme) provides a family of discrete spatial functions at each time index n , $0 \leq n < N$, from which a time–space function can be reconstructed.

Definition 3.4 (Time–reconstruct). *For a family of functions $(f_h^n)_{\{0 \leq n < N\}}$ on a set X , define the time–reconstruct $f_{h,\delta} : (0, T) \times X \rightarrow \mathbb{R}$ as $f_{h,\delta} := f_h^n$ on \mathcal{T}_n for $0 \leq n < N$.*

Definition 3.5 (Discrete solution). *The 4-tuple $(\alpha_{h,\delta}, u_{h,\delta}, c_{h,\delta}, \ell_{h,\delta})$, where $\alpha_{h,\delta}$, $u_{h,\delta}$, $c_{h,\delta}$, and $\ell_{h,\delta}$ are the respective time–reconstructs corresponding to the families $(\alpha_h^n)_n$, $(u_h^n)_n$, $(c_h^n)_n$, and $(\ell_h^n)_n$ obtained from (DS.a)–(DS.d), is called the discrete threshold solution.*

3.4.1 Physical properties of the threshold model

A few properties of the threshold model are discussed here. The numerical methods have been selected to preserve these properties as shown in this subsection. Define the continuous function spaces $\mathcal{C}^1(\overline{D_T})$ and $\mathcal{C}^{1,2}(\overline{D_T})$ by

$$\begin{aligned} \mathcal{C}^1(\overline{D_T}) &:= \left\{ c : \overline{D_T} \rightarrow \mathbb{R} : \frac{\partial c}{\partial t}, \frac{\partial c}{\partial x} \in \mathcal{C}(\overline{D_T}) \right\} \text{ and} \\ \mathcal{C}^{1,2}(\overline{D_T}) &:= \left\{ c : \overline{D_T} \rightarrow \mathbb{R} : \frac{\partial c}{\partial t}, \frac{\partial^2 c}{\partial x^2} \in \mathcal{C}(\overline{D_T}) \right\}. \end{aligned}$$

Conservation of mass by the cell volume fraction equation

Lemma 3.6 (Continuous case). *If (α, u, c, ℓ) is a solution of (3.1) such that α and u belong to $\mathcal{C}^1(\overline{D_T})$, then α satisfies the mass conservation property*

$$\int_0^{\ell(T)} \alpha(T, x) dx = \int_0^{\ell_0} \alpha_0(x) dx + \int_0^T \int_0^{\ell(t)} (\alpha - \alpha_{\text{thr}})^+ f(\alpha, c) dx dt.$$

Proof. Integrate (3.1a) over D_T to obtain

$$\int_0^T \int_0^{\ell(t)} (\alpha - \alpha_{\text{thr}})^+ f(\alpha, c) dx dt = \int_0^T \int_0^{\ell(t)} \frac{\partial \alpha}{\partial t} dx dt + \int_0^T \int_0^{\ell(t)} \frac{\partial}{\partial x} (u\alpha) dx dt. \quad (3.9)$$

In (3.9), apply Leibniz integral rule for the first term on the right–hand side and integrate $\frac{\partial}{\partial x} (u\alpha)$ in the second term over the interval $(0, \ell(t))$ to arrive at

$$\int_0^T \frac{\partial}{\partial t} \left(\int_0^{\ell(t)} \alpha(t, x) dx \right) dt - \int_0^T [\ell'(t) - u(t, \ell(t))] \alpha(t, \ell(t)) dt$$

$$-\int_0^T u(t,0)\alpha(t,0) dt = \int_0^T \int_0^{\ell(t)} (\alpha - \alpha_{\text{thr}})^+ f(\alpha, c) dx dt. \quad (3.10)$$

In the left hand side of (3.10), integrate the term over $(0, T)$, use $\ell'(t) = u(t, \ell(t))$ in the second term, and $u(t, 0) = 0$ in the third term to obtain the desired result. \square

Remark 3.7. Lemma 3.6 implies that the total cell volume fraction at time T is the sum of the total cell volume fraction present initially and the total cell volume fraction produced by the source term $(\alpha - \alpha_{\text{thr}})^+ f(\alpha, c)$ during the time interval $(0, T)$, which is precisely the mass conservation property.

Lemma 3.8 (Discrete case). Let $\alpha_{h,\delta}: \mathcal{D}_T \rightarrow \mathbb{R}$ and $c_{h,\delta}: \mathcal{D}_T \rightarrow \mathbb{R}$ be the time-reconstructions corresponding to the family of functions $(\alpha_h^n)_n$ obtained from (3.5) and $(c_h^n)_n$ obtained from (3.8), respectively. Then, $\alpha_{h,\delta}$ satisfies the discrete mass conservation property

$$\begin{aligned} \int_0^{\ell_m} \alpha_{h,\delta}(T, x) dx &= \int_0^{\ell_0} \alpha_0(x) dx \\ &+ \int_0^T \int_0^{\ell_m} (\alpha_{h,\delta}(t, x) - \alpha_{\text{thr}})^+ (1 - \alpha_{h,\delta}(t, x)) \frac{(1 + s_1)\Pi_{h,\delta} c_{h,\delta}(t, x)}{1 + s_1 \Pi_{h,\delta} c_{h,\delta}(t, x)} dx dt \\ &- \int_\delta^{T+\delta} \int_0^{\ell_m} (\alpha_{h,\delta}(t, x) - \alpha_{\text{thr}})^+ \frac{s_2 + s_3 \Pi_{h,\delta} c_{h,\delta}(t, x)}{1 + s_4 \Pi_{h,\delta} c_{h,\delta}(t, x)} dx dt. \end{aligned} \quad (3.11)$$

Proof. Multiply (3.5) by h and sum over $j = 0, \dots, J-1$ and $n = 1, \dots, N$ and use the fact that $u_0^{n-1} = 0 = u_J^{n-1}$ to obtain

$$\begin{aligned} \sum_{j=0}^{J-1} h \alpha_j^N - \sum_{j=0}^{J-1} h \alpha_j^0 &= \sum_{n=1}^N \delta \sum_{j=0}^{J-1} h (\alpha_j^{n-1} - \alpha_{\text{thr}})^+ (1 - \alpha_j^{n-1}) b_j^{n-1} \\ &- \sum_{n=1}^N \delta \sum_{j=0}^{J-1} h (\alpha_j^n - \alpha_{\text{thr}})^+ d_j^{n-1}. \end{aligned} \quad (3.12)$$

Note that each term in the sum $[u_{j+1}^{(n-1)+} \alpha_j^{n-1} - u_{j+1}^{(n-1)-} \alpha_{j+1}^{n-1} - u_j^{(n-1)+} \alpha_{j-1}^{n-1} + u_j^{(n-1)-} \alpha_j^{n-1}]$ in (3.5) cancels with the same term of opposite sign coming from (3.5) written for $j+1$ or $j-1$, and that the boundary terms vanish due to the boundary conditions. Use the definitions of b_j^n and d_j^n (see (DS.a) in Definition 3.2) and the definition of the time-reconstruction (see Definition 3.5) to arrive at (3.11) from (3.12). \square

Nonnegativity and boundedness of the nutrient concentration equation

Lemma 3.9 (Continuous case). If c satisfies (3.1c) with $\alpha \geq 0$ and belongs to $\mathcal{C}^{1,2}(\overline{D_T})$, then $0 \leq c \leq 1$.

Proof. Positivity: Multiply (3.1c) by the test function $-c^- = \min(c, 0)$ and integrate the product on the domain D_T to obtain

$$-\int_0^T \int_0^{\ell(t)} c^- \frac{\partial c}{\partial t} dx dt + \lambda \int_0^T \int_0^{\ell(t)} c^- \frac{\partial^2 c}{\partial x^2} dx dt = \int_0^T \int_0^{\ell(t)} c^- \frac{Q\alpha c}{1 + \widehat{Q}_1 |c|} dx dt. \quad (3.13)$$

In (3.13), use $-c^- \frac{\partial c}{\partial t} = \frac{1}{2} \frac{\partial}{\partial t} (c^-)^2$ to transform the first term on the left-hand side and apply integration by parts to the spatial integral in second term to obtain

$$\begin{aligned} \int_0^T \int_0^{\ell(t)} \frac{1}{2} \frac{\partial}{\partial t} (c^-)^2 dx dt + \lambda \int_0^T \int_0^{\ell(t)} \left| \frac{\partial c^-}{\partial x} \right|^2 dx dt + \lambda \int_0^T c^-(t, \ell(t)) \frac{\partial c}{\partial x}(t, \ell(t)) dt \\ - \lambda \int_0^T c^-(t, 0) \frac{\partial c}{\partial x}(t, 0) dt = \int_0^T \int_0^{\ell(t)} c^- \frac{Q\alpha c}{1 + \widehat{Q}_1 |c|} dx dt. \end{aligned} \quad (3.14)$$

Apply Leibniz integral rule on the first term in the left hand side of (3.14) and use the facts that $c^-(t, \ell(t)) = 0$ and $\frac{\partial c}{\partial x}(t, 0) = 0$ to arrive at

$$\begin{aligned} \frac{1}{2} \int_0^T \frac{\partial}{\partial t} \left(\int_0^{\ell(t)} (c^-)^2 dx \right) dt + \lambda \int_0^T \int_0^{\ell(t)} \left| \frac{\partial c^-}{\partial x} \right|^2 dx dt \\ = \int_0^T \int_0^{\ell(t)} c^- \frac{Q\alpha c}{1 + \widehat{Q}_1 |c|} dx dt. \end{aligned} \quad (3.15)$$

Carry out the time integration over the interval $(0, T)$ in first term in the left hand side of (3.15) and use the fact that $c^-(0, \cdot) = 0$ to obtain

$$\lambda \int_0^T \int_0^{\ell(t)} \left| \frac{\partial c^-}{\partial x} \right|^2 dx dt + \int_0^T \int_0^{\ell(t)} \frac{Q\alpha}{1 + \widehat{Q}_1 |c|} (c^-)^2 dx dt \leq 0.$$

Since $\alpha \geq 0$ this relation shows that $\partial_x c^- = 0$ and thus, since $c^-(t, \ell(t)) = 0$, that $c^- = 0$. This proves that $c \geq 0$ almost everywhere on D_T .

Boundedness: Multiply (3.1c) by the test function $(c-1)^+ = \max(c-1, 0)$ and integrate the product on the domain D_T to obtain

$$\begin{aligned} \int_0^T \int_0^{\ell(t)} (c-1)^+ \frac{\partial c}{\partial t} dx dt - \lambda \int_0^T \int_0^{\ell(t)} (c-1)^+ \frac{\partial^2 c}{\partial x^2} dx dt \\ = - \int_0^T \int_0^{\ell(t)} \frac{Q\alpha}{1 + \widehat{Q}_1 |c|} c(c-1)^+ dx dt. \end{aligned} \quad (3.16)$$

In (3.16), use $(c-1)^+ \frac{\partial c}{\partial t} = \frac{1}{2} \frac{\partial}{\partial t} ((c-1)^+)^2$ to transform the first term in the left-hand side, apply integration by parts to the spatial integral in the second term, and use the condition (3.1f) to obtain

$$\int_0^T \int_0^{\ell(t)} \frac{1}{2} \frac{\partial}{\partial t} ((c-1)^+)^2 dx dt + \int_0^T \int_0^{\ell(t)} \left| \frac{\partial}{\partial x} (c-1)^+ \right|^2 dx dt$$

$$= - \int_0^T \int_0^{\ell(t)} \frac{Q\alpha}{1 + \widehat{Q}_1|c|} c(c-1)^+ dx dt. \quad (3.17)$$

Apply the Leibniz integral rule on the first term in the left hand side of (3.17), carry out the time integration over the interval $(0, T)$, and use the condition (7.13f) to obtain

$$\int_0^T \int_0^{\ell(t)} \left| \frac{\partial}{\partial x} (c-1)^+ \right|^2 dx dt + \int_0^T \int_0^{\ell(t)} \frac{Q\alpha}{1 + \widehat{Q}_1|c|} ((c-1)^+)^2 dx dt \leq 0. \quad (3.18)$$

Result (3.18) implies that $(c-1)^+ = 0$, which yields that $c \leq 1$ almost everywhere on D_T . \square

The positivity and boundedness results corresponding to the discrete nutrient concentration $c_{h,\delta}$, obtained from the numerical scheme (3.8), is provided in Lemma 4.12 in Chapter 4.

3.4.2 Comments on the numerical method

This subsection substantiates the particular choices of numerical methods used to compute the discrete solution in Definition 3.5.

Volume fraction equation

The volume fraction equation (3.1a) is a continuity equation with the source term $\alpha f(\alpha, c)$, and the conserved variable α (see Lemma 3.6) is transported with a velocity u . Finite volume methods are the natural choice of numerical methods that preserve conservation property at the discrete level [107]. An upwinding finite volume scheme is used in (3.5). Upwinding treats the boundary flux values differently depending on the direction (sign) of the velocity as in (3.19), see [105, p. 159, Eq. (6.7)]. If the velocity at the node x_j is positive (resp. negative), then the material towards that node is upwinded from the control volume \mathcal{X}_{j-1} (resp. \mathcal{X}_j). This means that the flux at the boundary x_j between any two intervals \mathcal{X}_{j-1} and \mathcal{X}_j is approximated by: for any $t \in (0, T)$

$$(u_c \alpha)(t, \cdot)|_{x_j} \approx u_{h,\delta}(t, x_j)^+ \alpha_{h,\delta}(t, \cdot)|_{\mathcal{X}_{j-1}} - u_{h,\delta}(t, x_j)^- \alpha_{h,\delta}(t, \cdot)|_{\mathcal{X}_j}. \quad (3.19)$$

Therefore, the spatial difference $(u_c \alpha)(t, \cdot)|_{x_{j+1}} - (u_c \alpha)(t, \cdot)|_{x_j}$ at $t = t_{n-1}$ is approximated as

$$\begin{aligned} (u_c \alpha)(t, \cdot)|_{x_{j+1}} - (u_c \alpha)(t, \cdot)|_{x_j} &\approx \left(u_{j+1}^{(n-1)+} \alpha_j^{n-1} - u_{j+1}^{(n-1)-} \alpha_{j+1}^{n-1} \right) \\ &\quad - \left(u_j^{(n-1)+} \alpha_{j-1}^{n-1} - u_j^{(n-1)-} \alpha_j^{n-1} \right), \end{aligned}$$

which leads to (3.5).

Though the upwinding flux (3.19) is one of the simplest numerical fluxes that leads to a stable scheme, it introduces significant numerical diffusion in the discrete solution $\alpha_{h,\delta}$.

Hence, if we locate the time-dependent boundary ℓ_h^n as $\min\{x_j : \alpha_h^n = 0 \text{ on } (x_j, \ell_m]\}$, then $\ell_{h,\delta}$ will have notable deviation from the exact solution, which will further tamper the quality of the solutions $u_{h,\delta}$ and $c_{h,\delta}$. To eliminate this propagating error, the boundary point ℓ_h^n is located by $\min\{x_j : \alpha_h^n < \alpha_{\text{thr}} \text{ on } (x_j, \ell_m]\}$ (see Figure 3.3). However, the residual volume fraction of α_{thr} on $[\ell_h^n, \ell_m]$ might cause the reaction term $\alpha f(\alpha, c)$ to contribute a spurious growth; the modification $(\alpha - \alpha_{\text{thr}})^+ f(\alpha, c)$ overcomes this problem. More importantly, α_{thr} acts as a lower bound on the value of $\alpha_{h,\delta}$ on \mathcal{X}_{J_n-1} (the right most control volume in $(0, \ell_h^n)$) at each time t_n . A detailed numerical study of the dependence of the discrete solution on α_{thr} and the optimal choice of α_{thr} that minimises the error incurred in $\ell_{h,\delta}$ is done in Chapter 2.

Velocity equation

The velocity equation (3.1b) is elliptic with Dirichlet boundary condition at $x = 0$ and Neumann boundary condition at $x = \ell_h^n$ for each t_n , and hence the Lagrange \mathbb{P}_1 finite element method is used to discretise (3.1b). A specific benefit of using conforming finite elements for approximating the velocity is that it naturally provides nodal values (degrees of freedom of the scheme) of $u_{h,\delta}$ at the boundaries of each \mathcal{X}_j ; these nodal velocities can be directly used in the finite volume discretisation of (3.19) to compute fluxes at the control volume interfaces.

Nutrient concentration equation

The choice of time-implicit mass lumped finite element method [98, Section 7.3.5] for the nutrient concentration equation (3.1c) is substantiated mainly by two reasons. Firstly, the choice of mass lumping as opposed to a standard Lagrange \mathbb{P}_1 finite element method is important to obtain a discrete maximum principle for $c_{h,\delta}$. Secondly, the backward time procedure ensures the $L^2(0, T; H^1(0, \ell_m))$ stability of the mass lumped solutions. This is essential for the convergence analysis in Chapter 4. Also, the mass lumping operator Π_h used in (DS.d) preserves the L^1 norm of a piecewise linear function, and thus only locally redistributes the total amount of material whose concentration is specified by $c_{h,\delta}(t, \cdot)$ at each time $t \in (0, T)$.

3.5 Numerical example

The model and numerical parameter values used in the simulations shown in Figure 3.4 are provided in Table 3.2. Observe that all parameter values are dimensionless. The model values $k, \mu, Q, \hat{Q}_1, s_1, s_2, s_3, s_4$, and α^R are chosen from [1]. The threshold value α_{thr} and domain length ℓ_m are chosen based on the numerical experiments performed in [52]. The final time is set as $T_* = 50$.

The initial conditions employed in the simulations shown in Figure 3.4 are chosen from [1] and are as follows: for every $x \in (0, 1)$, $\alpha_0(x) = 0.8$ and $c_0(x) = 1$.

We plot the variation of $\alpha_{h,\delta}(t, \cdot)$, $u_{h,\delta}(t, \cdot)$ and $c_{h,\delta}(t, \cdot)$ for the times $t \in \{5, 10, \dots, 50\}$ on the corresponding domains $(0, \ell_{h,\delta}(t))$ in Figures 3.4(a), 3.4(b), and 3.4(c), respectively.

Parameter	Value	Parameter	Value
k	1	μ	1
Q	0.5	\widehat{Q}_1	0
s_1, s_4	10	s_2, s_3	0.5
α^R	0.8	ℓ_m	10
δ	10^{-3}	h	5×10^{-2}
ρ	0.1	α_{thr}	0.1

Table 3.2: The dimensionless model and numerical parameters values used in simulation shown in Figure 3.4.

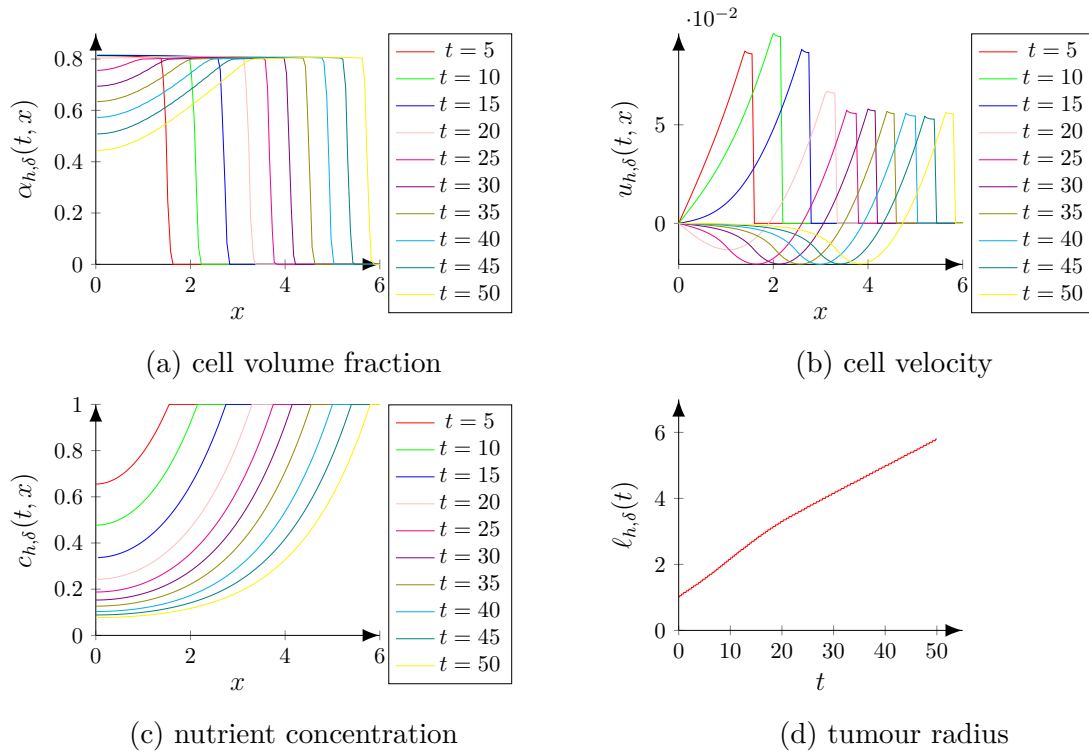


Figure 3.4: Numerical solution of the Definition 3.2 (discrete scheme) with $\delta = 10^{-3}$ and $h = 5 \times 10^{-2}$. A curve in each of the Figures 3.4(a), 3.4(b), and 3.4(c) represents the spatial variation of cell volume fraction, cell velocity, and nutrient concentration, respectively on the tumour domain $(0, \ell_{h,\delta}(t))$ at a time t as colour-coded in the legends. Figure 3.4(d) represents the evolution of the tumour radius $\ell(t)$ with respect to the time.

The variation of $\ell_{h,\delta}(t)$ with respect to time is depicted in 3.4(d). Observe from Figures 3.4(a) and 3.4(c) that the volume fraction and nutrient concentration decrease towards $x = 0$ due to the slower diffusion of nutrient towards $x = 0$ and the accelerated cell death owing to nutrient starvation. This effect is more noticeable in larger tumours than smaller

ones. The positive value of cell velocity towards the tumour boundary and negative value towards the interior suggests that the outermost cells flow outwards and the internal cells flow inwards. Note that $c_{h,\delta}$ is unity at $\ell_{h,\delta}(t)$, and this unlimited supply of nutrient results in the steady increase of tumour size as illustrated in Figure 3.4(d).

3.6 Conclusion

A variant of the extended model, termed as threshold model, is developed to mitigate the theoretical difficulties offered by extended model such as lack on uniform bounds on cell volume fraction and coercivity on cell velocity. An appropriate notion of a weak solution, called threshold solution characterised by the threshold value, is introduced. A discrete scheme that respects the physical properties of the model equations (3.1a)–(3.1c) is designed and implemented. The solutions obtained from the discrete scheme (Definition 3.2) are in very good agreement with the solutions obtained using standard techniques in Chapter 1 and using the discrete scheme (Definition 2.4) of Chapter 2.

Chapter 4

Convergence analysis of the numerical scheme for threshold model

4.1 Introduction

The main purpose of this chapter is to present an analytical framework, by which the existence of a threshold solution in Definition 3.1 can be established. The analysis in this chapter is novel and distinct from those available in the literature for free boundary problems, see Section 2.1.

Literature

Despite the fact that tumour growth models have been popular since the seventies [53, 54], the theoretical literature available on this field is very few. Recently, J. Zheng and S. Cui [55] considered existence of solutions for a tumour growth model with volume fraction and pressure in the tumour region as the unknown variables. The model equations in [55] are fully linear, while the boundary conditions are nonlinear, and a local well-posedness result is proved. A similar linear model is considered by C. Calzada et al. [56], and equivalence to an extended problem in a larger domain is proved. A more advanced model is considered by N. Zhang and Y. Tao [57], where the nutrient concentration is also considered as a variable and the existence of solutions is obtained by transforming the fixed domain to a unit ball in \mathbb{R} . Studies on convergence analysis are scarce. J. A. Mackenzie and A. Madzvamuse [12] have shown the convergence of a finite difference scheme for a single variable tumour growth model with a nonlinear source term on a time dependent boundary.

Contribution

This chapter aims to prove that the family of discrete solutions, see Definition 3.5, converge, up to a subsequence. Moreover, any limit of a convergent subsequence is established to be a threshold solution. Bounded variation estimates for the volume fraction, H^1 and L^∞ estimates for the cell velocity, and spatial and temporal estimates for the derivatives of nutrient concentration are obtained. The analysis in this chapter caters for the model

with all three variables (cell volume fraction, cell velocity, and nutrient concentration). To the best of our knowledge, it is the first convergence analysis of this kind.

Organisation

In Section 4.2, the main theorems are stated. The compactness and convergence properties of the numerical solutions from Definition 3.2 are derived in Section 4.3. In Section 4.4, we show that the limit of numerical solutions obtained in Section 4.3 is a threshold solution, see Definition 3.1. The maximal time of existence is discussed in Section 4.5.

4.2 Main theorems

In this chapter $(\alpha_{h,\delta}, u_{h,\delta}, c_{h,\delta}, \ell_{h,\delta})$ is a discrete solution from Definition 3.2 unless specified differently. Define the function $\hat{u}_{h,\delta}$ on \mathcal{D}_T such that for every $t \in (0, T)$,

$$\hat{u}_{h,\delta}(t, \cdot) := \begin{cases} u_{h,\delta}(t, \cdot) & \text{in } (0, \ell_{h,\delta}(t)], \\ u_{h,\delta}(t, \ell_{h,\delta}(t)) & \text{in } (\ell_{h,\delta}(t), \ell_m). \end{cases} \quad (4.1)$$

The function $\hat{u}_{h,\delta}$ is the constant extension of $u_{h,\delta}(t, \cdot)$ to $(\ell_{h,\delta}(t), \ell_m)$. Note that $\hat{u}_{h,\delta}$ is continuous on the contrary to $u_{h,\delta}$ (see Figure 4.1). This continuity is necessary to ensure the existence of a square integrable weak derivative.

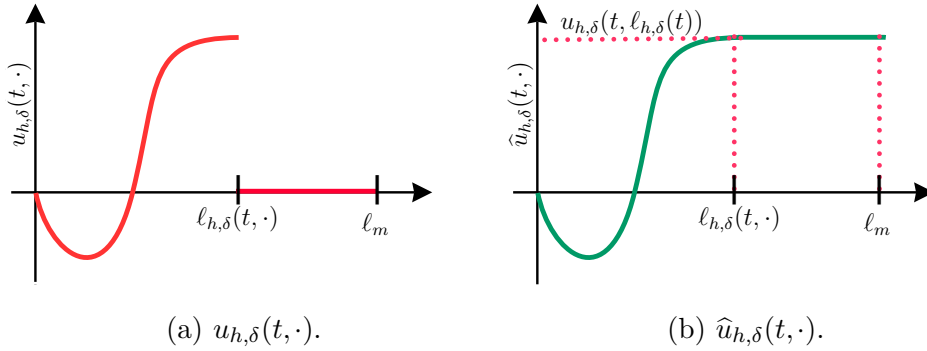


Figure 4.1: The left-hand side plot illustrates the discontinuous function $u_{h,\delta}$ and the right-hand side plot illustrates the continuous modification $\hat{u}_{h,\delta}$.

The notation $\Pi_{h,\delta}c_{h,\delta}$ denotes the mass lumping operator Π_h applied to $c_{h,\delta}(t, \cdot)$ for each $t \in (0, T)$. Define the Hilbert spaces:

$$\begin{aligned} L_c^2(0, T; H^1(0, \ell_m)) &:= \{f \in L^2(0, T; H^1(0, \ell_m)) : f(t, \ell(t)) = 0 \text{ for a.e. } t \in (0, T)\}, \\ L_u^2(0, T; H^1(0, \ell_m)) &:= \{f \in L^2(0, T; H^1(0, \ell_m)) : f(t, 0) = 0 \text{ for a.e. } t \in (0, T)\}. \end{aligned}$$

The main results of this chapter are stated in Theorem 4.2 and 4.3. Let $\hat{u}_{h,\delta}$ be defined by (4.1).

Remark 4.1 (Courant–Friedrichs–Lewy condition). *Theorems 4.2 depends on a Courant–Friedrichs–Lewy (CFL) condition (4.2) that restricts the possible choices of the spatial and temporal discretisation factors h and δ . This condition imparts stability to the finite volume scheme that discretises the hyperbolic conservation law (3.1a). The restriction on temporal discretisation factor due to (4.2) renders the schemes expensive. However, the condition is necessary and a characteristic feature of every explicit scheme [108].*

Theorem 4.2 (Compactness). *Let the properties stated below be true.*

- *The initial volume fraction α_0 belongs to $BV(0, \ell_m)$ and satisfies*

$$0 < m_{01} \leq \alpha_0 \leq m_{02} < 1 \quad \text{on } \widehat{\Omega}(0)$$

- *The discretisation parameters h and δ satisfy the following conditions:*

$$\rho \mathcal{C}_{\text{CFL}} \leq \frac{\delta}{h} \leq \mathcal{C}_{\text{CFL}} := \frac{\sqrt{a_*} \mu |1 - a^*|^2}{2\ell_m |a^* - \alpha^{\text{R}}|} \quad \text{and} \quad \delta < \min\left(\frac{1 - \rho}{s_2}, \frac{2(1 - \rho)}{1 + s_2}\right), \quad (4.2)$$

where ρ, a_ and a^* are constants chosen such that $\rho < 1$, $0 < a_* < m_{01}$, and $m_{02} < a^*$.*

Then, there exists a finite time T_ depending on the choice of ρ, a_* , and a^* , a subsequence (denoted by the same indices as of the sequence) of the family of functions $\{(\alpha_{h,\delta}, \widehat{u}_{h,\delta}, c_{h,\delta}, \ell_{h,\delta})\}_{h,\delta}$, and a 4-tuple of functions $(\alpha, \widehat{u}, c, \ell)$ such that, setting $\mathcal{D}_{T_*} = (0, T_*) \times (0, \ell_m)$, it holds*

$$\alpha \in BV(\mathcal{D}_{T_*}), \quad c \in L^2(0, T_*; H^1(0, \ell_m)), \quad \widehat{u} \in L^2_u(0, T_*; H^1(0, \ell_m)), \quad \ell \in BV(0, T_*),$$

and as $h, \delta \rightarrow 0$,

- $\alpha_{h,\delta} \rightarrow \alpha$ almost everywhere and in L^∞ -weak* on \mathcal{D}_{T_*} ,
- $\Pi_{h,\delta} c_{h,\delta} \rightarrow c$ strongly in $L^2(\mathcal{D}_{T_*})$ and $\partial_x c_{h,\delta} \rightharpoonup \partial_x c$ weakly in $L^2(\mathcal{D}_{T_*})$,
- $\widehat{u}_{h,\delta} \rightarrow \widehat{u}$ and $\partial_x \widehat{u}_{h,\delta} \rightharpoonup \partial_x \widehat{u}$ weakly in $L^2(\mathcal{D}_{T_*})$, and
- $\ell_{h,\delta} \rightarrow \ell$ almost everywhere in $(0, T_*)$.

The next theorem asserts that the functions (α, u, c, Ω) is a threshold solution, see Definition 3.1, introduced in Chapter 3.

Theorem 4.3 (Identification of the limit and convergence). *Let $(\alpha, \widehat{u}, c, \ell)$ be the limit, in the sense of Theorem 4.2, of any subsequence of the numerical approximations $(\alpha_{h,\delta}, \widehat{u}_{h,\delta}, c_{h,\delta}, \ell_{h,\delta})$. Define $\Omega(t) := (0, \ell(t))$ and the threshold domain $D_{T_*}^{\text{thr}} := \{(t, x) : x < \ell(t), t \in (0, T_*)\}$, and let $u := \widehat{u}$ on $D_{T_*}^{\text{thr}}$ and $u := 0$ on $\mathcal{D}_{T_*} \setminus D_{T_*}^{\text{thr}}$. Then, (α, u, c, Ω) is a threshold solution in the sense of Definition 3.1 with $T = T_*$.*

Remark 4.4 (Convergence up to a subsequence). *In the rest of the chapter, unless otherwise specified, “convergence” of sequences is to be understood up to a subsequence. Hence “a sequence $(a_n)_n$ converges to a limit a ” means that there exists a subsequence $(a_{k_n})_n \subseteq (a_n)_n$ such that $(a_{k_n})_n$ converges to a . This concept is classical when analysing the convergence of numerical approximations of non-linear equations, see, e.g., [58, Section 4.5], [109, Section 5.2] or [98, Chap. 5, 6].*

Remark 4.5 (Existence of a solution). *Existence of a threshold solution is ensured by Theorems 4.2 and 4.3. Theorem 4.3 also shows that if convergence is observed in a numerical simulation, then the limit is necessarily a solution to the threshold model. Finally, as usual in convergence by compactness arguments, if the solution to this model is proved to be unique then the entire sequence of approximations (not just a subsequence) converges to that solution.*

4.3 Proof of Theorem 4.2

The proof of Theorem 4.2 involves several steps, which are described here. In subsection 4.3.1, we prove the following:

- existence and uniqueness of the discrete solutions $\alpha_{h,\delta}$, $u_{h,\delta}$, and $c_{h,\delta}$ to the discrete scheme in Definition 3.2,
- boundedness of $u_{h,\delta}$ in various norms,
- positivity, boundedness, and bounded variation property of $\alpha_{h,\delta}$, and
- positivity and boundedness of $c_{h,\delta}$.

In subsection 4.3.2, we show that the families of functions $\{\alpha_{h,\delta}\}_{h,\delta}$, $\{u_{h,\delta}\}_{h,\delta}$, $\{c_{h,\delta}\}_{h,\delta}$, and $\{\ell_{h,\delta}\}_{h,\delta}$ are relatively compact in appropriate spaces.

4.3.1 Existence, uniqueness, and boundedness of the iterates

The proof of existence and uniqueness of the discrete solutions $\alpha_{h,\delta}$, $u_{h,\delta}$, and $c_{h,\delta}$ involves many interrelated results. For clarity, we provide a sketch of the steps involved.

Fix two constants $a^* \in (\max(\alpha^R, m_{02}), 1)$ and $a_* \in (0, \min(m_{01}, \alpha_{\text{thr}}))$. We establish the existence of a time T_* (explicitly determined in the analysis), which depends in particular on a_* and a^* , such that the following theorem holds.

Theorem 4.6. *For all $n \in \mathbb{N}$ such that $t_n \leq T_*$, $\alpha_{h,\delta}(t_n, \cdot)$ and $c_{h,\delta}(t_n, \cdot)$ are well defined. Also, it holds $a_* < \alpha_{h,\delta}(t_n, \cdot)|_{\Omega_h^n} < a^*$ and $0 \leq c_{h,\delta}(t_n, \cdot)|_{(0, \ell_m)} \leq 1$.*

The proof of Theorem 4.6 is done in several steps by strong induction on $n \in \mathbb{N}$. The base case obviously holds, for any choice of a_* and a^* as above. Let $n \in \mathbb{N}$ be such that $t_{n+1} \leq T_*$, and assume that Theorem 4.6 holds for the indices $0, \dots, n$. The steps (IS.1)–(IS.4) below show that Theorem 4.6 holds for $\alpha_{h,\delta}(t_{n+1}, \cdot)$ and $c_{h,\delta}(t_{n+1}, \cdot)$.

In the sequel, \mathcal{C} is a generic constant that depends on $T, \ell_m, \ell, \alpha^R, a_*, a^*$ and the model parameters, as explicitly defined in (4.5a)–(4.5c).

(IS.1) We establish that there exists a unique solution \tilde{u}_h^n for the variational problem (3.6) and derive energy estimates.

(IS.2) **Bounded variation and L^∞ estimates on $\alpha_{h,\delta}u_{h,\delta}$:** We show that

- (a) $\|\mu\alpha_{h,\delta}(t_n, \cdot)\partial_x u_{h,\delta}(t_n, \cdot) - \alpha_{h,\delta}(t_n, \cdot)\mathcal{H}(\alpha_{h,\delta}(t_n, \cdot))\|_{BV(0,\ell_m)} \leq \mathcal{C}$,
- (b) $\|(\mu\alpha_{h,\delta}(t_n, \cdot)\partial_x u_{h,\delta}(t_n, \cdot))^\ominus\|_{L^\infty(0,\ell_m)} \leq \mathcal{C}$, and
- (c) $\|\mu\alpha_{h,\delta}(t_n, \cdot)\partial_x u_{h,\delta}(t_n, \cdot)\|_{L^\infty(0,\ell_m)} \leq \mathcal{C}$,

where $\mathcal{H}(\alpha) = (\alpha - \alpha^R)^+ / (1 - \alpha)^2$.

(IS.3) L^∞ estimates on $\alpha_{h,\delta}$: It holds $a_* < \alpha_{h,\delta}(t_{n+1}, \cdot)|_{\Omega_h^{n+1}} < a^*$.

(IS.4) We show that there exists a unique solution $\tilde{c}_{h,\delta}(t_{n+1}, \cdot)$ to (3.8) and that $0 \leq \tilde{c}_{h,\delta}(t_{n+1}, \cdot)|_{(0,\ell_m)} \leq 1$.

The steps (IS.1)–(IS.4) are now performed in Lemmas 4.7, 4.9, 4.12 and Proposition 4.10, respectively. The time T_* is explicitly obtained in the proof of Proposition 4.10.

Lemma 4.7 (Step (IS.1)). *There exists a unique solution \tilde{u}_h^n to (3.6) and it satisfies the following estimates:*

$$\left\| \sqrt{\alpha_{h,\delta}(t_n, \cdot)} \partial_x \tilde{u}_h^n \right\|_{0,\Omega_h^n} + \left\| \frac{\sqrt{\alpha_{h,\delta}(t_n, \cdot)} \tilde{u}_h^n}{\sqrt{1 - \alpha_{h,\delta}(t_n, \cdot)}} \right\|_{0,\Omega_h^n} \leq \left(1 + \frac{1}{\sqrt{k}} \right) \frac{\sqrt{\ell_m} |a^* - \alpha^R|}{\mu |1 - a^*|^2}. \quad (4.3)$$

Proof. Coercivity and continuity of the bilinear form a_h^n and continuity of the linear form \mathcal{L}_h^n are clear from $0 < a_* \leq \alpha_{h,\delta}(t_n, \cdot) \leq a^* < 1$. An application of the Lax–Milgram lemma [97, p. 297] establishes the existence of a unique discrete solution to (3.6). A choice of $v_h^n = \tilde{u}_h^n$ in (3.6), the fact that $0 < \alpha_{h,\delta}(t_n, \cdot) < 1$, and Cauchy–Schwarz inequality in (3.7) yield the intermediate estimate

$$\begin{aligned} \mu \left\| \sqrt{\alpha_{h,\delta}(t_n, \cdot)} \partial_x \tilde{u}_h^n \right\|_{0,\Omega_h^n}^2 + k \left\| \frac{\sqrt{\alpha_{h,\delta}(t_n, \cdot)} \tilde{u}_h^n}{\sqrt{1 - \alpha_{h,\delta}(t_n, \cdot)}} \right\|_{0,\Omega_h^n}^2 \\ \leq \sqrt{\ell_m} \frac{|a^* - \alpha^R|}{|1 - a^*|^2} \left\| \sqrt{\alpha_{h,\delta}(t_n, \cdot)} \partial_x \tilde{u}_h^n \right\|_{0,\Omega_h^n}, \end{aligned}$$

which proves (4.3). □

Remark 4.8 (L^∞ estimate on velocity). *Since $\alpha_{h,\delta}(t_n, \cdot) \geq a_*$, the intermediate estimate yields an upper bound on $\|\partial_x \tilde{u}_h^n\|_{0,\Omega_h^n}$, which after an application of the boundary condition $\tilde{u}_h^n(0) = 0$ and a use of Cauchy–Schwarz inequality yields*

$$\|u_{h,\delta}(t_n, \cdot)\|_{L^\infty(0,\ell_m)} \leq \frac{\ell_m}{\sqrt{a_*} \mu} \frac{|a^* - \alpha^R|}{|1 - a^*|^2}. \quad (4.4)$$

Lemma 4.9 (Step (IS.2)). *It holds that*

$$\|\mu\alpha_{h,\delta}(t_n, \cdot)\partial_x u_{h,\delta}(t_n, \cdot) - \alpha_{h,\delta}(t_n, \cdot)\mathcal{H}(\alpha_{h,\delta}(t_n, \cdot))\|_{BV(0, \ell_m)} \leq \ell_m \sqrt{\frac{k}{\mu}} \frac{|a^* - \alpha^R|}{|1 - a^*|^{5/2}}, \quad (4.5a)$$

$$\|(\mu\alpha_{h,\delta}(t_n, \cdot)\partial_x u_{h,\delta}(t_n, \cdot))^\ominus\|_{L^\infty(0, \ell_m)} \leq \ell_m \sqrt{\frac{k}{\mu}} \frac{|a^* - \alpha^R|}{|1 - a^*|^{5/2}}, \quad \text{and} \quad (4.5b)$$

$$\|\mu\alpha_{h,\delta}(t_n, \cdot)\partial_x u_{h,\delta}(t_n, \cdot)\|_{L^\infty(0, \ell_m)} \leq \ell_m \sqrt{\frac{k}{\mu}} \frac{|a^* - \alpha^R|}{|1 - a^*|^{5/2}} + \frac{a^*(a^* - \alpha^R)}{(1 - a^*)^2}. \quad (4.5c)$$

Proof. Consider the Lagrange \mathbb{P}_1 nodal basis functions $\{\varphi_{h,j}^n\}_{\{1 \leq j \leq J_n\}}$ of $\mathcal{S}_{0,h}^n$, and choose $v_h^n = \varphi_{h,j}^n$ in (3.6) for $j \in \{1, \dots, J_n - 1\}$, where $J_n = \ell_h^n/h$, to obtain

$$\begin{aligned} \mu \left(\alpha_{j-1}^n \partial_x \tilde{u}_h^n|_{x_{j-1}} - \alpha_j^n \partial_x \tilde{u}_h^n|_{x_j} \right) - \left(\alpha_j^n \mathcal{H}(\alpha_j^n) - \alpha_{j-1}^n \mathcal{H}(\alpha_{j-1}^n) \right) \\ = -k \int_{x_{j-1}}^{x_{j+1}} \frac{\alpha_{h,\delta}(t_n, \cdot)}{1 - \alpha_{h,\delta}(t_n, \cdot)} \tilde{u}_h^n \varphi_{h,j}^n dx. \end{aligned} \quad (4.6a)$$

Choose $v_h^n = \varphi_{h,J_n}^n$ in (3.6) to obtain

$$\mu \alpha_j^n \partial_x \tilde{u}_h^n|_{x_{J_n-1}} - \alpha_{J_n-1}^n \mathcal{H}(\alpha_{J_n-1}^n) = -k \int_{x_{J_n-1}}^{x_{J_n}} \frac{\alpha_{h,\delta}(t_n, \cdot)}{1 - \alpha_{h,\delta}(t_n, \cdot)} \tilde{u}_h^n \varphi_{h,J_n}^n dx. \quad (4.6b)$$

Recall that $u_h^n = \tilde{u}_h^n$ on $(0, \ell_h^n)$, and that $u_h^n = 0 = \mathcal{H}(\alpha_j^n)$ outside this interval. Then, for any $j \in \{1, \dots, J-1\}$, (4.6a) and (4.6b) imply

$$\begin{aligned} \mu \left(\alpha_{j-1}^n \partial_x u_h^n|_{x_{j-1}} - \alpha_j^n \partial_x u_h^n|_{x_j} \right) - \left(\alpha_j^n \mathcal{H}(\alpha_j^n) - \alpha_{j-1}^n \mathcal{H}(\alpha_{j-1}^n) \right) \\ = -k \int_{x_{j-1}}^{x_{j+1}} \frac{\alpha_{h,\delta}(t_n, \cdot)}{1 - \alpha_{h,\delta}(t_n, \cdot)} u_h^n \varphi_{h,j}^n dx, \end{aligned}$$

where $\varphi_{h,j}^n = 0$ if $j \geq J_n + 1$. Then, taking the absolute value, summing over $j = 1, \dots, J-1$, applying Cauchy–Schwarz inequality, (4.3), and the observation that $0 \leq \varphi_{h,j-1}^n + \varphi_{h,j}^n \leq 1$ everywhere leads to (4.5a). As a consequence, since $\alpha_{h,\delta}(t_n, \cdot)(\mu\partial_x u_{h,\delta}(t_n, \cdot) - \mathcal{H}(\alpha_{h,\delta}(t_n, \cdot)))$ vanishes at $x = \ell_m$,

$$\|\mu\alpha_{h,\delta}(t_n, \cdot)\partial_x u_{h,\delta}(t_n, \cdot) - \alpha_{h,\delta}(t_n, \cdot)\mathcal{H}(\alpha_{h,\delta}(t_n, \cdot))\|_{L^\infty(0, \ell_m)} \leq \ell_m \sqrt{\frac{k}{\mu}} \frac{|a^* - \alpha^R|}{|1 - a^*|^{5/2}}.$$

Since $0 \leq \alpha_{h,\delta}(t_n, \cdot)\mathcal{H}(\alpha_{h,\delta}(t_n, \cdot)) \leq a^*(a^* - \alpha^R)/(1 - a^*)^2$, the bounds (4.5b) and (4.5c) follow. \square

The positivity and boundedness of $\alpha_{h,\delta}(t_{n+1}, \cdot)$ are shown next. The next proposition establishes the existence of a finite time T_* such that the strong induction assumption holds in $[0, T_*)$.

Proposition 4.10 (Step (IS.3)). *There exists $T_* > 0$ such that if $n+1 \leq N_* := T_*/\delta$, then*

$$a_* \leq \min_{j: x_j \in \Omega_h^{n+1}} \alpha_j^{n+1} \leq \max_{0 \leq j \leq J-1} \alpha_j^{n+1} \leq a^*.$$

Proof. Substitute $u_{j+1}^{n+} = u_{j+1}^n + u_{j+1}^{n-}$ and $u_j^{n-} = u_j^{n+} - u_j^n$ in (3.5) (written for $n+1$ instead of n) to obtain

$$\begin{aligned} \alpha_j^{n+1} + \delta(\alpha_j^{n+1} - \alpha_{\text{thr}})^+ d_j^n &= \alpha_j^n + \delta(\alpha_j^n - \alpha_{\text{thr}})^+ (1 - \alpha_j^n) b_j^n - \frac{\delta}{h} \alpha_j^n (u_{j+1}^n - u_j^n) \\ &\quad + \frac{\delta}{h} (u_{j+1}^{n-} (\alpha_{j+1}^n - \alpha_j^n) + u_j^{n+} (\alpha_{j-1}^n - \alpha_j^n)). \end{aligned} \quad (4.7)$$

Define the linear combination

$$\mathcal{L}(\alpha_{j-1}^n, \alpha_j^n, \alpha_{j+1}^n) := \frac{\delta}{h} u_j^{n+} \alpha_{j-1}^n + \left(1 - \frac{\delta}{h} u_{j+1}^{n-} - \frac{\delta}{h} u_j^{n+}\right) \alpha_j^n + \frac{\delta}{h} u_{j+1}^{n-} \alpha_{j+1}^n. \quad (4.8)$$

The conditions (4.2) and (4.4) show that all the coefficients in (4.8) are positive, and thus this linear combination is convex. Moreover, (4.7) can be recast as

$$\begin{aligned} \alpha_j^{n+1} + \delta(\alpha_j^{n+1} - \alpha_{\text{thr}})^+ d_j^n &= \mathcal{L}(\alpha_{j-1}^n, \alpha_j^n, \alpha_{j+1}^n) + \delta(\alpha_j^n - \alpha_{\text{thr}})^+ (1 - \alpha_j^n) b_j^n \\ &\quad - \delta \alpha_j^n \partial_x u_h^n|_{x_j}. \end{aligned} \quad (4.9)$$

Since $0 \leq c_h^n \leq 1$ (this is the induction hypothesis (IS.4) at step n), we have $0 \leq d_j^n \leq s_2$ and $b_j^n \geq 0$. Then, a use of (4.5c) and the positivity of $1 - \alpha_j^n$ in (4.9) yield

$$\alpha_j^{n+1} (1 + \delta s_2) \geq \min(\alpha_{j-1}^n, \alpha_j^n, \alpha_{j+1}^n) - \delta \mathcal{F}_{\min}, \quad (4.10)$$

where

$$\mathcal{F}_{\min} = \ell_m \frac{\sqrt{k}}{\mu^{3/2}} \frac{|a^* - \alpha^{\text{R}}|}{|1 - a^*|^{5/2}} + \frac{1}{\mu} \frac{a^* (a^* - \alpha^{\text{R}})}{(1 - a^*)^2}.$$

Step (DS.b) implies that $\alpha_{j-1}^n, \alpha_j^n, \alpha_{j+1}^n < \alpha_{\text{thr}}$ for $j \geq J_n + 1$. This fact along with an observation that $u_h^n = 0$ in $(0, \ell_m) \setminus \Omega_h^n$ ensures that the right hand side of (4.9) is strictly bounded above by α_{thr} (the linear combination remains, and the other terms vanish); hence $\alpha_j^{n+1} < \alpha_{\text{thr}}$, for all $j \geq J_{n+1}$. Thus the domain Ω_h^{n+1} is either a subset of Ω_h^n or equal to $\Omega_h^n \cup \mathcal{X}_{J_n}$. These two cases are considered separately.

Case 1 ($\Omega_h^{n+1} \subseteq \Omega_h^n$: tumour does not grow in the $(n+1)^{\text{th}}$ level). If $\Omega_h^{n+1} = \Omega_h^n$, the last value $\alpha_{J_{n+1}-1}^{n+1}$ depends on $\alpha_{J_n-2}^n, \alpha_{J_n-1}^n$, and $\alpha_{J_n}^n$ (see Figure 4.2(a)). The domain selection procedure (DS.b) shows $\alpha_{J_{n+1}-1}^{n+1} \geq \alpha_{\text{thr}}$. All other values α_j^{n+1} depend on α_k^n with $k \leq J_n-1$, which are values inside Ω_h^n . Therefore, for all $j \leq J_{n+1}-1$, by (4.10)

$$\alpha_j^{n+1} (1 + \delta s_2) \geq \min \left\{ \left(\min_{k: x_k \in \Omega_h^n} \alpha_k^n \right), \alpha_{\text{thr}} \right\} - \delta \mathcal{F}_{\min}. \quad (4.11)$$

The same argument follows in the case $\Omega_h^{n+1} \subset \Omega_h^n$ (see Figure 4.2(b)).

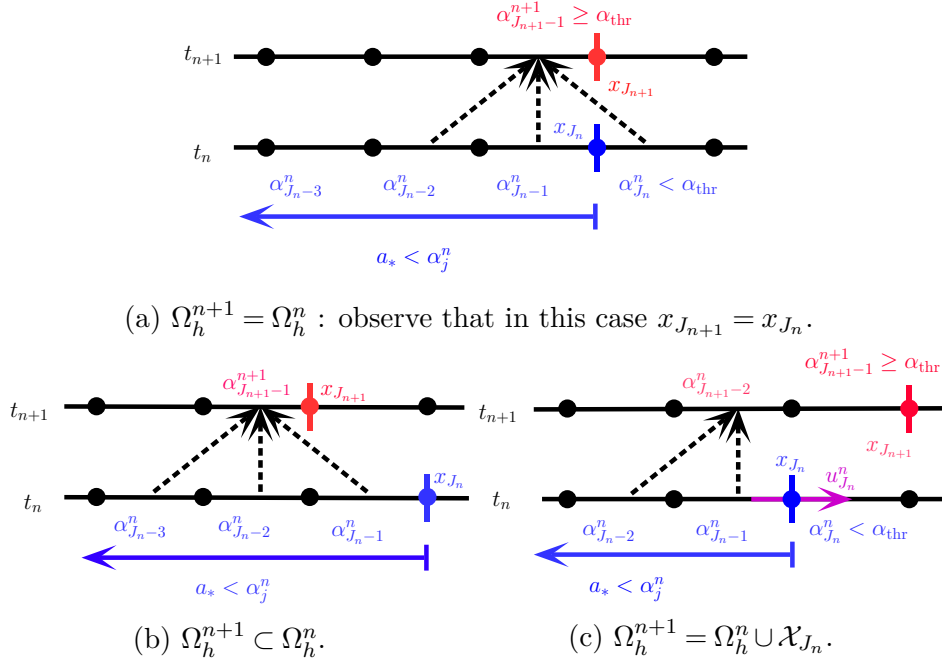


Figure 4.2: Dependency of α_j^{n+1} on α_j^n . Observe that in Figure 4.2(c) the direction of $u_{J_n}^n$ is rightwards, which eliminates the dependency of $\alpha_{J_{n+1}-2}^n$ on $\alpha_{J_n}^n$.

Case 2 ($\Omega_h^{n+1} = \Omega_h^n \cup \mathcal{X}_{J_n}$: tumour expands). By the domain selecting procedure (DS.b) we have $\alpha_{J_{n+1}-1}^{n+1} \geq \alpha_{\text{thr}}$ (see Figure 4.2(c)). This along with $\alpha_{J_n}^n < \alpha_{\text{thr}}$ and $u_j^n = 0$ for $j > J_n$, implies that some volume fraction must flow from Ω_h^n to \mathcal{X}_{J_n} . Hence, $u_{J_n}^n > 0$. We note here that our usage of $(\alpha - \alpha_{\text{thr}})^+$ in the source term cannot yield the growth above α_{thr} in \mathcal{X}_{J_n} . Therefore, since $J_{n+1} - 2 = J_n - 1$ in this case, choosing $j = J_n - 1$ in (4.9), the term involving α_{j+1}^n vanishes from $\mathcal{L}(\alpha_{j-1}^n, \alpha_j^n, \alpha_{j+1}^n)$ (since it is multiplied by $u_{J_n}^{n-}$) and we obtain

$$\alpha_{J_{n+1}-2}^{n+1}(1 + \delta s_2) \geq \min(\alpha_{J_n-2}^n, \alpha_{J_n-1}^n) - \delta \mathcal{F}_{\min}. \quad (4.12)$$

The values α_j^{n+1} with $j \leq J_{n+1} - 3$ can be dealt as in (4.11).

Combine (4.11) and (4.12) to obtain, for $j \leq J_{n+1} - 1$

$$\alpha_j^{n+1}(1 + \delta s_2) \geq \min \left\{ \left(\min_{k: x_k \in \Omega_h^n} \alpha_k^n \right), \alpha_{\text{thr}} \right\} - \delta \mathcal{F}_{\min}.$$

A use of $(1 + \delta s_2)^{-1} \geq \exp(-\delta s_2)$ yields

$$\min_{j: x_j \in \Omega_h^{n+1}} \alpha_j^{n+1} \geq \exp(-\delta s_2) \min \left\{ \left(\min_{k: x_k \in \Omega_h^n} \alpha_k^n \right), \alpha_{\text{thr}} \right\} - \delta \exp(-\delta s_2) \mathcal{F}_{\min}.$$

This relation is obviously also true if the left-hand side is replaced by α_{thr} , and therefore,

$$\min \left\{ \left(\min_{j: x_j \in \Omega_h^{n+1}} \alpha_j^{n+1} \right), \alpha_{\text{thr}} \right\} \geq \exp(-\delta s_2) \min \left\{ \left(\min_{k: x_k \in \Omega_h^n} \alpha_k^n \right), \alpha_{\text{thr}} \right\} - \delta \exp(-\delta s_2) \mathcal{F}_{\min}. \quad (4.13)$$

Define

$$y_n = \exp(s_2 n \delta) \min \left\{ \left(\min_{k: x_k \in \Omega_h^n} \alpha_k^n \right), \alpha_{\text{thr}} \right\}.$$

The estimate (4.13) shows that

$$y_{n+1} \geq y_n - \delta \exp(s_2 n \delta) \mathcal{F}_{\min}.$$

Write this relation for a generic $k \leq n$, and sum over $k = 0, \dots, n$ to obtain

$$y_{n+1} \geq y_0 - \sum_{n=0}^n \delta \exp(s_2 n \delta) \mathcal{F}_{\min}. \quad (4.14)$$

The fact that the sum in (4.14) is the lower Riemann sum for the function $\exp(s_2 \tau)$ from $\tau = 0$ to $\tau = (n+1)\delta$ yields

$$y_{n+1} \geq y_0 - \left(\frac{\exp(s_2(n+1)\delta) - 1}{s_2} \right) \mathcal{F}_{\min}.$$

Since $y_0 = \alpha_{\text{thr}}$, a selection of time $t_{n+1} = (n+1)\delta$ such that

$$t_{n+1} \leq T_m := \frac{1}{s_2} \ln \left(\frac{\mathcal{F}_{\min} + s_2 \alpha_{\text{thr}}}{\mathcal{F}_{\min} + a_* s_2} \right) \quad (4.15)$$

yields $y_{n+1} \geq a_* \exp(s_2 t_{n+1})$, and this leads to $\min\{\alpha_j^{n+1} : x_j \in \Omega_h^{n+1}\} \geq a_*$. To obtain an upper bound, note that (4.9) yields

$$\alpha_j^{n+1} \leq \max_{0 \leq k \leq J-1} \alpha_k^n + \delta(1 - \alpha_{\text{thr}}) + \frac{\delta}{\mu} \|(\mu \alpha_{h,\delta}(t_n, \cdot) \partial_x u_h^n)^-\|_{L^\infty(0, \ell_m)} \quad (4.16)$$

for every $0 \leq j \leq J-1$. Define the parameter

$$\mathcal{F}_{\max} = 1 - \alpha_{\text{thr}} + \frac{\ell_m \sqrt{k} |a^* - \alpha^{\text{R}}|}{a_* \mu^{3/2} |1 - a^*|^{5/2}}. \quad (4.17)$$

Then, (4.16) and (4.5b) imply

$$\max_{0 \leq j \leq J-1} \alpha_j^{n+1} \leq \max_{0 \leq j \leq J-1} \alpha_j^n + \delta \mathcal{F}_{\max}.$$

Write this relation for a generic $k \leq n$ and sum over $k = 0, \dots, n$ to obtain

$$\max_{0 \leq j \leq J-1} \alpha_j^{n+1} \leq \max_{0 \leq j \leq J-1} \alpha_j^0 + (n+1)\delta \mathcal{F}_{\max} \leq m_{02} + t_{n+1} \mathcal{F}_{\max}.$$

Selection of the time t_{n+1} such that

$$t_{n+1} \leq \frac{a^* - m_{02}}{\mathcal{F}_{\max}} := T_M \quad (4.18)$$

implies $\max_{0 \leq j \leq J-1} \alpha_j^{n+1} \leq a^*$. Finally to ensure that the extended domain $(0, \ell_m)$ contains the time-dependent domains $(0, \ell(t))$ for every $t \in [0, T_*]$ we impose a restriction on T_* . Since the domain size increases at most by h at each time step, and there are T_*/δ such time steps, we set $T_* < T_\ell := \rho \mathcal{C}_{\text{CFL}}(\ell_m - \ell_0) \leq \frac{\delta}{h}(\ell_m - \ell_0)$. Choose $T^* = \min(T_m, T_M, T_\ell)$ to conclude the proof. \square

Remark 4.11. The norm $\|\bullet\|_{0, \Omega_h^n}$ in the space \mathcal{S}_h^n is equivalent to the norm $\|\Pi_h \bullet\|_{0, \Omega_h^n}$. In fact, we have for all $w \in \mathcal{S}_h^n$, $(1/\sqrt{3})\|\Pi_h w\|_{0, \Omega_h^n} \leq \|w\|_{0, \Omega_h^n} \leq \|\Pi_h w\|_{0, \Omega_h^n}$. This is an easy consequence of estimating $\|w\|_{0, \Omega_h^n}$ by Simpson's quadrature rule, which is exact for second degree polynomials.

Lemma 4.12 (Step (IS.4)). The equation (3.8) has a unique solution \tilde{c}_h^{n+1} , and it holds $0 \leq c_h^{n+1} \leq 1$ for δ sufficiently small.

Proof. Recall that $x_{J_{n+1}} = \ell_h^{n+1}$, and for $r = n, n+1$, define the vector

$$\mathbf{c}_h^r := [c_h^r(x_0), c_h^r(x_1), \dots, c_h^r(x_{J_{n+1}-1})].$$

The vector \mathbf{c}_h^{n+1} contains the discrete unknowns at t_{n+1} . Note that we do not need to compute the nodal value $c_h^{n+1}(x_{J_{n+1}})$ at the discrete level since Dirichlet boundary condition holds at $x_{J_{n+1}}$. The matrix equation corresponding to (3.8) is

$$(M + \delta \lambda D + Q \delta S) \mathbf{c}_h^{n+1} = M \mathbf{c}_h^n - \delta \mathbf{b}_h,$$

where \mathbf{b}_h is the $J_{n+1} \times 1$ vector with entries $\mathbf{b}_{h,i} = 0$ for $0 \leq i \leq J_{n+1} - 2$ and $\mathbf{b}_{h, J_{n+1}-1} = -\lambda/h$. Here, M is the $J_{n+1} \times J_{n+1}$ positive, diagonal, lumped mass matrix. The matrix D is the stiffness matrix with all off-diagonal entries negative. The entries of the positive, diagonal, lumped mass matrix S are as follows:

$$S_{ii} = \sum_{\mathcal{X}_j \subset \text{supp}(\varphi_{i,h})} \frac{h \alpha_j^n}{2} \left\langle \frac{(\Pi_h \varphi_{i,h})^2}{1 + \widehat{Q}_1 |\Pi_h c_h^n|} \right\rangle_{\mathcal{X}_j}, \quad 0 \leq i \leq J_{n+1} - 1,$$

where $\{\varphi_{i,h}\}_{\{0 \leq i \leq J_{n+1}-1\}}$ is the canonical nodal basis of $\mathcal{S}_{h,0}^{n+1}$. The symbol $\langle f \rangle_{\mathcal{X}_j}$ denotes the average of f over the cell \mathcal{X}_j . An application of Lemma III(c) shows that the discrete operator $\epsilon_{h,\delta} := (\mathbb{I}_{J_{n+1}} + \delta M^{-1}(\lambda D + QS))^{-1}$ is positive. A use of the facts $\alpha_{h,\delta}(t_{n+1}, \cdot) >$

0, $\mathbf{c}_h^n \geq 0$, and $\mathbf{b}_h \leq 0$ yield $\mathbf{c}_h^{n+1} \geq 0$. Next, we obtain the upper bound for \mathbf{c}_h^{n+1} . For $r = n, n+1$, define

$$\widehat{\mathbf{c}}_h^r := [c_h^r(x_0) - 1, c_h^r(x_1) - 1, \dots, c_h^r(x_{J_{n+1}-1}) - 1].$$

It is easy to observe that $(M + \delta\lambda D + Q\delta S)\widehat{\mathbf{c}}_h^{n+1} = M\widehat{\mathbf{c}}_h^n - \delta\widehat{\mathbf{b}}_h$, where $\widehat{\mathbf{b}}_h$ is the vector of nonnegative entries

$$\widehat{\mathbf{b}}_{h,i} = \sum_{X_j \subset \text{supp}(\varphi_{i,h})} \frac{Q\alpha_j^n h}{2} \left\langle \frac{\Pi_h \varphi_{i,h}}{1 + \widehat{Q}|\Pi_h^n c_h^n|} \right\rangle_{\mathcal{X}_j}, \quad 0 \leq j \leq J_{n+1} - 1.$$

Then, the same reasoning is used to obtain the positivity and Lemma III(c) imply $\widehat{\mathbf{c}}_h^{n+1} \geq 0$ and $\mathbf{c}_h^{n+1} - 1 \leq 0$. \square

4.3.2 Compactness results

The next goal is to establish necessary compactness properties for the iterates, which enables us to extract a convergent subsequence of discrete solutions, whose limit is a threshold solution. We list the main steps involved in this section. We establish

- (CR.1) a uniform $L^2(0, T_*; H^1(0, \ell_m))$ estimate for the family $\{c_{h,\delta}\}_{h,\delta}$.
- (CR.2) a uniform spatial BV estimate for the family $\{\alpha_{h,\delta}\}_{h,\delta}$.
- (CR.3) a uniform temporal BV estimate for the family $\{\alpha_{h,\delta}\}_{h,\delta}$.
- (CR.4) a uniform $L^2(0, T_*; H^1(0, \ell_m))$ estimate for the family $\{\widehat{u}_{h,\delta}\}_{h,\delta}$.
- (CR.5) a uniform BV estimate for the family $\{\ell_{h,\delta}\}_{h,\delta}$.
- (CR.6) that the family $\{\Pi_{h,\delta} c_{h,\delta}\}_{h,\delta}$ is relatively compact in $L^2(\mathcal{D}_{T_*})$.
- (CR.7) Theorem 4.2 with the help of (CR.1)–(CR.6)

In this sequel, \mathcal{C}_1 denotes a generic constant that depends $\alpha_0, c_0, a_*, a^*, \ell_m, T_*$, and the model parameters. Let us start with a preliminary lemma, the proof of which is an easy consequence of local Taylor expansions.

Lemma 4.13. [98, Section 8.4] *For any $w \in H^1(0, \ell_m)$, the following estimates hold:*

$$\|w - \Pi_h w_h\|_{0,(0,\ell_m)} \leq \frac{h}{2} \|\partial_x w\|_{0,(0,\ell_m)} \quad \text{and} \quad (4.19)$$

$$\|\Pi_h w_h\|_{0,(0,\ell_m)} \leq \frac{h}{2} \|\partial_x w\|_{0,(0,\ell_m)} + \|w\|_{0,(0,\ell_m)}. \quad (4.20)$$

We now prove an $L^2(0, T_*; H^1(0, \ell_m))$ stability estimate for $c_{h,\delta}$.

Proposition 4.14 (Step (CR.1)). *It holds $\|c_{h,\delta}\|_{L^2(0,T_*;H^1(0,\ell_m))} \leq \mathcal{C}_1$.*

Proof. Define the continuous function \widehat{c}_h^n on $(0, \ell_m)$ by $\widehat{c}_h^n := \widetilde{c}_h^n - 1$ in Ω_h^n , and $\widehat{c}_h^n := 0$ on $(0, \ell_m) \setminus \Omega_h^n$. An application of Cauchy–Schwarz inequality and (1.1b) yields

$$2(\Pi_h \widehat{c}_h^{n-1}, \Pi_h \widehat{c}_h^n)_{\Omega_h^n} \leq \|\Pi_h \widehat{c}_h^{n-1}\|_{0, \Omega_h^n}^2 + \|\Pi_h \widehat{c}_h^n\|_{0, \Omega_h^n}^2. \quad (4.21)$$

If $\ell_h^n \leq \ell_h^{n-1}$, then $\|\Pi_h \widehat{c}_h^{n-1}\|_{0, \Omega_h^n}^2 \leq \|\Pi_h \widehat{c}_h^{n-1}\|_{0, \Omega_h^{n-1}}^2$ since $\Omega_h^n \subseteq \Omega_h^{n-1}$. If $\ell_h^n = \ell_h^{n-1} + h$, then $\Pi_h \widehat{c}_h^{n-1} = 0$ on $\Omega_h^n \setminus \Omega_h^{n-1}$, and $\|\Pi_h \widehat{c}_h^{n-1}\|_{0, \Omega_h^n}^2 = \|\Pi_h \widehat{c}_h^{n-1}\|_{0, \Omega_h^{n-1}}^2$. Hence by (4.21) in any case

$$2(\Pi_h \widehat{c}_h^{n-1}, \Pi_h \widehat{c}_h^n)_{\Omega_h^n} \leq \|\Pi_h \widehat{c}_h^{n-1}\|_{0, \Omega_h^{n-1}}^2 + \|\Pi_h \widehat{c}_h^n\|_{0, \Omega_h^n}^2. \quad (4.22)$$

Choose $v_h^n = \widehat{c}_h^n \in \mathcal{S}_{h,0}^n$ as the test function in (3.8) with a Dirichlet lift of -1 , and use (4.22) and the observation that, since $\widehat{c}_h^n \leq 0$ and $\alpha_h^n \geq 0$, $-\frac{Q\alpha_h^n \Pi_h \widehat{c}_h^n}{1 + \widehat{Q}_1 |\Pi_h \widehat{c}_h^{n-1}|} \leq -Q\alpha_h^n \Pi_h \widehat{c}_h^n$, to obtain

$$\frac{1}{2} \|\Pi_h \widehat{c}_h^n\|_{0, \Omega_h^n}^2 - \frac{1}{2} \|\Pi_h \widehat{c}_h^{n-1}\|_{0, \Omega_h^{n-1}}^2 + \delta \lambda \|\partial_x \widehat{c}_h^n\|_{0, \Omega_h^n}^2 \leq -Q\delta (\alpha_h^n, \Pi_h \widehat{c}_h^n)_{\Omega_h^n}.$$

A use of Young’s and Poincaré’s inequalities together with (4.20) and a summation on the index n yield

$$\frac{1}{2} \|\Pi_h \widehat{c}_h^n\|_{0, \Omega_h^n}^2 + \frac{\lambda \delta}{2} \sum_{r=0}^n \|\partial_x \widehat{c}_h^r\|_{0, \Omega_h^r}^2 \leq \mathcal{C}_1. \quad (4.23)$$

Since $\partial_x \widehat{c}_h^r = \partial_x c_h^r$ on Ω_h^r and $\partial_x c_h^r = 0$ outside this set, (4.23) yields a bound on $\partial_x c_{h,\delta}$ in $L^2(\mathcal{D}_{T_*})$. We obtain the desired conclusion from the fact $c_{h,\delta}(t, \ell_m) = 1$ for all $t \in (0, T_*)$ and a Poincaré inequality. \square

Proposition 4.14 is crucial in obtaining a bounded variation estimate for the piecewise constant function $\alpha_{h,\delta}$. The idea is then to use Helly’s selection theorem (see Theorem I) to extract an almost everywhere convergent subsequence of functions out of the family of functions $\{\alpha_{h,\delta}\}_{h,\delta}$. Spatial and temporal BV estimates for $\alpha_{h,\delta}$ are derived separately in Propositions 4.15 and 4.16 for this purpose.

Proposition 4.15 (Step (CR.2)). *For $t \in (0, T_*)$ it holds*

$$\|\alpha_{h,\delta}(t, \cdot)\|_{BV(0, \ell_m)} \leq \mathcal{C}_1. \quad (4.24)$$

Proof. Let $j \in \{1, \dots, J-1\}$ and subtract (4.9) for α_{j-1}^{n+1} from (4.9) for α_j^{n+1} . This yields $T_0 = T_1 + \delta T_2 - \delta T_3$, where

$$\begin{aligned} T_0 &= (\alpha_j^{n+1} - \alpha_{j-1}^{n+1}) + \delta((\alpha_j^{n+1} - \alpha_{\text{thr}})^+ d_j^n - (\alpha_{j-1}^{n+1} - \alpha_{\text{thr}})^+ d_{j-1}^n), \\ T_1 &= \mathcal{L}(\alpha_{j-1}^n, \alpha_j^n, \alpha_{j+1}^n) - \mathcal{L}(\alpha_{j-2}^n, \alpha_{j-1}^n, \alpha_j^n), \\ T_2 &= (\alpha_j^n - \alpha_{\text{thr}})^+ (1 - \alpha_j^n) b_j^n - (\alpha_{j-1}^n - \alpha_{\text{thr}})^+ (1 - \alpha_{j-1}^n) b_{j-1}^n, \text{ and} \end{aligned}$$

$$T_3 = \alpha_j^n \partial_x u_h^n|_{\mathcal{X}_j} - \alpha_{j-1}^n \partial_x u_h^n|_{\mathcal{X}_{j-1}}.$$

The terms in T_1 can be grouped in the following way:

$$\begin{aligned} T_1 &= (\alpha_j^n - \alpha_{j-1}^n) \left(1 - \frac{\delta}{h} u_j^{n-} - \frac{\delta}{h} u_j^{n+} \right) + \frac{\delta}{h} u_{j+1}^{n-} (\alpha_{j+1}^n - \alpha_j^n) \\ &\quad + \frac{\delta}{h} u_{j-1}^{n+} (\alpha_{j-1}^n - \alpha_{j-2}^n). \end{aligned} \quad (4.25a)$$

Split the terms in T_0 and T_2 using (1.1a) in Section 1.4.2 to obtain

$$\begin{aligned} T_0 &= (\alpha_j^{n+1} - \alpha_{j-1}^{n+1}) + \delta((\alpha_j^{n+1} - \alpha_{\text{thr}})^+ - (\alpha_{j-1}^{n+1} - \alpha_{\text{thr}})^+) \frac{d_j^n + d_{j-1}^n}{2} \\ &\quad + \delta((\alpha_j^{n+1} - \alpha_{\text{thr}})^+ + (\alpha_{j-1}^{n+1} - \alpha_{\text{thr}})^+) \frac{d_j^n - d_{j-1}^n}{2}, \text{ and} \end{aligned} \quad (4.25b)$$

$$\begin{aligned} T_2 &= ((\alpha_j^n - \alpha_{\text{thr}})^+ (1 - \alpha_j^n) + (\alpha_{j-1}^n - \alpha_{\text{thr}})^+ (1 - \alpha_{j-1}^n)) \frac{b_j^n - b_{j-1}^n}{2} \\ &\quad + ((\alpha_j^n - \alpha_{\text{thr}})^+ - (\alpha_{j-1}^n - \alpha_{\text{thr}})^+) (2 - \alpha_j^n - \alpha_{j-1}^n) \frac{b_j^n + b_{j-1}^n}{4} \\ &\quad + ((\alpha_j^n - \alpha_{\text{thr}})^+ + (\alpha_{j-1}^n - \alpha_{\text{thr}})^+) (\alpha_{j-1}^n - \alpha_j^n) \frac{b_j^n + b_{j-1}^n}{4}. \end{aligned} \quad (4.25c)$$

Substitute (4.25a), (4.25b), and (4.25c) in $T_0 = T_1 + \delta T_2 - \delta T_3$, use the facts that $0 \leq b_j^n \leq 1$, $0 \leq d_j^n \leq s_2$, $0 \leq \alpha_j^n \leq 1$, the CFL condition (4.2) together with the bound (4.4) on the velocity, the Lipschitz continuity of $x \mapsto (x - \alpha_{\text{thr}})^+$, and group the terms appropriately to obtain

$$\begin{aligned} (1 - \delta s_2) |\alpha_j^{n+1} - \alpha_{j-1}^{n+1}| &\leq |\alpha_j^n - \alpha_{j-1}^n| \left(1 - \frac{\delta}{h} u_j^{n-} - \frac{\delta}{h} u_j^{n+} \right) + \frac{\delta}{h} u_{j+1}^{n-} |\alpha_{j+1}^n - \alpha_j^n| \\ &\quad + \frac{\delta}{h} u_{j-1}^{n+} |\alpha_{j-2}^n - \alpha_{j-1}^n| + \delta |d_j^n - d_{j-1}^n| + \delta |b_j^n - b_{j-1}^n| \\ &\quad + 2\delta |\alpha_j^n - \alpha_{j-1}^n| + \delta |\alpha_j^n \partial_x u_h^n|_{\mathcal{X}_j} - \alpha_{j-1}^n \partial_x u_h^n|_{\mathcal{X}_{j-1}}|. \end{aligned} \quad (4.26)$$

Sum the expression (4.26) from $j = 1$ to $j = J$, and utilize $u_0^n = 0$, $u_J^n = 0$, $u_{J+1}^n = 0$ and $0 \leq (\delta/h) |\alpha_1^n - \alpha_0^n| u_0^{n-1}$ to obtain

$$\begin{aligned} (1 - \delta s_2) \sum_{j=1}^J |\alpha_j^{n+1} - \alpha_{j-1}^{n+1}| &\leq (1 + 2\delta) \sum_{j=1}^J |\alpha_j^n - \alpha_{j-1}^n| + \delta \sum_{j=1}^J |d_j^n - d_{j-1}^n| \\ &\quad + \delta \sum_{j=1}^J |b_j^n - b_{j-1}^n| + \delta \sum_{j=1}^J |\alpha_j^n \partial_x u_h^n|_{\mathcal{X}_j} - \alpha_{j-1}^n \partial_x u_h^n|_{\mathcal{X}_{j-1}}|. \end{aligned} \quad (4.27)$$

Further note that

$$\| \mu \alpha_{h,\delta}(t_n, \cdot) \partial_x u_{h,\delta}(t_n, \cdot) \|_{BV(0,\ell_m)} \leq \| \mu \alpha_{h,\delta}(t_n, \cdot) \partial_x u_{h,\delta}(t_n, \cdot) - \alpha_{h,\delta}(t_n, \cdot) \mathcal{H}(\alpha_{h,\delta}(t_n, \cdot)) \|_{BV(0,\ell_m)}$$

$$+ \|\alpha_{h,\delta}(t_n, \cdot) \mathcal{H}(\alpha_{h,\delta}(t_n, \cdot))\|_{BV(0, \ell_m)}.$$

A use of (4.5a) and the fact that \mathcal{H} is continuous and piecewise differentiable yield

$$\|\mu \alpha_{h,\delta}(t_n, \cdot) \partial_x u_{h,\delta}(t_n, \cdot)\|_{BV(0, \ell_m)} \leq \mathcal{C}_1 (1 + \|\alpha_{h,\delta}(t_n, \cdot)\|_{BV(0, \ell_m)}). \quad (4.28)$$

The CFL condition (4.2) yields $1 - \delta s_2 \geq \rho$. Moreover, there exists an $\eta > 0$ such that, for all admissible δ , $(1 + 2\delta)/(1 - s_2\delta) \leq 1 + \eta\delta$. Hence (4.27) and (4.28) imply

$$\begin{aligned} \|\alpha_{h,\delta}(t_{n+1}, \cdot)\|_{BV(0, \ell_m)} &\leq (1 + \eta\delta) \|\alpha_{h,\delta}(t_n, \cdot)\|_{BV(0, \ell_m)} + \delta \mathcal{C}_1 (\rho\mu)^{-1} \\ &\quad + \rho^{-1} \delta (\|d_{h,\delta}(t_n, \cdot)\|_{BV(0, \ell_m)} + \|b_{h,\delta}(t_n, \cdot)\|_{BV(0, \ell_m)}). \end{aligned}$$

Induction on the right hand side of the above expression yields

$$\begin{aligned} \|\alpha_{h,\delta}(t_{n+1}, \cdot)\|_{BV(0, \ell_m)} &\leq \exp(T_*\eta) (\|\alpha_{h,\delta}(0, \cdot)\|_{BV(0, \ell_m)} + \mathcal{C}_1 (\rho\mu)^{-1} T_*) \\ &\quad + \rho^{-1} \exp(T_*\eta) \int_0^{T_*} (\|b_{h,\delta}(t, \cdot)\|_{BV(0, \ell_m)} + \|d_{h,\delta}(t, \cdot)\|_{BV(0, \ell_m)}) dt, \end{aligned}$$

and since $d_{h,\delta}$ and $b_{h,\delta}$ are smooth functions of $c_{h,\delta}$ (see (DS.d) in Definition 3.2), the estimates for $c_{h,\delta}$ from Proposition 4.14 conclude the proof. \square

Proposition 4.16 (Step (CR.3)). *The function $\alpha_{h,\delta}$ satisfies the upper bound*

$$\int_0^{\ell_m} \|\alpha_{h,\delta}(\cdot, x)\|_{BV(0, T_*)} dx \leq \mathcal{C}_1.$$

Proof. Rearrange the terms (4.7) and appropriately group using (1.1a) to obtain

$$\begin{aligned} \alpha_j^{n+1} - \alpha_j^n &= \delta(\alpha_j^n - \alpha_{\text{thr}})^+ (1 - \alpha_j^n) b_j^n - \delta(\alpha_j^{n+1} - \alpha_{\text{thr}})^+ d_j^n + \frac{\delta}{h} u_{j+1}^{n-} (\alpha_{j+1}^n - \alpha_j^n) \\ &\quad + \frac{\delta}{h} u_j^{n+} (\alpha_{j-1}^n - \alpha_j^n) - \frac{\delta}{h} \alpha_j^n (u_{j+1}^n - u_j^n) \\ &= \delta((\alpha_j^n - \alpha_{\text{thr}})^+ + (\alpha_j^{n+1} - \alpha_{\text{thr}})^+) \frac{(1 - \alpha_j^n) b_j^n - d_j^n}{2} \\ &\quad + \delta((\alpha_j^n - \alpha_{\text{thr}})^+ - (\alpha_j^{n+1} - \alpha_{\text{thr}})^+) \frac{(1 - \alpha_j^n) b_j^n + d_j^n}{2} \\ &\quad + \frac{\delta}{h} u_{j+1}^{n-} (\alpha_{j+1}^n - \alpha_j^n) + \frac{\delta}{h} u_j^{n+} (\alpha_{j-1}^n - \alpha_j^n) - \frac{\delta}{h} \alpha_j^n (u_{j+1}^n - u_j^n). \end{aligned}$$

Use the facts that $0 \leq b_j^n \leq 1$, $0 \leq d_j^n \leq s_2$, $0 \leq \alpha_j^n \leq 1$, $x \mapsto (x - \alpha_{\text{thr}})^+$ is a Lipschitz function with Lipschitz constant one, and group the terms appropriately to obtain, for $j = 1, \dots, J-1$

$$|\alpha_j^{n+1} - \alpha_j^n| \leq \delta \left(1 + s_2 + |\alpha_j^n - \alpha_j^{n+1}| \frac{1 + s_2}{2} \right) + \frac{\delta}{h} \|u_{h,\delta}\|_{L^\infty(\mathcal{D}_{T_*})} |\alpha_{j+1}^n - \alpha_j^n|$$

$$+ \frac{\delta}{h} \| |u_{h,\delta}| \|_{L^\infty(\mathcal{D}_{T_*})} |\alpha_{j-1}^n - \alpha_j^n| + \delta \| |\alpha_{h,\delta} \partial_x u_{h,\delta}| \|_{L^\infty(\mathcal{D}_{T_*})}. \quad (4.29)$$

Since $u_0^n = 0$, for $j = 0$ an analogous estimate holds with $\alpha_{-1}^n := \alpha_0^n$. Multiply (4.29) by h and sum over $j = 0, \dots, J-1$ and $n = 0, \dots, N_* - 1$ with $N_* = T_*/\delta$ to obtain

$$\begin{aligned} \left(1 - \delta \frac{(1+s_2)}{2}\right) \sum_{j=0}^{J-1} h \sum_{n=0}^{N_*-1} |\alpha_j^{n+1} - \alpha_j^n| &\leq T_* \ell_m (1 + s_2 + \| |\alpha_{h,\delta} \partial_x u_{h,\delta}| \|_{L^\infty(\mathcal{D}_{T_*})}) \\ &\quad + 2 \| |u_{h,\delta}| \|_{L^\infty(\mathcal{D}_{T_*})} \sum_{n=0}^{N_*-1} \delta \sum_{j=0}^{J-1} |\alpha_{j+1}^n - \alpha_j^n|. \end{aligned}$$

A use of the estimates (4.4), (4.5c), (4.24), and (4.2) concludes the proof. \square

The next result is a direct consequence of Lemma 4.7, Proposition 4.10 and (4.4).

Proposition 4.17 (Step (CR.4)). *The family of functions $\{\widehat{u}_{h,\delta}\}_{h,\delta}$ is uniformly bounded in $L^2(0, T_*; H^1(0, \ell_m))$.*

Next, we need to obtain an estimate on the total variation of $\ell_{h,\delta}$. From Proposition 4.10 it is evident that at each time step, $\ell_{h,\delta}$ can either increase by h or decrease by any value. We show that $\ell_{h,\delta}$ can be expressed as sum of a decreasing function and a function bounded variation as discussed in the next proposition.

Proposition 4.18 (Step (CR.5)). *The piecewise constant function $\ell_{h,\delta} : [0, T_*] \rightarrow \mathbb{R}$ is of the form $\ell_{h,\delta} = \ell_{h,\delta,BV} + \ell_{h,\delta,D}$, where $\ell_{h,\delta,BV}$ is a function with uniformly bounded variation in $(0, T_*)$ and $\ell_{h,\delta,D}$ is a monotonically decreasing function. Consequently,*

$$\sum_{n=1}^{N_*} |\ell_h^n - \ell_h^{n-1}| \leq \mathcal{C}_1. \quad (4.30)$$

Proof. Define $\ell_{h,\delta,BV}(t) = (\rho \mathcal{C}_{\text{CFL}})^{-1} t$ and $\ell_{h,\delta,D}(t) = \ell_{h,\delta}(t) - (\rho \mathcal{C}_{\text{CFL}})^{-1} t$ where ρ and \mathcal{C}_{CFL} are defined in (4.2). Clearly, the function $\ell_{h,\delta,BV}$ has a uniformly bounded variation. For the function $\ell_{h,\delta,D}$ note that

$$\ell_{h,\delta,D}(t_{n+1}) - \ell_{h,\delta,D}(t_n) = \ell_h^{n+1} - \ell_h^n - (\rho \mathcal{C}_{\text{CFL}})^{-1} \delta.$$

If $\ell_h^{n+1} - \ell_h^n = h$, then by (4.2), $\ell_h^{n+1} - \ell_h^n \leq (\rho \mathcal{C}_{\text{CFL}})^{-1} \delta$ and thus $\ell_{h,\delta,D}(t_{n+1}) \leq \ell_{h,\delta,D}(t_n)$. If $\ell_h^{n+1} \leq \ell_h^n$, then $\ell_{h,\delta,D}(t_{n+1}) \leq \ell_{h,\delta,D}(t_n)$, trivially. Since $\ell_{h,\delta,D}$ is decreasing and uniformly bounded, the bounded variation estimate (4.30) follows. \square

The compactness results for the function $c_{h,\delta}$ are proved next. Note that Proposition 4.14 already guarantees that $c_{h,\delta} \in L^2(0, T_*; H^1(0, \ell_m))$, and the Hilbert space structure of this space allows us to extract a weakly convergent subsequence. However, (3.5) has non linear rational terms $b_{h,\delta}$ and $d_{h,\delta}$ that involve $\Pi_{h,\delta} c_{h,\delta}$. Hence, the weak convergence of

$\Pi_{h,\delta}c_{h,\delta}$ is not sufficient to prove that the limit of $\Pi_{h,\delta}c_{h,\delta}$ is a weak solution. Instead, strong $L^2(\mathcal{D}_{T_*})$ convergence is required. A standard method to achieve the strong $L^2(\mathcal{D}_{T_*})$ convergence for $\Pi_{h,\delta}c_{h,\delta}$ is to use a discrete Aubin–Simon theorem (see Theorem II in Section 1.4).

We state the definition of a compactly and continuously embedded sequence of Banach spaces next.

Definition 4.19 (Compactly–continuously embedded sequence). [98, Definition C.6]. *Let B be a Banach space. Let families of Banach spaces $\{X_h, \|\cdot\|_{X_h}\}_h$ and $\{Y_h, \|\cdot\|_{Y_h}\}_h$ be such that $X_h \subset Y_h \subset B$. We say that the family $\{(X_h, Y_h)\}_h$ is compactly–continuously embedded in B if the following conditions hold.*

- Any sequence $\{u_h\}_h$ such that $u_h \in X_h$ and $\{\|u_h\|_{X_h}\}_h$ uniformly bounded is relatively compact in B .
- Any sequence $\{u_h\}_h$ such that $u_h \in X_h$, $\{\|u_h\|_{X_h}\}_h$ uniformly bounded, $\{u_h\}_h$ converges in B , and $\|u_h\|_{Y_h} \rightarrow 0$, converges to zero in B .

Define $X_h := \Pi_h(H^1(0, \ell_m))$ with norm

$$\|u\|_{X_h} := \inf \left\{ \|w\|_{1,(0,\ell_m)} : w \in H^1(0, \ell_m), u = \Pi_h w \right\}. \quad (4.31a)$$

Set $Y_h := X_h$ with the discrete dual norm $\|\cdot\|_{Y_h}$ defined by: $\forall u \in Y_h$,

$$\|u\|_{Y_h} := \sup \left\{ \int_0^{\ell_m} u \Pi_h v \, dx : v \in H^1(0, \ell_m), \|v\|_{1,(0,\ell_m)} \leq 1 \right\}. \quad (4.31b)$$

Lemma 4.20. *The family of Banach spaces $\{(X_h, Y_h)\}$ with $X_h = \Pi_h(H^1(0, \ell_m)) = Y_h$ and $\|\cdot\|_{X_h}$ and $\|\cdot\|_{Y_h}$ as defined in (4.31a) and (4.31b), respectively, is compactly–continuously embedded in $B = L^2(0, \ell_m)$.*

Proof. We verify the conditions in Definition 4.19. Let $\{u_h\}_h \subset B$ be a sequence of functions such that $u_h \in X_h$ and $\{\|u_h\|_{X_h}\}_h$ is bounded. Consider the corresponding sequence $\{w_h\} \subset H^1(0, \ell_m)$ such that $u_h = \Pi_h w_h$ and $\|u_h\|_{X_h} = \|w_h\|_{1,(0,\ell_m)}$. The boundedness of $\{\|u_h\|_{X_h}\}_h$ shows that $\{\|w_h\|_{1,(0,\ell_m)}\}_h$ is also bounded. Since $H^1(0, \ell_m)$ is compactly embedded in $L^2(0, \ell_m)$, there exists a subsequence $\{w_h\}_h$ up to re-indexing such that $w_h \rightharpoonup w$ weakly in $H^1(0, \ell_m)$ and $w_h \rightarrow w$ strongly in $L^2(0, \ell_m)$. We claim that $u_h \rightarrow w$ strongly in $L^2(0, \ell_m)$. To prove this, use the triangle inequality and then apply (4.19) and (4.20) to obtain

$$\begin{aligned} \|u_h - w\|_{0,(0,\ell_m)} &\leq \|u_h - \Pi_h w\|_{0,(0,\ell_m)} + \|\Pi_h w - w\|_{0,(0,\ell_m)} \\ &\leq \|\Pi_h(w_h - w)\|_{0,(0,\ell_m)} + \|\Pi_h w - w\|_{0,(0,\ell_m)} \\ &\leq \|w_h - w\|_{0,(0,\ell_m)} + h \|\partial_x(w_h - w)\|_{0,(0,\ell_m)}. \end{aligned} \quad (4.32)$$

Since $w_h \rightarrow w$ in $L^2(0, \ell_m)$ while being bounded in $H^1(0, \ell_m)$, (4.32) shows that $\|u_h - w\|_{0,(0,\ell_m)} \rightarrow 0$ as $h \rightarrow 0$. This proves the first condition in Definition 4.19.

Let $\{u_h\} \subset B$ be such that $u_h \in X_h$, $\{\|u_h\|_{X_h}\}_h$ is bounded, $\|u_h\|_{Y_h} \rightarrow 0$ as $h \rightarrow 0$, and u_h converges in B . Let $w_h \in X_h$ be such that $\Pi_h w_h = u_h$ and $\|w_h\|_{1,(0,\ell_m)} = \|u_h\|_{X_h}$. Then, note that

$$\|u_h\|_{0,(0,\ell_m)}^2 = \int_0^{\ell_m} u_h \Pi_h w_h \, dx \leq \|u_h\|_{Y_h} \|w_h\|_{1,(0,\ell_m)} \leq \|u_h\|_{Y_h} \|u_h\|_{X_h}.$$

The assumed properties on $\{u_h\}_h$ then show that $u_h \rightarrow 0$ in $L^2(0, \ell_m)$, which concludes the proof. \square

To obtain the relative compactness of $\{\Pi_{h,\delta} c_{h,\delta}\}_{h,\delta}$ in $L^2(\mathcal{D}_{T_*})$, we start with an auxiliary function $\varphi_{h,\epsilon}^n : [0, \ell_m] \rightarrow [0, 1]$ defined by, for a fixed $\epsilon > 0$, (see Figure 4.3)

$$\varphi_{h,\epsilon}^n(x) = \begin{cases} 1 & 0 \leq x \leq \ell_h^n - \epsilon, \\ (\ell_h^n - x)/\epsilon & \ell_h^n - \epsilon < x \leq \ell_h^n, \\ 0 & \ell_h^n < x \leq \ell_m. \end{cases}$$

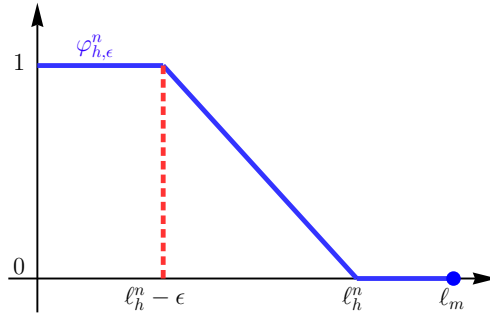


Figure 4.3: The auxiliary function $\varphi_{h,\epsilon}^n$.

For $\widehat{c}_{h,\delta} = c_{h,\delta} - 1$ the mass lumped function can be split into

$$\Pi_{h,\delta} \widehat{c}_{h,\delta} = \Pi_{h,\delta}(\widehat{c}_{h,\delta} \varphi_{h,\epsilon}) + \Pi_{h,\delta}(\widehat{c}_{h,\delta} (1 - \varphi_{h,\epsilon})),$$

where $\varphi_{h,\epsilon} = \varphi_{h,\epsilon}^n$ on $\mathcal{T}_n = (t_n, t_{n+1})$ for $0 \leq n \leq N_* - 1$. Consider the second term $\Pi_{h,\delta}(\widehat{c}_{h,\delta} (1 - \varphi_{h,\epsilon}))$, which is equal to $\Pi_h(\widehat{c}_h^n (1 - \varphi_{h,\epsilon}^n))$ on \mathcal{T}_n . A use of the facts $1 - \varphi_{h,\epsilon}^n = 0$ on $[0, \ell_h^n - \epsilon)$, $\Pi_h \widehat{c}_h^n = 0$ (see Figure 4.3) on $(\ell_h^n, \ell_m]$ and the property $\Pi_h(fg) = (\Pi_h f)(\Pi_h g)$ yield

$$\begin{aligned} \|\Pi_h(\widehat{c}_h^n (1 - \varphi_{h,\epsilon}^n))\|_{0,(0,\ell_m)}^2 &= \int_{\ell_h^n - \epsilon}^{\ell_h^n} |\Pi_h(\widehat{c}_h^n (1 - \varphi_{h,\epsilon}^n))|^2 \, dx \\ &\leq \epsilon \|\Pi_h(\widehat{c}_h^n (1 - \varphi_{h,\epsilon}^n))\|_{L^\infty(0,\ell_m)}^2. \end{aligned} \quad (4.33)$$

Multiply (4.33) by δ , sum over $n = 0, \dots, N_* - 1$, and use the bounds $\|\Pi_h(1 - \varphi_{h,\epsilon}^n)\|_{L^\infty(0,\ell_m)} \leq 1$ and $\|\Pi_h \widehat{c}_h^n\|_{L^\infty(0,\ell_m)} \leq 1$ to obtain

$$\|\Pi_{h,\delta}(\widehat{c}_{h,\delta} (1 - \varphi_{h,\epsilon}))\|_{L^2(\mathcal{D}_{T_*})} \leq \sqrt{T_*} \epsilon. \quad (4.34)$$

Proposition 4.23 below establishes that the family of functions $\{\Pi_{h,\delta}(\varphi_{h,\epsilon}\widehat{c}_{h,\delta})\}_{h,\delta}$ is relatively compact in $L^2(\mathcal{D}_{T_*})$. Then, Proposition 4.23 and (4.34) are used to prove Proposition 4.24.

Definition 4.21 (Discrete time derivative). *The discrete time derivative of a function f on \mathcal{D}_{T_*} is defined as follows: on \mathcal{T}_n ,*

$$D_{h,\delta}^n f := \frac{\Pi_h f(t_{n+1}, \cdot) - \Pi_h f(t_n, \cdot)}{\delta}. \quad (4.35)$$

Definition 4.22 (Piecewise linear interpolant operator). *The piecewise linear interpolant operator $\mathcal{I}_h : H^1(0, \ell_m) \rightarrow \mathcal{S}_h$ is defined by*

$$\mathcal{I}_h f(x) = f(x_j) \frac{x_{j+1} - x}{h} + f(x_{j+1}) \frac{x - x_j}{h} \quad \forall x \in \mathcal{X}_j, j = 0, \dots, J-1. \quad (4.36)$$

We are now in a position to prove the relative compactness of $\{\Pi_{h,\delta}(\varphi_{h,\epsilon}\widehat{c}_{h,\delta})\}_{h,\delta}$ in $L^2(\mathcal{D}_{T_*})$, which is required to prove Step (CR.5).

Proposition 4.23. *The family of functions $\{\Pi_{h,\delta}(\varphi_{h,\epsilon}\widehat{c}_{h,\delta})\}_{h,\delta}$ is relatively compact in $L^2(\mathcal{D}_{T_*})$.*

Proof. The desired result follows from the discrete Aubin–Simon theorem (see Theorem II), for which we need to verify the conditions (A.1)–(4.37b) with $B = L^2(0, \ell_m)$ and $Y_h = X_h = \Pi_h(H^1(0, \ell_m))$. The following conditions are verified for this:

$$\begin{aligned} &\{\Pi_{h,\delta}(\varphi_{h,\epsilon}\widehat{c}_{h,\delta})\}_{h,\delta} \text{ is bounded in } L^2(0, T_*; B), \\ &\{\|\Pi_{h,\delta}(\varphi_{h,\epsilon}\widehat{c}_{h,\delta})\|_{L^2(0, T_*; X_h)}\}_{h,\delta} \text{ is bounded, and} \end{aligned} \quad (4.37a)$$

$$\{\|D_{h,\delta}(\varphi_{h,\epsilon}\widehat{c}_{h,\delta})\|_{L^1(0, T_*; Y_h)}\}_{h,\delta} \text{ is bounded.} \quad (4.37b)$$

Proposition 4.14 and the bound $|\varphi_{h,\epsilon}| \leq 1$ yields (A.1). We have $|\varphi_{h,\epsilon}| \leq 1$ and $|\partial_x \varphi_{h,\epsilon}| \leq 1/\epsilon$, so for all $t \in (0, T_*)$,

$$|\varphi_{h,\epsilon}(t, \cdot)\widehat{c}_{h,\delta}(t, \cdot)|_{1,(0,\ell_m)} \leq |\widehat{c}_{h,\delta}(t, \cdot)|_{1,(0,\ell_m)} + \epsilon^{-1}|\widehat{c}_{h,\delta}(t, \cdot)|_{0,(0,\ell_m)}.$$

The facts $\|\widehat{c}_h^n\|_{L^\infty(0,\ell_m)} \leq 1$ and $\partial_x \varphi_{h,\epsilon}^n = 0$ on $[0, \ell_h^n - \epsilon - h) \cup (\ell_h^n + h, \ell_m)$ yield

$$\begin{aligned} |\varphi_{h,\epsilon}^n \widehat{c}_h^n|_{1,(0,\ell_m)}^2 &\leq 2 \int_0^{\ell_m} |\partial_x \widehat{c}_h^n|^2 dx + 2 \int_{\ell_h^n - \epsilon - h}^{\ell_h^n + h} \frac{1}{\epsilon^2} |\widehat{c}_h^n|^2 dx \\ &\leq 2|\widehat{c}_h^n|_{1,(0,\ell_m)}^2 + \frac{2(\epsilon + 2h)}{\epsilon^2}, \end{aligned}$$

and hence a use of (4.31a), Remark 4.11, and Proposition 4.14 leads to

$$\|\Pi_{h,\delta}(\varphi_{h,\epsilon}\widehat{c}_{h,\delta})\|_{L^2(0, T_*; X_h)} \leq \|\varphi_{h,\epsilon}\widehat{c}_{h,\delta}\|_{L^2(0, T_*; H^1(0, \ell_m))} \leq \mathcal{C}_1 + \frac{2T_*(\epsilon + 2h)}{\epsilon},$$

which verifies (4.37a). To verify (4.37b), we start with the estimation of $\|D_{h,\delta}^{n-1}(\varphi_{h,\epsilon}\widehat{c}_{h,\delta})\|_{Y_h}$. Let $v_h \in H^1(0, \ell_m)$ with $\|v_h\|_{1,(0,\ell_m)} \leq 1$. Note that (4.35) along with the identity (1.1b) yields

$$D_{h,\delta}^{n-1}(\varphi_{h,\epsilon}\widehat{c}_{h,\delta}) = (D_{h,\delta}^{n-1}\widehat{c}_{h,\delta})\Pi_h\varphi_{h,\epsilon}^n + (D_{h,\delta}^{n-1}\varphi_{h,\epsilon})\Pi_h\widehat{c}_h^{n-1},$$

and hence

$$\begin{aligned} \int_0^{\ell_m} D_{h,\delta}^{n-1}(\varphi_{h,\epsilon}\widehat{c}_{h,\delta})\Pi_h v_h dx &= \int_0^{\ell_m} (D_{h,\delta}^{n-1}\widehat{c}_{h,\delta})\Pi_h\varphi_{h,\epsilon}^n \Pi_h v_h dx \\ &\quad + \int_0^{\ell_m} (D_{h,\delta}^{n-1}\varphi_{h,\epsilon})\Pi_h\widehat{c}_h^{n-1} \Pi_h v_h dx =: T_1 + T_2. \end{aligned}$$

To estimate T_1 , observe that $\varphi_{h,\epsilon}^n$ is zero on $[\ell_h^n, \ell_m]$. Use the result $(\Pi_h f)(\Pi_h g) = \Pi_h(fg)$ to obtain

$$T_1 = \int_0^{\ell_h^n} (D_{h,\delta}\widehat{c}_h^{n-1})\Pi_h(\varphi_{h,\epsilon}^n v_h) dx.$$

Now observe that $\Pi_h(\varphi_{h,\epsilon}^n v_h) = \Pi_h(\mathcal{I}_h(\varphi_{h,\epsilon}^n v_h))$, where \mathcal{I}_h is defined by (4.36). Therefore, (3.8) with a Dirichlet lift of -1 tested against $\mathcal{I}_h(\varphi_{h,\epsilon}^n v_h) \in S_{h,0}^n$ yields

$$\begin{aligned} T_1 &= -\lambda \int_0^{\ell_h^n} \partial_x \widehat{c}_h^{n-1} \partial_x (\mathcal{I}_h(v_h \varphi_{h,\epsilon}^n)) dx - Q \int_0^{\ell_h^n} \frac{\alpha_{h,\delta}(t_n, \cdot) \Pi_h \widehat{c}_h^n}{1 + \widehat{Q}_1 |\Pi_h \widehat{c}_h^{n-1}|} \Pi_h(v_h \varphi_{h,\epsilon}^n) dx \\ &\quad - Q \int_0^{\ell_h^n} \frac{\alpha_{h,\delta}(t_n, \cdot)}{1 + \widehat{Q}_1 |\Pi_h \widehat{c}_h^{n-1}|} \Pi_h(v_h \varphi_{h,\epsilon}^n) dx. \end{aligned}$$

We have $\|\mathcal{I}_h w\|_{1,(0,\ell_h^n)} \leq \|w\|_{1,(0,\ell_h^n)}$ and $\|\varphi_{h,\epsilon}^n v_h\|_{1,(0,\ell_h^n)} \leq \mathcal{C}_2(\epsilon)$, where $\mathcal{C}_2(\epsilon)$ is a generic constant that depends on ϵ . Also, it holds $(1 + \widehat{Q}_1 |\Pi_h \widehat{c}_h^{n-1}|)^{-1} \leq 1$. Hence,

$$T_1 \leq \mathcal{C}_2(\epsilon) \|\partial_x \widehat{c}_h^{n-1}\|_{0,(0,\ell_h^n)} + \frac{3}{2} Q \|\Pi_h \widehat{c}_h^n\|_{0,(0,\ell_h^n)} + \frac{3}{2} Q \sqrt{\ell_m}. \quad (4.38)$$

The constant (3/2) in (4.38) results from the application of the Cauchy–Schwarz inequality to the integral $(\Pi_h \widehat{c}_h^n, \Pi_h(v_h \varphi_{h,\epsilon}^n))_{(0,\ell_m)}$, the facts $\Pi_h(v_h \varphi_{h,\epsilon}^n) = (\Pi_h v_h)(\Pi_h \varphi_{h,\epsilon}^n)$, $|\Pi_h \varphi_{h,\epsilon}^n| \leq 1$, and (4.20). Next, we estimate the term T_2 . The function $\varphi_{h,\epsilon}$ has the property $\varphi_{h,\epsilon}^{n-1}(x) = \varphi_{h,\epsilon}^n(x - \ell_h^{n-1} + \ell_h^n)$ by definition. Together with the fact that $\varphi_{h,\epsilon}^n$ is $1/\epsilon$ -Lipschitz, this implies $|D_{h,\delta}^{n-1}\varphi_{h,\epsilon}| \leq |\ell_h^n - \ell_h^{n-1}|/(\delta\epsilon)$. Consequently,

$$|T_2| \leq \frac{\ell_m}{\delta\epsilon} |\ell_h^n - \ell_h^{n-1}|. \quad (4.39)$$

Now let us conclude the argument. The estimates (4.38) and (4.39) yield

$$\begin{aligned} \int_0^{\ell_m} D_{h,\delta}(\varphi_{h,\epsilon}^n \widehat{c}_h^n)(t_{n-1}, \cdot) \Pi_h v_h dx &\leq \mathcal{C}_2(\epsilon) \|\partial_x \widehat{c}_h^{n-1}\|_{0,(0,\ell_h^n)} \\ &+ \frac{3}{2} Q \|\Pi_h \widehat{c}_h^n\|_{0,(0,\ell_h^n)} + \frac{3}{2} Q \sqrt{\ell_m} + \frac{\ell_m}{\delta \epsilon} |\ell_h^n - \ell_h^{n-1}|. \end{aligned} \quad (4.40)$$

Therefore, taking the supremum over the considered v_h , multiplying (4.40) by δ and summing over $n = 1, \dots, N_*$ yield

$$\begin{aligned} \int_0^{T_*} \|D_{h,\delta}(\varphi_{h,\epsilon} \widehat{c}_{h,\delta})\|_{Y_h} dt &\leq \mathcal{C}_2(\epsilon) \left[1 + \sum_{n=1}^{N_*} |\ell_h^n - \ell_h^{n-1}| \right. \\ &\quad \left. + \sum_{n=1}^{N_*} \delta (\|\Pi_h \widehat{c}_h^n\|_{0,(0,\ell_h^n)} + \|\partial_x \widehat{c}_h^n\|_{0,(0,\ell_h^n)}) \right]. \end{aligned}$$

Then, (4.37b) follows from an application of discrete Cauchy–Schwarz inequality, (4.30), and Proposition 4.14. \square

Proposition 4.24 (Step (CR.6)). *The family of functions $\{\Pi_{h,\delta} c_{h,\delta}\}_{h,\delta}$ is relatively compact in $L^2(\mathcal{D}_{T_*})$.*

Proof. Since (4.34) holds true, for any $\epsilon > 0$,

$$\{\Pi_{h,\delta} \widehat{c}_{h,\delta}\}_{h,\delta} \subset \{\Pi_{h,\delta}(\varphi_{h,\epsilon} \widehat{c}_{h,\delta})\}_{h,\delta} + B_{L^2(\mathcal{D}_{T_*})} \left(0; \sqrt{T_* \epsilon}\right), \quad (4.41)$$

where $B_{L^2(\mathcal{D}_{T_*})} \left(0; \sqrt{T_* \epsilon}\right)$ is the ball in $L^2(\mathcal{D}_{T_*})$ centered at the zero function with radius $\sqrt{T_* \epsilon}$. The relative compactness of the set $\{\Pi_{h,\delta}(\varphi_{h,\epsilon} \widehat{c}_{h,\delta})\}_{h,\delta}$ from Proposition 4.23 and (4.41) show that $\{\Pi_{h,\delta} \widehat{c}_{h,\delta}\}_{h,\delta}$ can be covered by finite number of $L^2(\mathcal{D}_{T_*})$ balls with radius η , for any $\eta > 0$, and hence is totally bounded in $L^2(\mathcal{D}_{T_*})$. This shows that $\{\Pi_{h,\delta} \widehat{c}_{h,\delta}\}$ is relatively compact. Then, the relation $c_{h,\delta} = \widehat{c}_{h,\delta} + 1$ yields the desired result. \square

We use Helly’s selection theorem for $\{\alpha_{h,\delta}\}$ and $\{\ell_{h,\delta}\}$, the weak compactness of $\{\widehat{u}_{h,\delta}\}$ in $L^2(0, T_*; H^1(0, \ell_m))$, and the relative compactness of $\{\Pi_{h,\delta} c_{h,\delta}\}$ in $L^2(\mathcal{D}_{T_*})$ to prove Theorem 4.2.

Proof of Theorem 4.2 (Step (CR.7). convergence of the iterates).

Proposition 4.10 establishes the existence of a time T_* such that $\alpha_{h,\delta} \in L^\infty(\mathcal{D}_{T_*})$. Propositions 4.15 and 4.16 show that $\alpha_{h,\delta} \in BV(\mathcal{D}_{T_*})$. Therefore, Helly’s selection theorem guarantees the existence of a subsequence $\{\alpha_{h,\delta}\}$ up to re-indexing and a function $\alpha \in BV(\mathcal{D}_{T_*}) \cap L^\infty(\mathcal{D}_{T_*})$ such that $\alpha_{h,\delta} \rightarrow \alpha$ in $L^1(\mathcal{D}_{T_*})$ and almost everywhere in \mathcal{D}_{T_*} .

Proposition 4.18 shows that the family $\{\ell_{h,\delta}\}_{h,\delta}$ is bounded in $BV(0, T_*)$. Therefore, Helly’s selection theorem guarantees the existence of a function $\ell \in BV(0, T_*) \cap L^\infty(0, T_*)$ such that $\ell_{h,\delta} \rightarrow \ell$ strongly in $L^1(0, T_*)$ and almost everywhere in $(0, T_*)$.

An application of Proposition 4.17 shows that there exist a subsequence $\{\widehat{u}_{h,\delta}\}_{h,\delta}$ and a function $\widehat{u} \in L^2(0, T_*; H^1(0, \ell_m))$ such that $\widehat{u}_{h,\delta} \rightharpoonup \widehat{u}$ weakly and $\partial_x \widehat{u}_{h,\delta} \rightharpoonup \partial_x \widehat{u}$ weakly in $L^2(\mathcal{D}_{T_*})$

Proposition 4.14 yields a subsequence $\{c_{h,\delta}\}_{h,\delta}$, up to re-indexing, and a function $c \in L^2(0, T_*; H^1(0, \ell_m))$ such that $c_{h,\delta} \rightharpoonup c$ and $\partial_x c_{h,\delta} \rightharpoonup \partial_x c$ weakly in $L^2(\mathcal{D}_{T_*})$. Proposition 4.24 establishes the strong convergence of $\Pi_{h,\delta} c_{h,\delta}$ in $L^2(\mathcal{D}_{T_*})$ and, by (4.19), $c_{h,\delta} - \Pi_{h,\delta} c_{h,\delta} \rightarrow 0$ in this space; hence, the strong limit of $\Pi_{h,\delta} c_{h,\delta}$ is c . \square

4.4 Proof of Theorem 4.3

In this section, the following assumption is used in Propositions 4.25, 4.26, 4.27, 4.31. Let $(\alpha, \hat{u}, c) : \mathcal{D}_{T_*} \rightarrow \mathbb{R}^3$ be a limit provided by Theorem 4.2 such that $\alpha_{h,\delta} \rightarrow \alpha$ almost everywhere in \mathcal{D}_{T_*} , $\hat{u}_{h,\delta} \rightharpoonup \hat{u}$ weakly in $L^2(\mathcal{D}_{T_*})$, $\partial_x \hat{u}_{h,\delta} \rightharpoonup \partial_x \hat{u}$ weakly in $L^2(\mathcal{D}_{T_*})$, $\Pi_{h,\delta} c_{h,\delta} \rightarrow c$ strongly in $L^2(\mathcal{D}_{T_*})$, and $\partial_x c_{h,\delta} \rightharpoonup \partial_x c$ weakly in $L^2(\mathcal{D}_{T_*})$. Also, let ℓ be a limit from Theorem 4.2 such that $\ell_{h,\delta} \rightarrow \ell$ almost everywhere in $(0, T_*)$.

The proof of Theorem 4.3 involves four main steps which are listed below.

- (CA.1) The domains $A_{h,\delta} := \{(t, x) : x < \ell_{h,\delta}(t), t \in (0, T_*)\}$ converge to $D_{T_*}^{\text{thr}} := \{(t, x) : x < \ell(t), t \in (0, T_*)\}$ as defined in Theorem 4.3.
- (CA.2) The limit function α satisfies (3.4a) with $T = T_*$.
- (CA.3) The restricted limit function $\hat{u}|_{D_{T_*}^{\text{thr}}}$ satisfies (3.4b) with $T = T_*$.
- (CA.4) The limit function $c|_{D_{T_*}^{\text{thr}}}$ satisfies (3.4c) with $T = T_*$.

Proposition 4.25 (Step (CA.1)). *The characteristic functions $\chi_{A_{h,\delta}}$ of $A_{h,\delta}$ converge (up to a subsequence) almost everywhere to the characteristic function $\chi_{D_{T_*}^{\text{thr}}}$ of $D_{T_*}^{\text{thr}}$.*

Proof. Theorem 4.3 starts on the assumption that there exists a converging subsequence $\{\ell_{h,\delta}\}$ (up to re-indexing) such that $\ell_{h,\delta} \rightarrow \ell$ almost everywhere, where $\ell \in BV(0, T_*)$. Define the set $E = \{t \in (0, T_*) : \ell_{h,\delta}(t) \not\rightarrow \ell(t)\}$. Let μ_d denotes the d -dimensional Lebesgue measure. The almost everywhere convergence of $\ell_{h,\delta}(t)$ to $\ell(t)$ implies that $\mu_1(E) = 0$. Tonelli's theorem applied to $\chi_{E \times (0, \ell_m)}$ yields $\mu_2(E \times (0, \ell_m)) = 0$. Define the graph of ℓ as $F_\ell = \{(t, x) \in \mathcal{D}_{T_*} : x = \ell(t), t \in (0, T_*)\}$ (see Figure 4.4). Again an application of the Tonelli's theorem shows $\mu_2(F_\ell) = 0$. Let $(t, x) \notin (E \times (0, \ell_m)) \cup F_\ell$. Then, either $\ell(t) > x$ or $\ell(t) < x$. When $\ell(t) < x$, $\chi_A(t, x) = 0$. Since $(t, x) \notin E \times (0, \ell_m)$, $\ell_{h,\delta}(t) \rightarrow \ell(t)$. Therefore, for h and δ small enough $\ell_{h,\delta}(t) < x$. That is, $\chi_{A_{h,\delta}}(t, x) = 0$, and hence $\chi_{A_{h,\delta}}(t, x) \rightarrow \chi_A(t, x)$. A similar argument yields the convergence for the case $\ell(t) > x$. Hence we have the almost everywhere convergence $\chi_{A_{h,\delta}} \rightarrow \chi_A$. \square

Proposition 4.26 (Step (CA.2)). *The function α satisfies (3.4a) with $T = T_*$ for every $\varphi \in \mathcal{C}_c^\infty([0, T_*] \times (0, \ell_m))$.*

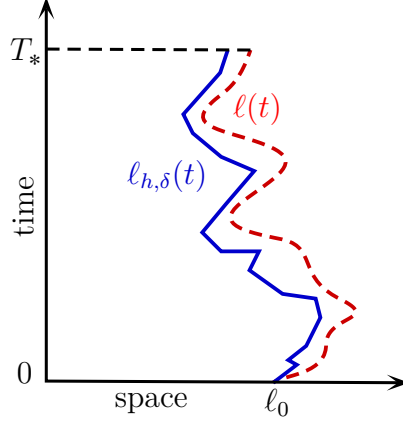


Figure 4.4: Continuous tumour radius ℓ and discrete tumour radius $\ell_{h,\delta}$.

Proof. Let $\varphi \in \mathcal{C}_c^\infty([0, T_*] \times (0, \ell_m))$. Multiply (3.5) between t_{n+1} and t_n by $\varphi_j^n := \langle \varphi(n\delta, \cdot) \rangle_{\mathcal{X}_j}$ and sum over the indices to obtain $T_1 + T_2 = T_3$, where

$$\begin{aligned} T_1 &:= h \sum_{n=0}^{N_*-1} \sum_{j=0}^{J-1} (\alpha_j^{n+1} - \alpha_j^n) \varphi_j^n, \\ T_2 &:= \delta \sum_{n=0}^{N_*-1} \sum_{j=0}^{J-1} (u_{j+1}^{n+} \alpha_j^n - u_{j+1}^{n-} \alpha_{j+1}^n - u_j^{n+} \alpha_{j-1}^n + u_j^{n-} \alpha_j^n) \varphi_j^n, \text{ and} \\ T_3 &:= h\delta \sum_{n=0}^{N_*-1} \sum_{j=0}^{J-1} ((\alpha_j^n - \alpha_{\text{thr}})^+ (1 - \alpha_i^n) b_j^n - (\alpha_j^{n+1} - \alpha_{\text{thr}})^+ d_j^n) \varphi_j^n, \end{aligned}$$

with $N_* = T_*/\delta$. The fact that $\varphi_j^{N_*} = 0$ for all j and a use of (1.4) yield

$$T_1 = -h \sum_{n=0}^{N_*-1} \sum_{j=0}^{J-1} (\varphi_j^{n+1} - \varphi_j^n) \alpha_j^{n+1} - \int_0^{\ell_0} \alpha_h^0(x) \varphi(0, x) dx, \quad (4.42)$$

where α_h^0 is a piecewise constant function defined by $\alpha_h^0|_{\mathcal{X}_j} = \langle \alpha_0 \rangle_{\mathcal{X}_j}$ for $j = 0, \dots, J-1$ (see Definition 3.2). A direct calculation shows the first term in the right hand side of (4.42) is equal to

$$- \sum_{n=0}^{N_*-1} \sum_{j=0}^{J-1} \alpha_j^{n+1} \int_{\mathcal{X}_j} \int_{n\delta}^{(n+1)\delta} \partial_t \varphi(t, x) dt = - \int_0^{\ell_m} \int_\delta^{T_*+\delta} \alpha_{h,\delta}(t, x) \partial_t \varphi(t - \delta, x) dt dx.$$

Since $\alpha_{h,\delta} \rightarrow \alpha$ almost everywhere by assumption (stated at the start of Section 4.4) as $h, \delta \rightarrow 0$, a use of Lebesgue's dominated convergence theorem shows that the first term in the right hand side of (4.42) converges to $-\int_0^{\ell_m} \int_0^{T_*} \alpha(t, x) \partial_t \varphi(t, x) dt dx$.

Since $\alpha_h^0 \rightarrow \alpha_0$ in $L^2(0, \ell_0)$, the second term in the right hand side of (4.42) converges to $-\int_0^{\ell_0} \alpha_0(x) \varphi(0, x) dx$. An application of (1.1a) on T_2 yields

$$\begin{aligned} T_2 &= \delta \sum_{n=0}^{N_*-1} \sum_{j=0}^{J-1} \varphi_j^n \left(|u_{j+1}^n| \frac{\alpha_j^n - \alpha_{j+1}^n}{2} - |u_j^n| \frac{\alpha_{j-1}^n - \alpha_j^n}{2} \right) \\ &\quad + \delta \sum_{n=0}^{N_*-1} \sum_{j=0}^{J-1} \varphi_j^n \left(u_{j+1}^n \frac{\alpha_j^n + \alpha_{j+1}^n}{2} - u_j^n \frac{\alpha_{j-1}^n + \alpha_j^n}{2} \right) =: T_{21} + T_{22}. \end{aligned}$$

A use of $u_0^n = 0$ and $u_J^n = 0$ leads to

$$\begin{aligned} |T_{21}| &= \left| \delta \sum_{n=0}^{N_*-1} \sum_{j=0}^{J-2} (\varphi_j^n - \varphi_{j+1}^n) |u_{j+1}^n| \frac{\alpha_j^n - \alpha_{j+1}^n}{2} \right| \\ &\leq \frac{h}{2} \|u_{h,\delta}\|_{L^\infty(\mathcal{D}_{T_*})} \|\partial_x \varphi(t, x)\|_{L^\infty(\mathcal{D}_{T_*})} \sum_{n=0}^{N_*-1} \delta \sum_{j=0}^{J-2} |\alpha_j^n - \alpha_{j+1}^n|, \end{aligned}$$

and hence (4.4) and (4.24) yield $|T_{21}| \rightarrow 0$ as $h \rightarrow 0$. Use (1.4) and $u_0^n = 0$ and $\varphi_J^n = 0$ to obtain

$$T_{22} = -\delta \sum_{n=0}^{N_*-1} \sum_{j=0}^{J-1} (\varphi_{j+1}^n - \varphi_j^n) u_{j+1}^n \frac{\alpha_j^n + \alpha_{j+1}^n}{2}. \quad (4.43)$$

Add and subtract $\delta \sum_{n=0}^{N_*-1} \sum_{j=0}^{J-1} (\varphi_{j+1}^n - \varphi_j^n) \frac{u_j^n}{2} \alpha_j^n$ to (4.43) to obtain

$$\begin{aligned} T_{22} &= \delta \sum_{n=0}^{N_*-1} \sum_{j=0}^{J-1} \frac{u_{j+1}^n \alpha_{j+1}^n}{2} (\varphi_{j+1}^n - \varphi_j^n - \varphi_{j+2}^n + \varphi_{j+1}^n) \\ &\quad - \delta \sum_{n=0}^{N_*-1} \sum_{i=0}^{J-1} (\varphi_{j+1}^n - \varphi_j^n) \frac{u_{j+1}^n + u_j^n}{2} \alpha_j^n. \end{aligned} \quad (4.44)$$

We show that the first term on the right hand side of (4.44) converges to zero. A use of the definition of φ_j^n , mean value theorem, and the CFL condition (4.2) yields

$$\begin{aligned} &\left| \delta \sum_{n=0}^{N_*-1} \sum_{j=0}^{J-1} \frac{u_{j+1}^n \alpha_{j+1}^n}{2} (\varphi_{j+1}^n - \varphi_j^n - \varphi_{j+2}^n + \varphi_{j+1}^n) \right| \\ &\leq \mathcal{C}_g \delta \|u_{h,\delta} \alpha_{h,\delta}\|_{L^\infty(\mathcal{D}_{T_*})} \|\partial_{xx} \varphi\|_{L^\infty(\mathcal{D}_{T_*})} \sum_{n=0}^{N_*-1} \delta \sum_{j=0}^J h \rightarrow 0 \text{ as } \delta \rightarrow 0, \end{aligned}$$

where \mathcal{C}_g is a constant independent of h and δ . Define $\partial_{h,\delta} \varphi : \mathcal{D}_{T_*} \rightarrow \mathbb{R}$ by $\partial_{h,\delta} \varphi := (\varphi_{j+1}^n - \varphi_j^n)/h$ on $\mathcal{T}_n \times \mathcal{X}_j$. Use the fact $u_{h,\delta} = \chi_{A_{h,\delta}} \hat{u}_{h,\delta}$ and the trapezoidal quadrature rule on the piecewise linear function $u_{h,\delta}$ to express the second term in the right hand side of (4.44) as

$$-\int_0^{T_*} \int_0^{\ell_m} u_{h,\delta} \alpha_{h,\delta} \partial_{h,\delta} \varphi dx dt = -\int_0^{T_*} \int_0^{\ell_m} \chi_{A_{h,\delta}} \hat{u}_{h,\delta} \alpha_{h,\delta} \partial_{h,\delta} \varphi dx dt$$

$$\rightarrow - \int_0^{T_*} \int_0^{\ell_m} u \alpha \partial_x \varphi \, dx \, dt,$$

where Lemmas III(a) and III(b) are applied in the last step. Write T_3 as

$$T_3 = h\delta \sum_{n=0}^{N_*-1} \sum_{j=0}^{J-1} (\alpha_j^n - \alpha_{\text{thr}})^+ (1 - \alpha_j^n) b_j^n \varphi_j^n - h\delta \sum_{n=0}^{N_*-1} \sum_{j=0}^{J-1} (\alpha_j^{n+1} - \alpha_{\text{thr}})^+ d_j^n \varphi_j^n. \quad (4.45)$$

Use definitions of b_j^n , d_j^n , and φ_j^n to rewrite the first term in the right hand side of (4.45) and use Lemmas III(a) and III(b) (see Section 1.4.3) to arrive at the following convergence

$$\begin{aligned} & \int_0^{T_*} \int_0^{\ell_m} (\alpha_{h,\delta}(t,x) - \alpha_{\text{thr}})^+ (1 - \alpha_{h,\delta}(t,x)) \frac{(1+s_1)\Pi_{h,\delta} c_{h,\delta}(t,x)}{1+s_1\Pi_{h,\delta} c_{h,\delta}(t,x)} \varphi(t,x) \, dx \, dt \\ & \rightarrow \int_0^T \int_0^{\ell_m} (\alpha - \alpha_{\text{thr}})^+ (1 - \alpha) \frac{(1+s_1)c}{1+s_1c} \varphi \, dx \, dt. \end{aligned}$$

A similar argument shows that the second term in the right hand side of (4.45) converges to $-\int_0^T \int_0^{\ell_m} (\alpha - \alpha_{\text{thr}})^+ \frac{s_2+s_3c}{1+s_1c} \varphi \, dx \, dt$. Plugging the above in $T_1 + T_2 = T_3$ concludes the proof. \square

Proposition 4.27 (Step (CA.3)). *For every $v \in H_{\partial x}^{1,u}(D_T^{\text{thr}})$ such that $v(\cdot, 0) = 0$, $\hat{u}|_{D_T^{\text{thr}}}$ satisfies (3.4b).*

Proof. Let $v \in \mathcal{C}^\infty(\overline{D_{T_*}^{\text{thr}}})$ with $v(\cdot, 0) = 0$. Redefine v to be a smooth extension to \mathcal{D}_{T_*} for ease of notation. Define $v_{h,\delta}(t,x) = \mathcal{I}_h v(t_n, x)$ on $\mathcal{T}_n \times \mathcal{X}_j$ for $n, j \geq 0$. The piecewise linear in space and piecewise constant in time function $v_{h,\delta}$ satisfies $v_{h,\delta} \rightarrow v$ and $\partial_x v_{h,\delta} \rightarrow \partial_x v$ strongly in $L^2(\mathcal{D}_{T_*})$.

Take the test function as $v_{h,\delta}(t_n, \cdot)$ in (3.6), multiply with $\delta \chi_{A_{h,\delta}}(t_n, \cdot)$, use the fact that $u_{h,\delta} = \chi_{A_{h,\delta}} \hat{u}_{h,\delta}$, and sum over $n = 1, \dots, N_* - 1$ to obtain $T_1 + T_2 = T_3$, where

$$\begin{aligned} T_1 &:= \int_0^{T_*} \int_0^{\ell_m} \chi_{A_{h,\delta}} \frac{k\alpha_{h,\delta}}{1 - \alpha_{h,\delta}} \hat{u}_{h,\delta} v_{h,\delta} \, dx \, dt, \\ T_2 &:= \int_0^{T_*} \int_0^{\ell_m} \chi_{A_{h,\delta}} \mu \alpha_{h,\delta} \partial_x \hat{u}_{h,\delta} \partial_x v_{h,\delta} \, dx \, dt, \text{ and} \\ T_3 &:= \int_0^{T_*} \int_0^{\ell_m} \chi_{A_{h,\delta}} \alpha_{h,\delta} \mathcal{H}(\alpha_{h,\delta}) \partial_x v_{h,\delta} \, dx \, dt. \end{aligned}$$

We have $\chi_{A_{h,\delta}} \rightarrow \chi_{D_{T_*}^{\text{thr}}}$ almost everywhere and $\alpha_{h,\delta} \rightarrow \alpha$ in $L^2(\mathcal{D}_{T_*})$. Therefore, Lemmas III(a) and III(b) show that

$$T_1 \rightarrow \int_0^{T_*} \int_0^{\ell_m} \chi_{D_{T_*}^{\text{thr}}} \frac{k\alpha}{1 - \alpha} \hat{u} v \, dx \, dt = \iint_{D_{T_*}^{\text{thr}}} \frac{k\alpha}{1 - \alpha} uv \, dx \, dt.$$

A similar argument for T_2 shows that

$$T_2 \rightarrow \int_0^{T_*} \int_0^{\ell_m} \chi_{D_{T_*}^{\text{thr}}} \mu \alpha \partial_x \hat{u} \partial_x v \, dx dt = \iint_{D_{T_*}^{\text{thr}}} \mu \alpha \partial_x u \partial_x v \, dx dt.$$

Since \mathcal{H} is continuous, $\mathcal{H}(\alpha_{h,\delta}) \rightarrow \mathcal{H}(\alpha)$ almost everywhere in \mathcal{D}_{T_*} . Therefore,

$$T_3 \rightarrow \int_0^{T_*} \int_0^{\ell_m} \chi_{D_{T_*}^{\text{thr}}} \alpha \mathcal{H}(\alpha) \partial_x v \, dx dt = \iint_{D_{T_*}^{\text{thr}}} \alpha \mathcal{H}(\alpha) \partial_x v \, dx dt.$$

These convergences, the relation $T_1 + T_2 = T_3$, and the density of $\mathcal{C}^\infty(\overline{D_{T_*}^{\text{thr}}})$ with zero value at $x = 0$ in $H_{\partial x}^{1,u}(D_T^{\text{thr}})$ yield the desired result. \square

To establish (3.4c) we start with a definition and a covering lemma.

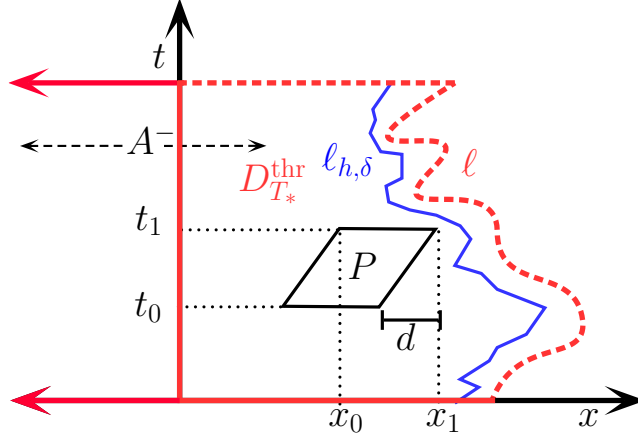


Figure 4.5: The domain A and A^- are the geometries described in Lemma 4.28, and P is a right-leaning parallelogram, and $d = (\rho \mathcal{C}_{\text{CFL}})^{-1}(t_1 - t_0)$.

Lemma 4.28 (Covering lemma). *For $x_0 < x_1$ and $t_0 < t_1$, let*

$$P := \bigcup_{t_0 \leq t \leq t_1} \{t\} \times [x_0 - (\rho \mathcal{C}_{\text{CFL}})^{-1}(t_1 - t), x_1 - (\rho \mathcal{C}_{\text{CFL}})^{-1}(t_1 - t)] \quad (4.46)$$

be a right-leaning parallelogram (see Figure 4.5) contained in $A^- := D_{T_}^{\text{thr}} \cup (\{0\} \times [0, \ell(0)]) \cup ([0, T] \times \mathbb{R}^-)$. Then, there exists an $h_P > 0$ and a $\delta_P > 0$ such that, for every $h \leq h_P$ and $\delta \leq \delta_P$, $P \subset A_{h,\delta}^- := A_{h,\delta} \cup (\{0\} \times [0, \ell(0)]) \cup ([0, T] \times \mathbb{R}^-)$.*

Proof. From (4.46) and $P \subset A^-$, we have $\ell(t_1) > x_1 + \epsilon$ for some $\epsilon > 0$. Without loss of generality, assume that $\ell_{h,\delta}(t_1) \rightarrow \ell(t_1)$ or consider a \tilde{t}_1 arbitrarily close to t_1 such that $\ell_{h,\delta}(\tilde{t}_1) \rightarrow \ell(\tilde{t}_1)$. The existence of \tilde{t}_1 is guaranteed by the fact that $\ell_{h,\delta} \rightarrow \ell$ almost everywhere. In this case, there exists an h_P and a δ_P such that $\ell_{h,\delta}(t_1) > x_1$ for every

$h \leq h_P$ and $\delta \leq \delta_P$, which means that $\ell_{h,\delta,D}(t_1) > x_1 - \ell_{h,\delta,BV}(t_1)$, where $\ell_{h,\delta,D}$ and $\ell_{h,\delta,BV}$ are obtained from the proof of Proposition 4.18. Since $\ell_{h,\delta,D}$ is decreasing, for $t \in [t_0, t_1]$ we have $\ell_{h,\delta,D}(t) > x_1 - \ell_{h,\delta,BV}(t_1)$ and

$$\begin{aligned} \ell_{h,\delta,D}(t) + \ell_{h,\delta,BV}(t) &> x_1 - \ell_{h,\delta,BV}(t_1) + \ell_{h,\delta,BV}(t) \\ &\geq x_1 - (\rho \mathcal{C}_{\text{CFL}})^{-1}(t_1 - t). \end{aligned}$$

Therefore, for $t \in [t_0, t_1]$, $\ell_{h,\delta}(t) > x_1 - (\rho \mathcal{C}_{\text{CFL}})^{-1}(t_1 - t)$, which yields $P \subset A_{h,\delta}^-$. \square

Remark 4.29. Let $v \in \mathcal{C}_c^\infty(A^-)$. Then, $\text{supp}(v)$ is compact in A^- and can be covered by a finite number of right leaning type parallelograms $\{P_i\}_i$. Since there exists a \mathcal{C}_c^∞ partition of unity $\{\zeta_i\}_i$ subordinate to $\{P_i\}_i$, we can write $v = \sum_i v \zeta_i$ and $\text{supp}(v \zeta_i) \subset P_i$. Then, for any $h < h_0$ and $\delta < \delta_0$, where $h_0 = \min_i h_{P_i}$, $\delta_0 = \min_i \delta_{P_i}$, the support of v is contained in $A_{h,\delta}^-$, and $v \in \mathcal{C}_c^\infty(A_{h,\delta}^-)$.

Remark 4.30. The fact that the nutrient concentration satisfies the Neumann boundary condition (7.13h) forces a test function in (3.4c) not to vanish at the boundary $(0, T_*] \times \{0\}$ of $D_{T_*}^{\text{thr}}$. This requirement requires us to consider A^- instead of $D_{T_*}^{\text{thr}}$ in Lemma 4.28. Since we can extend any function $v \in \mathcal{C}^\infty(D_{T_*}^{\text{thr}})$ with $v(t, \ell(t)) = 0$ smoothly to A^- , the proof of Proposition 4.31 is not affected by this consideration of A^- .

Next, we show that the nutrient concentration c satisfies (3.4c).

Proposition 4.31 (Step (CA.4)). For every $v \in H_{\partial x}^{1,c}(D_T^{\text{thr}})$ such that $\partial_t v \in L^2(D_{T_*}^{\text{thr}})$, $c|_{D_{T_*}^{\text{thr}}}$ satisfies (3.4c).

Proof. Since $v \in H_{\partial x}^{1,c}(D_T^{\text{thr}})$ can be approximated by functions in $\mathcal{C}^\infty(D_{T_*}^{\text{thr}})$ with $v(t, \ell(t)) = 0$ for all $t \in (0, T_*)$, by Remarks 4.29 and 4.30 it is sufficient to consider functions $v \in \mathcal{C}_c^\infty(P)$, where $P \subset A^-$ is a right-leaning parallelogram.

Choose $v \in \mathcal{C}_c^\infty(P)$. There exists an h and a δ small enough such that $v \in \mathcal{C}_c^\infty(A_{h,\delta}^-)$ by Remark 4.29. Define $v_{h,\delta}(t, x) = \mathcal{I}_h v(t_n, x)$ for $(t, x) \in \mathcal{T}_n \times \mathcal{X}_j$ for $n, j \geq 0$. The piecewise linear in space and piecewise constant in time function $v_{h,\delta}$ satisfies the following properties: (a) $v_{h,\delta} \in L^2(0, T_*; H^1(0, \ell_m))$, (b) for $n \geq 0$, $v_{h,\delta}(t_n, \ell_h^n) = 0$, (c) $v_{h,\delta} = 0$ on $\mathcal{D}_{T_*} \setminus \overline{A_{h,\delta}}$, and (d) $v_{h,\delta}(T_*, \cdot) = 0$.

In (3.8), take the test function as $v_{h,\delta}(t_n, \cdot)$ and sum over $n = 1, \dots, N_*$ to obtain $T_1 + T_2 = T_3$, where

$$\begin{aligned} T_1 &= \sum_{n=1}^{N_*} \int_0^{\ell_m} (\Pi c_{h,\delta}(t_n, x) - \Pi c_{h,\delta}(t_{n-1}, x)) \Pi v_{h,\delta}(t_n, x) dx, \\ T_2 &:= \sum_{n=1}^{N_*} \lambda \delta \int_0^{\ell_m} \partial_x c_{h,\delta}(t_n, x) \partial_x v_{h,\delta}(t_n, x) dx, \text{ and} \\ T_3 &:= -Q \sum_{n=1}^{N_*} \delta \int_0^{\ell_m} \frac{\alpha_{h,\delta}(t_n, x) \Pi_h c_{h,\delta}(t_n, x)}{1 + \widehat{Q}_1 |\Pi_h c_{h,\delta}(t_{n-1}, x)|} \Pi_h v_{h,\delta}(t_n, x) dx. \end{aligned}$$

Note that the space integrals in T_1 , T_2 , and T_3 are on $(0, \ell_h^n)$ for each t_n by the property (c). A use of (1.4) leads to

$$T_1 = - \sum_{n=1}^{N_*} \int_0^{\ell_m} (\Pi_h v_{h,\delta}(t_n, x) - \Pi_h v_{h,\delta}(t_{n-1}, x)) \Pi_h c_{h,\delta}(t_n, x) dx \\ + \int_0^{\ell_m} \Pi_h v_{h,\delta}(T_*, x) \Pi_h c_{h,\delta}(T_*, x) dx - \int_0^{\ell_m} \Pi_h v_{h,\delta}(0, x) \Pi_h c_{h,\delta}(0, x) dx.$$

Using the property (c) and the strong convergences $\Pi_h c_{h,\delta}(0, \cdot) \rightarrow c_0(\cdot)$, $\Pi_h v_{h,\delta}(0, \cdot) \rightarrow v(0, \cdot)$, $\partial_t v_{h,\delta} \rightarrow \partial_t v$, $\Pi_h c_{h,\delta} \rightarrow c$ in $L^2(\mathcal{D}_{T_*})$, we deduce

$$T_1 \rightarrow - \int_0^{T_*} \int_0^{\ell_m} c \partial_t v dx dt - \int_0^{\ell_m} c_0(x) v(0, x) dx \\ = - \iint_{D_{T_*}^{\text{thr}}} c \partial_t v dx dt - \int_0^{\ell(0)} c_0(x) v(0, x) dx.$$

The weak convergence $\partial_x c_{h,\delta} \rightharpoonup c$, the strong convergence $\partial_x v_{h,\delta} \rightarrow \partial_x v$ in $L^2(\mathcal{D}_{T_*})$, and an application of Lemma III(a) yield

$$T_2 = \lambda \int_0^{T_*} \int_0^{\ell_m} \partial_x c_{h,\delta} \partial_x v_{h,\delta} dx dt \rightarrow \lambda \int_0^{T_*} \int_0^{\ell_m} \partial_x c \partial_x v dx dt \\ = \lambda \iint_{D_{T_*}^{\text{thr}}} \partial_x c \partial_x v dx dt.$$

It is easily observed that $\Pi_{h,\delta} c_{h,\delta} / (1 + \widehat{Q}_1 |\Pi_{h,\delta} c_{h,\delta}|) \rightarrow c / (1 + \widehat{Q}_1 |c|)$ in $L^2(\mathcal{D}_{T_*})$. Then, use of Lemma III(b) shows that $\alpha_{h,\delta} \Pi_{h,\delta} c_{h,\delta} / (1 + \widehat{Q}_1 |\Pi_{h,\delta} c_{h,\delta}|) \rightarrow \alpha c / (1 + \widehat{Q}_1 |c|)$ in $L^2(\mathcal{D}_{T_*})$. Since $\Pi_h v_{h,\delta} \rightarrow v$ in $L^2(\mathcal{D}_{T_*})$ we obtain

$$T_3 \rightarrow -Q \int_0^{T_*} \int_0^{\ell_m} \frac{\alpha c}{1 + \widehat{Q}_1 |c|} v dx dt = -Q \iint_{D_{T_*}^{\text{thr}}} \frac{\alpha c}{1 + \widehat{Q}_1 |c|} v dx dt.$$

Plugging the above in $T_1 + T_2 = T_3$ yields the desired result. \square

This concludes the proof of Theorem 4.3, and thereby convergence of the Definition 3.2 to a threshold solution (see Definition 3.1).

4.5 Maximal time of existence

The time T_* below which a threshold solution exists (obtained in Proposition 4.10) depends on the parameters a_* , a^* , m_{02} , and α^R . We can always fix ℓ_m large enough so that $\rho \mathcal{C}_{\text{CFL}}(\ell_m - \ell_0)$ is larger than T_m and T_M , so that $T_* = \min(T_m, T_M)$ (see Proposition 4.10).

The time T_m provided by (4.15) is a decreasing function of \mathcal{F}_{\min} . The fact that $\mathcal{F}_{\min} \geq 0$ yields $T_m \leq \log(\alpha_{\text{thr}}/a_*)/s_2$, which precisely occurs when $a^* = \alpha^{\text{R}}$ (if and only if $\mathcal{F}_{\min} = 0$). The time T_M provided by (4.18) requires a more careful analysis. The domain of T_M as a function of a^* is $(m_{02}, 1]$. However, T_M is zero at both $a^* = m_{02}$ and $a^* = 1$ (since $\lim_{a^* \rightarrow 1} \mathcal{F}_{\max} = \infty$). Therefore, T_M has the maximum between $a^* = m_{02}$ and $a^* = 1$. Here, we need to consider three cases. If $m_{02} > \alpha^{\text{R}}$, then T_* attains the maximum at an a^* between m_{02} and 1 (see Figure 4.6). If $m_{02} = \alpha^{\text{R}}$, then T_M attains the maximum between

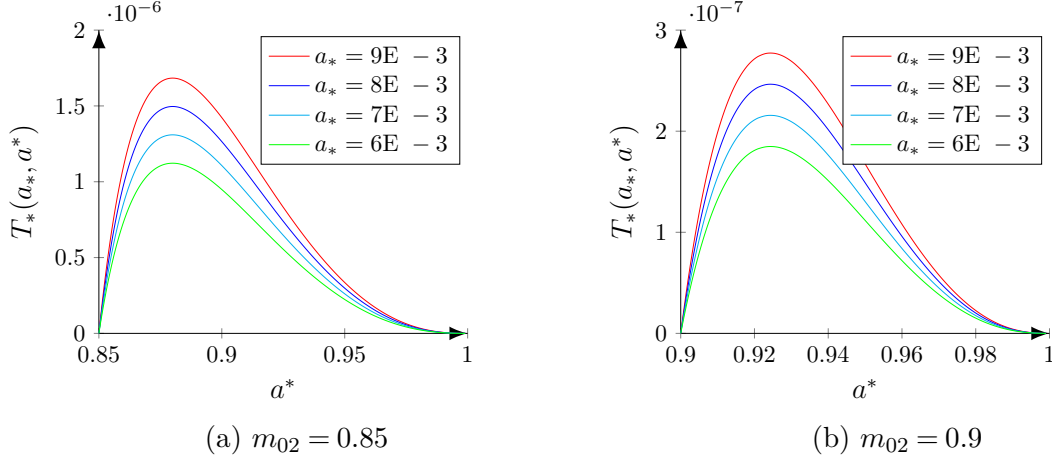


Figure 4.6: Variation of T_* with respect to a^* and a_* when $m_{02} > \alpha^{\text{R}} = 0.8$.

$a^* = \alpha^{\text{R}}$ and $a^* = 1$. Since T_m is decreasing on $[\alpha^{\text{R}}, 1]$, T_* attains the maximum at an a_* in $(\alpha^{\text{R}}, 1)$ (see Figure 4.7(a)). However, if $m_{02} < \alpha^{\text{R}}$, then T_* attains maximum exactly at

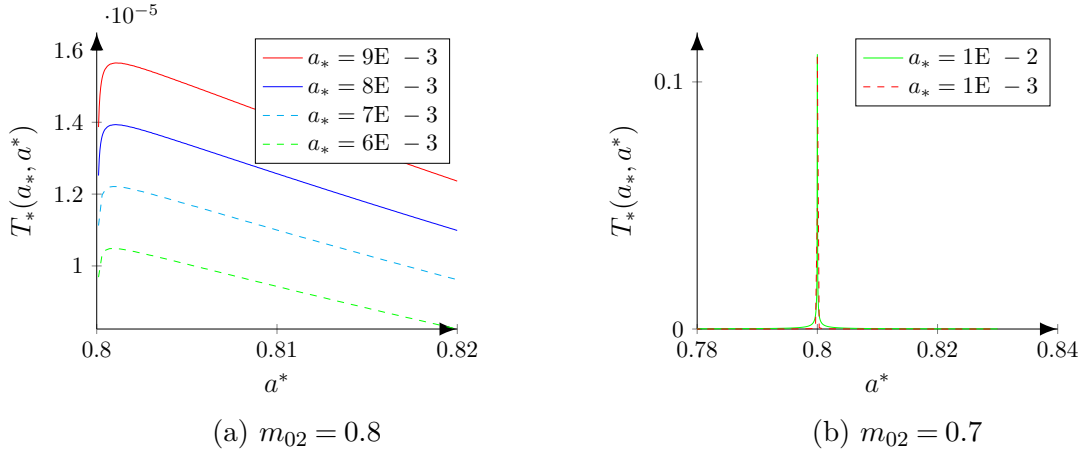


Figure 4.7: Variation of T_* with respect to a^* and a_* when $m_{02} \leq \alpha^{\text{R}} = 0.8$.

α^{R} since \mathcal{F}_{\max} is minimal at α^{R} and $a^* - m_{02}$ is increasing on $(m_{02}, 1)$ (see Figure 4.7(b)).

The time T_M depends also on the lower bound a_* . The range of a_* is $(0, \alpha_{\text{thr}})$. From (4.17) it is easy to observe that \mathcal{F}_{\max} is a decreasing function of a_* . Hence T_*

increases as a_* approaches α_{thr} which is evident from Figures 4.6, 4.7, and 4.8.

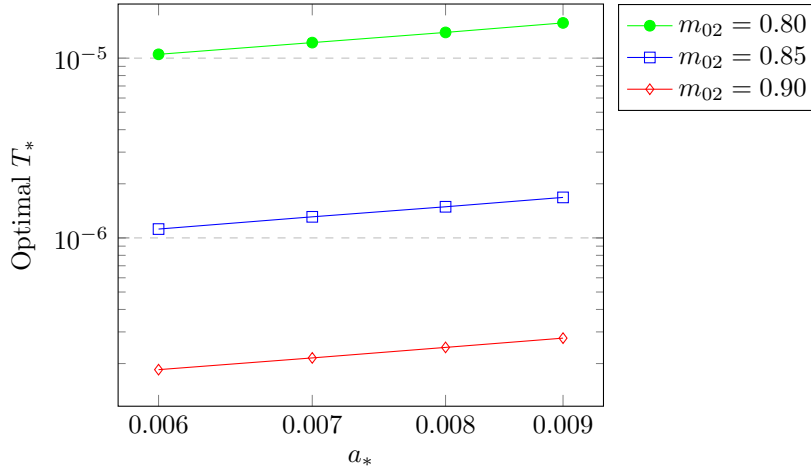


Figure 4.8: The dependence of optimal T_* on a_* .

Remark 4.32 (Sufficiency of Theorem 4.2). *The optimal value of T_* found here is of order of 10^{-7} to 10^{-5} , except when $m_{02} < \alpha^R$ in which case $T_* \approx 0.12$. However, in practice, we observe that the Discrete scheme 3.2 is stable, and thus convergent, up to at least a time of the order of 10^2 , as shown in Section 3.5. In other words, the time T_* derived in the proof of Proposition 4.10 is not restrictive, and only provides a sufficient condition for the convergence.*

Also, it must be noted that T_ is only restricted by the estimates on the model variables, in particular on cell volume fraction (see Proposition 4.10). The convergence analysis (Theorem 4.3 and proofs) does not impose any restriction on T_* . Consequently, if the Definition 3.2 is stable (the proper norms remain bounded) up to a certain time, which can be partially assessed during numerical simulations, then the convergence analysis shows the limits of subsequences are threshold solutions of the continuous model.*

4.6 Conclusion

In this chapter, the following objectives are achieved: (a) the convergence (up to a subsequence) of the discrete scheme is proved, and (b) the existence of a threshold solution up to a finite time is established. It is possible to extend the results derived in this chapter to similar models. Though extension to higher dimensional models has challenges, this chapter provides a frame work to approach similar coupled problems of elliptic, hyperbolic, and parabolic equations in single or several spatial dimensions. A general theory for problems with degenerate equations is open; for instance, (3.1b) which is only non-uniformly elliptic, defined in time-dependent domains, and includes the study of well-posedness, design, and analysis of numerical schemes.

Chapter 5

Numerical solution of a tumour growth model in two spatial dimensions

5.1 Introduction

The initial growth of a proliferating tumour does not contain vascular tissues, which forces the tumour to depend on diffused nutrients from the surrounding environment for its growth. The modelling and numerical simulations of this stage, namely the avascular growth stage, has been a frontier research area since the late 1970s [3, 8, 59]. Depending on the scale of observation – cellular level (microscopic) or aggregate level (tissue or macroscopic) – and nature of interactions between the constituents, several mathematical approaches and methods are used to model the avascular growth stage. A detailed review of various models can be found in T. Roose et al. [54] and R. P. Araujo et al. [60].

Literature

An extensive amount of scientific literature is available regarding the mathematical modelling of avascular tumour growth and multicellular spheroids [1, 6, 7, 33, 48, 61]. We focus on models based on mass balance equations, diffusion equations, and continuum mechanics [10]. Such models can be numerically implemented using appropriate combinations of finite element methods and finite volume methods.

This chapter complements the above mentioned works by relaxing several assumptions and extending to more general situations like asymmetric and irregular initial tumour geometries¹.

We consider a biphasic and viscous tumour model with a time-dependent spatial boundary in two and three spatial dimensions. The tumour cells constitute a viscous phase

¹The results in this chapter is published in J. Sci. Comput.: J. Droniou, J. A. Flegg, and G. C. Remesan, Numerical Solution of a Two Dimensional Tumour Growth Model with Moving Boundary. J. Sci. Comput. 85, 22 (2020). URL: <https://doi.org/10.1007/s10915-020-01326-6>

called the *cell phase* and the surrounding fluid medium constitute an inviscid phase called the *fluid phase*. The cell and fluid phases actively exchange matter through the processes of cell division and cell death. The diffusing nutrient controls the birth and death rates of the cells. H. M. Byrne et al. [7] considered an early version of this model and C. J. W. Beward et al. [1, 33] conducted a detailed study of the one-dimensional version. In these works, the authors present a detailed analysis of the effect of model parameters including the viscosity coefficient of the cell phase, drag coefficient between the cell and fluid phases, and parameters that determine attractive and repulsive forces between the tumour cells. A model based on multiphase mixture theory is described in the work by H. M. Byrne and L. Preziosi [6], in which they use a continuous cell–cell force term in contrast to the discontinuous force term in [1].

The previously mentioned models successfully describe the evolution of tumour radius and the effect of model parameters. However, to reduce a higher spatial dimensional model to a single spatial dimension, it is assumed that the tumour is growing radially symmetrically. This assumption is not valid if the initially seeded tumour is irregular in shape. Also, the time-dependent boundary is not well defined except in the radially symmetric case. In this chapter, we adapt and recast the model in [7], so that symmetry assumptions are relaxed, the ill-posedness of the time-dependent boundary is corrected, and numerical simulations are feasible without reducing the dimensionality.

J. M. Osborne and J. P. Whiteley [10] developed a generic numerical framework for multiphase viscous flow equations and applied it to simulate tissue engineering models and tumour growth models. Though the numerical scheme presented in [10] is robust, the tumour growth model considered is ill-posed. Here, the viscous system that governs the cell velocity has a solution unique only up to a (rigid-body motion) function of the form $\mathbf{u}(\mathbf{x}) = B\mathbf{x} + \boldsymbol{\beta}$, where B is a skew-symmetric matrix, $\mathbf{x} \in \mathbb{R}^d$, and $\boldsymbol{\beta} \in \mathbb{R}^d$ is a constant. This non-uniqueness for viscous equations with pure traction boundary condition is a well-established fact in the theory of continuum mechanics [99, p. 155]. At the discrete level, the resulting non-invertibility of the coefficient matrix is overcome by imposing an auxiliary condition. A natural approach is to set the cell velocity at the centre of the tumour to be zero. However, this approach has the following drawbacks. Firstly, the auxiliary condition is not inbuilt with the model; instead, it is a numerical fix. Secondly, in the case of an asymmetrically shaped tumour a well-defined centre is absent. Even if we define the centre in a mathematical way, say as the centre of mass, it will vary over time, and consequently, the auxiliary condition as well, thereby making the numerical algorithm computationally intense. Thirdly, fixing the velocity at a single point does not fully eliminate the non-uniqueness. In fact, in two dimensions, even after imposing this condition, solution of the viscous equation is unique only up to functions of the form $\mathbf{u}(x, y) = a(y_0 - y, x - x_0) + (\alpha_1, \alpha_2)$, where $a \in \mathbb{R}$ is an arbitrary constant and $\mathbf{u}(x_0, y_0) = (\alpha_1, \alpha_2)$ for fixed vectors (x_0, y_0) and (α_1, α_2) . The function \mathbf{u} can be decomposed into the form, $\mathbf{u}(x, y) = aB_{\pi/2}(x, y)^T + (ay_0 + \alpha_1, -ax_0 + \alpha_2)$, where the matrix $B_{\pi/2} = \begin{pmatrix} 0 & -1 \\ 1 & 0 \end{pmatrix}$ represents the anticlockwise rotation by $\pi/2$ radians. Therefore, \mathbf{u} is the sum of a scaled rotation and a translation in the Cartesian plane, and such functions constitute the null

space of the linear operator acting on \mathbf{u} . In the current work, we circumvent the need for any such numerical fix by ensuring the well-posedness of the viscous system. In particular, we employ appropriate boundary conditions arising from physical considerations on the model.

P. Macklin and J. Lowengrub [62] considered a ghost cell method for moving interface problems and applied it to a quasi-steady state reaction-diffusion model. However, the model is defined on a fixed domain, and the time-dependent interface is embedded in this fixed domain. The model we consider has an explicit moving boundary associated with it and hence the scheme in [62] does not directly apply. M. C. Calzada et al. [56] use a fictitious domain method to capture the time-dependent boundary. In a sense, we combine the synergy of both of these works: the time-dependent boundary problem is transformed to a fixed boundary problem without introducing any additional variables as in a level set method. Instead, we use one of the original unknown variables in the model itself to characterise the moving boundary.

Contributions

The major contributions of this chapter are as follows:

- (1) A mathematically well-defined model that does not assume symmetric tumour growth is developed by adapting previous models.
- (2) Two variants of this model depicting the tumour growth in (a) free suspension and (b) *in vivo* surrounded by tissues or *in vitro* in a passive polymeric gel are presented.
- (3) We construct an extended model defined in a fixed domain and solutions of this model are used to recover solutions of the original model. Since no additional variables are introduced to achieve this (as in level set methods), the complexity of the model is not increased.
- (4) We consider a numerical scheme based on finite volume methods, Lagrange $\mathbb{P}_2 - \mathbb{P}_1$ Taylor-Hood finite element method, and mass-lumped finite element methods. The numerical scheme eliminates the need for re-meshing the time-dependent domain at each time step, which makes the computations economical.
- (5) The numerical results are consistent with the findings from previous literature. We demonstrate the versatility of the scheme in simulating initial tumour geometries with irregular and asymmetric shape and tumours with a changing topological structure.

Organisation

The chapter is organised as follows. The dimensionless model is presented in Section 5.2. The preliminaries and notations are presented in Section 5.3. In Section 5.4, we present the notion of weak solutions and the main theorem that yields the equivalence between two different weak solutions in an appropriate sense. In Section 5.5, we provide the discretisation of the spatial and temporal domains and details of the numerical scheme. In

Section 5.6, we apply the numerical scheme presented in Section 5.5 to cases under different growth conditions and discuss the results in detail along with the scope for future research.

5.2 Model presentation

A brief derivation of the model is presented in Appendix B. The temporal and spatial variables are respectively denoted by t and $\mathbf{x} := (x_i)_{i=1,\dots,d}$ ($d = 2$ or 3) in the sequel. All equations and parameters are presented in dimensionless form. In the case $d = 2$, we take $\mathbf{x} = (x, y)$. At time $t \in (0, T)$, the tumour occupies the spatial domain $\Omega(t)$ in \mathbb{R}^d . The initial domain $\Omega(0)$ is a part of the given data. The tumour occupies the time–space domain $D_T := \cup_{t \in (0, T)} (\{t\} \times \Omega(t))$. We assume that $\Omega(t)$ is a bounded domain with a \mathcal{C}^1 –regular boundary [97, p. 627] given by $\Gamma(t) = \partial\Omega(t)$ for $t \in [0, T)$. The time–dependent boundary $B_T := \partial D_T \setminus ((\{0\} \times \Omega(0)) \cup (\{T\} \times \Omega(T)))$ of D_T is also assumed to be \mathcal{C}^1 –regular with respect to the time and space variables (see Figure 5.1). Let $\Omega_\ell = (-\ell, \ell)^d$ be a domain in \mathbb{R}^d such that $\Omega(t) \subset \Omega_\ell$ for every $t \in [0, T)$, which ensures $D_T \subset \mathcal{D}_T = (0, T) \times \Omega_\ell$. Let $\mathbf{n}_{|\Gamma(t)}$ be the unit normal to $\Gamma(t)$ pointing out of $\Omega(t)$ and $\mathbf{n}_{|B_T}$ be the (time–space) unit normal to B_T pointing out of D_T . If $\Omega(t) \subset \mathbb{R}^2$, then $\boldsymbol{\tau}_{|\Gamma(t)}$ denotes the unit tangent vector to $\Gamma(t)$. The projection of \mathbf{u} on the tangent space of ∂A , where $A \subset \mathbb{R}^d$ is denoted by $\mathbf{u}_{\partial A, \boldsymbol{\tau}}$, which is defined by $\mathbf{u}_{\partial A, \boldsymbol{\tau}} := (\mathbf{u}_{|\partial A} \cdot \boldsymbol{\tau}_{|\partial A}) \boldsymbol{\tau}_{|\partial A}$ in two spatial dimensions and $\mathbf{u}_{\partial A, \boldsymbol{\tau}} := \mathbf{n}_{|\partial A} \times (\mathbf{u}_{|\partial A} \times \mathbf{n}_{|\partial A})$ in three spatial dimensions.

The relative volume of tumour cells (cell phase) and extra–cellular fluid (fluid phase) are denoted by $\alpha := \alpha(t, \mathbf{x})$ and $\beta := \beta(t, \mathbf{x})$, respectively. We assume that the tumour does not contain any voids, which implies that $\alpha + \beta = 1$, and hence β can be determined using α . The velocity by which the cells are moving is denoted by $\mathbf{u} := \mathbf{u}(t, \mathbf{x})$. The average pressure experienced in the fluid phase is denoted by $p := p(t, \mathbf{x})$. The cell growth is controlled by a limiting nutrient and $c := c(t, \mathbf{x})$ represents its concentration.

Depending on the conditions in which the tumour is growing, the nutrient supply can be abundant or limited. For instance, when the growth is in free suspension, the external atmosphere acts as an unlimited source of nutrients, like oxygen. On the contrary, when the growth is *in vivo* (inside a living organism), the tissues and other biological materials around the tumour hinder the smooth diffusion of nutrients from the adjacent capillary tissues. Hence, the nutrient supply is limited in the *in vivo* case. A similar delay in nutrient supply is experienced in the *in vitro* (in a controlled laboratory environment) case as the surrounding polymeric growth medium hinders nutrient diffusion. We consider the three cases of free suspension, *in vitro*, and *in vivo* growth, and present two models to describe them.

Since the nutrient supply is unlimited in the free suspension growth, the model is referred to as *nutrient unlimited model* (NUM). On the contrary, the *in vitro* and *in vivo* cases are described by *nutrient limited model* (NLM).

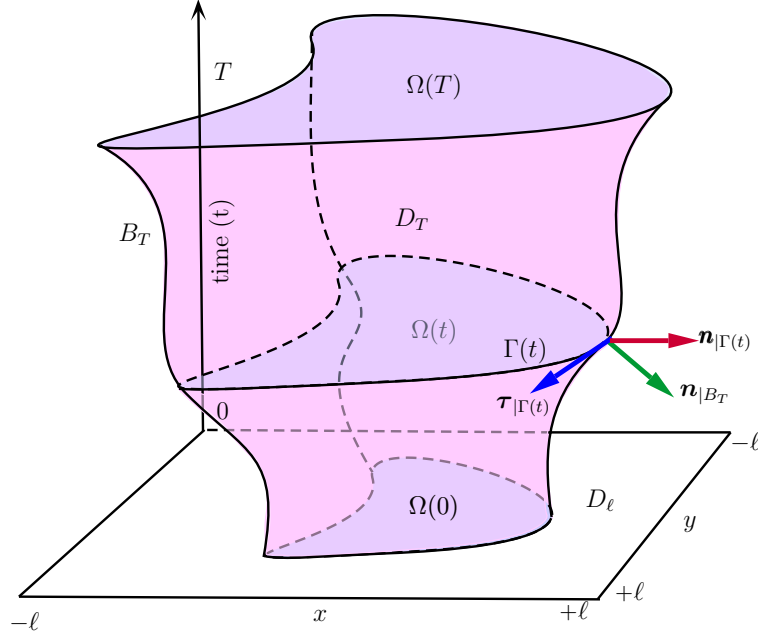


Figure 5.1: Three dimensional time–space domain occupied by the tumour. Here, 2ℓ is the side length of the square $\Omega_\ell \subset \mathbb{R}^2$, T is the final time of tumour growth, $\Omega(t) \subset \Omega_\ell$ is the domain occupied by the tumour at time t , $\Gamma(t)$ is the boundary of $\Omega(t)$, D_T is the time–space domain $\cup_{0 < t < T} (\{t\} \times \Omega(t))$, B_T is the evolving boundary given by $\partial D_T \setminus ((\{0\} \times \Omega(0)) \cup (\{T\} \times \Omega(T)))$, and \mathcal{D}_T is the time–space domain $(0, T) \times \Omega_\ell$.

5.2.1 Common features of NUM and NLM models

The free suspension model comes from [7], and the *in vivo/in vitro* one is a slight modification of this model. Both models are presented in dimensionless form and seek the variables $(\alpha, \mathbf{u}, p, c, \Omega)$ such that the mass balance on α and the momentum balance on (\mathbf{u}, p) hold in the moving domain: for every $t \in (0, T)$ and $\mathbf{x} \in \Omega(t)$,

$$\partial_t \alpha + \operatorname{div}(\alpha \mathbf{u}) = \alpha f(\alpha, c), \quad (5.1a)$$

$$-\operatorname{div}(\alpha \boldsymbol{\varepsilon}(\mathbf{u})) + \nabla p = -\nabla \mathcal{H}(\alpha), \text{ and} \quad (5.1b)$$

$$-\operatorname{div}\left(\frac{1-\alpha}{k\alpha} \nabla p\right) + \operatorname{div}(\mathbf{u}) = 0. \quad (5.1c)$$

The difference between the two models lies in the domain over which the nutrient concentration satisfies the following reaction–diffusion equation:

$$\partial_t c - \operatorname{div}(\eta \nabla c) = -\frac{Qc\alpha}{1 + \widehat{Q}_1 c}. \quad (5.1d)$$

Above, the function f is defined by $f(\alpha, c) := (1 - \alpha)b(c) - d(c)$, where $b(c) := (1 + s_1)c/(1 + s_1c)$, $d(c) := (s_2 + s_3c)/(1 + s_4c)$, and s_1, s_2, s_3 and s_4 are positive constants which control proliferation and death rates of the tumour cells. The operator $\boldsymbol{\varepsilon}$ is defined by

Equation	NUM	NLM
Evolution of α, \mathbf{u}, p , Eqs. (5.1a)–(5.1c)	$\mathbf{x} \in \Omega(t)$	
Boundary conditions α, \mathbf{u}, p	(5.1f)	
Initial conditions on α	(5.1e)	
Evolution of c , Eq. (5.1d)	For $\mathbf{x} \in \Omega(t)$	For $\mathbf{x} \in \Omega_\ell$
Initial conditions on c	(5.3) (on $\Omega(0)$)	(5.5) (on Ω_ℓ)
Boundary conditions c	(5.2) (on $\Gamma(t)$)	(5.4) (on $\partial\Omega_\ell$)

Table 5.1: Summary of NUM and NLM models.

$\varepsilon(\mathbf{u}) := 2\mu\nabla_s\mathbf{u} + \lambda\operatorname{div}(\mathbf{u})\mathbb{I}_d$, where \mathbb{I}_d is the d -dimensional identity tensor and $\nabla_s\mathbf{u} = \mu(\nabla\mathbf{u} + (\nabla\mathbf{u})^T)/2$. The scalar constants μ and λ are the shear and bulk viscosity coefficients, respectively and are related by $\lambda = -2\mu/3$ and $\mu > 0$. The function $\mathcal{H}(\alpha)$ is defined by $\alpha(\alpha - \alpha^*)^+ / (1 - \alpha)^2$, where α^* is a positive constant, $s^+ := \max(0, s)$, and $s^- := -\min(0, s)$ in the sequel. The positive constant k controls the traction between the cell and fluid phases. The constant $\eta > 0$ is the diffusivity coefficient of the limiting nutrient inside the tumour, and the constants $Q > 0$, further referred to as the absorptivity coefficient, and $\widehat{Q} \geq 0$ control the nutrient consumption by the cells.

The initial condition on α and the boundary conditions on (\mathbf{u}, p) are also common to both models:

$$\alpha(0, \mathbf{x}) = \alpha_0(\mathbf{x}) \quad \forall \mathbf{x} \in \Omega(0), \quad (5.1e)$$

$$(-\alpha\varepsilon(\mathbf{u}) + p\mathbb{I}_d)\mathbf{n}|_{\Gamma(t)} = -\mathcal{H}(\alpha)\mathbb{I}_d\mathbf{n}|_{\Gamma(t)}, \quad \mathbf{u}|_{\Gamma(t), \tau} = \mathbf{0}, \quad p|_{\Gamma(t)} = 0 \quad \forall t \in (0, T). \quad (5.1f)$$

The moving boundary is governed by the ordinary differential equation:

$$\partial_t\boldsymbol{\gamma} \cdot \mathbf{n}|_{\Gamma(t)} = \mathbf{u}|_{\Gamma(t)} \cdot \mathbf{n}|_{\Gamma(t)} \quad \forall t \in (0, T), \quad (5.1g)$$

where $\boldsymbol{\gamma}$ is a local parametrisation of B_T . We assume that $0 < m_{01} \leq \alpha_0(\mathbf{x}) \leq m_{02} < 1$ and $0 \leq c_0(\mathbf{x}) \leq 1$ for every $\mathbf{x} \in \Omega(0)$, where m_{01} and m_{02} are positive constants.

Remark 5.1. *Note that in (5.1g) we only specify the normal velocity of the moving boundary. The tangential velocity is not provided here. This is because tangential velocity does not change the topological structure of B_T , but changes only the parametrisation of B_T . Therefore, the domain D_T , that is the time-space region enclosed by B_T , is independent of the tangential velocity of the moving boundary. The extended solution presented in Definition 5.7 below recovers the domain D_T without resorting to an explicit parametrisation of the boundary B_T , and is an added advantage of the notion of the extended solution.*

The initial and boundary conditions for c are different for NUM and NLM and are made precise in the next sections. Table 5.1 summarises the two models.

5.2.2 Nutrient unlimited model (NUM)

In the *nutrient unlimited model* (NUM), we assume that the tumour grows in free space. Since the tumour has no voids within and is close-packed, it is reasonable to assume that the nutrient diffusion rate in the tumour is much lower than that of the free space outside the tumour. The nutrient consumed by the boundary cells is immediately replenished by the fast diffusing external nutrient supply. As a consequence, the nutrient concentration equation (5.1d) is only solved on the moving domain, for $t \in (0, T)$ and $\mathbf{x} \in \Omega(t)$, and at the boundary of this moving domain the nutrient concentration is set as the maximum value, which is unity after non-dimensionalisation. This leads to the following boundary and initial conditions for c :

$$c|_{\Gamma(t)} = 1 \quad \forall t \in (0, T), \quad (5.2)$$

$$c(0, \mathbf{x}) = c_0(\mathbf{x}) \quad \forall \mathbf{x} \in \Omega(0). \quad (5.3)$$

5.2.3 Nutrient limited model (NLM)

In the *nutrient limited model* (NLM), we assume that the tumour is growing inside a medium or a tissue. In this case, the nutrient diffusion rates in the exterior and interior regions of the tumour are in the same numerical range. Therefore, considerable delay can be expected for the nutrient to diffuse through the medium and reach the tumour. Consequently, the nutrient concentration at the tumour boundary is not unity at every time and one has to model the diffusion of the nutrient in the medium and in the tumour. Taking $\Omega_\ell = (-\ell, \ell)^d$ as the spatial region that encloses the tumour and the medium, the nutrient concentration equation (5.1d) is therefore solved for $t \in (0, T)$ and $\mathbf{x} \in \Omega_\ell$ (η could change between the external medium and the tumour), and the boundary and initial conditions on c are

$$c(t, \mathbf{x}) = c_b(\mathbf{x}) \quad \forall t \in (0, T), \forall \mathbf{x} \in \partial\Omega_\ell, \quad (5.4)$$

$$c(0, \mathbf{x}) = 0 \quad \forall \mathbf{x} \in \Omega_\ell. \quad (5.5)$$

This second condition means that no nutrient is available for the tumour cells initially. The boundary data satisfy $0 \leq c_b \leq 1$, and depends on the modelling situation under consideration. For illustrative purposes in two dimensions, we assume that blood vessels are present at $y = -\ell$ or $x = -\ell$ only. Therefore, the nutrient concentration at the boundary, c_b , is unity at $y = -\ell$ or $x = -\ell$ and zero at the other points in $\partial\Omega_\ell$.

5.3 Preliminaries and notations

We describe a smooth hypersurface $\mathcal{S} \subset \mathbb{R}^d$ and a local parametrisation of \mathcal{S} [110, Chapter 2]. The notion of local parametrisation of a smooth surface is crucial in extending the NUM and NLM models defined in D_T to \mathcal{D}_T , and thereby in eliminating the need for the evolving boundary B_T .

Definition 5.2 (\mathcal{C}^1 -smooth hypersurface). A set $\mathcal{S} \subset \mathbb{R}^d$ is said to be a \mathcal{C}^1 -smooth hypersurface in \mathbb{R}^d if the following conditions hold:

(SH.1) For each $\mathbf{z} \in \mathcal{S}$, there exists an open set $\mathcal{O}_{\mathbf{z}} \subset \mathbb{R}^d$ containing \mathbf{z} and a function $f_{\mathbf{z}} : \mathcal{O}_{\mathbf{z}} \rightarrow \mathbb{R}$ such that $\mathcal{S} \cap \mathcal{O}_{\mathbf{z}} = \{\mathbf{x} \in \mathcal{O}_{\mathbf{z}} : f_{\mathbf{z}}(\mathbf{x}) = 0\}$.

(SH.2) Each $f_{\mathbf{z}}$ in (SH.1) belongs to $\mathcal{C}^1(\mathcal{O}_{\mathbf{z}})$ and $\nabla f_{\mathbf{z}} \neq 0$ on $\mathcal{O}_{\mathbf{z}}$.

The collection $\{\mathcal{O}_{\mathbf{z}}, f_{\mathbf{z}}\}_{\mathbf{z} \in \mathcal{S}}$ is called a \mathcal{C}^1 -smooth local representation of \mathcal{S} .

Definition 5.3 (Regular surface and local parametrisation). A set $\mathcal{S} \subset \mathbb{R}^d$ is said to be a regular surface if for each $\mathbf{z} \in \mathcal{S}$, there exists open sets $U_{\mathbf{z}} \subset \mathbb{R}^{d-1}$ and $V_{\mathbf{z}} \subset \mathbb{R}^d$ with $\mathbf{z} \in V_{\mathbf{z}}$, and a diffeomorphism $\sigma_{\mathbf{z}} : U_{\mathbf{z}} \rightarrow V_{\mathbf{z}} \cap \mathcal{S}$. Each $\sigma_{\mathbf{z}}$ is called a coordinate chart, and the collection $\{U_{\mathbf{z}}, V_{\mathbf{z}}, \sigma_{\mathbf{z}}\}_{\mathbf{z} \in \mathcal{S}}$ is called a local parametrisation for \mathcal{S} .

If $\{\mathcal{O}_{\mathbf{z}}, f_{\mathbf{z}}\}_{\mathbf{z} \in \mathcal{S}}$ is a \mathcal{C}^1 -smooth local representation of the \mathcal{C}^1 -smooth hypersurface \mathcal{S} , then the normal to \mathcal{S} at a point $\mathbf{z} \in \mathcal{S}$ is given by $\nabla f_{\mathbf{z}}(\mathbf{z}) / \|\nabla f_{\mathbf{z}}(\mathbf{z})\|_2$, and this is meaningful since $\nabla f_{\mathbf{z}}(\mathbf{z}) \neq 0$ by Definition 5.2. An application of Theorem 3.27 in [110] shows that every \mathcal{C}^1 -smooth hypersurface is regular and therefore, has a local parametrisation.

5.3.1 Function spaces and norms

In this subsection, the definitions of function spaces and norms used in the remaining of this chapter are presented. Also, recall definitions from Section 1.4.

For a domain $A \subset \mathbb{R}^d$, $L^p(A)$ ($1 \leq p \leq \infty$) and $H^1(A)$ are standard Sobolev spaces of functions $f : A \rightarrow \mathbb{R}$. The notation $(\cdot, \cdot)_A$ stands for the standard $L^2(A)$ inner product. The space $\mathbf{H}_d^1(A) = (H^1(A))^d$ is the collection of functions $\mathbf{u} = (u_1, \dots, u_d)$ such that $u_i : A \rightarrow \mathbb{R}$ and $u_i \in H^1(A)$ for $i = 1, \dots, d$.

Define the norms $\|\mathbf{u}\|_{0,A} := (\mathbf{u}, \mathbf{u})_A^{1/2}$ and $\|\mathbf{u}\|_{k,A} := \sum_{i=1}^d \sum_{|\mathbf{j}| \leq k} \|\partial^{\mathbf{j}} u_i\|_{0,A}$, where \mathbf{j} is a multi-index. Define the subspace of functions in $\mathbf{H}_d^1(A)$ with homogeneous tangential component at ∂A , and the subspace of functions in $H^1(A)$ with homogeneous Dirichlet boundary condition ∂A , respectively, by

$$\mathbf{H}_{0,\tau}^1(A) := \{\mathbf{u} \in \mathbf{H}_d^1(A) : \mathbf{u}_{\partial A, \tau} = \mathbf{0}\} \quad \text{and} \quad H_0^1(A) := \{f \in H^1(A) : f|_{\partial A} = 0\}.$$

The space $BV(A)$ denotes the the space of all functions with bounded variation (see Sub-section 1.4.1) on the set A .

Let $A_T = \cup_{0 < t < T} (\{t\} \times X(t))$, where $\{X(t)\}_{t \in (0, T)}$ is a family of domains such that $X(t) \subset \mathbb{R}^d$ for every $t \in (0, T)$. Define the Hilbert spaces

$$\begin{aligned} \mathbf{H}_{\nabla}^{1,u}(A_T) &:= \{\mathbf{u} \in (L^2(A_T))^d : \partial_{x_j} u_i \in L^2(A_T), i, j = 1, \dots, d \\ &\quad \text{and } \mathbf{u}_{\partial X(t), \tau} = \mathbf{0} \forall t \in (0, T)\} \quad \text{and} \\ \mathbf{H}_{\nabla}^{1,c}(A_T) &:= \{c \in L^2(A_T) : \nabla c \in (L^2(A_T))^d \text{ and } c|_{\partial X(t)} = 0 \forall t \in (0, T)\}. \end{aligned}$$

5.4 Weak solutions and equivalence theorem

Recall that $D_T = \cup_{0 < t < T} (\{t\} \times \Omega(t))$ and $\mathcal{D}_T = (0, T) \times \Omega_\ell$. In this section, the well-posedness of the weak form of the velocity–pressure system is established and two weak formulations of the NUM model (in D_T and \mathcal{D}_T) (5.1)–(5.3) are presented. In the first one, the scalar conservation law (5.1a) is set on the moving domain $\Omega(t)$, while in the second one the velocity and nutrient concentration are extended to the entire box Ω_ℓ and the cell volume fraction α is set to satisfy the conservation law (5.1a) on this box. The interest of this second model, as already illustrated in the one–dimensional case in Chapter 2, is to enable the usage of a discrete scheme using a fixed background mesh, rather than a mesh that moves with the domain $\Omega(t)$. The moving meshes and re-meshing are technically more difficult and expensive in 2D than in 1D, and the approach in this chapter with second (extended) model that considers \mathcal{D}_T is more advantageous.

The two weak formulations are shown to be equivalent in Section 5.4.2. The key relation for proving this equivalence is Proposition 5.10, which establishes a formula for the outer normal to the time–space tumour domain in terms of the cell volume fraction, as well as the fact that if a piecewise smooth vector field \mathbf{F} has an L^2 divergence, then it has a zero normal jump across any hypersurface.

We only consider here the NUM model, the analogous proofs to NLM are straightforward. This is because the proof only depends on the divergence form of (5.1a), which reads $(\partial_t, \text{div})(\alpha, \alpha \mathbf{u}) = \alpha f(\alpha, c)$ and is same for NUM and NLM. However, in the proof for NUM model, the nutrient concentration needs to be extended as unity outside $\Omega(t)$. This extension is not required in NLM as the nutrient equation is defined in the extended domain \mathcal{D}_T .

5.4.1 Well–posedness of velocity–pressure system

We present the weak formulations of (5.1b) and (5.1c) with boundary conditions (5.1f), which remain the same for Definitions 5.6 and 5.7. Let $\mathbf{u} \in \mathbf{H}_{\nabla}^{1,u}(D_T)$ and $p \in H_{\nabla}^{1,c}(D_T)$. The weak formulation seeks (\mathbf{u}, p) such that for all $\mathbf{v} \in \mathbf{H}_{\nabla}^{1,u}(D_T)$ and $z \in H_{\nabla}^{1,c}(D_T)$, and for each $t \in (0, T)$ it holds

$$a_1^t(\mathbf{u}(t, \cdot), \mathbf{v}(t, \cdot)) - a_3^t(p(t, \cdot), \mathbf{v}(t, \cdot)) = \mathcal{L}_\alpha^t(\mathbf{v}(t, \cdot)) \quad \text{and} \quad (5.6a)$$

$$a_2^t(p(t, \cdot), z(t, \cdot)) + a_3^t(z(t, \cdot), \mathbf{u}(t, \cdot)) = 0, \quad (5.6b)$$

where $a_1^t : \mathbf{H}_{0,\tau}^1(\Omega(t)) \times \mathbf{H}_{0,\tau}^1(\Omega(t)) \rightarrow \mathbb{R}$, $a_2^t : H_0^1(\Omega(t)) \times H_0^1(\Omega(t)) \rightarrow \mathbb{R}$, and $a_3^t : H_0^1(\Omega(t)) \times \mathbf{H}_{0,\tau}^1(\Omega(t)) \rightarrow \mathbb{R}$ are bilinear forms defined by, for $j \in \{1, 2\}$,

$$a_1^t(\boldsymbol{\psi}_1, \boldsymbol{\psi}_2) = \int_{\Omega(t)} \alpha(t, \cdot) (2\mu \nabla_s \boldsymbol{\psi}_1 : \nabla_s \boldsymbol{\psi}_2 + \lambda \text{div}(\boldsymbol{\psi}_1) \text{div}(\boldsymbol{\psi}_2)) \, d\mathbf{x},$$

$$a_2^t(q_1, q_2) = \int_{\Omega(t)} \frac{1 - \alpha(t, \cdot)}{k\alpha(t, \cdot)} \nabla q_1 \cdot \nabla q_2 \, d\mathbf{x}, \quad \text{and}$$

$$a_3^t(q_1, \boldsymbol{\psi}_1) = \int_{\Omega(t)} q_1 \operatorname{div}(\boldsymbol{\psi}_1) \, d\mathbf{x}$$

for $\boldsymbol{\psi}_j \in \mathbf{H}_{0,\tau}^1(\Omega(t))$ and $q_j \in H_0^1(\Omega(t))$. The linear form $\mathcal{L}_\alpha^t : \mathbf{H}_d^1(\Omega(t)) \rightarrow \mathbb{R}$ is defined by

$$\mathcal{L}_\alpha^t(\boldsymbol{\psi}_1) = \int_{\Omega(t)} \mathcal{H}(\alpha(t, \cdot)) \operatorname{div}(\boldsymbol{\psi}_1) \, d\mathbf{x}.$$

Under the assumption that $\alpha : D_T \rightarrow \mathbb{R}$ is known and satisfies $0 < m_{11} \leq \alpha \leq m_{12} < 1$, we show that for each $t \in (0, T)$, (5.6a) and (5.6b) are well-posed. In the sequel, we suppress the time dependency for the ease of notation wherever there is no chance of confusion; for example \mathbf{v} in Lemma 5.4 stands for $\mathbf{v}(t, \cdot)$, and so do \mathbf{u}, p , and z .

Lemma 5.4. *If $\mathbf{v} \in \mathbf{H}_{0,\tau}^1(\Omega(t))$, then there exists a constant $\mathcal{C}_{KP} > 0$ such that*

$$\mathcal{C}_{KP} \|\mathbf{v}\|_{1,\Omega(t)} \leq \|\nabla_s \mathbf{v}\|_{0,\Omega(t)}.$$

Proof. Consider the spaces $X = \mathbf{H}_{0,\tau}^1(\Omega(t))$, $Y = [L^2(\Omega(t))]^{d \times d}$, and $Z = [L^2(\Omega(t))]^d$, and the linear map $A := \nabla_s : X \rightarrow Y$ and the natural embedding $T := id : X \rightarrow Z$. Theorem 13 in [63] shows that A is an injection. The natural embedding T is compact by Rellich-Kondrachov Theorem. Korn's second inequality (Theorem VI of Section 1.4) yields $\mathcal{C}_K \|\mathbf{v}\|_{1,\Omega} = \mathcal{C}_K \|\mathbf{v}\|_X \leq \|\nabla_s \mathbf{v}\|_{0,\Omega} + \|\mathbf{v}\|_{0,\Omega} = \|A\mathbf{v}\|_Y + \|T\mathbf{v}\|_Z$. An application of Petree–Tartar lemma (Theorem IV of Section 1.4) yields the desired conclusion. \square

Theorem 5.5 (Well-posedness). *Let $\mathbf{H}_{u,p}^t := \mathbf{H}_{0,\tau}^1(\Omega(t)) \times H_0^1(\Omega(t))$ and let the bilinear operator $\mathfrak{A}^t : \mathbf{H}_{u,p}^t \times \mathbf{H}_{u,p}^t \rightarrow \mathbb{R}$ be defined by*

$$\mathfrak{A}^t((\mathbf{u}, p), (\mathbf{v}, z)) = a_1^t(\mathbf{u}, \mathbf{v}) - a_3^t(p, \mathbf{v}) + a_2^t(p, z) + a_3^t(z, \mathbf{u}).$$

If $0 < m_{11} \leq \alpha \leq m_{12} < 1$, then \mathfrak{A}^t is a continuous and coercive bilinear form in $\mathbf{H}_{u,p}^t$, and the linear form $\mathfrak{L}^t : \mathbf{H}_{u,p}^t \rightarrow \mathbb{R}$ defined by $\mathfrak{L}^t(\mathbf{v}, z) = \mathcal{L}_\alpha^t(\mathbf{v})$ is continuous on $\mathbf{H}_{u,p}^t$. Hence, there exists a unique $(\mathbf{u}, p) \in \mathbf{H}_{u,p}^t$ such that for all $(\mathbf{v}, z) \in \mathbf{H}_{u,p}^t$,

$$\mathfrak{A}^t((\mathbf{u}, p), (\mathbf{v}, z)) = \mathfrak{L}^t((\mathbf{v}, z)). \quad (5.7)$$

Proof. Continuity of the bilinear form follows from the estimates below. Since $\|\operatorname{div}(\mathbf{u})\|_{0,\Omega(t)} \leq \sqrt{d} \|\mathbf{u}\|_{1,\Omega(t)}$,

$$\begin{aligned} \mathfrak{A}^t((\mathbf{u}, p), (\mathbf{v}, z)) &\leq 2m_{12}(\mu + \lambda) \|\mathbf{u}\|_{1,\Omega(t)} \|\mathbf{v}\|_{1,\Omega(t)} + \|p\|_{1,\Omega(t)} \sqrt{d} \|\mathbf{v}\|_{1,\Omega(t)} \\ &\quad + \frac{1 - m_{11}}{km_{11}} \|p\|_{1,\Omega(t)} \|z\|_{1,\Omega(t)} + \sqrt{d} \|z\|_{1,\Omega(t)} \|\mathbf{u}\|_{1,\Omega(t)} \\ &\leq \mathcal{C} (\|\mathbf{u}\|_{1,\Omega(t)}^2 + \|p\|_{1,\Omega(t)}^2)^{1/2} (\|\mathbf{v}\|_{1,\Omega(t)}^2 + \|z\|_{1,\Omega(t)}^2)^{1/2}, \end{aligned}$$

where \mathcal{C} is a constant. Set $\mathbf{v} = \mathbf{u}$ and $z = p$ in $\mathfrak{A}^t((\mathbf{u}, p), (\mathbf{v}, z))$ to obtain,

$$\mathfrak{A}^t((\mathbf{u}, p), (\mathbf{u}, p)) = a_1^t(\mathbf{u}, \mathbf{u}) + a_2^t(p, p)$$

$$\geq 2m_{11}\mu \int_{\Omega(t)} \nabla_s \mathbf{u} : \nabla_s \mathbf{u} \, d\mathbf{x} + \frac{1-m_{12}}{km_{12}} \|p\|_{1,\Omega(t)}^2.$$

Then, Lemma 5.4 yields the coercivity of \mathfrak{A}^t . The continuity of \mathfrak{L}^t follows from the estimate

$$\mathfrak{L}^t(\mathbf{v}, z) \leq \sqrt{2} \max(1, \mathcal{H}(m_{12}) \sqrt{d\mu_d(\Omega(t))}) (\|\mathbf{v}\|_{1,\Omega(t)}^2 + \|z\|_{1,\Omega(t)}^2)^{1/2},$$

where μ_d is the d -dimensional Lebesgue measure. An application of Lax-Milgram theorem (Theorem V of Section 1.4) establishes the existence of a unique $(\mathbf{u}, p) \in \mathbf{H}_{u,p}^t$ such that (5.7) (hence, (5.6a) and (5.6b)) holds. \square

Definition 5.6 (NUM–weak solution). *A weak solution of the NUM in D_T , further referred to as NUM–weak solution, is a five-tuple $(\alpha, \mathbf{u}, p, c, \Omega)$ such that (SW.1)–(SW.4) hold.*

(SW.1) *The volume fraction satisfies $\alpha \in L^\infty(D_T)$, $0 < m_{11} \leq \alpha \leq m_{12} < 1$, where $m_{11} \leq m_{01}$ and $m_{02} \leq m_{12}$ are constants, and $\forall \varphi \in \mathcal{C}_c^\infty(\overline{D_T} \setminus (\{T\} \times \Omega(T)))$*

$$\begin{aligned} \int_{D_T} (\alpha, \alpha \mathbf{u}) \cdot \nabla_{(t,\mathbf{x})} \varphi \, dt d\mathbf{x} + \int_{\Omega(0)} \varphi(0, \mathbf{x}) \alpha_0(\mathbf{x}) \, d\mathbf{x} + \int_{D_T} \alpha f(\alpha, c) \varphi \, dt d\mathbf{x}, \\ = \int_{B_T} (\alpha, \mathbf{u} \alpha) \cdot \mathbf{n}|_{B_T} \varphi \, ds. \end{aligned} \quad (5.8)$$

(SW.2) *The velocity $\mathbf{u} \in \mathbf{H}_{\nabla}^{1,u}(D_T)$ and pressure $p \in H_{\nabla}^{1,c}(D_T)$ satisfy (5.6a) and (5.6b) for every $\mathbf{v} \in \mathbf{H}_{\nabla}^{1,u}(D_T)$ and $z \in H_{\nabla}^{1,c}(D_T)$.*

(SW.3) *The nutrient concentration is such that $c - 1 \in H_{\nabla}^{1,c}(D_T)$, $c \geq 0$, and $\forall \zeta \in H_{\nabla}^{1,c}(D_T)$ with $\partial_t \zeta \in L^2(D_T)$*

$$\begin{aligned} - \int_{D_T} c \partial_t \zeta \, d\mathbf{x} \, dt - \int_{D_T} \eta \nabla c \cdot \nabla \zeta \, d\mathbf{x} \, dt + \int_{\Omega(0)} c_0(\mathbf{x}) \zeta(0, \mathbf{x}) \, d\mathbf{x} \\ + \int_{D_T} \frac{Qc\alpha}{1 + \widehat{Q}_1 c} \zeta \, d\mathbf{x} \, dt = 0. \end{aligned} \quad (5.9)$$

(SW.4) *The time-dependent boundary $\Gamma(t)$ is governed by (5.1g).*

Definition 5.7 (NUM–extended solution). *A weak solution of the NUM in \mathcal{D}_T , further referred to as NUM–extended solution, is a four-tuple $(\tilde{\alpha}, \tilde{\mathbf{u}}, \tilde{p}, \tilde{c})$ such that (SE.1)–(SE.4) hold.*

(SE.1) *The function $\tilde{\alpha}$ is such that $\tilde{\alpha} \in L^\infty(\mathcal{D}_T)$, $\tilde{\alpha} \geq 0$, and $\forall \tilde{\varphi} \in \mathcal{C}_c^\infty([0, T] \times \Omega_\ell)$:*

$$\int_{\mathcal{D}_T} (\tilde{\alpha}, \tilde{\mathbf{u}} \tilde{\alpha}) \cdot \nabla_{(t,\mathbf{x})} \tilde{\varphi} \, dt d\mathbf{x} + \int_{\Omega(0)} \tilde{\varphi}(0, \mathbf{x}) \alpha_0(\mathbf{x}) \, d\mathbf{x} + \int_{\mathcal{D}_T} \tilde{\alpha} f(\tilde{\alpha}, \tilde{c}) \tilde{\varphi} \, dt d\mathbf{x} = 0. \quad (5.10)$$

(SE.2) For a fixed t , define $\tilde{\Omega}(t) := \{(t, \mathbf{x}) : \tilde{\alpha}(t, \mathbf{x}) > 0\}$ and $\tilde{D}_T := \cup_{0 < t < T} (\{t\} \times \tilde{\Omega}(t))$. Then, it holds $\tilde{\mathbf{u}}|_{\partial_T \setminus \tilde{D}_T} = \mathbf{0}$, $\tilde{p}|_{\partial_T \setminus \tilde{D}_T} = 0$, and $\tilde{c}|_{\partial_T \setminus \tilde{D}_T} = 1$.

(SE.3) The functions $\tilde{\mathbf{u}}|_{\tilde{D}_T}$ and $\tilde{p}|_{\tilde{D}_T}$ are such that $\tilde{\mathbf{u}}|_{\tilde{D}_T} \in H_{\nabla}^{1,u}(\tilde{D}_T)$, $\tilde{p}|_{\tilde{D}_T} \in H_{\nabla}^{1,c}(\tilde{D}_T)$ and satisfy (5.6a)–(5.6b) with $\Omega(t)$, D_T , and α set as $\tilde{\Omega}(t)$, \tilde{D}_T , and $\tilde{\alpha}|_{\tilde{\Omega}(t)}$, respectively.

(SE.4) The function $\tilde{c}|_{\tilde{D}_T}$ is such that $\tilde{c}|_{\tilde{D}_T} - 1 \in H_{\nabla}^{1,c}(\tilde{D}_T)$ and satisfies (5.9) with D_T set as \tilde{D}_T for all $\zeta \in H_{\nabla}^{1,c}(\tilde{D}_T)$ with $\partial_t \zeta \in L^2(\tilde{D}_T)$.

5.4.2 Equivalence of weak solutions

In this subsection, we show that Definitions 5.6 and 5.7 are equivalent in an appropriate sense and under some regularity assumptions on B_T . In particular, we show that the recovered domain \tilde{D}_T in Definition 5.7 is equal to D_T in Definition 5.6.

Definition 5.8 (Time projection map). *The time projection map $\pi_t : \mathbb{R}^+ \times \mathbb{R}^{d-1} \rightarrow \mathbb{R}^+ \times \mathbb{R}^d$ is defined by $\pi_t(t, \mathbf{y}) = t$ for all $(t, \mathbf{y}) \in \mathbb{R}^+ \times \mathbb{R}^{d-1}$.*

Remark 5.9 (Time-slice property of B_T). *While constructing a local parametrisation for B_T in the sense of Definition 5.3, we use time also as a parameter through the time projection map π_t to preserve the ‘time-slice’ geometry of $B_T = \cup_t (\{t\} \times \partial\Omega(t))$ in the following sense. Let $(\mathbb{R}^+ \times U_{\omega}, \mathbb{R}^+ \times V_{\omega}, \sigma_{\omega} = (\pi_t, \gamma_{\omega}))$ be a local parametrisation around $\omega \in B_T$ of the evolving boundary B_T in the sense of Definition 5.3. Then, for a fixed time t , the restriction $\{U_{\omega}, V_{\omega}, \gamma_{\omega}(t, \cdot)\}_{\omega \in \{t\} \times \partial\Omega(t)}$ is a local parametrisation of $\partial\Omega(t)$. The time-slice structure of a local parametrisation for B_T is crucial in proving Proposition 5.10.*

The next proposition provides a formula for the unit normal vector to the hypersurface B_T in terms of local parametrisations.

Proposition 5.10. *Let $\{\mathbb{R}^+ \times U_{\omega}, \mathbb{R}^+ \times V_{\omega}, \sigma_{\omega} = (\pi_t, \gamma_{\omega})\}_{\omega}$ be a local parametrisation of B_T as in Remark 5.9 and $\{\mathcal{O}_{\omega}, f_{\omega}\}$ be a \mathcal{C}^1 -smooth local representation of it in the sense of Definition 5.2, where $\omega = (t, \mathbf{z}) \in B_T$. Then, the unit normal to the hypersurface B_T can be expressed as follows:*

$$\mathbf{n}_{B_T} = \frac{(-\nabla f_{\omega} \cdot \partial_t \gamma_{\omega}, \nabla f_{\omega})}{\|(-\nabla f_{\omega} \cdot \partial_t \gamma_{\omega}, \nabla f_{\omega})\|_2}. \quad (5.11)$$

Proof. A (non-unit) normal to B_T at the point $(t, \mathbf{z}) \in B_T \cap \mathcal{O}_{\omega}$ can be expressed as $\nabla_{(t, \mathbf{x})} f_{\omega}(t, \mathbf{z}) = (\partial_t f_{\omega}(t, \mathbf{z}), \nabla f_{\omega}(t, \mathbf{z}))$. Definition 5.3 yields a point $(t, \mathbf{y}) \in \mathbb{R}^+ \times U_{\omega}$ such that $(t, \mathbf{z}) = (t, \gamma_{\omega}(t, \mathbf{y}))$. Since f_{ω} is zero in $B_T \cap \mathcal{O}_{\omega}$ the time derivative $\frac{d}{dt} f_{\omega}(t, \gamma(t, \mathbf{y}))$ is also zero. Therefore, in $B_T \cap \mathcal{O}_{\omega}$

$$\partial_t f_{\omega}(t, \mathbf{z}) = -\nabla f_{\omega}(t, \mathbf{z}) \cdot \partial_t \gamma_{\omega}(t, \mathbf{y})$$

and a normal to B_T at (t, \mathbf{z}) is provided by

$$\nabla_{(t, \mathbf{x})} f_\omega(t, \mathbf{z}) = (-\nabla f_\omega(t, \mathbf{z}) \cdot \partial_t \boldsymbol{\gamma}_\omega(t, \mathbf{y}), \nabla f_\omega(t, \mathbf{z})),$$

normalisation of which yields (5.11). \square

Remark 5.11. *Since $\{\mathcal{O}_\omega, f_\omega\}$ is a \mathcal{C}^1 -smooth local representation of the hypersurface B_T , for a fixed time t , the unit normal to the boundary $\Gamma(t)$ is given by $-\nabla f_\omega / \|\nabla f_\omega\|_2$.*

Next, we present the equivalence between the weak formulations (SE.1) and (SW.1).

Theorem 5.12 (Equivalence). (ET.a) *Let B_T be \mathcal{C}^1 -regular and $(\alpha, \mathbf{u}, p, c, \Omega)$ be a NUM-weak solution. Set $\tilde{\alpha} := \alpha$, $\tilde{\mathbf{u}} := \mathbf{u}$, $\tilde{p} := p$, and $\tilde{c} := c$ in D_T ; $\tilde{\alpha} := 0$, $\tilde{\mathbf{u}} := \mathbf{0}$, $\tilde{p} := 0$, and $\tilde{c} := 1$ in $\mathcal{D}_T \setminus \overline{D_T}$. If $\alpha \in BV(D_T)$, then $(\tilde{\alpha}, \tilde{\mathbf{u}}, \tilde{p}, \tilde{c}, \tilde{\Omega})$ is a NUM-extended solution.*

(ET.b) *Let $(\tilde{\alpha}, \tilde{\mathbf{u}}, \tilde{p}, \tilde{c}, \tilde{\Omega})$ be a NUM-extended solution and assume that $\tilde{B}_T := \partial \tilde{D}_T \setminus (\{0\} \times \Omega(0)) \cup \{T\} \times \tilde{\Omega}(T)$ is \mathcal{C}^1 -regular, where \tilde{D}_T is given by (SE.2) in Definition 5.7 and $\tilde{\alpha}|_{\tilde{D}_T} > 0$ on \tilde{B}_T . If there exist constants $0 < \tilde{m}_{11} \leq m_{01}$ and $m_{02} \leq \tilde{m}_{12} < 1$ such that $\tilde{m}_{11} \leq \tilde{\alpha}|_{\tilde{D}_T} \leq \tilde{m}_{12}$ and $\tilde{\alpha} \in BV(\mathcal{D}_T)$, then $\tilde{D}_T = D_T$ and $(\tilde{\alpha}|_{D_T}, \tilde{\mathbf{u}}|_{D_T}, \tilde{p}|_{D_T}, \tilde{c}|_{D_T}, \tilde{\Omega})$ is a NUM-weak solution.*

Proof.

(ET.a) Let $\{\mathbb{R}^+ \times U_\omega, \mathbb{R}^+ \times V_\omega, \sigma_\omega = (\pi_t, \boldsymbol{\gamma}_\omega)\}_\omega$ be a local parametrisation of B_T . Choose $\tilde{\varphi}$ belonging to $\mathcal{C}_c^\infty([0, T] \times \Omega_\ell)$. Since $\tilde{\varphi}|_{D_T} \in \mathcal{C}_c^\infty(\overline{D_T} \setminus (\{T\} \times \Omega(T)))$ and $\tilde{\alpha} = 0$ in $\mathcal{D}_T \setminus \overline{D_T}$, the following holds:

$$\begin{aligned} \int_{D_T} (\tilde{\alpha}, \tilde{\alpha} \tilde{\mathbf{u}}) \cdot \nabla_{(t, \mathbf{x})} \tilde{\varphi} dt d\mathbf{x} + \int_{\Omega(0)} \tilde{\varphi}(0, \mathbf{x}) \alpha_0(\mathbf{x}) d\mathbf{x} + \int_{D_T} \tilde{\alpha} f(\tilde{\alpha}, \tilde{c}) \tilde{\varphi} dt d\mathbf{x} \\ = \int_{B_T} (\alpha, \alpha \mathbf{u}) \cdot \mathbf{n}_{B_T} \tilde{\varphi} ds \end{aligned} \quad (5.12a)$$

and

$$\int_{\mathcal{D}_T \setminus D_T} (\tilde{\alpha}, \tilde{\alpha} \tilde{\mathbf{u}}) \cdot \nabla_{(t, \mathbf{x})} \tilde{\varphi} dt d\mathbf{x} + \int_{\mathcal{D}_T \setminus D_T} \tilde{\alpha} f(\tilde{\alpha}, \tilde{c}) \tilde{\varphi} dt d\mathbf{x} = 0. \quad (5.12b)$$

A use of Proposition 5.10 and Remark 5.11 yields

$$K_N (\alpha, \alpha \mathbf{u})|_{B_T} \cdot \mathbf{n}_{B_T} = (\alpha, \alpha \mathbf{u})|_{B_T} \cdot \left(-\mathbf{n}_{|\Gamma(t)} \cdot \partial_t \boldsymbol{\gamma}_\omega, \mathbf{n}_{|\Gamma(t)} \right), \quad (5.13)$$

where $K_N \neq 0$ is a normalisation constant. We then use (5.1g) in (5.13) to obtain $(\alpha, \alpha \mathbf{u})|_{B_T} \cdot \mathbf{n}_{B_T} = 0$. Add (5.12b) and (5.12a) to arrive at (5.10). The conditions on $\tilde{\mathbf{u}}$, \tilde{p} , and \tilde{c} follow naturally from Definition 5.7.

(ET.b) Let $\{\mathbb{R}^+ \times U_{\boldsymbol{\omega}}, \mathbb{R}^+ \times V_{\boldsymbol{\omega}}, \sigma_{\boldsymbol{w}} = (\pi_t, \boldsymbol{\gamma}_{\boldsymbol{\omega}})\}_{\boldsymbol{\omega}}$ be a local parametrisation of \tilde{B}_T . Define a vector field $\mathbf{F} : \mathcal{D}_T \rightarrow \mathbb{R}^{d+1}$ by $\mathbf{F} := (\tilde{\alpha}, \tilde{\alpha}\tilde{\mathbf{u}})$. For $(t_0, \mathbf{x}_0) \in \tilde{B}_T$, define

$$\mathbf{F}|_{\tilde{B}_T^+}(t_0, \mathbf{x}_0) := \lim_{\substack{(t, \mathbf{x}) \rightarrow (t_0, \mathbf{x}_0) \\ (t, \mathbf{x}) \in \tilde{D}_T}} \mathbf{F}(t, \mathbf{x}), \quad \mathbf{F}|_{\tilde{B}_T^-}(t_0, \mathbf{x}_0) := \lim_{\substack{(t, \mathbf{x}) \rightarrow (t_0, \mathbf{x}_0) \\ (t, \mathbf{x}) \in \mathcal{D}_T \setminus \tilde{D}_T}} \mathbf{F}(t, \mathbf{x}).$$

The fact that $\mathbf{F} = \mathbf{0}$ in $\mathcal{D}_T \setminus \tilde{D}_T$ (since $\tilde{\alpha}|_{\mathcal{D}_T \setminus \tilde{D}_T} = 0$ from (SE.2)) yields $\mathbf{F}|_{\tilde{B}_T^-} = \mathbf{0}$ and hence,

$$\int_{\tilde{B}_T} \varphi(\tilde{\alpha}, \tilde{\alpha}\tilde{\mathbf{u}})|_{\tilde{D}_T} \cdot \mathbf{n}_{\tilde{B}_T} \, ds = \int_{\tilde{B}_T} \left(\mathbf{F}|_{\tilde{B}_T^+} - \mathbf{F}|_{\tilde{B}_T^-} \right) \cdot \mathbf{n}_{\tilde{B}_T} \varphi \, ds. \quad (5.14)$$

Since the weak divergence of \mathbf{F} given by $-\tilde{\alpha}f(\tilde{\alpha}, \tilde{c})$ belongs to $L^2(\mathcal{D}_T)$, the normal jump $(\mathbf{F}|_{\tilde{B}_T^+} - \mathbf{F}|_{\tilde{B}_T^-}) \cdot \mathbf{n}_{\tilde{B}_T}$ is zero. Consequently, $(\tilde{\alpha}, \tilde{\alpha}\tilde{\mathbf{u}})|_{\tilde{D}_T} \cdot \mathbf{n}_{\tilde{B}_T} = 0$ on \tilde{B}_T . Then, the fact that $\tilde{\alpha}|_{\tilde{D}_T} > 0$ on \tilde{B}_T , Proposition 5.10, and Remark 5.11 yield

$$\partial_t \tilde{\boldsymbol{\gamma}}_{\boldsymbol{\omega}} \cdot \mathbf{n}|_{\tilde{\Gamma}(t)} = \tilde{\mathbf{u}}|_{\tilde{\Gamma}(t)} \cdot \mathbf{n}|_{\tilde{\Gamma}(t)}. \quad (5.15)$$

Since $\tilde{\boldsymbol{\gamma}}_{\boldsymbol{\omega}}(0, \cdot) = \boldsymbol{\gamma}_{\boldsymbol{\omega}}(0, \cdot)$, (5.15) yields $\tilde{D}_T = D_T$. Choose $\tilde{\varphi} \in \mathcal{C}_c^\infty(\overline{D_T} \setminus (\{T\} \times \Omega(T)))$. Define $\varphi \in \mathcal{C}_c^\infty([0, T] \times \Omega_\ell)$ such that $\varphi = \tilde{\varphi}$ in D_T . Since $\tilde{D}_T = D_T$ and $\tilde{\alpha} = 0$ on $\mathcal{D} \setminus \tilde{D}_T$, (5.15) yields

$$\begin{aligned} \int_{D_T} (\tilde{\alpha}, \tilde{\mathbf{u}}\tilde{\alpha}) \cdot \nabla_{(t, \mathbf{x})} \tilde{\varphi} \, dt \, d\mathbf{x} + \int_{\Omega(0)} \tilde{\varphi}(0, \mathbf{x}) \alpha_0(\mathbf{x}) \, d\mathbf{x} + \int_{D_T} \tilde{\alpha} f(\tilde{\alpha}, \tilde{c}) \tilde{\varphi} \, dt \, d\mathbf{x} \\ = \int_{B_T} \tilde{\varphi}(\tilde{\alpha}, \tilde{\mathbf{u}}\tilde{\alpha}) \cdot \mathbf{n}_{B_T} \, ds. \end{aligned}$$

Therefore, $\tilde{\alpha}|_{D_T}$ satisfies (5.8). The conditions on $\tilde{\mathbf{u}}|_{D_T}$, $\tilde{p}|_{D_T}$, and $\tilde{c}|_{D_T}$ follow from Definition 5.6. \square

Remark 5.13. *The properties that $\alpha \in BV(D_T)$ and $\tilde{\alpha} \in BV(\mathcal{D}_T)$ are necessary in the proof of (ET.a) and (ET.b), respectively so that the boundary values in (5.13) and (5.14) are well defined in sense of traces (see Theorem 1 [101, p. 177]).*

5.5 Numerical scheme

5.5.1 Discretisation

Here, we consider for simplicity that the spatial dimension is equal to 2. The temporal domain $[0, T]$ is uniformly partitioned into N intervals, $\mathcal{T}_n = (t_n, t_{n+1})$, with $\delta = t_{n+1} - t_n$ for $n = 0, \dots, N-1$, where $t_0 = 0$ and $t_N = T$. Let $\mathcal{S} = \{K_j\}_{j=1, \dots, J}$ be a conforming Delaunay partition of the domain Ω_ℓ into triangles. The following notations will be followed in the sequel. For $i, j = 1, \dots, J$,

- \mathbf{z}_j : centroid of K_j , a_j : area of K_j ,
- $\mathcal{E}(j)$: set of all triangles sharing a common edge with K_j ; $\mathcal{V}(j)$: set of all vertices of the triangle K_j ,
- e_{ji} : common edge between the triangles K_j and K_i ; \mathbf{m}_{ji} : mid point of e_{ji} ; \mathbf{n}_{ji} : unit normal to the edge e_{ji} pointing from the triangle K_j ; ℓ_{ji} : length of e_{ji} ,
- $\mathcal{V} = (\mathbf{v}_j)_{j=1,\dots,M}$: collection of vertices of triangles in \mathcal{T} ,
- \mathcal{B}_e : set of all boundary edges in \mathcal{T} ; and \mathcal{B}_T : set of all boundary triangles.

Definition 5.14 (Discrete average). *For any real valued function f on \mathbb{R}^2 , define the discrete average of f on the triangle K_j by $\{\{f\}\}_{K_j} := \sum_{\mathbf{v}_i \in \mathcal{V}_j} f(\mathbf{v}_i)/3$, where $j = 1, \dots, J$.*

The following aspects need to be considered when choosing a proper triangulation for Ω_ℓ .

5.5.2 Mesh-locking effect

We use a finite volume scheme to approximate the hyperbolic conservation law (5.1a), and it is a well-known fact that finite volume solutions exhibit the mesh-locking effect, see [64] and references therein. That is, the computed solution is preferentially oriented in accordance with the orientation of the triangulation. Further, the domain $\tilde{\Omega}(t)$ obtained from (SE.1) in Definition 5.7 depends on $\tilde{\alpha}$. Therefore, the mesh-locking effect in $\tilde{\alpha}$ at the discrete level affects the accuracy of $\tilde{\Omega}$, and thus other variables as well. This error propagates at each time step in a compounding fashion. One way to eliminate this problem is to use a very refined triangulation, but this increases the computational cost. The natural and cost-effective way is to use an unstructured and random triangulation. Randomness avoids any particular orientation of the triangles and thus eliminates mesh-locking from the numerical solution.

5.5.3 Approximation of the initial domain

After triangulating Ω_ℓ , we approximate the initial domain $\Omega(0)$ by the set Ω_h^0 , where

$$\Omega_h^0 := \cup_{\{\mathbf{z}_j \in \Omega(0)\}} K_j. \quad (5.16)$$

However, this approximation of $\Omega(0)$ by Ω_h^0 is not accurate if the triangles are arranged in a structured manner. We illustrate this in Figure 5.2, where $\Omega(0)$, a circle centred at the origin with unit radius, is approximated by Ω_h^0 in different structured triangulations. Evidently, the coarse triangulations in Figures 5.2(d) and 5.2(e) with 1024 and 4096 triangles, respectively give a poor approximation of $\Omega(0)$. A reasonably good approximation is provided by the triangulation in Figure 5.2(f); however, this triangulation contains 16,384 triangles, which makes the computations expensive over multiple time steps. If the discrete

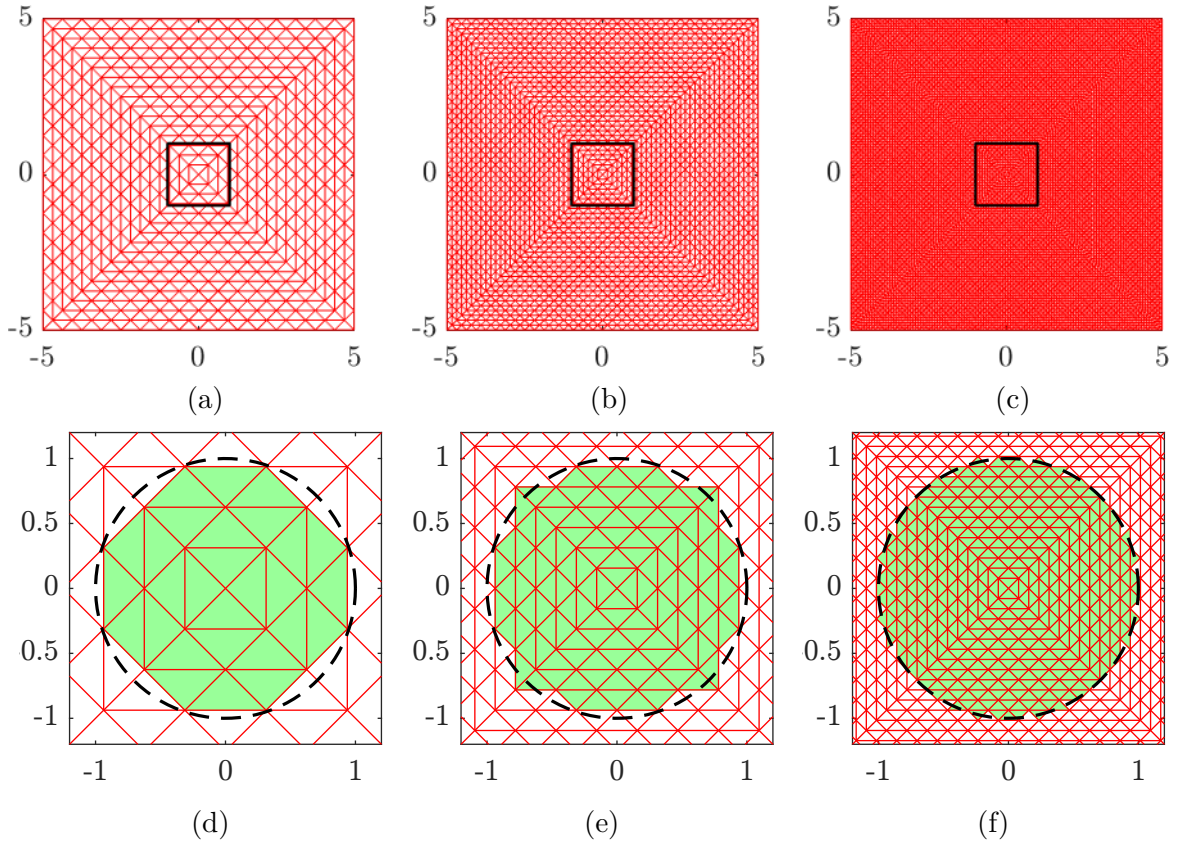


Figure 5.2: First row: Figures 5.2(a), 5.2(b) and 5.2(c) are structured triangulations of the domain $\Omega_\ell = (-5, 5)^2$. Triangulations in 5.2(d), 5.2(e), and 5.2(f), respectively contain 1024, 4096, and 16,384 triangles. Second row: Here, axes are limited to the region $(-1, 1)^2$ (black box in the first row) and corresponding approximations (green region) of an initial domain in the shape of a circle centred at origin with unit radius.

approximation of $\Omega(0)$ is not smooth enough, the discrete solution loses its symmetry as time evolves; this phenomenon is observed in the work by M. E. Hubbard and H. M. Byrne [11].

We overcome the issues discussed in Subsections 5.5.2 and 5.5.3 by using an adaptive and random triangulation. In particular, we employ the mesh generation of *Ruppert's algorithm* put forward by J. Ruppert [65]. This algorithm is based on Delaunay refinements, and produces quality triangulations without any skinny triangles; that is every angle in a triangle is greater than a preset value θ_{\min} . To obtain a good approximation of the domain $\Omega(0)$, we specify a finite number of nodes $\mathcal{N} = (\mathbf{N}_i)_{1 \leq i \leq N_0}$ (in anti-clockwise order) on $\partial\Omega(0)$, join the neighbouring nodes \mathbf{N}_i and \mathbf{N}_{i+1} by a straight line segment denoted by $\mathbf{N}_{i,i+1}$, and let this collection of straight edges be denoted by $\mathcal{L}(\mathcal{N})$. This procedure gives a piecewise affine approximation of $\partial\Omega(0)$. Ruppert's algorithm constructs a triangulation such that, corresponding to each straight edge $\mathbf{N}_{i,i+1} \in \mathcal{L}(\mathcal{N})$, there exists a triangle K_j

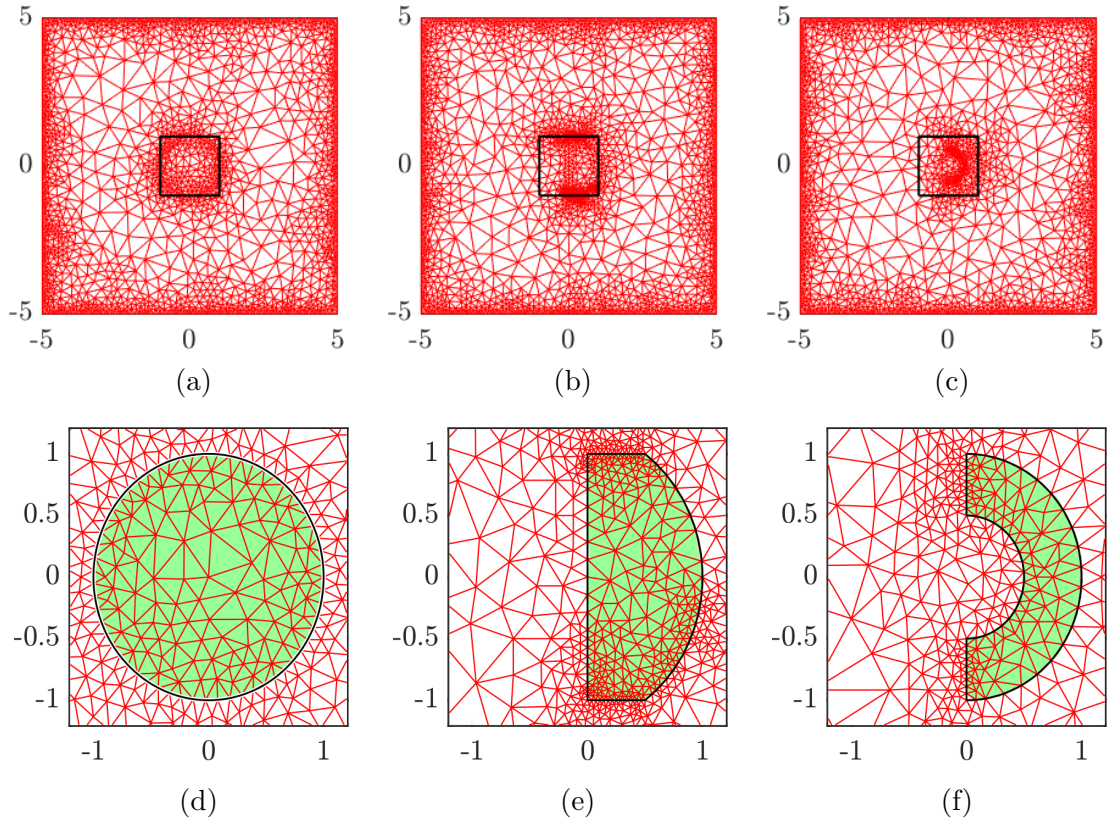


Figure 5.3: First row: Figures 5.3(a), 5.3(b), and 5.3(c) are the unstructured (Ruppert-Delaunay) triangulations of the domain $\Omega_\ell = (-5, 5)^2$ corresponding to initial domains with circular, bullet, and semi-annular shapes, respectively. The triangulations in 5.3(a), 5.3(b), and 5.3(c), respectively, contain 3492, 3642 and 4084 triangles. Second row: Here, axes are limited to the region $(-1, 1)^2$ (black box in the first row) to display the initial approximations (green region) better.

such that $N_{i,i+1}$ is an edge of K_j .

These aspects of Ruppert's algorithm help us to obtain a good approximation of $\Omega(0)$ irrespective of its shape. The fact that the algorithm uses reasonably few number of triangles is an added advantage. In Figure 5.3, we show the approximation of $\Omega(0)$ by Ω_h^0 , where the triangulations are obtained by Ruppert's algorithm. The circular, bullet-shaped and semi-annulus shaped domains, respectively shown in Figures 5.3(d), 5.3(e), and 5.3(f), are well approximated by the corresponding triangulations. In each case, we require fewer than 4100 triangles to obtain a good approximation of $\Omega(0)$ as opposed to 16,384 triangles in the case of a structured triangulation (see Figure 5.2(f)). This illustrates the economical advantage of Ruppert's algorithm.

Next, we present the numerical scheme. We discretise (5.1a) using a finite volume method, (5.1b)-(5.1c) using Lagrange $\mathbb{P}_2 - \mathbb{P}_1$ Taylor-Hood finite element method and (5.1d) using a backward Euler in time and mass lumped \mathbb{P}_1 finite element method.

Definition 5.15 (Discrete scheme for the NUM model). *Initial data approximation:*
Define

- α_h^0 by $\alpha_h^0 := \alpha_j^0$ on K_j , for $j = 1, \dots, J$, where $\alpha_j^0 := \int_{K_j} \alpha_0(\mathbf{x}) \, d\mathbf{x}$.
- c_h^0 by $c_{h|K_j}^0 \in \mathbb{P}_1(K_j)$ for $j = 1, \dots, J$, where $c_h^0(\mathbf{v}_i) = c_0(\mathbf{v}_i)$ for $i = 0, \dots, M$.
- Ω_h^0 is given by (5.16).
- The function \mathbf{u}_h^0 is obtained from (DS.c) by taking $n = 0$.

Updation: Fix a threshold $\alpha_{\text{thr}} \in (0, 1)$ and Ω_ℓ such that $\Omega_h^0 \subset \Omega_\ell$. Construct a finite sequence of functions $(\alpha_h^n, \mathbf{u}_h^n, p_h^n, c_h^n)_{\{1 \leq n \leq N\}}$ on Ω_ℓ such that for all $1 \leq n \leq N$, (DS.a)–(DS.d) hold.

(DS.a) $\alpha_h^n := \alpha_j^n$ on K_j for $j = 1, \dots, J$, where

$$\begin{aligned} \frac{1}{\delta}(\alpha_j^n - \alpha_j^{n-1}) + \frac{1}{a_j} \sum_{e_{ji} \in \mathcal{E}(j)} \ell_{ji} \mathcal{F}_{ji}^{n-1} \\ = (\alpha_j^{n-1} - \alpha_{\text{thr}})^+ (1 - \alpha_j^{n-1}) b_j^{n-1} - (\alpha_j^n - \alpha_{\text{thr}})^+ d_j^{n-1}, \end{aligned} \quad (5.17)$$

where \mathcal{F}_{ji}^{n-1} is the upwind flux between the triangles K_j and K_i through the common edge e_{ji} defined by

$$\mathcal{F}_{ji}^n := (\mathbf{u}_{ji}^n \cdot \mathbf{n}_{ji})^+ \alpha_j^n - (\mathbf{u}_{ji}^n \cdot \mathbf{n}_{ji})^- \alpha_i^n, \quad (5.18)$$

$$\mathbf{u}_{ij}^n = \mathbf{u}_h^n(\mathbf{m}_{ji}),$$

$$b_j^n = \left\{ \left\{ \frac{(1 + s_1)c_h^n}{(1 + s_1)c_h^n} \right\} \right\}_{K_j} \quad \text{and} \quad d_j^n = \left\{ \left\{ \frac{(s_2 + s_3)c_h^n}{(1 + s_4c_h^n)} \right\} \right\}_{K_j}.$$

If $e_{ji} \in \mathcal{B}_e$, then we set α_i^n to zero. This choice is justified since $\mathbf{u}_{ji}^n = \mathbf{0}$, so any choice of α_i^n does not change the value of the flux.

(DS.b) Ω_h^n is defined through the following process: starting from Ω_h^{n-1} ,

- (1) add all triangles $K_j \notin \Omega_h^{n-1}$ that have an edge on $\partial\Omega_h^{n-1}$ and such that $\alpha_j^n \geq \alpha_{\text{thr}}$;
- (2) remove all triangles $K_j \subset \Omega_h^{n-1}$ that have an edge on $\partial\Omega_h^{n-1}$ and such that $\alpha_j^n < \alpha_{\text{thr}}$;
- (3) Steps (1) and (2) lead to a new domain U ; repeat (2) with U instead of Ω_h^{n-1} until all triangles K_j that have an edge on ∂U satisfy $\alpha_j^n \geq \alpha_{\text{thr}}$, and define Ω_h^n as the resulting final set U .

(DS.c) Set the conforming finite element space of piecewise second degree polynomials from Ω_h^n to \mathbb{R}^2 with homogeneous tangential component on $\partial\Omega_h^n$ by

$$\mathbf{W}_{h,0}^n := \left\{ \boldsymbol{\varphi}_h^n \in (\mathcal{C}^0(\overline{\Omega_h^n}))^2 : \boldsymbol{\varphi}_h^n|_{K_j} \in (\mathbb{P}_2(K_j))^2 \forall K_j \subset \Omega_h^n, \boldsymbol{\varphi}_h^n|_{\partial\Omega_h^n} \cdot \boldsymbol{\tau}|_{\partial\Omega_h^n} = 0 \right\}.$$

Set the conforming finite element space of piecewise linear polynomials from Ω_h^n to \mathbb{R} and its subspace with homogeneous Dirichlet boundary condition on $\partial\Omega_h^n$ by

$$\begin{aligned} S_h^n &:= \left\{ v_h^n \in \mathcal{C}^0(\overline{\Omega_h^n}) : v_h^n|_{K_j} \in \mathbb{P}_1(K_j) \forall K_j \subset \Omega_h^n \right\} \text{ and} \\ S_{h,0}^n &:= \left\{ v_h^n \in S_h^n, v_h^n|_{\partial\Omega_h^n} = 0 \right\}. \end{aligned}$$

Then,

$$\mathbf{u}_h^n := \begin{cases} \tilde{\mathbf{u}}_h^n & \text{on } \Omega_h^n, \\ \mathbf{0} & \text{on } \Omega_\ell \setminus \overline{\Omega_h^n} \end{cases} \text{ and } p_h^n := \begin{cases} \tilde{p}_h^n & \text{on } \Omega_h^n, \\ 0 & \text{on } \Omega_\ell \setminus \overline{\Omega_h^n}, \end{cases}$$

where $(\tilde{\mathbf{u}}_h^n, \tilde{p}_h^n) \in \mathbf{W}_{h,0}^n \times S_{h,0}^n$ satisfies, for all $\boldsymbol{\varphi}_h^n \in \mathbf{W}_{h,0}^n$ and $v \in S_{h,0}^n$,

$$\begin{aligned} a_{1,h}^n(\tilde{\mathbf{u}}_h^n, \boldsymbol{\varphi}_h^n) - a_{3,h}^n(\tilde{p}_h^n, \boldsymbol{\varphi}_h^n) &= \mathcal{L}_h^n(\boldsymbol{\varphi}_h^n), \\ a_{2,h}^n(\tilde{p}_h^n, v_h^n) + a_{3,h}^n(v_h^n, \tilde{\mathbf{u}}_h^n) &= 0, \end{aligned}$$

with $a_{1,h}^n : \mathbf{W}_{h,0}^n \times \mathbf{W}_{h,0}^n \rightarrow \mathbb{R}$, $a_{2,h}^n : S_{h,0}^n \times \mathbf{W}_{h,0}^n \rightarrow \mathbb{R}$, $a_{3,h}^n : S_{h,0}^n \times S_{h,0}^n \rightarrow \mathbb{R}$ and $\mathcal{L}_h^n : \mathbf{W}_{h,0}^n \rightarrow \mathbb{R}$ are defined by

$$a_{1,h}^n(\mathbf{u}, \mathbf{v}) = \int_{\Omega_h^n} \alpha_h^n (2\mu \nabla_s \mathbf{u} : \nabla_s \mathbf{v} + \lambda \operatorname{div}(\mathbf{u}) \operatorname{div}(\mathbf{v})) \, d\mathbf{x}, \quad (5.19)$$

$$a_{2,h}^n(p, z) = \int_{\Omega_h^n} \frac{1 - \alpha_h^n}{k \alpha_h^n} \nabla p \cdot \nabla z \, d\mathbf{x},$$

$$a_{3,h}^n(z, \mathbf{w}) = \int_{\Omega_h^n} z \operatorname{div}(\mathbf{w}) \, d\mathbf{x}, \text{ and}$$

$$\mathcal{L}_h^n(\mathbf{v}) = \int_{\Omega_h^n} \mathcal{H}(\alpha_h^n) \operatorname{div}(\mathbf{v}) \, d\mathbf{x}. \quad (5.20)$$

(DS.d) Define the finite dimensional vector space of piecewise constant functions

$$S_{h,ML} := \left\{ w_h : w_h = \sum_{j=1}^M w_j \boldsymbol{\chi}_{\tilde{K}_j}, w_j \in \mathbb{R}, 1 \leq j \leq M \right\},$$

where, \tilde{K}_j is the convex polygon around the vertex \mathbf{v}_j defined by

$$\tilde{K}_j = \left\{ \mathbf{x} : \mathbf{x} = \sum_{\{i: \mathbf{v}_j \in \overline{K_i}\}} \lambda_i \mathbf{z}_i, 0 \leq \lambda_i \leq 1, \sum_i \lambda_i = 1 \right\}.$$

The mass lumping operator $\Pi_h : \mathcal{C}^0(\overline{\Omega_\ell}) \rightarrow S_{h,ML}$ is defined by $\Pi_h w = \sum_{j=1}^M w(\mathbf{v}_j) \chi_{\tilde{K}_j}$. Then,

$$c_h^n := \begin{cases} \tilde{c}_h^n & \text{on } \Omega_h^n, \\ 1 & \text{on } \Omega_\ell \setminus \Omega_h^n, \end{cases}$$

where $\tilde{c}_h^n \in S_h^n$ satisfies $\tilde{c}_h^n|_{\partial\Omega_h^n} = 1$ and, with $\Pi_h \tilde{c}_h^n := (\Pi_h c_h^n)|_{\Omega_h^n}$,

$$\begin{aligned} & \int_{\Omega_h^n} (\Pi_h \tilde{c}_h^n - \Pi_h c_h^{n-1}) \Pi_h v_h^n \, d\mathbf{x} + \delta \int_{\Omega_h^n} \eta \nabla \tilde{c}_h^n \cdot \nabla v_h^n \, d\mathbf{x} \\ &= -\delta \int_{\Omega_h^n} \frac{Q \alpha_h^n}{1 + \hat{Q}_1 \Pi_h c_h^{n-1}} \Pi_h \tilde{c}_h^n \Pi_h v_h^n \, d\mathbf{x} \quad \forall v_h^n \in S_{h,0}^n. \end{aligned} \quad (5.22)$$

Remark 5.16 (Scheme for the NLM model). Step (DS.d) needs to be modified in the case of numerical experiments for the NLM. In particular, we replace Ω_h^n in (5.22) by $\Omega_\ell = (-\ell, \ell)^2$ and \tilde{c}_h^n by c_h^n to incorporate the evolution of the nutrient in the entire domain \mathcal{D}_T . This modified (DS.d) reads

(DS.d) Define $S_h := \{v_h \in \mathcal{C}^0(\overline{\Omega_\ell}) : v_h^n|_{K_j} \in \mathbb{P}_1(K_j) \forall K_j \subset \Omega_\ell \text{ and } v_h|_{\partial\Omega_\ell} = 0\}$. The initial function c_h^0 is identically zero on Ω_ℓ . Then, $c_h^n \in S_{h,ML}$ with $c_h = c_{\mathbf{b}}$ on $\partial\Omega_\ell$ satisfies

$$\begin{aligned} & \int_{\Omega_\ell} (\Pi_h c_h^n - \Pi_h c_h^{n-1}) \Pi_h v_h \, d\mathbf{x} + \delta \int_{\Omega_\ell} \eta \nabla c_h^n \cdot \nabla v_h \, d\mathbf{x} \\ &= -\delta \int_{\Omega_\ell} \frac{Q \alpha_h^n}{1 + \hat{Q}_1 \Pi_h c_h^{n-1}} \Pi_h c_h^n \Pi_h v_h \, d\mathbf{x} \quad \forall v_h \in S_{h,0}. \end{aligned}$$

The boundary condition, $c_{\mathbf{b}}$, imposed on $\partial\Omega_\ell$ represents the supply of nutrient through blood vessels at the boundary of the domain.

Remark 5.17 (Determining Ω_h^n). The step (DS.b) determines the tumour domain. The volume fraction of tumour cells outside Ω_h^n is numerically close to zero while it is significant on the boundary of Ω_h^n . That is, the boundary of Ω_h^n is the interface beyond which the cell volume fraction reduces to a numerically small value. However, we allow the volume fraction of the tumour cells to become close to zero in some internal parts of Ω_h^n , and still remain as integral parts of Ω_h^n .

To ensure the stability of the finite volume discretisation of (5.1a), the time stepping used in simulations must be chosen so that the CFL condition holds; as a consequence, the tumour can only grow by one layer of triangles at each time step, which justifies the choice in Step (1) in (DS.b). Additionally, in our simulations we noticed that multiple iterations of Step (2) in (DS.b) are not required: after one iteration only, all the resulting boundary triangles have a tumour volume fraction larger than α_{thr} .

Remark 5.18 (3D setting). *The discrete schemes presented here in 2D for the NUM and NLM models extend in a straightforward way to three-dimensional models, since they are based on methods (finite volume, finite elements) that can be applied to 2D and 3D equations, and have the same presentation in both dimensions.*

Definition 5.19 (Discrete solution for the NUM model). *The functions $(\alpha_{h,\delta}, \mathbf{u}_{h,\delta}, p_{h,\delta}, c_{h,\delta})$ defined by $(\alpha_{h,\delta}, \mathbf{u}_{h,\delta}, p_{h,\delta}, c_{h,\delta}) := (\alpha_h^n, \mathbf{u}_h^n, p_h^n, c_h^n)$ on \mathcal{T}_n for $0 \leq n \leq N-1$, where the finite sequence $(\alpha_h^n, \mathbf{u}_h^n, p_h^n, c_h^n)_{\{0 \leq n \leq N-1\}}$ is obtained from Definition 5.15, is said to be the discrete solution of the NUM model (5.1)–(5.3) with respect to the time discretisation $(\mathcal{T}_n)_{n=0,\dots,N-1}$ and the triangulation \mathcal{T} .*

A few aspects of the numerical scheme need to be discussed briefly. For more details, the reader may refer to Chapter 2.

Threshold value

The threshold value $\alpha_{\text{thr}} \in (0, 1)$ plays an important role in obtaining accurate numerical solutions. The finite volume method used in (DS.a) introduces significant numerical diffusion while computing α_h^n , due to upwinding of the fluxes. If we define the discrete domain Ω_h^n as the union of all triangle K_j with $\alpha_{h|K_j}^n > 0$, the domain Ω_h^n might be significantly larger than the exact domain $\Omega(t_n)$. Since the computation of \mathbf{u}_h^n, p_h^n , and c_h^n depends crucially on Ω_h^n , the error in Ω_h^n affects the accuracy of these functions as well. Further, α_h^{n+1} depends on \mathbf{u}_h^n, p_h^n , and c_h^n . So the error propagates over time steps, finally reducing the quality of numerical solutions significantly. To avoid this, we compare α_h^n with a small positive number, α_{thr} . The tumour boundary $\partial\Omega_h^n$ is the polygonal curve constituted by the edges of triangles in \mathcal{T} such that $\alpha_j^n \geq \alpha_{\text{thr}}$ in the boundary triangles K_j internal to Ω_h^n , and $\alpha_j^n < \alpha_{\text{thr}}$ in every triangle external to $\partial\Omega_h^n$. However, the triangles in $\Omega_\ell \setminus \Omega_h^n$ have volume fraction in the range $(0, \alpha_{\text{thr}})$. This residual volume fraction causes a spurious growth from the term $\alpha f(\alpha, c)$ in the right hand side of (5.1a) and this effect is eliminated by modifying $\alpha f(\alpha, c)$ to $(\alpha - \alpha_{\text{thr}})^+ f(\alpha, c)$ in the right hand side of (5.17).

Numerical methods

The volume fraction equation (5.1a) is a hyperbolic conservation law. Therefore, we use a finite volume scheme with piecewise constant solutions on each triangle K_j . The piecewise constant solutions α_h^n have the added advantage of easy computation of the integrals in (5.19)–(5.20). The Lagrange $\mathbb{P}_2 - \mathbb{P}_1$ Taylor-Hood method ensures the stability of the solutions (\mathbf{u}_h^n, p_h^n) obtained from (DS.c); note that when α_h^n approaches unity, (5.1b) and (5.1c) become a Stokes system. Moreover, taking the values of \mathbf{u}_h^n at the edge mid points facilitates a straightforward computation of the numerical flux defined by (5.18). The backward in time Euler method ensures the stability of the numerical solutions c_h^n obtained from (DS.d). The mass lumped \mathbb{P}_1 finite element method and the Delaunay based triangulation are used to obtain the positivity and boundedness (by unity) of c_h^n [32].

5.6 Numerical results

The tests conducted in this section are categorised into two sets, Set-NUM and Set-NLM, corresponding to NUM and NLM models. The values of the parameters that remain the same in Set-NUM and Set-NLM are tabulated in Table 5.2. The numerical values in the

Parameter	Value	Parameter	Value
δ	0.1	μ	1
s_1, s_4	10	λ	-2/3
s_2, s_3	0.5	α_{thr}	0.01
\widehat{Q}	0	α^*	0.8

Table 5.2: Dimensionless parameters used in the numerical experiments for Set-NUM and Set-NLM.

below table are adapted from [1] in which a similar model in one spatial dimension is considered. Values of the parameters Q and η depend on specific cases and are provided in the later experiments. In all sets of experiments, the initial volume fraction is given by $\alpha(0, \mathbf{x}) = 0.8$ when $\mathbf{x} \in \Omega_h^0$ and $\alpha(0, \mathbf{x}) = 0$ when $\mathbf{x} \notin \Omega_h^0$, and the time step δ is set as 0.1 (see Remark 5.17). In all simulations, the images are represented in a large enough box that contains tumour domain depicted therein well in its interior. The MATLAB code for NUM simulations can be found at https://github.com/gopikrishnancr/2D_tumour_growth_FEM_FVM.

5.6.1 Setting for NUM simulations (Set-NUM)

We simulate the evolution of tumours starting with initial domains of the shapes as in Figures 5.3(d)–5.3(f). In all the simulations, the dimension of the square Ω_ℓ is $(-5, 5)^2$. The final time is set at $T = 20$. The triangulations are as in Figures 5.3(a)–5.3(c).

In the simulations corresponding to Figure 5.4, we set $Q = 0.5$ and $\eta = 1$. This figure shows the state of the variables: volume fraction, nutrient concentration, negative pressure, and the momentum – defined as the product of the volume fraction and the cell velocity vector field – at the time $T = 20$ from the top row to the bottom row, respectively. The columns from the left to the right depict the evolution of a tumour initially seeded with cells in the shape of a circle, bullet and semi-annulus, respectively.

5.6.2 Setting for NLM simulations (Set-NLM)

In Set-NLM tests, we study the evolution of a tumour that was initially circular. The dimension of the square Ω_ℓ is $(-5, 5)^2$ and the final time $T = 30$. We set $Q = 0.01$ and $\eta = 2$. It is worthwhile to notice that we keep η to be the same inside and outside the tumour region for simplicity. However, in a more generic situation, η will vary between the tumour region and external medium. In this set of experiments, volume fraction and nutrient

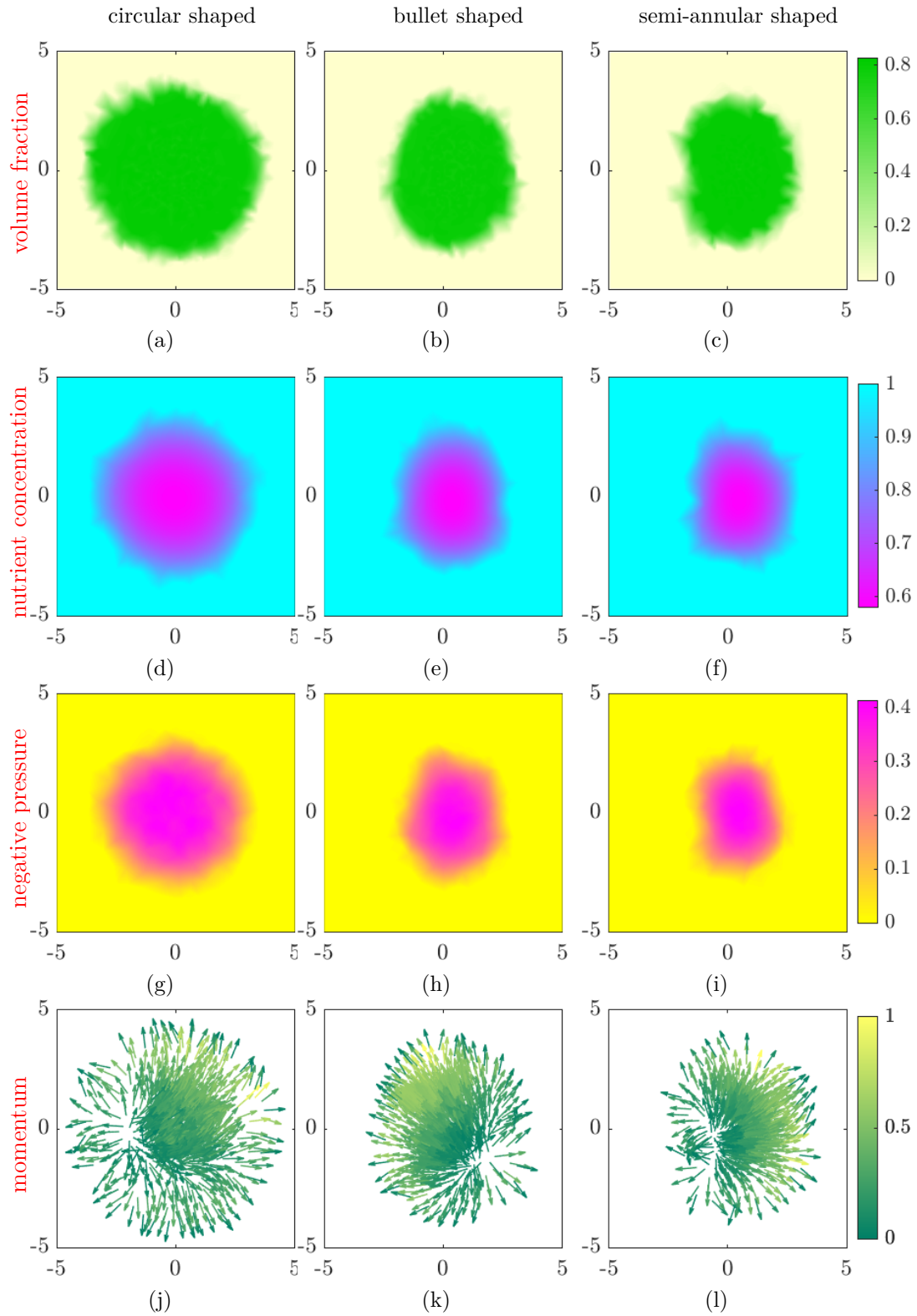


Figure 5.4: Set-NUM: Rows one to four illustrate the volume fraction, nutrient concentration, negative pressure, and cell momentum at $T = 20$, respectively. The variables in columns one to three correspond to an initial domain, $\Omega(0)$, in the shape of a circle, bullet, and semi-annulus, respectively.

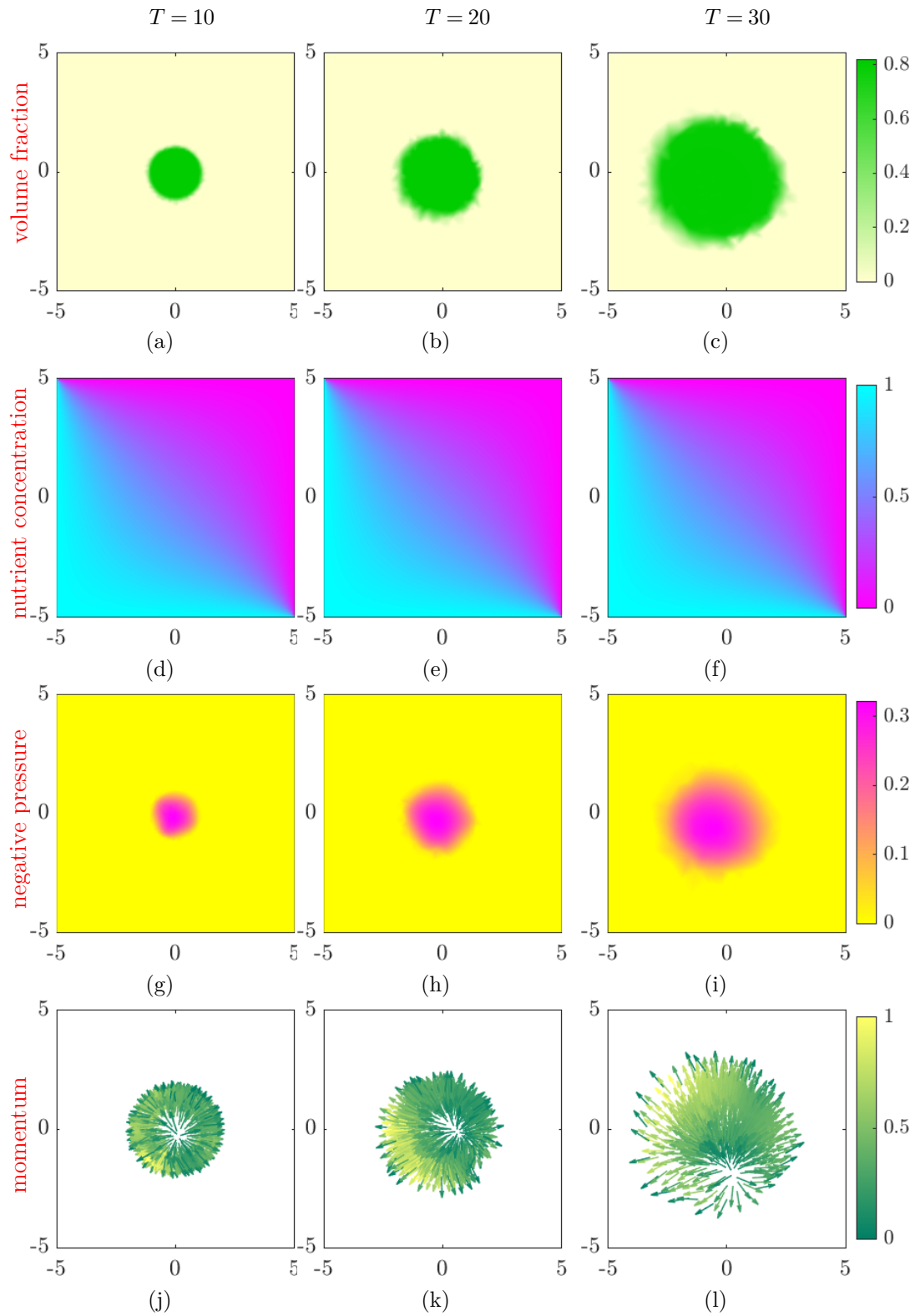


Figure 5.5: Set-NLM: Evolution of a tumour with a circular initial geometry. Rows one to four illustrate the variables volume fraction, nutrient concentration, negative pressure and cell momentum, respectively and columns one to three illustrate state of the variables at times $T = 10, 20,$ and $30,$ respectively.

concentration are solved in the entire spatial domain Ω_ℓ , while cell velocity and pressure are solved in Ω_h^n at each t_n . We set the boundary values of the nutrient concentration c as follows: $c = 0$ on $y = 5$ and $x = 5$, and $c = 1$ on $y = -5$ and $x = -5$. The initial nutrient concentration is given by $c_0(0, \mathbf{x}) = 0$. In Figure 5.5, the columns from the left to the right show the state of the variables at time $T = 10, 20$ and 30 , respectively. The rows from the top to the bottom represent, volume fraction, nutrient concentration, negative pressure, and cell momentum vector field, respectively.

5.6.3 Discussion on numerical results

Set-NUM, effect of initial tumour shape

Numerical experiments in Subsections 5.6.1 and 5.6.2 substantiate the beneficial aspects of the discrete scheme (Definition 5.15) developed in Section 5.5. This scheme is able to simulate tumour geometries with arbitrary shapes (see Figure 5.4). Firstly, we considered a tumour with unit circular shaped initial geometry in Set-NUM and in this case, the initial volume fraction is uniform and symmetric about the origin. The nutrient concentration at the boundary of the tumour is unity throughout the simulation. Therefore, the tumour does not experience any unbalanced force that disturbs its symmetry and we expect radially symmetric growth. The numerical results in Figure 5.4(a), 5.4(d), 5.4(g), and 5.4(j) confirm this argument. It is clear that the tumour is growing with radial symmetry as the volume fraction distribution in Figure 5.4(a) indicates. However, such symmetry cannot be expected for the cases with asymmetric initial geometries. This is corroborated by the numerical experiments with the bullet shaped and semi-annular shaped initial geometry. In the case of a bullet shaped initial geometry, since much of the volume fraction is distributed along the y -axis rather than along the x -axis, a natural expectation is that the vertical dimension of the tumour is longer than the horizontal dimension, which the numerical simulations show. The asymmetric growth in the case of the tumour with semi-annular initial geometry arises in a different way. The convex side of the tumour with apex at $x = 1$ grows normally outwards, while the non-convex side grows into the semi-annular gap between $y = -0.5$ and $y = 0.5$, and $x = 0$ and $x = 0.5$ (see Figure 5.4(c) and 5.4(l)).

As the tumour proliferates and expands, it becomes more difficult for the nutrient to diffuse into the interior region of tumour. The nutrient concentration distribution in Figures 5.4(d), 5.4(e), and 5.4(f) show the decreasing value of concentration towards the interior of the tumour irrespective of the initial geometry. The depletion of nutrient level inside the tumour causes cell necrosis and as result, the extra-cellular fluid tends to fill the space generated. This is clearly reflected by the fact that the fluid pressure is more negative (see Figures 5.4(g), 5.4(h), and 5.4(i)) towards the interior of the tumour and hence the fluid flow direction is from outside to inside. The cell velocity vector field shows the direction in which the cells are moving. When the initial geometry of the tumour is circular, the cells move in a radial direction with roughly equal magnitude (see Figure 5.4(j)). However, in the case of asymmetric initial geometries the cell velocity vector field is also asymmetric

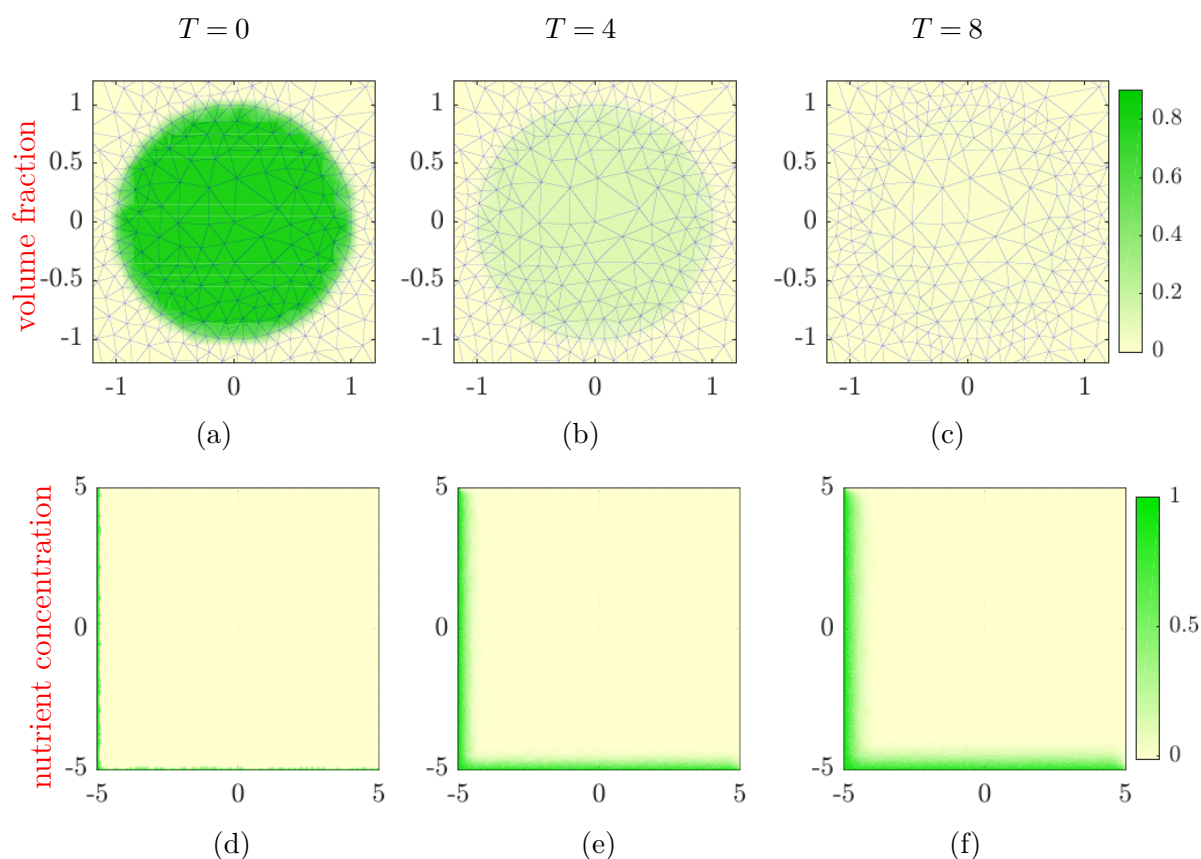


Figure 5.6: The evolution of volume fraction and nutrient concentration with $\eta = 0.1$ and $Q = 0.01$ in NLM. Observe that the cells undergo necrosis before the nutrient can reach the tumour.

(see Figures 5.4(k) and 5.4(l)).

Set-NLM, attraction towards nutrient source

The simulations for the Set-NLM test give interesting results. It can be observed from the volume fraction at times 10, 20, and 30 that the tumour grows towards the south-west corner. This affinity can be explained using the differential supply of the nutrient. The only source of the nutrient for the tumour comes from the left and bottom boundaries of the square Ω_ℓ . As Figures 5.5(d), 5.5(e) and 5.5(f) show, the nutrient diffuses from the left and the bottom boundaries towards the tumour. The tumour starts to grow when this diffused nutrient reaches its vicinity. From Figure 5.5(a), we see that the tumour has not grown, until $T = 10$, the time at which the diffused nutrient just meets the tumour boundary. The tumour starts to grow after this time as observed from Figures 5.5(b) and 5.5(c). The numerical values of Q and η are crucial in determining the fate of the tumour. In fact, the diffusivity, η , which controls the ease of nutrient to diffuse into the

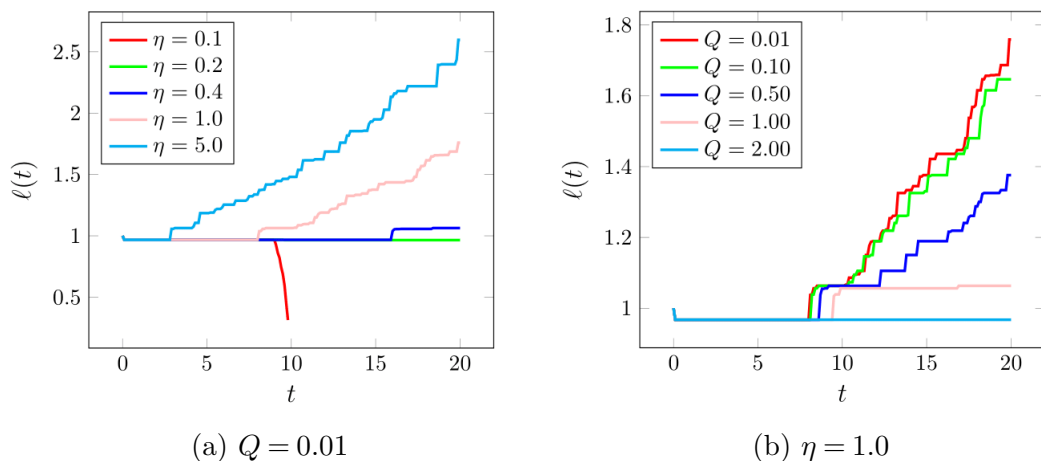


Figure 5.7: Variation of the tumour radius, $\ell(t)$ with respect to the time for different values of η and Q .

tumour and the surrounding medium needs to be high enough so that the nutrient is able to reach the tumour vicinity before all the cells die. This situation occurs with numerical values $Q = 0.01$ and $\eta = 0.1$. Here, the low value of η prevents the nutrient from reaching the tumour cells in adequate time (see Figures 5.6(d)-5.6(f)), and as a result the volume fraction of the tumour cells gradually decreases (see Figures 5.6(a)-5.6(c)). Moreover, this suggests that a higher value of η facilitates faster tumour growth owing to faster diffusion of the nutrient, and is supported by the numerical results in Figure 5.7(a). Here, the growth (set-NLM) of a tumour with circular initial geometry is studied, and we quantify the tumour size by the tumour radius, $\ell(t)$. Furthermore, we see that the tumour size decreases as Q increases, indicated by Figure 5.7(b). We note that, broadly speaking, increasing η and decreasing Q have a similar effect in producing a larger tumour volume (see Figures 5.7(a)-5.7(b)). In this way, identifiability issues may be encountered when estimating these two parameters from data that solely measures tumour size over time. However, supplementing with additional data on oxygen perfusion through cancer tissue (see, for example, [66]), we expect that both parameters could be estimated.

Grid orientation effect

The orientation of the triangulation has little effect in determining the tumour radius as illustrated in Figure 5.8. In these simulations, three rotated versions (by angles 0 , $\pi/2$ and π) of a random triangulation are used for Set-NUM experiments, with an initial tumour in the form of a disk (this ensures that the rotated triangulations remain suitable for this initial shape, see Section 5.5.3). The resulting volume fraction profiles remain mostly circular, with slight effects of the rotations but no change in the final tumour radius.

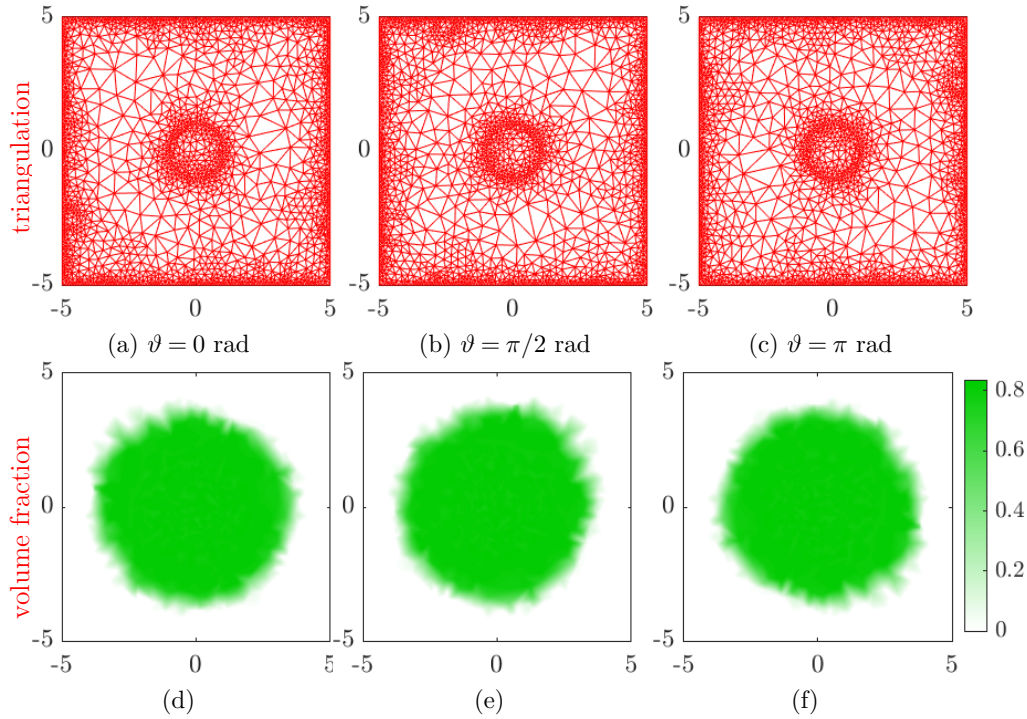


Figure 5.8: Effect of orientation of the triangulation on tumour radius. In Figures 5.8(a)–5.8(c) the triangulation is rotated anticlockwise by the angles $\vartheta = 0, \pi/2$ and π radians. The corresponding volume fraction profile at $T = 20$ with temporal discretisation factor $\delta = 0.1$ is provided in Figures 5.8(d)–5.8(f).

Handling topology changes of tumour

Another notable feature of scheme is that it can simulate tumour growth starting from highly irregular initial geometries with multiple disconnected components. Consider the growth of a tumour initially having three disconnected components with irregular boundaries. The irregularity of the initial tumour geometry is shown in Figure 5.9(a). The cell volume fraction at times $T = 0, 5, 10, 20, 20, 30,$ and 40 is plotted in Figure 5.9. As the tumour grows the multiple components merge and the tumour continues to grow as a single entity. The numerical scheme is designed in such a way that intrinsic changes in the tumour geometry like the variation in the number of connected components is seamlessly dealt with and the numerical results in Figure 5.9 support this. It can be observed from Figure 5.9(f) that a necrotic core of dead cells has developed owing to the nutrient starvation experienced at the tumour centre due to its large size. The numerical scheme captures a broad spectrum of features as discussed previously for both symmetric and asymmetric initial geometries. A key factor that helps to achieve this is the implicit recovery of the boundary using the volume fraction. In the scheme it is not required to follow the movement of each point in the boundary, which may result in overlapping of edges and other similar complexities. Defining the interior of the tumour as the union of triangles with active cell volume fraction

eliminates these issues, thereby making the numerical scheme versatile for a wide range of scenarios.

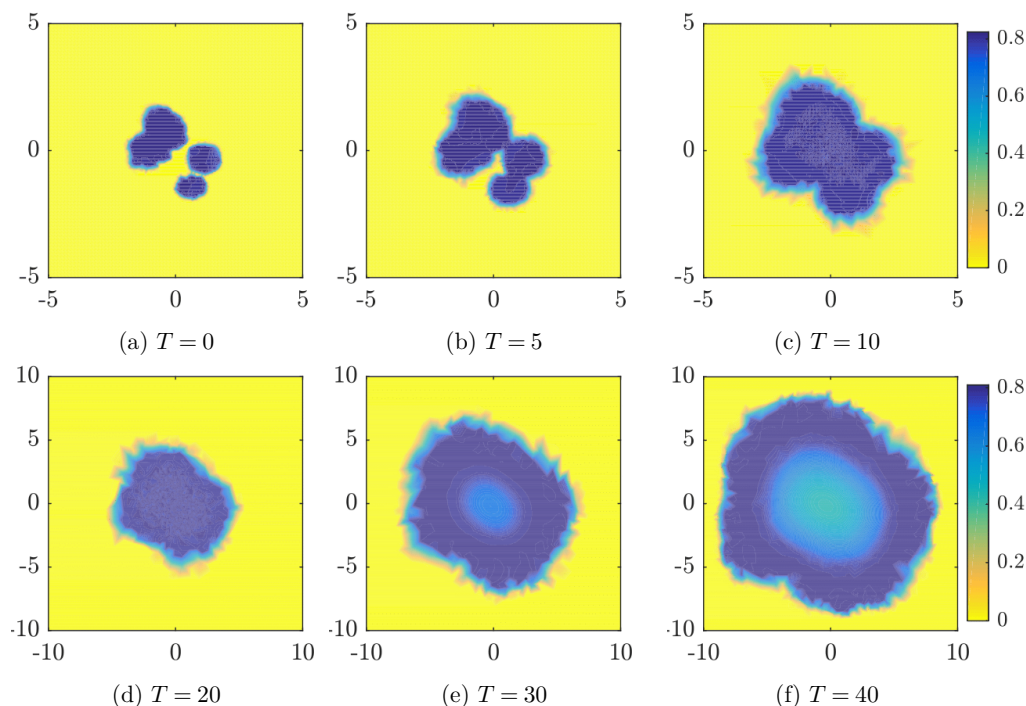


Figure 5.9: Stages of cell volume fraction for tumour growth (NUM) with an irregular initial shape having multiple initial components.

Using structured meshes

The use of a random Delaunay mesh is critical in obtaining good solutions that have minimal mesh-locking. We present the evolution of the volume fraction of a tumour starting with a circular initial geometry, simulated using structured triangulations with 1024, 4096, and 16,384 triangles in Figures 5.10(a)– 5.10(c), Figures 5.10(d)– 5.10(f), and Figures 5.10(g)– 5.10(i), respectively. The final time is set as $T = 20$, and the time step is $\delta = 0.1$. The initial geometry is circular (see Figure 5.10(g)). As the triangulations become more refined, it can be observed that the tumour becomes more radially symmetrical. This observation indicates the convergence of the discrete solutions to the radially symmetric solution as the spatial discretisation factor approaches zero. However, the tumour also becomes more squarish as time increases, as shown in Figure 5.10, showing that, for a long time, an extremely fine structure triangulation would have to be used to obtain a reasonable solution. Such refinement would come at a great cost, whereas the use of a random mesh (with adaptation only to the initial shape) provides suitable solutions with relatively few triangles.

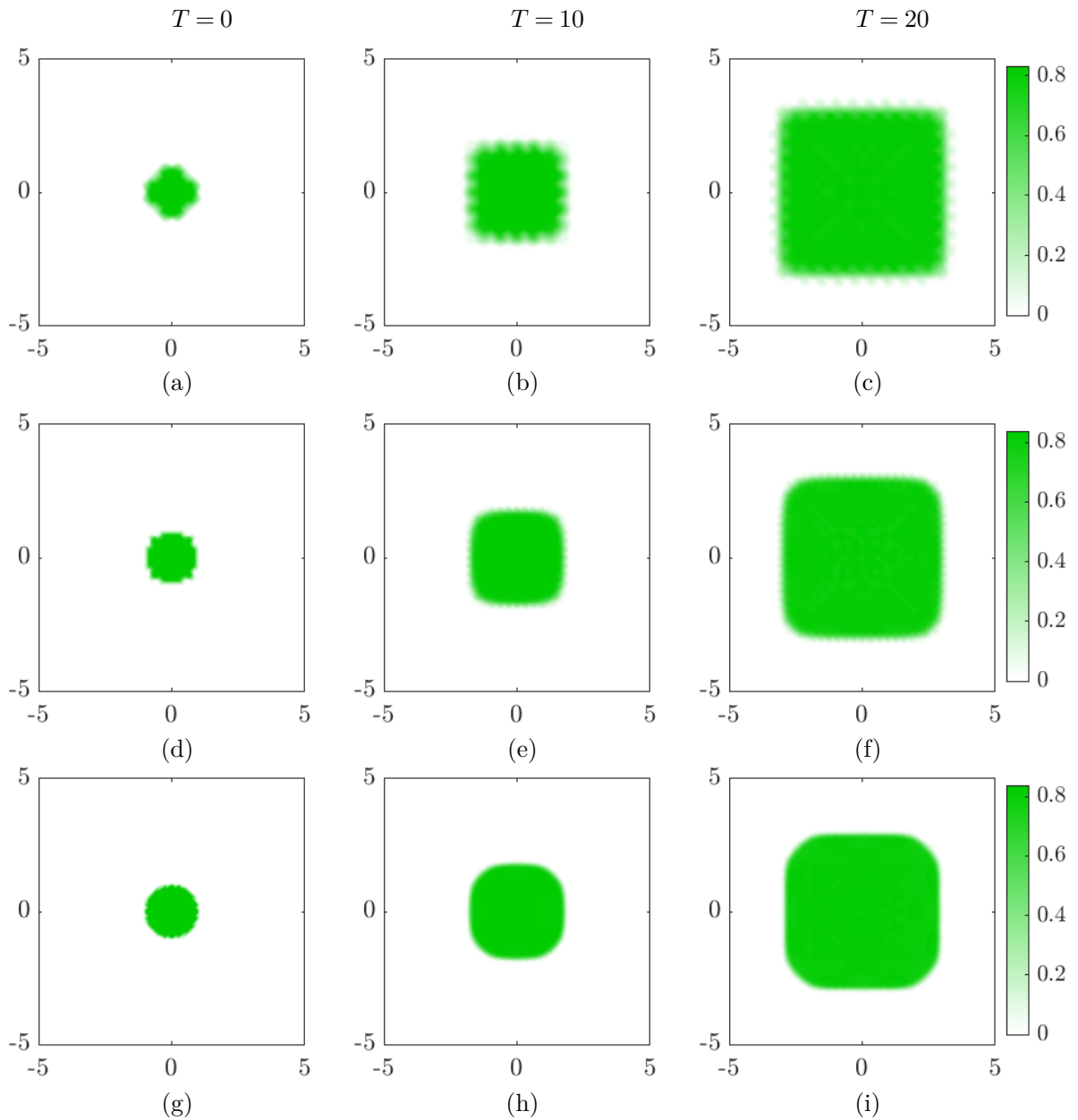


Figure 5.10: Evolution of volume fraction with respect to time on structured triangulation. The initial domain is a circle centred at origin with unit radius. Figures 5.10(a)– 5.10(c) are computed using the triangulation in Figure 5.2(a), Figures 5.10(d)– 5.10(f) are computed using the triangulation in Figure 5.2(b), and Figures 5.10(g)– 5.10(i) are computed using the triangulation in Figure 5.2(c).

Assessment of convergence

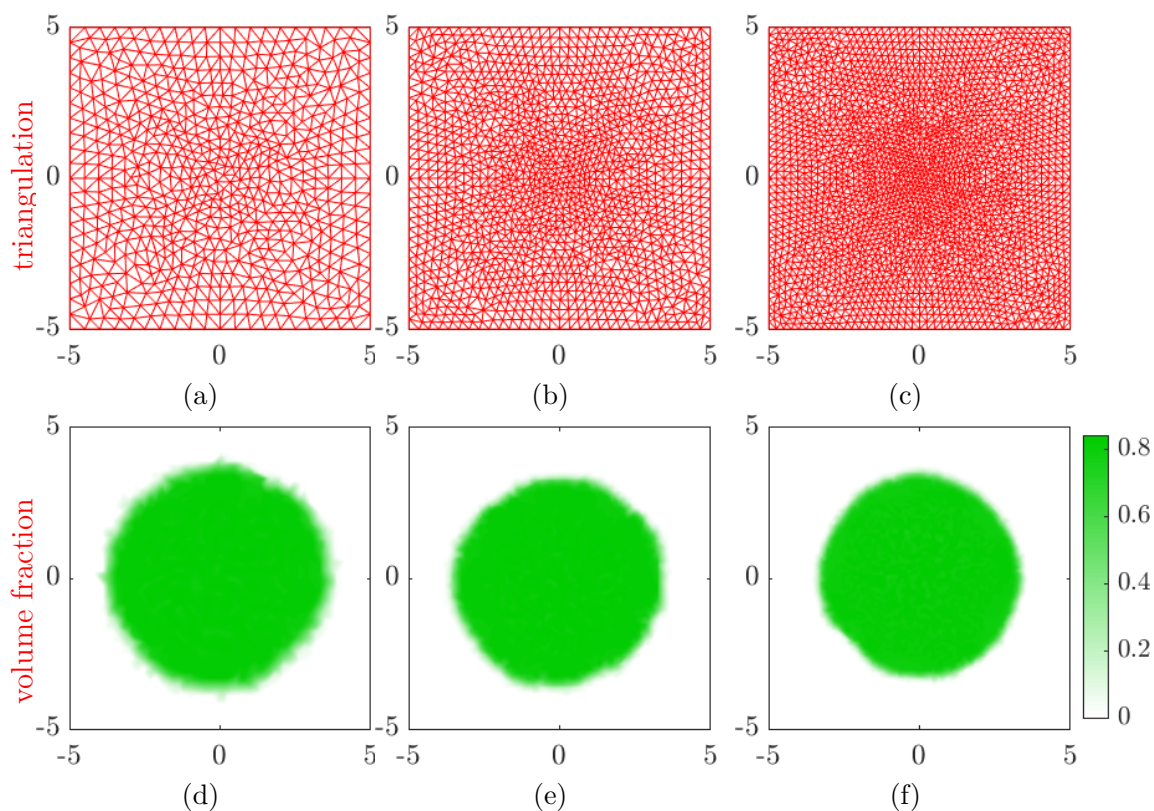


Figure 5.11: Convergence of cell volume fraction for Set-NLM with respect to the spatial discretisation factor. The triangulations in Figures 5.11(a), 5.11(b), and 5.11(c) contains 1248, 2084, and 4996 triangles. The volume fractions for Set-NLM are computed at the time $T = 20$.

The convergence of the scheme, as the grid size is reduced, is clearly observable in the case of random triangulations; see Figure 5.11. However, this convergence requires uniform refinements of the mesh, because it depends on both on a Courant–Friedrichs–Lewy (CFL) (see Remark 4.1) and on an inverse CFL relation, as demonstrated in Chapter 4. These conditions take the form

$$\underbrace{C_{\text{ICFL}} \leq \max_{0 \leq n \leq N} \sup_{\Omega_h^n} \|\mathbf{u}_h^n\|_2 \frac{\delta}{a_{\max}}}_{\text{inverse CFL condition}} \leq \overbrace{\max_{0 \leq n \leq N} \sup_{\Omega_h^n} \|\mathbf{u}_h^n\|_2 \frac{\delta}{a_{\min}}}_{\text{CFL condition}} \leq C_{\text{CFL}}, \quad (5.23)$$

where C_{ICFL} and C_{CFL} are positive constants, $a_{\max} = \max_j a_j$, $a_{\min} = \min_j a_j$, $\|\cdot\|_2$ is the Euclidean norm; recall that a_j is the area of triangle j . The temporal discretisation factor δ is fixed by the smallest triangle through the CFL condition (5.23). With this δ , at each time

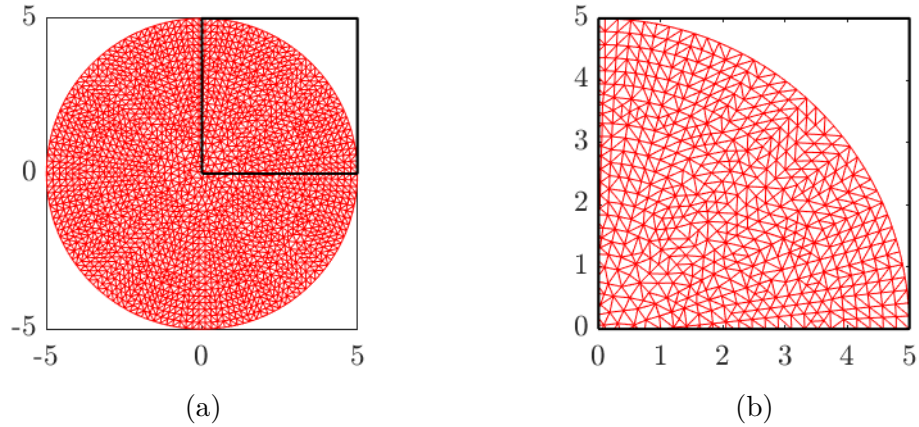


Figure 5.12: Radially aligned triangulation - Figure 5.12(a) shows the triangulation on the domain $\Omega_\ell = (-5, 5)^2$ and Figure 5.12(b) shows an enlarged view of the first quadrant.

step the diffusion of tumour cells inside the larger triangles would not be sufficient to create a volume fraction α_h^n larger than the threshold, and the tumour would not expand. Such a situation is avoided by the inverse CFL condition (5.23), which ensures a lower bound on numerical diffusion on large triangles also. Nevertheless, the CFL and inverse CFL condition together restrict the possible choices of temporal discretisation factor. Since Ruppert's algorithm performs a fine refinement on triangles near the boundaries of the initial domain and bounding box, and a relatively coarser refinement on the triangles in between these two boundaries, it leads to a refined triangulation with considerable difference in the sizes of triangles within. Therefore, in the case of very fine refinements, it is better to consider a structured triangulation well adapted to the initial condition, and then perturb the vertices of triangles randomly to remove the mesh-locking effect (see Figures 5.11(a)–5.11(c)). It can be observed from Figures 5.11(d)–5.11(f) that the volume fractions are indeed converging with mesh refinement.

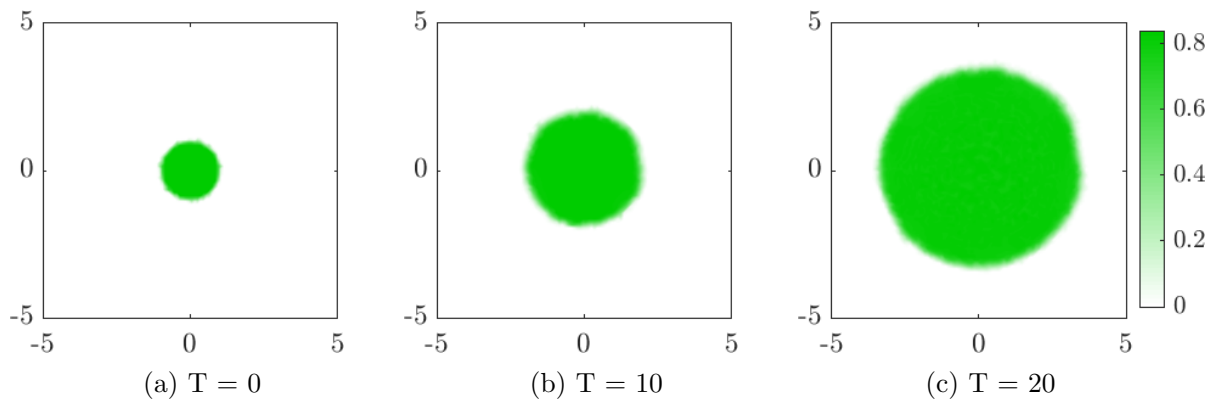
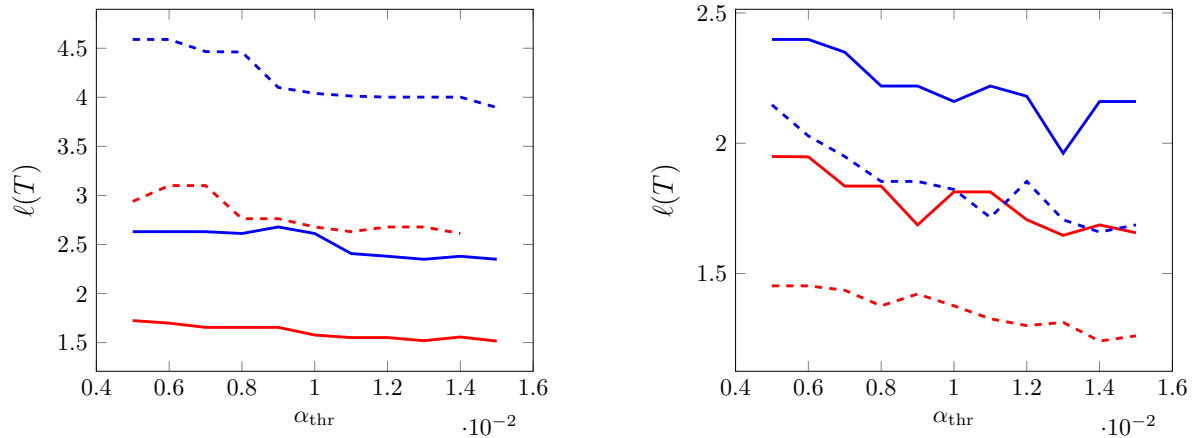


Figure 5.13: Evolution of volume fraction obtained from Set-NUM experiment on the radially aligned triangulation in Figure 5.12(a).

Mesh locking and loss of radial symmetry in the case of structured triangulations is not due to the procedure using a threshold value to capture the boundary of a tumour. Instead, this is a classical problem associated with the nature of triangulations and finite volume schemes (see subsection 5.5.2 also). If the symmetry of a discrete solution is known *a priori* and we use a triangulation that respects this symmetry, then the discrete scheme in Definition 5.15 preserves this symmetry. For instance, consider the evolution of a tumour with an initial geometry of a unit circle centred at the origin. Since the tumour is expected to evolve with a radial symmetry, we use a triangulation wherein the triangles are aligned with concentric circles centred at the origin (see Figure 5.12(a)). In this case, it can be observed from Figures 5.13(a)–5.13(c) that the discrete volume fraction remains radially symmetrical. However, this method cannot be used in the case of initial geometries like the bullet or semi-annular shape since the symmetry properties of discrete solutions are not known *a priori*. Additionally, meshing a domain respecting a present internal geometry can be complicated. In such cases, the most economically viable choice is to resort to a random triangulation.

Influence of threshold value



(a) Set-NUM: $Q = 5$ – solid lines, $Q = 0.5$ – dashed lines, $\eta = 1$ – blue lines, and $\eta = 0.1$ – red lines. (b) Set-NLM: $Q = 0.01$ – solid lines, $Q = 0.5$ – dashed lines, $\eta = 1$ – blue lines, and $\eta = 2$ – red lines.

Figure 5.14: Dependence of $\ell(T)$, where $T = 20$ on α_{thr} .

The choice of threshold value, α_{thr} , influences the evolution of the tumour radius and hence, by extension, the other variables. We cannot choose the threshold value to be too large or too small. Such a choice will incur a cascading array of high errors on the tumour radius and other variables as the time increases. A very small threshold value implies that the volume fraction is too small on triangles closer to the boundary, thus forcing the velocity–pressure system to be singular. The variation of tumour radius at the time $T = 20$

with respect to the threshold value over the range $[0.005, 0.015]$ for Set-NUM and Set-NLM experiments is provided in Figure 5.14. The radius varies by a maximum of about 15% for Set-NUM and 20% for Set-NLM as the threshold value varies from 0.005 to 0.015. Therefore, deviation in the tumour radius with respect to the threshold value is present. But, with a proper choice of the threshold value, it is possible to minimise the error in the tumour radius from the exact value [52]. Moreover, one of the main motivations for simulating cancer growth is perhaps not to get an extremely accurate representation of the tumour radius, but more to study the effect of drugs; in this situation, the simulation of the current model would serve as a baseline, to be compared with simulations obtained with a model including said drug effect, and run using the same threshold value.

5.7 Conclusions

In this chapter, a mathematically well-defined model is developed which can replicate the evolution of an avascular tumour that grows from a variety of initial geometries. The equivalent formulation in Section 5.4 and Theorem 5.12 yield a framework to design a numerical scheme that does not require explicit tracking of the time-dependent boundary associated with the tumour. The tumour domain is recovered as the union of all triangles in which the volume fraction of the tumour is greater than a fixed threshold value. While implementing the scheme, a multitude of factors, like the nature of triangulation and the threshold value need to be taken into account. For instance, we illustrate the mesh-locking effect associated with the use of structured triangulations and the advantage of using a random triangulation. The numerical results for both NUM and NLM models support the heuristic expectations and results from previous literature [1, 11]. The tests also illustrate the nutrient dependent growth of the tumour as in Figure 5.5. In addition to this, the numerical scheme seamlessly deals with the complex tumour geometries in Figure 5.9, including initially disconnected tumour groups that merge later on. The numerical results justify the ability of the scheme to take care of different irregular tumour geometries and topological structures, which in turn shows its practical applicability in simulating tumour growth from real-time clinical data. As such, the work presented here could be extended to quantify the effect of drug treatment on an evolving tumour.

Chapter 6

Strong BV estimates for FV approximations of scalar conservation laws and applications

6.1 Introduction

Consider the following scalar hyperbolic conservation law in \mathbb{R}^2 with a homogeneous source term and an initial data of bounded variation (BV):

$$\left. \begin{aligned} \partial_t \alpha + \operatorname{div}(\mathbf{u}f(\alpha)) &= 0 \text{ in } \Omega_T \text{ and} \\ \alpha(0, \cdot) &= \alpha_0 \text{ in } \Omega, \mathbf{u} = 0 \text{ in } \partial\Omega. \end{aligned} \right\} \quad (6.1)$$

where α is the unknown, $\alpha_0 : \Omega \rightarrow \mathbb{R}$ is a known *a priori* function of BV , $\mathbf{u} = (u, v)$ is the advecting velocity, $\Omega_T := (0, T) \times \Omega$, $\Omega := I \times J$, $I := (a, b) \subset \mathbb{R}$ and $J := (c, d) \subset \mathbb{R}$ are intervals. Here the divergence $\operatorname{div}(\mathbf{u})$ is not zero. The function f quantifies the amount of material advected with the velocity \mathbf{u} and is called the *flux function*. It is assumed that f is Lipschitz continuous with Lipschitz constant $\operatorname{Lip}(f)$, which is a classical assumption in literature [105]. Finite volume methods are extensively used to compute numerical solutions to (6.1) since such schemes respect the conservation of mass property associated with the underlying partial differential equation. The homogeneous boundary condition $\mathbf{u} = 0$ is only for technical simplicity. The analysis in this chapter extends to the general case with $\mathbf{u} = \mathbf{u}_b$ on $\partial\Omega$ ¹.

Literature

Total variation properties of weak and entropy solutions of (6.1) are rather classical results.

¹The work in this chapter has been accepted to publish in ESAIM: Mathematical Modelling and Numerical Analysis.: Remesan, G. C. Strong bounded variation estimates for the multi-dimensional finite volume approximation of scalar conservation laws, (36 pages), June 2021. URL: <https://arxiv.org/abs/2004.12346>

E. Conway and J. Smoller [67] studied conservation laws of the form

$$\partial_t \alpha + \sum_{j=1}^d \partial_{x_j} f_j(\alpha) = 0, \quad (6.2)$$

where BV initial data and $(f_j)_{j=1,\dots,d}$ are assumed to be in $\mathcal{C}^1(\mathbb{R};\mathbb{R})$. They studied a finite difference scheme on a uniform Cartesian grid (see Definition 6.2) and showed that discrete solutions have uniform BV . The limit solution obtained from a strongly convergent subsequence is then showed to be a weak solution and is a function with BV . N. Kuznetsov [68] provided early results on BV properties of entropy solutions of (6.2). This article [68] establishes that the BV seminorm of the entropy solution to (6.2) at any time is bounded by the BV seminorm of the initial data. M. G. Crandall and A. Majda [69] considered monotone finite difference approximations of (6.2) with BV initial data on uniform Cartesian meshes and established uniform BV estimate for discrete solutions. This estimate is used to prove the convergence of the discrete solutions to the unique entropy solution in strong L^1 -norm and to prove that the entropy solution also inherits the BV property of the discrete solutions. Later, this work was extended to nonuniform Cartesian meshes by R. Sanders [70]. B. Merlet and J. Vovelle [71, 72] considered linear advection equations of the form (6.1) with $f(\alpha) = \alpha$, $\mathbf{u} \in W^{1,\infty}(\mathbb{R}^+ \times \mathbb{R}^d; \mathbb{R}^d)$, and $\operatorname{div}(\mathbf{u}(t, \cdot)) = 0$. The BV seminorm of the unique weak solution of this problem, constructed using the characteristic method, is bounded and the bound depends on the BV seminorm of the initial data. However, discrete solutions corresponding to this problem obtained by using finite volume schemes on general polygonal meshes are not proved to satisfy a uniform BV estimate (see the Remark 1.5 in [72, p. 7]). In fact, to show that the finite volume solutions converge to the entropy solution, whose existence is known *a priori*, it is enough to have a weak BV estimate [73, p. 143][105, p. 161] of the following form

$$\sum_{n=0}^N \delta \sum_{e \in \mathcal{E}} |f(\alpha_e^n) - f(\alpha_e^{n+1})| \left| \int_e \mathbf{u}(t_n, \cdot) \cdot \mathbf{n}_e \, ds \right| \leq Ch^{-1/2}, \quad (6.3)$$

where δ is the temporal discretisation factor, h is the spatial discretisation factor, \mathcal{E} is the set of mesh edges, \mathbf{n}_e is a unit normal to e , $\alpha_e^{(p/n)}$ are the values of the discrete solution on the neighbouring polygons of e . The weak BV estimate ensures convergence in nonlinear weak- $*$ sense (see Definition 6.3 in [105, p. 100]) to a Young measure, called a *process solution*. In this scenario, the nonlinear weak- $*$ convergence actually becomes strong L^p convergence (see Theorem 6.4 and 6.5 in [105, p. 187-188]). Uniqueness of the process solution is crucial in this technique and hence, it is difficult to use it in the case of coupled systems like those appearing in tumour growth models. The relationship between process solution and function solution is not very clear in this case and an *a priori* compactness result like a uniform BV estimate appears necessary to obtain strong L^p convergence.

A recent uniform BV estimate on finite volume solutions of conservation laws of the form (6.2) on uniform Cartesian grid is obtained by K. H. Karlsen and J. D. Towers [74].

They consider (6.2) with an auxiliary boundary condition $\mathbf{f} \cdot \mathbf{n}_\Omega = 0$, where \mathbf{n}_Ω is the outward unit normal to $\partial\Omega$. C. Chainais-Hillairet [75] also provides a uniform BV estimate on finite volume solutions of fully nonlinear conservation laws on uniform square Cartesian grids (see subsection 6.5 for details).

In [105, p. 153], it is stated that weak BV estimates may be extended to the case with $\operatorname{div}(\mathbf{u}) \neq 0$. It is also mentioned in [105, p. 154] that BV estimates in higher dimensional Cartesian grids reduces to a one dimensional discretisation. However, the corresponding proofs are not provided.

Contributions

In all of the works reviewed above, either the advecting velocity vector is component-wise constant (see (6.2)) or the advecting velocity is assumed to be divergence-free. However, these may not be realistic assumptions in applications as evident from (6.5) below. While discretising physical models, it is imperative to refine the regions where discontinuities of the solution are expected and to retain other regions relatively coarse so that the scheme remains economical. A uniform BV estimate is crucial in enabling the nonlinear terms to converge and hence to prove existence of a solution.

The main contributions of this chapter are stated below.

- A standard assumption in the literature that deals with hyperbolic conservation laws is that $\operatorname{div}(\mathbf{u}) = 0$. This assumption is relaxed for the conservation law (6.1) and subsequent analysis in this chapter.
- A finite volume scheme on nonuniform Cartesian grids in two-dimensions is considered, and the analysis holds in general for the class of monotone numerical fluxes. The nonuniformity of Cartesian grid can be used to refine the mesh adaptively and economically.
- A strong BV estimate for nonlinear conservation laws in three spatial dimensions is derived.
- Finite volume solutions satisfy a uniform BV estimate in space and time and this result is extended to the case of fully nonlinear conservation laws [75].
- The existence of a weak solution for a tumour growth model is shown by utilising the BV estimates on Cartesian grids. Compactness results rendered by uniform BV estimates present a convergent subsequence out of a family of discrete solutions constructed by applying a finite volume scheme to (6.5a) to the model.

The uniform BV estimate in space and time for linear and nonlinear conservation laws is obtained by computing the variation of the discrete solution along orthogonal Cartesian axes separately. This method has two major difficulties. Firstly, the term $\alpha \operatorname{div}(\mathbf{u})$ serves as an additional source function since divergence of the velocity field is not zero. The difference of $\alpha \operatorname{div}(\mathbf{u})$ at time step t_{n+1} across neighbouring control volumes is estimated in terms of

the BV seminorm of $\operatorname{div}(\mathbf{u})$ and L^∞ bound of α at time step t_n . Secondly, while estimating the difference of the discrete solution across two control volumes in one direction, we obtain terms that contain differences of numerical fluxes across the other orthogonal direction and vice-versa. This is a potential obstacle to the standard technique of writing the variation of the discrete solution at t_{n+1} across two control volumes as a convex linear combination of variations of the discrete solutions across neighbouring control volumes at t_n . We introduce the idea of an intermediate nodal (edge) flux in two (three) spatial dimensions, which is the numerical flux across control volumes sharing only a single vertex (edge), to transform the differences along y and z directions into that along x direction and vice-versa. This helps to obtain a relation of the form

$$BV(n+1) \leq BV(n) + \int_{t_n}^{t_{n+1}} A(t) dt, \quad (6.4)$$

where $BV(n)$ is the BV seminorm of the discrete solution at t_n , and $A(t)$ depends on BV seminorm of $\operatorname{div}(\mathbf{u})$ and $\|\nabla \mathbf{u}(t, \cdot)\|_{L^\infty(\Omega)}$. Finally, an application of induction on (6.4) yields the BV estimate on the discrete solution.

Organisation

This chapter is organised in the following fashion. The models are presented in Section 6.2. In Section 6.3, we present the necessary notations, assumptions, function spaces, and the finite volume scheme. Section 6.3 also presents the main results. This includes the strong BV estimates on finite volume solution of nonlinear conservation laws in 2D and 3D and existence of a weak solution for a tumour growth model in 2D. The proofs of uniform BV estimate of finite volume solutions of (6.1) is presented in Section 6.4. In Section 6.5, we show the uniform BV estimate for conservation laws with fully nonlinear flux. The numerical results and discussion are presented in Section 6.6. The uniform BV estimate for scalar conservation laws in three spatial dimensions is presented in Section 6.7. The semi-discrete analysis that proves the existence of a weak solution of the tumour growth model is conducted in Section 6.8. The conclusions are presented in Section 6.9.

6.2 Applications

Conservation laws of the form (6.1) are crucial in practical applications. Usually they model density or concentration of a conserved quantity in a coupled system, where the conservation law is strongly entangled with the equation that governs the advecting velocity, and with other governing equations, if present. This coupled nature renders the advecting velocity as a nonlinear function of the concentration of the conserved variable. Moreover, the velocity vector field \mathbf{u} is not necessarily divergence-free, see (6.5b). The divergence of the velocity field manifests as a source term in (6.1). Hence, while attempting to obtain a uniform BV estimate on discrete solutions of (6.1), we need to also account for divergent velocity vector fields. As a result the current BV results available in the literature with the assumption

$\operatorname{div}(\mathbf{u}) = 0$ cannot be directly applied to such conservation laws. Two examples are provided next. The existence of a weak solution to the first example is proved in this chapter. The second example is more complex than the first one and is a subject of future research.

Example 1. A wide class tumour growth models based on multiphase mixture theory [6] contain a coupled system of a conserved variable and corresponding advecting velocity. For instance consider an *in vivo* model developed by S. J. Franks et al. [29] that depicts *ductal carcinoma in situ* – the initial stage of breast cancer. In two spatial dimensions, the model describes the evolution of an advancing tissue in a cylindrical domain with rigid walls, see Figure 6.1.

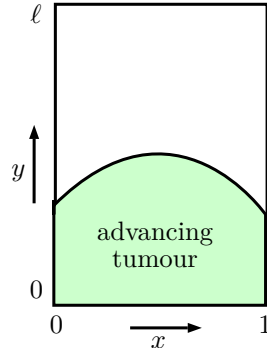


Figure 6.1: Advancing tumour in the duct $(0, 1) \times (0, \ell)$

To keep the discussion simple, we consider the model with simplified kinetics, wherein the viscosity, denoted by μ , inside and outside the tumour is assumed to be uniform and divergence of the velocity field is assumed to depend only on nutrient concentration. The domain of tumour growth is denoted by $\Omega = \{\mathbf{x} := (x, y) : 0 \leq x \leq 1, 0 \leq y \leq \ell\}$. Here, x is the radial distance, y is the axial distance, and $\ell > 2$ is the duct length. For $T < \infty$, the time–space domain is denoted by $\Omega_T = (0, T) \times \Omega$ and $t \in (0, T)$ is the time variable. Model variables are the concentration of the tumour cells $\alpha(t, \mathbf{x})$, the velocity of the tumour cells $\mathbf{u}(t, \mathbf{x}) := (u(t, \mathbf{x}), v(t, \mathbf{x}))$, pressure inside the tumour $p(t, \mathbf{x})$, and the nutrient concentration $c(t, \mathbf{x})$. The model seeks a four tuple $(\alpha, p, \mathbf{u}, c)$ such that, in Ω_T it holds

$$\text{tumour cell concentration} \begin{cases} \frac{\partial \alpha}{\partial t} + \operatorname{div}(\mathbf{u}\alpha) = \gamma\alpha(1 - c), \end{cases} \quad (6.5a)$$

$$\text{velocity – pressure system} \begin{cases} -\mu \left(\Delta \mathbf{u} + \frac{1}{3} \nabla(\operatorname{div}(\mathbf{u})) \right) + \nabla p = \mathbf{0}, \\ \operatorname{div}(\mathbf{u}) = \gamma(1 - c), \text{ and} \end{cases} \quad (6.5b)$$

$$\text{nutrient concentration} \begin{cases} -\Delta c = Q\alpha, \end{cases} \quad (6.5c)$$

with appropriate boundary conditions. In (6.5a), γ is a positive constant that controls the rate of cell division and in (6.5c), Q is a positive constant that controls the nutrient intake by the cells.

Example 2. Another example is the two-phase tumour spheroid growth problem, see Chapter 5, where the velocity of the tumour cells \mathbf{u} is governed by

$$\left. \begin{aligned} -\operatorname{div}\left(\mu\alpha(\nabla\mathbf{u}+(\nabla\mathbf{u})^T)+\lambda\alpha\operatorname{div}(\mathbf{u})\mathbb{I}_2\right)+\nabla p &= -\nabla\left(\frac{(\alpha-\alpha^*)^+}{(1-\alpha)^2}\right) \text{ and} \\ -\operatorname{div}\left(\frac{1-\alpha}{k\alpha}\nabla p\right)+\operatorname{div}(\mathbf{u}) &= 0, \end{aligned} \right\}$$

where μ and λ are the viscosity coefficients, k is the traction coefficient, α^* is a positive parameter that controls intra-cellular attraction, p is the pressure, \mathbb{I}_2 is the 2×2 identity tensor, and α evolves with respect to (6.1) with a nonlinear source function in α .

An interesting non-biological example is the compressible magento-hydrodynamic system. P. Chandrashekar and C. Klingenberg has studied finite volume solutions of this system in [76] and several numerical examples are presented. To show that a possible limit of discrete solutions obtained from a finite volume scheme applied to (6.1) satisfies (6.5) and hence to prove the existence of a solution, we need to establish that the discrete solutions converge to the limit in strong L^p -norm, where $p \geq 1$. Otherwise, it becomes challenging, and perhaps infeasible, to apply pass to the limit arguments on functions of α appearing in (6.5). A possible way to obtain strong L^p -norm convergence is to show that the discrete solutions have uniform BV and invoke Helly's selection theorem (Theorem I of Section 1.4) to extract a strongly converging subsequence.

6.3 Main results

Four main results are presented in this chapter. The first three results establish uniform bounded variation estimates in space and time for

- conservation laws in two spatial dimensions of the form $\partial_t\alpha + \operatorname{div}(\mathbf{u}f(\alpha)) = 0$ in Theorem 6.4.
- conservation laws in two spatial dimensions with fully nonlinear flux of the form $\partial_t\alpha + \operatorname{div}(\mathbf{F}(t, \mathbf{x}, \alpha)) = 0$ in Theorem 6.9.
- conservation laws in three spatial dimensions of the form $\partial_t\alpha + \operatorname{div}(\mathbf{u}f(\alpha)) = 0$ in Theorem 6.48.

The fourth main result, see Theorem 6.24, presented in Section 6.8 applies Theorem 6.4 to establish the existence of a weak solution to the practical problem of interest (6.5).

6.3.1 Preliminaries

Definition 6.1. A function $\beta \in L^1(\mathcal{A})$, where \mathcal{A} is an open set in \mathbb{R}^d with $d \geq 1$, is of BV if $|\beta|_{BV_{\mathbf{x}}(\mathcal{A})} < \infty$, where

$$|\beta|_{BV_{\mathbf{x}}(\mathcal{A})} := \sup \left\{ \int_{\mathcal{A}} \beta \operatorname{div}(\boldsymbol{\varphi}) \, d\mathbf{x} : \boldsymbol{\varphi} \in \mathcal{C}_c^1(\mathcal{A}; \mathbb{R}^d), |\boldsymbol{\varphi}|_{L^\infty(\mathcal{A})} \leq 1 \right\}.$$

The space $BV_{\mathbf{x}}(\mathcal{A})$ is the vector space of functions $\beta \in L^1(\mathcal{A})$ with BV . Recall that in this chapter $\Omega_T = (0, T) \times \Omega$, where $\Omega = (a, b) \times (c, d)$. Then, define the following BV seminorms for a function $\beta : \Omega_T \rightarrow \mathbb{R}$:

$$\begin{aligned} |\beta(t, \cdot)|_{L_y^1 BV_x} &:= \int_{\mathbf{J}} |\beta(t, \cdot, y)|_{BV_x(\mathbf{I})} dy, & |\beta(t, \cdot)|_{L_x^1 BV_y} &:= \int_{\mathbf{I}} |\beta(t, x, \cdot)|_{BV_y(\mathbf{J})} dx, \\ |\beta(t, \cdot)|_{BV_{x,y}} &:= |\beta(t, \cdot)|_{L_y^1 BV_x} + |\beta(t, \cdot)|_{L_x^1 BV_y}, \\ |\beta|_{L_t^1 BV_{x,y}} &:= \int_0^T |\beta(t, \cdot)|_{BV_{x,y}} dt, & |\beta|_{L_{x,y}^1 BV_t} &:= \int_{\Omega} |\beta(\cdot, x, y)|_{BV_t(0,T)} dx dy, \text{ and} \\ |\beta|_{BV_{x,y,t}} &:= |\beta|_{L_{x,y}^1 BV_t} + |\beta|_{L_t^1 BV_{x,y}}. \end{aligned} \quad (6.6)$$

Also, define the following norms for a function $v : X_T \rightarrow \mathbb{R}^d$ ($d \geq 1$), where $X_T := (0, T) \times X$:

$$\|v\|_{L_t^1 L^\infty(X_T)} := \int_0^T \|v(t, \cdot)\|_{L^\infty(X)} dt \quad \text{and} \quad \|v\|_{L_t^\infty L^1(X_T)} := \sup_{0 < t < T} \|v(t, \cdot)\|_{L^1(X)}.$$

For a function $\beta : (a, b) \rightarrow \mathbb{R}$, define the total variation by $\text{TV}(\beta) := \sup_P \sum_{i=0}^I |\beta(x_{i+1}) - \beta(x_i)|$, where $P := \{a = x_0, \dots, x_{I+1} = b\}$ is any partition of (a, b) . It is a classical result that $|\beta|_{BV_x(a,b)} = \text{TV}(\beta)$ [111, Appendix A].

Definition 6.2 (two dimensional admissible grid). *Let $X_k := \{x_{-1/2}, \dots, x_{I+1/2}\}$ and $Y_h := \{y_{-1/2}, \dots, y_{J+1/2}\}$, where $x_{-1/2} = a$, $x_{I+1/2} = b$, $y_{-1/2} = c$, $y_{J+1/2} = d$, $k_i = x_{i+1/2} - x_{i-1/2}$, $h_j = y_{j+1} - y_{j-1/2}$, $h = \max_i h_i$, and $k = \max_j k_j$. The Cartesian grid $X_k \times Y_h$ is said to be a two dimensional admissible grid if for a fixed constant $\tilde{c} > 0$, it holds that $\tilde{c}^{-1} \leq \frac{h_j}{k_i} \leq \tilde{c} \forall i, j$. If $k_i = k \forall i$ and $h_j = h \forall j$, then $X_k \times Y_h$ is called a uniform Cartesian grid and otherwise a nonuniform Cartesian grid, see Figure 6.2.*

We assume that (AS.1)–(AS.3) below hold.

- (AS.1) The flux $f : \mathbb{R} \rightarrow \mathbb{R}$ and the numerical flux $g : \mathbb{R}^2 \rightarrow \mathbb{R}$ are Lipschitz continuous with Lipschitz constants $\text{Lip}(f)$ and $\text{Lip}(g)$, respectively.
- (AS.2) The numerical flux g is monotonically nondecreasing in the first variable and nonincreasing in the second variable, and satisfies $g(a, a) = f(a) \forall a \in \mathbb{R}$.
- (AS.3) There exists a constant $\mathcal{C} \geq 0$ such that

$$\max \left(\|\mathbf{u}\|_{L_t^1 L^\infty(\Omega_T)}, \|\nabla \mathbf{u}\|_{L_t^1 L^\infty(\Omega_T)}, |\text{div}(\mathbf{u})|_{L_t^1 BV_{x,y}} \right) \leq \mathcal{C} < \infty.$$

6.3.2 Presentation of the numerical scheme

Define the spatial discretisation factor h_{\max} by $h_{\max} = \max_{i,j} \{k_i, h_j\}$, which quantifies the size of the Cartesian grid $X_k \times Y_h$. Let T_δ defined by $T_\delta := \{t_0, \dots, T_N\}$ be a discretisation

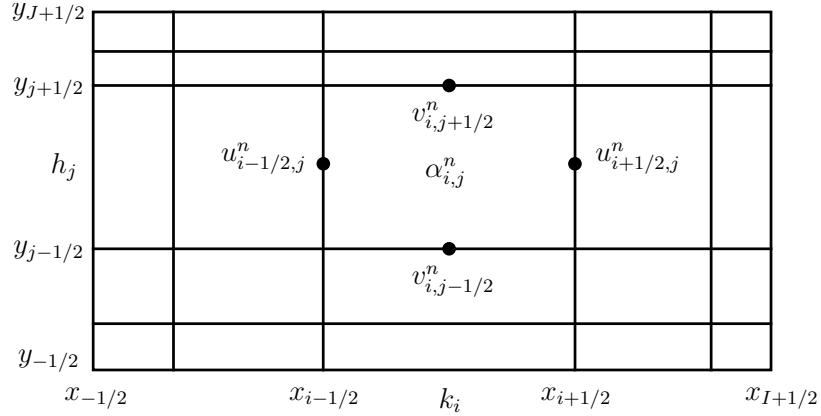


Figure 6.2: Rectangular grid and locations of the velocities and discrete unknowns $\alpha_{i,j}^n$.

of $(0, T)$, where $t_0 = 0$ and $t_N = T$. Define the temporal discretisation factor by $\delta = \max_n \delta_n$, where $\delta_n = t_{n+1} - t_n$. For technical simplicity a uniform temporal discretisation is taken, wherein $\delta_n = \delta \forall n$. However, note that the results in this chapter hold with a nonuniform temporal discretisation also.

Integrate (6.1) over $(t_{n+1}, t_n) \times K_{ij}$, where $K_{ij} = (x_{i-1/2}, x_{i+1/2}) \times (y_{j-1/2}, y_{j+1/2})$, and apply the divergence theorem to obtain

$$0 = \int_{t_n}^{t_{n+1}} \int_{K_{ij}} \partial_t \alpha \, d\mathbf{x} dt + \int_{t_n}^{t_{n+1}} \int_{\partial K_{ij}} f(\alpha)(u, v) \cdot \mathbf{n}_{ij} \, ds dt =: I_1 + I_2, \quad (6.7)$$

where \mathbf{n}_{ij} is the outward unit normal to ∂K_{ij} and $\mathbf{u} = (u, v)$. Replace I_1 by the difference formula $k_i h_j (\alpha_{i,j}^{n+1} - \alpha_{i,j}^n)$. Term I_2 in (6.7) is approximated by the numerical flux $g: \mathbb{R}^2 \rightarrow \mathbb{R}$ as $\delta h_j (F_{i+1/2,j}^n - F_{i-1/2,j}^n) + \delta k_i (G_{i,j+1/2}^n - G_{i,j-1/2}^n)$, where

$$\begin{aligned} F_{i-1/2,j}^n &:= \left(u_{i-1/2,j}^{n+} g(\alpha_{i-1,j}^n, \alpha_{i,j}^n) - u_{i-1/2,j}^{n-} g(\alpha_{i,j}^n, \alpha_{i-1,j}^n) \right), \\ G_{i,j-1/2}^n &:= \left(v_{i,j-1/2}^{n+} g(\alpha_{i,j-1}^n, \alpha_{i,j}^n) - v_{i,j-1/2}^{n-} g(\alpha_{i,j}^n, \alpha_{i,j-1}^n) \right), \end{aligned} \quad (6.8)$$

$a^+ = \max(a, 0)$, and $a^- = -\min(a, 0)$ for $a \in \mathbb{R}$,

$$u_{i-1/2,j}^n = \int_{t_n}^{t_{n+1}} \int_{y_{j-1/2}}^{y_{j+1/2}} u(t, x_{i-1/2}, s) \, ds dt \quad \text{and} \quad v_{i,j-1/2}^n = \int_{t_n}^{t_{n+1}} \int_{x_{i-1/2}}^{x_{i+1/2}} v(t, s, y_{j-1/2}) \, ds dt,$$

where \int_A is the averaging integral over the set A . Locations of the discrete unknowns $\alpha_{i,j}^n$, velocities $u_{i-1/2,j}$ and $v_{i,j-1/2}$ in a two dimensional admissible grid is shown in Figure 6.2. A substitution of approximations of I_1 and I_2 in (6.7) leads to

$$\alpha_{i,j}^{n+1} = \alpha_{i,j}^n - \mu_i (F_{i+1/2,j}^n - F_{i-1/2,j}^n) - \lambda_j (G_{i,j+1/2}^n - G_{i,j-1/2}^n), \quad (6.9a)$$

where $\mu_i = \delta/k_i$ and $\lambda_j = \delta/h_j$. We set the discrete initial data as follows

$$\alpha_{i,j}^0 := \int_{K_{i,j}} \alpha_0(\mathbf{x}) d\mathbf{x}. \quad (6.9b)$$

The terms $F_{i,j}^n$ and $G_{i,j}^n$ can be expressed as, for $s \in \{-1, 1\}$,

$$F_{i+s/2,j}^n = M_{i+s/2,j}^x \left[\frac{(1-s)}{2} (\alpha_{i-1,j}^n - \alpha_{i,j}^n) + \frac{(1+s)}{2} (\alpha_{i,j}^n - \alpha_{i+1,j}^n) \right] + u_{i+s/2,j}^n f(\alpha_{i,j}^n) \quad \text{and} \quad (6.10a)$$

$$G_{i,j+s/2}^n = M_{i,j+s/2}^y \left[\frac{(1-s)}{2} (\alpha_{i,j-1}^n - \alpha_{i,j}^n) + \frac{(1+s)}{2} (\alpha_{i,j}^n - \alpha_{i,j+1}^n) \right] + v_{i,j+s/2}^n f(\alpha_{i,j}^n), \quad (6.10b)$$

where

$$M_{i-1/2,j}^x := \left[u_{i-1/2,j}^{n+} D_{i,j}^n(\alpha_{i-1,j}^n, \alpha_{i,j}^n) + u_{i-1/2,j}^{n-} D_{i,j}^n(\alpha_{i,j}^n, \alpha_{i-1,j}^n) \right],$$

$$M_{i,j-1/2}^y := \left[v_{i,j-1/2}^{n+} D_{i,j}^n(\alpha_{i,j-1}^n, \alpha_{i,j}^n) + v_{i,j-1/2}^{n-} D_{i,j}^n(\alpha_{i,j}^n, \alpha_{i,j-1}^n) \right],$$

and the difference quotient $D_{i,j}^n : \mathbb{R}^2 \rightarrow \mathbb{R}$ is defined by

$$D_{i,j}^n(a, b) = \begin{cases} \frac{g(a, b) - g(\alpha_{i,j}^n, \alpha_{i,j}^n)}{a - b} & \text{if } a \neq b, \text{ and} \\ 0 & \text{if } a = b. \end{cases}$$

Observe that $D_{i,j}^n(\alpha_{i-1,j}^n, \alpha_{i,j}^n)$, $D_{i,j}^n(\alpha_{i,j}^n, \alpha_{i-1,j}^n)$, $D_{i,j}^n(\alpha_{i,j}^n, \alpha_{i,j-1}^n)$, and $D_{i,j}^n(\alpha_{i,j-1}^n, \alpha_{i,j}^n)$, (hence, $M_{i-1/2,j}^x$ and $M_{i,j-1/2}^y$) are nonnegative due to the monotonicity of g . Use (6.10a) and (6.10b) to transform the right hand side of (6.9a) into a convex linear combination of the terms $\alpha_{l,m}^n$, where $(l, m) \in \{(i, j), (i-1, j), (i+1, j), (i, j+1), (i, j-1)\}$, and this yields an alternate form of the discrete scheme (6.9a)

$$\begin{aligned} \alpha_{i,j}^{n+1} &= \alpha_{i,j}^n \left(1 - \mu_i M_{i+1/2,j}^x - \lambda_j M_{i,j+1/2}^y - \mu_i M_{i-1/2,j}^x - \lambda_j M_{i,j-1/2}^y \right) \\ &\quad + \alpha_{i+1,j}^n \mu_i M_{i+1/2,j}^x + \alpha_{i,j+1}^n \lambda_j M_{i,j+1/2}^y + \alpha_{i-1,j}^n \mu_i M_{i-1/2,j}^x + \alpha_{i,j-1}^n \lambda_j M_{i,j-1/2}^y \\ &\quad - f(\alpha_{i,j}^n) \left(\int_{t_n}^{t_{n+1}} \int_{K_{i,j}} \operatorname{div}(\mathbf{u})(t, \mathbf{x}) dt d\mathbf{x} \right). \end{aligned} \quad (6.11)$$

Definition 6.3 (Time-reconstruct). *For a sequence of functions $(f_n)_{\{n \geq 0\}}$, where $f_n : X \rightarrow \mathbb{R}$, define the corresponding time-space reconstruct $f_{h,\delta} : (0, T) \times X \rightarrow \mathbb{R}$ almost everywhere in time by $f(t, \cdot) := f_n(\cdot)$ for every $t \in (t_n, t_{n+1})$.*

The function $\alpha_{h,\delta} : \Omega_T \rightarrow \mathbb{R}$ is the time-space reconstruct corresponding to the sequence of functions $(\alpha_{h,k}^n)_{\{n \geq 0\}}$, where $\alpha_{h,k}^n(\mathbf{x}) := \alpha_{i,j}^n$ on $K_{i,j}$.

Theorem 6.4 (bounded variation). *Let $X_k \times Y_h$ be a two-dimensional admissible grid, and assumptions (AS.1)–(AS.3) and the Courant–Friedrichs–Lewy (CFL) condition*

$$4\delta \max_{i,j} \left(\frac{1}{k_i} + \frac{1}{h_j} \right) \text{Lip}(g) \|\mathbf{u}\|_{L^\infty(\Omega_T)} \leq 1$$

hold. If $\alpha_0 \in L^\infty(\Omega) \cap BV_{\mathbf{x}}(\Omega)$, then $\alpha_{h,\delta}$ satisfies $|\alpha_{h,\delta}|_{BV_{x,y,t}} \leq \mathcal{C}_{\text{BV}}$, where \mathcal{C}_{BV} depends on T , α_0 , f , g , $\|\nabla \mathbf{u}\|_{L_t^1 L^\infty(\Omega_T)}$, and $|\text{div}(\mathbf{u})|_{L_t^1 BV_{x,y}}$.

Remark 6.5 (Boundedness constant \mathcal{C}_{BV}). *The exact dependency of \mathcal{C}_{BV} on the factors T , α_0 , and Lipschitz continuity of fluxes is obtained from the proofs of Propositions 6.7 and 6.8. The final expression for \mathcal{C}_{BV} is described by*

$$\mathcal{C}_{\text{BV}} \leq TB_{\mathbf{u}} B_{\alpha, \mathbf{u}} \left(1 + 4\text{Lip}(g) \int_0^T \|\mathbf{u}\|_{L^\infty(\Omega)} dt \right) + (\text{Lip}(f)\alpha_M + f_0) \|\text{div}(\mathbf{u})\|_{L^1(\Omega_T)},$$

where $\mathcal{C} := \max(\text{Lip}(f)\alpha_M + f_0, 3\text{Lip}(f) + 4\text{Lip}(g)(\tilde{c} + 1) + 1)$, $B_{\mathbf{u}} := \exp(\mathcal{C} \|\nabla \mathbf{u}\|_{L_t^1 L^\infty(\Omega_T)})$, $B_{\alpha, \mathbf{u}} := |\alpha_0|_{BV_{x,y}} + \mathcal{C} \|\text{div}(\mathbf{u})\|_{L_t^1 BV_{x,y}}$, and $f_0 := f(0)$. However, the precise form of \mathcal{C}_{BV} has little impact on compactness arguments used to extract a strongly convergent subsequence from the family of time–space functions $\{\alpha_{h,\delta}\}$ – for this purpose it is sufficient to bound $|\alpha_{h,\delta}|_{BV_{x,y,t}}$ by a global constant independent of the discretisation factors.

Assumptions (AS.1), (AS.2), and the boundedness of $\|\mathbf{u}\|_{L_t^1 L^\infty(\Omega_T)}$ described by (AS.3) are classical in the literature (see [105, p. 153] and [75, p. 130] for more details). The crucial assumptions of Theorem 6.4 are the boundedness of (a) $\|\nabla \mathbf{u}\|_{L_t^1 L^\infty(\Omega_T)}$ and (b) $|\text{div}(\mathbf{u})|_{L_t^1 BV_{x,y}}$ described by (AS.3). Condition (a) is expected since a conventional assumption in estimating BV seminorms of finite volume approximations of nonlinear conservation laws of the form (6.1) is that $\mathbf{u} \in \mathcal{C}^1(\mathbb{R}^d \times \mathbb{R}^+)$ [105, 75], which yields (a) on compact subsets of $\mathbb{R}^d \times \mathbb{R}^+$. Though (b) apparently seems to be restrictive, it is pivotal in bounding the difference of $\text{div}(\mathbf{u})$ between two control volumes (see (6.29)). Indeed, we can relax this assumption to $\text{div}(\mathbf{u}) \in L_t^1 L^\infty(\Omega_T)$, which is the formally correct choice and is used in the seminal work [77] by DiPerna and Lions. However, with this less restrictive assumption, Proposition II.1 in DiPerna and Lions [77] only guarantees the existence of a weak solution $\alpha \in L_t^\infty L^1(\Omega_T)$. Therefore, (b) is justified for establishing a stronger convergence of the finite volume solutions and the higher BV regularity of the limiting solution.

In the one–dimensional case, the regularity of the advection velocity can be slightly relaxed. Adimurty et al. has studied conservation laws of the form $u_t + \partial_x f(k(x), u) = 0$, where k is a piecewise smooth function with finitely many discontinuities and f is $\mathcal{C}^{1,1}$ with respect to k and Lipschitz with respect to u [78]. Similar results and BV estimates on finite volume solutions has been presented in the works [79–82].

6.4 Proof of Theorem 6.4

We let the hypotheses of Theorem 6.4 to hold throughout the sequel of this chapter and recall that $\alpha_{h,\delta}$ is the time-reconstruct in the sense of Definition 6.3. The proof of Theorem 6.4 is accomplished through three steps: establish the

- boundedness of $\alpha_{h,\delta}$ in Proposition 6.6,
- spatial BV estimate of $\alpha_{h,\delta}$ in Proposition 6.7, and
- temporal BV estimate of $\alpha_{h,\delta}$ in Proposition 6.8.

Proposition 6.6 (boundedness). *The function $\alpha_{h,\delta}$ satisfies, for every $0 \leq t \leq T$,*

$$\left| \alpha_{h,\delta}(t, \cdot) \right|_{L^\infty(\Omega)} \leq B_{f,\mathbf{u}} \left(\|\alpha_0\|_{L^\infty(\Omega)} + f_0 \|\operatorname{div}(\mathbf{u})\|_{L_t^1 L^\infty(\Omega_T)} \right), \quad (6.13)$$

where $B_{f,\mathbf{u}} := \exp \left(\operatorname{Lip}(f) \|\operatorname{div}(\mathbf{u})\|_{L_t^1 L^\infty(\Omega_T)} \right)$, and $f_0 = f(0)$.

Proof. The Lipschitz continuity of the function g yields $|\mathbb{M}_{i-1/2,j}^x| \leq \operatorname{Lip}(g) |u_{i-1/2,j}^n|$ and $|\mathbb{M}_{i,j-1/2}^y| \leq \operatorname{Lip}(g) |v_{i,j-1/2}^n|$ for $i = 0, \dots, I$ and $j = 0, \dots, J$. The CFL condition in Theorem 6.4 ensures that the coefficient of $\alpha_{i,j}^n$ in (6.11) is nonnegative. Use the properties of convex linear combination of $\{\alpha_{l,m}^n\}$, where $(l, m) \in \{(i, j-1), (i, j+1), (i-1, j), (i+1, j)\}$ in (6.11) and the Lipschitz continuity of f to obtain

$$\begin{aligned} \sup_{i,j} |\alpha_{i,j}^{n+1}| &\leq \sup_{i,j} |\alpha_{i,j}^n| \left[1 + \operatorname{Lip}(f) \int_{t_n}^{t_{n+1}} \|\operatorname{div}(\mathbf{u})(t, \cdot)\|_{L^\infty(\Omega)} dt \right] \\ &\quad + f_0 \int_{t_n}^{t_{n+1}} \|\operatorname{div}(\mathbf{u})(t, \cdot)\|_{L^\infty(\Omega)} dt. \end{aligned} \quad (6.14)$$

An application of induction on (6.14) with n as the index and (6.9b) yield (6.13). \square

Proposition 6.7 (spatial variation). *The function $\alpha_{h,\delta}$ satisfies*

$$\left| \alpha_{h,\delta}(t, \cdot) \right|_{BV_{x,y}} \leq B_{\mathbf{u}} \left(|\alpha_0|_{BV_{x,y}} + \mathcal{C} \|\operatorname{div}(\mathbf{u})\|_{L_t^1 BV_{x,y}} \right)$$

for every $0 \leq t \leq T$, where $B_{\mathbf{u}} := \exp \left(\mathcal{C} \|\nabla \mathbf{u}\|_{L_t^1 L^\infty(\Omega_T)} \right)$ and \mathcal{C} is defined in Remark 6.5.

The proof of Proposition 6.7 is achieved in five intermediate steps, which are as follows.

Step 1 Write the difference $\alpha_{i,j}^{n+1} - \alpha_{i-1,j}^{n+1}$ as $\alpha_{i,j}^{n+1} - \alpha_{i-1,j}^{n+1} := \alpha_{i,j}^n - \alpha_{i-1,j}^n - \mathbb{H}_{i,j} - \mathbb{J}_{i,j}$, where $\mathbb{H}_{i,j}$ collects the variation of $\alpha_{i,j}^n$ in x -direction and $\mathbb{J}_{i,j}$ the variation of $\alpha_{i,j}^n$ in y -direction.

Step 2 Use the intermediate nodal fluxes (see Figure 6.4) to transform the vertical differences in $\mathbb{J}_{i,j}$ into horizontal differences.

Step 3 Use **Step 1** and **Step 2** to write $\alpha_{i,j}^{n+1} - \alpha_{i-1,j}^{n+1}$ as a sum of (a) convex linear combinations of $\alpha_{i,j}^n - \alpha_{l,m}^n$, where $(l,m) \in \{(i,j-1), (i,j+1), (i-1,j), (i+1,j)\}$ and (b) the variations of $\partial_x u$ and $\partial_y v$ (recall that $\mathbf{u} = (u, v)$).

Step 4 Estimate the variations of $\partial_x u$ and $\partial_y v$ in terms of the BV seminorm of $\text{div}(\mathbf{u})$.

Step 5 Combine the estimates from **Step 3** and **Step 4** to bound $|\alpha_{h,\delta}(t_{n+1}, \cdot)|_{BV_{x,y}}$ in terms of $|\alpha_{h,\delta}(t_n, \cdot)|_{BV_{x,y}}$ and $|\text{div}(\mathbf{u})|_{L_t^1 BV_{x,y}}$ (see (6.31a)) and apply induction on n to obtain the desired conclusion.

Proof. **Step 1:** Consider the difference between the scheme (6.9a) written for $\alpha_{i,j}^{n+1}$ and $\alpha_{i-1,j}^{n+1}$

$$\begin{aligned} \alpha_{i,j}^{n+1} - \alpha_{i-1,j}^{n+1} &= \alpha_{i,j}^n - \alpha_{i-1,j}^n - \left[\mu_i (F_{i+1/2,j} - F_{i-1/2,j}) - \mu_{i-1} (F_{i-1/2,j} - F_{i-3/2,j}) \right] \\ &\quad - \left[\lambda_j (G_{i,j+1/2} - G_{i,j-1/2}) - \lambda_j (G_{i-1,j+1/2} - G_{i-1,j-1/2}) \right] \\ &=: \alpha_{i,j}^n - \alpha_{i-1,j}^n - H_{i,j} - J_{i,j}. \end{aligned} \quad (6.15)$$

The term $H_{i,j}$ gathers the variation in the x -direction; use (6.10a) to rewrite $H_{i,j}$ as

$$\begin{aligned} H_{i,j} &= \mu_i M_{i-1/2,j}^x (\alpha_{i,j}^n - \alpha_{i-1,j}^n) + \mu_i M_{i+1/2,j}^x (\alpha_{i,j}^n - \alpha_{i+1,j}^n) \\ &\quad + \mu_{i-1} M_{i-1/2,j}^x (\alpha_{i,j}^n - \alpha_{i-1,j}^n) + \mu_{i-1} M_{i-3/2,j}^x (\alpha_{i-2,j}^n - \alpha_{i-1,j}^n) + K_{i,j}^f, \end{aligned} \quad (6.16a)$$

where

$$K_{i,j}^f := f(\alpha_{i,j}^n) \int_{t_n}^{t_{n+1}} \int_{K_{i,j}} \partial_x u(t, \mathbf{x}) \, d\mathbf{x} \, dt - f(\alpha_{i-1,j}^n) \int_{t_n}^{t_{n+1}} \int_{K_{i-1,j}} \partial_x u(t, \mathbf{x}) \, d\mathbf{x} \, dt. \quad (6.16b)$$

Step 2: The goal of this step is to transform the horizontal difference of variations

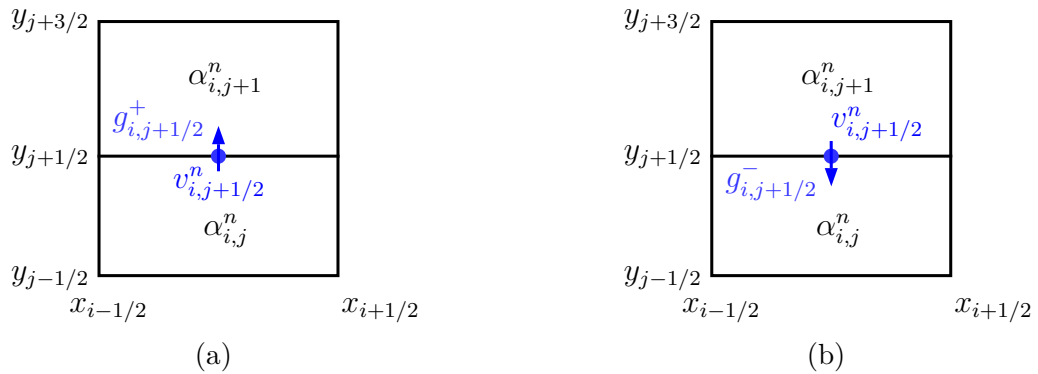


Figure 6.3: Spatial locations of the numerical fluxes $g_{i,j+1/2}^+$ and $g_{i,j+1/2}^-$.

between the vertical levels $(i-r, j+s)$ and $(i-r, j-s)$, where $(r, s) \in \{(0, 1/2), (-1, -1/2)\}$

appearing in $J_{i,j}$ of (6.15) so that the resulting terms can be combined to form a convex linear combination of differences of $\alpha_{h,\delta}(t_n, \cdot)$ between neighbouring rectangles. Define $g_{i,j+1/2}^+ := g(\alpha_{i,j}^n, \alpha_{i,j+1}^n)$ and $g_{i,j+1/2}^- := g(\alpha_{i,j+1}^n, \alpha_{i,j}^n)$. Use (6.8) to rewrite $J_{i,j} = J_{i,j}^+ - J_{i,j}^-$, where

$$J_{i,j}^\star := \lambda_j \left(v_{i,j+1/2}^{n\star} g_{i,j+1/2}^\star - v_{i,j-1/2}^{n\star} g_{i,j-1/2}^\star \right) - \lambda_j \left(v_{i-1,j+1/2}^{n\star} g_{i-1,j+1/2}^\star - v_{i-1,j-1/2}^{n\star} g_{i-1,j-1/2}^\star \right)$$

with $\star \in \{+, -\}$. The numerical fluxes involved in $J_{i,j}^+$ and $J_{i,j}^-$ can be assigned with spatial locations as in Figures 6.3(a) and 6.3(b). A re-grouping of $J_{i,j}^\star$ leads to

$$\begin{aligned} J_{i,j}^\star &:= \lambda_j \left(v_{i,j+1/2}^{n\star} g_{i,j+1/2}^\star - v_{i-1,j+1/2}^{n\star} g_{i-1,j+1/2}^\star \right) - \lambda_j \left(v_{i,j-1/2}^{n\star} g_{i,j-1/2}^\star - v_{i-1,j-1/2}^{n\star} g_{i-1,j-1/2}^\star \right) \\ &=: \lambda_j (\mathfrak{T}_1^\star - \mathfrak{T}_2^\star). \end{aligned} \quad (6.17)$$

Observe that $J_{i,j}^\star/\lambda_j$ is the horizontal variation between differences across two vertical levels as in Figure 6.5(a). However, this form does not yield any terms like $\alpha_{i,r}^n - \alpha_{p,r}^n$, where $p \in \{i+1, i-1\}$ and $r \in \{j+1, j, j-1\}$, and thereby annihilates any chance of expressing $\alpha_{i,j}^{n+1} - \alpha_{i-1,j}^{n+1}$ as a linear combination of such terms, which is crucial in controlling the growth of spatial variation over time. This problem can be fixed by considering the terms $J_{i,j}^+$ and $J_{i,j}^-$ as vertical variations between differences across two horizontal levels, see (6.17), as in Figure 6.5(b).

We consider horizontal difference $\mathfrak{T}_1^+ = v_{i,j+1/2}^{n+} g(\alpha_{i,j}^n, \alpha_{i,j+1}^n) - v_{i-1,j+1/2}^{n+} g(\alpha_{i-1,j}^n, \alpha_{i-1,j+1}^n)$ for clarity. Grouping the terms appropriately yields

$$\begin{aligned} v_{i,j+1/2}^{n+} g(\alpha_{i,j}^n, \alpha_{i,j+1}^n) - v_{i-1,j+1/2}^{n+} g(\alpha_{i-1,j}^n, \alpha_{i-1,j+1}^n) &= (v_{i,j+1/2}^{n+} - v_{i-1,j+1/2}^{n+}) g(\alpha_{i,j}^n, \alpha_{i,j+1}^n) \\ &\quad + v_{i-1,j+1/2}^{n+} \left(g(\alpha_{i,j}^n, \alpha_{i,j+1}^n) - g(\alpha_{i-1,j}^n, \alpha_{i-1,j+1}^n) \right). \end{aligned} \quad (6.18)$$

Introduce an artificial nodal flux $g(\alpha_{i-1,j}^n, \alpha_{i,j+1}^n)$ arising from two diagonally opposite control volumes as in Figure 6.4. The nodal flux, splitting as in (6.18), and some manipulations

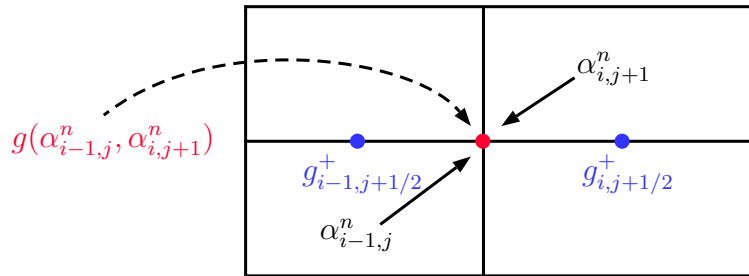


Figure 6.4: Intermediate nodal flux connecting the fluxes on edges.

lead to

$$J_{i,j}^\star = \lambda_j \left((v_{i,j+1/2}^{n\star} - v_{i-1,j+1/2}^{n\star}) g_{i,j+1/2}^\star - (v_{i,j-1/2}^{n\star} - v_{i-1,j-1/2}^{n\star}) g_{i,j-1/2}^\star \right)$$

$$\begin{aligned}
& + \lambda_j \left[v_{i-1,j+1/2}^{n\star} E_{\star}(\alpha_{i,j}^n, \alpha_{i-1,j}^n, \alpha_{i,j+1}^n) (\alpha_{i,j}^n - \alpha_{i-1,j}^n) \right. \\
& \quad \left. - v_{i-1,j-1/2}^{n\star} E_{\star}(\alpha_{i,j-1}^n, \alpha_{i-1,j-1}^n, \alpha_{i,j}^n) (\alpha_{i,j-1}^n - \alpha_{i-1,j-1}^n) \right. \\
& + v_{i-1,j+1/2}^{n\star} E_{-\star}(\alpha_{i,j+1}^n, \alpha_{i-1,j+1}^n, \alpha_{i-1,j}^n) (\alpha_{i,j+1}^n - \alpha_{i-1,j+1}^n) \\
& \quad \left. - v_{i-1,j-1/2}^{n\star} E_{-\star}(\alpha_{i,j}^n, \alpha_{i-1,j}^n, \alpha_{i-1,j-1}^n) (\alpha_{i,j}^n - \alpha_{i-1,j-1}^n) \right], \quad (6.19a)
\end{aligned}$$

where the difference quotients $E_{\star} : \mathbb{R}^3 \rightarrow \mathbb{R}$ are defined by

$$E_{\star}(a, b, c) := \begin{cases} \frac{(1 + \star)(g(a, c) - g(b, c)) + (1 - \star)(g(c, a) - g(c, b))}{2(a - b)} & \text{if } a \neq b, \text{ and} \\ 0 & \text{if } a = b. \end{cases} \quad (6.19b)$$

Note that the sums $(1 \pm (\pm))$ used in (6.19b) are understood as $(1 \pm (\pm 1))$. Use the identity $a^+ = a + a^-$ to transform the differences $(v_{i,j+1/2}^{n+} - v_{i-1,j+1/2}^{n+})$ and $(v_{i,j-1/2}^{n+} - v_{i-1,j-1/2}^{n+})$ in $J_{i,j}^+$ and combine the resulting negative parts with the corresponding negative parts in $J_{i,j}^-$. This yields

$$\begin{aligned}
& \left(\lambda_j (v_{i,j+1/2}^{n+} - v_{i-1,j+1/2}^{n+}) g_{i,j+1/2}^+ - \lambda_j (v_{i,j-1/2}^{n+} - v_{i-1,j-1/2}^{n+}) g_{i,j-1/2}^+ \right) \\
& - \left(\lambda_j (v_{i,j+1/2}^{n-} - v_{i-1,j+1/2}^{n-}) g_{i,j+1/2}^- - \lambda_j (v_{i,j-1/2}^{n-} - v_{i-1,j-1/2}^{n-}) g_{i,j-1/2}^- \right) \\
& = \left(\begin{aligned} & \frac{g_{i,j+1/2}^+}{h_j} \int_{t_n}^{t_{n+1}} \left(\int_{x_{i-1/2}}^{x_{i+1/2}} v(t, s, y_{j+1/2}) ds - \int_{x_{i-3/2}}^{x_{i-1/2}} v(t, s, y_{j+1/2}) ds \right) dt \\ & - \frac{g_{i,j-1/2}^+}{h_j} \int_{t_n}^{t_{n+1}} \left(\int_{x_{i-1/2}}^{x_{i+1/2}} v(t, s, y_{j-1/2}) ds - \int_{x_{i-3/2}}^{x_{i-1/2}} v(t, s, y_{j-1/2}) ds \right) dt \end{aligned} \right) \Bigg\} =: K_{i,j}^g \\
& + \lambda_j (v_{i,j+1/2}^{n-} - v_{i-1,j+1/2}^{n-}) (g_{i,j+1/2}^+ - g_{i,j+1/2}^-) \\
& - \lambda_j (v_{i,j-1/2}^{n-} - v_{i-1,j-1/2}^{n-}) (g_{i,j-1/2}^+ - g_{i,j-1/2}^-). \quad (6.20)
\end{aligned}$$

Step 3: Combine (6.15), (6.16a), (6.19a), (6.20) and re-group the terms to obtain

$$\begin{aligned}
\alpha_{i,j}^{n+1} - \alpha_{i-1,j}^{n+1} & = (\alpha_{i,j}^n - \alpha_{i-1,j}^n) (1 - c_{i,j}) - \mu_i M_{i+1/2,j}^x (\alpha_{i,j}^n - \alpha_{i+1,j}^n) \\
& \quad - \mu_{i-1} M_{i-3/2,j}^x (\alpha_{i-2,j}^n - \alpha_{i-1,j}^n) \\
& + \lambda_j \left[\sum_{\star \in \{+, -\}} (\star) v_{i-1,j-1/2}^{n\star} E_{\star}(\alpha_{i,j-1}^n, \alpha_{i-1,j-1}^n, \alpha_{i,j}^n) (\alpha_{i,j-1}^n - \alpha_{i-1,j-1}^n) \right. \\
& \quad \left. - \sum_{\star \in \{+, -\}} (\star) v_{i-1,j+1/2}^{n\star} E_{-\star}(\alpha_{i,j+1}^n, \alpha_{i-1,j+1}^n, \alpha_{i-1,j}^n) (\alpha_{i,j+1}^n - \alpha_{i-1,j+1}^n) \right] \\
& - \lambda_j \left[(v_{i,j+1/2}^{n-} - v_{i-1,j+1/2}^{n-}) (g_{i,j+1/2}^+ - g_{i,j+1/2}^-) \right. \\
& \quad \left. + (v_{i,j-1/2}^{n-} - v_{i-1,j-1/2}^{n-}) (g_{i,j-1/2}^+ - g_{i,j-1/2}^-) \right] - (K_{i,j}^f + K_{i,j}^g), \quad (6.21a)
\end{aligned}$$

$$\begin{aligned}
\text{where } c_{i,j} := & \mu_i M_{i-1/2,j}^x + \mu_{i-1} M_{i-1/2,j}^x + \lambda_j \left[v_{i-1,j+1/2}^{n+} E_+(\alpha_{i,j}^n, \alpha_{i-1,j}^n, \alpha_{i,j+1}^n) \right. \\
& - v_{i-1,j-1/2}^{n+} E_-(\alpha_{i,j}^n, \alpha_{i-1,j}^n, \alpha_{i-1,j-1}^n) - v_{i-1,j+1/2}^{n-} E_-(\alpha_{i,j}^n, \alpha_{i-1,j}^n, \alpha_{i,j+1}^n) \\
& \left. + v_{i-1,j-1/2}^{n-} E_+(\alpha_{i,j}^n, \alpha_{i-1,j}^n, \alpha_{i-1,j-1}^n) \right]. \tag{6.21b}
\end{aligned}$$

Note that in (6.21b) the terms E_- are nonpositive and E_+ are nonnegative. This fact along with the CFL condition ensures that $1 - c_{i,j}$ is nonnegative. Take absolute value on both sides of (6.21a), multiply by h_j , sum on $i = 1, \dots, I$ and $j = 0, \dots, J$, and use the condition that $\mathbf{u} = \mathbf{0}$ on $\partial\Omega$ to change the indices appropriately to obtain

$$\begin{aligned}
\sum_{j=0}^J h_j \sum_{i=1}^I |\alpha_{i,j}^{n+1} - \alpha_{i-1,j}^{n+1}| & \leq \sum_{j=0}^J h_j \sum_{i=1}^I |\alpha_{i,j}^n - \alpha_{i-1,j}^n| (1 - c_{i,j}) \\
& + \sum_{j=0}^J h_j \left[\sum_{i=1}^I \mu_{i-1} M_{i-1/2,j}^x |\alpha_{i,j}^n - \alpha_{i-1,j}^n| + \sum_{i=1}^I \mu_i M_{i-1/2,j}^x |\alpha_{i,j}^n - \alpha_{i-1,j}^n| \right] \\
& + \sum_{* \in \{+, -\}} \sum_{j=0}^J h_j \sum_{i=1}^I \left[\lambda_j v_{i-1,j+1/2}^{n*} (*) E_{*}(\alpha_{i,j}^n, \alpha_{i-1,j}^n, \alpha_{i,j+1}^n) |\alpha_{i,j}^n - \alpha_{i-1,j}^n| \right. \\
& \quad \left. + v_{i-1,j-1/2}^{n*} (-*) E_{-*}(\alpha_{i,j}^n, \alpha_{i-1,j}^n, \alpha_{i-1,j-1}^n) |\alpha_{i,j}^n - \alpha_{i-1,j}^n| \right] \\
& + \sum_{j=0}^{J-1} h_j \sum_{i=1}^I \lambda_j |v_{i,j+1/2}^{n-} - v_{i-1,j+1}^{n-}| |g(\alpha_{i,j}^n, \alpha_{i,j+1}^n) - g(\alpha_{i,j+1}^n, \alpha_{i,j}^n)| \\
& + \sum_{j=1}^J h_j \sum_{i=1}^I \lambda_j |v_{i,j-1/2}^{n-} - v_{i-1,j-1/2}^{n-}| |g(\alpha_{i,j-1}^n, \alpha_{i,j}^n) - g(\alpha_{i,j}^n, \alpha_{i,j-1}^n)| \\
& + \sum_{j=1}^J h_j \sum_{i=1}^I (|K_{i,j}^f| + |K_{i,j}^g|). \tag{6.22}
\end{aligned}$$

The term $1 - c_{i,j}$ and coefficients of $|\alpha_{i,j}^n - \alpha_{i-1,j}^n|$ in the second and third sum on the right hand side of (6.22) add up to one, and this yields

$$\begin{aligned}
\sum_{j=0}^J h_j \sum_{i=1}^I |\alpha_{i,j}^{n+1} - \alpha_{i-1,j}^{n+1}| & \leq \sum_{j=0}^J h_j \sum_{i=1}^I |\alpha_{i,j}^n - \alpha_{i-1,j}^n| \\
& + \sum_{j=0}^{J-1} h_j \sum_{i=1}^I \lambda_j |v_{i,j+1/2}^{n-} - v_{i-1,j+1/2}^{n-}| |g(\alpha_{i,j}^n, \alpha_{i,j+1}^n) - g(\alpha_{i,j+1}^n, \alpha_{i,j}^n)| \\
& + \sum_{j=1}^J h_j \sum_{i=1}^I \lambda_j |v_{i,j-1/2}^{n-} - v_{i-1,j-1/2}^{n-}| |g(\alpha_{i,j-1}^n, \alpha_{i,j}^n) - g(\alpha_{i,j}^n, \alpha_{i,j-1}^n)| \\
& + \delta \sum_{j=1}^J h_j \sum_{i=1}^I (|K_{i,j}^f| + |K_{i,j}^g|). \tag{6.23}
\end{aligned}$$

Use the Lipschitz continuity of the negative part $a \rightarrow a^-$ (with constant 1) and g , the Lipschitz continuity of v in the x -direction, and the grid regularity condition of Definition 6.2 to obtain

$$\begin{aligned} \lambda_j \left| v_{i,j-1/2}^{n-} - v_{i-1,j-1/2}^{n-} \right| \left| g(\alpha_{i,j-1}^n, \alpha_{i,j}^n) - g(\alpha_{i,j}^n, \alpha_{i,j-1}^n) \right| \leq \\ \tilde{c} \left| \alpha_{i,j}^n - \alpha_{i,j-1}^n \right| \text{Lip}(g) \int_{t_n}^{t_{n+1}} \|\partial_x v(t, \cdot)\|_{L^\infty(\Omega)} dt. \end{aligned} \quad (6.24)$$

Step 4: Apply (1.1a) on $K_{i,j}^g$ (see (6.20)) to obtain

$$\begin{aligned} K_{i,j}^g &= \frac{g_{i,j+1/2}^+ - g_{i,j-1/2}^+}{2h_j} \left[\int_{t_n}^{t_{n+1}} \left(\int_{x_{i-1/2}}^{x_{i+1/2}} v(t, s, y_{j+1/2}) ds - \int_{x_{i-3/2}}^{x_{i-1/2}} v(t, s, y_{j+1/2}) ds \right) dt \right. \\ &\quad \left. + \int_{t_n}^{t_{n+1}} \left(\int_{x_{i-1/2}}^{x_{i+1/2}} v(t, s, y_{j-1/2}) ds - \int_{x_{i-3/2}}^{x_{i-1/2}} v(t, s, y_{j-1/2}) ds \right) dt \right] \\ &\quad + \frac{g_{i,j+1/2}^+ + g_{i,j-1/2}^+}{2} \left[\int_{t_n}^{t_{n+1}} \int_{K_{i,j}} \partial_y v(t, \cdot) d\mathbf{x} dt - \int_{t_n}^{t_{n+1}} \int_{K_{i-1,j}} \partial_y v(t, \cdot) d\mathbf{x} dt \right] \\ &=: K_{i,j}^{g,1} + K_{i,j}^{g,2}. \end{aligned}$$

Write the term $K_{i,j}^f$ (see (6.16b)) as

$$\begin{aligned} K_{i,j}^f &= \left(f(\alpha_{i,j}^n) \int_{t_n}^{t_{n+1}} \int_{K_{i,j}} \text{div}(\mathbf{u})(t, \cdot) d\mathbf{x} dt - f(\alpha_{i-1,j}^n) \int_{t_n}^{t_{n+1}} \int_{K_{i-1,j}} \text{div}(\mathbf{u})(t, \cdot) d\mathbf{x} dt \right) \\ &\quad - \left(f(\alpha_{i,j}^n) \int_{t_n}^{t_{n+1}} \int_{K_{i,j}} \partial_y v(t, \cdot) d\mathbf{x} dt - f(\alpha_{i-1,j}^n) \int_{t_n}^{t_{n+1}} \int_{K_{i-1,j}} \partial_y v(t, \cdot) d\mathbf{x} dt \right) \\ &=: K_{i,j}^{f,1} + K_{i,j}^{f,2}. \end{aligned}$$

Use the Lipschitz continuity of g , the Lipschitz continuity of v in the x -direction, and Definition 6.2 to obtain

$$|K_{i,j}^{g,1}| \leq \tilde{c} \text{Lip}(g) \left(|\alpha_{i,j}^n - \alpha_{i,j-1}^n| + |\alpha_{i,j+1}^n - \alpha_{i,j}^n| \right) \int_{t_n}^{t_{n+1}} \|\partial_x v(t, \cdot)\|_{L^\infty(\Omega)} dt. \quad (6.25)$$

A use of (1.1a) on $K_{i,j}^{f,1}$ yields

$$\begin{aligned} K_{i,j}^{f,1} &= \frac{f(\alpha_{i,j}^n) - f(\alpha_{i-1,j}^n)}{2} \left[\int_{t_n}^{t_{n+1}} \int_{K_{i,j}} \text{div}(\mathbf{u})(t, \cdot) d\mathbf{x} dt + \int_{t_n}^{t_{n+1}} \int_{K_{i-1,j}} \text{div}(\mathbf{u})(t, \cdot) d\mathbf{x} dt \right] \\ &\quad + \frac{f(\alpha_{i,j}^n) + f(\alpha_{i-1,j}^n)}{2} \left[\int_{t_n}^{t_{n+1}} \int_{K_{i,j}} \text{div}(\mathbf{u})(t, \cdot) d\mathbf{x} dt - \int_{t_n}^{t_{n+1}} \int_{K_{i-1,j}} \text{div}(\mathbf{u})(t, \cdot) d\mathbf{x} dt \right], \end{aligned}$$

Therefore, $|\mathbf{K}_{i,j}^{f,1}|$ can be bounded by

$$\begin{aligned} |\mathbf{K}_{i,j}^{f,1}| &\leq \text{Lip}(f)|\alpha_{i,j}^n - \alpha_{i-1,j}^n| \int_{t_n}^{t_{n+1}} \|\text{div}(\mathbf{u})(t, \cdot)\|_{L^\infty(\Omega)} dt \\ &\quad + (\text{Lip}(f)\alpha_M + f_0) \int_{t_n}^{t_{n+1}} \left| \int_{K_{i,j}} \text{div}(\mathbf{u})(t, \cdot) d\mathbf{x} - \int_{K_{i-1,j}} \text{div}(\mathbf{u})(t, \cdot) d\mathbf{x} \right| dt. \end{aligned} \quad (6.26)$$

The sum $\mathbf{K}_{i,j}^{g,2} + \mathbf{K}_{i,j}^{f,2}$ can be written as

$$\begin{aligned} \mathbf{K}_{i,j}^{g,2} + \mathbf{K}_{i,j}^{f,2} &= \frac{-2f(\alpha_{i,j}^n) + g_{i,j+1/2}^+ + g_{i,j-1/2}^+}{2} \int_{t_n}^{t_{n+1}} \int_{K_{i,j}} \partial_y v(t, \cdot) d\mathbf{x} dt \\ &\quad + \frac{2f(\alpha_{i-1,j}^n) - g_{i,j+1/2}^+ - g_{i,j-1/2}^+}{2} \int_{t_n}^{t_{n+1}} \int_{K_{i-1,j}} \partial_y v(t, \cdot) d\mathbf{x} dt. \end{aligned} \quad (6.27)$$

The Lipschitz continuity of g and f and $g(a, a) = f(a)$ yield

$$|-2f(\alpha_{i,j}^n) + g_{i,j+1/2}^+ + g_{i,j-1/2}^+| \leq \text{Lip}(g)|\alpha_{i,j}^n - \alpha_{i,j-1}^n| + \text{Lip}(g)|\alpha_{i,j}^n - \alpha_{i,j+1}^n|, \quad (6.28a)$$

$$\begin{aligned} |2f(\alpha_{i-1,j}^n) + g_{i,j+1/2}^+ + g_{i,j-1/2}^+| &\leq 2\text{Lip}(f)|\alpha_{i,j}^n - \alpha_{i-1,j}^n| \\ &\quad + \text{Lip}(g)|\alpha_{i,j}^n - \alpha_{i,j-1}^n| + \text{Lip}(g)|\alpha_{i,j}^n - \alpha_{i,j+1}^n|. \end{aligned} \quad (6.28b)$$

Combine the bounds (6.25), (6.26), (6.27), (6.28a), and (6.28b) to obtain

$$\begin{aligned} |\mathbf{K}_{i,j}^f + \mathbf{K}_{i,j}^g| &\leq |\mathbf{K}_{i,j}^{f,1}| + |\mathbf{K}_{i,j}^{g,1}| + |\mathbf{K}_{i,j}^{f,2} + \mathbf{K}_{i,j}^{g,2}| \\ &\leq \text{Lip}(f)|\alpha_{i,j}^n - \alpha_{i-1,j}^n| \left(\int_{t_n}^{t_{n+1}} \|\text{div}(\mathbf{u})(t, \cdot)\|_{L^\infty(\Omega)} dt + 2 \int_{t_n}^{t_{n+1}} \|\partial_y v(t, \cdot)\|_{L^\infty(\Omega)} dt \right) \\ &\quad + \text{Lip}(g) \left(|\alpha_{i,j}^n - \alpha_{i,j-1}^n| + |\alpha_{i,j+1}^n - \alpha_{i,j}^n| \right) \left(\tilde{c} \int_{t_n}^{t_{n+1}} \left(\|\partial_x v(t, \cdot)\|_{L^\infty(\Omega)} + 2\|\partial_y v(t, \cdot)\|_{L^\infty(\Omega)} \right) dt \right) \\ &\quad + (\text{Lip}(f)\alpha_M + f_0) \int_{t_n}^{t_{n+1}} \left| \int_{K_{i,j}} \text{div}(\mathbf{u})(t, \cdot) d\mathbf{x} - \int_{K_{i-1,j}} \text{div}(\mathbf{u})(t, \cdot) d\mathbf{x} \right| dt. \end{aligned} \quad (6.29)$$

Step 5: Use (6.23), (6.24), and (6.29) to obtain

$$\begin{aligned} |\alpha_{h,\delta}(t_{n+1}, \cdot)|_{L_y^1 BV_x} &\leq |\alpha_{h,\delta}(t_n, \cdot)|_{L_y^1 BV_x} + 4(\tilde{c} + 1) \text{Lip}(g) |\alpha_{h,\delta}(t_n, \cdot)|_{L_x^1 BV_y} \int_{t_n}^{t_{n+1}} \|\nabla \mathbf{u}\|_{L^\infty(\Omega)} dt \\ &\quad + 3\text{Lip}(f) |\alpha_{h,\delta}(t_n, \cdot)|_{L_y^1 BV_x} \int_{t_n}^{t_{n+1}} \|\nabla \mathbf{u}\|_{L^\infty(\Omega)} dt \\ &\quad + (\text{Lip}(f)\alpha_M + f_0) \int_{t_n}^{t_{n+1}} |\Pi_h^0(\text{div}(\mathbf{u}))(t, \cdot)|_{L_y^1 BV_x} dt, \end{aligned} \quad (6.30)$$

where the piecewise constant projection $\Pi_{h,k}^0 : BV_{\mathbf{x}}(\Omega) \rightarrow BV_{\mathbf{x}}(\Omega)$ for an admissible grid $X_k \times Y_h$ is defined by, for $\beta \in BV_{\mathbf{x}}(\Omega)$, $(\Pi_{h,k}^0(\beta))(\mathbf{x}) := \int_{K_{i,j}} \beta d\mathbf{x} \quad \forall \mathbf{x} \in K_{i,j}$. A similar argument can be obtained with i and j interchanged and when combined with (6.30) yields

$$\begin{aligned} |\alpha_{h,\delta}(t_{n+1}, \cdot)|_{BV_{x,y}} &\leq |\alpha_{h,\delta}(t_n, \cdot)|_{BV_{x,y}} \left(1 + \mathcal{C} \int_{t_n}^{t_{n+1}} \|\nabla \mathbf{u}(t, \cdot)\|_{L^\infty(\Omega)} dt \right) \\ &\quad + \mathcal{C} \int_{t_n}^{t_{n+1}} |\Pi_{h,k}^0(\operatorname{div}(\mathbf{u}))|_{BV_{x,y}} dt, \end{aligned} \quad (6.31a)$$

where $\mathcal{C} = \max(\operatorname{Lip}(f)\alpha_M + f_0, 3\operatorname{Lip}(f) + 4\operatorname{Lip}(g)(\tilde{c} + 1) + 1)$. Apply induction on (6.31a) with n as the index and use the fact that $|\Pi_{h,k}^0(\operatorname{div}(\mathbf{u}))|_{BV_{x,y}} \leq |\operatorname{div}(\mathbf{u})|_{BV_{x,y}}$ to obtain

$$|\alpha_{h,\delta}(t_n, \cdot)|_{BV_{x,y}} \leq \mathbf{B}\mathbf{u} \left(|\alpha_{h,\delta}(t_0, \cdot)|_{BV_{x,y}} + \mathcal{C} \int_0^T |\operatorname{div}(\mathbf{u})|_{BV_{x,y}} dt \right). \quad (6.31b)$$

The desired conclusion follows from (6.31b) and (6.9b). \square

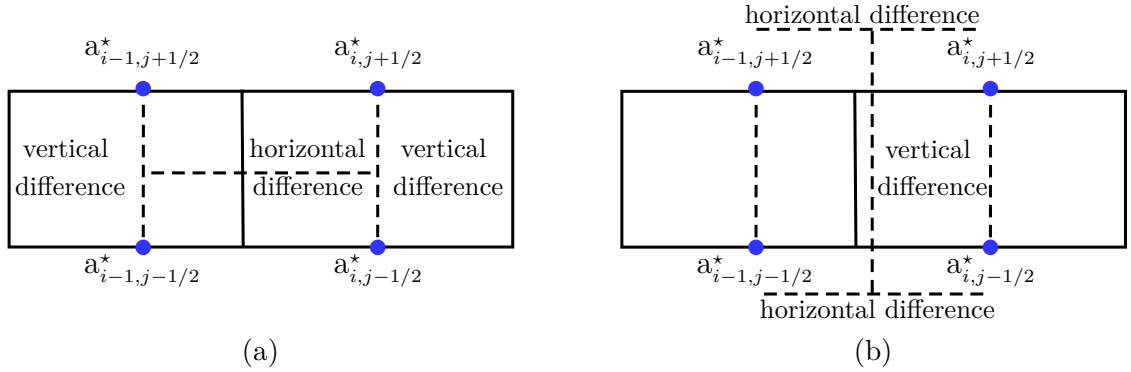


Figure 6.5: Differences between horizontal and vertical levels. Here, $a_{i,j+1/2}^* = v_{i,j+1/2}^{n*} g_{i,j+1/2}^*$, where $g_{i,j+1/2}^+ = g(\alpha_{i,j}^n, \alpha_{i,j+1}^n)$ and $g_{i,j+1/2}^- = g(\alpha_{i,j+1}^n, \alpha_{i,j}^n)$.

Proposition 6.8 (temporal variation). *The function $\alpha_{h,\delta}$ satisfies*

$$\begin{aligned} |\alpha_{h,\delta}|_{L_{x,y}^1 BV_t} &\leq 4\mathbf{B}\mathbf{u} \left(|\alpha_0|_{BV_{x,y}} + \mathcal{C} |\operatorname{div}(\mathbf{u})|_{L_t^1 BV_{x,y}} \right) \operatorname{Lip}(g) \|\mathbf{u}\|_{L_t^1 L^\infty(\Omega_T)} \\ &\quad + (\operatorname{Lip}(f)\alpha_M + f_0) |\operatorname{div}(\mathbf{u})|_{L^1(\Omega_T)}. \end{aligned}$$

The proof of Proposition 6.8 is obtained by writing $\alpha_{i,j}^{n+1} - \alpha_{i,j}^n$ in terms of the differences $\alpha_{i,j}^n - \alpha_{l,m}^n$, where $(l, m) \in \{(i, j-1), (i, j+1), (i-1, j), (i+1, j)\}$ and by applying Proposition 6.7.

Proof. Use (6.11) to write

$$\begin{aligned} \alpha_{i,j}^{n+1} - \alpha_{i,j}^n &= \mu_i M_{i+1/2,j}^x (\alpha_{i+1,j}^n - \alpha_{i,j}^n) + \lambda_j M_{i,j+1/2}^y (\alpha_{i,j+1}^n - \alpha_{i,j}^n) \\ &\quad + \mu_i M_{i-1/2,j}^x (\alpha_{i-1,j}^n - \alpha_{i,j}^n) + \lambda_j M_{i,j-1/2}^y (\alpha_{i,j-1}^n - \alpha_{i,j}^n) \\ &\quad - f(\alpha_{i,j}^n) \left(\int_{t_n}^{t_{n+1}} \int_{K_{i,j}} \operatorname{div}(\mathbf{u})(t, \mathbf{x}) \, d\mathbf{x} \, dt \right). \end{aligned} \quad (6.32)$$

Multiply both sides of (6.32) by $h_j k_i$, sum over $n = 0, \dots, N$, $i = 0, \dots, I$ and $j = 0, \dots, J$, and use the homogeneous boundary condition on \mathbf{u} to obtain

$$\begin{aligned} \sum_{j=0}^J \sum_{i=0}^I h_j k_i \sum_{n=0}^N |\alpha_{i,j}^{n+1} - \alpha_{i,j}^n| &\leq \sum_{n=0}^N \delta \sum_{j=0}^J h_j \sum_{i=0}^{I-1} M_{i+1/2,j}^x |\alpha_{i+1,j}^n - \alpha_{i,j}^n| \\ &\quad + \sum_{n=0}^N \delta \sum_{i=0}^I k_i \sum_{j=0}^{J-1} M_{i,j+1/2}^y |\alpha_{i,j+1}^n - \alpha_{i,j}^n| + \sum_{n=0}^N \delta \sum_{j=0}^J h_j \sum_{i=1}^I M_{i-1/2,j}^x |\alpha_{i-1,j}^n - \alpha_{i,j}^n| \\ &\quad + \sum_{n=0}^N \delta \sum_{i=0}^I k_i \sum_{j=1}^J M_{i,j-1/2}^y |\alpha_{i,j-1}^n - \alpha_{i,j}^n| + \sum_{j=0}^J \sum_{i=0}^I \sum_{n=0}^N f(\alpha_{i,j}^n) \left(\int_{t_n}^{t_{n+1}} \int_{K_{i,j}} \operatorname{div}(\mathbf{u})(t, \mathbf{x}) \, d\mathbf{x} \, dt \right). \end{aligned} \quad (6.33)$$

Use the Lipschitz continuity of the functions f and g and (6.33) to obtain

$$\begin{aligned} \int_{\Omega} |\alpha_{h,\delta}(\cdot, x, y)|_{BV_i(0,T)} \, dx \, dy &\leq 4 \operatorname{Lip}(g) \int_0^T \|\mathbf{u}(t, \cdot)\|_{L^\infty(\Omega)} |\alpha_{h,\delta}(t, \cdot)|_{BV_{x,y}} \, dt \\ &\quad + (\operatorname{Lip}(f)\alpha_M + f_0) \|\operatorname{div}(\mathbf{u})\|_{L^1(\Omega_T)}. \end{aligned} \quad (6.34)$$

Use (6.34) and Proposition 6.7 to arrive at the desired result. \square

Theorem 6.4 follows from Propositions 6.7, 6.8, and (6.6). The homogeneous source term in (6.1) can be replaced with a function $\mathfrak{S}(t, \mathbf{x}, \alpha)$ that satisfies the assumption:

- (AS.4) $\mathfrak{S} \in L_t^1 L^\infty(\Omega_T)$ and $\mathfrak{S}(t, \mathbf{x}, z)$ is Lipschitz continuous with respect to z (with constant $\operatorname{Lip}_z(\mathfrak{S})$), uniformly with respect to t and \mathbf{x} , and is Lipschitz continuous with respect to \mathbf{x} (with constant $\operatorname{Lip}_{\mathbf{x}}(\mathfrak{S})$), uniformly with respect to t and z .

In this case, we obtain the following corollary to Theorem 6.4.

Corollary 1. *Let (AS.1)–(AS.4) and the Courant–Friedrichs–Lewy (CFL) condition*

$$4\delta \max_{i,j} \left(\frac{1}{k_i} + \frac{1}{h_j} \right) \operatorname{Lip}(g) \|\mathbf{u}\|_{L^\infty(\Omega_T)} \leq 1$$

hold. If $\alpha_0 \in L^\infty(\Omega) \cap BV_{\mathbf{x}}(\Omega)$ then, the time-reconstruct $\alpha_{h,\delta} : \Omega_T \rightarrow \mathbb{R}$ reconstructed from the values $\alpha_{i,j}^n$ obtained from the scheme

$$\alpha_{i,j}^{n+1} = \alpha_{i,j}^n - \mu_i (F_{i+1/2,j} - F_{i-1/2,j}) - \lambda_j (G_{i,j+1/2} - G_{i,j-1/2}) + \int_{t_n}^{t_{n+1}} \int_{K_{i,j}} \mathfrak{S}(t, \mathbf{x}, \alpha_{i,j}^n) \, dt \, d\mathbf{x}$$

satisfies $|\alpha_{h,\delta}|_{BV_{x,y,t}} \leq \mathcal{C}_{BV}$, where \mathcal{C}_{BV} depends on T , α_0 , f , g , $\|\nabla \mathbf{u}\|_{L_t^1 L^\infty(\Omega_T)}$, $|\operatorname{div}(\mathbf{u})|_{L_t^1 BV_{x,y}}$, $\operatorname{Lip}_{\mathbf{x}}(\mathfrak{S})$, $\operatorname{Lip}_z(\mathfrak{S})$, and $|\mathfrak{S}|_{L_t^1 BV_{x,y}}$.

Proof. It is enough to estimate variation of the source term in the x direction, which can be written as

$$V_{i,j} := \int_{t_n}^{t_{n+1}} \int_{K_{i,j}} \mathfrak{S}(t, \mathbf{x}, \alpha_{i,j}^n) dt d\mathbf{x} - \int_{t_n}^{t_{n+1}} \int_{K_{i-1,j}} \mathfrak{S}(t, \mathbf{x}, \alpha_{i-1,j}^n) dt d\mathbf{x}. \quad (6.35)$$

Add and subtract $\int_{t_n}^{t_{n+1}} \int_{K_{i,j}} \mathfrak{S}(t, \mathbf{x}, \alpha_{i-1,j}^n) dt d\mathbf{x}$ to (6.35) and group the terms appropriately to obtain

$$\begin{aligned} |V_{i,j}| &\leq \int_{t_n}^{t_{n+1}} \int_{K_{i,j}} \left| \mathfrak{S}(t, \mathbf{x}, \alpha_{i,j}^n) - \mathfrak{S}(t, \mathbf{x}, \alpha_{i-1,j}^n) \right| dt d\mathbf{x} \\ &\quad + \int_{t_n}^{t_{n+1}} \left| \int_{K_{i,j}} \mathfrak{S}(t, \mathbf{x}, \alpha_{i-1,j}^n) d\mathbf{x} - \int_{K_{i-1,j}} \mathfrak{S}(t, \mathbf{x}, \alpha_{i-1,j}^n) d\mathbf{x} \right| dt =: V_1 + V_2. \end{aligned} \quad (6.36)$$

Use the Lipschitz continuity of \mathfrak{S} with respect to the third argument to bound V_1 by $\delta \operatorname{Lip}_z(\mathfrak{S}) |\alpha_{i,j}^n - \alpha_{i-1,j}^n|$. Sum (6.36) for $i = 1, \dots, I$ to obtain

$$\sum_{i=1}^I |V_{i,j}| \leq \delta \operatorname{Lip}_z(\mathfrak{S}) |\alpha_{h,\delta}(t_n, \cdot)|_{BV_x} + \operatorname{Lip}_{\mathbf{x}}(\mathfrak{S}) \int_{t_n}^{t_{n+1}} \left| \Pi_h^0(\mathfrak{S}) \right|_{BV_x} dt. \quad (6.37)$$

Rest of the proof follows by adding the terms in the right hand side of (6.37) to the right hand side of (6.30) and by following the steps from there on. \square

6.5 BV estimate for conservation laws with fully nonlinear flux

Several practical problems presents a nonlinear flux dependent on time, space, and the conserved variable. Continuous sedimentation problems [83] and oil reservoir simulations [84] are examples of such systems. Theorem 6.4 can be extended to the case with fully nonlinear flux such as

$$\left. \begin{aligned} \partial_t \alpha + \operatorname{div}(\mathbf{F}(t, \mathbf{x}, \alpha)) &= 0 \text{ in } \Omega_T \text{ and} \\ \alpha(0, \cdot) &= \alpha_0 \text{ in } \Omega. \end{aligned} \right\} \quad (6.38)$$

The strong BV estimate on finite volume schemes for (6.38) on square Cartesian grids is obtained by C. Chainais-Hilaret [75] under the assumption that $\operatorname{div}_{\mathbf{x}}(\mathbf{F}) = 0$. In this chapter, we relax this condition and obtain bounded variation estimates for α under the following assumptions.

(AS.5) $\mathbf{F}(t, \mathbf{x}, z)$ is $\mathcal{C}^1(\overline{\Omega_T} \times \mathbb{R})$ and is Lipschitz continuous with respect to z (with constant $\text{Lip}(\mathbf{F})$), uniformly with respect to (t, \mathbf{x}) , and $\partial_z \mathbf{F}$ is Lipschitz continuous with respect to \mathbf{x} (with constant $\text{Lip}(\partial_s \mathbf{F})$), uniformly with respect to t and z ,

(AS.6) $|\text{div}_{\mathbf{x}}(\mathbf{F})|_{L_t^1 BV_{x,y}} < \infty$ and $\text{div}_{\mathbf{x}}(\mathbf{F})$ is Lipschitz continuous with respect to z (with constant $\text{Lip}(\text{div}_{\mathbf{x}}(\mathbf{F}))$), uniformly with respect to t and \mathbf{x} .

Use (AS.5) to write the flux \mathbf{F} as $\mathbf{F} := (F_1, F_2)$, $F_1 = \mathcal{A} + \mathcal{B}$, and $F_2 = \mathcal{C} + \mathcal{D}$, where \mathcal{A} and \mathcal{C} are monotonically nondecreasing and \mathcal{B} and \mathcal{D} are monotonically nonincreasing in z , uniformly with respect to t and \mathbf{x} . In this case, we can set the following finite volume scheme on an admissible grid $X_h \times Y_k$:

$$\begin{aligned} \alpha_{i,j}^{n+1} = & \alpha_{i,j}^n - \frac{1}{k_i} \left(a_{i+1/2,j}^n(\alpha_{i,j}^n) - a_{i-1/2,j}^n(\alpha_{i-1,j}^n) + b_{i+1/2,j}^n(\alpha_{i+1,j}^n) - b_{i-1/2,j}^n(\alpha_{i,j}^n) \right) \\ & - \frac{1}{h_j} \left(c_{i,j+1/2}^n(\alpha_{i,j}^n) - c_{i,j-1/2}^n(\alpha_{i,j-1}^n) + d_{i,j+1/2}^n(\alpha_{i,j+1}^n) - d_{i,j-1/2}^n(\alpha_{i,j}^n) \right) \end{aligned} \quad (6.39)$$

with the initial condition (6.9b), where the numerical fluxes are defined, for $\gamma \in \{\mathcal{A}, \mathcal{B}\}$, and $\varrho \in \{\mathcal{C}, \mathcal{D}\}$, by

$$\begin{aligned} \gamma_{i+1/2,j}^n(s) &= \int_{t_n}^{t_{n+1}} \int_{y_{j-1/2}}^{y_{j+1/2}} \gamma(t, x_{i+1/2}, y, s) dy dt \quad \text{and} \\ \varrho_{i,j+1/2}^n(s) &= \int_{t_n}^{t_{n+1}} \int_{x_{i-1/2}}^{x_{i+1/2}} \varrho(t, x, y_{j+1/2}, s) dx dt. \end{aligned}$$

Theorem 6.9 (bounded variation for fully nonlinear flux). *Let the assumptions (AS.5)–(AS.6) and the following CFL condition hold:*

$$4\delta \text{Lip}(\mathbf{F}) \max_{i,j} \left(\frac{1}{k_i} + \frac{1}{h_j} \right) \leq 1.$$

Then the piecewise time-reconstruct $\alpha_{h,\delta} : \Omega_T \rightarrow \mathbb{R}$ re-constructed from the values $\alpha_{i,j}^n$ obtained from the scheme (6.39) satisfies $|\alpha_{h,\delta}|_{BV_{x,y,t}(\Omega_T)} \leq \mathcal{C}$, where \mathcal{C} depends on T , α_0 , $|\text{div}_{\mathbf{x}}(\mathbf{F})|_{L_t^1 BV_{x,y}}$, and $\text{Lip}(\text{div}_{\mathbf{x}}(\mathbf{F}))$.

The proof of Theorem 6.9 is based on two main ideas. Firstly, the terms in the scheme (6.39) are re-arranged and grouped appropriately so that the term $\int_{t_n}^{t_n} \int_{K_{i,j}} \text{div}_{\mathbf{x}}(\mathbf{F})(t, \mathbf{x}, \alpha_{i,j}^n) d\mathbf{x} dt$ can be separately estimated (see (6.41)). Secondly, we employ the Lipschitz continuity of $\text{div}_{\mathbf{x}}(\mathbf{F})$ to bound difference of the terms $\{\int_{t_n}^{t_{n+1}} \int_{K_{l,j}} \text{div}_{\mathbf{x}}(\mathbf{F})(t, \mathbf{x}, \alpha_{l,j}^{n+1}) d\mathbf{x} dt : l = i, i+1\}$ by the BV seminorms $\int_{t_n}^{t_{n+1}} |\alpha_{h,\delta}(t, \cdot)|_{BV_x} dt$ and $\int_{t_n}^{t_{n+1}} |\text{div}_{\mathbf{x}}(\mathbf{F})(t, \cdot, \cdot)|_{BV_x} dt$.

Proof. The scheme (6.39) can be expressed as

$$\alpha_{i,j}^{n+1} = \left(\begin{array}{c} \alpha_{i,j}^n - \Delta_{i,j}^{1,n}(\alpha_{i,j}^n, \alpha_{i-1,j}^n)(\alpha_{i,j}^n - \alpha_{i-1,j}^n) - \Delta_{i,j}^{2,n}(\alpha_{i,j}^n, \alpha_{i+1,j}^n)(\alpha_{i,j}^n - \alpha_{i+1,j}^n) \\ - \frac{1}{h_j} \left(c_{i,j-1/2}^n(\alpha_{i,j}^n) - c_{i,j-1/2}^n(\alpha_{i,j-1}^n) + d_{i,j+1/2}^n(\alpha_{i,j+1}^n) - d_{i,j+1/2}^n(\alpha_{i,j}^n) \right) \end{array} \right)$$

$$- \left(\int_{t_n}^{t_{n+1}} \int_{K_{i,j}} \operatorname{div}_{\mathbf{x}}(\mathbf{F})(t, \mathbf{x}, \alpha_{i,j}^n) d\mathbf{x} dt, \right) =: T_{1,i} - T_{2,i} \quad (6.41)$$

where

$$\Delta_{i,j}^{1,n}(p, q) = \frac{\mathcal{A}_{i-1/2,j}^n(p) - \mathcal{A}_{i-1/2,j}^n(q)}{p - q} \quad \text{and} \quad \Delta_{i,j}^{2,n}(p, q) = \frac{\mathcal{B}_{i+1/2,j}^n(p) - \mathcal{B}_{i+1/2,j}^n(q)}{q - p}.$$

It is enough to estimate $|\alpha_{h,\delta}|_{L_y^1 BV_x}$ as we did in the proof of Proposition 6.7. Take the difference between the scheme (6.41) written for $\alpha_{i+1,j}^{n+1}$ and $\alpha_{i,j}^{n+1}$. The difference $T_{1,i+1} - T_{1,i}$ can be estimated exactly as in the proof of [75, Lemma 8], wherein the CFL condition in Theorem 6.9 enables us to express $\alpha_{i,j}^{n+1} - \alpha_{i-1,j}^{n+1}$ as a convex linear combination of differences at the previous time step n . Consider the difference $|T_{2,i+1} - T_{2,i}|$:

$$\begin{aligned} |T_{2,i+1} - T_{2,i}| &\leq \int_{t_n}^{t_{n+1}} \left| \int_{K_{i+1,j}} \operatorname{div}_{\mathbf{x}}(\mathbf{F})(t, \mathbf{x}, \alpha_{i+1,j}^n) d\mathbf{x} - \int_{K_{i,j}} \operatorname{div}_{\mathbf{x}}(\mathbf{F})(t, \mathbf{x}, \alpha_{i+1,j}^n) d\mathbf{x} \right| dt \\ &+ \int_{t_n}^{t_{n+1}} \left| \int_{K_{i,j}} \operatorname{div}_{\mathbf{x}}(\mathbf{F})(t, \mathbf{x}, \alpha_{i+1,j}^n) d\mathbf{x} - \int_{K_{i,j}} \operatorname{div}_{\mathbf{x}}(\mathbf{F})(t, \mathbf{x}, \alpha_{i,j}^n) d\mathbf{x} \right| dt =: Q_1 + Q_2. \end{aligned} \quad (6.42)$$

The term Q_2 can be estimated as

$$Q_2 \leq \delta |\operatorname{Lip}(\operatorname{div}_{\mathbf{x}}(\mathbf{F}))| |\alpha_{i+1,j}^n - \alpha_{i,j}^n|. \quad (6.43)$$

Follow the proof of [75, Lemma 8] and use (6.42) and (6.43) to obtain

$$\begin{aligned} |\alpha_{h,\delta}(t_{n+1}, \cdot)|_{BV_{x,y}} &\leq |\alpha_{h,\delta}(t_n, \cdot)|_{BV_{x,y}} (1 + 6\delta \operatorname{Lip}(\partial_s \mathbf{F}) + \delta \operatorname{Lip}(\operatorname{div}_{\mathbf{x}}(\mathbf{F}))) \\ &+ \int_{t_n}^{t_{n+1}} |\Pi_h^0(\operatorname{div}_{\mathbf{x}}(\mathbf{F}))|_{BV_{x,y}} dt. \end{aligned}$$

Apply induction on the above result and use similar arguments as in the proof of Proposition 6.8 to obtain the desired result. \square

6.6 Numerical examples

We consider three examples to demonstrate the conclusions of Theorems 6.4 and 6.9. In Example 6.10, we manufacture a source term such that the conservation law (6.44) has a smooth solution. In Example 6.11, the source term is set to be zero and a discontinuous function is chosen as the initial data, and as a result the exact solution also becomes discontinuous. Example 6.11 helps to understand how the discontinuities in the solution affect the growth of BV seminorm. In Example 6.12, we consider a conservation law with fully nonlinear flux with an exact solution and illustrate the conclusions of Theorems 6.9.

Example 6.10 (smooth solution). We consider the spatial domain $\Omega = (-1, 1)^2$, temporal domain $(0, 1)$, velocity vector field $\mathbf{u} = (u, v)$ defined by

$$u(t, x, y) := t \sin(\pi x) \cos(\pi y/2)/16 \quad \text{and} \quad v(t, x, y) := t \sin(\pi y) \cos(\pi x/2)/16,$$

initial data $\alpha_0(x, y) := 1 \quad \forall (x, y) \in \Omega$, and an appropriate source term \mathfrak{S} such that the problem

$$\left. \begin{aligned} \partial_t \alpha + \operatorname{div}(\mathbf{u}f(\alpha)) &= \mathfrak{S} \text{ in } \Omega_1 \text{ and} \\ \alpha(0, x, y) &= \alpha_0(x, y) \quad \forall (x, y) \in \Omega, \end{aligned} \right\} \quad (6.44)$$

has the unique smooth solution $\alpha(t, x, y) = \exp(t(x+y)) \quad \forall (t, x, y) \in \Omega_1$, where $\Omega_1 = (0, 1) \times \Omega$.

Example 6.11 (discontinuous solution). The spatial domain is $\Omega = (-3, 3)^2$ and the temporal domain is $(0, 2)$. In the case where the flux function f in (6.44) is linear, then we set the velocity vector field \mathbf{u} as $(1, 1)$ and the source term \mathfrak{S} as zero so that the problem (6.44) has the unique solution $\alpha(t, x, y) := \alpha_0(x-t, y-t)$. The initial data considered is $\alpha_0(x, y) = \mathbf{1}_{[x > -1/4]}/2 + \mathbf{1}_{[y > -1/4]}/2$, where $\mathbf{1}_A$ is the characteristic function of the set A . In the case where the flux function f is nonlinear, then we set the velocity vector field $\mathbf{u} = (u, v)$ as

$$u(t, x, y) = \sin(\pi x) \cos(\pi y/2)/20 \quad \text{and} \quad v(t, x, y) = \sin(\pi y) \cos(\pi x/2)/20.$$

Note that in the case of nonlinear flux, the vector \mathbf{u} is zero on the boundary of the square $(-3, 3)^2$, and as a result we can take the boundary data $(\alpha \mathbf{u})|_{\partial\Omega} \cdot \mathbf{n}|_{\partial\Omega} = 0$, where $\mathbf{n}|_{\partial\Omega}$ is the outward normal to $\partial\Omega$. This homogeneous boundary condition on \mathbf{u} is useful since the exact solution to the problem (6.44) with a nonlinear flux is not available. The source term and the initial condition remain the same as in the case of linear flux.

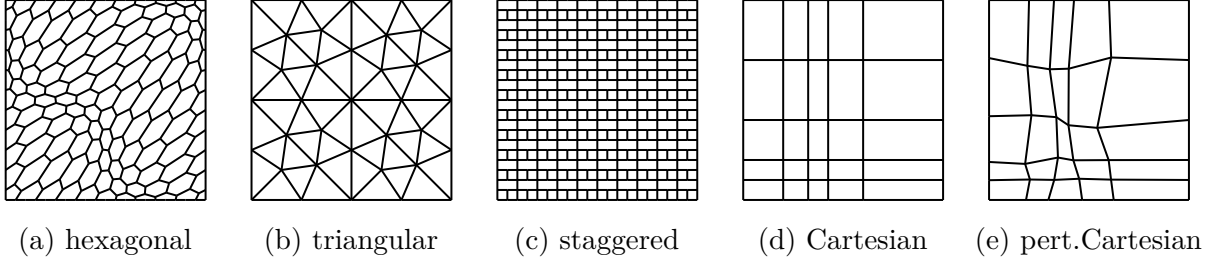
Example 6.12 (fully nonlinear flux). The spatial and temporal domains, initial data, and exact solution are chosen as in Example 6.10. The nonlinear conservation law considered is

$$\left. \begin{aligned} \partial_t \alpha + \operatorname{div}(\sin((x-t)\alpha), \cos((y-t)\alpha)) &= \mathfrak{S}_N \text{ in } \Omega_1 \text{ and} \\ \alpha(0, x, y) &= \alpha_0(x, y) \quad \forall (x, y) \in \Omega. \end{aligned} \right\} \quad (6.45)$$

The source term \mathfrak{S}_N is chosen such that (6.45) has the smooth solution $\alpha(t, x, y) = \exp(t(x+y))$. Note that the divergence of the flux $\operatorname{div}(\sin((x-t)\alpha), \cos((y-t)\alpha)) = \alpha \cos((x-t)\alpha) - \alpha \sin((y-t)\alpha)$ is not identically zero.

We consider two fluxes in the tests: (i) linear flux, $f(s) = s$ and (ii) sinusoidal flux, $f(s) = \sin(2\pi s)$. The numerical flux used is the Godunov flux defined by

$$g(a, b) = \begin{cases} \max_{b < s < a} (f(s)) & \text{if } b < a, \\ \min_{a < s < b} (f(s)) & \text{if } a < b. \end{cases}$$



The families of meshes considered are (a) hexagonal, (b) triangular, (c) staggered, (d) Cartesian, and (e) perturbed Cartesian (see Figures 6.6(a)–6.6(e)).

The BV and L^1 rates are defined by

$$BV \text{ rate} = \frac{\log \left| \alpha_{h_{k+1}, \delta_{k+1}}(T, \cdot) \right|_{BV_{x,y}} - \log \left| \alpha_{h_k, \delta_k}(T, \cdot) \right|_{BV_{x,y}}}{\log(h_{k+1}/h_k)} \text{ and}$$

$$L^1 \text{ rate} = \frac{\log \left| \alpha_{h_{k+1}, \delta_{k+1}}(T, \cdot) \right|_{L^1(\Omega)} - \log \left| \alpha_{h_k, \delta_k}(T, \cdot) \right|_{L^1(\Omega)}}{\log(h_{k+1}/h_k)}.$$

Discretisation factors, BV norms, and BV rates corresponding to Cartesian and perturbed Cartesian grids are presented in Tables 6.2–6.5 and Tables 6.7–6.10. The L^1 errors and L^1 rates are also included whenever an exact solution is available. Arrangement of the contents in Tables 6.2–6.10 are outlined in Table 6.1 for clarity. The BV rates corresponding to hexagonal, triangular, and staggered are presented in Table 6.6 and Table 6.11. The quantities L^1 error and L^1 rate are omitted for these three families of meshes since they follow a trend exactly similar to that of perturbed Cartesian grids. The L^1 and BV rates of the discrete solutions obtained by applying the scheme (6.39) to Example 6.12 are provided in Table 6.12.

Tables showing L^1 and BV rates		continuous flux	grid
Example 6.10	Example 6.11		
Table 6.2	Table 6.7	linear, $f(s) = s$	Cartesian
Table 6.3	Table 6.8	sinusoidal, $f(s) = \sin(2\pi s)$	Cartesian
Table 6.4	Table 6.9	linear, $f(s) = s$	perturbed Cartesian
Table 6.5	Table 6.10	sinusoidal, $f(s) = \sin(2\pi s)$	perturbed Cartesian

Table 6.1: Arrangement of contents in Tables 6.2–6.5 and Tables 6.7–6.10.

The captions of Tables 6.2–6.5 and Tables 6.7–6.10 are in the following format: *example, continuous flux function, grid type*.

6.6.1 Observations

We recall three classical results from the theory of convergence analysis of finite volume schemes for conservation laws of the type (6.1).

- (R.1) For a BV initial data, finite volume approximations of conservation laws of the type (6.1) on structured Cartesian meshes converge with $h^{1/2}$ rate with respect to $L_t^\infty L^1$ norm [68], and this result is extended to nearly Cartesian meshes by B. Cockburn et al. [85]. For generic meshes the $L_t^\infty L^1$ convergence rate is $h^{1/4}$ [105, p. 188].
- (R.2) The BV seminorm of the finite volume solution grows with a rate not greater than $h^{-1/2}$ [105, p. 168]. Further details can be found in [85, p. 1777] and the references therein.
- (R.3) For BV initial data, finite volume approximations of nonlinear conservation laws of the type (6.45) converge with $h^{1/2}$ rate with respect to $L_1(\Omega_T)$ norm (see Theorem 4 and Remark 1 in [75]).

In Tables 6.2–6.9, it can be observed that the order of convergence with respect to the L^1 -norm is well above $1/4$. The BV seminorm grows as h decreases indicated by the negative values of BV rate in Tables 6.2–6.9. But the growth rate is well below $-1/2$ except in the case of initial coarse meshes. The trend in L^1 rate is related to the trend in BV rate. A reduced L^1 rate is attributed to the fact that finite volume solutions on generic grids lack a uniform strong BV estimate. The weak BV estimate (6.3) diminishes the L^1 rate from $h^{1/2}$ to $h^{1/4}$ in the case of non-Cartesian meshes.

When the flux is linear, the mesh is Cartesian (uniform or nonuniform), and (6.1) possesses a smooth solution, we obtain first order L^1 rate and the BV rate decreases in magnitude (but with oscillations), which indicates that the BV seminorm seems to not blow up. In the case of sinusoidal flux, the L^1 rate shows a slight reduction for coarse meshes but readily becomes well above $h^{1/2}$, which is the theoretical L^1 rate. Here also, BV rate decreases in magnitude but with oscillations as h decreases.

The numerical tests with perturbed Cartesian meshes also shows a similar behaviour. The linear flux exhibits first order L^1 rate and the sinusoidal flux a slightly reduced L^1 rate but well above $h^{1/2}$. However, the BV rate shows a steady reduction in magnitude in both the linear and sinusoidal case. The BV rate for hexagonal, triangular, and staggered meshes also show a steady decrease in magnitude as provided in Table 6.11.

In Example 6.11, we see a prominent reduction in the L^1 rate and this is due to the discontinuities in the weak solution to (6.1). The explicit finite volume scheme introduces considerable numerical diffusion in the discrete solution by smearing out the sharp fronts, thereby reducing the convergence rate. This reduction in the L^1 rate is visible in both the Cartesian and perturbed Cartesian cases (see Tables 6.7 and 6.9). The BV rate is also decreasing in magnitude but with oscillations. In the sinusoidal flux case also BV rates show the same pattern (see Tables 6.8 and 6.10). For other non-Cartesian meshes also the BV rate seems to be decreasing in magnitude as presented in Table 6.11.

In the of conservation laws with fully nonlinear flux, it is clear from Table 6.12 that the BV rate is decreasing in magnitude steadily as h decreases. This complements the uniform BV estimates in Theorem 6.9. The L^1 rate is also greater than the theoretical rate of $h^{1/2}$

h	δ	error	rate	BV seminorm	BV rate
		L^1	L^1		
5.00E-01	2.50E-01	1.37E-01	-	2.02E+01	-
2.50E-01	1.25E-01	7.19E-02	9.30E-01	2.31E+01	-1.92E-01
1.25E-01	6.25E-02	3.82E-02	9.08E-01	3.06E+01	-4.07E-01
6.25E-02	3.12E-02	1.98E-02	9.50E-01	3.53E+01	-2.05E-01
3.12E-02	1.56E-02	1.01E-02	9.72E-01	3.79E+01	-1.03E-01

Table 6.2: Example 6.10, linear, Cartesian

h	δ	error	rate	BV seminorm	BV rate
		L^1	L^1		
5.00E-01	3.97E-02	3.32E-02	-	2.42E+01	-
2.50E-01	1.98E-02	3.35E-02	-1.02E-02	3.20E+01	-3.99E-01
1.25E-01	9.94E-03	2.59E-02	3.71E-01	3.78E+01	-2.41E-01
6.25E-02	4.97E-03	1.64E-02	6.53E-01	4.03E+01	-9.13E-02
3.12E-02	2.48E-03	9.58E-03	7.81E-01	4.12E+01	-3.13E-02

Table 6.3: Example 6.10, sinusoidal, Cartesian

h	δ	error	rate	BV seminorm	BV rate
		L^1	L^1		
5.70E-01	2.85E-01	1.54E-01	-	1.97E+01	-
3.01E-01	1.50E-01	8.76E-02	8.95E-01	2.71E+01	-4.99E-01
1.52E-01	7.62E-02	4.65E-02	9.26E-01	3.30E+01	-2.88E-01
8.40E-02	4.20E-02	2.61E-02	9.68E-01	3.64E+01	-1.65E-01
4.21E-02	2.10E-02	1.33E-02	9.80E-01	3.84E+01	-7.84E-02

Table 6.4: Example 6.10, linear, perturbed Cartesian

h	δ	Error	rate	BV seminorm	BV rate
		L^1	L^1		
5.70E-01	4.54E-02	5.44E-02	-	2.42E+01	-
3.01E-01	2.40E-02	3.74E-02	5.87E-01	3.31E+01	-4.91E-01
1.52E-01	1.21E-02	2.69E-02	4.81E-01	3.73E+01	-1.75E-01
8.40E-02	6.68E-03	1.77E-02	7.06E-01	4.13E+01	-1.70E-01
4.21E-02	3.35E-03	1.01E-02	8.11E-01	4.19E+01	-1.84E-02

Table 6.5: Example 6.10, sinusoidal, perturbed Cartesian

h decreasing	BV rate (linear)			BV rate (sinusoidal)		
	hexagonal	triangular	staggered	hexagonal	triangular	staggered
	-2.49E-01	-2.43E-01		-1.46E-01	-2.39E-01	
	-1.62E-01	-1.26E-01	-1.77E-01	-6.87E-02	-1.27E-01	-9.39E-02
	-1.04E-01	-6.79E-02	-8.83E-02	-2.41E-02	-4.01E-02	-3.10E-02
-2.62E-01	-3.80E-02	-2.59E-02	-1.28E-03	-5.11E-03	-1.13E-02	

Table 6.6: Example 6.10 – Trend in the rate of BV norm for a smooth solution of (6.1).

h	δ	error	rate	BV seminorm	BV rate
		L^1	L^1		
3.00E+00	9.37E-02	4.14E-01	-	4.26E+00	-
1.50E+00	4.68E-02	8.16E-01	-9.78E-01	5.57E+00	-3.85E-01
7.50E-01	2.34E-02	4.74E-01	7.81E-01	6.33E+00	-1.85E-01
3.75E-01	1.17E-02	3.70E-01	3.59E-01	7.69E+00	-2.80E-01
1.87E-01	5.85E-03	2.87E-01	3.66E-01	8.75E+00	-1.86E-01

Table 6.7: Example 6.11, linear, Cartesian

h	δ	BV seminorm	BV rate
3.00E+00	1.49E-02	6.32E+00	-
1.50E+00	7.46E-03	6.35E+00	-7.31E-03
7.50E-01	3.73E-03	6.60E+00	-5.44E-02
3.75E-01	1.86E-03	6.76E+00	-3.52E-02
1.87E-01	9.32E-04	7.08E+00	-6.64E-02

Table 6.8: Example 6.11, sinusoidal, Cartesian

h	δ	error	rate	BV seminorm	BV rate
		L^1	L^1		
3.42E+00	1.06E-01	3.98E-01	-	4.68E+00	-
1.81E+00	5.65E-02	7.24E-01	-9.38E-01	6.23E+00	-4.49E-01
9.14E-01	2.85E-02	4.61E-01	6.59E-01	6.48E+00	-5.70E-02
5.04E-01	1.57E-02	3.70E-01	3.69E-01	8.77E+00	-5.07E-01
2.53E-01	7.91E-03	2.85E-01	3.78E-01	9.51E+00	-1.17E-01

Table 6.9: Example 6.11, linear, perturbed Cartesian

h	δ	BV seminorm	BV rate
3.42E+00	1.06E-01	6.32E+00	-
1.81E+00	5.65E-02	6.54E+00	-4.95E-02
9.14E-01	2.85E-02	6.70E+00	-3.51E-02
5.04E-01	1.57E-02	7.57E+00	-2.05E-01
2.53E-01	7.91E-03	7.28E+00	-5.75E-02

Table 6.10: Example 6.11, sinusoidal, perturbed Cartesian

h decreasing	BV rate (linear flux)		BV rate (sinusoidal flux)			
	hexagonal	triangular	square	hexagonal	triangular	staggered
	-4.32E-01	-3.90E-01	6.54E-02	-7.19E-02	-4.91E-01	
	-3.77E-01	-3.61E-01	-1.89E-01	-6.92E-02	1.93E-01	1.46E-01
	-3.14E-01	-6.60E-02	-4.14E-02	-3.16E-02	-2.39E-02	-1.24E-01
	-3.11E-01	-1.71E-01	-4.88E-03	-1.10E-03	-9.69E-03	-1.24E-04

Table 6.11: Example 6.11 – Trend in BV rate for a discontinuous solution of (6.1).

h	δ	error	rate	BV seminorm	BV rate
		L^1	L^1		
5.00E-01	3.97E-02	1.47E-01	-	2.45E+00	-
2.50E-01	1.98E-02	1.08E-01	4.35E-01	3.58E+00	-5.43E-01
1.25E-01	9.94E-03	7.48E-02	5.40E-01	4.57E+00	-3.54E-01
6.25E-02	4.97E-03	4.74E-02	6.58E-01	5.33E+00	-2.21E-01
3.12E-02	2.48E-03	2.80E-02	7.58E-01	5.88E+00	-1.40E-01

Table 6.12: Example 6.12 – Fully nonlinear flux and Cartesian grid.

except for the initial coarse mesh (see result (R.3)). Table 6.12 also complements in [75, Lemma 8, Theorem 4], which provide the boundedness of the BV seminorm of discrete solutions corresponding to uniform square Cartesian grids.

Remark 6.13. *The choice of the functions \mathcal{A} , \mathcal{B} , \mathcal{C} , and \mathcal{D} for the scheme (6.39) is not arbitrary. It is crucial that \mathcal{A} and \mathcal{C} are nondecreasing, \mathcal{B} and \mathcal{D} are nonincreasing, and the CFL condition in Theorem 6.9 holds. We use the following pairs to obtain the results provided in Table 6.12:*

$$\begin{aligned} \mathcal{A}(t, x, y, z) &= (\sin((x-t)z) + \mathfrak{M}z)/2, & \mathcal{B}(t, x, y, z) &= (\sin((x-t)z) - \mathfrak{M}z)/2, \\ \mathcal{C}(t, x, y, z) &= (\cos((y-t)z) + \mathfrak{M}z)/2, & \mathcal{D}(t, x, y, z) &= (\cos((y-t)z) - \mathfrak{M}z)/2, \end{aligned}$$

where $\mathfrak{M} = \text{Lip}(\mathbf{F})$. This choice of \mathfrak{M} ensures the monotonicity conditions required by

\mathcal{A} , \mathcal{B} , \mathcal{C} , and \mathcal{D} . Moreover, \mathcal{A} , \mathcal{B} , \mathcal{C} , and \mathcal{D} become Lipschitz continuous with Lipschitz constant $Lip(\mathbf{F})$ so that the CFL condition in Theorem 6.9 holds.

6.6.2 A remark on strong BV estimate for non-Cartesian grids

In the case of Cartesian mesh, note that the BV rate decreases in magnitude as h decreases and the BV seminorm stabilises eventually, which agrees with the conclusion of Theorem 6.4. This is also supported by the higher values of L^1 rate than the theoretically predicted ones and the fact that the reduced convergence rate stems from lack of a strong BV estimate (see result (R.1)).

Similar trends can be observed in the case of perturbed Cartesian grids also. These trends indicate that the BV bounds established here would possibly also hold for certain non-Cartesian grids. Any such uniform estimate on strong BV immediately provides a proof for the improved convergence rates. However, as of now any analytical proof of a strong BV estimate on meshes other than nonuniform Cartesian grids is not available in the literature. A strong challenge in this direction is the counterexample provided by B. Després [86]. This article presents an analytical example that shows the BV seminorms of finite volume solutions on a staggered grid, see Figure 6.6(c). The example consists of the problem

$$\left. \begin{aligned} \partial_t \alpha + u \partial_x \alpha &= 0, \text{ for } (x, y) \in (-\ell, \ell)^2, \ 0 < t < T \\ \alpha(t, x, y) &= \alpha_0(x, y) \text{ for } (x, y) \in (-\ell, \ell)^2, \end{aligned} \right\} \quad (6.46)$$

with $\ell = 1$, $u = 1$, and $\alpha_0(x, y) = H(x - 1/2)$, where H is the Heaviside step function may blow up with an order greater than $-1/2$. This is supported by numerical experiments also. In Table 6.13 it is evident that the BV seminorm is increasing and the rate of increase is also growing towards the theoretical rate of $h^{-1/2}$. Considering this result, the uniform BV estimate on non-Cartesian grids needs a deeper investigation.

h	δ	BV seminorm	BV rate
1.00E-01	1.00E-01	3.90E+00	-
5.00E-02	5.00E-02	5.65E+00	-5.36E-01
2.50E-02	2.50E-02	6.86E+00	-2.78E-01
1.25E-02	1.25E-02	9.00E+00	-3.92E-01
6.25E-03	6.25E-03	1.19E+01	-4.14E-01

Table 6.13: BV seminorms of the finite volume solutions corresponding to (6.46) on staggered meshes. The parameters used are $\ell = 1$ and $T = 1/4$.

6.7 Extension to three spatial dimensions

An analogous result to Theorem 6.4 can be derived in a three spatial dimensional setting. The main result is stated in Theorem 6.48. The proof is not included here since it is similar to the proof of Theorem 6.4 and only more technical as a result of an extra spatial dimension. A brief sketch is provided in Appendix A.2. Consider the partial differential equation on the time–space domain $\widehat{\Omega}_T = (0, T) \times \widehat{\Omega}$, wherein $\widehat{\Omega} := (a_L, a_R) \times (b_L, b_R) \times (c_L, c_R)$ described by

$$\left. \begin{aligned} \partial_t \alpha + \operatorname{div}(\mathbf{u}f(\alpha)) &= 0 \text{ in } \widehat{\Omega}_T \text{ and} \\ \alpha(0, \cdot) &= \alpha_0 \text{ in } \widehat{\Omega}, \end{aligned} \right\}$$

where $\mathbf{u} = (u, v, w)$. The assumptions (AS.1), (AS.2), and the condition $\mathbf{u}|_{\partial\widehat{\Omega}} = \mathbf{0}$ hold. In addition to assume (AS.3*) below.

(AS.3*) There exists a generic constant $\mathcal{C} \geq 0$ such that

$$\max \left(\|\mathbf{u}\|_{L_t^1 L^\infty(\widehat{\Omega}_T)}, \|\nabla \mathbf{u}\|_{L_t^1 L^\infty(\widehat{\Omega}_T)}, |\operatorname{div}(\mathbf{u})|_{L_t^1 BV_{x,y,z}} \right) \leq \mathcal{C} < \infty.$$

The temporal grid is same as in Section 6.3.2. An admissible grid on the cube, $\widehat{\Omega}$, is defined next.

Definition 6.14 (three dimensional admissible grid). *Define the one dimensional discretisations $X_k := \{x_{-1/2}, \dots, x_{I+1/2}\}$, $Y_h := \{y_{-1/2}, \dots, y_{J+1/2}\}$, and $Z_l := \{z_{-1/2}, \dots, z_{L+1/2}\}$, where $x_{-1/2} = a_L$, $x_{I+1/2} = a_R$, $y_{-1/2} = b_L$, $y_{J+1/2} = b_R$, $z_{-1/2} = c_L$, $z_{L+1/2} = c_R$, $k_i = x_{i+1/2} - x_{i-1/2}$, $h_j = y_{j+1/2} - y_{j-1/2}$, $l_m = z_{m+1/2} - z_{m-1/2}$, $k := \max k_i$, $h := \max h_j$, and $l := \max l_m$. The Cartesian grid $X_k \times Y_h \times Z_l$ is said to be a three dimensional admissible grid if the following hold: for a fixed constant $\tilde{c} > 0$, $(\tilde{c})^{-1} \leq \frac{h_j}{k_i} + \frac{k_i}{l_m} + \frac{l_m}{h_j} \leq \tilde{c} \forall i, j, l$.*

Define the control volumes $K_{i,j,m} := (x_{i-1/2}, x_{i+1/2}) \times (y_{j-1/2}, y_{j+1/2}) \times (z_{m-1/2}, z_{m+1/2})$, for $0 \leq i \leq I$, $0 \leq j \leq J$, and $0 \leq m \leq L$.

Definition 6.15 (three dimensional discrete solution). *Set the discrete initial data as $\alpha_{i,j,m}^0 := \int_{K_{i,j,m}} \alpha_0(\mathbf{x}) d\mathbf{x}$. The three dimensional discrete solution at the time step $n+1$, $\alpha_h^{n+1} : \widehat{\Omega} \rightarrow \mathbb{R}$, $n \geq 0$ is defined by $\alpha_h^{n+1}|_{K_{i,j,m}} = \alpha_{i,j,m}^{n+1}$, where*

$$\begin{aligned} \alpha_{i,j,m}^{n+1} &= \alpha_{i,j,m}^n - \mu_i \left(F_{i+1/2,j,m}^x - F_{i-1/2,j,m}^x \right) - \lambda_j \left(F_{i,j+1/2,m}^y - F_{i,j-1/2,m}^y \right) \\ &\quad - \nu_m \left(F_{i,j,m+1/2}^z - F_{i,j,m-1/2}^z \right), \end{aligned} \tag{6.47a}$$

where $\mu_i = \delta/k_i$, $\lambda_j = \delta/h_j$, $\nu_m = \delta/l_m$,

$$\begin{aligned} F_{i-1/2,j,m}^x &:= \left(u_{i-1/2,j,m}^{n+} g(\alpha_{i-1,j,m}^n, \alpha_{i,j,m}^n) - u_{i-1/2,j,m}^{n-} g(\alpha_{i,j,m}^n, \alpha_{i-1,j,m}^n) \right), \\ F_{i,j-1/2,m}^y &:= \left(v_{i,j-1/2,m}^{n+} g(\alpha_{i,j-1,m}^n, \alpha_{i,j,m}^n) - v_{i,j-1/2,m}^{n-} g(\alpha_{i,j,m}^n, \alpha_{i,j-1,m}^n) \right), \\ F_{i,j,m-1/2}^z &:= \left(w_{i,j,m-1/2}^{n+} g(\alpha_{i,j,m-1}^n, \alpha_{i,j,m}^n) - w_{i,j,m-1/2}^{n-} g(\alpha_{i,j,m}^n, \alpha_{i,j,m-1}^n) \right), \end{aligned} \tag{6.47b}$$

and for $a \in \mathbb{R}$,

$$\begin{aligned} u_{i-1/2,j,m}^n &= \int_{t_n}^{t_{n+1}} \int_{y_{j-1/2}}^{y_{j+1/2}} \int_{z_{m-1/2}}^{z_{m+1/2}} u(t, x_{i-1/2}, s, r) dr ds dt, \\ v_{i,j-1/2,m}^n &= \int_{t_n}^{t_{n+1}} \int_{x_{i-1/2}}^{x_{i+1/2}} \int_{z_{m-1/2}}^{z_{m+1/2}} v(t, s, y_{j-1/2}, r) dr ds dt, \quad \text{and} \\ w_{i,j,m-1/2}^n &= \int_{t_n}^{t_{n+1}} \int_{x_{i-1/2}}^{x_{i+1/2}} \int_{y_{j-1/2}}^{y_{j+1/2}} w(t, s, r, z_{m-1/2}) dr ds dt. \end{aligned}$$

Recall the time-reconstruct in Definition 6.3. Let $\alpha_{h,\delta} : \widehat{\Omega}_T \rightarrow \mathbb{R}$ be the time-reconstruct corresponding to the family of functions $\{\alpha_h^n\}_{n \geq 0}$. Define the BV in the time-space domain $\widehat{\Omega}_T$ for a function $\beta : \widehat{\Omega}_T \rightarrow \mathbb{R}$ by

$$|\beta|_{BV_{x,y,z,t}} := |\beta|_{L_x^1 L_y^1 L_z^1 BV_t} + |\beta|_{L_t^1 L_x^1 L_y^1 BV_z} + |\beta|_{L_t^1 L_y^1 L_z^1 BV_x} + |\beta|_{L_t^1 L_z^1 L_x^1 BV_y}.$$

The next theorem shows that $\alpha_{h,\delta}$ is a function of BV . The proof follows analogous to Theorem 6.4. [bounded variation] Let $X_k \times Y_h \times Z_l$ be a three dimensional admissible grid. Assume (AS.1), (AS.2), (AS.3*), and the Courant–Friedrichs–Lewy (CFL) condition

$$4\delta \max_{i,j} \left(\frac{1}{k_i} + \frac{1}{h_j} + \frac{1}{\nu_m} \right) \text{Lip}(g) \|\mathbf{u}\|_{L^\infty(\Omega_T)} \leq 1. \quad (6.48a)$$

If $\alpha_0 \in L^\infty(\widehat{\Omega}) \cap BV_{\mathbf{x}}(\widehat{\Omega})$, then $\alpha_{h,\delta}$ satisfies $|\alpha_{h,\delta}|_{BV_{x,y,z,t}} \leq \widehat{\mathcal{C}}_{BV}$, where $\widehat{\mathcal{C}}_{BV}$ depends on T , α_0 , f , g , $\|\nabla \mathbf{u}\|_{L_t^1 L^\infty(\widehat{\Omega}_T)}$, and $|\text{div}(\mathbf{u})|_{L_t^1 BV_{x,y,z}}$.

6.8 Existence result for a ductal carcinoma model

Set $\Omega = (0, 1) \times (0, \ell)$ in the sequel. Recall the *ductal carcinoma in situ* model (6.5). The model seeks a four tuple $(\alpha, p, \mathbf{u}, c)$ such that, in $\Omega_T = (0, T) \times \Omega$ it holds

$$\begin{aligned} \text{tumour cell concetration} &\left\{ \begin{array}{l} \frac{\partial \alpha}{\partial t} + \text{div}(\mathbf{u}\alpha) = \gamma\alpha(1-c), \end{array} \right. \\ \text{velocity – pressure system} &\left\{ \begin{array}{l} -\mu \left(\Delta \mathbf{u} + \frac{1}{3} \nabla(\text{div}(\mathbf{u})) \right) + \nabla p = \mathbf{0}, \\ \text{div}(\mathbf{u}) = \gamma(1-c), \text{ and} \end{array} \right. \\ \text{nutrient concentration} &\left\{ \begin{array}{l} -\Delta c = Q\alpha, \end{array} \right. \end{aligned}$$

A crucial application of Theorem 6.4 is that it enables us to prove the existence of a weak solution to coupled problems involving α and \mathbf{u} , such as (6.5). In this section, we apply Theorem 6.4 to establish the existence of a solution to the *ductal carcinoma in situ* problem (6.5). The main idea is to combine a finite volume discretisation of (6.5a) and

semi-discrete variational formulation of (6.5b), and thereby reduce the interdependence between α and \mathbf{u} to a semi-discrete relation $(\alpha_h^{n+1}, \mathbf{u}_h^{n+1}) = \mathbf{F}(\alpha_h^n, \mathbf{u}_h^n)$, where $(\alpha_h^n, \mathbf{u}_h^n)$ is the discrete solution at time step n and h is the discretisation factor. Then, an inductive argument is used to show that the BV norm of the time-reconstruct $\alpha_{h,\delta}$, see Definition 6.3, constructed from $(\alpha_h^n)_{n \geq 0}$ is independent of h and δ . Finally, Helly's selection theorem, see Theorem I, is invoked to obtain a convergent subsequence of $\{\alpha_{h,\delta}\}_{h,\delta}$ and the limit function is proved to be a weak solution of (6.5a).

Initial and boundary conditions

Fix an ε such that $0 < \varepsilon < (\ell - 1)/2$ and define the auxiliary domain $\Omega(\varepsilon) := (0, 1) \times (0, \ell - \varepsilon)$. Recall that for any $A \subset \mathbb{R}^d$, the set A_T is defined by $A_T = (0, T) \times A$. In the sequel, x (resp. y) component of \mathbf{u} is denoted by u (resp. v).

The initial concentration of the tumour cells and nutrient are $\alpha(0, \mathbf{x}) = \alpha_0(\mathbf{x})$ and $c(0, \mathbf{x}) = c_0(\mathbf{x})$, respectively. We assume that $\alpha_{0|(0,1) \times (1,\ell)} = 0$, which means the initial tumour occupies only a subset of $(0, 1) \times (0, 1)$ and later spreads throughout the duct Ω as time evolves. In Proposition 6.22, we obtain a time T_* such that the concentration of tumour cells remains zero for every $(t, x, y) \in (0, T_*) \times (0, 1) \times (\ell - 2\varepsilon, 1)$. This temporal restriction is imperative as it enables us to obtain a uniform BV estimate on the finite volume solutions. The boundary conditions on (6.5b) and (6.5c) are as follows:

$$\text{on } x \in \{0, 1\} : \quad \mathbf{u} \cdot \mathbf{n} = 0, \quad \nabla v \cdot \mathbf{n} = 0, \quad \nabla c \cdot \mathbf{n} = 0, \quad (6.50)$$

$$\text{on } y = 0 : \quad \mathbf{u} \cdot \mathbf{n} = 0, \quad \nabla u \cdot \mathbf{n} = 0, \quad \nabla c \cdot \mathbf{n} = 0, \quad \text{and} \quad (6.51)$$

$$\text{on } y = \ell : \quad \mathbf{u} \cdot \boldsymbol{\tau} = 0, \quad \nabla v \cdot \mathbf{n} = 0, \quad \nabla u \cdot \boldsymbol{\tau} = \gamma, \quad c = 0, p = 0, \quad (6.52)$$

where $\boldsymbol{\tau}$ and \mathbf{n} are the unit tangent and unit normal vectors to $\partial\Omega$, respectively. The boundary condition $c = 0$ at $y = 0$ used in [29] is replaced by $\nabla c \cdot \mathbf{n} = 0$ in (6.51), which indicates that nutrient cannot enter or leave the interior of duct through the duct wall at $y = 0$. The supplementary condition $\nabla u \cdot \boldsymbol{\tau} = \gamma$ in (6.52) is obtained from (6.5c) and the boundary condition $c = 0$ at $y = \ell$. These changes are reasonable from the modelling perspective, and aid in obtaining the minimal regularity on \mathbf{u} and c that guarantees the convergence of discrete solutions.

Recall the following definitions from Section 1.4. The Sobolev spaces $W^{m,p}(\Omega)$, $H^m(\Omega) := W^{m,2}(\Omega)$, and $L^p(\Omega)$, where $1 \leq p \leq \infty$, are defined in the standard way. Set the product spaces $\mathbf{W}^{m,p}(\Omega) := W^{m,p}(\Omega) \times W^{m,p}(\Omega)$ and $\mathbf{H}^m(\Omega) := H^m(\Omega) \times H^m(\Omega)$. For $\mathbf{u} = (u_1, \dots, u_d) \in \prod_{i=1}^d W^{m,p}(\Omega)$, $d \in \{1, 2\}$, define the norm $\|\mathbf{u}\|_{m,p,\Omega} := \sum_{i=1}^d \sum_{|\boldsymbol{\beta}| \leq m} \|\partial^{\boldsymbol{\beta}} u_i\|_{L^p(\Omega)}$, where $\boldsymbol{\beta} \in \mathbb{N}^2$ is a multi-index. Let $X_{\text{loc}}(\Omega) := \{v \in L^2(\Omega) : v|_{\omega} \in X(\omega) \quad \forall \omega \subset\subset \Omega\}$, where $X = H^m$ or $X = \mathbf{H}^m$. Define the Hilbert spaces \mathbf{H} and V by

$$\mathbf{H} := \left\{ \mathbf{u} := (u, v) \in \mathbf{H}^1(\Omega) \left| \begin{array}{l} \mathbf{u} \cdot \mathbf{n} = 0 \text{ at } x = 0, x = 1, y = 0, \\ \text{and } \mathbf{u} \cdot \boldsymbol{\tau} = 0 \text{ at } y = \ell \end{array} \right. \right\} \quad \text{and}$$

$$V := \{v \in H^1(\Omega) : v = 0 \text{ at } y = \ell\}.$$

For ease of notations, the explicit dependence of variables $(\alpha, \mathbf{u}, p, c)$ on time is skipped. For instance, in (6.54), \mathbf{u} stands for $\mathbf{u}(t, \cdot)$.

Definition 6.16 (weak solution). *A weak solution of the problem (6.5a)–(6.5c) is a four tuple $(\alpha, \mathbf{u}, p, c)$ such that the following conditions hold:*

1. *For $\nabla_{t,\mathbf{x}} = (\partial_t, \nabla)$, the tumour cell concentration $\alpha \in L^\infty(\Omega_T)$ is such that, for every $\vartheta \in \mathcal{C}_c^\infty([0, T] \times \Omega)$,*

$$\int_{\Omega_T} ((\alpha, \mathbf{u}\alpha) \cdot \nabla_{t,\mathbf{x}}\vartheta + \gamma\alpha(1-c)\vartheta) \, d\mathbf{x} \, dt + \int_{\Omega} \alpha_0(\mathbf{x})\vartheta(0, \mathbf{x}) \, d\mathbf{x} = 0. \quad (6.53)$$

2. *The velocity–pressure system is such that $\mathbf{u} \in L^2(0, T; \mathbf{H})$, $p \in L^2(0, T; L^2(\Omega))$, and for every $\boldsymbol{\psi} := (\psi_1, \psi_2) \in L^2(0, T; \mathbf{H})$, $w \in L^2(0, T; L^2(\Omega))$,*

$$\begin{aligned} \int_0^T \mu \mathbf{a}(\mathbf{u}, \boldsymbol{\psi}) \, d\mathbf{x} - \int_{\Omega_T} p \operatorname{div}(\boldsymbol{\psi}) \, d\mathbf{x} \, dt &= \int_0^T \int_{y=\ell} \frac{\gamma\mu}{3} \psi_2 \, ds \, dt, \quad \text{and} \quad (6.54) \\ \int_{\Omega_T} \operatorname{div}(\mathbf{u}) w \, d\mathbf{x} \, dt &= \int_{\Omega_T} \gamma(1-c) w \, d\mathbf{x} \, dt, \end{aligned}$$

where

$$\mathbf{a}(\mathbf{v}, \mathbf{w}) := \int_{\Omega} (\nabla \mathbf{v} : \nabla \mathbf{w} + \frac{1}{3} \operatorname{div}(\mathbf{v}) \operatorname{div}(\mathbf{w})) \, d\mathbf{x}$$

for $\mathbf{v}, \mathbf{w} \in \mathbf{H}^1(\Omega)$.

3. *The variable $c \in L^2(0, T; V)$ satisfies, for every $\varphi \in L^2(0, T; V)$*

$$\int_0^T \int_{\Omega} \nabla c \cdot \nabla \varphi \, d\mathbf{x} \, dt = \int_0^T \int_{\Omega} Q \alpha \varphi \, d\mathbf{x} \, dt. \quad (6.55)$$

We define a semi–discrete scheme for (6.5), where the tumour cell concentration is discrete and other variables are kept continuous. The tumour cell concentration is discretised using a finite volume method, and the velocity–pressure and nutrient concentration are obtained from the corresponding weak formulations and boundary conditions (6.50)–(6.52).

Semi–discrete scheme: *Let $X_h \times Y_h$ be a uniform grid on $\Omega(\varepsilon)$ with $h < \varepsilon$ and $0 = t_0 < \dots < T_N = T$ be a uniform temporal discretisation with $\delta = t_{n+1} - t_n$. Construct a finite sequence of functions $(\alpha_h^n, \mathbf{u}_h^n, p_h^n, c_h^n)_{\{0 \leq n < N\}}$ on Ω as follows. For $n = 0$, define $\alpha_h^0 : \Omega \rightarrow \mathbb{R}$ by $\alpha_h^0 := \alpha_{i,j}^0$, where $\alpha_{i,j}^0 := \int_{K_{i,j}} \alpha_0(\mathbf{x}) \, d\mathbf{x}$. For $0 \leq n < N$, define the iterates as follows.*

1. *The function $c_h^n \in V$ is defined by: for every $\varphi \in V$,*

$$\int_{\Omega} (\nabla c_h^n \cdot \nabla \varphi - Q \alpha_h^n \varphi) \, d\mathbf{x} = 0. \quad (6.56)$$

2. The functions $(\mathbf{u}_h^n, p_h^n) \in \mathbf{H} \times L^2(\Omega)$ is defined by: for every $(\boldsymbol{\varphi}, q) \in \mathbf{H} \times L^2(\Omega)$ with $\boldsymbol{\varphi} = (\varphi_1, \varphi_2)$,

$$\mu \mathbf{a}(\mathbf{u}_h^n, \boldsymbol{\varphi}) - \int_{\Omega} p_h^n \operatorname{div}(\boldsymbol{\varphi}) \, d\mathbf{x} = \int_{y=\ell} \frac{\gamma \mu}{3} \varphi_2 \, ds, \quad \text{and} \quad (6.57)$$

$$\int_{\Omega} \operatorname{div}(\mathbf{u}_h^n) q \, d\mathbf{x} = \int_{\Omega} \gamma (1 - c_h^n) q \, d\mathbf{x}. \quad (6.58)$$

3. Define α_h^{n+1} as the trivial extension of $\hat{\alpha}_h^{n+1} : \Omega(\varepsilon) \rightarrow \mathbb{R}$, where $\hat{\alpha}_h^{n+1} := \hat{\alpha}_{i,j}^{n+1}$ on $K_{i,j} = (x_{i-1/2}, x_{i+1/2}) \times (y_{j-1/2}, y_{j+1/2})$ is obtained by

$$\begin{aligned} \hat{\alpha}_{i,j}^{n+1} &= \hat{\alpha}_{i,j}^n - \frac{\delta}{h} \left[(\hat{\mathbb{F}}_{i+1/2,j}^n - \hat{\mathbb{F}}_{i-1/2,j}^n) + (\hat{\mathbb{G}}_{i,j+1/2}^n + \hat{\mathbb{G}}_{i,j-1/2}^n) \right] \\ &\quad + \gamma \delta \int_{K_{i,j}} \hat{\alpha}_{i,j}^n (1 - c_h^n) \, d\mathbf{x}, \end{aligned} \quad (6.59)$$

where

$$\hat{\mathbb{F}}_{i-1/2,j}^n := u_{i-1/2,j}^{n+} \alpha_{i-1,j}^n - u_{i-1/2,j}^{n-} \alpha_{i,j}^n, \quad \hat{\mathbb{G}}_{i,j-1/2}^n := v_{i,j-1/2}^{n+} \alpha_{i,j-1}^n - v_{i,j-1/2}^{n-} \alpha_{i,j}^n,$$

$$u_{i-1/2,j}^n = \int_{t_n}^{t_{n+1}} \int_{y_{j-1/2}}^{y_{j+1/2}} u_h^n(x_{i-1/2}, s) \, ds \, dt, \quad \text{and}$$

$$v_{i,j-1/2}^n = \int_{t_n}^{t_{n+1}} \int_{x_{i-1/2}}^{x_{i+1/2}} v_h^n(s, y_{j-1/2}) \, ds \, dt.$$

6.8.1 Compactness

The functions $\alpha_{h,\delta}$, $\mathbf{u}_{h,\delta}$, $p_{h,\delta}$, and $c_{h,\delta}$ are the time-reconstructs, see Definition 6.3, corresponding to the family of functions $(\alpha_h^n)_{\{n \geq 0\}}$, $(\mathbf{u}_h^n)_{\{n \geq 0\}}$, $(p_h^n)_{\{n \geq 0\}}$, and $(c_h^n)_{\{n \geq 0\}}$, respectively.

Theorem 6.17 (Compactness). *Fix a positive number $\alpha_M > a^0 = \sup_{\Omega} |\alpha_0|$. Assume that $\alpha_0|_{(0,1) \times (1,\ell)} = 0$ and the following property on the discretisation factors δ and h :*

$$\mathcal{C}_{\text{ICFL}}^\varepsilon \leq \frac{\delta}{h} \leq \gamma \mathcal{C}_{\text{emb},\varepsilon} \mathcal{C}_\varepsilon (1 + Q \mathcal{C} \sqrt{2\ell} \alpha_M). \quad (6.60a)$$

where the constants $\mathcal{C} > 0$ and $\mathcal{C}_{\text{emb},\varepsilon} \mathcal{C}_\varepsilon > 0$ are specified in Lemmas 6.20 and 6.21, respectively. Here, \mathcal{C}_ε , $\mathcal{C}_{\text{emb},\varepsilon}$ and $\mathcal{C}_{\text{ICFL}}^\varepsilon$ depends on ε , but not on h and δ . Then, there exists a finite time $T_* < \infty$, a subsequence – denoted with the same indices – of the family of functions $\{(\alpha_{h,\delta}, \mathbf{u}_{h,\delta}, p_{h,\delta}, c_{h,\delta})\}_{h,\delta}$ obtained from the semi-discrete scheme, and a four tuple of functions $(\alpha, \mathbf{u}, p, c)$ such that

$$\alpha \in BV(\Omega_{T_*}), \quad \mathbf{u} \in L^2(0, T_*; \mathbf{H}), \quad p \in L^2(0, T_*; L^2(\Omega)), \quad c \in L^2(0, T_*; V)$$

and as $h, \delta \rightarrow 0$

- $\alpha_{h,\delta} \rightarrow \alpha$ almost everywhere and in L^∞ weak- \star on Ω_{T_*} ,
- $\mathbf{u}_{h,\delta} \rightharpoonup \mathbf{u}$ weakly in $L^2(0, T_*; \mathbf{H})$, $p_{h,\delta} \rightharpoonup p$ weakly in $L^2(0, T_*; L^2(\Omega))$, and
- $c_{h,\delta} \rightharpoonup c$ weakly in $L^2(0, T_*; V)$.

Remark 6.18 (Necessity of strong BV estimate on $\alpha_{h,\delta}$). *The uniform boundedness on $\alpha_{h,\delta}$ directly yields a subsequence that converges in weak- \star topology. However, this is not sufficient to show that the second term in the right hand side of (6.59) converges weakly. It is shown that $c_{h,\delta}$ converges weakly in $L^2(0, T_*; H^1(\Omega))$. Therefore, to establish that $\alpha_{h,\delta}(1 - c_{h,\delta})$ converges weakly to $\alpha(1 - c)$, the strong convergence of $\alpha_{h,\delta}$ is required. We employ Theorem I of Section 6.3.1 to extract a subsequence of $\{\alpha_{h,\delta}\}$ that converges almost everywhere and in $L^1(\Omega_{T_*})$, for which a strong uniform BV estimate is necessary.*

The proof of Theorem 6.17 is achieved over multiple steps. We establish the following properties.

- in Lemma 6.20: c_h^n has $W^{2,p}(\Omega)$ regularity, which yields an estimate on $\|c_h\|_{1,\infty,\Omega}$
- in Lemma 6.21: \mathbf{u}_h^n has $\mathbf{H}_{\text{loc}}^3(\Omega)$ regularity, which yields a local estimate on $\|\mathbf{u}_h^n\|_{1,\infty}$
- in Proposition 6.22: the finite volume solution $\alpha_{h,\delta}$ is bounded, and
- in Proposition 6.23: Corollary 1 and the above steps are employed to prove that $\alpha_{h,\delta}$ is a function with BV.

Define the extended functions \bar{c}_h^n , $\bar{\mathbf{u}}_h^n := (\bar{u}_h^n, \bar{v}_h^n)$, and \bar{p}_h^n on $\Omega_{\text{ext}} := (-1, 2) \times (-\ell, \ell)$ using even and odd reflections as follows. Let $a \in \{0, 1, 2\}$ and $b \in \{0, \ell\}$. Then, on $(a - 1, a) \times (b - \ell, b)$ set $(\tilde{x}, \tilde{y}) := (x(-2a^2 + 4a - 1) + (a^2 - a), (2b - \ell)y/\ell)$ and define

$$\left. \begin{aligned} \bar{\alpha}_h^n(x, y) &:= \alpha_h^n(\tilde{x}, \tilde{y}), \quad \bar{c}_h^n(x, y) := c_h^n(\tilde{x}, \tilde{y}), \quad \bar{p}_h^n(x, y) := p_h^n(\tilde{x}, \tilde{y}), \quad \text{and} \\ \bar{u}_h^n(x, y) &:= (-2a^2 + 4a - 1)u_h^n(\tilde{x}, \tilde{y}), \quad \bar{v}_h^n(x, y) := (2b/\ell - 1)v_h^n(\tilde{x}, \tilde{y}). \end{aligned} \right\} \quad (6.61)$$

In (6.61), we have a compact representation of all reflections employed to construct the extended functions. A pictorial representation of (6.61) is provided in Figure 6.7 for clarity. We introduced three spatial domains so far and relations between them are represented in Figure 6.8.

Remark 6.19 (auxiliary domain $\Omega(\varepsilon)$). *The internal regularity result, see Theorem III, only grants $\mathbf{u}_h^n \in \mathbf{H}^3(\Omega(\varepsilon))$. The discontinuity in normal gradient of the even reflection of c about $y = \ell$ prevents us from extending this local regularity of \mathbf{u}_h^n up to $y = \ell$. As a result, it is necessary to keep $\Omega(\varepsilon)$ to have enough regularity of \mathbf{u}_h^n to move the analysis forward. We use the Sobolev embedding theorem to obtain $\mathbf{u}_h^n \in \mathbf{H}^3(\Omega(\varepsilon)) \hookrightarrow \mathbf{W}^{1,\infty}(\Omega(\varepsilon))$, from which a BV estimate on $\alpha_{h,\delta}|_{\Omega(\varepsilon)}$ is derived, see Corollary 1. By imposing a restriction on time, the BV regularity of $\alpha_{h,\delta}$ is extended to Ω .*

ℓ	$\bar{\alpha}_h^n = \alpha_h^n(-x, y)$ $\bar{c}_h^n = c_h^n(-x, y)$ $\bar{p}_h^n = p_h^n(-x, y)$ $\bar{u}_h^n = -u_h^n(-x, y)$ $\bar{v}_h^n = v_h^n(-x, y)$	$\bar{\alpha}_h^n = \alpha_h^n(x, y)$ $\bar{c}_h^n = c_h^n(x, y)$ $\bar{p}_h^n = p_h^n(x, y)$ $\bar{u}_h^n = u_h^n(x, y)$ $\bar{v}_h^n = v_h^n(x, y)$	$\bar{\alpha}_h^n = \alpha_h^n(2-x, y)$ $\bar{c}_h^n = c_h^n(2-x, y)$ $\bar{p}_h^n = p_h^n(2-x, y)$ $\bar{u}_h^n = -u_h^n(2-x, y)$ $\bar{v}_h^n = v_h^n(2-x, y)$
$y \uparrow$ 0	$\bar{\alpha}_h^n = \alpha_h^n(-x, -y)$ $\bar{c}_h^n = c_h^n(-x, -y)$ $\bar{p}_h^n = p_h^n(-x, -y)$ $\bar{u}_h^n = -u_h^n(-x, -y)$ $\bar{v}_h^n = -v_h^n(-x, -y)$	$\bar{\alpha}_h^n = \alpha_h^n(x, -y)$ $\bar{c}_h^n = c_h^n(x, -y)$ $\bar{p}_h^n = p_h^n(x, -y)$ $\bar{u}_h^n = u_h^n(x, -y)$ $\bar{v}_h^n = -v_h^n(x, -y)$	$\bar{\alpha}_h^n = \alpha_h^n(2-x, -y)$ $\bar{c}_h^n = c_h^n(2-x, -y)$ $\bar{p}_h^n = p_h^n(2-x, -y)$ $\bar{u}_h^n = -u_h^n(2-x, -y)$ $\bar{v}_h^n = -v_h^n(2-x, -y)$
$-\ell$	-1	0	1 2
	$x \rightarrow$		

Figure 6.7: Extended functions on the rectangle $(-1, 2) \times (-\ell, \ell)$

Lemma 6.20. *For every $n \geq 0$, (6.56) has a unique solution $c_h^n \in V$. Moreover, it holds $\bar{c}_h^n \in H_{\text{loc}}^2(\Omega_{\text{ext}})$, $c_h^n \in W^{2,p}(\Omega)$ for any $p \geq 2$, and $\|c_h^n\|_{2,p,\Omega} \leq \mathcal{C}Q(2\ell)^{1/p}\|\alpha_h^n\|_{0,\infty,\Omega}$, where $\mathcal{C} > 0$ is a constant that depends only on Ω .*

Proof. An application of the Lax–Milgram theorem ensures the existence of a unique $c_h^n \in V$ that satisfies (6.56). Observe that $\bar{c}_h^n \in H_{\text{ext}} := \{v \in H^1(\Omega_{\text{ext}}) : v = 0 \text{ at } y = \ell, -\ell\}$. Apply change of variables to establish $\int_{\Omega_{\text{ext}}} \nabla \bar{c}_h^n \cdot \nabla v \, d\mathbf{x} = Q \int_{\Omega_{\text{ext}}} \bar{\alpha}_h^n v \, d\mathbf{x}$ for every $v \in H_{\text{ext}}$. Therefore, Theorem I yields $\bar{c}_h^n \in H_{\text{loc}}^2(\Omega_{\text{ext}})$.

The $W^{2,p}(\Omega)$ regularity of c_h^n is obtained by an application of odd reflection on c_h^n about $y = \ell$. Set $\Lambda := (0, 1) \times (0, 2\ell)$. Define the function $\hat{c}_h^n : \Lambda \rightarrow \mathbb{R}$ by

$$\hat{c}_h^n := \begin{cases} c_h^n(x, y) & \text{if } y \leq \ell, \text{ and} \\ -c_h^n(x, 2-y) & \text{if } y > \ell. \end{cases}$$

Let $f(x, y) = Q\alpha_h^n(x, y)$ if $y \leq \ell$ and $f(x, y) = -Q\alpha_h^n(x, 2-y)$ if $y > \ell$. Then, note that $\hat{c}_h^n \in H^1(\Lambda)$ and $\int_{\Lambda} \nabla \hat{c}_h^n \cdot \nabla v \, d\mathbf{x} = \int_{\Lambda} f v \, d\mathbf{x}$ holds for every $v \in H^1(\Lambda)$. Hence, Theorem II shows that $\hat{c}_h^n \in W^{2,p}(\Lambda)$, $p \geq 1$, and that $\|c_h^n\|_{2,p,\Omega} \leq \mathcal{C}(2\ell)^{1/p}Q\|\alpha_h^n\|_{0,\infty,\Omega}$. \square

Lemma 6.21. *For every $n \geq 0$, there exists a unique $(\mathbf{u}_h^n, p_h^n) \in \mathbf{H} \times L^2(\Omega)$ that satisfies (6.57)–(6.58) for every $(\boldsymbol{\varphi}, q) \in \mathbf{H} \times L^2(\Omega)$. Moreover, it holds $\bar{\mathbf{u}}_h^n \in \mathbf{H}_{\text{loc}}^3(\Omega_{\text{ext}})$ and for each $\varepsilon > 0$*

$$\|\mathbf{u}_h^n\|_{3,2,\Omega(\varepsilon)} \leq \gamma \mathcal{C}_\varepsilon (1 + \mathcal{C}Q\sqrt{2\ell}\|\alpha_h^n\|_{0,\infty,\Omega}),$$

where $\mathcal{C}_\varepsilon > 0$ depends only on ε .

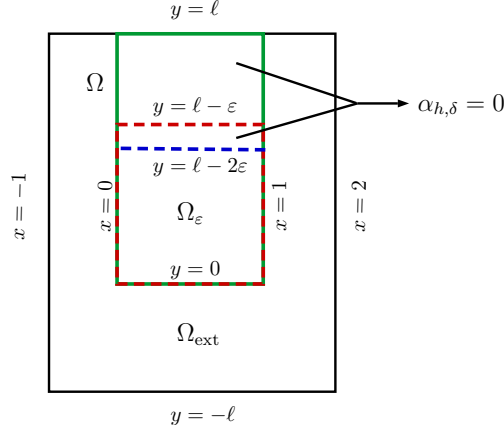


Figure 6.8: Relationship with domains

Proof. The existence of a unique solution $(\mathbf{u}_h^n, p_h^n) \in \mathbf{H} \times L^2(\Omega)$ follows from the Ladyshenzkaya–Babuska–Brezzi theorem [112, p. 227]. Set the space

$$\mathbf{H}_{\text{ext}} := \left\{ \mathbf{u} := (u, v) \in \mathbf{H}^1(\Omega_{\text{ext}}) \mid \begin{array}{l} \mathbf{u} \cdot \mathbf{n} = 0 \text{ at } x = -1, x = 2, \\ \text{and } \mathbf{u} \cdot \boldsymbol{\tau} = 0 \text{ at } y = l, y = -l \end{array} \right\}.$$

Then, observe that the extended function $(\bar{\mathbf{u}}_h^n, \bar{p}_h^n)$ belongs to $\mathbf{H}_{\text{ext}} \times L^2(\Omega_{\text{ext}})$ and satisfies for every $(\boldsymbol{\varphi}, q) \in \mathbf{H}_{\text{ext}} \times L^2(\Omega_{\text{ext}})$

$$\begin{aligned} \mu \int_{\Omega_{\text{ext}}} \left(\nabla \bar{\mathbf{u}}_h^n : \nabla \boldsymbol{\varphi} + \frac{1}{3} \operatorname{div}(\bar{\mathbf{u}}_h^n) \operatorname{div}(\boldsymbol{\varphi}) \right) d\mathbf{x} - \int_{\Omega_{\text{ext}}} \bar{p}_h^n \operatorname{div}(\boldsymbol{\varphi}) d\mathbf{x} &= \int_{y=l, -l} \frac{\gamma \mu}{3} \varphi_2 ds, \quad \text{and} \\ \int_{\Omega_{\text{ext}}} \operatorname{div}(\bar{\mathbf{u}}_h^n) q d\mathbf{x} &= \int_{\Omega_{\text{ext}}} \gamma(1 - \bar{c}_h^n) q d\mathbf{x}. \end{aligned}$$

Since Lemma 6.20 yields $\gamma(1 - \bar{c}_h^n) \in H_{\text{loc}}^2(\Omega_{\text{ext}})$, apply Theorem III to conclude the proof. \square

Lemmas 6.20 and 6.21 are crucial in obtaining the supremum norm estimates on c_h^n and $\operatorname{div}(\mathbf{u}_h^n)$ on $\Omega(\varepsilon)$. Since $\bar{c}_h^n \in W^{2,p}(\Omega)$ and $\mathbf{u}_h^n \in \mathbf{H}^3(\Omega(\varepsilon))$, the Sobolev embedding theorem with $p > 2$ yields, with \mathcal{C}_{emb} and $\mathcal{C}_{\text{emb},\varepsilon}$ are the embedding constants that depends only on Ω and Ω_ε , respectively

$$\|c_h^n\|_{1,\infty,\Omega} \leq \mathcal{C}_{\text{emb}} \|\bar{c}_h^n\|_{2,p,\Omega} \leq \mathcal{C}_{\text{emb}} \mathcal{C} Q (2\ell)^{1/p} \|\alpha_h^n\|_{0,\infty,\Omega}, \quad \text{and} \quad (6.62)$$

$$\|\mathbf{u}_h^n\|_{1,\infty,\Omega(\varepsilon)} \leq \mathcal{C}_{\text{emb},\varepsilon} \|\bar{\mathbf{u}}_h^n\|_{3,2,\Omega(\varepsilon)} \leq \gamma \mathcal{C}_{\text{emb},\varepsilon} \mathcal{C}_\varepsilon (1 + \mathcal{C} Q \sqrt{2\ell} \|\alpha_h^n\|_{0,\infty,\Omega}). \quad (6.63)$$

Proposition 6.22. *Fix a positive number $\alpha_M > a_0$. There exists a finite time $T_* > 0$ such that for every $t \leq T_*$, $\sup_\Omega |\alpha_{h,\delta}(t, \cdot)| \leq \alpha_M$ holds.*

Proof. Step 1: The proof employs strong induction on the time index n . Since $a^0 < \alpha_M$, the base case holds. To establish the inductive case, assume that $\sup_{\Omega(\varepsilon)} |\alpha_{h,\delta}(t_k, \cdot)| \leq \alpha_M$

for every $k \leq n$. We establish that $\sup_{\Omega(\varepsilon)} |\alpha_{h,\delta}(t_{n+1}, \cdot)| \leq \alpha_M$ holds for every $t_{n+1} < T_1$, for a fixed time $T_1 > 0$.

Step 2: Recall $\|v\|_{L_t^1 L^\infty(\Omega(\varepsilon)_T)} := \int_0^T \|v(t, \cdot)\|_{L^\infty(\Omega(\varepsilon))} dt$. The results in (6.63) and (6.60a) imply the CFL condition in Theorem 6.4. Then, Proposition 6.6 applied to (6.59) yields, for any finite time $t < T$

$$\|\alpha_{h,\delta}(t, \cdot)\|_{L^\infty(\Omega(\varepsilon))} \leq B \left(a_0 + \|\operatorname{div}(\mathbf{u}_h^n)\|_{L_t^1 L^\infty(\Omega(\varepsilon)_T)} \right), \quad (6.64)$$

where $B = \exp(\|\operatorname{div}(\mathbf{u}_h^n)\|_{L_t^1 L^\infty(\Omega(\varepsilon)_T)} + \gamma(T + \|c_h^n\|_{L_t^1 L^\infty(\Omega(\varepsilon)_T)}))$. Then (6.62), (6.63), and (6.64) imply $\|\alpha_{h,\delta}(t, \cdot)\|_{L^\infty(\Omega(\varepsilon))} \leq \mathcal{F}(T)$, where

$$\begin{aligned} \mathcal{F}(T) := & \exp(T\gamma \mathcal{C}_{\text{emb},\varepsilon} \mathcal{C}_\varepsilon (1 + \mathcal{C} Q \sqrt{2\ell} \alpha_M) + \\ & TQ \mathcal{C}_{\text{emb}} \mathcal{C} (2\ell)^{1/p} \alpha_M) \left(a_0 + T\gamma \mathcal{C}_{\text{emb},\varepsilon} \mathcal{C}_\varepsilon (1 + Q\mathcal{C} \sqrt{2\ell} \alpha_M) \right). \end{aligned}$$

Since $\mathcal{F}(0) - \alpha_M < 0$ and \mathcal{F} is continuous, there exists a finite time T_1 such that for every $t \in [0, T_1]$ it holds $\|\alpha_{h,\delta}(t, \cdot)\|_{L^\infty(\Omega(\varepsilon))} \leq \mathcal{F}(T_1) \leq \alpha_M$.

Step 3: Next, we need to show that $\alpha_{h,\delta}$ is bounded on $\Omega \setminus \Omega(\varepsilon)$. Note that $\alpha_0(x, y) = 0$ for $y \geq 1$. The finite speed of propagation of the scheme (6.59) on $\Omega(\varepsilon)$ and (6.60a) yield $\alpha_{h,\delta} = 0$ on $(0, T_2) \times (\ell - 2\varepsilon, \ell)$, where $T_2 := (\ell - 2\varepsilon - 1) / (\gamma \mathcal{C}_{\text{emb},\varepsilon} \mathcal{C}_\varepsilon (1 + Q\mathcal{C} \sqrt{2\ell} \alpha_M))$. Since $h < \varepsilon$, $\alpha_{i,j}^n = 0$ for every $K_{i,j} \subset (\ell - 2\varepsilon, \ell)$, see Figure 6.8. Define $T_* = \min(T_1, T_2)$ to obtain the conclusion. \square

Observe that for every $(t, \mathbf{x}, z) \in (0, T_*) \times \Omega \times (-\alpha_M, \alpha_M)$, the function $\mathfrak{S}(t, \mathbf{x}, z) = \gamma(1 - c_{h,\delta})z$ is Lipschitz continuous with respect to z , uniformly with respect to t and \mathbf{x} and Lipschitz continuous with respect to \mathbf{x} , uniformly with respect to t and z . This is a direct consequence of (6.62).

Proposition 6.23. *The function $\alpha_{h,\delta} : (0, T_*) \times \Omega \rightarrow \mathbb{R}$ has bounded variation. Moreover, on $(0, T_*) \times \Omega$ it holds $|\alpha_{h,\delta}|_{BV_{x,y,t}} \leq \mathcal{C}_{BV}$, where \mathcal{C}_{BV} is independent of h and δ .*

The proof of Proposition 6.23 follows from an application of Corollary 1, the Lipschitz continuity of $\gamma(1 - c_{h,\delta}(t, \mathbf{x}))z$ of (t, \mathbf{x}, z) on $(0, T_*) \times \Omega \times (-\alpha_M, \alpha_M)$, and the fact that $\alpha_{h,\delta} = 0$ on $(0, 1) \times (\ell - 2\varepsilon, \ell)$, see Figure 6.8.

Proof of Theorem 6.17

Recall that $\Omega_{T_*} = (0, T_*) \times \Omega$. Proposition 6.23 shows that $\alpha_{h,\delta} \in BV(\Omega_{T_*})$. Therefore, an application of Theorem I provides the existence of subsequence of $\{\alpha_{h,\delta}\}$ – assigned with the same indices – and a function $\alpha \in BV(\Omega_{T_*})$ such that $\alpha_{h,\delta} \rightarrow \alpha$ almost everywhere and L^∞ weak- \star on Ω_{T_*} . Lemma 6.20 and Lemma 6.21 show that $c_{h,\delta} \in L^2(0, T_*; V)$ and $(\mathbf{u}_{h,\delta}, p_{h,\delta}) \in L^2(0, T_*; \mathbf{H}) \times L^2(0, T_*; L^2(\Omega))$ for every h and δ . Observe that $L^2(0, T_*; V)$ and $L^2(0, T_*; \mathbf{H}) \times L^2(0, T_*; L^2(\Omega))$ are Hilbert spaces. Hence, there exist subsequences of $\{c_{h,\delta}\}$ and $\{(\mathbf{u}_{h,\delta}, p_{h,\delta})\}$, and functions $c \in L^2(0, T_*; V)$ and $(\mathbf{u}, p) \in L^2(0, T_*; \mathbf{H}) \times L^2(0, T_*; L^2(\Omega))$ such that $c_{h,\delta} \rightharpoonup c$ weakly in $L^2(0, T_*; V)$ and $(\mathbf{u}_{h,\delta}, p_{h,\delta}) \rightharpoonup (\mathbf{u}, p)$ weakly in $L^2(0, T_*; \mathbf{H}) \times L^2(0, T_*; L^2(\Omega))$.

6.8.2 Convergence

Theorem 6.24 (Convergence). *Let $(\alpha, \mathbf{u}, p, \mathbf{c})$ be a limit of any subsequence of $\{(\alpha_{h,\delta}, \mathbf{u}_{h,\delta}, p_{h,\delta}, c_{h,\delta})\}_{h,\delta}$ obtained from the semi-discrete scheme in the sense of Theorem 6.17. Then, $(\alpha, \mathbf{u}, p, \mathbf{c})$ is a solution to the problem (6.5a)–(6.5c) for the finite time $T_* < \infty$.*

Proof of Theorem 6.24. The proof of Theorem 6.24 has two steps.

Step 1. (Convergence of tumour cell concentration) Let $\alpha : \Omega_{T_*} \rightarrow \mathbb{R}$ be a limit provided by Theorem 6.17 such that $\alpha_{h,\delta} \rightarrow \alpha$ almost everywhere in Ω_{T_*} . Then, we show that α satisfies (6.53) for every $\vartheta \in \mathcal{C}_c^\infty([0, T_*] \times \Omega)$.

Set $\varphi \in \mathcal{C}_c^\infty([0, T_*] \times \Omega)$ and $N_* = T_*/\delta$. For ease of notations, let $\varphi(t, \cdot)$ denote its trivial extension on \mathbb{R}^2 , for every $t \geq 0$. Multiply (6.59) by $h^2 \vartheta_{i,j}^n$, $\vartheta_{i,j}^n := \int_{K_{i,j}} \vartheta(t_n, \cdot) d\mathbf{x}$ and sum over the indices to obtain $T_1 + T_2^x + T_2^y = T_3$, where

$$\begin{aligned} T_1 &:= h^2 \sum_{n=0}^{N_*-1} \sum_{i=0}^I \sum_{j=0}^J (\alpha_{i,j}^{n+1} - \alpha_{i,j}^n) \vartheta_{i,j}^n, \\ T_2^x &:= h^2 \delta \sum_{n=0}^{N_*-1} \sum_{i=0}^I \sum_{j=0}^J \left(u_{i+1/2,j}^{n+} \alpha_{i,j}^n - u_{i+1/2,j}^{n-} \alpha_{i+1/2,j}^n - u_{i-1/2,j}^{n+} \alpha_{i-1,j}^n + u_{i-1/2,j}^{n-} \alpha_{i,j}^n \right) \vartheta_{i,j}^n, \\ T_2^y &:= h^2 \delta \sum_{n=0}^{N_*-1} \sum_{i=0}^I \sum_{j=0}^J \left(v_{i,j+1/2}^{n+} \alpha_{i,j}^n - v_{i,j+1/2}^{n-} \alpha_{i,j+1}^n - v_{i,j-1/2}^{n+} \alpha_{i,j-1}^n + v_{i,j-1/2}^{n-} \alpha_{i,j}^n \right) \vartheta_{i,j}^n, \text{ and} \\ T_3 &:= h^2 \delta \sum_{n=0}^{N_*-1} \sum_{i=0}^{I-1} \sum_{j=0}^{J-1} \gamma \vartheta_{i,j}^n \int_{t_n}^{t_{n+1}} \int_{K_{i,j}} \alpha_{h,\delta} (1 - c_{h,\delta}) d\mathbf{x}, dt. \end{aligned}$$

Define the piecewise constant function $\alpha_h^0|_{K_{i,j}} := \int_{K_{i,j}} \alpha_0(\mathbf{x}) d\mathbf{x}$ for $0 \leq i \leq I$ and $0 \leq j \leq J$. Since $\vartheta_{i,j}^{N_*} = 0$ for all i, j , use discrete integration by parts (IV) in Section 1.4 to arrive at

$$T_1 = -h^2 \sum_{n=0}^{N_*-1} \sum_{i=0}^I \sum_{j=0}^J (\vartheta_{i,j}^{n+1} - \vartheta_{i,j}^n) \alpha_{i,j}^{n+1} - \int_{\Omega} \alpha_h^0(\mathbf{x}) \vartheta(0, \mathbf{x}) d\mathbf{x}. \quad (6.65)$$

A direct calculation shows the first term in the right hand side of (6.65) is equal to

$$- \sum_{n=0}^{N_*-1} \sum_{i=0}^I \sum_{j=0}^J \alpha_{i,j}^{n+1} \int_{t_n}^{t_{n+1}} \int_{K_{i,j}} \partial_t \vartheta(t, \mathbf{x}) d\mathbf{x} dt = - \int_{\delta}^{T_*+\delta} \int_{\Omega} \alpha_{h,\delta}(t, \mathbf{x}) \partial_t \vartheta(t - \delta, \mathbf{x}) d\mathbf{x} dt.$$

Note that $\alpha_{h,\delta} \rightarrow \alpha$ almost everywhere (see Theorem 6.17) as $h, \delta \rightarrow 0$. Then, apply Lebesgue's dominated convergence theorem to show that the first term in the right hand side of (6.65) converges to $-\int_{\Omega_{T_*}} \alpha(t, \mathbf{x}) \partial_t \vartheta(t, \mathbf{x}) dt d\mathbf{x}$. Since $\alpha_h^0 \rightarrow \alpha_0$ in $L^2(\Omega)$, the second term in the right hand side of (6.65) converges to $-\int_{\Omega} \alpha_0(\mathbf{x}) \vartheta(0, \mathbf{x}) d\mathbf{x}$.

The convergence of T_2^y is shown next. The steps for T_2^x follow similar steps. An application (IV) in Section 1.4 on T_2^y leads to

$$\begin{aligned} T_2^y &= \delta h^2 \sum_{n=0}^{N_*-1} \sum_{i=0}^I \sum_{j=0}^J \vartheta_{i,j}^n \left(|v_{i,j+1/2}^n| \frac{\alpha_{i,j}^n - \alpha_{i,j+1}^n}{2} - |v_{i,j-1/2}^n| \frac{\alpha_{i,j-1}^n - \alpha_{i,j}^n}{2} \right) \\ &\quad + \delta h^2 \sum_{n=0}^{N_*-1} \sum_{i=0}^I \sum_{j=0}^J \vartheta_{i,j}^n \left(v_{i,j+1/2}^n \frac{\alpha_{i,j}^n + \alpha_{i,j+1}^n}{2} - v_{i,j-1/2}^n \frac{\alpha_{i,j-1}^n + \alpha_{i,j}^n}{2} \right) =: T_{21} + T_{22}. \end{aligned}$$

Set $\alpha_{i,J+1}^n = 0$ and $\alpha_{i,-1}^n = 0$. Then,

$$\begin{aligned} |T_{21}| &\leq \left| \delta h^2 \sum_{n=0}^{N_*-1} \sum_{i=0}^I \sum_{j=0}^{J-1} (\vartheta_{i,j+1}^n - \vartheta_{i,j}^n) |v_{i,j+1/2}^n| \frac{\alpha_{i,j}^n - \alpha_{i,j+1}^n}{2} \right| + \mathcal{O}(h) \\ &\leq \frac{h}{2} \|\mathbf{u}_{h,\delta}\|_{L^\infty(\Omega_{T_*})} \|\partial_x \vartheta(t, \mathbf{x})\|_{L^\infty(\Omega_{T_*})} \sum_{n=0}^{N_*-1} \delta \sum_{i=0}^I h \sum_{j=0}^{J-1} |\alpha_{i,j}^n - \alpha_{i,j+1}^n| + \mathcal{O}(h), \end{aligned}$$

and hence (6.63) and Proposition 6.23 imply $|T_{21}| \rightarrow 0$ as $h \rightarrow 0$. Use (IV) in Section 1.4 to obtain

$$T_{22} = -\delta h^2 \sum_{n=0}^{N_*-1} \sum_{i=0}^I \sum_{j=0}^J (\vartheta_{i,j+1}^n - \vartheta_{i,j}^n) v_{i,j+1/2}^n \frac{\alpha_{i,j}^n + \alpha_{i,j+1}^n}{2} + \mathcal{O}(h).$$

Add and subtract $\delta \sum_{n=0}^{N_*-1} \sum_{i=0}^I \sum_{j=0}^J (\vartheta_{i,j+1}^n - \vartheta_{i,j}^n) \frac{v_{i,j-1/2}^n}{2} \alpha_{i,j}^n$ to (4.43) to arrive at

$$\begin{aligned} T_{22} &= \delta h^2 \sum_{n=0}^{N_*-1} \sum_{i=0}^I \sum_{j=0}^J \frac{v_{i,j+1/2}^n \alpha_{i,j+1}^n}{2} (\vartheta_{i,j+1}^n - \vartheta_{i,j}^n - \vartheta_{i,j+2}^n + \vartheta_{i,j+1}^n) \\ &\quad - \delta h^2 \sum_{n=0}^{N_*-1} \sum_{i=0}^I \sum_{j=0}^J (\vartheta_{i,j+1}^n - \vartheta_{i,j}^n) \frac{v_{i,j+1/2}^n + v_{i,j-1/2}^n}{2} \alpha_{i,j}^n. \end{aligned} \quad (6.66)$$

Use of the definition of $\vartheta_{i,j}^n$, mean value theorem, and CFL condition (6.60a) to show that the first term in the right hand side of (6.66) converges to zero. Define $\partial_{h,\delta} \varphi : \Omega_{T_*} \rightarrow \mathbb{R}$ by $\partial_{h,\delta} \varphi := (\vartheta_{i,j+1}^n - \vartheta_{i,j}^n)/h$ on $(t_n, t_{n+1}) \times K_{i,j}$. Then the second term in the right hand side of (6.66) can be expressed as

$$- \int_0^{T_*} \int_{\Omega} v_{h,\delta} \alpha_{h,\delta} \partial_{h,\delta} \vartheta \, d\mathbf{x} \, dt \rightarrow - \int_0^{T_*} \int_{\Omega} v \alpha \partial_x \vartheta \, d\mathbf{x} \, dt,$$

where Lemmas III(a) and III(b) are applied in the last step. Follow the same steps for T_2^x to obtain $T_2 \rightarrow - \int_0^{T_*} \int_{\Omega} \alpha \mathbf{u} \cdot \nabla \vartheta \, d\mathbf{x} \, dt$. Rewrite T_3 and apply Lemma III(a)

$$\int_0^{T_*} \int_{\Omega} \gamma \alpha_{h,\delta} (1 - c_{h,\delta}) \, d\mathbf{x} \, dt \rightarrow \int_0^T \int_{\Omega} \gamma \alpha (1 - c) \, d\mathbf{x} \, dt.$$

Plug the above in $T_1 + T_2^x + T_2^y = T_3$ to arrive the desired conclusion.

The proofs of step 2 and step 3 follows from a direct application of weak convergence of $(u_{h,\delta}, p_{h,\delta})$ and $c_{h,\delta}$. Hence, we omit the proofs.

Step 2. (Convergence of pressure–velocity system) Let $(\mathbf{u}, p) : \Omega_{T_*} \rightarrow \mathbb{R}^3$ be a limit provided by Theorem 6.17 such that $\mathbf{u}_{h,\delta} \rightharpoonup \mathbf{u}$ weakly in $L^2(0, T_*; \mathbf{H})$ and $p_{h,\delta} \rightharpoonup p$ weakly in $L^2(0, T_*; L^2(\Omega))$. Then, (\mathbf{u}, p) satisfies (6.5b) for every $(\boldsymbol{\psi}, q) \in L^2(0, T_*; \mathbf{H}) \times L^2(0, T; L^2(\Omega))$. The proof directly follows from the weak convergences on $\mathbf{u}_{h,\delta}$ and $p_{h,\delta}$.

Step 3. (Convergence of nutrient concentration) Let $c : \Omega_{T_*} \rightarrow \mathbb{R}$ be a limit provided by Theorem 6.17 such that $c_{h,\delta} \rightharpoonup c$ weakly in $L^2(0, T_*; V)$. Then c satisfies (6.55) for every $\varphi \in L^2(0, T_*; V)$. The proof is straightforward from the weak convergence of $c_{h,\delta}$.

6.9 Conclusions

A uniform estimate on total variation of discrete solutions obtained by applying finite volume schemes on conservation laws of the form (6.1) in two and three spatial dimensions for nonuniform Cartesian grids is proved. We relaxed the standard assumption that the advecting velocity vector is divergence free. This enables us to apply the finite volume scheme to problems in which the advecting velocity vector is a nonlinear function of the conserved variable. Since the underlying meshes are nonuniform Cartesian it is possible to adaptively refine the mesh on regions where the solution is expected to have sharp fronts. A uniform BV estimate is also obtained for finite volume approximations of conservation laws of the type (6.38) that has a fully nonlinear flux on nonuniform Cartesian grids. Numerical experiments support the theoretical findings. The counterexample by B. Després and numerical evidence from Table 6.13 indicate that nonuniform Cartesian grids are the current limit on which we can obtain uniform BV estimates. Extending Theorem 6.4 to perturbed Cartesian grids (Figure 6.6(e)) might be the immediate future step. Theorem 6.24, which proves the existence of a weak solution to the tumour growth model (6.5), attests to the applicability of Theorem 6.4 in the analytical study of coupled systems involving conservation laws and elliptic equations.

Chapter 7

Two-phase model of compressive stress induced on a surrounding hyperelastic medium by an expanding tumour

This chapter presents a mathematical model of *in vitro* tumour growth in an external polymeric medium in 1D. The tumour is modelled as a biphasic mixture. Nonlinear elasticity is employed to model the external medium, referred to as hydrogel. The models considered in Chapters 1–3 account for tumour growth in free suspension. The influence of external medium on nutrient diffusion is captured by the *nutrient limited model* (NLM) in Chapter 5. The work in this chapter quantifies the sole effect of compressive stress induced on the polymeric medium on tumour growth. To isolate the influence of compressive stress the effect on nutrient diffusion is not included in the current model.

7.1 Introduction

The compressive stress induced in the external medium controls tumour topology. Moreover, it has significant medical and genetic consequences. For instance, brain tumour and subsequent oedema generate abnormally high intracranial pressure, which may lead to severe headaches, nausea, seizures, and even death [87]. The mechanical stress activates oncogenes, which triggers signalling pathways that modify cellular mechanical response and tissue geometry [88]. The reduction in tumour spheroid sizes due to the mechanical stress in external polymeric medium or soft tissues has been well known since the late 1990s [89–91]. Recent studies have shown that external mechanical stress has a necrotic effect on breast and other types of cancer cells, see S. Takao et al. [92] and references therein. The biological significance of the impact of compressive stress on tumour growth justifies the

need for modelling and computational studies along with experimental research¹.

To study the effect of hydrogel on a proliferating tumour (and vice versa), we require a combined model of two processes; the tumour growth and the mechanical deformations occurring in the hydrogel. These two processes operate in an entangled fashion, wherein one acts as a feedback to the other.

The modelling of tumour spheroids is a well-developed subject in mathematical biology, see for example the reviews [53, 54] and Chapter 1. In this chapter, the framework used in the BBL model of Section 1.5 is used to model a growing tumour. The cells and fluid medium constitute the cell and fluid phase, respectively. The proliferation rate of tumour cells is controlled by an external nutrient, which follows a diffusion process. We apply conservation of mass and momentum to the cell and fluid phases to obtain the governing equations for tumour growth. The model variables associated with tumour growth are the volume fraction of tumour cells, the velocity of tumour cells, nutrient concentration, and tumour radius.

Hydrogel belongs to the class of hyperelastic materials, which means it follows a nonlinear stress-strain relationship [113], [114, p. 136-149]. Moreover, hyperelastic materials are characterised by a stored energy density, the derivative of which with respect to the deformation gradient yields the stress tensor. This characterisation is an advantage in the sense that it is sufficient to know the energy density in terms of the deformation gradient; the stress tensor can be computed from the energy density and rules of equilibrium classical mechanics can be applied to obtain the governing equation. However, the selection of an appropriate energy density is mostly heuristic and phenomenological. A review of energy density functionals that can be employed to model the mechanical behaviour of soft biological tissues is provided in G. Chagnon et al. [93].

In this chapter, we develop a biphasic model for tumour growth based on the works described in [7]. The hydrogel is modelled as a compressible hyperelastic material. In practice, the hydrogel is a mixture of absorbed fluid and the polymeric material. When a compressive force is applied, two mechanisms occur in the hydrogel. Firstly, the compressive force deforms the polymeric scaffold in the hydrogel. Secondly, the hydrogel registers a volumetric change since a part of the solvent is absorbed into the tumour. The absorbed fluid is utilised by tumour cells to facilitate cell proliferation and growth. However, in this chapter, the fluid dynamic effects in the hydrogel are ignored in conformity with previous works [30]. Instead, we only focus on the mechanical deformation in the hydrogel to gain a clear understanding of the effect of compressive stress on tumour growth.

Since the tumour is expanding, the interface between the tumour and hydrogel is a time-dependent unknown variable associated with the model. At a fixed time, the location of this interface is characterised by the continuity of the normal stress in the tumour and that in the hydrogel. Here, a major difference from the BBL model in Section 1.5 is that the Neumann boundary condition associated with the cell velocity equation is no more

¹The work in this chapter is to be submitted: G. C. Remesan, J. A. Flegg, and H. Byrne, *Two-phase model of compressive stress induced on a surrounding hyperelastic medium by an expanding tumour*, (25 pages), 2021.

homogeneous.

Literature

The use of multiphase mixture theory and conservation equations in individual phases to model tumour spheroid growth started in the 1970s with the work by H. P. Greenspan [59]. Mathematical modelling of tumours has witnessed significant progress since the second half of the 1990s with the emergence of many publications with sophisticated models [1, 4–7, 11, 33, 53]. The biphasic framework of avascular tumour growth is extensively studied in [1] for a single spatial dimension and in [7] for higher spatial dimensions, see Chapters 1, 2, and 5 for further details. The viscous cell phase and inviscid fluid phase obey the principles of mass and momentum conservation. The model further reduces to a system of a hyperbolic, generalised viscous Stokes, and parabolic equations.

An early experimental work on how the compressive stress affects the tumour growth was conducted by G. Helminger et al. [89], where the authors report that tumours growing in a polymeric medium eventually attains a steady state. The steady state radius decreases as the polymer concentration in the hydrogel increases. An initial work describing the mechanical effect of an external medium on a growing tumour is conducted by C. Y. Chen et al. in 2001 [30]. The authors assume that tumour growth is radially symmetric in space and consequently, the deformation in the hydrogel is also radially symmetric. This radial symmetry makes the off-diagonal entries of the deformation gradient vanish in spherical polar coordinates. Consequently, model equations that govern the hydrogel dynamics reduce to a system of steady-state partial differential equations at each fixed time. The computed radius determines the pressure experienced by the tumour cells at the hydrogel–tumour interface, which acts as a boundary condition for the equations governing the tumour growth. The effect of stress on the surrounding soft biological tissues by an expanding tumour has also been investigated. In the work by I. C. Sorribes et al. [87], the authors derive a mathematical model for the intracranial pressure and oedema induced by brain tumours. The model also accurately captures how the healthy neurons compensate for the abnormal intracranial pressure induced by the tumour and describes the variation of intracranial pressure with respect to the severity of the tumour. The effect of stress induced on an elastic and incompressible medium by avascular tumours and vice versa is studied by F. Valdés-Ravelo et al. [94], wherein a higher dimensional model is constructed and reduced to single dimension using symmetry arguments.

A generic and robust framework to compute numerical solutions of a multiphase fluid flow model is provided in [10] (also see Chapter 5). In [10] the authors employ a combination of finite volume and finite element methods to compute the approximate solutions. However, the underlying model employed in [10] is ill-posed and the procedure is computationally expensive since the time-dependent boundary is explicitly tracked. A well-posed model for avascular tumour growth and improved computational procedure in one and two spatial dimensions are presented in Chapters 2 and 5, respectively.

Contributions

- (1) A model in one spatial dimension is presented. This model describes the influence

of stress imparted by an external medium – in this case, a polymeric hydrogel – on different properties of a proliferating tumour such as tumour radius, cell volume fraction, cell velocity, and stress inside the tumour is presented. The time–dependent boundary is eliminated using a transformation to the unit domain, see Chapter 1.

- (2) The cell volume fraction, cell velocity, and nutrient concentration are discretised using an upwind finite volume method, Lagrange \mathbb{P}_1 conforming finite element method, and \mathbb{P}_1 mass-lumped finite element method, respectively.
- (3) The exact expression for the deformation in the hydrogel is derived. The effect of various parameters involved in the model on tumour growth is examined, and the outcomes agree with the experimental results available from the literature.

Organisation

The mathematical model is derived in Section 7.2. The dimensionless model is presented in Section 7.3. The detailed discrete scheme used to compute the numerical solutions and a notion of weak solution is provided in Section 7.4. The numerical solutions are presented in Section 7.5.

7.2 Mathematical model

Define the time–space domain $\mathcal{D}_T := (0, T) \times I_\ell$, where $I_\ell := (0, \ell_m)$. The spatial bounding box I_ℓ contains the tumour and hydrogel, see Figure 7.1.

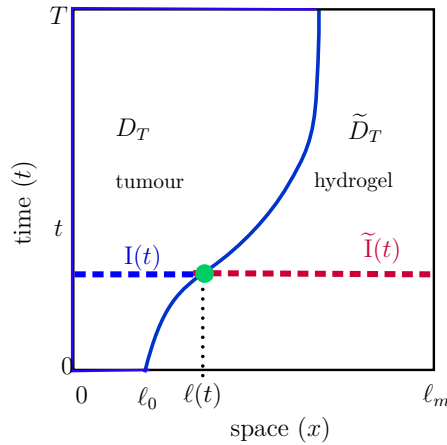


Figure 7.1: Tumour and hydrogel domains.

At a fixed time $t \in (0, T)$, tumour cells occupy the domain $I(t) := (0, \ell(t))$ and the hydrogel occupies the complementary domain $\tilde{I}(t) := (\ell(t), \ell_m)$. The time–space domain of tumour growth is defined by $D_T := \cup_{0 < t < T} (\{t\} \times I(t))$. Define $\tilde{D}_T := \mathcal{D}_T \setminus \overline{D_T}$, where $\overline{D_T}$ is the closure of D_T in \mathbb{R}^2 . The domain $I(0) := (0, \ell_0) \subset I_\ell$ contains the initially seeded tumour

cells and $\tilde{\mathbb{I}}(0) := I_\ell \setminus \overline{\mathbb{I}(0)}$, where $\overline{\mathbb{I}(0)} := [0, \ell_0]$, contains the undeformed hydrogel. Here, ℓ_0 is the initial tumour radius.

Summary of the model

The tumour and hydrogel form a continuum in I_ℓ , separated by the interphase $\ell(t) \in (0, \ell_m)$, referred to as the tumour boundary. The tumour contained in the spatial domain $(0, \ell(t))$ is a biphasic mixture of viscous tumour cells and inviscid extra-cellular fluid. The mass and momentum balance applied to cells and extra cellular-fluid and further simplification yield governing equations for the volume fraction (hyperbolic conservation law) and velocity (elliptic) of tumour cells. An external nutrient that follows a diffusion equation (parabolic) controls the tumour growth. The tumour boundary $\ell(t)$ propagates with a velocity equal to that of tumour cells present at $\ell(t)$. At each time $t \in (0, T)$, the hydrogel initially located in $(\ell(0), \ell_m)$ is deformed to $(\ell(t), \ell_m)$. This deformation builds up stress in the hydrogel, which is computed using hyper elasticity theory. The stress in the hydrogel is calculated as the gradient of the strain energy density, which is a functional of the deformation gradient. The tumour and hydrogel kinetics are coupled together by the continuity of the stress experienced by the tumour cells and that by the hydrogel at $\ell(t)$. The model is closed by appropriate initial and boundary conditions. The model assumptions are presented in appropriate locations in the sequel enumerated as (A.x), $x = 1, 2, \dots$

7.2.1 Deformations in the hydrogel

Coordinates of the undeformed hydrogel are denoted by $X \in \tilde{\mathbb{I}}(0)$ and that of the deformed hydrogel at a time $t \in (0, T)$ by $x \in \tilde{\mathbb{I}}(t)$. The *deformation map* is a function $\chi : (0, T) \times \tilde{\mathbb{I}}(0) \rightarrow \tilde{D}_T$. At each time $t \in (0, T)$, $\chi(t, \cdot)$ maps $\tilde{\mathbb{I}}(0)$ onto $\tilde{\mathbb{I}}(t)$. The deformation gradient, denoted by G , is the spatial derivative of χ , that is $G(t, X) = \frac{\partial \chi}{\partial X}(t, X)$ for every $X \in \tilde{\mathbb{I}}(0)$ and $t \in (0, T)$.

Strain energy density is the work done per unit volume in deforming the hydrogel material. The choice of strain energy density is based on phenomenological and empirical evidences. A wide range of strain energy density functionals are available in the literature [115, 116]. We consider the following strain energy density suggested by P. J. Flory [117, 95]:

$$\mathcal{W}_G = \frac{\nu}{2} G^2 - \frac{3}{2} N k_B \mathfrak{T}_{\text{abs}} - \vartheta \log(G), \quad (7.1)$$

where ν and ϑ are nonnegative constants with the dimension of stress (force/area), N is the ratio between the number of hydrogel polymer chains and the volume of the hydrogel in dry state, k_B is the Boltzmann constant, and $\mathfrak{T}_{\text{abs}}$ is the absolute temperature considered as a constant in this work. The formula (7.1) is obtained from applying thermodynamic principles to stretching of a lattice consisting of polymer fibres. The energy density functional (7.1) is also used to model the stretching in a polymer lattice due to absorption of a solvent with small molecular size such as water, which is known as Flory–Huggins solution theory [117].

The equations of motion that govern the kinetics of the hydrogel particles are formulated in the material or Lagrangian coordinates. The hydrogel deformations attain steady-state much faster than the tumour, which leads to, for every $(t, X) \in (0, T) \times \tilde{\mathbb{I}}(0)$

$$\frac{\partial \sigma^{\text{H}}}{\partial X} = 0, \quad (7.2)$$

where $\sigma^{\text{H}} := \frac{\partial \mathcal{W}_G}{\partial G}$ is the first Piola–Kirchoff stress tensor. It follows from (7.1) that

$$\sigma^{\text{H}} = \nu G - \vartheta G^{-1}. \quad (7.3)$$

Substitute (7.3) in (7.2) to obtain

$$\nu \frac{\partial^2 \chi}{\partial X^2} + \vartheta \left(\frac{\partial \chi}{\partial X} \right)^{-2} \frac{\partial^2 \chi}{\partial X^2} = 0. \quad (7.4)$$

Since $\frac{\partial \chi}{\partial X}$ is the ratio of two infinitesimal lengths and the linear ordering of the material in the hydrogel is preserved under any admissible transformations (compression and stretching), we impose the auxiliary condition $\frac{\partial \chi}{\partial X} > 0$. For instance, a complete self-folding transformation such as $\chi(X) = \ell_m(X - \ell_m)/(\ell_0 - \ell_m) + \ell_0(X - \ell_0)/(\ell_m - \ell_0)$, which reverses the location of hydrogel particles at $X = \ell_0$ and $X = \ell_m$ to $X = \ell_m$ and $X = \ell_0$, respectively is not allowed. At each time $t \in (0, T)$, the boundary points of the undeformed hydrogel ℓ_0 and ℓ_m are transformed to $\ell(t)$ and ℓ_m . This leads to the boundary conditions

$$\chi(t, \ell_0) = \ell(t) \quad \text{and} \quad \chi(t, \ell_m) = \ell_m. \quad (7.5)$$

With the condition $\frac{\partial \chi}{\partial X} > 0$ and boundary conditions (7.5), (7.4) has the unique linear solution described by

$$\chi(t, X) = \frac{\ell_m - \ell(t)}{\ell_m - \ell_0} X + \frac{\ell(t) - \ell_0}{\ell_m - \ell_0}. \quad (7.6)$$

Use this and (7.3) to obtain the following expression for the stress in the hydrogel, for every $X \in (\ell(t), \ell_m)$

$$\sigma^{\text{H}}(X) = \nu \frac{\ell_m - \ell(t)}{\ell_m - \ell_0} - \vartheta \left(\frac{\ell_m - \ell(t)}{\ell_m - \ell_0} \right)^{-1}. \quad (7.7)$$

Dimensions of σ_{H} , ν , and ϑ are presented in Table 7.1.

Remark 7.1 (Spatial variation of stress in the hydrogel). *Note that for a fixed time, σ^{H} is a constant as in (7.7) and depends only on the tumour radius $\ell(t)$. The spatial constancy of σ^{H} results from (7.3), wherein G is the spatial derivative of deformation in the hydrogel. Since the deformation is linear as provided in (7.6), the derivative $G = (\ell_m - \ell(t))/(\ell_m - \ell_0)$ is a constant at each time.*

In the sequel, it is assumed that

$$(A.1) \quad \vartheta \geq \nu, \text{ so that } \sigma^H \text{ is negative.}$$

Assumption (A.1) ensures that the stress generated in the hydrogel always acts against the tumour growth. If $\nu > \vartheta$, then σ^H becomes positive for $\ell(t) < \ell_m - (\ell_m - \ell_0)\sqrt{\vartheta/\nu}$, see Figure 7.2(b), and it asserts that the stress in the hydrogel favours tumour growth, which is physically not possible.

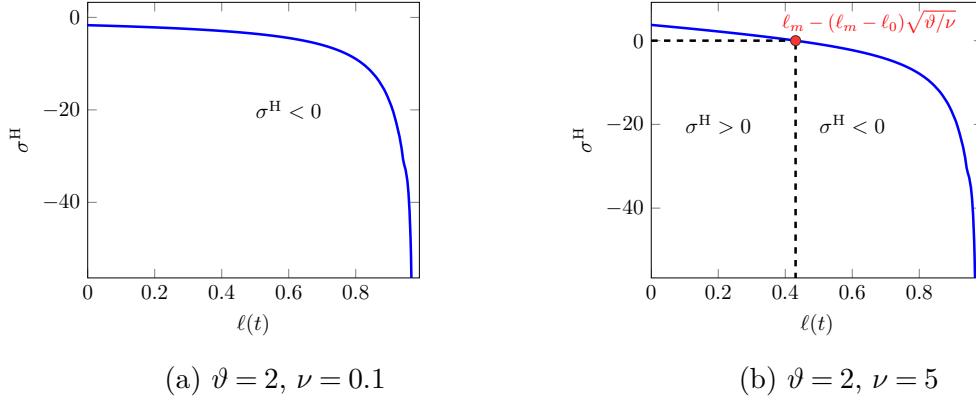


Figure 7.2: Variation of σ^H with respect to $\ell(t) \in (0, 1)$ for $\nu < \vartheta$ and $\vartheta < \nu$.

7.2.2 Biphasic tumour growth

The tumour is construed as an agglomeration of two interacting phases. The tumour cells constitute the cell phase and the fluid medium in which the cells are suspended constitute the fluid phase. The model variables are described in Table 7.1, and they are functions of time and space. Observe that the tumour growth variables in Table 7.1 are the same as that of the BBL model, see Table 1.2.

The main assumptions on tumour growth are as follows:

- (A.2) The tumour comprises only cells and fluid, and hence no voids are present. This leads to $\alpha + \beta = 1$.
- (A.3) The cell and fluid phases are incompressible with the same constant densities.
- (A.4) The cell phase is viscous and the fluid phase is inviscid.
- (A.5) The tumour is symmetric with respect to $x = 0$, which leads to $u_\alpha(t, 0) = 0 = u_\beta(t, 0)$ and $\frac{\partial c}{\partial x}(t, 0) = 0$.

The derivation of the model equations are detailed in Section 1.5. The governing equations for the tumour is defined in the time-space domain D_T . The coordinates in D_T are denoted by (t, x) . Then, it holds for every $(t, x) \in D_T$

$$\frac{\partial \alpha}{\partial t} + \frac{\partial}{\partial x}(u_\alpha \alpha) = q_\alpha \quad (7.8)$$

	Variable or Parameter	Notation		Dimension
		Cell phase	Fluid phase	
Tumour	Volume fraction	α	β	1
	Velocity	u_α	u_β	LT^{-1}
	Pressure	p_α	p_β	$\text{ML}^{-1}\text{T}^{-2}$
	Stress	σ_α	σ_β	$\text{ML}^{-1}\text{T}^{-2}$
	Force exerted by one phase on the other	$F_{\alpha\beta}$	$F_{\beta\alpha}$	$\text{ML}^{-2}\text{T}^{-2}$
	Net production rate	\mathcal{F}_α	\mathcal{F}_β	T^{-1}
	Viscosity	μ_α	-	$\text{ML}^{-1}\text{T}^{-1}$
	Intracellular force coefficient	γ	-	$\text{ML}^{-1}\text{T}^{-2}$
	Traction coefficients		k, k_1	$\text{ML}^{-3}\text{T}^{-1}$
	Cell close packing density		α^{R}	1
	Hydrogel	Hydrogel stress		σ^{H}
Compressibility parameters			ϑ, ν	$\text{ML}^{-1}\text{T}^{-2}$

Table 7.1: Model variables, parameters, and source terms. Here, M, L, and T, refer to mass, length, and time.

$$2\mu_\alpha \frac{\partial}{\partial x} \left(\alpha \frac{\partial u_\alpha}{\partial x} \right) = \frac{k_1 \alpha}{1 - \alpha} u_\alpha + \frac{\partial}{\partial x} (\alpha \gamma \mathcal{H}(\alpha)), \quad (7.9)$$

$$\frac{\partial c}{\partial t} = \frac{\partial}{\partial x} \left(\eta \frac{\partial c}{\partial x} \right) - \frac{Q_0 \alpha c}{1 + Q_1 c}, \quad (7.10)$$

$$\ell'(t) = u_\alpha(t, \ell(t)). \quad (7.11)$$

Recall that

$$q_\alpha = \underbrace{\alpha(1 - \alpha) \frac{S_0 c}{1 + S_1 c}}_{\mathfrak{B}(\alpha, c)\text{-birth rate}} - \underbrace{\frac{S_2 + S_3 c}{1 + S_4 c} \alpha}_{\mathfrak{D}(\alpha, c)\text{-death rate}} \quad \text{and} \quad \mathcal{H}(\alpha) = \frac{(\alpha - \alpha^{\text{R}})^+}{(1 - \alpha)^2}$$

Remark 7.2 (variability of η). *In general, η may not be a constant since the rate of diffusion depends on the medium through which the nutrient diffuses. The tumour becomes more closely packed as the cell volume fraction increases, and it impedes the diffusion of the nutrient. This scenario can be modelled by setting the diffusivity as a function of the cell volume fraction. Also, the nutrient may be advected with the phase in which it is distributed. The advection term is excluded in (7.10) as it is considered negligible compared to the diffusion.*

Initial and boundary conditions

The initial conditions are, for every $x \in (0, \ell_0)$

$$\alpha(0, x) = \alpha_0(x) \text{ and } c(0, x) = c_0(x).$$

The assumption (A.5) yields the following two boundary conditions at $x = 0$; for every $t \in (0, T)$

$$u_\alpha(t, 0) = 0 = \frac{\partial c}{\partial x}(t, 0).$$

The fluid is allowed to freely flow across the boundary $x = \ell(t)$ and hence $p_{\beta|\ell(t)} = 0$. However, we neglect the fluid pore pressure experienced in the hydrogel. The continuity of stress at the tumour–hydrogel interface yields, for each $t \in (0, T)$ and $x = \ell(t)$

$$2\mu_\alpha \frac{\partial u_\alpha}{\partial x}(t, \ell(t)) - \gamma \mathcal{H}(\alpha(t, \ell(t))) = \sigma_{|\ell(t)}^H, \quad (7.12)$$

where σ^H is given in (7.7). The left hand side of (7.12) is the stress in the cell phase at $x = \ell(t)$ (sum of viscous effects and fluid pressure). The nutrient concentration is assumed to be a constant maximum at $x = 0$, which yields for every $t \in (0, T)$

$$c(t, \ell(t)) = c_{out}.$$

Interaction between hydrogel and tumour

The tumour and hydrogel kinetics are coupled through (7.12) (continuity of stress) and (7.7) (stress in hydrogel), see Figure 7.3. We note that:

- Since σ^H is negative, see assumption (A.1), (7.12) shows that the cell phase stress, σ_α , is negative at $x = \ell(t)$. This implies that the tumour cells experience a force (acting to the left) against their outward growth at $x = \ell(t)$, see Figure 7.1, which retards the growth rate. The growth rate becomes slower as σ^H becomes more negative.
- Tumour growth affects the stress in the hydrogel through (7.7). Observe that σ^H is a function of $\ell(t)$. Let $d_{\ell(t)}\sigma^H$ be the derivative of σ^H with respect to $\ell(t)$. Since $d_{\ell(t)}\sigma^H < 0$, σ^H decreases as $\ell(t)$ increases, see Figure 7.2(a), and the tumour receives a higher opposing force against its growth.

Since the above two kinetics are opposite to each other, two possibilities exists: (a) the tumour grows till a steady state radius is achieved, wherein stress in the tumour is just adequate enough to resist the compressive stress in the hydrogel and not able to further compress the hydrogel or (b) stress in the hydrogel is too strong so that it compresses (and eventually annihilates) the tumour.

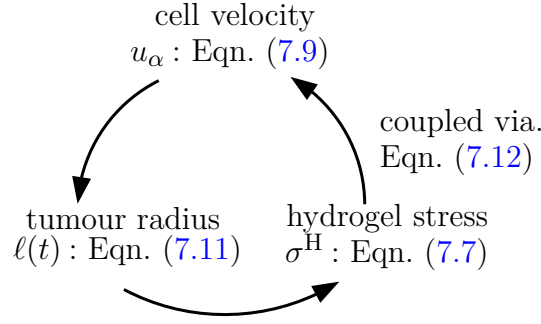


Figure 7.3: Mutual coupling between cell velocity, hydrogel stress, and tumour radius.

Consolidated model

The model variables of tumour growth are cell volume fraction, cell velocity, nutrient concentration and tumour radius governed by (7.8), (7.9), (7.10), and (7.11), respectively. The stress generated in the hydrogel at $x = \ell(t)$ interacts with the tumour model variables through (7.12).

7.3 Dimensionless model

The rescaled dimensionless variables are provided in Table 7.2. Here, t_{dim} is $(1 +$

Dimensional quantities	Dimensionless quantities
Space and time	$x' = \frac{x}{\ell_{\text{dim}}}, t' = \frac{t}{t_{\text{dim}}}$
cell volume fraction	$\alpha' = \alpha, s_1 = S_1 c_{\text{out}}, s_2 = t_{\text{dim}} S_2, s_3 = \frac{t_{\text{dim}} S_3}{c_{\text{out}}}, s_4 = S_4 c_{\text{out}}$
cell velocity	$u'_\alpha = \frac{t_{\text{dim}}}{\ell_d} u_\alpha, k' = \frac{k_1 \ell_{\text{dim}}^2}{\gamma t_{\text{dim}}}, \mu = \frac{2\mu_\alpha}{\gamma t_{\text{dim}}}, \gamma' = \gamma/\gamma = 1.$
nutrient concentration	$c' = \frac{c}{c_{\text{out}}}, Q = Q_0 t_{\text{dim}}, \hat{Q}_1 = Q_1 c_{\text{out}}, \eta' = \frac{t_{\text{dim}} \eta}{\ell_{\text{dim}}^2}$
tumour radius	$\ell' = \frac{\ell}{\ell_{\text{dim}}}, \text{ and } \ell'_0 = \frac{\ell_0}{\ell_{\text{dim}}}$
hydrogel	$\nu' = \frac{\nu}{\gamma}, \vartheta' = \frac{\vartheta}{\gamma}, \ell'_m = \frac{\ell_m}{\ell_{\text{dim}}}$

Table 7.2: Dimensionless variables and parameters

$S_1 c_{\text{out}})/S_0 c_{\text{out}}$, which is the time required to produce unit volume fraction of cells at the highest nutrient concentration. The space scaling ℓ_{dim} is taken as ℓ_m so that the scaled box dimension ℓ'_m becomes unity. Also, we define $\mathcal{H}(\alpha) := \Sigma(\alpha)/\gamma = (\alpha - \alpha^R)^+/(1 - \alpha)^2$. Variables with prime symbols are dimensionless. The prime symbols, subscripts α and β are dropped in the dimensionless model for notational simplicity. In what follows, the

rescaled domains $\mathcal{D}_T = (0, T) \times (0, 1)$ and $D_T \subset \mathcal{D}_T$ are dimensionless. The nutrient diffuses at a rate much faster than that of tumour cells mitosis, which justifies the quasi-steady state assumption that has been applied to (7.13c) in the following.

The dimensionless model for tumour-hydrogel dynamics is as follows: for all $(t, x) \in D_T$ it holds

$$\frac{\partial \alpha}{\partial t} + \frac{\partial}{\partial x}(u\alpha) = \alpha f(\alpha, c), \quad (7.13a)$$

$$-\mu \frac{\partial}{\partial x} \left(\alpha \frac{\partial u}{\partial x} \right) + \frac{k\alpha u}{1-\alpha} = -\frac{\partial}{\partial x}(\alpha \mathcal{H}(\alpha)), \quad (7.13b)$$

$$\frac{\partial}{\partial x} \left(\eta \frac{\partial c}{\partial x} \right) = \frac{Q\alpha c}{1 + \widehat{Q}_1 c}, \quad (7.13c)$$

$$\ell'(t) = u(t, \ell(t)), \quad (7.13d)$$

where the stress in the hydrogel, σ^H is

$$\sigma^H = \nu \frac{1 - \ell(t)}{1 - \ell_0} - \vartheta \left(\frac{1 - \ell(t)}{1 - \ell_0} \right)^{-1}. \quad (7.13e)$$

The initial conditions are

$$\alpha(0, x) = \alpha_0(x), \quad c(0, x) = c_0(x) \quad \forall x \in (0, \ell_0), \quad \ell(0) = \ell_0, \quad (7.13f)$$

and boundary conditions are

$$u(t, 0) = 0, \quad \mu \frac{\partial u}{\partial x}(t, \ell(t)) - \mathcal{H}(\alpha(t, \ell(t))) = \sigma^H, \quad (7.13g)$$

$$\frac{\partial c}{\partial x}(t, 0) = 0, \quad \text{and} \quad c(t, \ell(t)) = 1 \quad \forall t \in (0, T). \quad (7.13h)$$

Here,

$$f(\alpha, c) = \frac{(1 + s_1)(1 - \alpha)c}{(1 + s_1 c)} - \frac{(s_2 + s_3 c)}{(1 + s_4 c)}.$$

Differences between BBL model and (7.13)

The total stress experienced at the tumour boundary is the sum of mechanical stress and fluid pressure, see LHS of second equation in (7.13g). The total stress at the tumour boundary is zero in the BBL model from the balance of stresses and since external stresses are absent. However, in (7.13) this is not zero but σ^H . The nondimensionalisation employed in (7.13) is also different from that in the BBL model. The variables in BBL model are spatially scaled using the initial tumour radius, ℓ_0 . In (7.13), size of the box, ℓ_m , is used to scale the model variables. This difference in scaling is reflected in the numerical values of k , η , and ℓ_0 in (7.13), see Tables 7.2 and 7.3. In the BBL model (k, η, ℓ_0) is $(1, 1, 1)$, while the corresponding values in (7.13) are $(1600, 1/1600, 1/40)$.

Remark 7.3 (Dimensionless compressibility parameters). *Observe that the dimensionless compressibility parameters ν and ϑ in (7.13e) do not explicitly depend on ℓ_m . This may strike as counter-intuitive since the rescaled hydrogel ought to exhibit a lesser or higher compressibility upon stretching or compressing, respectively, since any quantity v with the dimension of stress is rescaled into a dimensionless version by the formula*

$$v' = v \times (\text{length scale} \times (\text{time scale})^2) / (\text{mass scale}).$$

The dependence of ν and ϑ on ℓ_m is hidden in the rescaling using the intercellular force coefficient, γ . Note that γ also depends on the box dimension ℓ_m and achieves a lesser or higher value when rescaled to a larger or smaller domain. Since γ and the compressibility parameters are rescaled using the same length scale, the effect of box dimension is made implicit while taking the fractions γ/γ , ν/γ , and ϑ/γ as displayed in rows three and six in Table 7.2.

7.4 Discrete scheme

In the discrete scheme, see Definition 7.5, the tumour boundary $\ell(t)$ is explicitly tracked using (7.14d). In other chapters, the model is recast into an extended domain and the ODE (7.14d) is eliminated. Then, the tumour boundary is recovered using the discrete cell volume fraction and the threshold value. The reason to explicitly track the tumour boundary is to isolate the effect of hydrogel compressibility parameters ϑ and ν on the tumour radius. To the best of our knowledge, the influence of these parameters on the tumour size have not been investigated before. Since the threshold value also influences the location of tumour radius, it becomes difficult to study the individual effect of hydrogel compressibility. Since the model is purely 1D the scaling and explicit tracking is feasible.

The model (7.13a)–(7.13d) is defined on the time dependent domain $(0, \ell(t))$ for each time $t \in (0, T)$. The domain $(0, \ell(t))$ is rescaled to the unit interval $(0, 1)$ by using the transformation, $\xi = x/\ell(t)$ for every $x \in (0, \ell(t))$, see Section 1.5 for further details. The rescaled model reads as, for every $D_{1,T} := (t, \xi) \in (0, T) \times (0, 1)$, it holds

$$\frac{\partial \alpha}{\partial t} - \frac{\xi}{\ell} \frac{d\ell}{dt} \frac{\partial \alpha}{\partial \xi} + \frac{1}{\ell} \frac{\partial (u\alpha)}{\partial \xi} = \alpha f(\alpha, c), \quad (7.14a)$$

$$\frac{\ell^2 k \alpha u}{1 - \alpha} - \mu \frac{\partial}{\partial \xi} \left(\alpha \frac{\partial u}{\partial \xi} \right) = -\ell \frac{\partial}{\partial \xi} \mathcal{H}(\alpha), \quad (7.14b)$$

$$\frac{\partial}{\partial \xi} \left(\eta \frac{\partial c}{\partial \xi} \right) = \frac{Q \ell^2 \alpha c}{1 + \widehat{Q}_1 c}, \text{ and} \quad (7.14c)$$

$$\ell'(t) = u(t, 1). \quad (7.14d)$$

The transformed initial conditions are

$$\alpha(0, \xi) = \alpha_0(\xi), \quad c(0, \xi) = c_0(\xi) \quad \forall \xi \in \Omega(0), \quad \ell(0) = \ell_0,$$

and the boundary conditions are

$$\begin{aligned} u(t, 0) = 0, \quad \mu\alpha(t, 1) \frac{\partial u}{\partial \xi}(t, 1) &= \ell(t) \left(\mathcal{H}(\alpha(t, 1)) + \sigma_{|\xi=1}^H \right), \\ \frac{\partial c}{\partial \xi}(t, 0) = 0, \quad \text{and } c(t, 1) &= 1 \quad \forall t \in (0, T). \end{aligned} \quad (7.15)$$

Observe that (7.14a) can be written in the following conservative form

$$\frac{\partial \alpha}{\partial t} + \frac{\partial}{\partial \xi} \left(\frac{\alpha}{\ell(t)} (u - \xi u(t, 1)) \right) = \alpha f(\alpha, c) - \frac{\alpha}{\ell(t)} u(t, 1). \quad (7.16)$$

Since (7.16) is a hyperbolic conservation law, it is discretised using an upwind finite volume method. Let $0 = \xi_{-1/2} < \dots < \xi_{J+1/2} = 1$ and $0 = t_0 < \dots < t_N = T$ be uniform spatial and temporal discretisations, respectively. Define $h = \xi_{j+1/2} - \xi_{j-1/2}$ and $\delta = t_{n+1} - t_n$. Define $K_j := (\xi_{j-1/2}, \xi_{j+1/2})$ for $0 \leq j \leq J$ and $\mathcal{T}_n := (t_n, t_{n+1})$ for $0 \leq n < N$.

Definition 7.4 (Discrete average). *For any real valued function f on \mathbb{R} , define the discrete average of f on the interval K_j by $\{\{f\}\}_{K_j} := (f(\xi_{j-1/2}) + f(\xi_{j+1/2}))/2$, where $j = 0, \dots, J$.*

The cell velocity equation (7.14b) is discretised using Lagrange \mathbb{P}_1 finite element method and the nutrient equation (7.14c) using the mass lumped \mathbb{P}_1 finite element method. Recall that $a^+ = \max(a, 0)$ and $a^- = -\min(a, 0)$ from Section 1.4.

Definition 7.5 (Discrete scheme). **Initial data approximation:** *Define:*

- α_h^0 by $\alpha_h^0 := \alpha_j^0$ on K_j , for $j = 0, \dots, J$, where $\alpha_j^0 = \int \alpha_0(\xi) d\xi$.
- c_h^0 by $c_{h|K_j} \in \mathbb{P}_1(K_j)$ for $j = 0, \dots, J$ where $c_h^0(x_{j-1/2}) = c_0(x_{j-1/2})$ for $j = 0, \dots, J+1$.

Updation: *Construct a finite sequence of four tuple of functions $(\alpha_h^n, u_h^n, c_h^n, \ell_h^n)_{\{1 \leq n \leq N\}}$ on $(0, 1)$ such that for every $1 \leq n \leq N$, it holds:*

(DS.a) *Define $\ell_h^n := \ell_h^{n-1} + \delta u_h^{n-1}(1)$.*

(DS.b) *Set for $j = 0, \dots, J$*

$$\begin{aligned} v_{j+1/2}^{n-1} &:= \frac{1}{\ell_h^n} \left(u_h^{n-1}(\xi_{j+1/2}) - \xi_{j+1/2} u_h^{n-1}(1) \right), \\ b_j^{n-1} &:= \{\{(1 + s_1)c_h^{n-1}/(1 + s_1 c_h^{n-1})\}\}_{K_j}, \quad \text{and} \\ d_j^{n-1} &:= \{\{(s_2 + s_3 c_h^{n-1})/(1 + s_4 c_h^{n-1})\}\}_{K_j}. \end{aligned}$$

For $j = 0, \dots, J$ define $\alpha_h^n := \alpha_j^n$ on K_j , where

$$\begin{aligned} \alpha_j^n &= \alpha_j^{n-1} - \frac{\delta}{h} \left((v_{j+1/2}^{n-1,+} \alpha_j^{n-1} - v_{j+1/2}^{n-1,-} \alpha_{j+1}^{n-1}) - (v_{j-1/2}^{n-1,+} \alpha_{j-1}^{n-1} - v_{j-1/2}^{n-1,-} \alpha_j^{n-1}) \right) \\ &\quad + \delta \alpha_j^{n-1} (1 - \alpha_j^{n-1}) b_j^{n-1} - \delta \alpha_j^n d_j^{n-1} - \frac{\delta}{\ell_h^n} \left(u_h^{n-1,+}(t, 1) \alpha_j^{n-1} - u_h^{n-1,-}(t, 1) \alpha_j^n \right). \end{aligned}$$

(DS.c) Set the finite element space of piecewise affine polynomials from $(0,1)$ to \mathbb{R} with homogeneous boundary condition at $\xi = 0$ by

$$V_h = \left\{ v_h \in \mathcal{C}^0([0,1]) : v_h|_{K_j} \in \mathbb{P}_1(K_j), 0 \leq j \leq J, v_h(0) = 0 \right\}.$$

Define $u_h^n \in V_h$ such that, for every $v_h \in V_h$, it holds $a_u(u_h^n, v_h) = \mathcal{L}_h(v_h)$, where

$$\begin{aligned} a_u(u_h^n, v_h) &:= \int_0^1 k(\ell_h^n)^2 \frac{\alpha_h^n}{1 - \alpha_h^n} u_h^n v_h \, d\xi + \mu \int_0^1 \alpha_h^n \frac{\partial u_h^n}{\partial \xi} \frac{\partial v_h}{\partial \xi} \, d\xi, \text{ and} \\ \mathcal{L}_h(v_h) &:= \int_0^1 \ell_h^n \mathcal{H}(\alpha_h^n) \frac{\partial v_h}{\partial \xi} \, d\xi + \ell_h^n \left(\nu \frac{1 - \ell_h^n}{1 - \ell_0} - \vartheta \left(\frac{1 - \ell_h^n}{1 - \ell_0} \right)^{-1} \right) v_h(1). \end{aligned}$$

(DS.d) Set $K_j = (\xi_{j-1/2} - h/2, \xi_{j-1/2} + h/2)$, $1 \leq j \leq J$, $\tilde{K}_0 = (0, h/2)$, and $\tilde{K}_{J+1} = (1 - h/2, 1)$. Define the following finite dimensional vector spaces on $(0,1)$ by

$$\begin{aligned} W_h &:= \left\{ w_h \in \mathcal{C}^0([0,1]) : w_h|_{K_j} \in \mathbb{P}_1(K_j), 0 \leq j \leq J \right\}, \\ W_{h,0} &:= \left\{ w_h \in W_h : w_h(1) = 0 \right\}, \text{ and} \\ W_{h,\text{ML}} &:= \left\{ w_h : w_h = \sum_{j=0}^J w_j \chi_{\tilde{K}_j}, w_j \in \mathbb{R}, 0 \leq j \leq J \right\}, \end{aligned}$$

and the mass lumping operator $\Pi_h : \mathcal{C}^0([0,1]) \rightarrow \mathcal{S}_{h,\text{ML}}$ by $\Pi_h w := \sum_{j=0}^J w(x_j) \chi_{\tilde{K}_j}$. Then, $c_h^n \in W_h$ satisfies $c_h^n(1) = 1$ and for every $w_h \in W_h$, $a_2^n(c_h^n, w_h) = 0$, where

$$a_2^n(c_h^n, w_h) = \eta \int_0^1 \frac{\partial c_h^n}{\partial \xi} \frac{\partial w_h}{\partial \xi} \, d\xi + \int_0^1 \frac{Q(\ell_h^n)^2 \alpha_h^n}{1 + \hat{Q}_1 \Pi_h c_h^{n-1}} \Pi_h c_h^n \Pi_h w_h \, d\xi.$$

Differences between schemes in Definitions 7.5 and 2.4

The discrete schemes in Definitions 7.5 and 2.4 are different in three aspects.

- The upwind finite volume scheme is different as the flux function in (7.16) is $\frac{\alpha}{\ell(t)}(u - \xi u(t, 1))$, which was $u\alpha$ in the hyperbolic conservation laws in BBL, extended, and threshold models.
- The Neumann boundary condition for the velocity equation is not homogeneous as the stress in the hydrogel is nonzero, see (7.15).
- The ordinary differential equation $\ell'(t) = u(t, \ell(t))$ is solved using an explicit Euler scheme, instead of extending the model and recovering the tumour radius using the cell volume fraction and threshold value.

Parameter	Value	Parameter	Value
k	1600	μ	1
Q	1	\widehat{Q}_1	0
s_1, s_4	10	s_2, s_3	0.5
α^R	0.8	η	1/1600
α_0, c_0	1	ℓ_0	1

Table 7.3: Model parameters (source: see [1])

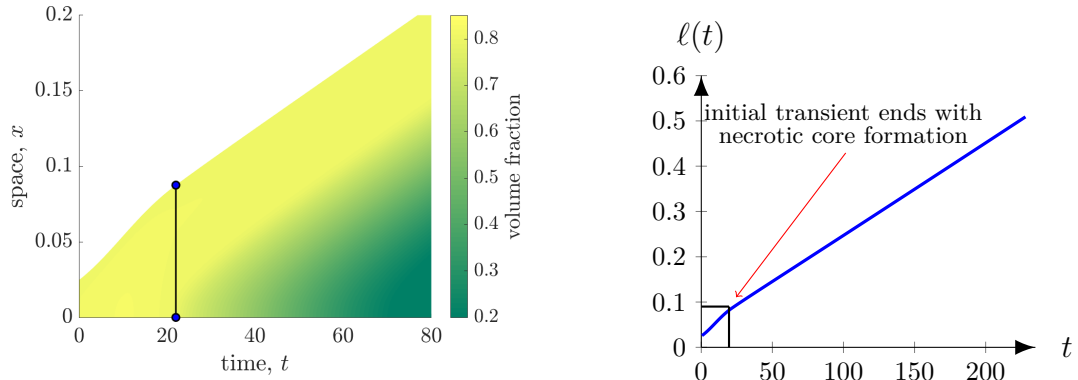
7.5 Numerical simulations

The parameters used for the numerical simulations are dimensionless. The values that are fixed in this section are given in Table 7.3. Two sets of numerical experiments are conducted in this section. In Subsection 7.5.1, the growth in free suspension, wherein hydrogel is absent, is simulated. The effect of stress from the hydrogel on tumour growth is studied in Subsection 7.5.2.

7.5.1 Free suspension growth

The absence of hydrogel is simulated by setting $\vartheta = 0 = \nu$. It follows that $\sigma^H = 0$ and the tumour does not experience an opposing stress against its growth. Therefore, the tumour can grow freely if sufficient nutrient is available. It is well known that sufficiently large tumours develop a central zone of dead cells, called the necrotic core, due to nutrient deficiency. In Figure 7.4(a), the formation of necrotic core can be observed near $t = 20$, where the volume fraction at the tumour centre and its vicinity significantly reduces. The formation of the necrotic core also influences the velocity of tumour boundary, see Figure 7.4(b); the slope of the function $\ell(t)$ vs. t curve decreases at $t = 20$. The formation of the necrotic core aids to release tumour stress by redistributing cells at the boundary $x = \ell(t)$ and the necrotic core. Small tumours cannot release stress by distributing cells at the necrotic core. As a result, stress is predominantly directed towards the periphery, which accelerates the tumour growth. The qualitative behaviour of the model variables are different before and after the formation of the necrotic core. To show this difference, enlarged graphs of model variables on $0 \leq t \leq 20$ are displayed in the second row of Figure 7.5. The initial transient before the formation of the necrotic core is a characteristic feature of small sized tumours.

Nutrient concentration follows the same profile at every time; it monotonically increases from $x = 0$ to $x = \ell(t)$. The volume fraction monotonically decreases from $x = 0$ to $x = \ell(t)$ before the formation of the necrotic core, see Figure 7.5(f). Once the necrotic core forms, cell volume fraction follows a travelling wave pattern with respect to time, in which the volume fraction is minimal at the tumour center $x = 0$, increasing and stabilising towards $x = \ell(t)$, see Figure 7.5(b). The velocity is positive and monotonically increasing before the formation of the necrotic core, see Figure 7.5(g). This explains the rightward



(a) Volume fraction as a function of space (distance from tumour center) and time for free suspension growth. (b) Tumour radius vs. time for free suspension growth.

Figure 7.4: Formation of necrotic core in free suspension growth

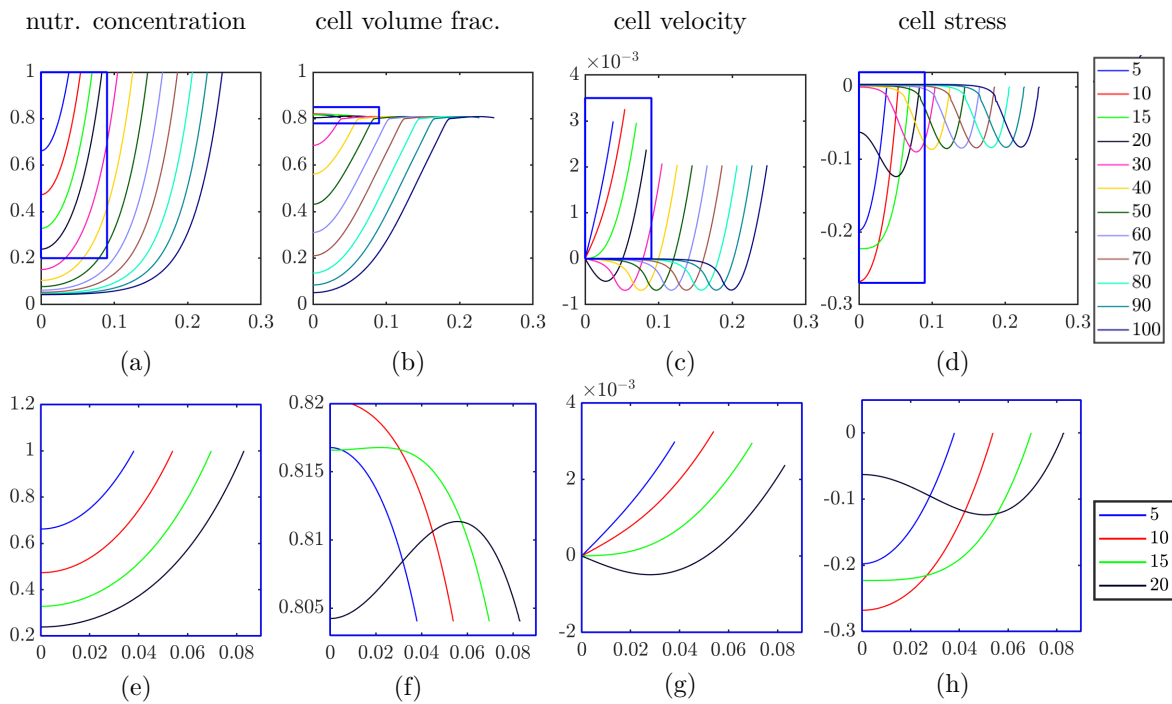


Figure 7.5: In each subfigure, the x -axis represents the distance from the tumour center ($x = 0$) and y -axis the model variable captioned above in the respective column. Upper row: spatial variation of model variables at time steps $t \in \{5, 10, 15, 20, 30, 40, 50, 60, 70, 80, 90, 100\}$ indicated by the legends on the last column. Lower row: Enlarged view of (blue box in the upper row) spatial variation of model variables at time steps $t \in \{5, 10, 15, 20\}$.

motion of cells, see Figure 7.1. The cell velocity is zero in the necrotic region. It then decreases to a negative minimum showing movement of cells towards the necrotic region, and increases to attain a positive maximum at $x = \ell(t)$, see Figure 7.5(c), indicating the movement of cells towards $x = \ell(t)$. This trend is supported by the stress profiles, σ_α , in Figures 7.5(d) and 7.5(h). The stress is negative, which shows compression in the tumour. The stress reaches a negative maximum at the tumour centre and increases to zero at $x = \ell(t)$ before the formation of the necrotic core. The development of the necrotic core reduces the stress there to zero. The stress attains a negative maximum in the actively proliferating region and increases to zero at $x = \ell(t)$. The vanishing stresses at $x = \ell(t)$ and in the necrotic centre points to the redistribution of cells towards these two regions.

Remark 7.6 (BBL model as a special case of (7.13)). *The BBL mode manifests as a special case of (7.13) by setting $\vartheta = \nu = 0$. The profiles of the model variables α , u , and c , displayed in Figure 7.5 are same as that of in Chapter 1 (see Figure 1.7) up to a scaling of the x -axis. The scale difference in x -axis is due to the difference in nondimensionalisation employed in these two models. In this sense, (7.13) is more generic than the previous works and presents a more realistic version of in vitro tumour growth.*

7.5.2 Stress controlled growth for tumours

In a stress controlled environment tumour exhibits three types of qualitative behaviours depending on the compressibility parameters, ν and ϑ . These are illustrated in Figure 7.6. All experiments in Figure 7.6 are conducted with $\nu = 0$. Since the nutrient concentration exhibits the same behaviour as shown in Figure 7.5(a) in all experiments, its graphs are not included in the sequel. The first to fourth columns in Figure 7.6 represent the variation of volume fraction, cell velocity, stress in tumour-hydrogel continuum, and tumour radius, respectively.

The y -axis in the third column is σ_{TG} , where $\sigma_{TG} := \sigma_\alpha$ if $0 \leq x \leq \ell(t)$ and $\sigma_{TG} := \sigma^H$ if $\ell(t) \leq x \leq 1$. It can be observed that σ_{TG} is continuous at the tumour boundary, indicated by coloured circles in each line plot of Figures 7.6(c), 7.6(g), and 7.6(k), and it follows that $\sigma_\alpha = \sigma^H$ at $x = \ell(t)$. Since σ_α is strictly negative at $x = \ell(t)$, tumour growth is impeded. On the contrary, in free suspension growth, the compressive stress vanishes at $x = \ell(t)$, see Figure 7.5(d), which allows unhindered growth.

When ϑ is adequately low ($\vartheta = 0.5$), the tumour grows to a size that allows the formation of the necrotic core as shown in the first row of Figure 7.6. The volume fraction, velocity, and stress follows a wave like behaviour (with a time dependent wave speed). Since the stress becomes more negative as $\ell(t)$ increases as in Figure 7.6(c), the cell velocity approaches zero and the tumour radius slowly stabilises. Along with this wave like behaviour pattern this negative stress stacks the line plots in Figures 7.6(a), 7.6(b), and 7.6(c) closer as time evolves. Such a growth pattern is referred to as *post-necrotic growth* in the sequel.

For moderately high values of ϑ ($\vartheta = 2$), the tumour grows but cannot reach a size that facilitates the formation of a necrotic core as shown in the second row of Figure 7.6. Here, the cell volume fraction, velocity, and stress profiles remain in the initial transient

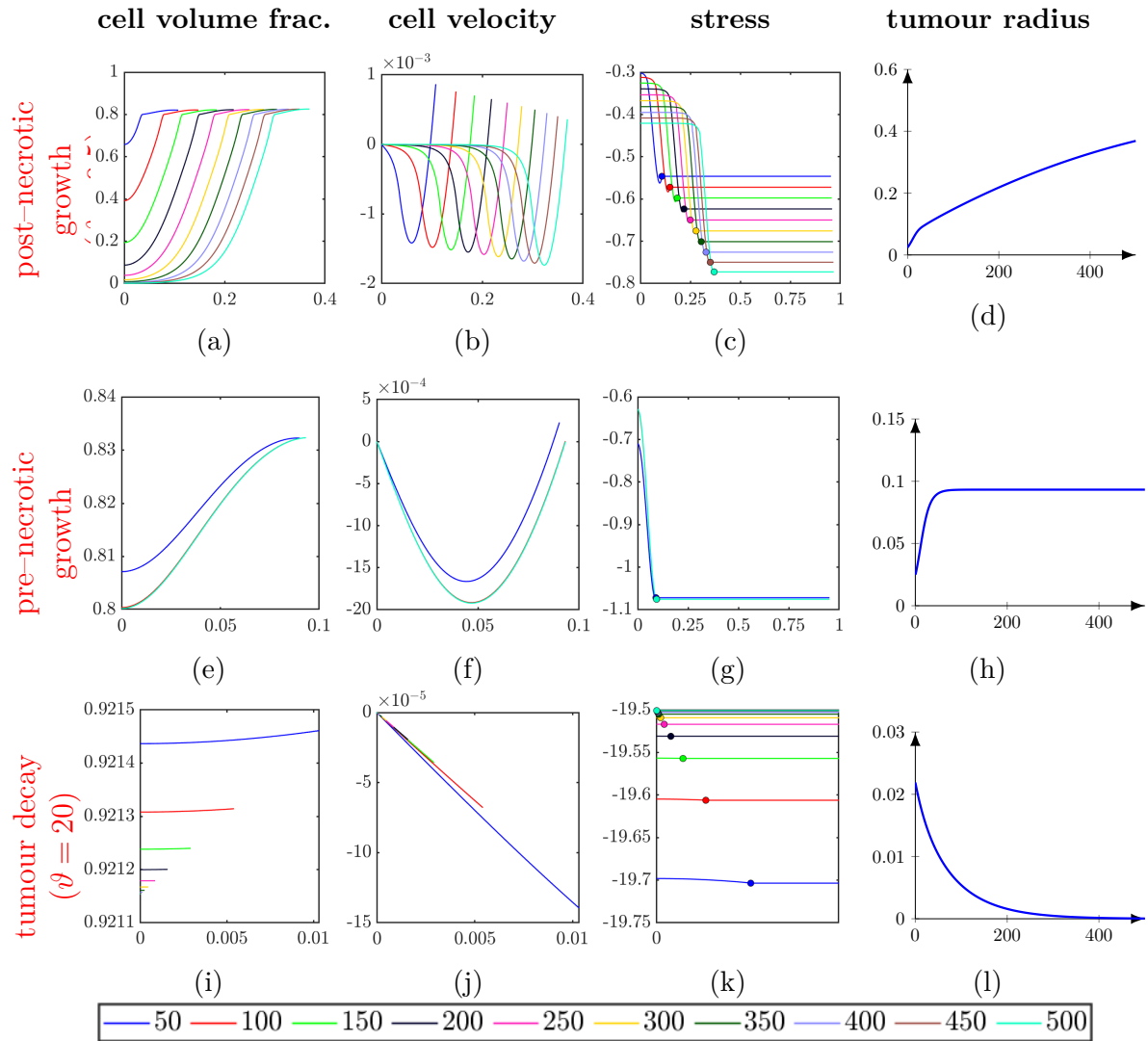


Figure 7.6: Effect of ϑ on tumour growth (here $\nu = 0$). The variables are indicated by the title of each row. From the first to third columns, the x -axis is the distance from the tumour centre. In the fourth column, the x -axis is time. Each coloured line in the first to third columns represent the variation of the respective variable at a time as indicated in the legend.

stage. The tumour stabilises much faster, see Figure 7.6(h), than in the case of $\vartheta = 0.5$. Since the compressive stress from the hydrogel is much higher the stabilising radius is smaller than that when $\vartheta = 0.5$. This behaviour is termed as *pre-necrotic growth* in the sequel.

When ϑ is large ($\vartheta = 20$), the hydrogel stress becomes exceedingly negative and the tumour fails to grow. In this case, the hydrogel compresses the tumour, which leads to its eventual decay as shown in the third row of Figure 7.6. This growth pattern is termed as *tumour decay*.

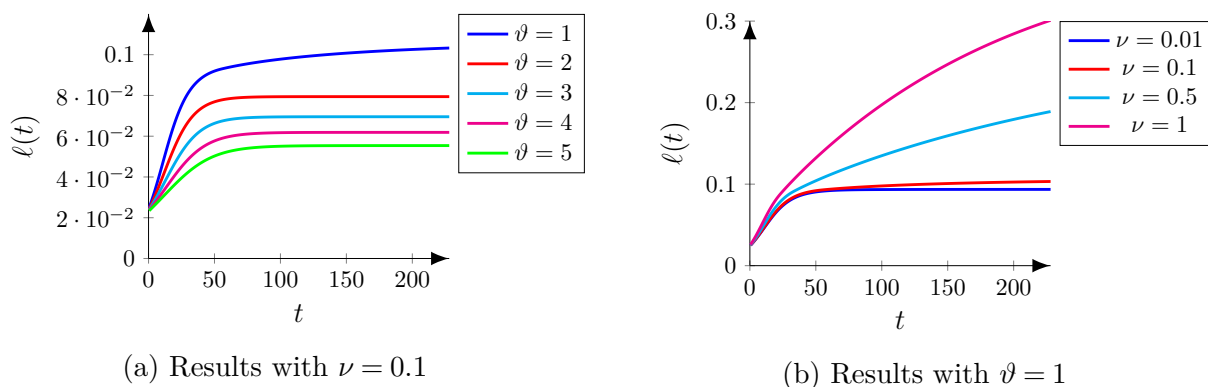


Figure 7.7: Effect of compressibility parameters on $\ell(t)$ profiles.

The effect of ν on tumour growth is opposite to that of ϑ . A high value of ν asserts that the hydrogel is more compressible and favours tumour growth. This is illustrated in Figure 7.7(b), wherein ϑ is set as unity. It can be observed that the tumour radius stabilises to higher values as ν increases. On the contrary, the tumour radius stabilises to smaller values as ϑ increases as shown in Figure 7.7(a), where ν is set as 0.1.

The variation of limiting radius ($\ell_s = \lim_{t \rightarrow \infty} \ell(t)$) with respect to ν and ϑ is illustrated in Figure 7.8. To numerically compute the limiting radius, the model (7.13) is solved for a sufficiently large time – in this case, $T = 1000$ – and the limiting radius is defined as the truncated value $\ell_s = \ell(1000)$. The values of ϑ and ν for which the tumour exhibits post and pre-necrotic growth behaviours are shown as two separate zones in Figure 7.8. For (ϑ, ν) above the red line in Figure 7.8, the tumour achieves a limiting size greater than $\ell_s = 0.01$ (see Figure 7.4(b)), which marks the onset of post-necrotic growth behaviour, see Figure 7.6. For (ϑ, ν) below the red line, the tumour fails to attain this size and remains in the pre-necrotic growth behaviour forever (at least until $T = 1000$). Also, it is worth noticing that the tumour attains a limiting radius close to $\ell_s = 0.9$ only for very small values of ϑ (towards the bottom-left corner in Figure 7.8). Otherwise, the tumour attains a limiting radius less than approximately $\ell_s = 0.4$, which indicates the predominant effect of external stress in controlling the tumour size. In Figure 7.8, the decay zone for the tumour is not indicated to obtain a better resolution of the post and pre-necrotic growth behaviours. It has been observed numerically that for $\vartheta \geq 11.75$ the tumour exhibits a decay behaviour.

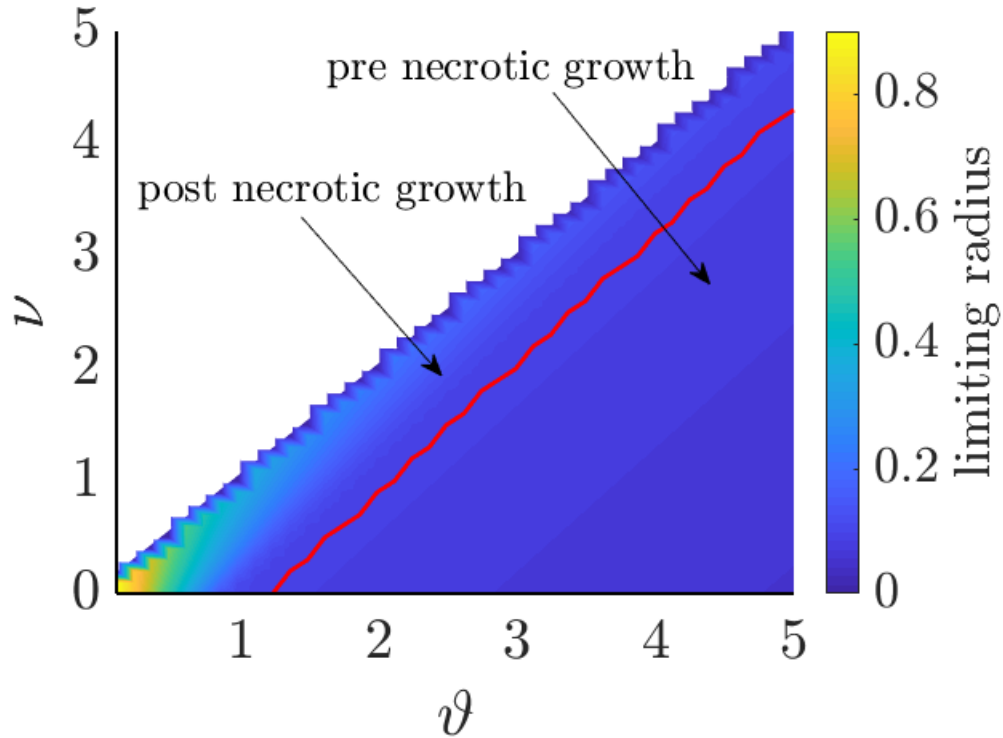


Figure 7.8: Variation of the limiting radius with respect to ϑ and ν for $\nu \leq \vartheta$. The region above and below the red demarcation indicates the values of (ϑ, ν) , where the tumour attains post and pre necrotic behaviours, respectively.

7.5.3 Behaviour of tumour radius near the box boundary

The evolution of tumour radius in free suspension and in hydrogel medium are different. When the tumour grows in free suspension, depending on the choice of parameters it may evolve to a travelling wave solution or a steady state solution (due to the counter-acting effects of tumour expansion and the necrotic core). In the former case, the tumour radius increases monotonically and in the latter case the tumour radius becomes a constant eventually.

When tumour grows in a hydrogel, then the tumour radius is bound to attain a steady state. If $u(t, \ell(t))$ is nonpositive for every t , then the tumour will eventually decay as shown in Figure 7.6(1).

When $u(t, \ell(t))$ is nonnegative for every t , it can be proved that $u(t, \ell(t))$ asymptotes to zero as $\ell(t)$ approaches the box dimension, see Figure 7.1. An analytical proof of this is presented in Theorem 7.7. Here, we assume that the volume fraction is bounded. Then, it is established that the boundary velocity $u(t, \ell(t))$ approaches zero as $\ell(t)$ approaches the box dimension, unity in this case. As the tumour expands, the polymer molecules in the hydrogel are stacked together and forced to occupy a smaller physical space. Eventually, a

stage will be attained, wherein the short range molecular repulsion between the hydrogel molecules are dominant and the hydrogel becomes incompressible. Since the hydrogel occupies a 1D domain in this model, this incompressibility leads to length invariance of the hydrogel and hence the tumour.

Theorem 7.7 (Steady state of tumour radius). *Let (α, u, c, ℓ) be a solution of (7.13) such that $u(t, \ell(t)) \geq 0$ for every $t \geq 0$. If $\vartheta \geq \nu$, then it holds $\lim_{\ell(t) \rightarrow 1} \ell'(t) = 0$.*

Proof. Multiply (7.13b) by $u(t, x)$ on both sides and apply integration by parts to obtain

$$\int_0^{\ell(t)} \frac{k\alpha}{1-\alpha} u^2 dx + \int_0^{\ell(t)} \mu\alpha \left(\frac{\partial u}{\partial x} \right)^2 dx = \int_0^{\ell(t)} \mathcal{H}(\alpha) \frac{\partial u}{\partial x} dx + u(t, \ell(t)) \sigma_{|\ell(t)}^H. \quad (7.17)$$

Since $u(t, \ell(t)) \geq 0$ (by assumption), it follows $u(t, \ell(t)) \sigma_{|\ell(t)}^H \leq 0$, whence

$$\int_0^{\ell(t)} \frac{k\alpha}{1-\alpha} u^2 dx + \int_0^{\ell(t)} \mu\alpha \left(\frac{\partial u}{\partial x} \right)^2 dx \leq \int_0^{\ell(t)} \mathcal{H}(\alpha) \frac{\partial u}{\partial x} dx.$$

Use Cauchy–Schwartz inequality and $0 < \alpha_m \leq \alpha \leq \alpha_M < 1$ to arrive at

$$\mu\alpha_m \left(\int_0^{\ell(t)} \left(\frac{\partial u}{\partial x} \right)^2 dx \right)^{1/2} \leq \sqrt{\ell(t)} \frac{\alpha_M |\alpha_M - \alpha^R|}{|1 - \alpha_M|^2}. \quad (7.18)$$

Since the left hand side of (7.17) is nonnegative, we obtain $u(t, \ell(t)) \leq \frac{1}{|\sigma_{|\ell(t)}^H|} \int_0^{\ell(t)} \mathcal{H}(\alpha) \frac{\partial u}{\partial x} dx$. Then, Cauchy–Schwartz inequality and (7.18) leads to

$$u(t, \ell(t)) \leq \frac{1}{\mu\alpha_m |\sigma_{|\ell(t)}^H|} \left(\frac{\alpha_M |\alpha_M - \alpha^R|}{|1 - \alpha_M|^2} \right)^2.$$

Since $|\sigma_{|\ell(t)}^H|$ approaches infinity as $\ell(t)$ tends to 1, it follows $\lim_{\ell(t) \rightarrow 1} u(t, \ell(t)) = 0$, and thereby $\lim_{\ell(t) \rightarrow 1} \ell'(t) = 0$. \square

Remark 7.8. *Theorem 7.7 does not explicitly describe the behaviour of the tumour radius as time evolves. Rather, it asserts that the cell velocity asymptotically becomes zero as $\ell(t)$ approaches the box dimension (unity here). That is, the tumour radius is bound to follow a profile as in Figure 7.6(h), wherein $\ell(t)$ monotonically increases first and then plateaus into a stationary value. This theoretical inference is consistent with the experimental observations in G. Helminger [89]. This is applicable when $u(t, \ell(t))$ is nonpositive as well, since (7.17) and $\sigma_{|\ell(t)}^H \neq 0$ implies $u(t, \ell(t))$ asymptotes to zero as $\ell(t)$ vanishes. As a result, the tumour decay also shows a semi-sigmoid shape as in Figure 7.6(l).*

7.6 Conclusions

In this chapter a continuum model of tumour growth in a hydrogel medium is derived. The tumour is modelled as a biphasic mixture of cell and fluid phases and the hydrogel as a nonlinear elastic material. The tumour and hydrogel kinetics are coupled through a Neumann boundary condition, which asserts the continuity of the stress at tumour-hydrogel interface. The model is discretised using a combination of finite volume and finite element schemes. It has been observed that the tumour exhibits three different types of behaviours depending on the hydrogel compressibility; (a) travelling wave with necrotic core for compressible hydrogels (b) initial transient without necrotic core for moderately incompressible hydrogels, and (c) tumour decay for highly incompressible hydrogels. Theorem 7.7 shows that the tumour radius is bound to attain a steady state profile near the box boundary.

Chapter 8

Summary and future work

This chapter summarises the results and conclusions in this thesis and presents some possible future extensions.

8.1 Summary

In this thesis three aspects of mathematical study of tumour growth are explored:

- mathematical modelling in Chapters 2, 3, and 7,
- scientific computing in Chapters 2 and 5, and
- convergence analysis and existence of solutions in Chapters 4 and 6.

The summary and applications of models in each chapter is presented in Table 8.1. The basic modelling framework in this thesis is obtained from the BBL model in (1.21). The time-dependent boundary in the BBL model offers several numerical and theoretical challenges such as re-meshing, ill-posed models due to degenerate coefficients, and uncontrollable error propagation (see Section 2.1). To mitigate a few of these, a different variant of the BBL model (1.21), termed as *extended model*, is presented in Chapter 2. In the extended model, the cell volume fraction equation is defined on a fixed domain $(0, \ell_m)$ and the tumour radius, $\ell(t)$, is characterised as $\ell(t) := \min\{y : \forall y \leq x \leq \ell_m, \alpha(t, x) = 0\}$ (see Section 2.2). In Theorem 2.3, BBL and extended models are established to be equivalent under appropriate conditions. Several numerical experiments are conducted to verify the robustness of the proposed numerical scheme (see Section 2.4). Here, a fixed discretisation of the domain $(0, \ell_m)$ is used. The cell volume fraction equation is approximated using upwind and MUSCL schemes. The discrete tumour boundary is defined as $\ell(t_n) := \min\{y : \forall y \leq x \leq \ell_m, \alpha_h(t_n, x) \leq \alpha_{\text{thr}}\}$ at a time step t_n , where $\alpha_h(t_n, \cdot)$ is the discrete volume fraction at time t_n and α_{thr} is a small positive number. The elliptic equation (on the cell velocity) and parabolic equation (on the nutrient concentration) are solved using Lagrange \mathbb{P}_1 finite element method and a mass lumped \mathbb{P}_1 finite element method, respectively. The threshold value, α_{thr} , is crucial in improving the accuracy of $\ell(t_n)$ and

Chapter	Model type	Relevance/Applications
1– 4	free suspension growth	Basic framework for complex and realistic models in multidimensions, idea of extended and threshold models that eliminates re-meshing, proof of existence of a weak solution.
5	free suspension growth (NUM), <i>in vitro</i> and <i>in vivo</i> (NLM)	Well defined model in 2D and 3D, idea of threshold model is extended to 2D and 3D, inclusion of diffusivity of nutrient across the tissue or medium surrounding a tumour.
6	<i>in vivo</i>	strong BV estimate on FV solutions of nonlinear conservation laws, existence of a weak solution for the ductal carcinoma model
7	<i>in vitro</i>	Biphasic–hyperelastic model of tumour in a polymeric medium, the effect of compressibility is studied, potential extension by including the effect of drugs, basic framework for stress–dependent growth models such as brain tumours.

Table 8.1: Applicability of models in each chapter

obtaining many theoretical results on the model. The numerical solutions are tested against a simplified model with *a priori* known exact solutions. The results showed that the numerical solutions provide a good approximation of the exact solution. The scheme is used to obtain the numerical solution of the extended model and the results were in agreement with that from Section 1.5.

The extended model and the subsequent numerical scheme presented in Chapter 2 helps to eliminate the time–dependent boundary from the BBL model. However, the lack of uniform bounds of cell volume fraction and coercivity of the cell velocity inside the computational domain $\mathcal{D}_T := (0, T) \times (0, \ell_m)$ are two major drawbacks of the extended model. In Chapter 3, another variant of the BBL model called the *threshold model* is presented. In the threshold model, the tumour boundary is defined as $\tilde{\ell}(t) = \min\{x : \alpha(t, x) \leq \alpha_{\text{thr}} \text{ on } (x, \ell_m)\}$. The source term in the volume fraction equation is modified as $(\alpha - \alpha_{\text{thr}})f(\alpha, c)$ and force term $\mathcal{H}(\alpha)$ in the cell velocity equation is modified as $(\alpha - \alpha_{\text{thr}})^+ / (1 - \alpha)^2$. The justifications for these modifications are explained in Section 3.4.2. A weak solution for the threshold model, termed as *threshold solution*, is introduced in Chapter 3. A discrete scheme is presented for the threshold model, which is based on the scheme introduced in Chapter 2 for the extended model. The discrete schemes in Definitions 2.4 and 3.2 differ in the source terms of (3.5) and (3.8). The numerical solutions obtained Section 3.5 are in very good agreement with those from Chapters 1 and 2.

In Chapter 4, it is established that the discrete solutions from Chapter 3 converge (up to a subsequence) to a threshold solution. This process also proves the existence

of a threshold solution. Uniform bounds of the discrete solution in appropriate normed spaces are presented in Theorem 4.2. The convergence of discrete solutions and existence of a threshold solution are presented in Theorem 4.3. The main challenge in proving Theorem 4.2 is to obtain a uniformly bounded variation estimate on the discrete volume fraction, which is achieved in Propositions 4.15 and 4.16. A discrete Aubin-Simon theorem is used to obtain strong convergence of the discrete nutrient concentration in Proposition 4.24. This is crucial as the source terms of (3.5) involve nonlinear terms of discrete nutrient concentration and cell volume fraction. The proof of Theorem 4.3 starts by establishing convergence of the discrete time-space domains in Proposition 4.25. This follows by the convergences of discrete cell volume fraction, cell velocity, and nutrient concentration in Propositions 4.26, 4.27, and 4.31, respectively. A brief discussion on the maximal time that admits the existence of a threshold solution is provided in Section 4.5.

Chapter 5 presents a biphasic continuum model (5.1) for avascular tumour growth in 2D and 3D, in which the cell and fluid phases follow conservation of mass and momentum. The model variables are the cell volume fraction, cell velocity–fluid pressure system, and nutrient concentration. A coupled system of a hyperbolic conservation law, a Stokes equation, and a parabolic diffusion equation governs the dynamics of the model variables. The tumour boundary moves with the normal velocity of the outermost layer of cells, and this time-dependence is a challenge in designing and implementing a stable and fast numerical scheme. Similar to the work in Chapter 2, the model is recast into a form where the hyperbolic equation is defined on a fixed extended domain and we retrieve the tumour boundary as the interface at which the cell volume fraction becomes zero, see Section 5.4. The equivalence between the variants is proved in Theorem 5.12. This procedure eliminates the need to track the tumour boundary explicitly and the computationally expensive re-meshing of the time-dependent domains. A numerical scheme based on an upwind finite volume method for the hyperbolic conservation law, Lagrange $\mathbb{P}_2 - \mathbb{P}_1$ Taylor–Hood finite element method for the viscous Stokes system, and mass-lumped finite element method for the parabolic equation is implemented in two spatial dimensions, and several cases are studied, see Section 5.5. The versatility of the numerical scheme in catering for irregular and asymmetric initial tumour geometries is demonstrated. When the nutrient diffusion equation is defined only in the tumour region, the model depicts growth in free suspension. On the contrary, when the nutrient diffusion equation is defined in a larger fixed domain, the model depicts tumour growth in a polymeric gel. Numerical simulations for both cases are presented and the results are consistent with theoretical and heuristic expectations such as early linear growth rate and preservation of radial symmetry when the boundary conditions are symmetric.

The main purpose of Chapter 6 is to derive a strong bounded variation estimate for finite volume solutions of nonlinear hyperbolic conservation laws of the form $\partial_t \alpha + \mathbf{F}(t, \mathbf{x}, \alpha) = 0$ and $\alpha(0, \cdot) = \alpha_0$ in Ω on nonuniform Cartesian grids in \mathbb{R}^d , $d \geq 2$. This result is crucial in proving the existence of a weak solution for tumour growth models in higher dimensions. In this chapter, the classical assumption that $\operatorname{div}_{\mathbf{x}} \mathbf{F} = 0$ is relaxed to $\operatorname{div}_{\mathbf{x}} \mathbf{F} \in BV(\Omega)$. The strong BV estimate on finite volume schemes for nonlinear scalar conservation

laws in 3D over nonuniform Cartesian grids is also described. A two dimensional tumour growth model first proposed by S. J. Frank et al. [29] is studied as a prototype. A hyperbolic conservation law, viscous stokes system, and Poisson equation that respectively governs the cell volume fraction, cell velocity–pressure system, and nutrient concentration constitute the model. The existence of weak solution to this model is proved by employing the strong bounded variation estimate on the cell volume fraction (concentration).

Chapter 7 deals with the mathematical modelling of tumour growth in an external polymeric medium referred to as *hydrogel*. The hydrogel is modelled as a nonlinear elastic material. The tumour is modelled using the framework described in Section 1.5. A Cartesian geometry is considered to simplify the modelling and subsequent numerical simulations. The model variables are cell volume fraction, cell velocity, nutrient concentration, and tumour radius. These variables are respectively governed by a hyperbolic conservation law, a generalised Stokes equation, a parabolic diffusion equation, and an ordinary differential equation. The tumour and hydrogel are coupled through a Neumann boundary condition, which asserts the continuity of stress at the tumour–hydrogel interface. The numerical scheme employed is a combination of upwind finite volume and finite element schemes. The qualitative behaviour of tumour growth depends on the hydrogel compressibility. In the case of highly compressible hydrogel, the tumour grows to a size that admits a travelling wave profile. In this case, the tumour will develop a well differentiated central necrotic core. For a moderately compressible hydrogel, the tumour fails to grow to an adequate size that allows a travelling wave profile and exhibits initial transient behaviour. A nearly incompressible hydrogel compresses the tumour, which leads to its eventual elimination.

8.2 Future Work

The models, numerical schemes, and theoretical results in this thesis present the following further research problems. In general, the results in this thesis can be adapted to the study of vascular tumour growth, wound healing closure study, and multiphase mixture models.

- **Existence of a threshold solution in 2D and 3D:** The existence of a threshold solution in 2D and 3D suffers many critical challenges. An initial step would be to derive an appropriate compactness result for the discrete time–space domains $\cup_{0 \leq n \leq N} ((t_n, t_{n+1}) \times \Omega_h^n)$ (see Definition 5.15). A more demanding task is to derive a strong bounded variation estimate for the finite volume solution of the cell volume fraction equation. This in turn requires uniformly bounded supremum norm estimates on cell velocity and its gradient. The current Sobolev embedding results do not guarantee any such estimates. Completion of the aforementioned tasks and establishing the existence of a threshold solution would be a significant step in the state of the art of mathematical analysis associated with tumour growth models and probably a number of other nonlinear systems of PDEs with moving boundaries.
- **Stress mediated growth in 2D and 3D:** The stress dependent growth of a tumour in a hydrogel medium, see Chapter 7, is the simplified version in a 1D Cartesian system

of a 3D phenomenon. A model has been derived in 2D and 3D. The computations and analysis are more difficult in the higher dimensional setting. The explicit tracking of the tumour–hydrogel boundary is necessary to compute the stress in the hydrogel in 2D and 3D. This leads to either re-meshing of time–dependent domains at each time step or re-mapping of triangles from a reference domain to the time–dependent domains. The first method is computationally intense and in the second method the shape–regularity of the reference triangulation will be maintained only for a small time. Both of these are not ideal for the long time scales associated with a tumour growth problem. The construction of a proper numerical scheme using finite volume and finite element methods is also not straight forward on time-dependent meshes. In Chapter 7, the most convenient result was the exact solution for the deformation map, which simplified the computations to a great extent. In the 2D and 3D systems a nonlinear finite element solver is required to account for the nonlinear elasticity. To the best of our knowledge, satisfactory computational results and numerical analysis on the aforementioned problems are not available in the literature.

- **Four phase model for stress dependent growth:** The model presented in Chapter 7 does not consider the fluid dynamic effects in the hydrogel. Experimentally, it is observed that the hydrogel can absorb and retain a large amount of water. As a result, there is a continuous exchange of the fluid medium between the hydrogel and tumour depending upon the pressure gradient. It is also observed that a tumour releases protein digesting enzymes that can disintegrate the molecular framework of the hydrogel near the tumour–hydrogel interface. Consequently, the compressibility of hydrogel needs to be treated as a nonuniform function of space. An explicit model describing these phenomena is not derived yet.

Appendix A

A.1 Monotone upwind scheme for conservation laws

Monotone upwind scheme for conservation laws (MUSCL) provides more accurate solutions to scalar conservation laws compared to upwind schemes. Given a source function f consider a prototype conservation law in one spatial and temporal dimension that seeks α such that for every $(t, x) \in (0, T) \times (a, b)$

$$\begin{aligned}\partial_t \alpha + \partial_x(u\alpha) &= f(t, x) \text{ and} \\ \alpha(0, x) &= \alpha_0(x),\end{aligned}\tag{9.1}$$

where $u : (0, T) \times (a, b) \rightarrow \mathbb{R}$ is the advection velocity. The interval (a, b) is uniformly discretised into $a = x_0 < x_1 < \dots < x_I = b$ and $(0, T)$ into $0 = t_0 < t_1 < \dots < t_N = T$. Define $h := x_{i+1} - x_i$ and $\delta := t_{n+1} - t_n$. Integrate (9.1) over the control volume $(t_n, t_{n+1}) \times (x_i, x_{i+1})$ to arrive at

$$\begin{aligned}\int_{x_i}^{x_{i+1}} \alpha(t_{n+1}, x) dx - \int_{x_i}^{x_{i+1}} \alpha(t_n, x) dx + \int_{t_n}^{t_{n+1}} (v(t, x_{i+1})\alpha(t, x_{i+1}) - v(t, x_i)\alpha(t, x_i)) dt \\ = \int_{t_n}^{t_{n+1}} \int_{x_i}^{x_{i+1}} f(t, x) dx dt.\end{aligned}\tag{9.2}$$

In (9.2) approximate $\int_{x_i}^{x_{i+1}} \alpha(t_n, x) dx$ by $h\alpha_i^n$, $\int_{t_n}^{t_{n+1}} v(t, x_i)\alpha(t, x_i) dt$ by $\delta v(t_n, x_i)\alpha(t_n, x_i)$, and $\int_{t_n}^{t_{n+1}} \int_{x_i}^{x_{i+1}} f(t, x) dx dt$ by $h\delta f(t_n, x_i)$ to obtain

$$h(\alpha_i^{n+1} - \alpha_i^n) + \delta(v(t_n, x_{i+1})\alpha(t_n, x_{i+1}) - v(t_n, x_i)\alpha(t_n, x_i)) = h\delta f(t_n, x_i).$$

In upwind method, the boundary flux term $v(t_n, x_i)\alpha(t_n, x_i)$ is approximated as

$$v(t_n, x_i)\alpha(t_n, x_i) \approx v(t_n, x_i)^+ \alpha_{i-1}^n - v(t_n, x_i)^- \alpha_i^n,$$

where $v(t_n, x_i)^+$ and $v(t_n, x_i)^-$ are positive and negative parts of $v(t_n, x_i)$. In this approximation, it is assumed that the finite volume solution $\alpha_{h,\delta}$ is piecewise constant with $\alpha_{h,\delta|(t_n, t_{n+1}) \times (x_i, x_{i+1})} = \alpha_i^n$. The resulting finite volume scheme (upwind) has linear order

of convergence. This can be improved by relaxing and replacing the piecewise constant approximation by a piecewise linear approximation. The piecewise linear approximation on (x_i, x_{i+1}) is constructed as, for every $(t, x) \in [t_n, t_{n+1}) \times (x_i, x_{i+1})$

$$\widetilde{\alpha}_{h,\delta}(t_n, x) := p_i^n \left(x - \frac{x_i + x_{i+1}}{2} \right) + \alpha_i^n, \quad (9.3)$$

where p_i^n is the slope to be determined so that scheme remains stable. Then, the boundary flux term is approximated with upwinding as

$$v(t_n, x_i) \alpha(t_n, x_i) \approx v(t_n, x_i)^+ \left(p_{i-1}^n (h/2) + \alpha_{i-1}^n \right) - v(t_n, x_i)^- \left(-p_i^n (h/2) + \alpha_i^n \right).$$

The slope p_i^n is defined by

$$p_i^n := \text{minmod} \left(\frac{\alpha_{i+1}^n - \alpha_i^n}{h}, \frac{\alpha_i^n - \alpha_{i-1}^n}{h} \right), \quad (9.4)$$

where, for every $a, b \in \mathbb{R}$

$$\text{minmod}(a, b) := \begin{cases} \text{sgn}(a) \min(|a|, |b|) & \text{if } ab \geq 0, \\ 0 & \text{otherwise.} \end{cases}$$

The slope can be defined in different ways as well. Definition (9.4) is employed as it ensures discrete stability with minimal numerical diffusion. The final scheme is as follows: find $\{\alpha_i^n : 1 \leq i \leq I, 0 < n \leq N\}$ such that

$$\begin{aligned} \text{scheme:} \quad & \alpha_i^{n+1} = \alpha_i^n - \frac{h}{\delta} (f_{i+1}^n - f_i^n) + \delta f(t_n, x_i), \\ \text{flux:} \quad & f_i^n := v(t_n, x_i)^+ \left(p_{i-1}^n (h/2) + \alpha_{i-1}^n \right) - v(t_n, x_i)^- \left(-p_i^n (h/2) + \alpha_i^n \right), \text{ and} \\ \text{slope:} \quad & p_i^n = \text{minmod} \left(\frac{\alpha_{i+1}^n - \alpha_i^n}{h}, \frac{\alpha_i^n - \alpha_{i-1}^n}{h} \right). \end{aligned}$$

The initial condition is discretised as $\alpha_i^0 = \frac{1}{h} \int_{x_i}^{x_{i+1}} \alpha_0(x) dx$. The piecewise linear solution $\widetilde{\alpha}_{h,\delta} : (0, T) \times (a, b) \rightarrow \mathbb{R}$ is reconstructed from the discrete data $\{\alpha_i^n : 1 \leq i \leq I, 0 < n \leq N\}$ using (9.3).

A.2 BV estimate for 3D conservation laws

The terms $F_{i-1/2,j,m}^\vartheta$ in (6.47b), where $\vartheta \in \{x, y, z\}$ can be written as, for $s \in \{-1, 1\}$

$$\begin{aligned} F_{i+s/2,j,m}^x = M_{i+s/2,j,m}^x & \left[\frac{(1-s)}{2} \left(\alpha_{i-1,j,m}^n - \alpha_{i,j,m}^n \right) + \frac{(1+s)}{2} \left(\alpha_{i,j,m}^n - \alpha_{i+1,j,m}^n \right) \right] \\ & + u_{i+s/2,j,m}^n f(\alpha_{i,j,m}^n), \end{aligned} \quad (9.5)$$

$$\begin{aligned} F_{i,j+s/2,m}^y &= M_{i,j+s/2,m}^y \left[\frac{(1-s)}{2} (\alpha_{i,j-1,m}^n - \alpha_{i,j,m}^n) + \frac{(1+s)}{2} (\alpha_{i,j,m}^n - \alpha_{i,j+1,m}^n) \right] \\ &\quad + v_{i,j+s/2,m}^n f(\alpha_{i,j,m}^n), \end{aligned} \quad (9.6)$$

$$\begin{aligned} F_{i,j,m+s/2}^z &= M_{i,j,m+s/2}^z \left[\frac{(1-s)}{2} (\alpha_{i,j,m-1}^n - \alpha_{i,j,m}^n) + \frac{(1+s)}{2} (\alpha_{i,j,m}^n - \alpha_{i,j,m+1}^n) \right] \\ &\quad + w_{i,j,m+s/2}^n f(\alpha_{i,j,m}^n), \end{aligned} \quad (9.7)$$

where

$$\begin{aligned} M_{i-1/2,j,m}^x &:= \left[u_{i-1/2,j,m}^{n+} D_{i,j,m}(\alpha_{i-1,j,m}^n, \alpha_{i,j,m}^n) + u_{i-1/2,j,m}^{n-} D_{i,j,m}(\alpha_{i,j,m}^n, \alpha_{i-1,j,m}^n) \right], \\ M_{i,j-1/2,m}^y &:= \left[v_{i,j-1/2,m}^{n+} D_{i,j,m}(\alpha_{i,j-1,m}^n, \alpha_{i,j,m}^n) + v_{i,j-1/2,m}^{n-} D_{i,j,m}(\alpha_{i,j,m}^n, \alpha_{i,j-1,m}^n) \right], \\ M_{i,j,m-1/2}^z &:= \left[w_{i,j,m-1/2}^{n+} D_{i,j,m}(\alpha_{i,j,m-1}^n, \alpha_{i,j,m}^n) + w_{i,j,m-1/2}^{n-} D_{i,j,m}(\alpha_{i,j,m}^n, \alpha_{i,j,m-1}^n) \right], \end{aligned}$$

and the difference quotient $D_{i,j} : \mathbb{R}^2 \rightarrow \mathbb{R}$ is defined by

$$D_{i,j,m}(a, b) = \begin{cases} \frac{g(a, b) - f(\alpha_{i,j,m}^n)}{a - b} & \text{if } a \neq b, \text{ and} \\ 0 & \text{if } a = b. \end{cases}$$

Observe that $D_{i,j,m}(\gamma_1, \gamma_2)$ and $D_{i,j,m}(\gamma_2, \gamma_1)$, where

$$(\gamma_1, \gamma_2) \in \{(\alpha_{i-1,j,m}^n, \alpha_{i,j,m}^n), (\alpha_{i,j-1,m}^n, \alpha_{i,j,m}^n), (\alpha_{i,j,m-1}^n, \alpha_{i,j,m}^n)\},$$

and hence $M_{i-1/2,j,m}^x, M_{i,j-1/2,m}^y, M_{i,j,m-1/2}^z$, are nonnegative due to the monotonicity of g and $g(\alpha_{i,j,m}^n, \alpha_{i,j,m}^n) = f(\alpha_{i,j,m}^n)$. Use (9.5)–(9.7) to transform the right side of (6.47a) into a convex linear combination of the terms $\alpha_{p,q,r}^n$, where $(p, q, r) \in \{(i, j, m), (i-1, j, m), (i+1, j, m), (i, j-1, m), (i, j+1, m), (i, j, m-1), (i, j, m+1)\}$ described by

$$\begin{aligned} \alpha_{i,j,m}^{n+1} &= \alpha_{i,j,m}^n (1 - \mu_i M_{i+1/2,j,m}^x - \lambda_j M_{i,j+1/2,m}^y - \nu_m M_{i,j,m+1/2}^z - \mu_i M_{i-1/2,j,m}^x \\ &\quad - \lambda_j M_{i,j-1/2,m}^y - \nu_m M_{i,j,m-1/2}^z) \\ &\quad + \mu_i \alpha_{i+1,j,m}^n M_{i+1/2,j,m}^x + \lambda_j \alpha_{i,j+1,m}^n M_{i,j+1/2,m}^y + \nu_m \alpha_{i,j,m+1}^n M_{i,j,m+1/2}^z \\ &\quad + \mu_i \alpha_{i-1,j,m}^n M_{i-1/2,j,m}^x + \lambda_j \alpha_{i,j-1,m}^n M_{i,j-1/2,m}^y + \nu_m \alpha_{i,j,m-1}^n M_{i,j,m-1/2}^z \\ &\quad - f(\alpha_{i,j,m}^n) \left(\int_{t_n}^{t_{n+1}} \int_{K_{i,j,m}} \operatorname{div}(\mathbf{u})(t, \mathbf{x}) dt d\mathbf{x} \right). \end{aligned} \quad (9.8)$$

A crucial estimate that is used many times in this section is obtained from the Lipschitz continuity of the function g , which is $|M_{i-1/2,j,m}^x| \leq \operatorname{Lip}(g)|u_{i-1/2,j,m}^n|$, $|M_{i,j-1/2,m}^y| \leq \operatorname{Lip}(g)|v_{i,j-1/2,m}^n|$, and $|M_{i,j,m-1/2}^z| \leq \operatorname{Lip}(g)|w_{i,j,m-1/2}^n|$ for $i = 0, \dots, I$, $j = 0, \dots, J$, and $m = 0, \dots, L$.

Proposition 9.1 (boundedness). *The function $\alpha_{h,\delta}$ satisfies, for every $0 \leq t \leq T$,*

$$\left| \alpha_{h,\delta}(t, \cdot) \right|_{L^\infty(\Omega)} \leq B_{f,\mathbf{u}} \left(a^0 + f_0 \|\operatorname{div}(\mathbf{u})\|_{L_t^1 L^\infty(\Omega_T)} \right),$$

where $B_{f,\mathbf{u}} := \exp \left(\operatorname{Lip}(f) \|\operatorname{div}(\mathbf{u})\|_{L_t^1 L^\infty(\Omega_T)} \right)$, $a^0 = \|\alpha_0\|_{L^\infty(\Omega)}$, and $f_0 = f(0)$.

The proof of Proposition 9.1 is based on writing $\alpha_{i,j,m}^{n+1}$ as convex linear combination of values of $\alpha_{h,\delta}$ at the previous time step as in (9.8). The steps are similar to the proof of Proposition 6.6 and hence the details are skipped.

Proposition 9.2 (spatial variation). *The function $\alpha_{h,\delta}$ satisfies, for every $0 \leq t \leq T$,*

$$\left| \alpha_{h,\delta}(t, \cdot) \right|_{BV_{x,y,z}} \leq B_{\mathbf{u}} \left(|\alpha_0|_{BV_{x,y,z}} + \mathcal{C} \|\operatorname{div}(\mathbf{u})\|_{L_t^1 BV_{x,y,z}} \right), \quad (9.9)$$

where $B_{\mathbf{u}} := \exp \left(\mathcal{C} \|\nabla \mathbf{u}\|_{L_t^1 L^\infty(\widehat{\Omega}_T)} \right)$ and \mathcal{C} has the same dependencies as in Theorem 6.48.

Proof. Step 1: Consider the difference between the scheme (6.47a) written for $\alpha_{i,j,m}^{n+1}$ and $\alpha_{i-1,j,m}^{n+1}$

$$\begin{aligned} \alpha_{i,j,m}^{n+1} - \alpha_{i-1,j,m}^{n+1} &= \alpha_{i,j,m}^n - \alpha_{i-1,j,m}^n \\ &\quad - \left[\mu_i (\mathbb{F}_{i+1/2,j,m}^x - \mathbb{F}_{i-1/2,j,m}^x) - \mu_{i-1} (\mathbb{F}_{i-1/2,j,m}^x - \mathbb{F}_{i-3/2,j,m}^x) \right] \\ &\quad - \left[\lambda_j (\mathbb{F}_{i,j+1/2,m}^y - \mathbb{F}_{i,j-1/2,m}^y) - \lambda_j (\mathbb{F}_{i-1,j+1/2,m}^y - \mathbb{F}_{i-1,j-1/2,m}^y) \right] \\ &\quad - \left[\nu_m (\mathbb{F}_{i,j,m+1/2}^z - \mathbb{F}_{i,j,m-1/2}^z) - \nu_m (\mathbb{F}_{i-1,j,m+1/2}^z - \mathbb{F}_{i-1,j,m-1/2}^z) \right] \\ &=: \alpha_{i,j,m}^n - \alpha_{i-1,j,m}^n - H_{i,j,m}^x - H_{i,j,m}^y - H_{i,j,m}^z. \end{aligned} \quad (9.10)$$

Use (9.5) to write

$$\begin{aligned} H_{i,j,m}^x &= \mu_i M_{i-1/2,j,m}^x \left(\alpha_{i,j,m}^n - \alpha_{i-1,j,m}^n \right) + \mu_i M_{i+1/2,j,m}^x \left(\alpha_{i,j,m}^n - \alpha_{i+1,j,m}^n \right) \\ &\quad + \mu_{i-1} M_{i-1/2,j,m}^x \left(\alpha_{i,j,m}^n - \alpha_{i-1,j,m}^n \right) + \mu_{i-1} M_{i-3/2,j,m}^x \left(\alpha_{i-2,j,m}^n - \alpha_{i-1,j,m}^n \right) + K_{i,j,m}^f, \end{aligned}$$

where

$$K_{i,j,m}^f := f(\alpha_{i,j,m}^n) \int_{t_n}^{t_{n+1}} \int_{K_{i,j,m}} \partial_x u(t, \mathbf{x}) \, d\mathbf{x} \, dt - f(\alpha_{i-1,j,m}^n) \int_{t_n}^{t_{n+1}} \int_{K_{i-1,j,m}} \partial_x u(t, \mathbf{x}) \, d\mathbf{x} \, dt.$$

Step 2: Consider the term $H_{i,j,m}^y$. Transform the differences along y - direction into x - direction as in **Step 2** of Proposition 6.7, and use the definition of E_{\pm} to write

$$\begin{aligned} H_{i,j,m}^y &= \lambda_j v_{i-1,j+1/2,m}^{n+} E_+ \left(\alpha_{i,j,m}^n, \alpha_{i-1,j,m}^n, \alpha_{i,j+1,m}^n \right) \left(\alpha_{i,j,m}^n - \alpha_{i-1,j,m}^n \right) \\ &\quad - \lambda_j v_{i-1,j-1/2,m}^{n+} E_+ \left(\alpha_{i,j-1,m}^n, \alpha_{i-1,j-1,m}^n, \alpha_{i,j,m}^n \right) \left(\alpha_{i,j-1,m}^n - \alpha_{i-1,j-1,m}^n \right) \end{aligned}$$

$$\begin{aligned}
& + \lambda_j v_{i-1,j+1/2,m}^{n+} \mathbf{E}_-(\alpha_{i,j+1,m}^n, \alpha_{i-1,j+1,m}^n, \alpha_{i-1,j,m}^n) (\alpha_{i,j+1,m}^n - \alpha_{i-1,j+1,m}^n) \\
& \quad - \lambda_j v_{i-1,j-1/2}^{n*} \mathbf{E}_-(\alpha_{i,j,m}^n, \alpha_{i-1,j,m}^n, \alpha_{i-1,j-1,m}^n) (\alpha_{i,j,m}^n - \alpha_{i-1,j,m}^n) \\
& - \lambda_j v_{i-1,j+1/2,m}^{n-} \mathbf{E}_-(\alpha_{i,j,m}^n, \alpha_{i-1,j,m}^n, \alpha_{i,j+1,m}^n) (\alpha_{i,j,m}^n - \alpha_{i-1,j,m}^n) \\
& \quad + \lambda_j v_{i-1,j-1/2,m}^{n-} \mathbf{E}_-(\alpha_{i,j-1,m}^n, \alpha_{i-1,j-1,m}^n, \alpha_{i,j,m}^n) (\alpha_{i,j-1,m}^n - \alpha_{i-1,j-1,m}^n) \\
& - \lambda_j v_{i-1,j+1/2,m}^{n-} \mathbf{E}_+(\alpha_{i,j+1,m}^n, \alpha_{i-1,j+1,m}^n, \alpha_{i-1,j,m}^n) (\alpha_{i,j+1,m}^n - \alpha_{i-1,j+1,m}^n) \\
& \quad + \lambda_j v_{i-1,j-1/2,m}^{n-} \mathbf{E}_+(\alpha_{i,j,m}^n, \alpha_{i-1,j,m}^n, \alpha_{i-1,j-1,m}^n) (\alpha_{i,j,m}^n - \alpha_{i-1,j,m}^n) \\
& + \lambda_j (v_{i,j+1/2,m}^{n-} - v_{i-1,j+1/2,m}^{n-}) (g_{i,j+1/2,m}^+ - g_{i,j+1/2,m}^-) \\
& \quad - \lambda_j (v_{i,j-1/2,m}^{n-} - v_{i-1,j-1/2,m}^{n-}) (g_{i,j-1/2,m}^+ - g_{i,j-1/2,m}^-) + \mathbf{K}_{i,j,m}^{g,y}, \quad (9.11)
\end{aligned}$$

where

$$\begin{aligned}
\mathbf{K}_{i,j,m}^{g,y} & := \frac{g_{i,j+1/2,m}^+}{h_j} \int_{t_n}^{t_{n+1}} \int_{z_{m-1/2}}^{z_{m+1/2}} \left(\int_{x_{i-1/2}}^{x_{i+1/2}} v(t, s, y_{j+1/2}, r) ds - \int_{x_{i-3/2}}^{x_{i-1/2}} v(t, s, y_{j+1/2}, r) ds \right) dr dt \\
& - \frac{g_{i,j-1/2,m}^+}{h_j} \int_{t_n}^{t_{n+1}} \int_{z_{m-1/2}}^{z_{m+1/2}} \left(\int_{x_{i-1/2}}^{x_{i+1/2}} v(t, s, y_{j-1/2}, r) ds - \int_{x_{i-3/2}}^{x_{i-1/2}} v(t, s, y_{j-1/2}, r) ds \right) dr dt.
\end{aligned}$$

By applying the same operations used to write (9.11), we can transform $\mathbf{H}_{i,j,m}^z$. To obtain the resultant expression for $\mathbf{H}_{i,j,m}^z$ apply the swap operations in (9.12) to the terms in the right hand side of (9.11): with $* \in \{+, -\}$

$$\text{in } \mathbf{H}_{i,j,m}^y \left\{ \begin{array}{ll} \alpha_{i+p,j+q,m+r}^n & \leftrightarrow \alpha_{i+p,j+r,m+q}^n \\ v_{i+p,j+r,m+q}^{n*} & \leftrightarrow w_{i+p,j+q,m+r}^{n*} \\ g_{i+p,j+r,m+q}^* & \leftrightarrow g_{i+p,j+q,m+r}^* \\ \int_{z_{m-1/2}}^{z_{m+1/2}} v(t, s, y_{j+q}, r) dr & \leftrightarrow \int_{y_{j-1/2}}^{y_{j+1/2}} w(t, s, r, z_{m+q}) dr \\ \mathbf{K}_{i,j,m}^{g,y} & \leftrightarrow \mathbf{K}_{i,j,m}^{g,z} \end{array} \right\} \text{in } \mathbf{H}_{i,j,m}^z \quad (9.12)$$

Step 3: Combine (9.10)–(9.11) to write

$$\begin{aligned}
\alpha_{i,j,m}^{n+1} - \alpha_{i-1,j,m}^{n+1} & = (\alpha_{i,j,m}^n - \alpha_{i-1,j,m}^n) (1 - c_{i,j,m}) \\
& - \mu_i \mathbf{M}_{i+1/2,j,m}^x (\alpha_{i,j,m}^n - \alpha_{i+1,j,m}^n) - \mu_{i-1} \mathbf{M}_{i-3/2,j,m}^x (\alpha_{i-2,j,m}^n - \alpha_{i-1,j,m}^n) \\
& + \lambda_j v_{i-1,j-1/2,m}^{n+} \mathbf{E}_+(\alpha_{i,j-1,m}^n, \alpha_{i-1,j-1,m}^n, \alpha_{i,j,m}^n) (\alpha_{i,j-1,m}^n - \alpha_{i-1,j-1,m}^n) \\
& - \lambda_j v_{i-1,j+1/2,m}^{n+} \mathbf{E}_-(\alpha_{i,j+1,m}^n, \alpha_{i-1,j+1,m}^n, \alpha_{i-1,j,m}^n) (\alpha_{i,j+1,m}^n - \alpha_{i-1,j+1,m}^n) \\
& - \lambda_j v_{i-1,j-1/2,m}^{n-} \mathbf{E}_-(\alpha_{i,j-1,m}^n, \alpha_{i-1,j-1,m}^n, \alpha_{i,j}^n) (\alpha_{i,j-1,m}^n - \alpha_{i-1,j-1,m}^n) \\
& + \lambda_j v_{i-1,j+1/2,m}^{n-} \mathbf{E}_+(\alpha_{i,j+1,m}^n, \alpha_{i-1,j+1,m}^n, \alpha_{i-1,j,m}^n) (\alpha_{i,j+1,m}^n - \alpha_{i-1,j+1,m}^n)
\end{aligned}$$

$$\begin{aligned}
& + \nu_m v_{i-1,j,m-1/2}^{n+} \mathbf{E}_+ (\alpha_{i,j,m-1}^n, \alpha_{i-1,j,m-1}^n, \alpha_{i,j,m}^n) (\alpha_{i,j,m-1}^n - \alpha_{i-1,j,m-1}^n) \\
& - \nu_m v_{i-1,j,m+1/2}^{n+} \mathbf{E}_- (\alpha_{i,j,m+1}^n, \alpha_{i-1,j,m+1}^n, \alpha_{i-1,j,m}^n) (\alpha_{i,j,m+1}^n - \alpha_{i-1,j,m+1}^n) \\
& - \nu_m v_{i-1,j,m-1/2}^{n-} \mathbf{E}_- (\alpha_{i,j,m-1}^n, \alpha_{i-1,j,m-1}^n, \alpha_{i,j,m}^n) (\alpha_{i,j,m-1}^n - \alpha_{i-1,j,m-1}^n) \\
& + \nu_m v_{i-1,j,m+1/2}^{n-} \mathbf{E}_+ (\alpha_{i,j,m+1}^n, \alpha_{i-1,j,m+1}^n, \alpha_{i-1,j,m}^n) (\alpha_{i,j,m+1}^n - \alpha_{i-1,j,m+1}^n) \\
& \quad - \lambda_j (v_{i,j+1/2,m}^{n-} - v_{i-1,j+1/2,m}^{n-}) (g_{i,j+1/2,m}^+ - g_{i,j+1/2,m}^-) \\
& \quad + \lambda_j (v_{i,j-1/2,m}^{n-} - v_{i-1,j-1/2,m}^{n-}) (g_{i,j-1/2,m}^+ - g_{i,j-1/2,m}^-) \\
& \quad - \nu_m (v_{i,j,m+1/2}^{n-} - v_{i-1,j,m+1/2}^{n-}) (g_{i,j,m+1/2}^+ - g_{i,j,m+1/2}^-) \\
& + \nu_m (v_{i,j,m-1/2}^{n-} - v_{i-1,j,m-1/2}^{n-}) (g_{i,j,m-1/2}^+ - g_{i,j,m-1/2}^-) - (\mathbf{K}_{i,j,m}^f + \mathbf{K}_{i,j,m}^{g,y} + \mathbf{K}_{i,j,m}^{g,z}), \tag{9.13}
\end{aligned}$$

where

$$\begin{aligned}
c_{i,j,m} & := \mu_i M_{i-1/2,j,m}^x + \mu_{i-1} M_{i-1/2,j,m}^x + \lambda_j v_{i-1,j+1/2,m}^{n+} \mathbf{E}_+ (\alpha_{i,j,m}^n, \alpha_{i-1,j,m}^n, \alpha_{i,j+1,m}^n) \\
& - \lambda_j v_{i-1,j-1/2,m}^{n+} \mathbf{E}_- (\alpha_{i,j,m}^n, \alpha_{i-1,j,m}^n, \alpha_{i-1,j-1,m}^n) - \lambda_j v_{i-1,j+1/2,m}^{n-} \mathbf{E}_- (\alpha_{i,j,m}^n, \alpha_{i-1,j,m}^n, \alpha_{i,j+1,m}^n) \\
& + \lambda_j v_{i-1,j-1/2,m}^{n-} \mathbf{E}_+ (\alpha_{i,j,m}^n, \alpha_{i-1,j,m}^n, \alpha_{i-1,j-1,m}^n) + \nu_m v_{i-1,j,m+1/2}^{n+} \mathbf{E}_+ (\alpha_{i,j,m}^n, \alpha_{i-1,j,m}^n, \alpha_{i,j,m+1}^n) \\
& - \nu_m v_{i-1,j,m-1/2}^{n+} \mathbf{E}_- (\alpha_{i,j,m}^n, \alpha_{i-1,j,m}^n, \alpha_{i-1,j,m-1}^n) - \nu_m v_{i-1,j,m+1/2}^{n-} \mathbf{E}_- (\alpha_{i,j,m}^n, \alpha_{i-1,j,m}^n, \alpha_{i,j,m+1}^n) \\
& \quad + \nu_m v_{i-1,j,m-1/2}^{n-} \mathbf{E}_+ (\alpha_{i,j,m}^n, \alpha_{i-1,j,m}^n, \alpha_{i-1,j,m-1}^n).
\end{aligned}$$

The CFL condition (6.48a) implies that $1 - c_{i,j,m}$ is nonnegative. Take absolute value on both sides of (9.13), multiply by $h_j l_m$, sum over $i = 1, \dots, I$, $j = 0, \dots, J$, and $m = 0, \dots, L$, use the condition that $\mathbf{u} = 0$ on $\partial\tilde{\Omega}$, and follow the same indicial transformations employed to arrive at (6.22) in **Step 3** of the proof of Proposition 6.7 to obtain

$$\begin{aligned}
& \sum_{m=0}^L l_m \sum_{j=0}^J h_j \sum_{i=1}^I |\alpha_{i,j,m}^{n+1} - \alpha_{i-1,j,m}^{n+1}| \leq \sum_{m=0}^L l_m \sum_{j=0}^J h_j \sum_{i=1}^I |\alpha_{i,j,m}^n - \alpha_{i-1,j,m}^n| \\
& + \sum_{m=0}^L l_m \sum_{j=0}^{J-1} h_j \sum_{i=1}^I \lambda_j |v_{i,j+1/2,m}^{n-} - v_{i-1,j+1/2,m}^{n-}| |g(\alpha_{i,j,m}^n, \alpha_{i,j+1,m}^n) - g(\alpha_{i,j+1,m}^n, \alpha_{i,j,m}^n)| \\
& + \sum_{m=0}^L l_m \sum_{j=1}^J h_j \sum_{i=1}^I \lambda_j |v_{i,j-1/2,m}^{n-} - v_{i-1,j-1/2,m}^{n-}| |g(\alpha_{i,j-1,m}^n, \alpha_{i,j,m}^n) - g(\alpha_{i,j,m}^n, \alpha_{i,j-1,m}^n)| \\
& + \sum_{m=0}^{L-1} l_m \sum_{j=0}^J h_j \sum_{i=1}^I \nu_m |w_{i,j,m+1/2}^{n-} - w_{i-1,j,m+1/2}^{n-}| |g(\alpha_{i,j,m}^n, \alpha_{i,j,m+1}^n) - g(\alpha_{i,j,m+1}^n, \alpha_{i,j,m}^n)| \\
& + \sum_{m=1}^L l_m \sum_{j=0}^J h_j \sum_{i=1}^I \nu_m |w_{i,j,m-1/2}^{n-} - w_{i-1,j,m-1/2}^{n-}| |g(\alpha_{i,j,m-1}^n, \alpha_{i,j,m}^n) - g(\alpha_{i,j,m}^n, \alpha_{i,j,m-1}^n)|
\end{aligned}$$

$$+ \delta \sum_{m=1}^L l_m \sum_{j=1}^J h_j \sum_{i=1}^I \left(|K_{i,j,m}^f + K_{i,j,m}^{g,y} + K_{i,j,m}^{g,z}| \right). \quad (9.14)$$

The Lipschitz continuity of $x \rightarrow x^-$ and g , Lipschitz continuity of v and w in the x -direction, and grid regularity condition in Definition 6.14 imply

$$\begin{aligned} & \lambda_j \left| v_{i,j-1/2,m}^{n-} - v_{i-1,j-1/2,m}^{n-} \right| \left| g(\alpha_{i,j-1,m}^n, \alpha_{i,j,m}^n) - g(\alpha_{i,j,m}^n, \alpha_{i,j-1,m}^n) \right| \leq \\ & \quad \tilde{c} |\alpha_{i,j-1,m}^n - \alpha_{i,j,m}^n| \text{Lip}(g) \int_{t_n}^{t_{n+1}} \|\partial_x v(t, \cdot)\|_{L^\infty(\Omega)} dt \quad \text{and} \\ & \nu_m \left| w_{i,j,m+1/2}^{n-} - w_{i-1,j,m+1/2}^{n-} \right| \left| g(\alpha_{i,j,m}^n, \alpha_{i,j,m+1}^n) - g(\alpha_{i,j,m+1}^n, \alpha_{i,j,m}^n) \right| \leq \\ & \quad \tilde{c} |\alpha_{i,j,m-1}^n - \alpha_{i,j,m}^n| \text{Lip}(g) \int_{t_n}^{t_{n+1}} \|\partial_x w(t, \cdot)\|_{L^\infty(\Omega)} dt. \end{aligned}$$

Step 4: Write the term $K_{i,j,m}^f$ as

$$\begin{aligned} K_{i,j,m}^f &= \left(f(\alpha_{i,j,m}^n) \int_{t_n}^{t_{n+1}} \int_{K_{i,j,m}} \text{div}(\mathbf{u})(t, \cdot) d\mathbf{x} dt - f(\alpha_{i-1,j,m}^n) \int_{t_n}^{t_{n+1}} \int_{K_{i-1,j,m}} \text{div}(\mathbf{u})(t, \cdot) d\mathbf{x} dt \right) \\ & \quad - \left(f(\alpha_{i,j,m}^n) \int_{t_n}^{t_{n+1}} \int_{K_{i,j,m}} \partial_y v(t, \cdot) d\mathbf{x} dt - f(\alpha_{i-1,j,m}^n) \int_{t_n}^{t_{n+1}} \int_{K_{i-1,j,m}} \partial_y v(t, \cdot) d\mathbf{x} dt \right) \\ & \quad - \left(f(\alpha_{i,j,m}^n) \int_{t_n}^{t_{n+1}} \int_{K_{i,j,m}} \partial_z w(t, \cdot) d\mathbf{x} dt - f(\alpha_{i-1,j,m}^n) \int_{t_n}^{t_{n+1}} \int_{K_{i-1,j,m}} \partial_z w(t, \cdot) d\mathbf{x} dt \right) \\ & =: K_{i,j,m}^{f,1} + K_{i,j,m}^{f,2} + K_{i,j,m}^{f,3}. \end{aligned}$$

Use the grouping identity (1.1a) to split the terms $K_{i,j,m}^{g,y}$ and $K_{i,j,m}^{g,z}$ as follows:

$$\begin{aligned} K_{i,j,m}^{g,y} &= \frac{g_{i,j+1/2,m}^+ - g_{i,j-1/2,m}^+}{2h_j} \left[\int_{t_n}^{t_{n+1}} \int_{z_{m-1/2}}^{z_{m+1/2}} \left(\int_{x_{i-1/2}}^{x_{i+1/2}} v(t, s, y_{j+1/2}, r) ds \right. \right. \\ & \quad \left. \left. - \int_{x_{i-3/2}}^{x_{i-1/2}} v(t, s, y_{j+1/2}, r) ds \right) dr dt \right. \\ & \quad \left. + \int_{t_n}^{t_{n+1}} \int_{z_{m-1/2}}^{z_{m+1/2}} \left(\int_{x_{i-1/2}}^{x_{i+1/2}} v(t, s, y_{j-1/2}, r) ds - \int_{x_{i-3/2}}^{x_{i-1/2}} v(t, s, y_{j-1/2}, r) ds \right) dr dt \right] \\ & \quad + \frac{g_{i,j+1/2,m}^+ + g_{i,j-1/2,m}^+}{2} \left[\int_{t_n}^{t_{n+1}} \int_{K_{i,j,m}} \partial_y v(t, \cdot) d\mathbf{x} dt - \int_{t_n}^{t_{n+1}} \int_{K_{i-1,j,m}} \partial_y v(t, \cdot) d\mathbf{x} dt \right] \end{aligned}$$

$$=: K_{i,j,m}^{g,y,1} + K_{i,j,m}^{g,y,2} \quad \text{and}$$

$$\begin{aligned} K_{i,j,m}^{g,z} &= \frac{g_{i,j,m+1/2}^+ - g_{i,j,m-1/2}^+}{2\nu_m} \left[\int_{t_n}^{t_{n+1}} \int_{y_{j-1/2}}^{y_{j+1/2}} \left(\int_{x_{i-1/2}}^{x_{i+1/2}} w(t,s,r,z_{m+1/2}) ds \right. \right. \\ &\quad \left. \left. - \int_{x_{i-3/2}}^{x_{i-1/2}} w(t,s,r,z_{m+1/2}) ds \right) dr dt \right. \\ &\quad \left. + \int_{t_n}^{t_{n+1}} \int_{y_{j-1/2}}^{y_{j+1/2}} \left(\int_{x_{i-1/2}}^{x_{i+1/2}} w(t,s,r,z_{m-1/2}) ds - \int_{x_{i-3/2}}^{x_{i-1/2}} v(t,s,r,z_{m-1/2}) ds \right) dr dt \right] \\ &\quad + \frac{g_{i,j,m+1/2}^+ + g_{i,j,m-1/2}^+}{2} \left[\int_{t_n}^{t_{n+1}} \int_{K_{i,j,m}} \partial_z w(t,\cdot) d\mathbf{x} dt - \int_{t_n}^{t_{n+1}} \int_{K_{i-1,j,m}} \partial_z w(t,\cdot) d\mathbf{x} dt \right] \\ &=: K_{i,j,m}^{g,z,1} + K_{i,j,m}^{g,z,2}. \end{aligned}$$

Apply analogous arguments used to bound $K_{i,j}^{f,1}$ and $K_{i,j}^{g,1}$ (see (6.25) and (6.26)) to obtain

$$\begin{aligned} |K_{i,j,m}^{f,1}| &\leq \text{Lip}(f) |\alpha_{i,j,m}^n - \alpha_{i-1,j,m}^n| \int_{t_n}^{t_{n+1}} \|\text{div}(\mathbf{u})(t,\cdot)\|_{L^\infty(\Omega)} dt \\ &\quad + (\text{Lip}(f)\alpha_M + f_0) \int_{t_n}^{t_{n+1}} \left| \int_{K_{i,j,m}} \text{div}(\mathbf{u})(t,\cdot) d\mathbf{x} - \int_{K_{i-1,j,m}} \text{div}(\mathbf{u})(t,\cdot) d\mathbf{x} \right| dt. \\ |K_{i,j,m}^{g,y,1}| &\leq \tilde{c} \text{Lip}(g) \left(|\alpha_{i,j,m}^n - \alpha_{i,j-1,m}^n| + |\alpha_{i,j+1,m}^n - \alpha_{i,j,m}^n| \right) \int_{t_n}^{t_{n+1}} \|\partial_x v(t,\cdot)\|_{L^\infty(\Omega)} dt. \\ |K_{i,j,m}^{g,z,1}| &\leq \tilde{c} \text{Lip}(g) \left(|\alpha_{i,j,m}^n - \alpha_{i,j,m-1}^n| + |\alpha_{i,j,m+1}^n - \alpha_{i,j,m}^n| \right) \int_{t_n}^{t_{n+1}} \|\partial_x w(t,\cdot)\|_{L^\infty(\Omega)} dt. \end{aligned}$$

Use combined estimates on $K_{i,j,m}^{g,y,2} + K_{i,j,m}^{f,2}$ and $K_{i,j,m}^{g,z,2} + K_{i,j,m}^{f,3}$ and similar arguments used to bound $|K_{i,j}^{f,2} + K_{i,j}^{g,2}|$ (see (6.29)) to arrive at

$$\begin{aligned} |K_{i,j,m}^f + K_{i,j,m}^{g,y} + K_{i,j,m}^{g,z}| &\leq |K_{i,j,m}^{f,1}| + |K_{i,j,m}^{g,y,1}| + |K_{i,j,m}^{f,2} + K_{i,j,m}^{g,y,2}| + |K_{i,j,m}^{g,z,1}| + |K_{i,j,m}^{f,3} + K_{i,j,m}^{g,z,2}| \\ &\leq \text{Lip}(f) |\alpha_{i,j,m}^n - \alpha_{i-1,j,m}^n| \left(\int_{t_n}^{t_{n+1}} \|\text{div}(\mathbf{u})(t,\cdot)\|_{L^\infty(\Omega)} dt + 2 \int_{t_n}^{t_{n+1}} \|\partial_y v(t,\cdot)\|_{L^\infty(\Omega)} dt \right. \\ &\quad \left. + 2 \int_{t_n}^{t_{n+1}} \|\partial_z w(t,\cdot)\|_{L^\infty(\Omega)} dt \right) \\ &\quad + \text{Lip}(g) \left(|\alpha_{i,j}^n - \alpha_{i,j-1}^n| + |\alpha_{i,j+1}^n - \alpha_{i,j}^n| \right) \left(\tilde{c} \int_{t_n}^{t_{n+1}} \left(\|\partial_x v(t,\cdot)\|_{L^\infty(\Omega)} + 2\|\partial_y v(t,\cdot)\|_{L^\infty(\Omega)} \right) dt \right) \\ &\quad + \left[\text{Lip}(g) \left(|\alpha_{i,j,m}^n - \alpha_{i,j,m-1}^n| + |\alpha_{i,j,m+1}^n - \alpha_{i,j,m}^n| \right) \times \right. \end{aligned}$$

$$\begin{aligned} & \left(\tilde{c} \int_{t_n}^{t_{n+1}} \left(\|\partial_x w(t, \cdot)\|_{L^\infty(\Omega)} + 2\|\partial_z w(t, \cdot)\|_{L^\infty(\Omega)} \right) dt \right) \Big] \\ & + (\text{Lip}(f)\alpha_M + f_0) \int_{t_n}^{t_{n+1}} \left| \int_{K_{i,j,m}} \text{div}(\mathbf{u})(t, \cdot) d\mathbf{x} - \int_{K_{i-1,j,m}} \text{div}(\mathbf{u})(t, \cdot) d\mathbf{x} \right| dt. \end{aligned} \quad (9.15)$$

Step 5: Use (9.14)–(9.15) to obtain

$$\begin{aligned} |\alpha_{h,\delta}(t_{n+1}, \cdot)|_{L_z^1 L_y^1 BV_x} & \leq |\alpha_{h,\delta}(t_n, \cdot)|_{L_z^1 L_y^1 BV_x} \\ & + 4(\tilde{c} + 1) \text{Lip}(g) |\alpha_{h,\delta}(t_n, \cdot)|_{L_z^1 L_x^1 BV_y} \int_{t_n}^{t_{n+1}} \|\nabla \mathbf{u}\|_{L^\infty(\Omega)} dt \\ & + 4(\tilde{c} + 1) \text{Lip}(g) |\alpha_{h,\delta}(t_n, \cdot)|_{L_y^1 L_x^1 BV_z} \int_{t_n}^{t_{n+1}} \|\nabla \mathbf{u}\|_{L^\infty(\Omega)} dt \\ & + 5\text{Lip}(f) |\alpha_{h,\delta}(t_n, \cdot)|_{L_z^1 L_y^1 BV_x} \int_{t_n}^{t_{n+1}} \|\nabla \mathbf{u}\|_{L^\infty(\Omega)} dt \\ & + (\text{Lip}(f)\alpha_M + f_0) \int_{t_n}^{t_{n+1}} |\tilde{\Pi}_h^0(\text{div}(\mathbf{u}))(t, \cdot)|_{L_y^1 BV_x} dt, \end{aligned} \quad (9.16)$$

where the piecewise constant projection $\tilde{\Pi}_h^0 : BV_{\mathbf{x}}(\Omega) \rightarrow BV_{\mathbf{x}}(\Omega)$ for an admissible grid $X_k \times Y_h \times Z_l$ is defined by, for $\beta \in BV_{\mathbf{x}}(\Omega)$,

$$(\tilde{\Pi}_h^0(\beta))(\mathbf{x}) := \int_{K_{i,j,m}} \beta d\mathbf{x} \quad \forall \mathbf{x} \in K_{i,j,m}.$$

Along with similar estimates on $|\alpha_{h,\delta}(t_{n+1}, \cdot)|_{L_z^1 L_x^1 BV_y}$ and $|\alpha_{h,\delta}(t_{n+1}, \cdot)|_{L_y^1 L_x^1 BV_z}$ (9.16) yields

$$\begin{aligned} |\alpha_{h,\delta}(t_{n+1}, \cdot)|_{BV_{x,y,z}} & \leq |\alpha_{h,\delta}(t_n, \cdot)|_{BV_{x,y,z}} \left(1 + \mathcal{C} \int_{t_n}^{t_{n+1}} \|\nabla \mathbf{u}(t, \cdot)\|_{L^\infty(\Omega)} dt \right) \\ & + \mathcal{C} \int_{t_n}^{t_{n+1}} |\tilde{\Pi}_h^0(\text{div}(\mathbf{u}))|_{BV_{x,y}} dt, \end{aligned} \quad (9.17)$$

where $\mathcal{C} := \max(\text{Lip}(f)\alpha_M + f_0, 5\text{Lip}(f) + 4\text{Lip}(g)(\tilde{c} + 1) + 1)$. An application of induction on (9.17) yields (9.9). \square

Proposition 9.3 (temporal variation for the three dimensional scheme). *The function $\alpha_{h,\delta}$ satisfies*

$$\begin{aligned} |\alpha_{h,\delta}|_{L_{x,y,z}^1 BV_t} & \leq \mathbf{B}_{\mathbf{u}} \left(|\alpha_0|_{BV_{x,y,z}} + \mathcal{C} |\text{div}(\mathbf{u})|_{L_t^1 BV_{x,y,z}} \right) \text{Lip}(g) \|\nabla \mathbf{u}\|_{L_t^1 L^\infty(\hat{\Omega}_T)} \\ & + (\text{Lip}(f)\alpha_M + f_0) |\text{div}(\mathbf{u})|_{L^1(\hat{\Omega}_T)}. \end{aligned} \quad (9.18)$$

The proof of Proposition 9.3 is similar to the proof of Proposition 6.8. A use of the results (9.9) and (9.18) establishes Theorem 6.48.

Appendix B

Biphasic model formulation in higher spatial dimensions

A brief derivation of the model considered in Chapter 5 is provided in this appendix. The principles involved in modelling tumour growth in two and three dimensions are similar to that of the one-dimensional case in Chapter 1. However, the final system that describes the evolution of cell velocity and pressure differs from the one-dimensional version. In one dimension, it is possible to eliminate the pressure variable using velocity, see (1.17) and thus reduce the number of unknown variables to three; cell volume fraction, cell velocity, and nutrient concentration. In a higher-dimensional setting, the dimensionality constrains forbids such a reduction. Instead, cell velocity and pressure are governed by a generalised viscous Stokes system. The first version of the model considered in Chapter 5 is proposed H M. Byrne et al. [61].

The tumour growth is studied over the finite duration $(0, T)$, $T > 0$. The tumour at each fixed time $t \in (0, T)$ occupies the time-dependent domain $\Omega(t) \subset \mathbb{R}^d$, where $d \in \{2, 3\}$. The boundary of $\Omega(t)$ is denoted by $\Gamma(t)$. We set the normal velocity of $\Gamma(t)$ equal to the normal component of the velocity of cells present at $\Gamma(t)$ for every $t \in (0, T)$. That is,

$$\mathbf{u}_c(t, \gamma(t)) \cdot \mathbf{n}_{|\Gamma(t)} = \frac{\partial \gamma'(t)}{\partial t} \cdot \mathbf{n}_{|\Gamma(t)},$$

where $\gamma(t)$ is a local parametrization of $\Gamma(t)$ and $\mathbf{n}_{|\Gamma(t)}$ is the unit normal vector to $\Gamma(t)$. Here, \mathbf{u}_c is the velocity of the tumour cells.

Conservation laws

Mass conservation applied to cell and fluid phases yields the following hyperbolic conservation laws

$$\frac{\partial \alpha}{\partial t} + \operatorname{div}(\mathbf{u}_c \alpha) = q_c \quad \text{and} \quad \frac{\partial \alpha}{\partial t} + \operatorname{div}(\mathbf{u}_w \beta) = q_w, \quad (10.1)$$

where \mathbf{u}_c and \mathbf{u}_w are cell and fluid velocity vector fields and $q_c = -q_w$ is the net production of tumour cells. In higher dimensional setting also, it is assumed that $\alpha + \beta = 1$. The stress tensors in cell and fluid phases are denoted by $\boldsymbol{\sigma}_c$ and $\boldsymbol{\sigma}_w$, respectively. Corresponding momentum source terms are denoted by \mathbf{F}_c and \mathbf{F}_w . Neglect inertial effects to obtain the momentum conservation laws as follows

$$\operatorname{div}(\alpha\boldsymbol{\sigma}_c) + \mathbf{F}_c = \mathbf{0} \quad \text{and} \quad \operatorname{div}(\beta\boldsymbol{\sigma}_w) + \mathbf{F}_w = \mathbf{0}. \quad (10.2)$$

The balance of forces gives $\mathbf{F}_c = -\mathbf{F}_w$. Let \mathbb{I}_d be the d -dimensional identity tensor, $d \in \{2, 3\}$. The cell phase is assumed to be viscous, and the associated stress tensor is described by

$$\boldsymbol{\sigma}_c = -p_c\mathbb{I}_d + \mu_c(\nabla\mathbf{u}_c + \nabla\mathbf{u}_c^T) + \lambda_c\operatorname{div}(\mathbf{u}_c)\mathbb{I}_d, \quad (10.3)$$

where p_c is cell pressure, μ_c is shear viscosity coefficient, and λ_c is the bulk viscosity coefficient. The shear and bulk viscosity coefficients are thermodynamically related by $\lambda_c = -2\mu_c/3$. The fluid phase is assumed to be inviscid, which yields,

$$\boldsymbol{\sigma}_w = -p_w\mathbb{I}_d \quad (10.4)$$

where p_w is the fluid pressure. The nutrient follows the diffusion equation

$$\frac{\partial c}{\partial t} - \operatorname{div}(\bar{\eta}\nabla c) = -Q_c, \quad (10.5)$$

where $Q_c = Q_0c\alpha/(1 + Q_1c)$ is the nutrient consumption rate and $\bar{\eta}$ is the diffusivity constant.

Constitutive assumptions

Recall that $\mathcal{H}(\alpha) = \gamma(\alpha - \alpha^R)^+ / (1 - \alpha)^2$ from Section 1.5. Add the two equations in (10.2) to obtain $\operatorname{div}(\alpha\boldsymbol{\sigma}_c + \beta\boldsymbol{\sigma}_w) = 0$. Substitute (10.3) and (10.4) in $\operatorname{div}(\alpha\boldsymbol{\sigma}_c + \beta\boldsymbol{\sigma}_w) = 0$ and use $p_c = p_w + \gamma\mathcal{H}(\alpha)$ and $\alpha + \beta = 1$ to arrive at

$$\operatorname{div}\left(-p_w\mathbb{I}_d + \mu_c(\nabla\mathbf{u}_c + (\nabla\mathbf{u}_c)^T) + \lambda_c\operatorname{div}(\mathbf{u}_c)\mathbb{I}_d - \alpha\gamma\mathcal{H}(\alpha)\mathbb{I}_d\right) = \mathbf{0}. \quad (10.6)$$

The momentum source terms are modelled as $\mathbf{F}_c = p_w\nabla\alpha + k_1\alpha\beta(\mathbf{u}_w - \mathbf{u}_c)$ and $\mathbf{F}_w = p_w\nabla\beta + k_1\alpha\beta(\mathbf{u}_w - \mathbf{u}_c)$. Use \mathbf{F}_w and $\boldsymbol{\sigma}_w$ in (10.2) to obtain

$$-\nabla p_w = k_1\alpha(\mathbf{u}_w - \mathbf{u}).$$

Add the two equations in (10.1) to arrive at

$$\operatorname{div}(\alpha\mathbf{u}_c + \beta\mathbf{u}_w) = 0. \quad (10.7)$$

The final model is described by (10.1)–(10.7).

Initial and boundary conditions

Since (10.1) and (10.5) are evolution equations, initial conditions need to be specified: $\alpha(0, \mathbf{x}) = \alpha_0(\mathbf{x})$ and $c(0, \mathbf{x}) = c_0(\mathbf{x})$ for every $\mathbf{x} \in \Omega(0)$. On the boundary, the internal and external nutrient concentration coincides, which yields $c|_{\Gamma(t)} = c_{out}$ for every $t > 0$. Since the fluid pressure is zero outside the tumour, $p_w|_{\Gamma(t)} = 0$ holds. The continuity of normal stress across the tumour boundary and since stress is zero outside the tumour, it follows

$$(\mu_c(\nabla \mathbf{u}_c + (\nabla \mathbf{u}_c)^T) + \lambda_c \operatorname{div}(\mathbf{u}_c) \mathbb{I}_d) \mathbf{n}|_{\Gamma(t)} = \mathbf{0}.$$

Nondimensionalisation and simplification

Rescale the variables as follows

$$\begin{aligned} \mathbf{x}' &= \frac{1}{\ell_0} \mathbf{x}, \quad t = t' t_{\dim}, \quad \alpha' = \alpha, \quad \mathbf{u}'_c = \frac{t_{\dim}}{\ell_0} \mathbf{u}_c, \quad \mathbf{u}'_w = \frac{t_{\dim}}{\ell_0} \mathbf{u}_w, \\ p'_w &= \frac{p_w}{\gamma}, \quad p'_c = \frac{p_c}{\gamma}, \quad c' = \frac{c}{c_{out}}, \quad \mu'_c = \frac{\mu_c}{(\gamma t_{\dim})}, \quad \text{and} \quad \lambda'_c = \frac{\lambda_c}{(\gamma t_{\dim})}, \end{aligned}$$

where ℓ_0 is the circumradius of $\Omega(0)$ and t_{\dim} is $(1 + S_1 c_{out})/S_0 c_{out}$. Variables with prime symbols are dimensionless. Set $\operatorname{div}' = \ell_0 \operatorname{div}$, $\nabla' = \ell_0 \nabla$, and $\frac{\partial}{\partial t'} = t_{\dim} \frac{\partial}{\partial t}$. The cell volume fraction satisfies the following dimensionless equation

$$\frac{\partial \alpha}{\partial t'} + \operatorname{div}'(\mathbf{u}'_c \alpha) = \frac{(1 + s_1) c'}{1 + s_1 c'} \alpha (1 - \alpha) - \frac{s_2 + s_3 c'}{(1 + s_4 c')} \alpha,$$

where s_1, s_2, s_3 , and s_4 are defined by (1.5.3). Divide (10.6) by γ to obtain the dimensionless version

$$\operatorname{div} \left(-p'_w \mathbb{I}_d + \mu'_c \alpha (\nabla' \mathbf{u}'_c + (\nabla' \mathbf{u}'_c)^T) + \lambda'_c \alpha \operatorname{div}'(\mathbf{u}'_c) \mathbb{I} - \alpha \mathcal{H}(\alpha) \mathbb{I}_d \right) = \mathbf{0}. \quad (10.8)$$

Combine the dimensionless equations $-\nabla' p'_w = k \alpha (\mathbf{u}'_w - \mathbf{u}'_c)$ and $\operatorname{div}'(\alpha \mathbf{u}'_c + \beta \mathbf{u}'_w) = 0$ to arrive at

$$\operatorname{div} \left(\frac{1 - \alpha}{k \alpha} \nabla' p'_w \right) + \operatorname{div}(\mathbf{u}'_c) = 0. \quad (10.9)$$

The relations (10.8) and (10.9) eliminate \mathbf{u}_w and p_c from the combined system. The dimensionless version of (10.5) is

$$\frac{\partial c'}{\partial t'} - \operatorname{div}'(\eta \nabla' c') = -\frac{Q c' \alpha}{1 + \widehat{Q}_1 c'},$$

where $\eta = \bar{\eta} t_{\dim} / \ell_0^2$. The prime symbols are dropped for notational simplicity. Since \mathbf{u}_w and p_c are eliminated from the final system, the subscripts used to differentiate cell and fluid phases can also be dropped. The final dimensionless system is as follows:

$$\frac{\partial \alpha}{\partial t} + \operatorname{div}(\mathbf{u} \alpha) = \alpha f(\alpha, c),$$

$$\begin{aligned}
\operatorname{div}\left(-p\mathbb{I}_d + \mu\alpha(\nabla\mathbf{u} + (\nabla\mathbf{u})^T) + \lambda\alpha\operatorname{div}(\mathbf{u})\mathbb{I}_d - \alpha\mathcal{H}(\alpha)\mathbb{I}_d\right) &= 0, \\
-\operatorname{div}\left(\frac{1-\alpha}{k\alpha}\nabla p\right) + \operatorname{div}(\mathbf{u}) &= 0, \quad \text{and} \\
\frac{\partial c}{\partial t} - \operatorname{div}(\eta\nabla c) &= -\frac{Qc\alpha}{1 + \widehat{Q}_1 c}.
\end{aligned}$$

The initial conditions are

$$\alpha(0, \mathbf{x}) = \alpha_0(\mathbf{x}), \quad c(0, \mathbf{x}) = c_0(\mathbf{x}) \quad \forall \mathbf{x} \in \Omega(0),$$

and boundary conditions are, $\forall t \in (0, T)$

$$p|_{\Gamma(t)} = 0, \quad (\mu(\nabla\mathbf{u} + (\nabla\mathbf{u})^T) + \lambda_c\operatorname{div}(\mathbf{u})\mathbb{I}_d - \alpha\mathcal{H}(\alpha)\mathbb{I}_d)\mathbf{n}|_{\Gamma(t)} = \mathbf{0}, \quad \text{and} \quad c|_{\Gamma(t)} = 1.$$

Bibliography

Articles

- [1] C. J. W. Breward, H. M. Byrne, and C. E. Lewis. “The role of cell-cell interactions in a two-phase model for avascular tumour growth”. In: *J. Math. Biol.* 45.2 (2002), pp. 125–152. URL: <https://doi.org/10.1007/s002850200149> (pages 1, 4, 8, 9, 17, 18, 25, 27, 33, 34, 49, 59, 91, 92, 112, 124, 168, 180).
- [2] H. P. Greenspan. “Models for the growth of a solid tumour by diffusion”. In: *Studies. Appl. Math.* 51.4 (1972), pp. 431–473. URL: <https://doi.org/10.1002/sapm1972514317> (page 3).
- [3] J. Ward and J. R. King. “Mathematical modelling of avascular–tumour growth”. In: *IMA J. Math. Appl. Med. Bio.* 14.1 (1997), pp. 39–69. URL: <https://doi.org/10.1093/imammb14.1.39> (pages 4, 35, 91).
- [4] H. M. Byrne and P. Matthews. “Asymmetric growth of models of avascular solid tumours: Exploiting symmetries”. In: *IMA J. Math. Appl. in Med. Biol.* 19.1 (2002), pp. 1–29. URL: <https://doi.org/10.1093/imammb/19.1.1> (pages 4, 46, 168).
- [5] C. J. W. Breward, H. M. Byrne, and C. E. Lewis. “Modelling the interactions between tumour cells and a blood vessel in a microenvironment within a vascular tumour”. In: *European J. Appl. Math.* 12.5 (2001), pp. 529–556. URL: <https://doi.org/10.1017/S095679250100448X> (pages 4, 34, 168).
- [6] H. M. Byrne and L. Preziosi. “Modelling solid tumour growth using the theory of mixtures”. In: *Math. Med. Bio.* 20.4 (2003), pp. 341–366. URL: <https://doi.org/10.1093/imammb/20.4.341> (pages 4, 5, 34, 91, 92, 129, 168).
- [7] H. M. Byrne, J. R. King, D. L. S. McElwain, and L. Preziosi. “A two-phase model of solid tumour growth”. In: *Appl. Math. Lett.* 16.4 (2003), pp. 567–573. URL: [https://doi.org/10.1016/S0893-9659\(03\)00038-7](https://doi.org/10.1016/S0893-9659(03)00038-7) (pages 4, 8, 11, 25, 34, 91, 92, 95, 167, 168).
- [8] J. Ward and J. R. King. “Mathematical modelling of avascular–tumor growth II: Modelling growth saturation”. In: *IMA J. Math. Appl. Med. Bio.* 16.2 (1999), pp. 171–211. URL: <https://doi.org/10.1093/imammb16.2.171> (pages 4, 35, 91).
- [9] S. Astanin and L. Preziosi. “Multiphase models of tumour growth”. In: *Model. Simul. Sci. Eng. Technol.* (2008), pp. 223–253. URL: https://doi.org/10.1007/978-0-8176-4713-1_9 (pages 5, 34).
- [10] J. M. Osborne and J. P. Whiteley. “A numerical method for the multiphase viscous flow equations”. In: *Comput. Methods Appl. Mech. Engg.* 199.49 (2010), pp. 3402–3417. ISSN: 0045-7825. URL: <https://doi.org/10.1016/j.cma.2010.07.011> (pages 5, 8, 91, 92, 168).

- [11] M. E. Hubbard and H. M. Byrne. “Multiphase modelling of vascular tumour growth in two spatial dimensions”. In: *J. Theoret. Biol.* 316 (2013), pp. 70–89. URL: <https://doi.org/10.1016/j.jtbi.2012.09.031> (pages 5, 8, 46, 106, 124, 168).
- [12] J. A. MacKenzie and A. Madzvamuse. “Analysis of stability and convergence of finite-difference methods for a reaction-diffusion problem on a one-dimensional growing domain”. In: *IMA J. of Numer. Anal.* 31 (2011), pp. 212–232. URL: <https://doi.org/10.1093/imanum/drp030> (pages 5, 62).
- [13] B. Bazaliy and A. Friedman. “Global existence and asymptotic stability for an elliptic-parabolic free boundary problem: an application to a model of tumor growth”. In: *Indiana University Mathematics Journal* 52.5 (2003), pp. 1265–1304. URL: <https://www.jstor.org/stable/24903448> (page 5).
- [14] S. Cui and A. Friedman. “A hyperbolic free boundary problem modeling tumor growth”. In: *Interfaces and Free Boundaries* 5.2 (2003), pp. 159–181. URL: <https://doi.org/10.4171/IFB/76> (page 5).
- [15] A. Friedman. “Free boundary problems arising in tumor models”. In: *Atti della Accademia Nazionale dei Lincei. Classe di Scienze Fisiche, Matematiche e Naturali. Rendiconti Lincei. Matematica e Applicazioni* 15.3-4 (2004), pp. 161–168. URL: <http://eudml.org/doc/252409> (page 6).
- [16] X. Chen, S. Cui, and A. Friedman. “A hyperbolic free boundary problem modeling tumor growth: Asymptotic behavior”. In: *Transactions of the American Mathematical Society* 357.12 (2005), pp. 4771–4804. URL: <https://doi.org/10.1090/S0002-9947-05-03784-0> (page 6).
- [17] Y. Tao, N. Yoshida, and Q. Guo. “Nonlinear analysis of a model of vascular tumour growth and treatment”. In: *Nonlinearity* 17.3 (2004), pp. 867–895. URL: <https://doi.org/10.1088/0951-7715/17/3/008> (page 6).
- [18] P. Colli, G. Gilardi, and D. Hilhorst. “On a Cahn-Hilliard type phase field system related to tumor growth”. In: *Discrete Contin. Dyn. Syst.* 35.6 (2015), pp. 2423–2442. URL: <https://doi.org/10.3934/dcds.2015.35.2423> (page 6).
- [19] H. Garcke and K. F. Lam. “Global weak solutions and asymptotic limits of a Cahn-Hilliard-Darcy system modelling tumour growth”. In: *AIMS Mathematics* 1.3 (2016), pp. 318–360. URL: <https://doi.org/10.3934/Math.2016.3.318> (page 6).
- [20] M. Dai, E. Feireisl, E. Rocca, G. Schimperna, and M. E. Schonbek. “Analysis of a diffuse interface model of multispecies tumor growth”. In: *Nonlinearity* 30.4 (2017), pp. 1639–1658. URL: <https://doi.org/10.1088/1361-6544/aa6063> (page 6).
- [21] I. C. Kim, B. Perthame, and P. E. Souganidis. “Free boundary problems for tumor growth: a viscosity solutions approach”. In: *Nonlinear Anal.* 138 (2016), pp. 207–228. URL: <https://doi.org/10.1016/j.na.2016.01.019> (page 6).

- [22] A. Belmiloudi. “Mathematical modeling and optimal control problems in brain tumour targeted drug delivery strategies”. In: *Int. J. Biomath.* 10.4 (2017), pp. 1750056, 62. URL: <https://doi.org/10.1142/S1793524517500565> (page 7).
- [23] S. I. Oke, M. B. Matadi, and S. S. Xulu. “Optimal control analysis of a mathematical model for breast cancer”. In: *Math. Comput. Appl.* 23.2 (2018), pp. 21–28. URL: <https://doi.org/10.3390/mca23020021> (page 7).
- [24] T. Hillen, H. Enderling, and P. Hahnfeldt. “The tumor growth paradox and immune system-mediated selection for cancer stem cells”. In: *Bull. Math. Bio.* 75 (2013), pp. 161–184. URL: <https://doi.org/10.1007/s11538-012-9798-x> (page 7).
- [25] I. Padilla and R. G. Plaza. “On the role of cancer cells’ diffusion in the tumor growth paradox”. In: *arXiv preprint arXiv:1903.04537* (2019). URL: <https://arxiv.org/abs/1903.04537> (page 7).
- [26] L. Maddalena. “Analysis of an integro-differential system modeling tumor growth”. In: *Appl. Math. Comput.* 245 (2014), pp. 152–157. URL: <https://doi.org/10.1016/j.amc.2014.07.081> (page 7).
- [27] A. Fasano, A. Mancini, and M. Primicerio. “Tumours with cancer stem cells: a PDE model”. In: *Math. Biosci.* 272 (2016), pp. 76–80. URL: <https://doi.org/10.1016/j.mbs.2015.12.003> (page 7).
- [28] I. Borsi, A. Fasano, M. Primicerio, and T. Hillen. “A non-local model for cancer stem cells and the tumour growth paradox”. In: *Math. Med. Biol.* 34.1 (2017), pp. 59–75. URL: <https://doi.org/10.1093/imammb/dqv037> (page 7).
- [29] S. J. Franks, H. M. Byrne, J. R. King, J. C. E. Underwood, and C. E. Lewis. “Modelling the early growth of ductal carcinoma in situ of the breast”. In: *J. Math. Biol.* 47.5 (2003). URL: <https://doi.org/10.1007/s00285-003-0214-x> (pages 8, 12, 129, 156, 191).
- [30] C. Y. Chen, H. M. Byrne, and J. R. King. “The influence of growth-induced stress from the surrounding medium on the development of multicell spheroids”. In: *J. Math. Biol.* 43.3 (2001), pp. 191–220. URL: <https://doi.org/10.1007/s002850100091> (pages 8, 167, 168).
- [31] H. Song, B. Hu, and Z. Wang. “Stationary solutions of a free boundary problem modeling the growth of vascular tumors with a necrotic core”. In: *Dis. Cont. Dyn. Sys. - B* 22 (2020). URL: <https://doi.org/10.3934/dcdsb.2020084> (page 7).
- [32] V. Thomée and L. B. Wahlbin. “On the existence of maximum principles in parabolic finite element equations”. In: *Math. Comp.* 77.261 (2008), pp. 11–19. URL: <https://doi.org/10.1090/S0025-5718-07-02021-2> (pages 16, 111).
- [33] C. J. W. Beward, H. M. Byrne, and C. E. Lewis. “A multiphase model describing vascular tumour growth”. In: *Bull. of Math. Bio.* 65.4 (2003), pp. 609–640. ISSN: 1522-9602. URL: [https://doi.org/10.1016/S0092-8240\(03\)00027-2](https://doi.org/10.1016/S0092-8240(03)00027-2) (pages 34, 35, 91, 92, 168).

- [34] H. B. Stewart and B. Wendroff. “Two-phase flow: models and methods”. In: *J. Comp. Phys.* 56 (1984), pp. 363–409. URL: [https://doi.org/10.1016/0021-9991\(84\)90103-7](https://doi.org/10.1016/0021-9991(84)90103-7) (page 34).
- [35] D. A. Drew. “Mathematical Modeling of Two-Phase Flow”. In: *Annual Review of Fluid Mechanics* 15.1 (1983), pp. 261–291. URL: <https://doi.org/10.1146/annurev.fl.15.010183.001401> (page 34).
- [36] A. Caboussat. “A numerical simulation of two-phase free surface flows”. In: *Arch. Comput. Meth. Engng.* 12 (2005), pp. 165–224. URL: <https://doi.org/10.1007/BF03044518> (page 35).
- [37] E. W. Grald and J. W. Macarthur. “A moving-boundary formulation for modeling time-dependent two-phase flows”. In: *Int. J. Heat and Fluid Flow* 13 (1992), pp. 266–272. URL: [https://doi.org/10.1016/0142-727X\(92\)90040-G](https://doi.org/10.1016/0142-727X(92)90040-G) (page 35).
- [38] D. Li, K. Luo, and J. Dang. “A moving boundary model for two-phase flow heat exchanger incorporated with relative velocities between boundaries and fluid”. In: *Int. J. Heat and Mass Transf.* 95 (2016), pp. 35–44. URL: <https://doi.org/10.1016/j.ijheatmasstransfer.2015.11.095> (page 35).
- [39] L. Yao and C. Zhu. “Free boundary value problem for a viscous two-phase model with mass-dependent viscosity”. In: *J. Differ. Equ.* 247 (2009), pp. 2705–2739. URL: <https://doi.org/10.1016/j.jde.2009.07.013> (page 35).
- [40] G. H. Meyer. “A numerical method for two-phase Stefan problems”. In: *SIAM J. Numer. Anal.* 8.3 (1971), pp. 555–568. URL: <https://doi.org/10.1137/0708053> (page 35).
- [41] L. Wenchao, Y. Bowen, and Y. Wang. “Numerical solution of a moving boundary problem of one-dimensional flow in semi-infinite long porous media with threshold pressure gradient”. In: *Int. J. of Heat and Mass Transfer* 55 (2012), pp. 60176022. URL: <https://doi.org/10.1016/j.ijheatmasstransfer.2012.06.012> (page 35).
- [42] B. van Leer. “Towards the ultimate conservative difference scheme. V. A second-order sequel to Godunov’s method”. In: *J. Comput. Phys.* 32.1 (1979), pp. 101–136. URL: [https://doi.org/10.1016/0021-9991\(79\)90145-1](https://doi.org/10.1016/0021-9991(79)90145-1) (page 42).
- [43] J. A. Adam. “A simplified mathematical model of tumour growth”. In: *Math. Biosci.* 81 (1986), pp. 229–244. URL: [https://doi.org/10.1016/0025-5564\(86\)90119-7](https://doi.org/10.1016/0025-5564(86)90119-7) (page 46).
- [44] S. R. Mahmoud, S. A. Ghaleb, A. K. Alzahrani, and E. Ghandourah. “Mathematical approach for effect of growth on the mechanical stresses during soft tissues and avascular tumour”. In: *Appl. Math. Inf. Sci.* 11 (2017), pp. 1353–1360. URL: <https://doi.org/10.18576/amis/110512> (page 46).
- [45] Y. Zhuang. “Asymptotic behaviour of solutions of a free-boundary tumour model with angiogenesis”. In: *Nonlinear Anal. Real World Appl.* 44 (2018), pp. 86–105. URL: <https://doi.org/10.1016/j.nonrwa.2018.05.003> (page 46).

- [46] C. S. Hoguea, B. T. Murray, and J. A. Sethian. “Simulating complex tumour dynamics from avascular to vascular growth using a general level-set method”. In: *J. Math. Biol.* 53.1 (2006), pp. 86–134. ISSN: 1432-1416. URL: <https://doi.org/10.1007/s00285-006-0378-2> (page 46).
- [47] H. Perfahl, H. M. Byrne, T. Chen, V. C. Estrella, T. Alarcón, A. Lapin, R. A. Gatenby, R. J. Gillies, M. C. Lloyd, P. K. Maini, M. Reuss, and M. R. Owen. “Multiscale modelling of vascular tumour growth in 3D: the roles of domain size and boundary Conditions”. In: *Plos one* 6 (2011), pp. 1–17. URL: <https://doi.org/10.1371/journal.pone.0014790> (page 46).
- [48] G. Sciumè, S. Shelton, W. G Gray, C. T. Miller, F. Hussain, M. Ferrari, P. Decuzzi, and B. A. Schrefler. “A multiphase model for three-dimensional tumour growth”. In: *New J. Phy.* 15 (2013), p. 015005. URL: <https://doi.org/10.1088/1367-2630/15/1/015005> (pages 46, 91).
- [49] D. Kroener and S. Luckhaus. “Flow of oil and water in a porous medium”. In: *J. Differential Equations* 55.2 (1984), pp. 276–288. ISSN: 0022-0396. URL: [https://doi.org/10.1016/0022-0396\(84\)90084-6](https://doi.org/10.1016/0022-0396(84)90084-6) (page 46).
- [50] X. Cao and I. S. Pop. “Degenerate two-phase porous media flow model with dynamic capillarity”. In: *J. Differential Equations* 260.3 (2016), pp. 2418–2456. ISSN: 0022-0396. URL: <https://doi.org/10.1016/j.jde.2015.10.008> (page 46).
- [51] J. Folkman and M. Hochberg. “Self-regulation of growth in three dimensions”. In: *J. Exp. Med.* 138.4 (1973), pp. 745–753. URL: <https://doi.org/10.1084/jem.138.4.745> (page 49).
- [52] G. C. Remesan. “Numerical solution of the two-phase tumour growth model with moving boundary”. In: *ANZIAM J.* 60 (2019). Ed. by B. Lamichane, T. Tran, and J. Bunder, pp. C1–C15. URL: <https://doi.org/10.21914/anziamj.v60i0.13936> (pages 59, 124).
- [53] H. M. Byrne, T. Alarcon, M. R. Owen, S. D. Webb, and P. K. Maini. “Modelling aspects of cancer dynamics: A review”. In: *Philos. Trans. Roy. Soc. A* 364.1843 (2006), pp. 1563–1578. URL: <https://doi.org/10.1098/rsta.2006.1786> (pages 62, 167, 168).
- [54] T. Roose, S. J. Chapman, and P. K. Maini. “Mathematical models of avascular tumour growth”. In: *SIAM Rev.* 49 (2007), pp. 179–208. URL: <https://doi.org/10.1137/S0036144504446291> (pages 62, 91, 167).
- [55] J. Zheng and S. Cui. “Analysis of a tumour-model free boundary problem with a non-linear boundary condition”. In: *J. Math. Anal. Appl.* 478 (2019), pp. 806–824. URL: <https://doi.org/10.1016/j.jmaa.2019.05.056> (page 62).
- [56] M. C. Calzada, G. Camacho, E. Fernández-Cara, and M. Marín. “Fictitious domains and level sets for moving boundary problems. Applications to the numerical simulation of tumour growth”. In: *J. Comput. Phys.* 230 (2011), pp. 1335–1358. URL: <https://doi.org/10.1016/j.jcp.2010.11.005> (pages 62, 93).

- [57] N. Zhang and Y. Tao. “A free boundary problem modelling tumour growth with different chemotactic responses and random motions for various cell types”. In: *J. Math. Anal. Appl.* 398 (2013), pp. 534–541. URL: <https://doi.org/10.1016/j.jmaa.2012.09.013> (page 62).
- [58] E. Tadmor. “A review of numerical methods for nonlinear partial differential equations”. In: *Bull. Amer. Math. Soc. (N.S.)* 49.4 (2012), pp. 507–554. URL: <https://doi-org.ezproxy.lib.monash.edu.au/10.1090/S0273-0979-2012-01379-4> (page 64).
- [59] H. P. Greenspan. “On the growth and stability of cell cultures and solid tumors”. In: *J. Theoret. Bio.* 56.1 (1976), pp. 229–242. URL: [https://doi.org/10.1016/s0022-5193\(76\)80054-9](https://doi.org/10.1016/s0022-5193(76)80054-9) (pages 91, 168).
- [60] R. P. Araujo and D. L. S. McElwain. “A history of the study of solid tumour growth: The contribution of mathematical modelling”. In: *Bull. Math. Bio.* 66.5 (2004), pp. 1039–1091. URL: <https://doi.org/10.1016/j.bulm.2003.11.002> (page 91).
- [61] H. M. Byrne and M. A. J. Chaplain. “Free boundary value problems associated with the growth and development of multicellular spheroids”. In: *European J. Appl. Math.* 8.6 (1997), pp. 639–658. URL: <https://doi.org/10.1017/S0956792597003264> (pages 91, 202).
- [62] P. Macklin and J. Lowengrub. “Nonlinear simulation of the effect of microenvironment on tumor growth”. In: *J. Theoret. Bio.* 245.4 (2007), pp. 677–704. URL: <https://doi.org/10.1016/j.jtbi.2006.12.004> (page 93).
- [63] S. Bauer and D. Pauly. “On Korn’s first inequality for mixed tangential and normal boundary conditions on bounded Lipschitz domains in \mathbb{R}^N ”. In: *Ann. Univ. Ferrara Sez. VII Sci. Mat* 62.2 (2016), pp. 173–188. URL: <https://doi.org/10.1007/s11565-016-0247-x> (page 100).
- [64] R. Eymard, C. Guichard, and R. Masson. “Grid orientation effect in coupled finite volume schemes”. In: *IMA J. Numer. Anal.* 33.2 (2013), pp. 582–608. ISSN: 0272-4979. DOI: 10.1093/imanum/drs016. URL: <https://doi-org.ezproxy.lib.monash.edu.au/10.1093/imanum/drs016> (page 105).
- [65] J. Ruppert. “A Delaunay refinement algorithm for quality 2-dimensional mesh generation”. In: *J. Algor.* 18.3 (1995), pp. 548–585. DOI: 10.1006/jagm.1995.1021. URL: <https://doi.org/10.1006/jagm.1995.1021> (page 106).
- [66] D. R. Grimes, P. Kannan, D. R. Warren, B. Markelc, R. Bates, R. Muschel, and M. Partridge. “Estimating oxygen distribution from vasculature in three-dimensional tumour tissue”. In: *J. R. Soc. Interface* 13.116 (2016), pp. 20160–070. URL: <https://doi.org/10.1098/rsif.2016.0070> (page 117).
- [67] E. Conway and J. Smoller. “Global solutions of the Cauchy problem for quasi-linear first-order equations in several space variables”. In: *Comm. Pure Appl. Math.* 19.1 (1966), pp. 95–105. URL: <https://doi.org/10.1002/cpa.3160190107> (page 126).

- [68] N. N. Kuznetsov. “Accuracy of some approximate methods for computing the weak solutions of a first-order quasi-linear equation”. In: *USSR Comp. Math. Math. Phy.* 16.6 (1976), pp. 105–119. URL: [https://doi.org/10.1016/0041-5553\(76\)90046-X](https://doi.org/10.1016/0041-5553(76)90046-X) (pages 126, 149).
- [69] M. G. Crandall and A. Majda. “Monotone difference approximations for scalar conservation laws”. In: *Math. Comp.* 34.149 (1980), pp. 1–21. URL: <https://doi.org/10.2307/2006218> (page 126).
- [70] R. Sanders. “On convergence of monotone finite difference schemes with variable spatial differencing”. In: *Math. Comp.* 40.161 (1983), pp. 91–106. URL: <https://doi.org/10.1090/S0025-5718-1983-0679435-6> (page 126).
- [71] B. Merlet. “ L^∞ - and L^2 -error estimates for a finite volume approximation of linear advection”. In: *SIAM J. Numer. Anal.* 46.1 (2007), pp. 124–150. URL: <https://doi.org/10.1137/060664057> (page 126).
- [72] B. Merlet and J. Vovelle. “Error estimate for finite volume scheme”. In: *Numer. Math.* 106.1 (2007), pp. 129–155. URL: <https://doi.org/10.1007/s00211-006-0053-y> (page 126).
- [73] S. Champier, T. Gallouët, and R. Herbin. “Convergence of an upstream finite volume scheme for a nonlinear hyperbolic equation on a triangular mesh”. In: *Numer. Math.* 66.1 (1993), pp. 139–157. URL: <https://doi.org/10.1007/BF01385691> (page 126).
- [74] K. H. Karlsen and J. D. Towers. “Convergence of monotone schemes for conservation laws with zero-flux boundary conditions”. In: *Adv. Appl. Math. Mech.* 9.3 (2017), pp. 515–542. URL: <https://doi.org/10.4208/aamm.2016.m-s1> (page 126).
- [75] C. Chainais-Hillairet. “Finite volume schemes for a nonlinear hyperbolic equation. Convergence towards the entropy solution and error estimate”. In: *M2AN Math. Model. Numer. Anal.* 33.1 (1999), pp. 129–156. URL: <https://doi.org/10.1051/m2an:1999109> (pages 127, 134, 144, 146, 149, 152).
- [76] P. Chandrashekar and C. Klingenberg. “Entropy stable finite volume scheme for ideal compressible MHD on 2-D Cartesian meshes”. In: *SIAM J. Numer. Anal.* 54.2 (2016), pp. 1313–1340. URL: <https://doi.org/10.1137/15M1013626> (page 130).
- [77] R. J. DiPerna and P. L. Lions. “Ordinary differential equations, transport theory and Sobolev spaces”. In: *Invent. Math.* 98.3 (1989), pp. 511–547. URL: <https://doi.org/10.1007/BF01393835> (page 134).
- [78] Adimurthi, S. Mishra, and G. D. V. Gowda. “Convergence of Godunov type methods for a conservation law with a spatially varying discontinuous flux function”. In: *Math. Comp.* 76.259 (2007), pp. 1219–1242. URL: <https://doi.org/10.1090/S0025-5718-07-01960-6> (page 134).

- [79] Adimurthi, R Dutta, G. D. V. Gowda, and J. Jaffré. “Monotone (A, B) entropy stable numerical scheme for scalar conservation laws with discontinuous flux”. In: *ESAIM Math. Model. Numer. Anal.* 48.6 (2014), pp. 1725–1755. URL: <https://doi.org/10.1051/m2an/2014017> (page 134).
- [80] Adimurthi, S. Mishra, and G. D. V. Gowda. “Conservation law with the flux function discontinuous in the space variable. II. Convex-concave type fluxes and generalized entropy solutions”. In: *J. Comput. Appl. Math.* 203.2 (2007), pp. 310–344. URL: <https://doi.org/10.1016/j.cam.2006.04.009> (page 134).
- [81] Adimurthi, S. K. Kumar, and G. D. V. Gowda. “Second order scheme for scalar conservation laws with discontinuous flux”. In: *Appl. Numer. Math.* 80 (2014), pp. 46–64. URL: <https://doi.org/10.1016/j.apnum.2014.02.004> (page 134).
- [82] Adimurthi, J. Jaffré, and G. D. V. Gowda. “Godunov-type methods for conservation laws with a flux function discontinuous in space”. In: *SIAM J. Numer. Anal.* 42.1 (2004), pp. 179–208. URL: <https://doi.org/10.1137/S003614290139562X> (page 134).
- [83] S. Diehl. “A conservation law with point source and discontinuous flux function modelling continuous sedimentation”. In: *SIAM J. Appl. Math.* 56.2 (1996), pp. 388–419. URL: <https://doi.org/10.1137/S0036139994242425> (page 144).
- [84] T. Gimse and N. H. Risebro. “Solution of the Cauchy problem for a conservation law with a discontinuous flux function”. In: *SIAM J. Math. Anal.* 23.3 (1992), pp. 635–648. URL: <https://doi.org/10.1137/0523032> (page 144).
- [85] B. Cockburn, P. A. Gremaud, and J. X. Yang. “A priori error estimates for numerical methods for scalar conservation laws. III. Multidimensional flux-splitting monotone schemes on non-Cartesian grids”. In: *SIAM J. Numer. Anal.* 35.5 (1998), pp. 1775–1803. URL: <https://doi.org/10.1137/S0036142997316165> (page 149).
- [86] B. Després. “An explicit a priori estimate for a finite volume approximation of linear advection on non-Cartesian grids”. In: *SIAM J. Numer. Anal.* 42.2 (2004), pp. 484–504. URL: <https://doi.org/10.1137/S0036142901394558> (page 153).
- [87] I. C. Sorribes, M. N. J. Moore, H. M. Byrne, and H. V. Jain. “A Biomechanical Model of Tumor-Induced Intracranial Pressure and Edema in Brain Tissue”. In: *Biophys. J.* 116.8 (2019), pp. 1560–157. URL: <https://doi.org/10.1016/j.bpj.2019.02.030> (pages 166, 168).
- [88] J. M. Northcott, I. S. Dean, J. K. Mouw, and V. M. Weaver. “Feeling Stress: The Mechanics of Cancer Progression and Aggression”. In: *Front. Cell Dev. Biol.* 6 (2018), p. 17. URL: <https://doi.org/10.3389/fcell.2018.00017> (page 166).

- [89] G. Helmlinger, P. A. Netti, H. C. Lichtenbeld, R. J. Melder, and R. K. Jain. “Solid stress inhibits the growth of multicellular tumor spheroids”. In: *Nature Biotechnology* 15.8 (1997), pp. 778–783. URL: <https://doi.org/10.1038/nbt0897-778> (pages 166, 168, 186).
- [90] G. Cheng, J. Tse, R. K. Jain, and L. L. Munn. “Micro-Environmental Mechanical Stress Controls Tumor Spheroid Size and Morphology by Suppressing Proliferation and Inducing Apoptosis in Cancer Cells”. In: *PLoS ONE* 4.2 (2009), pp. 17–28. URL: <https://doi.org/10.1371/journal.pone.0004632> (page 166).
- [91] M. Delarue, F. Montel, D. Vignjevic, J. Prost, J. F. Joanny, and G. Cappello. “Compressive stress inhibits proliferation in tumor spheroids through a volume limitation”. In: *Biophys. J.* 107.8 (2014), pp. 1821–1828. URL: <https://doi.org/10.1016/j.bpj.2014.08.031> (page 166).
- [92] S. Takao, M. Taya, and C. Chiew. “Mechanical stress-induced cell death in breast cancer cells”. In: 8.8 (2019). URL: <https://doi.org/10.1242/bio.043133> (page 166).
- [93] G. Chagnon, M. Rebouah, and D. Favier. “Hyperelastic energy densities for soft biological tissues: a review”. In: *J. Elasticity* 120.2 (2015), pp. 129–160. URL: <https://doi.org/10.1007/s10659-014-9508-z> (page 167).
- [94] F. Valdés-Ravelo, A. Ramírez-Torres, R. Rodríguez-Ramos, J. Bravo-Castillero, R. Guinovart-Díaz, J. Merodio, R. Penta, A. Conci, F. J. Sabina, and C. García-Reimbert. “Mathematica modeling of the interplay between stress and anisotropic growth of avascular tumors”. In: *J. Mech. Med. Biol.* 18.01 (2018), p. 1850006. URL: <https://doi.org/10.1142/S0219519418500069> (page 168).
- [95] W. Hong, X. Zhao, J. Zhou, and Z. Suo. “A theory of coupled diffusion and large deformation in polymeric gels”. In: *J. Mech. Phys. Solids* 56.5 (2008), pp. 1779–1793. URL: <https://doi.org/10.1016/j.jmps.2007.11.010> (page 170).

Books and monographs

- [96] H. Brezis. *Functional analysis, Sobolev spaces and partial differential equations*. Universitext. Springer, New York, 2011. URL: <https://doi.org/10.1007/978-0-387-70914-7> (pages 13, 15).
- [97] L. C. Evans. *Partial differential equations*. Vol. 19. Graduate Studies in Mathematics. American Mathematical Society, Providence, RI, 2010. URL: <https://doi.org/10.1090/gsm/019> (pages 13, 17, 66, 94).
- [98] J. Droniou, R. Eymard, T. Gallouët, C. Guichard, and R. Herbin. *The gradient discretisation method*. Vol. 82. Mathématiques & Applications. Springer, Cham, 2018. URL: <https://doi.org/10.1007/978-3-319-79042-8> (pages 15, 16, 59, 64, 72, 77).
- [99] A. Ern and J. L. Guermond. *Theory and practice of finite elements*. Vol. 159. Applied Mathematical Sciences. Springer-Verlag, New York, 2004. URL: <https://doi.org/10.1007/978-1-4757-4355-5> (pages 15, 17, 92).
- [100] S. Kesavan. *Topics in functional analysis and applications*. John Wiley & Sons, Inc., New York, 2015 (page 15).
- [101] L. C. Evans and R. F. Gariepy. *Measure theory and fine properties of functions*. Studies in Advanced Mathematics. CRC Press, Boca Raton, FL, 1992. URL: <https://doi.org/10.1201/b18333> (pages 15, 104).
- [102] F. Boyer and P. Fabrie. *Mathematical tools for the study of the incompressible Navier-Stokes equations and related models*. Vol. 183. Applied Mathematical Sciences. Springer, New York, 2013. URL: <https://doi.org/10.1007/978-1-4614-5975-0> (page 17).
- [103] V. Maz'ya and J. Rossmann. *Elliptic equations in polyhedral domains*. Vol. 162. Mathematical Surveys and Monographs. American Mathematical Society, Providence, RI, 2010. URL: <https://doi.org/10.1090/surv/162> (page 17).
- [104] L. G. Leal. *Advanced transport phenomena: Fluid mechanics and convective transport processes*. Cambridge Series in Chemical Engineering. Cambridge University Press, 2007. URL: <https://doi.org/10.1017/CB09780511800245> (page 19).
- [105] R. Eymard, T. Gallouët, and R. Herbin. *Finite volume methods*. Handb. Numer. Anal., VII. North-Holland, Amsterdam, 2000, pp. 713–1020. URL: <https://doi.org/10.1086/phos.67.4.188705> (pages 40, 58, 125–127, 134, 149).
- [106] S. Salsa, F. M. G. Vegni, A. Zaretti, and P. Zunino. *A primer on PDEs*. Italian. Vol. 65. Unitext. Models, methods, simulations, La Matematica per il 3+2. Springer, Milan, 2013. URL: <https://doi.org/10.1007/978-88-470-2862-3> (page 47).
- [107] R. J. LeVeque. *Finite volume methods for hyperbolic problems*. Cambridge Texts in Applied Mathematics. Cambridge University Press, Cambridge, 2002. URL: <https://doi.org/10.1017/CB09780511791253> (page 58).

- [108] K. Schneider, D. Kolomenskiy, and E. Deriaz. *Is the CFL condition sufficient? Some remarks*. Birkhäuser/Springer, New York, 2013, pp. 139–146. URL: https://doi.org/10.1007/978-0-8176-8394-8_9 (page 64).
- [109] D. A. Di Pietro and A. Ern. *Mathematical aspects of discontinuous Galerkin methods*. Vol. 69. Mathématiques & Applications. Springer, Heidelberg, 2012. URL: <https://doi.org/10.1007/978-3-642-22980-0> (page 64).
- [110] K. Tapp. *Differential geometry of curves and surfaces*. Undergraduate Texts in Mathematics. Springer International Publishing, 2016. URL: <https://doi.org/10.1007/978-3-319-39799-3> (pages 97, 98).
- [111] H. Holden and N. H. Risebro. *Front tracking for hyperbolic conservation laws*. Second. Vol. 152. Applied Mathematical Sciences. Springer, Heidelberg, 2015. URL: <https://doi.org/10.1007/978-3-662-47507-2> (page 131).
- [112] D. Boffi, F. Brezzi, and M. Fortin. *Mixed finite element methods and applications*. Vol. 44. Springer Series in Computational Mathematics. Springer, Heidelberg, 2013. URL: <https://doi.org/10.1007/978-3-642-36519-5> (page 161).
- [113] J. Bergström. *Mechanics of solid polymers*. Ed. by J. Bergström. Vol. 4. Continuum mechanics foundations. William Andrew Publishing, 2015, pp. 131–207. URL: <https://doi.org/10.1016/B978-0-323-31150-2.00004-2> (page 167).
- [114] A. J. M. Spencer. *Continuum Mechanics*. Dover books on physics. Dover Publications, 2004 (page 167).
- [115] J. Bergström. *Mechanics of solid polymers*. Ed. by J. Bergström. Vol. 5. Elasticity/Hyperelasticity. William Andrew Publishing, 2015, pp. 209–307. URL: <https://doi.org/10.1016/B978-0-323-31150-2.00005-4> (page 170).
- [116] O. H. Yeoh. *Comprehensive Polymer Science and Supplements*. Ed. by Geoffrey Allen and John C. Bevington. Vol. 12. Phenomenological Theory of Rubber Elasticity. Amsterdam: Pergamon, 1989, pp. 425–439. URL: <https://doi.org/10.1016/B978-0-08-096701-1.00251-2> (page 170).
- [117] P. J. Flory. *Principles of Polymer Chemistry*. Baker lectures 1948. Cornell University Press, 1953 (page 170).

Subject index

- $BV(\Omega)$, 14
- $H^m(\Omega)$, 14
- $W^{m,p}(\Omega)$, 14
- $W_0^{m,p}(\Omega)$, 14
- $\mathbf{H}^m(\Omega)$, 14
- $\mathbf{W}^{m,p}(\Omega)$, 14
- $\mathcal{C}^\infty(\Omega)$, 14
- $\mathcal{C}^k(\Omega)$, 14
- $\mathcal{C}_c^1(\Omega; \mathbb{R}^d)$, 14
- $\mathcal{C}_c^\infty(\Omega)$, 14

- Avascular, 1
- Avascular tumour, 1

- BBL model, 17, 35
- Biphasic model, 17
- Birth rate, 20
- Bounded variation, 131
- Bounded variation seminorm, 14
- Bounded–strong convergence lemma, 16
- Breward–Byrne–Lewis model, 17

- Cahn–Hilliard models, 6
- Compactly–continuously embedded sequence, 16, 77
- Compactness theorem, 64, 158
- Compressible Stokes system, 17
- Convergence theorem, 64, 163
- Courant–Friedrichs–Lewy (CFL) condition, 63, 121
- Covering lemma, 86
- Cut-off models, 47

- Death rate, 20

- Deformation, 170
- Discrete Aubin–Simon theorem, 16
- Discrete average, 105
- Discrete integration by parts, 15
- Discrete positivity lemma, 16
- Discrete scheme, 40, 53, 107, 179
- Discrete time derivative, 79
- Domain fixing transformation, 26, 35
- Ductal carcinoma, 129, 155

- Elliptic–Hyperbolic–Parabolic models, 5
- Equivalence theorem, 39, 99, 103
- Euclidean norm, 13
- Extended model, 36

- FDM (BBL model), 27
- Fick’s law, 23
- Finite volume scheme, 132
- Flory energy density, 170
- Flux function, 125
- Free suspension growth, 94, 180
- Fully nonlinear flux, 144

- Global regularity of Poisson equation, 17
- Godunov flux, 40
- Grid orientation effect, 117
- Grouping identity, 14

- Hölder’s inequalities, 15
- Heaviside function, 21
- Helly’s selection theorem, 15
- Hydrogel, 167
- Hypersurface, 98

- In vitro, 1, 94

In vivo, [1](#), [94](#)
 Integro-differential equation models, [7](#)
 Internal regularity of Stokes equation, [17](#)
 Internal regularity of Poisson equation, [17](#)

 Korn's second inequality, [15](#)

 Lax-Milgram Theorem, [17](#)
 Lebesgue measure, [13](#)
 Linear interpolant, [79](#)
 Locally regular Sobolev space, [14](#)

 Max-Min identities, [15](#)
 Maximal time of existence, [88](#)
 Mesh-locking effect, [105](#)
 Method M, [40](#)
 Method U, [40](#)
 Modified numerical scheme (BBL model), [30](#)
 Momentum source terms, [22](#)
 Multi-index, [13](#)
 Multiphase models, [3](#), [35](#)
 MUSCL method, [40](#), [194](#)

 Nodal flux, [137](#)
 Nondimensionalisation, [24](#), [175](#), [204](#)
 Nonlinear conservation law, [125](#)
 Nonlinear models, [7](#)
 NUM-extended solutions, [101](#)
 NUM-weak solution, [101](#)
 Nutrient consumption rate, [23](#)
 Nutrient limited model (NLM), [95](#), [97](#), [112](#)
 Nutrient unlimited model (NUM), [95](#), [97](#), [112](#)

 Optimal control models, [7](#)

 Petree-Tartar lemma, [17](#)

 Phase field models, [6](#)
 Piola-Kirchoff stress, [171](#)
 Poincaré inequality, [15](#)
 Porous media models, [6](#)

 Reflection technique, [159](#)
 Reynold's transportation theorem, [19](#)
 Right-leaning parallelogram, [86](#)
 Ruppert's algorithm, [106](#)

 Semi-discrete scheme, [158](#)
 Sobolev spaces, [13](#), [98](#)
 Steady state, [186](#)
 Stress controlled growth, [182](#)
 Stress tensors, [21](#)
 Structured meshes, [119](#)

 Tangent space, [94](#)
 Three-dimensional BV estimate, [154](#), [194](#)
 Threshold domain, [47](#)
 Threshold model, [47](#)
 Threshold solution, [51](#)
 Threshold value, [47](#), [111](#), [123](#)
 Time projection map, [102](#)
 Time-reconstruct, [55](#)
 Time-slice property, [102](#)
 Time-space normal, [102](#)
 Two-dimensional model, [94](#), [202](#)

 Upwind method, [193](#)

 Vascular, [1](#)
 Vasculature, [1](#)

 Weak solution (BBL model), [38](#)
 Weak solution (extended model), [38](#)
 Weak-strong convergence lemma, [16](#)

 Young's inequalities, [15](#)

Author index

- Adam, J. A., 46
Adimurthi, 134
Alarcon, T., 62, 167, 168
Alarcón, T., 46
Alzahrani, A. K., 46
Araujo, R. P., 91
Astanin, S., 5, 34
- Bates, R., 117
Bauer, S., 100
Bazaliy, B., 5
Belmiloudi, A., 7
Bergström, J., 167, 170
Boffi, D., 161
Borsi, I., 7
Bowen, Y., 35
Boyer, F., 17
Bravo-Castillero, J., 168
Breward, C. J. W., v, 1, 4, 8, 9, 17, 18,
25, 27, 33–35, 49, 59, 91, 92, 112,
124, 168, 180
Brezis, H., 13, 15
Brezzi, F., 161
Byrne, H. M., v, 1, 4, 5, 8, 9, 11, 12, 17,
18, 25, 27, 33–35, 46, 49, 59, 62,
91, 92, 95, 106, 112, 124, 129,
156, 166–168, 180, 191, 202
- Caboussat, A., 35
Calzada, M. C., 62, 93
Camacho, G., 62, 93
Cao, X., 46
Cappello, G., 166
- Chagnon, G., 167
Chainais-Hillairet, C., 127, 134, 144, 146,
149, 152
Champier, S., 126
Chandrashekar, P., 130
Chaplain, M. A. J., 91, 202
Chapman, S. J., 62, 91, 167
Chen, C. Y., 8, 167, 168
Chen, T., 46
Chen, X., 6
Cheng, G., 166
Chiew, C., 166
Cockburn, B., 149
Colli, P., 6
Conci, A., 168
Conway, E., 126
Crandall, M. G., 126
Cui, S., 5, 6, 62
- Dai, M., 6
Dang, J., 35
Dean, I. S., 166
Decuzzi, P., 46, 91
Delarue, M., 166
Deriaz, E., 64
Després, B., 153
Di Pietro, D. A., 64
Diehl, S., 144
DiPerna, R. J., 134
Drew, D. A., 34
Droniou, J., 15, 16, 59, 64, 72, 77
Dutta, R., 134

Enderling, H., 7
 Ern, A., 15, 17, 64, 92
 Estrella, V. C., 46
 Evans, L. C., 13, 15, 17, 66, 94, 104
 Eymard, R., 15, 16, 40, 58, 59, 64, 72, 77,
 105, 125–127, 134, 149

 Fabrie, P., 17
 Fasano, A., 7
 Favier, D., 167
 Feireisl, E., 6
 Fernández-Cara, E., 62, 93
 Ferrari, M., 46, 91
 Flory, P. J., 170
 Folkman, J., 49
 Fortin, M., 161
 Franks, S. J., 8, 12, 129, 156, 191
 Friedman, A., 5, 6

 Gallouët, T., 15, 16, 40, 58, 59, 64, 72,
 77, 125–127, 134, 149
 García-Reimbert, C., 168
 Garcke, H., 6
 Gariépy, R. F., 15, 104
 Gatenby, R. A., 46
 Ghaleb, S. A., 46
 Ghandourah, E., 46
 Gilardi, G., 6
 Gillies, R. J., 46
 Gimse, T., 144
 Gowda, G. D. V., 134
 Grald, E. W., 35
 Gray, W. G., 46, 91
 Greenspan, H. P., 3, 91, 168
 Gremaud, P. A., 149
 Grimes, D. R., 117
 Guermond, J. L., 15, 17, 92
 Guichard, C., 15, 16, 59, 64, 72, 77, 105
 Guinovart-Díaz, R., 168
 Guo, Q., 6

 Hahnfeldt, P., 7
 Helmlinger, G., 166, 168, 186

 Herbin, R., 15, 16, 40, 58, 59, 64, 72, 77,
 125–127, 134, 149
 Hilhorst, D., 6
 Hillen, T., 7
 Hochberg, M., 49
 Hogeia, C. S., 46
 Holden, H., 131
 Hong, W., 170
 Hu, B., 7
 Hubbard, M. E., 5, 8, 46, 106, 124, 168
 Hussain, F., 46, 91

 Jaffré, J., 134
 Jain, H. V., 166, 168
 Jain, R. K., 166, 168, 186
 Joanny, J. F., 166

 Kannan, P., 117
 Karlsen, K. H., 126
 Kesavan, S., 15
 Kim, I. C., 6
 King, J. R., 4, 8, 11, 12, 25, 34, 91, 92,
 95, 129, 156, 167, 168, 191
 Klingenberg, C., 130
 Kolomenskiy, D., 64
 Kroener, D., 46
 Kumar, S. K., 134
 Kuznetsov, N. N., 126, 149

 Lam, K. F., 6
 Lapin, A., 46
 Leal, L. G., 19
 Leer, B. van, 42
 LeVeque, R. J., 58
 Lewis, C. E., v, 1, 4, 8, 9, 12, 17, 18, 25,
 27, 33–35, 49, 59, 91, 92, 112,
 124, 129, 156, 168, 180, 191
 Li, D., 35
 Lichtenbeld, H. C., 166, 168, 186
 Lions, P. L., 134
 Lloyd, M. C., 46
 Lowengrub, J., 93
 Luckhaus, S., 46

Luo, K., 35
 Macarthur, J. W., 35
 MacKenzie, J. A., 5, 62
 Macklin, P., 93
 Maddalena, L., 7
 Madzvamuse, A., 5, 62
 Mahmoud, S. R., 46
 Maini, P. K., 46, 62, 91, 167, 168
 Majda, A., 126
 Mancini, A., 7
 Markelc, B., 117
 Marín, M., 62, 93
 Masson, R., 105
 Matadi, M. B., 7
 Matthews, P., 4, 46, 168
 Maz'ya, V., 17
 McElwain, D. L. S., 4, 8, 11, 25, 34, 91, 92, 95, 167, 168
 Melder, R. J., 166, 168, 186
 Merlet, B., 126
 Merodio, J., 168
 Meyer, G. H., 35
 Miller, C. T., 46, 91
 Mishra, S., 134
 Montel, F., 166
 Moore, M. N. J., 166, 168
 Mouw, J. K., 166
 Munn, L. L., 166
 Murray, B. T., 46
 Muschel, R., 117
 Netti, P. A., 166, 168, 186
 Northcott, J. M., 166
 Oke, S. I., 7
 Osborne, J. M., 5, 8, 91, 92, 168
 Owen, M. R., 46, 62, 167, 168
 Padilla, I., 7
 Partridge, M., 117
 Pauly, D., 100
 Penta, R., 168
 Perfahl, H., 46
 Perthame, B., 6
 Plaza, R. G., 7
 Pop, I. S., 46
 Preziosi, L., 4, 5, 8, 11, 25, 34, 91, 92, 95, 129, 167, 168
 Primicerio, M., 7
 Prost, J., 166
 R. King, J., 4, 35, 91
 Ramírez-Torres, A., 168
 Rebouah, M., 167
 Remesan, G. C., 59, 124
 Reuss, M., 46
 Risebro, N. H., 131, 144
 Rocca, E., 6
 Rodríguez-Ramos, R., 168
 Roose, T., 62, 91, 167
 Rossmann, J., 17
 Ruppert, J., 106
 Sabina, F. J., 168
 Salsa, S., 47
 Sanders, R., 126
 Schimperna, G., 6
 Schneider, K., 64
 Schonbek, M. E., 6
 Schrefler, B. A., 46, 91
 Sciumè, G., 46, 91
 Sethian, J. A., 46
 Shelton, S., 46, 91
 Smoller, J., 126
 Song, H., 7
 Sorribes, I. C., 166, 168
 Souganidis, P. E., 6
 Spencer, A. J. M., 167
 Stewart, H. B., 34
 Suo, Z., 170
 Tadmor, E., 64
 Takao, S., 166
 Tao, Y., 6, 62
 Tapp, K., 97, 98
 Taya, M., 166

Thom e, V., 16, 111
Towers, J. D., 126
Tse, J., 166
Underwood, J. C. E., 8, 12, 129, 156, 191
Vald es-Ravelo, F., 168
Vegni, F. M. G., 47
Vignjevic, D., 166
Vovelle, J., 126
Wahlbin, L. B., 16, 111
Wang, Y., 35
Wang, Z., 7
Ward, J., 4, 35, 91
Warren, D. R., 117
Weaver, V. M., 166
Webb, S. D., 62, 167, 168
Wenchao, L., 35
Wendroff, B., 34
Whiteley, J. P., 5, 8, 91, 92, 168
Xulu, S. S., 7
Yang, J. X., 149
Yao, L., 35
Yeoh, O. H., 170
Yoshida, N., 6
Zaretti, A., 47
Zhang, N., 62
Zhao, X., 170
Zheng, J., 62
Zhou, J., 170
Zhu, C., 35
Zhuang, Y., 46
Zunino, P., 47

List of publications

- [1] J. Droniou, N. Nataraj, and G. C. Remesan. “Convergence analysis of a numerical scheme for a tumour growth model”. In: *IMA J. Numer. Anal.* (2021), (49 pages), URL <https://doi.org/10.1093/imanum/drab016>.
- [2] J. Droniou, J. Flegg, and G. C. Remesan. “Numerical solution of a two dimensional tumour growth model with moving boundary”. In: *J. Sci. Comput.* 85.22 (2020), (31 pages), URL <https://doi.org/10.1007/s10915-020-01326-6>.
- [3] G. C. Remesan. “Numerical solution of the two-phase tumour growth model with moving boundary”. In: *Proceedings of the 18th Biennial Computational Techniques and Applications Conference, CTAC-2018*, Ed. by B. Lamichane, T. Tran, and J. Bunder. Vol. 60. ANZIAM J. (2019), pp. C1–C15, (15 pages). URL: <https://doi.org/10.21914/anziamj.v60i0.13936>.
- [4] G. C. Remesan. Strong bounded variation estimates for the multi-dimensional finite volume approximation of scalar conservation laws. In: ArXiv: abs/2004.12346 (2020), (36 pages). URL <https://arxiv.org/abs/2004.12346>. [**Accepted on June 2021: M2AN: Math. Model. Anal**].
- [5] G. C. Remesan, J. A. Flegg, and H. M. Byrne. Two-phase model of compressive stress induced on a surrounding medium by an expanding tumour, (2021), (25 pages). [**In preparation**].